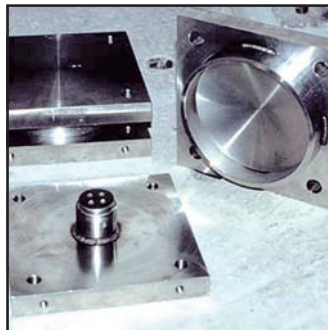
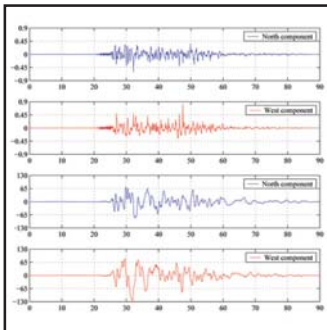


Performance Estimates for Seismically Isolated Bridges

by
Gordon P. Warn and Andrew S. Whittaker



Technical Report MCEER-07-0024

December 30, 2007

NOTICE

This report was prepared by the University at Buffalo, State University of New York as a result of research sponsored by MCEER through a contract from the Federal Highway Administration. Neither MCEER, associates of MCEER, its sponsors, the University at Buffalo, State University of New York, nor any person acting on their behalf:

- a. makes any warranty, express or implied, with respect to the use of any information, apparatus, method, or process disclosed in this report or that such use may not infringe upon privately owned rights; or
- b. assumes any liabilities of whatsoever kind with respect to the use of, or the damage resulting from the use of, any information, apparatus, method, or process disclosed in this report.

Any opinions, findings, and conclusions or recommendations expressed in this publication are those of the author(s) and do not necessarily reflect the views of MCEER or the Federal Highway Administration.

Performance Estimates for Seismically Isolated Bridges

by

Gordon P. Warn¹ and Andrew S. Whittaker²

Publication Date: December 30, 2007

Submittal Date: June 21, 2007

Technical Report MCEER-07-0024

Task Number 094-D-1.3

FHWA Contract Number DTFH61-98-C-00094

- 1 Post-Doctoral Research Associate, Department of Civil, Structural and Environmental Engineering, University at Buffalo, State University of New York
- 2 Professor, Department of Civil, Structural and Environmental Engineering, University at Buffalo, State University of New York

MCEER

University at Buffalo, The State University of New York

Red Jacket Quadrangle, Buffalo, NY 14261

Phone: (716) 645-3391; Fax (716) 645-3399

E-mail: mceer@buffalo.edu; WWW Site: <http://mceer.buffalo.edu>

Preface

The Multidisciplinary Center for Earthquake Engineering Research (MCEER) is a national center of excellence in advanced technology applications that is dedicated to the reduction of earthquake losses nationwide. Headquartered at the University at Buffalo, State University of New York, the Center was originally established by the National Science Foundation in 1986, as the National Center for Earthquake Engineering Research (NCEER).

Comprising a consortium of researchers from numerous disciplines and institutions throughout the United States, the Center's mission is to reduce earthquake losses through research and the application of advanced technologies that improve engineering, pre-earthquake planning and post-earthquake recovery strategies. Toward this end, the Center coordinates a nationwide program of multidisciplinary team research, education and outreach activities.

MCEER's research is conducted under the sponsorship of two major federal agencies, the National Science Foundation (NSF) and the Federal Highway Administration (FHWA), and the State of New York. Significant support is also derived from the Federal Emergency Management Agency (FEMA), other state governments, academic institutions, foreign governments and private industry.

The Center's Highway Project develops improved seismic design, evaluation, and retrofit methodologies and strategies for new and existing bridges and other highway structures, and for assessing the seismic performance of highway systems. The FHWA has sponsored three major contracts with MCEER under the Highway Project, two of which were initiated in 1992 and the third in 1998.

Of the two 1992 studies, one performed a series of tasks intended to improve seismic design practices for new highway bridges, tunnels, and retaining structures (MCEER Project 112). The other study focused on methodologies and approaches for assessing and improving the seismic performance of existing "typical" highway bridges and other highway system components including tunnels, retaining structures, slopes, culverts, and pavements (MCEER Project 106). These studies were conducted to:

- assess the seismic vulnerability of highway systems, structures, and components;
- develop concepts for retrofitting vulnerable highway structures and components;
- develop improved design and analysis methodologies for bridges, tunnels, and retaining structures, which include consideration of soil-structure interaction mechanisms and their influence on structural response; and
- develop, update, and recommend improved seismic design and performance criteria for new highway systems and structures.

The 1998 study, “Seismic Vulnerability of the Highway System” (FHWA Contract DTFH61-98-C-00094; known as MCEER Project 094), was initiated with the objective of performing studies to improve the seismic performance of bridge types not covered under Projects 106 or 112, and to provide extensions to system performance assessments for highway systems. Specific subjects covered under Project 094 include:

- development of formal loss estimation technologies and methodologies for highway systems;
- analysis, design, detailing, and retrofitting technologies for special bridges, including those with flexible superstructures (e.g., trusses), those supported by steel tower substructures, and cable-supported bridges (e.g., suspension and cable-stayed bridges);
- seismic response modification device technologies (e.g., hysteretic dampers, isolation bearings); and
- soil behavior, foundation behavior, and ground motion studies for large bridges.

In addition, Project 094 includes a series of special studies, addressing topics that range from non-destructive assessment of retrofitted bridge components to supporting studies intended to assist in educating the bridge engineering profession on the implementation of new seismic design and retrofitting strategies.

This research investigated key assumptions inherent in the equation for calculation of displacements in seismically isolated bridges (Equation 3 of the 1999 AASHTO Guide Specifications), and the validity of the current testing protocol for full-scale prototype seismic isolators for seismic loading as specified in AASHTO 1999. To facilitate response-history analysis, earthquake ground motions were collected and organized into eight bins. For each bin, the seismic hazard was characterized using the mean and median spectrum. Mean and median spectra were used to calculate the maximum design displacement using the static analysis procedures given in AASHTO 1999. Nonlinear response-history analysis was performed considering a simple isolated bridge model and twenty combinations of isolator properties subjected to unidirectional and bidirectional seismic excitation using 77 pairs of earthquake ground motion records. These properties of the seismic isolators, namely, the characteristic strength normalized by the weight acting on the isolator and the second slope-period, were varied widely to represent most bridge isolation systems. The results of the response-history analyses were mined to determine maximum isolator displacements and energy demands imposed on seismic isolators during maximum earthquake shaking. Energy demands were quantified using two metrics: (1) the total energy dissipated by the seismic isolator normalized by the energy dissipated by one fully reversed cycle to the maximum displacement and (2) the rate-of-energy dissipated.

ABSTRACT

This report presents an analytical study investigating the performance of an isolated bridge structure subjected to seismic excitation. Here performance is being assessed using the following descriptors: maximum horizontal displacements and cumulative energy dissipated by an individual seismic isolator. Twenty different isolation systems are considered with varied parameters, namely, characteristic strength (Q_d) and second-slope stiffness (K_d). Unidirectional and bi-directional response-history analysis was performed considering nonlinear systems and eight bins of earthquake ground motions. Results of the response-history analysis are being used to: (1) determine the increase in maximum horizontal displacement of a seismic isolator due to bi-directional seismic excitation utilizing a coupled plasticity model with a circular yield function to represent the seismic isolator elements, and (2) review the accuracy of the current AASHTO equation for the calculation of displacements in isolated bridge structures which assumes unidirectional seismic excitation and linearly increasing displacements for periods greater than 1-second, and (3) develop prototype testing requirements for seismic isolators in terms of an equivalent number of harmonic cycles to the maximum displacement and an equivalent testing frequency based on the observed energy demand imposed on individual isolators and isolation systems from numerical simulation of maximum earthquake events.

ACKNOWLEDGEMENT

The research presented in this report was supported in whole through Task D1.3 of the Federal Highway Administration through Contract DTFH 61-98-C-0094 to the Multidisciplinary Center for Earthquake Engineering Research. However, the opinions expressed in this dissertation are those of the author and do not reflect the opinions of the Multidisciplinary Center for Earthquake Engineering Research or the Federal Highway Administration. No guarantee regarding the results, findings, and recommendations are offered by either the Multidisciplinary Center for Earthquake Engineering Research or the Federal Highway Administration.

TABLE OF CONTENTS

SECTION	TITLE	PAGE
1	INTRODUCTION	1
1.1	General	1
1.2	Displacements in Seismically Isolated Bridges	2
1.3	Performance Characterization of Seismic Isolators	3
1.4	Report Organization	4
2	MODELING AND ANALYSIS OF SEISMIC ISOLATION SYSTEMS	5
2.1	General	5
2.2	Mokha, Constantinou, and Reinhorn (1993)	6
2.3	Huang, Fenves, Whittaker, and Mahin (2000)	7
2.4	Mosqueda, Whittaker, and Fenves (2003)	8
3	EARTHQUAKE GROUND MOTIONS AND ELASTIC RESPONSE SPECTRA	11
3.1	General	11
3.2	Ground Motions	11
3.2.1	General	11
3.2.2	Organization	12
3.2.3	Near-Field Ground Motions	12
3.2.4	Soft-Soil Ground Motions	13
3.2.5	Soil Classification	14
3.3	Elastic Response Spectra	14
3.3.1	General	14
3.3.2	Characterization of the Elastic Response Spectra	15
3.3.3	Directivity of Response Spectrum	15
3.3.4	Effects of Forward Rupture Directivity on the Response Spectrum	16
3.3.5	Identification of Spectral Regions	16
3.3.6	Linear Regression Analysis Performed on the Logarithm of the Mean Acceleration Spectrum	18

TABLE OF CONTENTS (CONT'D)

SECTION	TITLE	PAGE
4	RESPONSE-HISTORY ANALYSIS	55
4.1	General	55
4.2	Nonlinear Response-History Analysis	55
4.2.1	General	55
4.2.2	Simple Bridge Model	55
4.2.3	Isolation Paramters	57
4.2.4	Mathematical Model for Isolator Elements	58
4.2.5	Equation of Motion	62
5	DISPLACEMENT ESTIMATES IN SEISMICALLY ISOLATED BRIDGES	65
5.1	General	65
5.2	Static Analysis Procedure	65
5.2.1	General	65
5.2.2	Results of the Static Analysis Procedure	66
5.2.3	Design Displacement Considering Directivity of Ground Motion Components	66
5.3	Results of Unidirectional Nonlinear Response-History Analysis (URHA)	67
5.3.1	General	67
5.3.2	Comparison of Displacement Results Determined from URHA and Static Analysis Procedure	68
5.4	Results of Bi-directional Nonlinear Response-History Analysis (BRHA)	69
5.4.1	General	69
5.4.2	Comparison of Displacement Results Determined from BRHA and Static Analysis Procedure	70
5.5	Unidirectional Displacement Multiplier	71
5.5.1	General	71
5.5.2	Estimates of the Maximum Horizontal Displacement	73
5.6	Conclusion	74

TABLE OF CONTENTS (CONT'D)

SECTION	TITLE	PAGE
6	ENERGY DEMANDS IMPOSED ON SEISMIC ISOLATORS SUBJECTED TO EARTHQUAKE EXCITATION	97
6.1	General	97
6.2	Energy Demands on Seismic Isolators	97
6.2.1	General	97
6.2.2	Normalized Energy Dissipated	98
6.2.2.1	General	98
6.2.2.2	Unidirectional Seismic Excitation	99
6.2.2.3	Bi-directional Seismic Excitation	100
6.2.3	Rate-of-Energy Dissipated	102
6.2.3.1	General	102
6.2.3.2	Unidirectional Seismic Excitation	103
6.2.3.3	Bi-directional Seismic Excitation	104
6.2.3.4	Equivalent Harmonic Frequency	105
6.3	Conclusions	107
6.3.1	General	107
6.3.2	Current Prototype Testing Requirements	108
6.3.3	Conclusions Regarding the Current Prototype Testing Requirements	109
6.3.4	Recommendations for the Prototype Testing of Seismic Isolators	111
7	SUMMARY, CONCLUSIONS, AND RECOMMENDATIONS	153
7.1	Summary	153
7.2	Conclusions	154
7.3	Recommendations	155
7.3.1	Future Research	155
7.3.2	Prototype Testing Protocol	156
8	REFERENCES	157

TABLE OF CONTENTS (CONT'D)

SECTION	TITLE	PAGE
APPENDIX A	EARTHQUAKE GROUND MOTIONS	161
APPENDIX B	INVESTIGATION OF THE DISTRIBUTION OF SPECTRAL ACCELERATION DATA	201
B.1	Introduction	201
B.2	Organization of Spectral Acceleration Data	201
B.3	Continuous Distribution Functions	202
B.4	Qualitative Assessment of the Distribution of Spectral Acceleration Data	203
B.5	Quantitative Analysis of Spectral Acceleration Data	204
B.6	Results of the Goodness-of-Fit Test	205
B.7	Conclusions	206
APPENDIX C	NUMERICAL PROCEDURE FOR NONLINEAR RESPONSE-HISTORY ANALYSIS AND VERIFICATION USING SAP2000	213
C.1	Introduction	213
C.2	Numerical Procedure	213
C.2.1	General	213
C.2.2	Newmark's Method	213
C.2.3	Coupled-Plasticity Model	214
C.2.4	Stability and Accuracy of Solution	216
C.3	Verification using SAP2000	217
C.4	Conclusion	219
APPENDIX D	SAMPLE CALCULATIONS TO DETERMINE ISOLATOR DISPLACEMENTS USING THE AASHTO PROCEDURE AND EQUATION 3B FROM THE GUIDE SPECIFICATIONS	229
D.1	Sample calculations considering the 1-second mean spectral acceleration from Bin 2M and isolator properties: $Q_d / W = 0.06$ and $T_d = 4.0$ sec. Values of B determined using Table 7.1-1 of the AASHTO Guide Specifications	229

TABLE OF CONTENTS (CONT'D)

SECTION	TITLE	PAGE
D.2	Sample calculations considering the 1-second mean spectral acceleration from Bin 7 and isolator properties: $Q_d/W = 0.03$ and $T_d = 3.0$ sec. Values of B determined using Table 7.1-1 of the AASHTO Guide Specifications	231
	APPENDIX E MAXIMUM ISOLATOR DISPLACEMENT DATA	235
	APPENDIX F NORMALIZED ENERGY DISSIPATED AND RATE-OF-ENERGY DISSIPATED DATA	249

LIST OF FIGURES

FIGURE	TITLE	PAGE
3.1	Acceleration, velocity, and displacement traces for record TCU065	29
3.2	Acceleration, velocity, and displacement traces for record TCU075	30
3.3	Elastic response spectra for Bin 1 ground motions and 5% critical damping using a normal characterization	31
3.4	Elastic response spectra for Bin 2 ground motions and 5% critical damping using a normal characterization	32
3.5	Elastic response spectra for Bin 2M ground motions and 5% critical damping using a normal characterization	33
3.6	Elastic response spectra for Bin 3 ground motions and 5% critical damping using a normal characterization	34
3.7	Elastic response spectra for Bin 4 ground motions and 5% critical damping using a normal characterization	35
3.8	Elastic response spectra for Bin 5 ground motions and 5% critical damping using a normal characterization	36
3.9	Elastic response spectra for Bin 6 ground motions and 5% critical damping using a normal characterization	37
3.10	Elastic response spectra for Bin 7 ground motions and 5% critical damping using a normal characterization	38
3.11	Elastic response spectra for Bin 1 ground motions and 5% critical damping using a lognormal characterization	39
3.12	Elastic response spectra for Bin 2 ground motions and 5% critical damping using a lognormal characterization	40
3.13	Elastic response spectra for Bin 2M ground motions and 5% critical damping using a lognormal characterization	41
3.14	Elastic response spectra for Bin 3 ground motions and 5% critical damping using a lognormal characterization	42
3.15	Elastic response spectra for Bin 4 ground motions and 5% critical damping using a lognormal characterization	43
3.16	Elastic response spectra for Bin 5 ground motions and 5% critical damping using a lognormal characterization	44
3.17	Elastic response spectra for Bin 6 ground motions and 5% critical damping using a lognormal characterization	45
3.18	Elastic response spectra for Bin 7 ground motions and 5% critical damping using a lognormal characterization	46

LIST OF FIGURES (CONT'D)

FIGURE	TITLE	PAGE
3.19	Mean elastic response spectra for 1st, 2nd, and all, ground motion components and 5% critical damping for Bins 1 and 2	47
3.20	Mean elastic response spectra for 1st, 2nd, and all, ground motion components and 5% critical damping for Bins 2M and 3	48
3.21	Mean elastic response spectra for 1st, 2nd, and all, ground motion components and 5% critical damping for Bins 4 and 5	49
3.22	Mean elastic response spectra for 1st, 2nd, and all, ground motion components and 5% critical damping for Bins 6 and 7	50
3.23	Median elastic response spectra for 1st, 2nd, and all, ground motion components and 5% critical damping for Bins 1 and 6	51
3.24	Elastic response spectra for record TCU065 and 5% critical damping	52
3.25	Elastic response spectra for record TCU075 and 5% critical damping	53
3.26	Estimated periods for the transition of spectral regions	54
4.1	Simple bridge model based on: ATC example bridge	56
4.2	Bilinear characterization of an isolation bearing	58
4.3	Comparison of the response of an isolator using coupled and uncoupled plasticity models for box shape displacement orbit	63
4.4	Comparison of the response of an isolator using coupled and uncoupled plasticity models for hourglass shape displacement orbit	64
5.1	Maximum isolator displacements calculated using Equation 3b from the AASHTO Guide Specifications and the <i>mean</i> 1-second spectral acceleration	84
5.2	Maximum isolator displacements calculated using Equation 3b from the AASHTO Guide Specifications and the <i>median</i> 1-second spectral acceleration	85
5.3	Maximum isolator displacements calculated using Equation 3b from the AASHTO Guide Specifications using the 1-second spectral acceleration from the <i>mean</i> and <i>median</i> first component spectrum for Bins 1 and 6	86
5.4	Comparison of maximum isolator displacements determined from unidirectional response-history analysis with the results of the AASHTO procedure using a mean characterization of the hazard and six bins of ground motions	87

LIST OF FIGURES (CONT'D)

FIGURE	TITLE	PAGE
5.5	Comparison of maximum isolator displacements determined from unidirectional response-history analysis with the results of the AASHTO procedure using a median characterization of the hazard and six bins of ground motions	88
5.6	Comparison of maximum isolator displacements calculated using the AASHTO procedure and the results of nonlinear response-history analysis using a <i>mean</i> and <i>median</i> characterization of the hazard considering the first ground motion components contained in Bins1 and 6	89
5.7	Comparison of maximum isolator displacements determined from bi-directional response-history analysis with the results of the AASHTO procedure using a mean characterization of the hazard and six bins of ground motions	90
5.8	Comparison of maximum isolator displacements determined from bi-directional response-history analysis with the results of the AASHTO procedure using a median characterization of the hazard and six bins of ground motions	91
5.9	Unidirectional displacement multiplier calculated for each isolation system and six bins of ground motions	92
5.10	Modified unidirectional displacement multiplier calculated for each isolation system and ground motion bins 1 and 6	93
5.11	Comparison of maximum isolator displacements using median statistics considering six bins of ground motions	94
5.12	Comparison of maximum isolator displacements using median statistics considering the first ground motion components from Bins 1 and 6	95
6.1	Cumulative energy histories calculated from the results of unidirectional response-history analysis considering two sets of isolator properties and a ground motion record from the 1992 Cape Mendocino Earthquake, Petrolia Station, (nf08) and included in Bin 1	121
6.2	Normalized energy dissipated (<i>NED</i>) based on the results of unidirectional response-history analysis and Bin 1 ground motions	122
6.3	Normalized energy dissipated (<i>NED</i>) based on the results of unidirectional response-history analysis and Bin 2 ground motions	123
6.4	Normalized energy dissipated (<i>NED</i>) based on the results of unidirectional response-history analysis and Bin 2M ground motions	124

LIST OF FIGURES (CONT'D)

FIGURE	TITLE	PAGE
6.5	Normalized energy dissipated (<i>NED</i>) based on the results of unidirectional response-history analysis and Bin 3 ground motions	125
6.6	Normalized energy dissipated (<i>NED</i>) based on the results of unidirectional response-history analysis and Bin 6 ground motions	126
6.7	Normalized energy dissipated (<i>NED</i>) based on the results of unidirectional response-history analysis and Bin 7 ground motions	127
6.8	Normalized energy dissipated (<i>NED</i>) based on the results of bi-directional response-history analysis and Bin 1 ground motions	128
6.9	Normalized energy dissipated (<i>NED</i>) based on the results of bi-directional response-history analysis and Bin 2 ground motions	129
6.10	Normalized energy dissipated (<i>NED</i>) based on the results of bi-directional response-history analysis and Bin 2M ground motions	130
6.11	Normalized energy dissipated (<i>NED</i>) based on the results of bi-directional response-history analysis and Bin 3 ground motions	131
6.12	Normalized energy dissipated (<i>NED</i>) based on the results of bi-directional response-history analysis and Bin 6 ground motions	132
6.13	Normalized energy dissipated (<i>NED</i>) based on the results of bi-directional response-history analysis and Bin 7 ground motions	133
6.14	Comparison of the mean normalized energy dissipated (<i>NED</i>) calculated for unidirectional and bi-directional excitation considering all values of Q_d / W , $T_d = 1.5$ seconds and $T_d = 2.0$ seconds, for ground motion bins, 1, 2, 2M, 3, 6, and 7	134
6.15	Comparison of the mean normalized energy dissipated (<i>NED</i>) calculated for unidirectional and bi-directional excitation considering all values of Q_d / W , $T_d = 2.5$ seconds and $T_d = 3.0$ seconds, for ground motion bins, 1, 2, 2M, 3, 6, and 7	135
6.16	Comparison of the mean normalized energy dissipated (<i>NED</i>) calculated for unidirectional and bi-directional excitation considering all values of Q_d / W , and $T_d = 4.0$ seconds, for ground motion bins, 1, 2, 2M, 3, 6, and 7	136
6.17	Comparison of the mean + 1σ normalized energy dissipated (<i>NED</i>) calculated for unidirectional and bi-directional excitation considering all values of Q_d / W , $T_d = 1.5$ seconds and $T_d = 2.0$ seconds, for ground motion bins, 1, 2, 2M, 3, 6, and 7	137

LIST OF FIGURES (CONT'D)

FIGURE	TITLE	PAGE
6.18	Comparison of the mean + 1σ normalized energy dissipated (NED) calculated for unidirectional and bi-directional excitation considering all values of Q_d / W , $T_d = 2.5$ seconds and $T_d = 3.0$ seconds, for ground motion bins, 1, 2, 2M, 3, 6, and 7	138
6.19	Comparison of the mean + 1σ normalized energy dissipated (NED) calculated for unidirectional and bi-directional excitation considering all values of Q_d / W , and $T_d = 4.0$ seconds, for ground motion bins, 1, 2, 2M, 3, 6, and 7	139
6.20	Sample energy history results from unidirectional response-history analysis performed using a ground motion record from the Cape Mendocino earthquake, Rio Dell Over Pass station (RIO360), incorporated into Bin 2M	140
6.21	Two definitions for the rate-of-energy dissipated by a seismic isolator (R_E) using a sample energy history calculated considering isolator properties: $Q_d / W = 0.06$ and $T_d = 2.5$ sec., and ground motion RIO360 from Bin 2M	141
6.22	Normalized rate-of-energy dissipated calculated using <i>Definition 1</i> (R_E^{90}) and the results of unidirectional response-history analysis	142
6.23	Normalized rate-of-energy dissipated calculated using <i>Definition 2</i> (R_E^{50}) and the results of unidirectional response-history analysis	143
6.24	Normalized rate-of-energy dissipated calculated using <i>Definition 1</i> (R_E^{90}) and the results of bi-directional response-history analysis	144
6.25	Normalized rate-of-energy dissipated calculated using <i>Definition 2</i> (R_E^{50}) and the results of bi-directional response-history analysis	145
6.26	Comparison of mean normalized rate-of-energy dissipated (R_E) data calculated using two definitions (R_E^{90} and R_E^{50}) and the results of unidirectional and bi-directional response-history analysis considering ground motion bins 1 and 2	146
6.27	Comparison of mean normalized rate-of-energy dissipated (R_E) data calculated using two definitions (R_E^{90} and R_E^{50}) and the results of unidirectional and bi-directional response-history analysis considering ground motion bins 2M and 3	147
6.28	Comparison of mean normalized rate-of-energy dissipated (R_E) data calculated using two definitions (R_E^{90} and R_E^{50}) and the results of unidirectional and bi-directional response-history analysis considering ground motion bins 6 and 7	148

LIST OF FIGURES (CONT'D)

FIGURE	TITLE	PAGE
6.29	Comparison of mean + 1σ normalized rate-of-energy dissipated (R_E) data calculated using two definitions (R_E^{90} and R_E^{50}) and the results of unidirectional and bi-directional response-history analysis considering ground motion bins 1 and 2	149
6.30	Comparison of mean + 1σ normalized rate-of-energy dissipated (R_E) data calculated using two definitions (R_E^{90} and R_E^{50}) and the results of unidirectional and bi-directional response-history analysis considering ground motion bins 2M and 3	150
6.31	Comparison of mean + 1σ normalized rate-of-energy dissipated (R_E) data calculated using two definitions (R_E^{90} and R_E^{50}) and the results of unidirectional and bi-directional response-history analysis considering ground motion bins 6 and 7	151
6.32	Schematic of the equivalent frequency (f_{eq}) determined using two definitions of the rate-of-energy (R_E) dissipated for isolator properties: $Q_d / W = 0.06$ and $T_d = 4.0$ seconds, and ground motion record RIO360 from Bin 2M	152

LIST OF TABLES

TABLE	TITLE	PAGE
1.1	Damping Coefficient B (Adopted from AASHTO 1999)	3
3.1	Near-field ground motions (Bin 1)	20
3.2	Large-magnitude, small-distance ground motions (Bin 2)	21
3.3	Large-magnitude, small-distance ground motions (Bin 2M)	22
3.4	Large-magnitude, large-distance ground motions (Bin 3)	23
3.5	Small-magnitude, small-distance ground motions (Bin 4)	24
3.6	Small-magnitude, large-distance ground motions (Bin 5)	25
3.7	Near-field, soft-soil ground motions (Bin 6)	26
3.8	Large-magnitude, soft-soil ground motions (Bin 7)	27
3.9	Spectral ordinates $S_{0.2}$ and S_1	28
3.10	Estimated transition periods for the spectral regions	28
3.11	Estimated values of the period exponent	28
4.1	Isolator parameter matrix	57
5.1	Results of the AASTHO design calculation using a mean characterization of the seismic hazard	76
5.2	Results of the AASTHO design calculation using a median characterization of the seismic hazard	77
5.3	Results of the AASHTO design calculation using a mean characterization of the seismic hazard considering directivity of the ground motion components	78
5.4	Results of the AASHTO design calculation using a median characterization of the seismic hazard considering directivity of the ground motion components	78
5.5	Mean and mean + 1σ maximum isolator displacements determined from unidirectional response-history analysis	79
5.6	Median and 84th percentile maximum isolator displacements determined from unidirectional response-history analysis	80
5.7	Mean and mean + 1σ maximum isolator displacements determined from bi-directional response-history analysis	81

LIST OF TABLES (CONT'D)

TABLE	TITLE	PAGE
5.8	Median and 84th percentile maximum isolator displacements determined from bi-directional response-history analysis	82
5.9	Unidirectional displacement multiplier	83
5.10	Modified definition of the unidirectional displacement multiplier	83
6.1	Mean and mean + 1σ normalized energy dissipated (<i>NED</i>) determined from the results of unidirectional response-history analysis for six bins of ground motions	113
6.2	Mean and mean + 1σ normalized energy dissipated (<i>NED</i>) determined from the results of bi-directional response-history analysis for six bins of ground motions	114
6.3	Mean and mean + 1σ normalized rate-of-energy dissipated data calculated using <i>Definition 1</i> and the results of unidirectional response-history analysis for six bins of ground motions	115
6.4	Mean and mean + 1σ normalized rate-of-energy dissipated data calculated using <i>Definition 2</i> and the results of unidirectional response-history analysis for six bins of ground motions	116
6.5	Mean and mean + 1σ normalized rate-of-energy dissipated data calculated using <i>Definition 1</i> and the results of bi-directional response-history analysis for six bins of ground motions	117
6.6	Mean and mean + 1σ normalized rate-of-energy dissipated data calculated using <i>Definition 2</i> and the results of bi-directional response-history analysis for six bins of ground motions	118
6.7	Sample calculation for the equivalent frequency (f_{eq}) using results of unidirectional response-history analysis and ground motion RIO360 from Bin 2M	119
6.8	Sample calculation for the equivalent frequency (f_{eq}) using results of unidirectional response-history analysis and ground motion CNP196 from Bin 2M	120

SECTION 1

INTRODUCTION

1.1 General

Seismic isolation is employed for new and retrofit bridge construction in many countries, including the United States, Greece, Italy, Japan, New Zealand, South Korea, and Turkey. Isolation systems are used to reduce force demands on bridge substructures to the point where substructures can be designed to remain elastic in maximum earthquake shaking. Force demands are reduced through the installation of vertically stiff but horizontally flexible components (isolators) between the superstructure and the substructure. Damping is generally an integral part of a bridge seismic isolator and serves the primary purpose of reducing the isolator displacements.

There are three broad classes of seismic isolator used for bridge construction in the United States and Japan at this time: the (elastomeric) Lead-Rubber (LR) bearing, the (sliding) Friction Pendulum (FP) bearing, and the (elastomeric) High-Damping Rubber (HDR) bearing. The most popular seismic isolation bridge bearings in the United States are the LR and FP bearings because both types of bearing have large initial stiffness, which is needed to prevent movement under service (braking) loads.

The current design procedures for seismic isolation systems for bridge structures are given by the American Association of State Highway and Transportation Officials (AASHTO) Guide Specification for Seismic Isolation Design (AASHTO, 1999). The Guide Specifications provide procedures for the analysis of isolation systems, design of isolation systems and individual seismic isolators, and full-scale testing of seismic isolators. Many of the procedures presented in the Guide Specification can be traced back to either the first edition of the Guide Specification (AASHTO, 1991) or the seismic isolation design provisions included in the 1997 Uniform Building Code (ICBO, 1997) for building structures.

This report presents new information that will have an impact on two aspects of the Guide Specification, namely, (1) displacement estimates in seismically isolated bridges, and (2) prototype testing of seismic isolation bearings. Summary information on each of these aspects of the Guide Specification is presented in the following two sections.

1.2 Displacements in Seismically Isolated Bridges

The key design variable for seismic isolation systems is displacement over the isolation interface. Isolator displacement dictates (a) the space around the isolated superstructure to facilitate unrestricted movement of the superstructure, (b) the shear strain in elastomeric isolators and isolator stability, (c) the plan geometry of sliding isolators, and (d) forces transmitted to the bridge substructure (piers and abutments) for given isolator stiffness.

The Uniform Load Method of the Guide Specification presents the basic method for estimating displacements in seismically isolated bridges. Specifically, equation (3) of the Guide Specification writes (in SI units of millimeters) that the isolator displacement d (or the deck displacement relative to the ground if the substructure is flexible) is equal to

$$d = \frac{250AS_i T_{eff}}{B} \quad (1.1)$$

where T_{eff} is the effective period at maximum displacement (based on the secant stiffness at the maximum displacement); $250AS_i$ is the 5-percent damped spectral displacement at 1-second, and B is a damping coefficient that modifies the design spectrum for values of equivalent viscous damping other than 5 percent. The 1-second spectral displacement is a function of the acceleration coefficient, A , and the site coefficient, S_i . Values of A and S_i are given in Division 1-A: Seismic Design of the AASHTO Standard Specifications for Highway Bridges (AASHTO, 1996). Equation (1.1) assumes that the isolated period falls in the constant velocity portion of the design spectrum in which spectral displacements are assumed to increase linearly with period.

Values for the damping coefficient B are presented in Table 7.1 of the Guide Specification, which is reproduced in Table 1.1 to illustrate the reduction in displacements afforded by the provision of damping in the isolation system.

Table 1.1. Damping Coefficient B (adopted from AASHTO 1999).

	Damping (Percentage of Critical)						
	≤ 2	5	10	20	30	40	50
B	0.8	1.0	1.2	1.5	1.7	1.9	2.0

The procedures for analysis and design of seismically isolated building structures are similar in part to those used for bridge structures. A benchmark estimate of isolator displacement is calculated using an equation similar to (1.1). Superstructure and substructure forces are tied to displacements calculated by alternate means (such as response-history analysis) that are limited as a percentage of the displacement of (1.1). Accordingly, it is of significant import to both bridge and building isolation construction that an estimate of isolator displacement established using the Uniform Load Method (or the building Equivalent Lateral Force Procedure) is accurate.

Two of the basic assumptions inherent in (1.1) are studied in this report, namely, (1) that on average, displacements increase linearly in the range of interest for isolated bridges, and (2) the effect of bi-directional horizontal shaking on the displacement estimate d , can be ignored.

1.3 Performance Characterization of Seismic Isolators

The performance of seismic isolators is checked prior to fabrication of production isolators and their installation in a bridge through prototype testing. Section 13.2 of the Guide Specification include requirements for prototype testing that include multiple cycles of seismic testing to the maximum isolator displacement, d . Specifically, the Guide Specification in Section 13.2 writes that a prototype isolator be subjected to (a) three fully reversed cycles at the following multiples of the total design displacement: 1.0, 0.25, 0.50, 0.75, 1.0, and 1.25, (b) not less than 10 and not more than 25 fully reversed cycles of loading at the design displacement, d , and (c) three fully reversed cycles of loading at the total design displacement. All of the prototype tests are typically executed at low maximum speeds.

Because isolation prototype testing is intended to judge the performance of the prototype isolator with respect to the mechanical properties assumed for the analysis and design of the isolation system, it is legitimate to question the prototype test sequence presented in the Guide Specifications. One objective of the research work described in this report was to better understand the energy demands on bridge seismic isolation bearings and to translate those estimates of energy demand into a recommended protocol for testing seismic isolation bearings.

1.4 Report Organization

This report contains 7 sections, a list of references, and 6 appendices. Section 2 presents a brief summary of research related to the modeling and analysis of seismic isolation systems. Section 3 describes the organization of earthquake ground motions utilized for response-history analysis and characterization of the seismic hazard using mean and median response spectrum. Section 4 discusses the simple mathematical model of the isolated bridge structures assumed for response-history analysis. Displacement estimates in seismically isolated bridge structures are addressed in Section 5. Energy demands on seismic isolation bearings and recommended testing protocols for seismic isolation bearings are described in Section 6. A summary of the research work, key conclusions, and recommendations for future studies are presented in Section 7. The appendices present: earthquake records used for response-history analysis (Appendix A), an investigation of the distribution of spectral acceleration data (Appendix B), verification of the mathematical model of the isolated bridge structure and a discussion of the numerical procedures used for response-history analysis (Appendix C), calculation of the maximum isolator displacement using the AASHTO procedure (Appendix D), maximum isolator displacement data (Appendix E), and data for the total energy dissipated and rate-of-energy dissipated by seismic isolators (Appendix F).

SECTION 2

MODELING AND ANALYSIS OF SEISMIC ISOLATION SYSTEMS

2.1 General

Over the past decade there have been significant advances in the understanding of the behavior of seismic isolators subjected to earthquake loading. Two of the most popular types of seismic isolation hardware are elastomeric (Lead-Rubber) and sliding (Friction Pendulum) bearings. These two types of seismic isolators have been and continue to be implemented in buildings and bridges around the world. For the design and analysis of seismically isolated structures, it is important to have mathematical models that accurately capture the behavior of these isolator elements. With sufficiently accurate models, numerical analysis of simplified isolated structures can be performed to determine important response quantities such as maximum isolator displacement and maximum shear force transmitted to the super- and substructure. Mathematical models such as the *coupled-plasticity* and *Bouc Wen* have been used to represent Lead-Rubber (LR) and Friction Pendulum (FP) isolation bearings and incorporated in computer routines to enable dynamic analysis of isolated structures subjected to earthquake loading. Such programs include 3D-BASIS (Nagarajaiah et al., 1989) and SAP2000 (CSI, 2000). The capability of these models to predict the response of seismic isolation systems subjected to earthquake loading, including prediction of the maximum force and maximum displacement information has been demonstrated through experimental testing.

A few examples of research related to the modeling, analysis, and behavior of seismic isolation systems subjected to one or more components of earthquake excitation are presented in this section. Results of this research have shown that well developed mathematical models are capable of predicting the behavior of seismically isolated structures subjected to earthquake excitation accurately. These models have been calibrated and verified through extensive experimental testing using earthquake simulators at the State University of New York at Buffalo and the University of California, Berkeley.

2.2 Mokha, Constantinou, and Reinhorn (1993)

This research study verified a mathematical model of frictional sliding bearings proposed by Constantinou, Mokha, and Reinhorn (1990) subjected to compressive loads and high velocity bi-directional motion. The mathematical model accounted for variation in normal load, bearing pressure, velocity and direction of sliding. Model parameters were calibrated experimentally by applying unidirectional sinusoidal motion with a specific amplitude and frequency to a bearing with Teflon and stainless steel contact surfaces. These materials are typically used for the contact surfaces of Friction Pendulum isolators, which have been implemented in a large number of buildings and bridges around the world.

An experimental program was conducted consisting of two sets of bi-directional motions: (1) harmonic motion with out-of-phase components and (2) random earthquake type motions. [It is important to note that the authors use the term “out-of-phase” to describe the two horizontal displacement components with respect to time. However, out-of-phase in this context does not necessarily results in simultaneous displacement demand in both horizontal directions. This is demonstrated in Section 4 of this report where a box shape displacement orbit is investigated.] Results of the experimental program were compared with the predictions of the mathematical model. This comparison proved qualitatively that the mathematical model was capable of predicting the response of the bearing subjected to harmonic and random bi-directional excitation. However, no quantitative comparison was provided. These results, both analytical and experimental, demonstrated the importance of bi-directional interaction in sliding isolation systems.

Bi-directional interaction was further investigated by analyzing a model structure supported by 45 isolators using nine pairs of earthquake ground motions. The isolators were modeled using the previously mentioned mathematical model considering bi-directional interaction (circular yield function) and neglecting bi-directional interaction (square yield function). The ground motions used for the analyses were scaled to have consistent amplitude and frequency content with a target spectrum over the period range of interest. Results of this supplemental analytical investigation showed that neglecting the bi-directional interaction resulted in an *overestimation* of the lateral forces transmitted

to the super- and substructure and an *underestimation* of the maximum displacement. This overestimation of the structural shear and underestimation of the maximum displacement was observed to be as large as 20 percent. The authors determined that this was significant and that bi-directional interaction in sliding isolation systems should be considered.

2.3 Huang, Fenves, Whittaker, and Mahin (2000)

An experimental and analytical investigation of the bi-directional behavior of Lead-Rubber bearings was conducted. The experimental component of this research used a rigid-frame supported by 4 Lead-Rubber bearings subjected to four defined displacement orbits and five pairs of earthquake ground motion records. The displacement orbits were varied to obtain displacement demand in either of the horizontal directions independently or in both simultaneously. The earthquake ground motions represented different intensity, duration, soil type, and source mechanism. For the analytical component, a bi-linear rate-independent plasticity model was considered. For this model both coupled (circular yield function) and uncoupled (square yield function) were considered. Further, a 4-parameter model based on bounding surface theory, was proposed and investigated.

A comparison of the experimental and analytical results for the pre-defined displacement orbits showed that the bi-linear plasticity model with circular yield function (coupled) was capable of prediction the force response of the Lead-Rubber bearing with reasonable accuracy. The bi-linear plasticity model with square yield function (uncoupled) was unable to accurately reproduce the force response of the Lead-Rubber bearing. A comparison of the experimental and analytical results using the five pairs of earthquake ground motions showed that the coupled plasticity model reproduced the force and displacement response with reasonable accuracy and the uncoupled plasticity model again was unable to reproduce the force or displacement response when compared to the experimental results. However, the uncoupled plasticity model was able to predict maximum isolator displacements with reasonable accuracy for at least one ground motion pair.

An improved model for Lead-Rubber isolation bearing was proposed. This model uses strain independent parameters and is based on bounding surface theory. Numerical simulations were performed using the improved model subjected to a unidirectional sinusoidal displacement time history with varying displacement amplitudes. Results of this analysis were compared with experimental results of a Lead-Rubber bearing isolated structure subjected to the same unidirectional sinusoidal displacement time history with varying amplitude corresponding to 25, 50, 100, and 150 percent shear strain. This comparison showed that the improved model was capable of predicting the response of the Lead-Rubber bearing over a wide range of strain levels.

2.4 Mosqueda, Whittaker, and Fenves (2003)

The behavior of Friction Pendulum bearings subjected to multiple components of excitation was investigated in this research. Both experimental and numerical simulations of a rigid-frame model representing a rigid bridge super-structure supported by four Friction Pendulum bearings were conducted. Results of the experimental simulations were used to evaluate the efficacy of five mathematical models.

The experimental component utilized both displacement controlled orbits and scaled earthquake ground motions. Six displacement orbits were used to evaluate the response of Friction Pendulum bearings subjected to bi-directional motion. Data from the experimental simulation was used to calibrate the mathematical model, namely, the coefficient of friction and the threshold velocities for which the coefficient of friction can be assumed constant. Five pairs of earthquake ground motions were used to evaluate the response of the isolated bridge model subjected to unidirectional and bi-directional seismic excitation. Tri-directional tests were also performed to evaluate the effect of vertical ground motion on the response of the isolated bridge model. Experimental data was used to evaluate five mathematical models for the Friction Pendulum isolators.

Five mathematical models were used to represent the Friction Pendulum isolators: (1) a coupled plasticity model with varying axial load; (2) a coupled plasticity model with constant axial load; (3) an uncoupled plasticity model with varying axial load; (4) an uncoupled plasticity model with constant axial load; and (5) a linear viscous

representation. The five models were subjected to the pre-defined displacement orbits and the five pairs of earthquake histories using numerical simulation. Results of the experimental simulations were used to evaluate the ability of the five mathematical models to predict the response of the Friction Pendulum isolators subjected to multiple components of excitation as well as the prediction of maximum isolator displacements and maximum resisting forces. From this comparison it was determined that the coupled plasticity model with varying axial load predicted the response of the isolators and isolation system with the greatest accuracy. However, the coupled plasticity model with constant axial load was capable of predicting maximum displacement with reasonable accuracy, however, the maximum restoring force of the system was underestimated. Both uncoupled plasticity models were observed to underestimate maximum displacements and overestimate the maximum restoring force. The linear viscous model was unable to accurately predict maximum isolator displacement or the maximum restoring force.

It was concluded that the coupled plasticity model with varying axial force yields the best prediction of the response of the Friction Pendulum isolation system subjected to bi-directional excitation and predicts the maximum isolator displacements and maximum restoring force within 10 percent accuracy. The linear viscous model was unable to capture the response of the isolator subjected to bi-directional seismic excitation and predicted the maximum displacement and maximum restoring force with an unacceptable level of accuracy. The researchers also concluded that such a model should not be used to represent Friction Pendulum isolators for dynamic response-history analysis.

SECTION 3

EARTHQUAKE GROUND MOTIONS AND ELASTIC RESPONSE SPECTRA

3.1 General

This section presents information about the earthquake ground motions used for response-history analysis performed for this study. A brief explanation regarding the organization of the ground motions into eight bins is presented. Elastic, 5% damped response spectrum were generated for each ground motion component. Response spectra contained in a particular bin were statistically organized to characterize the seismic hazard. The eight bins of ground motions represent a broad range of seismic demand such that the results of analyses performed using the bins of ground motions will, on average, be applicable to the design of isolated bridges throughout the United States.

Presented at the end of this section is an investigation of the spectral regions and associated transition periods for five of the eight bins of ground motions. Results of this investigation were used to determine the constant velocity portions of the mean spectra and to verify the linearly increasing displacements assumed by the AASHTO design spectrum.

3.2 Ground Motions

3.2.1 General

A total of 77 earthquake ground motion pairs were utilized for this study. Ground motions were organized into eight bins, five of which were based on moment magnitude and distance-to-fault. Acceleration time histories were extracted from two sources: the Pacific Earthquake Engineering Research (PEER) database, <http://peer.berkeley.edu/smcat/> (PEER, 2000); the SAC Steel Project database, <http://eerc.berkeley.edu:8080/index.html/> (SAC, 1997). One pair of soft soil ground motions was obtained from Miranda (Personal communication, 2002).

3.2.2 Organization

Ground motions were organized into 8 bins: (1) Near-Field, (2) Large-Magnitude Small-Distance, (2M) Large-Magnitude Small-Distance, (3) Large-Magnitude Large-Distance, (4) Small-Magnitude Small-Distance, (5) Small-Magnitude Large-Distance, (6) Near-Field Soft-Soil, and (7) Large-Magnitude Soft-Soil. Bin descriptions (2) through (5) are those adopted by Krawinkler (Personal communication, 2001). The bin descriptions represent parameters such as: distance-to-fault, moment magnitude and soil type, which were used to organize the ground motions. For instance, large-magnitude describes events greater than 6.5, while small-magnitude refers to events ranging from 5.2 to 6.6. Similarly, small-distance ranges from 10 to 30 km and large-distance refers to distances greater than 30 km. The near-field bin contains ground motions ranging from 6.7 to 7.6 in magnitude and distances-to-fault of less than 10 km.

Each bin contains 20 horizontal ground motion components corresponding to 10 earthquake events with the exception of the near-field bin, which contains 24 ground motions. Also, Bin 2 was modified to form Bin 2M, replacing five pairs of ground motion to achieve a mean 1-second spectral acceleration of approximately 0.4g. Lists of ground motion components by bin are presented in Tables 3.1 through 3.8 including information such as: event, moment-magnitude, distance-to-fault, peak ground acceleration, and soil type (SAC, 1997; PEER, 2000). Acceleration time histories for each ground motion component are presented in Appendix A.

3.2.3 Near-Field Ground Motions

The first twenty ground motion components listed in Table 3.1 were obtained from the SAC Steel Project database. Of these twenty motions, ten of the motions were recorded and ten were simulated. For the recorded ground motions, some were originally recorded on soil conditions corresponding to site class: D, as designated by the National Earthquake Hazard Reduction Program, and some were modified to represent these soil conditions (SAC, 1997).

The last four ground motions of Table 3.1: TCU065N, TCU065W, TCU075N and TCU075W, are from the 1999 Chi-Chi (Taiwan) earthquake. These two ground motion

pairs were extracted from the PEER database and incorporated into Bin 1. Acceleration, velocity and displacement time histories for each component of TCU065 and TCU075 are presented in Figures 3.1 and 3.2, respectively. These motions have been incorporated into Bin 1 in an effort to increase the diversity of the near-field strong motion data used for this study.

One of the ground motion pairs selected from the Chi-Chi data set was found to contain directivity effects. Specifically, forward rupture directivity (FRD) which is typically found on the fault normal component of strike-slip faulting for near-field ground motions. The presence of FRD is determined by the alignment of slip and the direction of propagation of the rupture front (Somerville, 2000). Forward rupture directivity is characterized by a large, two sided velocity pulse appearing on the fault normal component of the record. The fault parallel component is usually absent of this pulse with a velocity time history more commonly found from vibratory earthquake ground motions. Referring to the components of TCU075, the North and West components are approximately aligned in the fault parallel and fault normal direction, respectively. From the velocity time history traces of record TCU075 (see Figure 3.2) a large two sided velocity pulse is observed on the West component between 26 and 32 seconds with a maximum velocity of 88 cm/s. The velocity trace of the North component is more uniform in amplitude over the duration of strong motion with a maximum velocity of 38 cm/s. Based on these observations TCU075 was believed to contain directivity effects and therefore incorporated in the near-field bin used in this study. Elastic response spectra were generated to further investigate the presence of forward rupture directivity.

3.2.4 Soft-Soil Ground Motions

Ground motion comprising bins 6 and 7 represent soft-soil site conditions. The ground motions contained in Bin 6 were obtained from the SAC Steel Project database. These ground motions were simulated using a nonlinear model of a soil column and stiff-soil ground motions as input at the base of the soil column. The soil column model was intended to represent soil conditions with: a depth to firm ground of 46 m (150ft) and an average shear wave velocity of 152 m/s (497 fps) (SAC, 1997). Presented in Table 3.7 is a list of the near-field soft-soil ground motions and information corresponding to the

original input ground motions. Bin 7 ground motions were collected from the PEER database with the exception of the SCT ground motion pair, which was obtained from Miranda et al. (Personal communication 2002). Table 3.8 presents a list of the large-magnitude soft-soil ground motions and corresponding information.

3.2.5 Soil Classification

The first twenty motions of the near-field bin were classified with a soil type of D as designated by the National Earthquake Hazard Reduction Program (FEMA, 2001). Site class D corresponds to a stiff soil profile with an average shear wave velocity ranging from 180-360 m/s. Soil conditions for ground motion bins 2-5 have been classified by United States Geological Survey (USGS) as either type A or type C, corresponding to rock (average shear wave velocities >750 m/s) and stiff soil profiles (average shear wave velocities ranging from 180-360 m/s), respectively. The ground motions of Bin 6 represent site class, F, using the NEHRP designation (SAC, 1997). Site class information for the first four ground motion pairs of Bin 7 are based on descriptions of the local soil conditions (Benuska, 1990; Miranda, 1991). Site class information for the remaining six pairs of ground motions in Bin 7 is based on the USGS Classification corresponding to C (average shear wave velocity between 180-360 m/s) and D (average shear wave velocity <180 m/s). Soil classification information has been included in Tables 3.1 through 3.8.

3.3 Elastic Response Spectra

3.3.1 General

Elastic response spectra were generated for each ground motion component used in this study. All spectra were generated for 5% critical damping. For brevity, not all spectra are presented. However, the seismic hazard for each bin has been characterized by two means: first, as the *mean* of all spectra contained in a particular bin assuming the spectral acceleration data follow a normal distribution and second, as the *median* assuming the spectral acceleration data follow a lognormal distribution.

3.3.2 Characterization of the Elastic Response Spectra

Based on an investigation of the probabilistic distribution of spectral acceleration data, presented in Appendix B, a lognormal characterization of the spectral acceleration data was determined to be the better of the two models considered. However, because the normal distribution is commonly used to characterize the dispersion of elastic spectra, both normal and lognormal characterizations of the elastic design spectrum are presented.

Presented in Figures 3.3 through 3.10 are: mean; mean plus and minus one standard deviation ($\text{mean} \pm 1\sigma$); and maximum and minimum (*max/min*) spectra, for Bins 1 through 7. The spectra were determined assuming the spectral acceleration data to be normally distributed. The mean and standard deviation were calculated as the sample mean and sample standard deviation of the spectral acceleration data.

Figures 3.11 through 3.18 present: median; 84th percentile; and 16th percentile spectra, for Bins 1 through 7. These spectra were determined assuming a lognormal characterization of the spectral acceleration data. The parameters of the lognormal distribution were estimated from the spectral acceleration data samples. A more detailed explanation regarding the characterization of the distribution of spectral acceleration data is presented in Appendix B.

3.3.3 Directivity of Response Spectrum

The mean spectrum for each bin represent *null* directivity spectrum with the exceptions of Bin 1 (Near-Field) and Bin 6 (Near-Field Soft-Soil) where component orientation with respect to the fault has been preserved in an approximate fault normal and fault parallel orientation. Plotted in Figures 3.19 through 3.22 are the mean of the first component, the mean of the second component, and, the mean of all components for each bin. Plotted in Figure 3.23 are the median of the first component, the median of the second component, and the median spectra for Bins 1 and 6. Referring to the spectra of Bin 1 shown in Figure 3.19a, the mean first component spectrum is observed to lie significantly above the mean spectrum. This is due to the strong directivity effects exhibited by six of the ten pairs of ground motions in Bin 1. Referring to the spectra of Bin 6, shown in Figure 3.22a, there appears to be some directivity effect contained in the Bin 6 ground motions

components. This directivity effect is a result of the input ground motions used for the nonlinear analysis of a soil column previously mentioned. For Bins 2 through 5, the similarity of the first component, second component and mean spectra can be seen in Figures 3.19b through 3.21b. These figures suggest that the mean spectrum represents a *null* directivity spectrum. Note the vertical axes in Figures 3.19b through 3.21b and 3.22b are plotted at the same scale for comparison between bins and the scale of the vertical axis in Figures 3.19a and 3.22a are different. Spectral acceleration data for 0.2 and 1.0 second periods considering mean and median spectrum for Bins 1 through 7 is presented in Table 3.9. Also presented in Table 3.9 is spectral acceleration data for 0.2 and 1.0 seconds considering the mean and median of the 1st component for Bins 1 and 6.

3.3.4 Effects of Forward Rupture Directivity on Elastic Response Spectrum

Typically, the effect of forward rupture directivity on the elastic response spectrum is to increase the response of the horizontal fault normal component for periods greater than 0.5 second with the peak response of the fault normal component typically shifted to longer periods (Somerville, 2000).

Response spectra generated from the North and West components of TCU075 further indicate the presence of forward rupture directivity. An increase in the response of the West component is evident from the displacement, velocity and acceleration spectra shown in Figure 3.25. This increase in the fault normal component over the fault parallel component is observed for periods greater than 1.25 seconds for the displacement and velocity response spectrum. At a period of 4.0 seconds, a typical upper bound for isolated structures, the West component is approximately two times larger than the North component for both the displacement and velocity spectra, clearly indicating that directivity effects will have a significant effect on an isolated structure located in close proximity to a major fault and that component orientation relative to the fault must be considered for the analysis and design of these structures.

3.3.5 Identification of Spectral Regions

An investigation of the spectral regions of the mean spectrum for six of the eight bins of ground motions is presented. The spectral regions were investigated for two reasons: (1)

to identify the constant velocity portion of the mean spectrum and to determine whether this range is consistent with the effective period of plausible isolation systems, and (2) to facilitate linear regression analysis on the constant velocity portion of the log acceleration response spectrum to assess the validity of the assumed linearly increasing displacements assumed by the current AASHTO design spectrum. That is, if the spectral acceleration is shown to decay at a rate proportional to $1.0/T$, the linearly increasing displacement assumption is verified.

Estimates of the transition periods, and thus the spectral regions, were determined by performing an iterative tri-linear regression analysis on the logarithm of the mean velocity spectrum for each bin considered. Plotted in Figure 3.26 are mean velocity spectra for each of the six bins considered. Note the velocity spectra are plotted on a log-log scale. Also included on each plot are the estimates of the transition periods, namely, T_{AV} the transition period between the acceleration and velocity sensitive regions, and T_{VD} the transition period between the velocity and displacement sensitive regions. Estimates of T_{AV} and T_{VD} , were determined to be the intersection of adjacent linear best-fit lines from the converged tri-linear regression analysis.

Values of T_{VD} for Bins 1, 2, 2M and 3, were determined to be 3.5, 4.75, 5.0, and 3.75 respectively. For Bin 4 and Bin 5, the value of T_{VD} was determined to be 1.0 and 1.15 respectively. However, this discussion will focus on the results from Bins 1, 2, 2M and 3, as seismic isolation is viable for this level of seismic hazard, and unlikely to be used to protect against an earthquake hazard represented by bins 4 and 5.

From the results shown in Figures 3.26a and 3.26c, the velocity spectrum of Bin 1 (near-field) and Bin 3 (far-field) show the transition from the acceleration sensitive to velocity sensitive region occurs at a much lower period for Bin 3 than Bin 1, 0.25 and 0.75 seconds respectively. Values of the transition period from the velocity sensitive region to the displacement sensitive region calculated for Bin 1 and Bin 3 yield similar values of 3.5 and 3.75 seconds respectively. The velocity plateau of the far-field motions (Bin 3) is observed to be much larger than the plateau for the near-field motions (Bin 1). These results are in agreement with recent research comparing the response of near-field and

far-field ground motions (Chopra and Chintanapakdee, 2001). To estimate the transition period, T_{VD} , for the mean spectrum of Bins 2 and 2M, the velocity response was calculated over a period range of approximately 20 seconds. The response was calculated to a maximum period of 20 seconds to ensure sufficient information in the displacement sensitive region to facilitate the iterative tri-linear regression analysis. From the results of the regression analysis, values of T_{VD} for Bins 2 and 2M were determined to be 4.75 and 5, respectively. Estimates of the transition period from the velocity to the displacement sensitive region, T_{VD} , for ground motion bins 1, 2, 2M, and 3 corresponds to the upper-limit of the effective period of plausible seismic isolation systems. This observation indicates that the effective period of feasible isolation systems considered here lie within constant velocity region of the design spectrum.

Results of the tri-linear regression analysis were utilized to determine an appropriate period range to facilitate linear regression analysis on the logarithm of the mean acceleration spectrum. This is discussed in greater detail in the next section. Values of T_{AV} and T_{VD} and the ratio T_{AV}/T_{VD} are given in Table 3.10 for Bins 1 through 5.

3.3.6 Linear Regression Analysis Performed on the Logarithm of the Mean Acceleration Spectrum

The current design spectrum for isolated bridge structures assumes the acceleration response of a single degree-of-freedom system subjected to earthquake excitation decays at a rate proportional to $1.0/T$ in the constant-velocity region of the design spectrum (AASHTO, 1999). To investigate the validity of this assumption the following relationship was investigated

$$S_a = \frac{S_1}{T^\alpha} \quad (3.1)$$

where S_a is the spectral acceleration; S_1 is the 1-second spectral acceleration; T is the period of vibration, and α an exponent greater than or equal to unity. To estimate the value of α , linear regression analysis was performed on the log of the acceleration data over a range consistent with the constant-velocity region determined from the

investigation of the transitions periods. Taking the log of both sides of (3.1) yields the relationship

$$\log(S_a) = -\alpha \cdot \log(T) + \log(S_1) \quad (3.2)$$

where α was determined as the slope of the best-fit line of the transformed acceleration data. Results of the linear regression analysis are given in Table 3.11. Values of α shown in this table range from 1.05 to 1.28 for the six bins of ground motions considered. The results of this investigation suggest that the mean spectrum calculated for the six bins of ground motions considered match reasonably well the assumed shape of the AASHTO design spectrum over a period range consistent with the effective period of typical isolated bridges. Performing this analysis on the mean spectrum and not each individual spectrum contained in a particular ground motion bin may explain the deviation of the observed value of α from unity. However no further investigation is provided here.

Table 3.1. Near-field ground motions (Bin 1).

Record	Event	Year	Moment Magnitude	Station	Orientation ¹	PGA (g)	Distance to Fault ² (km)	Site Class ³
NF01	Tabas, Iran	1978	7.4	Tabas	FP	0.90	1.2	D
NF02	Tabas, Iran	1978	7.4	Tabas	FN	0.98	1.2	D
NF03	Loma Prieta	1989	7.0	Los Gatos	FN	0.72	3.5	D
NF04	Loma Prieta	1989	7.0	Los Gatos	FP	0.46	3.5	D
NF05	Loma Prieta	1989	7.0	Lex Dam	FN	0.69	6.3	D
NF06	Loma Prieta	1989	7.0	Lex Dam	FP	0.37	6.3	D
NF07	Cape Mendocino	1992	7.1	Petrolia	FN	0.64	8.5	D
NF08	Cape Mendocino	1992	7.1	Petrolia	FP	0.65	8.5	D
NF09	Erzincan, Turkey	1992	6.7	Erzincan	FN	0.43	2	D
NF10	Erzincan, Turkey	1992	6.7	Erzincan	FP	0.46	2	D
NF11	Landers	1992	7.3	Lucerne	FP	0.71	1.1	D
NF12	Landers	1992	7.3	Lucerne	FN	0.80	1.1	D
NF13	Northridge	1994	6.7	Rinaldi	FN	0.89	7.5	D
NF14	Northridge	1994	6.7	Rinaldi	FP	0.39	7.5	D
NF15	Northridge	1994	6.7	Olive View	FP	0.73	6.4	D
NF16	Northridge	1994	6.7	Olive View	FN	0.60	6.4	D
NF17	Kobe	1995	6.9	JMA	FN	1.09	3.4	D
NF18	Kobe	1995	6.9	JMA	FP	0.57	3.4	D
NF19	Kobe	1995	6.9	Takatori	FN	0.79	4.3	D
NF20	Kobe	1995	6.9	Takatori	FP	0.42	4.3	D
TCU065-N	Chi Chi, Taiwan	1999	7.6	TCU065	North	0.81	0.98	C*
TCU065-W	Chi Chi, Taiwan	1999	7.6	TCU065	West	0.60	0.98	C*
TCU075-N	Chi Chi, Taiwan	1999	7.6	TCU075	North	0.33	1.49	C*
TCU075-N	Chi Chi, Taiwan	1999	7.6	TCU075	West	0.26	1.49	C*

Notes:

¹ FN - Fault Normal, FP - Fault Parallel

² Closest to fault rupture

³ Site classification per 2000 NEHRP; * denotes USGS classification

Table 3.2. Large-magnitude, small-distance ground motions (Bin 2).

Record	Event	Year	Moment Magnitude	Station	Orientation ¹	PGA (g)	Distance to Fault ² (km)	Site Class
G01000	Loma Prieta	1989	6.9	Gilroy Array #1 47379	0	0.41	11.2	A
G01090	Loma Prieta	1989	6.9	Gilroy Array #1 47379	90	0.47	11.2	A
SGI270	Loma Prieta	1989	6.9	1032 Hollister: SAGO Vault	270	0.04	29.9	A
SGI360	Loma Prieta	1989	6.9	1032 Hollister: SAGO Vault	360	0.06	29.9*	A
L09000	Northridge	1994	6.7	127 Lake Hughes #9	0	0.17	29.9*	A
L09090	Northridge	1994	6.7	127 Lake Hughes #9	90	0.22	26.8	A
WON095	Northridge	1994	6.7	90017 LA Wonderlnd Ave	95	0.11	22.7	A
WON185	Northridge	1994	6.7	90017 LA Wonderlnd Ave	185	0.17	22.7	A
L09021	San Fernando	1971	6.6	127 Lake Hughes #9	21	0.16	23.5	A
L09291	San Fernando	1971	6.6	127 Lake Hughes #9	291	0.13	23.5	A
G02000	Loma Prieta	1989	6.9	47380 Gilroy Array #2	0	0.37	12.7	C
G02090	Loma Prieta	1989	6.9	47380 Gilroy Array #2	90	0.32	12.7	C
YER270	Landers	1992	7.3	22074 Yermo Fire Station	270	0.24	24.9	C
YER360	Landers	1992	7.3	22074 Yermo Fire Station	360	0.15	24.9	C
ABN000	Kobe	1995	6.9	Abeno	0	0.22	23.8	C
ABN090	Kobe	1995	6.9	Abeno	90	0.23	23.8	C
A-E01140	Imperial Valley	1979	6.5	El Centro Array #1 5056	140	0.08	15.5	C
A-E01230	Imperial Valley	1979	6.5	El Centro Array #1 5056	230	0.03	15.5	C
CNP106	Northridge	1994	6.7	90053 Canoga Park	106	0.36	15.8	C
CNP196	Northridge	1994	6.7	90053 Canoga Park	196	0.42	15.8	C

Notes:

¹ Orientation with respect to an arbitrary reference

² Closest fo fault rupture; * closest to surface projection of rupture

³ Site classification per USGS

Table 3.3. Large-magnitude, small-distance ground motions (Bin 2M).

Record	Event	Year	Moment Magnitude	Station	Orientation ¹	PGA (g)	Distance to Fault ² (km)	Site Class ³
G01000	Loma Prieta	1989	6.9	Gilroy Array #1 47379	0	0.41	11.2	A
G01090	Loma Prieta	1989	6.9	Gilroy Array #1 47379	90	0.47	11.2	A
GBZ000	Kocaeli, Turkey	1999	7.4	Gebze	0	0.24	17	A
GBZ270	Kocaeli, Turkey	1999	7.4	Gebze	270	0.14	17	A
STG000	Loma Prieta	1989	6.9	58065 Saratoga Aloha Ave	0	0.51	13	B
STG090	Loma Prieta	1989	6.9	58065 Saratoga Aloha Ave	90	0.32	13	B
RIO270	Cape Mendocino	1992	7.1	89324 Rio Dell Over Pass FF	270	0.39	18.5	B
RIO360	Cape Mendocino	1992	7.1	89324 Rio Dell Over Pass FF	360	0.55	18.5	B
JOS000	Landers	1992	7.3	22170 Joshua Tree	0	0.27	11.6	B
JOS090	Landers	1992	7.3	22170 Joshua Tree	90	0.28	11.6	B
G02000	Loma Prieta	1989	6.9	47380 Gilroy Array #2	0	0.37	12.7	C
G02090	Loma Prieta	1989	6.9	47380 Gilroy Array #2	90	0.32	12.7	C
YER270	Landers	1992	7.3	22074 Yermo Fire Station	270	0.25	24.9	C
YER360	Landers	1992	7.3	22074 Yermo Fire Station	360	0.15	24.9	C
ABN000	Kobe	1995	6.9	Abeno	0	0.22	23.8	C
ABN090	Kobe	1995	6.9	Abeno	90	0.24	23.8	C
BOL000	Duzce, Turkey	1999	7.1	Bolu	0	0.73	17.6	C
BOL090	Duzce, Turkey	1999	7.1	Bolu	90	0.82	17.6	C
CNP106	Northridge	1994	6.7	90053 Canoga Park Topanga Can	106	0.36	15.8	C
CNP196	Northridge	1994	6.7	90053 Canoga Park Topanga Can	196	0.42	15.8	C

Notes:

¹ Orientation with respect to an arbitrary reference

² Closest fo fault rupture

³ Site classification per USGS

Table 3.4 Large-magnitude, large-distance ground motions (Bin 3).

Record	Event	Year	Moment Magnitude	Station	Orientation ¹	PGA (g)	Distance to Fault ² (km)	Site Class ³
CHY000	Kobe	1995	6.9	Chihaya	0	0.09	48.7	A
CHY090	Kobe	1995	6.9	Chihaya	90	0.11	48.7	A
29P000	Landers	1992	7.3	22161 Twentynine Palms	0	0.08	42.2	A
29P090	Landers	1992	7.3	22161 Twentynine Palms	90	0.06	42.2	A
MCH000	Loma Prieta	1989	6.9	47377 Monterey City Hall	0	0.07	44.8	A
MCH090	Loma Prieta	1989	6.9	47377 Monterey City Hall	90	0.06	44.8	A
MTW000	Northridge	1994	6.7	Mt Wilson - CIT Seis Sta	0	0.23	36.1	A
MTW090	Northridge	1994	6.7	Mt Wilson - CIT Seis Sta	90	0.13	36.1	A
GRN180	Northridge	1994	6.7	San Gabriel - E. Grand Ave	180	0.14	41.7	A
GRN270	Northridge	1994	6.7	San Gabriel - E. Grand Ave	270	0.26	41.7	A
TDO000	Kobe	1995	6.9	Tadoka	0	0.29	30.5	C
TDO090	Kobe	1995	6.9	Tadoka	90	0.20	30.5	C
PSA000	Landers	1992	7.3	12025 Palm Springs Airport	0	0.08	37.5	C
PSA090	Landers	1992	7.3	12025 Palm Springs Airport	90	0.09	37.5	C
SLC270	Loma Prieta	1989	6.9	1601 Palo Alto SLAC Lab	270	0.19	36.3	C
SLC360	Loma Prieta	1989	6.9	1601 Palo Alto SLAC Lab	360	0.28	36.3	C
CAS000	Northridge	1994	6.7	Compton Castlegate St.	0	0.09	49.6	C
CAS270	Northridge	1994	6.7	Compton Castlegate St.	270	0.14	49.6	C
H-VCT075	Imperial Valley	1979	6.5	6610 Victoria	75	0.12	54.1	C
H-VCT345	Imperial Valley	1979	6.5	6610 Victoria	345	0.17	54.1	C

Notes:

¹ Orientation with respect to an arbitrary reference

² Closest fo fault rupture

³ Site classification per USGS

Table 3.5. Small-magnitude, small-distance ground motions (Bin 4).

Record	Event	Year	Moment Magnitude	Station	Orientation ¹	PGA (g)	Distance to Fault ² (km)	Site Class ³
MH-G01230	Morgan Hill	1984	6.2	47379 Gilroy Array #1	230	0.07	16.2	A
MH-G01320	Morgan Hill	1984	6.2	47379 Gilroy Array #1	320	0.10	16.2	A
SIL000	North Palm Springs	1986	6.0	Silent Valley - Poppet F	0	0.14	25.8	A
SIL090	North Palm Springs	1986	6.0	Silent Valley - Poppet F	90	0.11	25.8	A
A-WON075	Whittier Narrows	1987	6.0	90017 LA - Wonderland Ave	75	0.04	24.6	A
A-WON165	Whittier Narrows	1987	6.0	90017 LA - Wonderland Ave	165	0.05	24.6	A
B-MTW000	Whittier Narrows	1987	5.3	Mt Wilson - CIT Seis Sta	0	0.16	21.2	A
B-MTW090	Whittier Narrows	1987	5.3	Mt Wilson - CIT Seis Sta	90	0.14	21.2	A
G01230	Coyote Lake	1979	5.7	47379 Gilroy Array #1	230	0.10	9.3	A
G01320	Coyote Lake	1979	5.7	47379 Gilroy Array #1	320	0.13	9.3	A
HVR150	Coyote Lake	1979	5.7	57191 Halls Valley	150	0.04	31.2	C
HVR240	Coyote Lake	1979	5.7	57191 Halls Valley	240	0.05	31.2	C
A-CX0225	Imperial Valley	1979	5.2	Calexico Fire Station	225	0.12	15	C
A-CX0315	Imperial Valley	1979	5.2	Calexico Fire Station	315	0.07	15	C
G02000	Morgan Hill	1984	6.2	47380 Gilroy Array #2	0	0.16	15.1	C
G02090	Morgan Hill	1984	6.2	47380 Gilroy Array #2	90	0.21	15.1	C
A-SRM070	Livermore	1980	5.4	San Ramon Fire Station	70	0.06	20.7	C
A-SRM340	Livermore	1980	5.4	San Ramon Fire Station	340	0.04	20.7	C
A-BUE250	Whittier Narrows	1987	6.0	Burbank - N Buena Vista	250	0.23	23.7	C
A-BUE340	Whittier Narrows	1987	6.0	Burbank - N Buena Vista	340	0.19	23.7	C

Notes:

¹ Orientation with respect to an arbitrary reference

² Closest fo fault rupture

³ Site classification per USGS

Table 3.6. Small-magnitude, large-distance ground motions (Bin 5).

Record	Event	Year	Moment Magnitude	Station	Orientation ¹	PGA (g)	Distance to Fault ² (km)	Site Class ³
AZF225	North Palm Springs	1986	6.0	5160 Anza Fire Station	225	0.10	46.7	A
AZF315	North Palm Springs	1986	6.0	5160 Anza Fire Station	315	0.07	46.7	A
ARM270	North Palm Springs	1986	6.0	5224 Anza - Red Mountain	270	0.10	45.6	A
ARM360	North Palm Springs	1986	6.0	5224 Anza - Red Mountain	360	0.13	45.6	A
H02000	North Palm Springs	1986	6.0	Winchester Bergman Ran	0	0.07	57.6	A
H02090	North Palm Springs	1986	6.0	Winchester Bergman Ran	90	0.09	57.6	A
H01000	North Palm Springs	1986	6.0	Murrieta Hot Springs	0	0.05	63.3	A
H01090	North Palm Springs	1986	6.0	Murrieta Hot Springs	90	0.05	63.3	A
SOD015	San Fernando	1971	6.6	Upland - San Antonio Dam	15	0.06	58.1	A
SOD285	San Fernando	1971	6.6	Upland - San Antonio Dam	285	0.08	58.1	A
H-C08000	Coalinga	1983	6.4	Parkfield - Cholame 8W	0	0.10	50.7	C
H-C08270	Coalinga	1983	6.4	Parkfield - Cholame 8W	270	0.10	50.7	C
H06270	North Palm Springs	1986	6.0	San Jacinto Valley Cem.	270	0.07	39.6	C
H06360	North Palm Springs	1986	6.0	San Jacinto Valley Cem.	360	0.06	39.6	C
HCH001	Morgan Hill	1984	6.2	Hollister City Hall	1	0.07	32.5	C
HCH271	Morgan Hill	1984	6.2	Hollister City Hall	271	0.07	32.5	C
A-CNP106	Whittier Narrows	1987	6.0	Canoga Park Topanga	106	0.12	47.4	C
A-CNP196	Whittier Narrows	1987	6.0	Canoga Park Topanga	196	0.11	47.4	C
A-STP093	Livermore	1980	5.8	Tracy -Sewage Treatm. Plant	93	0.05	37.3	C
A-STP183	Livermore	1980	5.8	Tracy -Sewage Treatm. Plant	183	0.07	37.3	C

Notes:

¹ Orientation with respect to an arbitrary reference

² Closest fo fault rupture

³ Site classification per USGS

Table 3.7. Near-field, soft-soil ground motions¹ (Bin 6)

Record	Event	Year	Moment Magnitude	Station	Orientation ²	PGA (g)	Distance to Fault ³ (km)
LS01C	Imperial Valley	1940	6.9	EI Centro	FN	0.33	10
LS02C	Imperial Valley	1940	6.9	EI Centro	FP	0.34	10
LS03C	Imperial Valley	1979	6.5	Array #05	FN	0.38	4.1
LS04C	Imperial Valley	1979	6.5	Array #05	FP	0.31	4.1
LS05C	Imperial Valley	1979	6.5	Array #06	FN	0.34	1.2
LS06C	Imperial Valley	1979	6.5	Array #06	FP	0.28	1.2
LS07C	Landers	1992	7.3	Barstow	FN	0.39	36
LS08C	Landers	1992	7.3	Barstow	FP	0.22	36
LS09C	Landers	1992	7.3	Yermo	FN	0.44	25
LS10C	Landers	1992	7.3	Yermo	FP	0.35	25
LS11C	Loma Prieta	1989	7.0	Gilroy	FN	0.58	12
LS12C	Loma Prieta	1989	7.0	Gilroy	FP	0.40	12
LS13C	Northridge	1994	6.7	Newhall	FN	0.57	6.7
LS14C	Northridge	1994	6.7	Newhall	FP	0.34	6.7
LS15C	Northridge	1994	6.7	Rinaldi RS	FN	0.57	7.5
LS16C	Northridge	1994	6.7	Rinaldi RS	FP	0.28	7.5
LS17C	Northridge	1994	6.7	Sylmar	FN	0.52	6.4
LS18C	Northridge	1994	6.7	Sylmar	FP	0.42	6.4
LS19C	North Palm Springs	1986	6.0	NA	FN	0.56	6.7
LS20C	North Palm Springs	1986	6.0	NA	FP	0.35	6.7

Notes:

¹ Tabulated ground motion information is that of the original event used to simulate a soft soil record corresponding to a depth to firm ground of 150 feet and an average shear wave velocity of 497 fps. (SAC, 1997)

² FN - Fault Normal, FP - Fault Parallel

³ Closest to fault rupture

Table 3.8. Large-magnitude, soft soil ground motions (Bin 7)

Record	Event	Year	Moment Magnitude ¹	Station	Orientation ²	PGA (g)	Distance to Fault ³ (km)	Site Class ⁴
SCTEW	Mexico City	1985	8.1*	SCT	EW	0.17	385	E**
SCTNS	Mexico City	1985	8.1*	SCT	NS	0.10	385	E**
MEN270	Loma Prieta	1989	6.9	1515 Foster City - 355 Menhaden	270	0.11	51.2	F*
MEN360	Loma Prieta	1989	6.9	1515 Foster City - 355 Menhaden	360	0.12	51.2	F*
EMV260	Loma Prieta	1989	6.9	Emeryville	260	0.24	96	F*
EMV350	Loma Prieta	1989	6.9	Emeryville	350	0.21	96	F*
OHW035	Loma Prieta	1989	6.9	Oakland (Outer Harbor Wharf)	35	0.29	76	F*
OHW305	Loma Prieta	1989	6.9	Oakland (Outer Harbor Wharf)	305	0.27	76	F*
RWC043	Loma Prieta	1989	6.9	Redwood City	43	0.28	47.9	D
RWC233	Loma Prieta	1989	6.9	Redwood City	233	0.23	47.9	D
SFA000	Loma Prieta	1989	6.9	S.F. International Airport	0	0.24	64.4	C
SFA090	Loma Prieta	1989	6.9	S.F. International Airport	90	0.33	64.4	C
TRI000	Loma Prieta	1989	6.9	Treasure Island (Fire Station)	0	0.10	82.9	D
TRI090	Loma Prieta	1989	6.9	Treasure Island (Fire Station)	90	0.16	82.9	D
ATS000	Turkey, Kocaeli	1999	7.4	Ambarli Termik Santrali	0	0.25	78.9	D
ATS090	Turkey, Kocaeli	1999	7.4	Ambarli Termik Santrali	90	0.19	78.9	D
DZC180	Turkey, Kocaeli	1999	7.4	Duzce	180	0.31	12.7	C
DZC270	Turkey, Kocaeli	1999	7.4	Duzce	270	0.36	12.7	C
YPT060	Turkey, Kocaeli	1999	7.4	Yarimca	60	0.27	2.6	C
YPT330	Turkey, Kocaeli	1999	7.4	Yarimca	330	0.35	2.6	C

Notes:

¹ * denotes surface wave magnitude (M_S) used

² Orientation with respect to an arbitrary reference

³ Closest to fault rupture

⁴ Site classification per USGS; * based on description of local soil conditions (Benuska, 1990);

** based on description of local soil conditions (Miranda, 1991)

Table 3.9. Spectral ordinates $S_{0.2}$ and S_1 .

Bin	Normal Characterization				Lognormal Characterization			
	All Components		1st Components		All Components		1st Components	
	$S_{0.2}$	S_1	$S_{0.2}$	S_1	$S_{0.2}$	S_1	$S_{0.2}$	S_1
	(g)	(g)	(g)	(g)	(g)	(g)	(g)	(g)
1	1.13	1.01	1.09	1.35	1.01	0.83	1.03	1.26
2	0.52	0.20			0.38	0.12		
2M	0.78	0.41			0.71	0.36		
3	0.43	0.14			0.36	0.09		
4	0.25	0.05			0.21	0.04		
5	0.18	0.05			0.16	0.04		
6	0.50	0.81	0.53	0.98	0.49	0.76	0.54	0.98
7	0.44	0.36			0.37	0.30		

Table 3.10. Estimated transition periods for the spectral regions.

Bin	Description	T_{AV} (seconds)	T_{VD} (seconds)	T_{VD} / T_{AV}
1	Near-field	0.75	3.45	4.6
2	Large-magnitude, small-distance	0.29	4.75	16.3
2M	Large-magnitude, small-distance	0.35	5.07	14.6
3	Large-magnitude, large-distance	0.25	3.74	14.96
4	Small-magnitude, small-distance	0.21	1.02	4.86
5	Small-magnitude, large-distance	0.31	1.15	3.71

Table 3.11. Estimated values of the period exponent.

Bin	Description	α ($T_{AV} < T < T_{VD}$)
1	Near-field	1.12
2	Large-magnitude, small-distance	1.28
2M	Large-magnitude, small-distance	1.26
3	Large-magnitude, large-distance	1.05
4	Small-magnitude, small-distance	1.09
5	Small-magnitude, large-distance	1.21

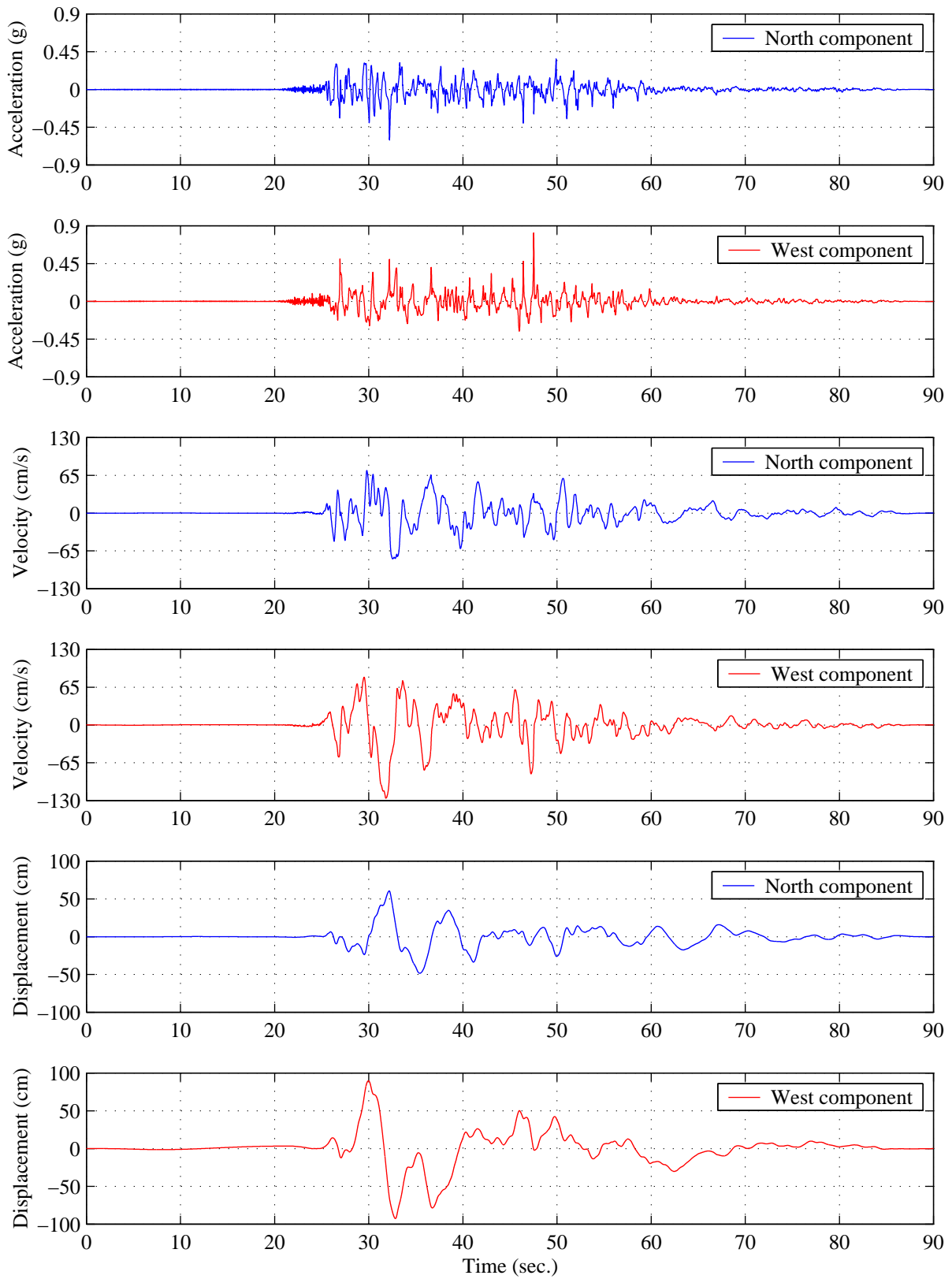


Figure 3.1. Acceleration, velocity, and displacement traces for record TCU065.

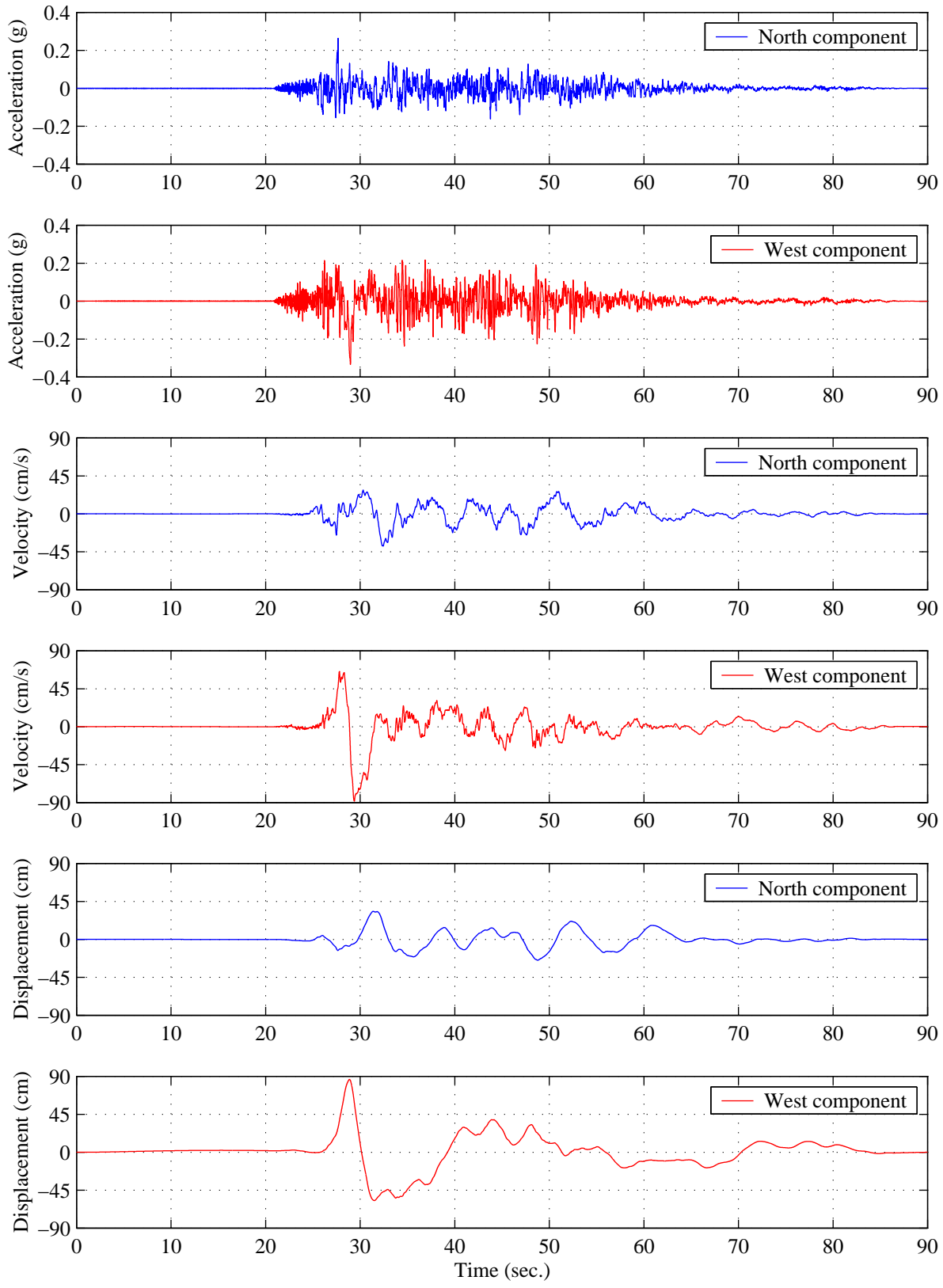
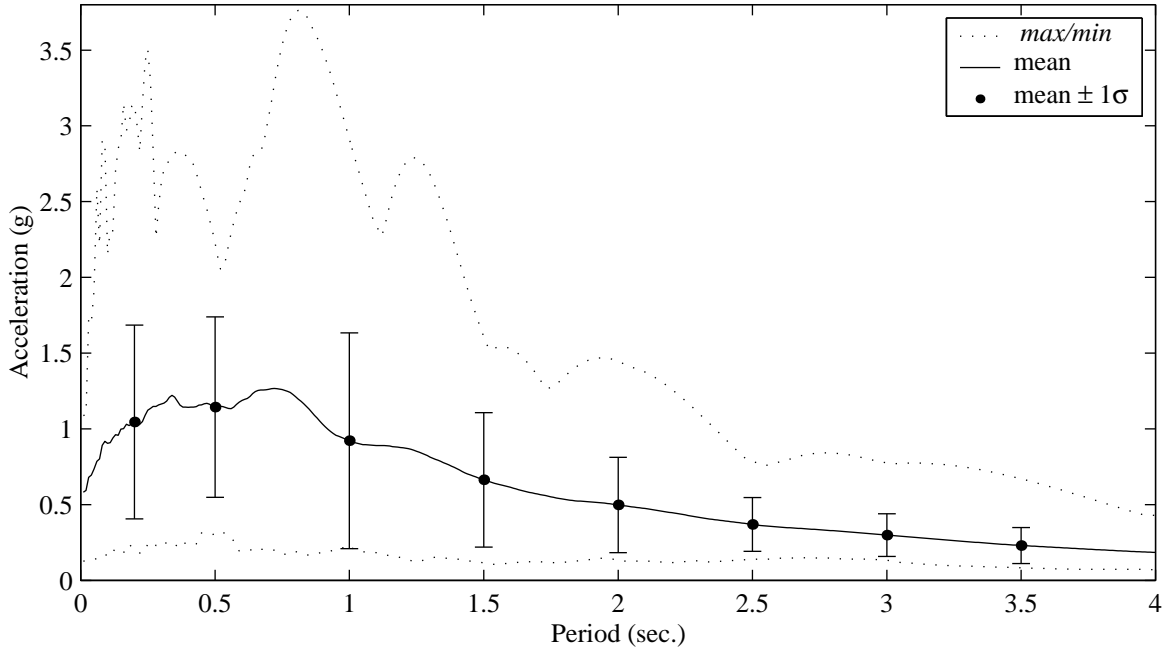
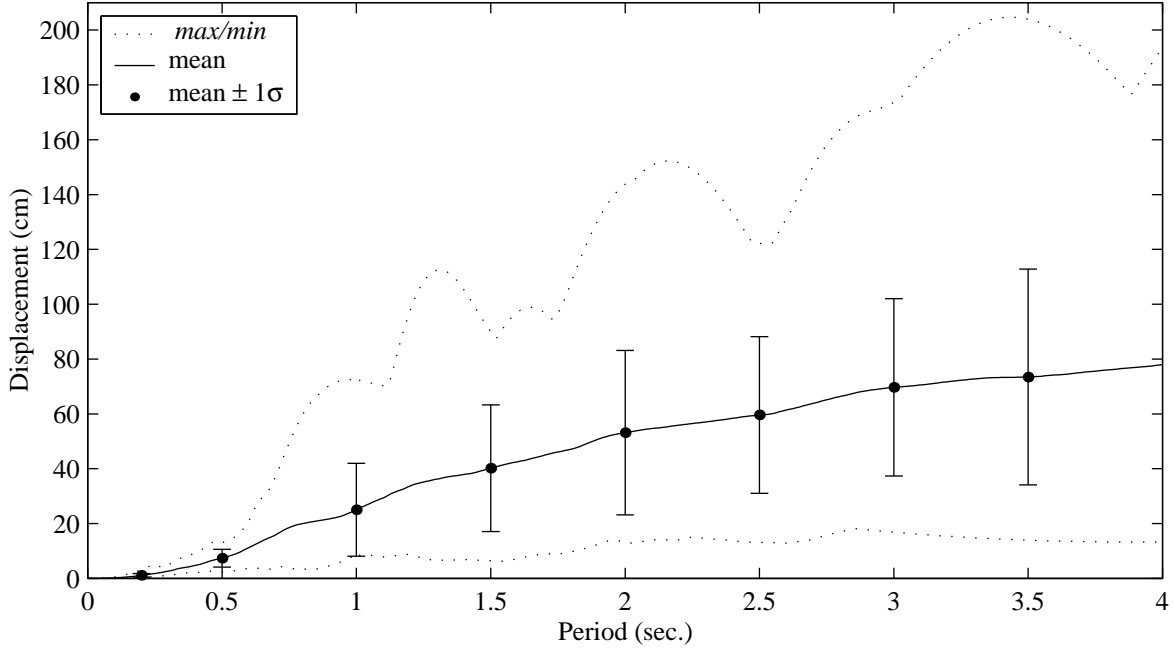


Figure 3.2. Acceleration, velocity, and displacement traces for record TCU075.

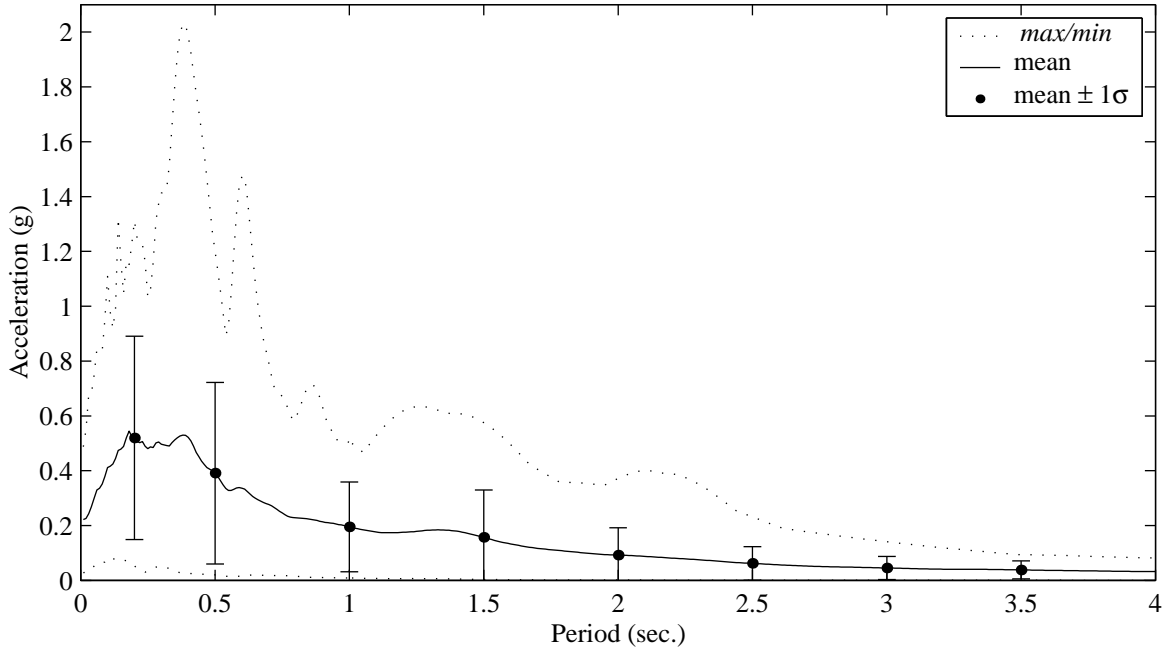


a. acceleration response spectra

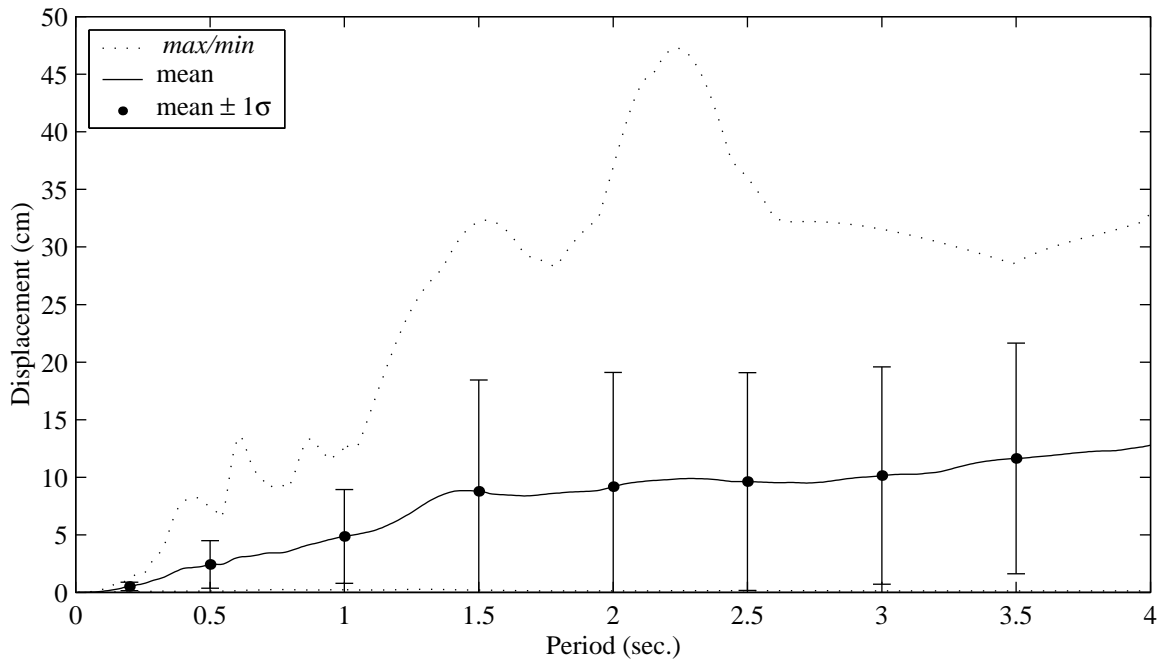


b. displacement response spectra

Figure 3.3. Elastic response spectra for Bin 1 ground motions and 5% critical damping using a normal characterization.

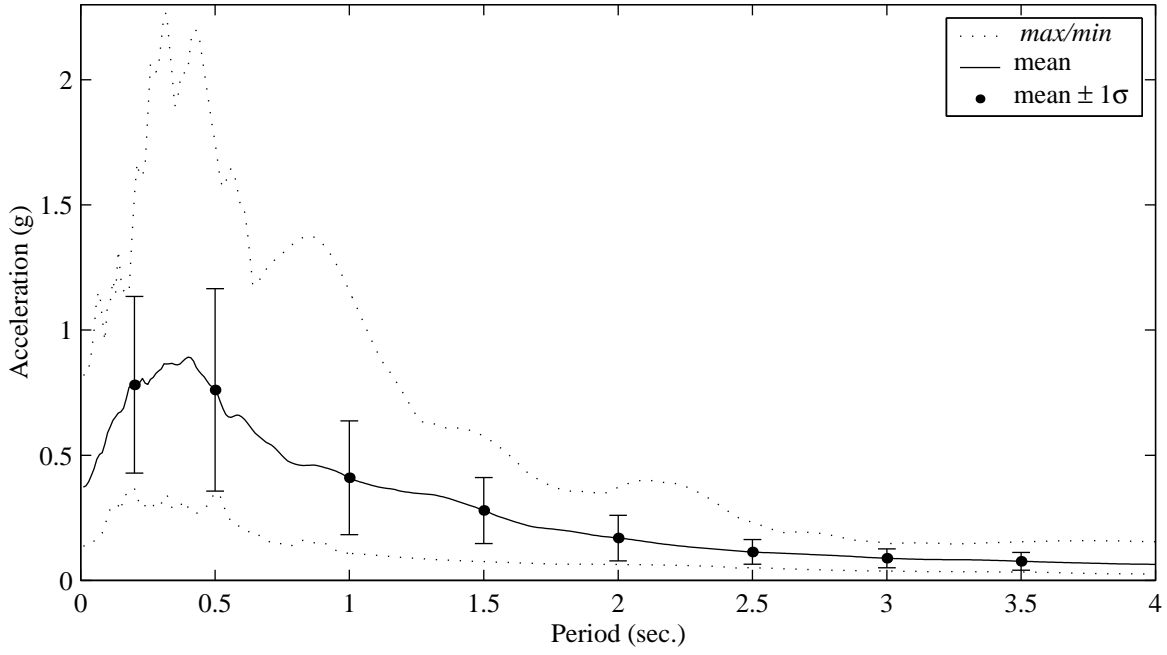


a. acceleration response spectra

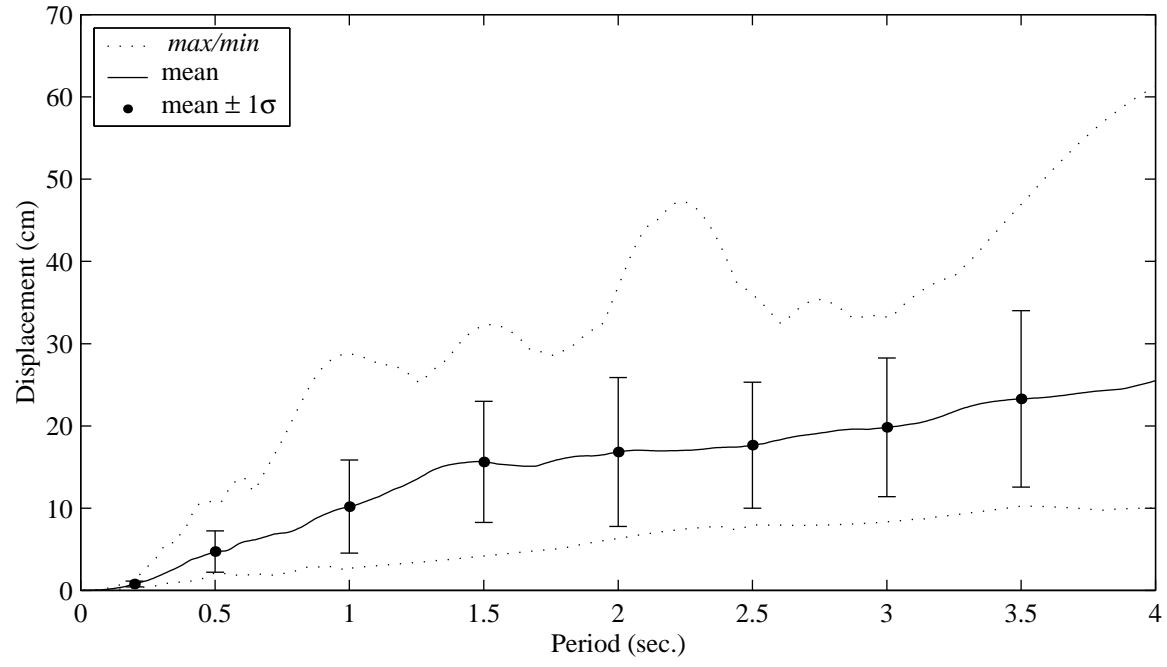


b. displacement response spectra

Figure 3.4. Elastic response spectra for Bin 2 ground motions and 5% critical damping using a normal characterization.

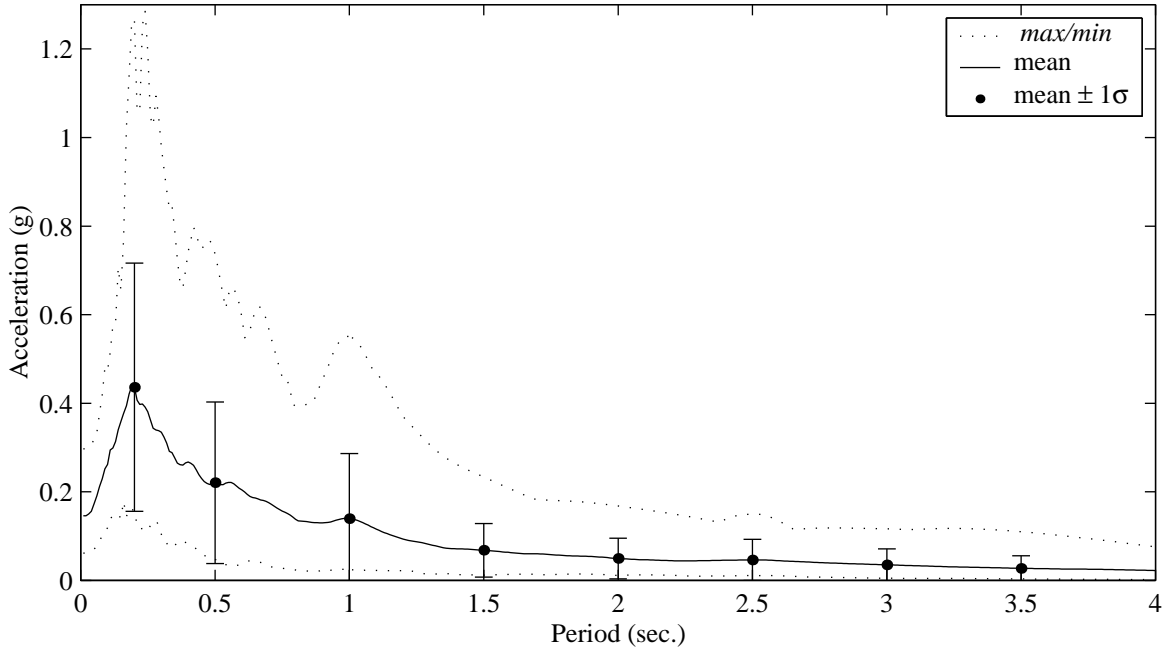


a. acceleration response spectra

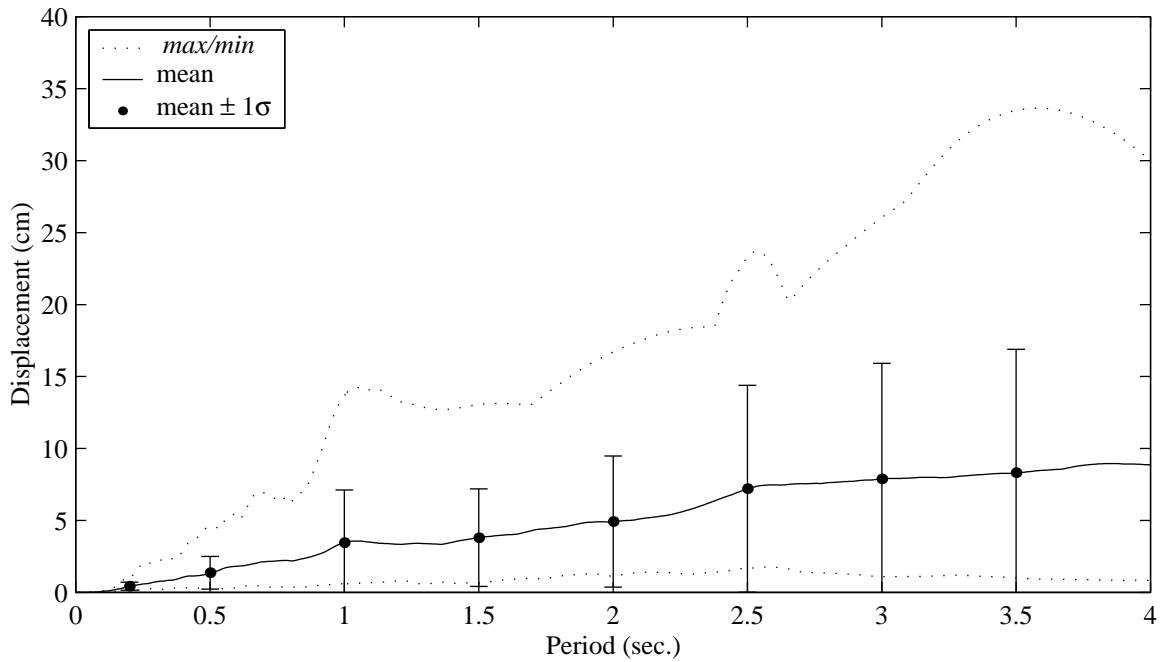


b. displacement response spectra

Figure 3.5. Elastic response spectra for Bin 2M ground motions and 5% critical damping using a normal characterization.

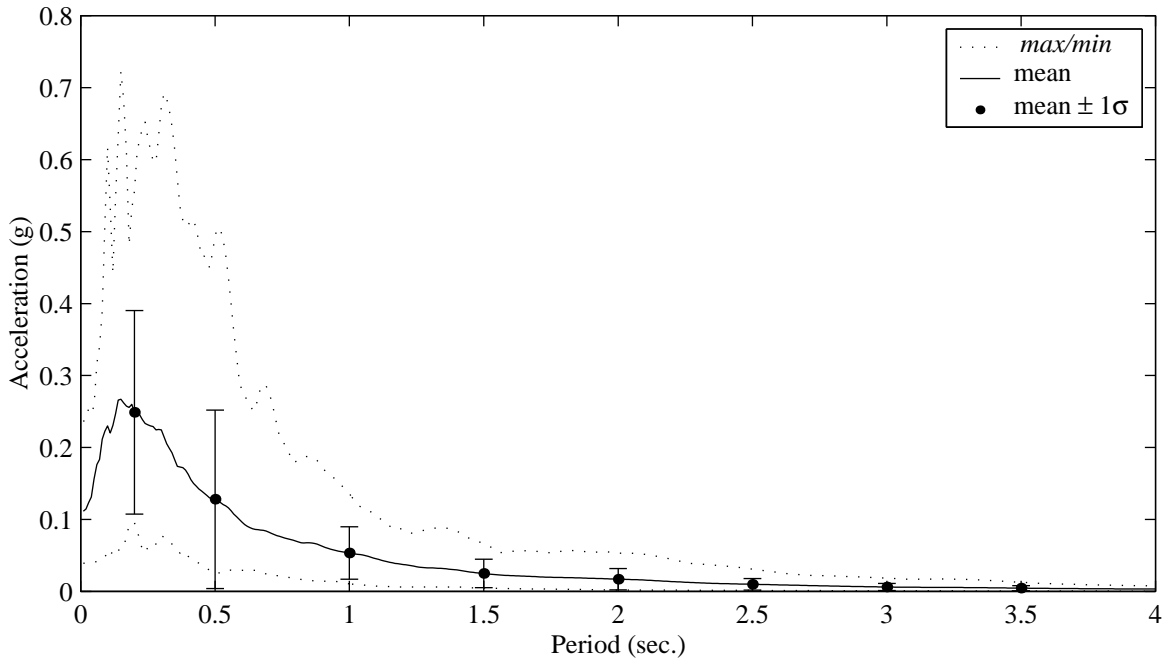


a. acceleration response spectra

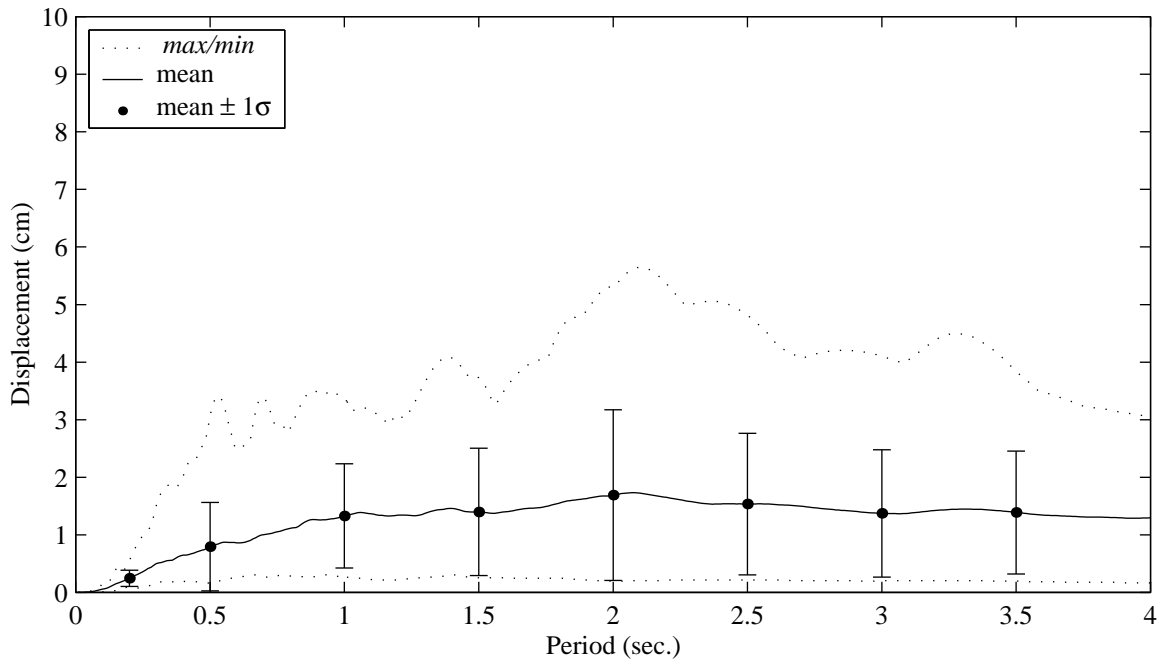


b. displacement response spectra

Figure 3.6. Elastic response spectra for Bin 3 ground motions and 5% critical damping using a normal characterization.

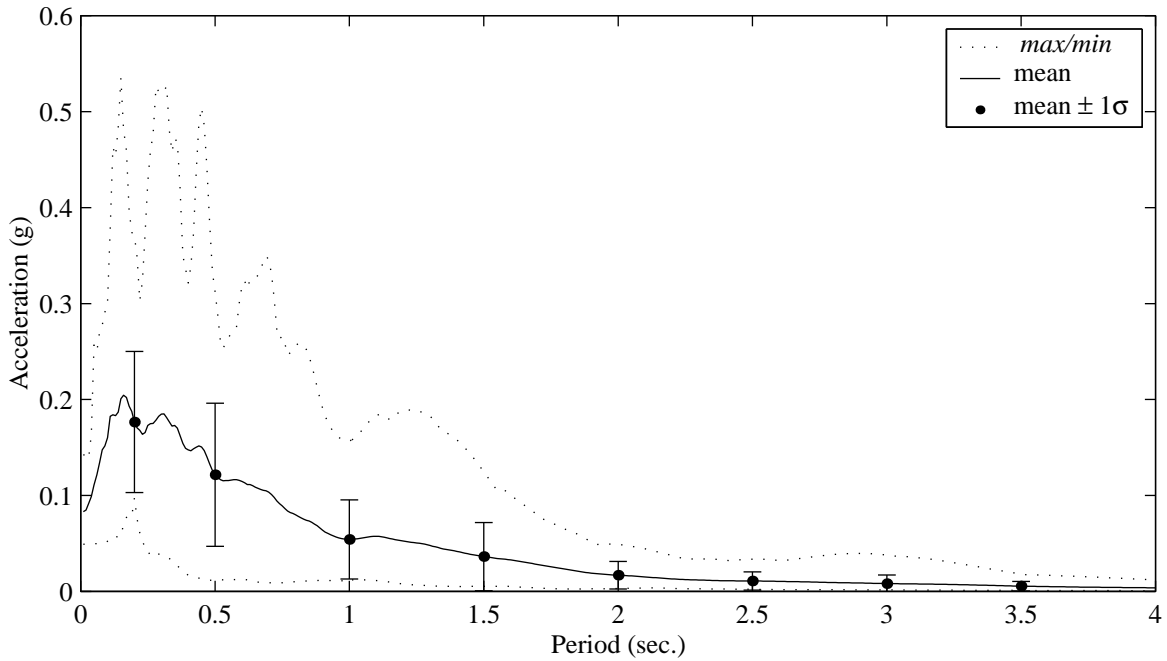


a. acceleration response spectra

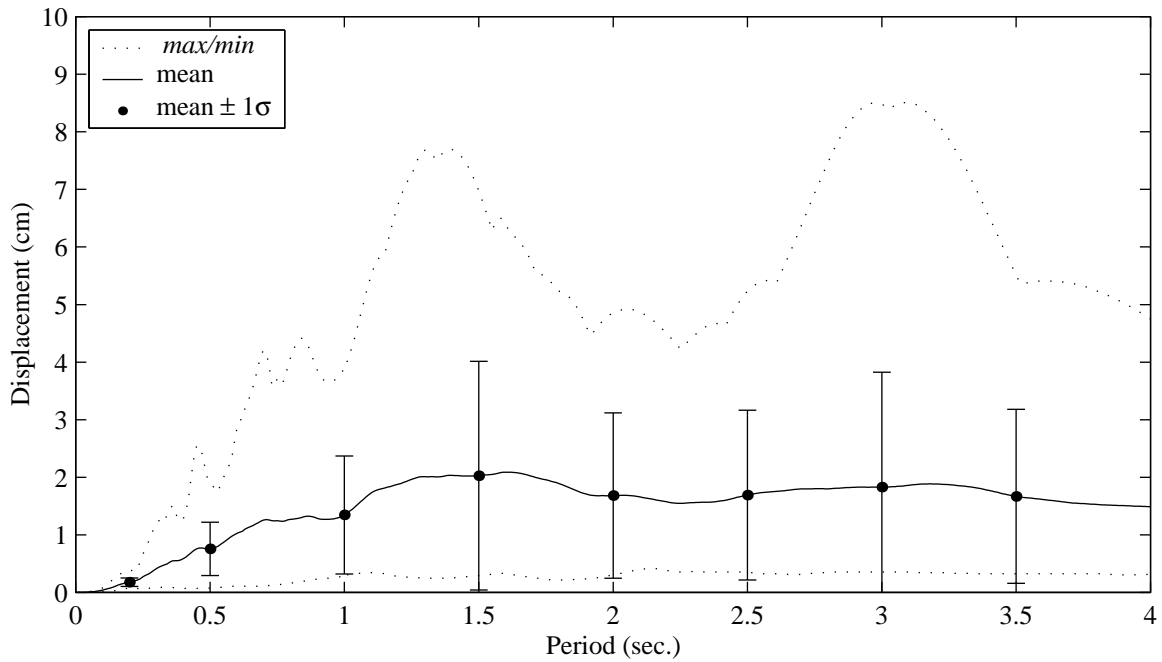


b. displacement response spectra

Figure 3.7. Elastic response spectra for Bin 4 ground motions and 5% critical damping using a normal characterization.

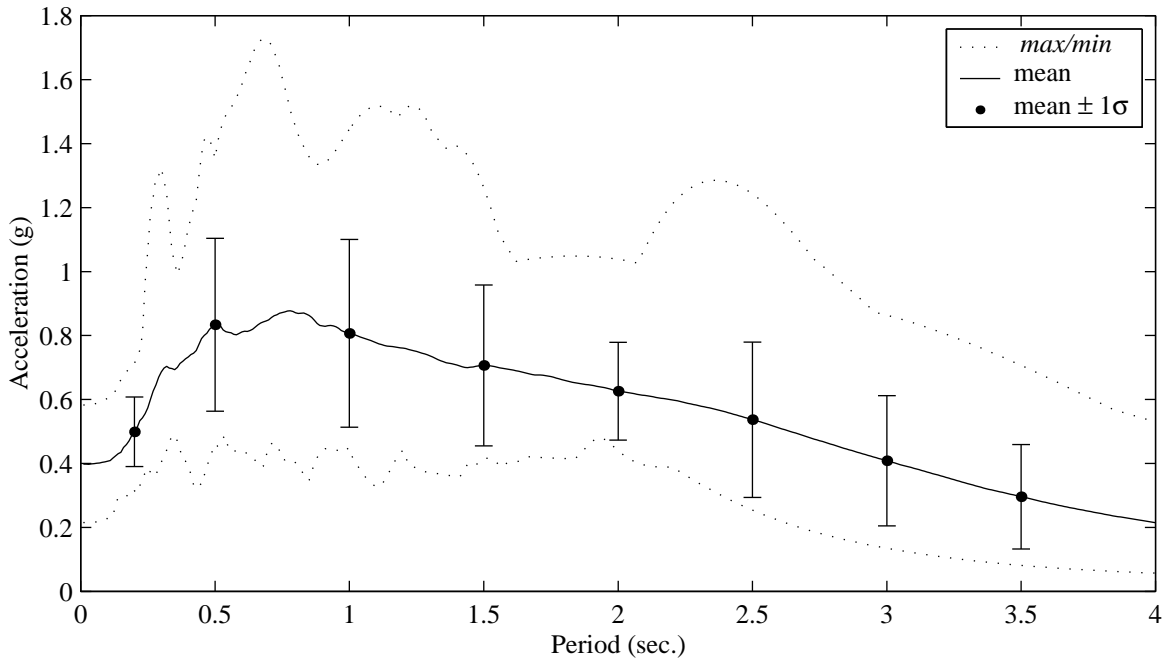


a. acceleration response spectra

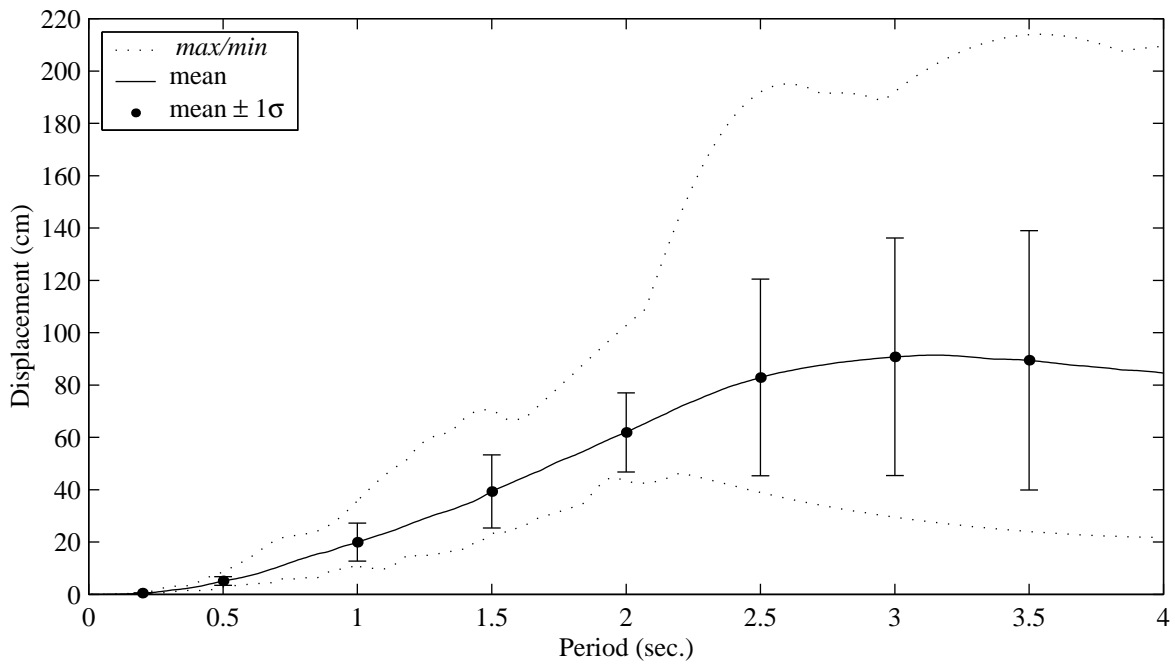


b. displacement response spectra

Figure 3.8. Elastic response spectra for Bin 5 ground motions and 5% critical damping using a normal characterization.

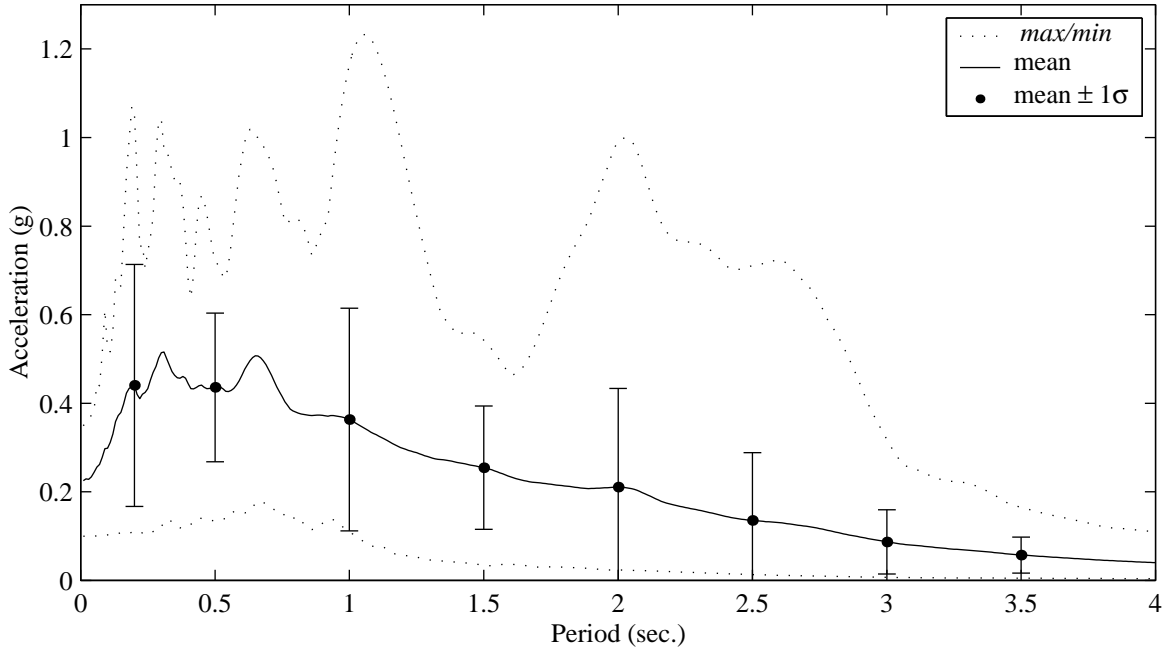


a. acceleration response spectra

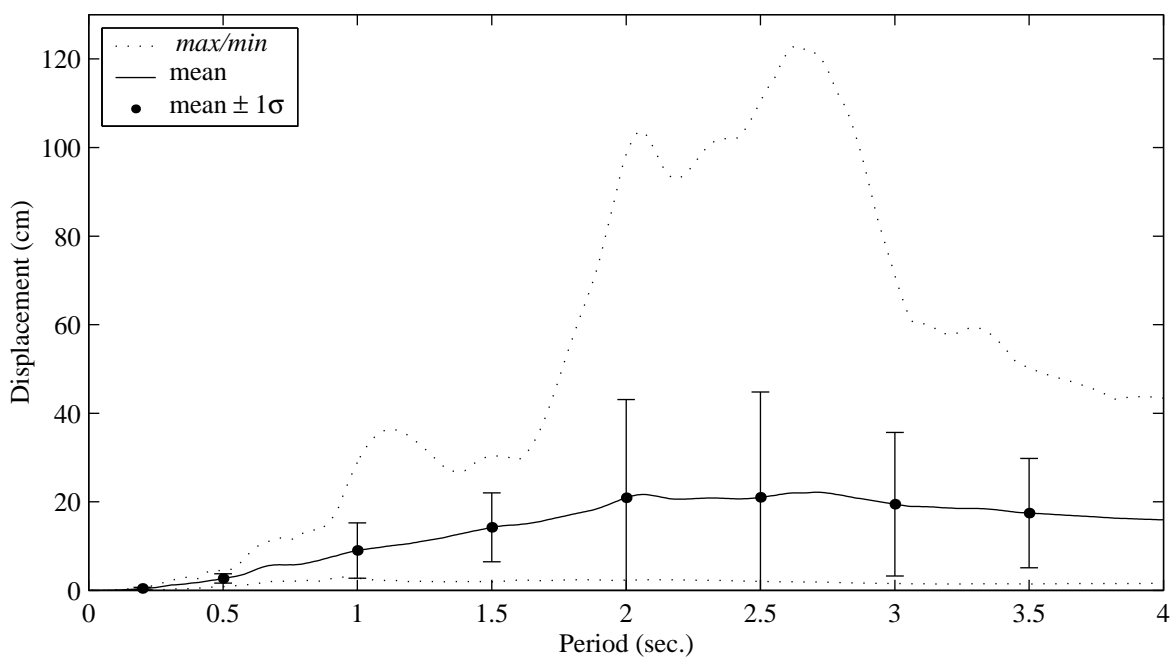


b. displacement response spectra

Figure 3.9. Elastic response spectra for Bin 6 ground motions and 5% critical damping using a normal characterization.

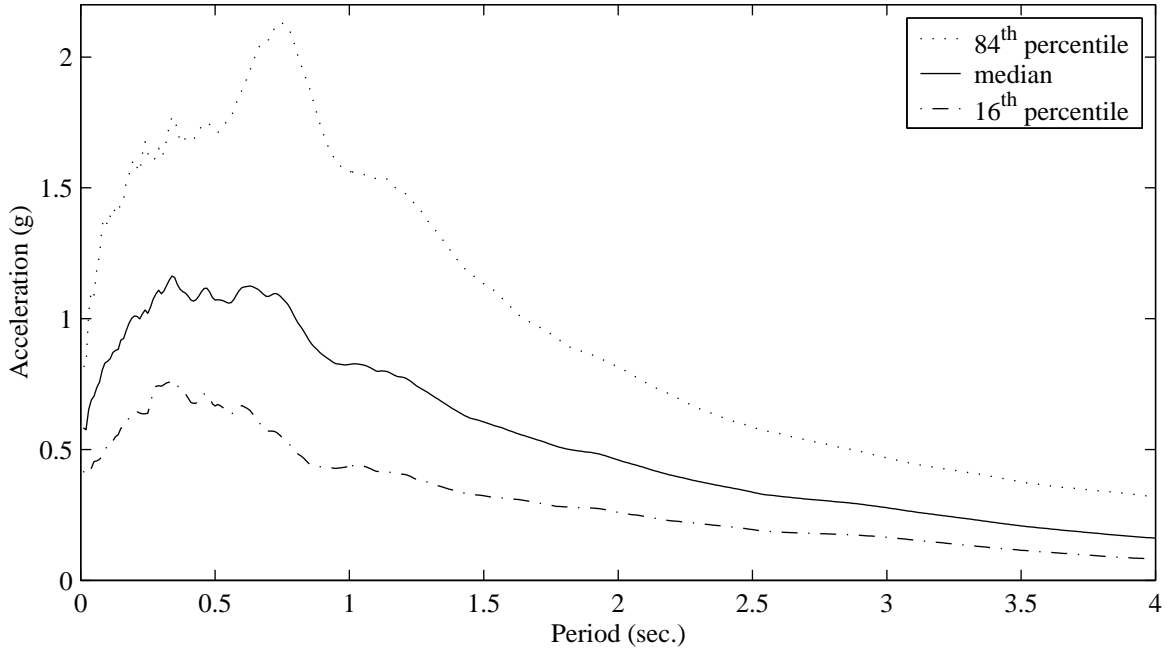


a. acceleration response spectra

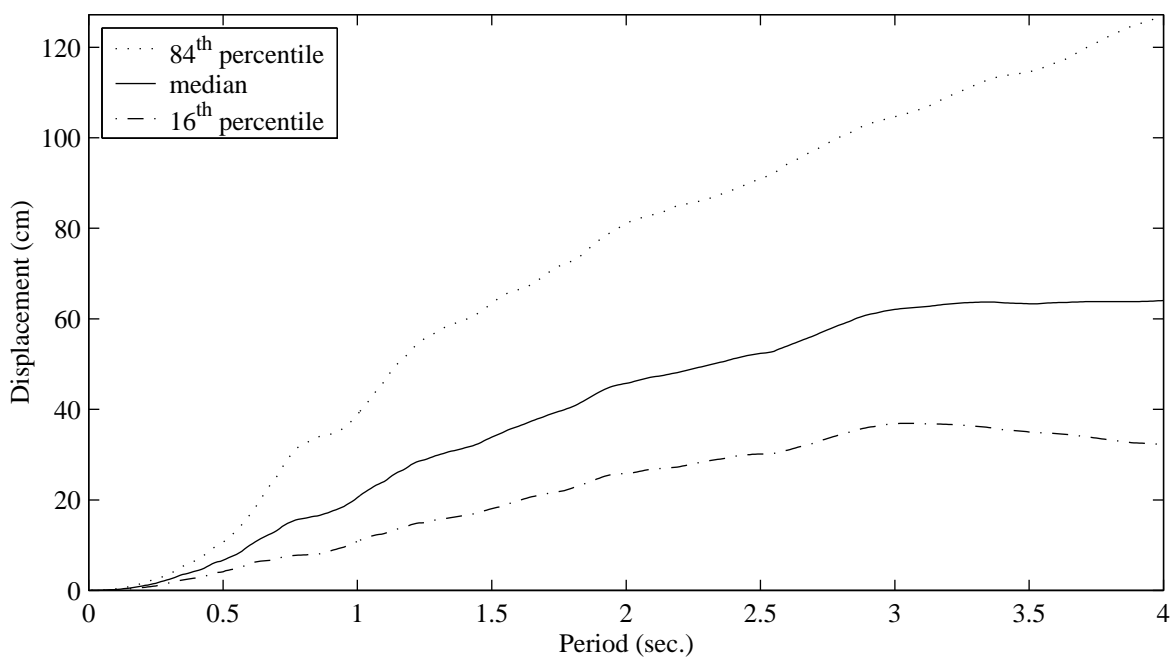


b. displacement response spectra

Figure 3.10. Elastic response spectra for Bin 7 ground motions and 5% critical damping using a normal characterization.

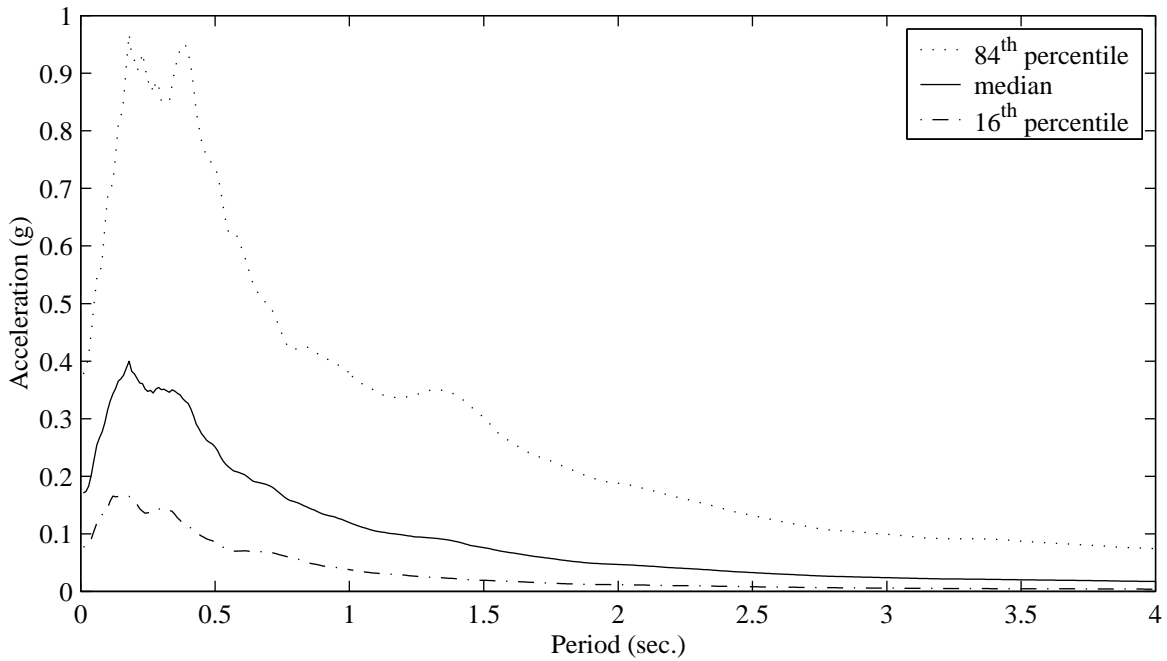


a. acceleration response spectra

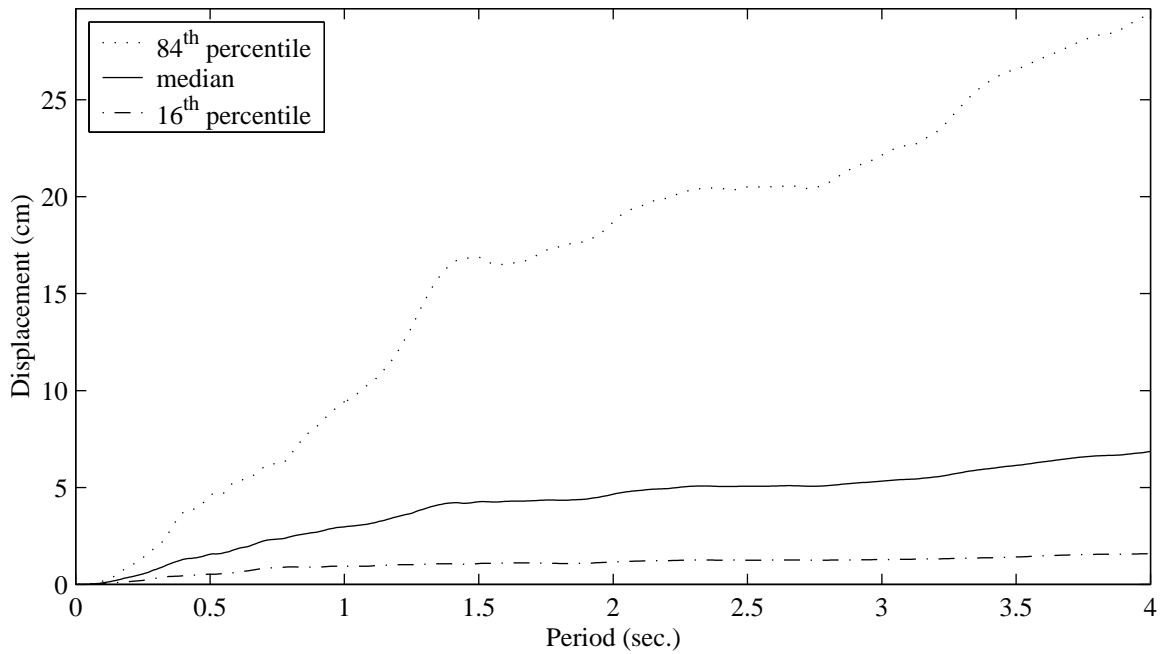


b. displacement response spectra

Figure 3.11. Elastic response spectra for Bin 1 ground motions and 5% critical damping using a lognormal characterization.

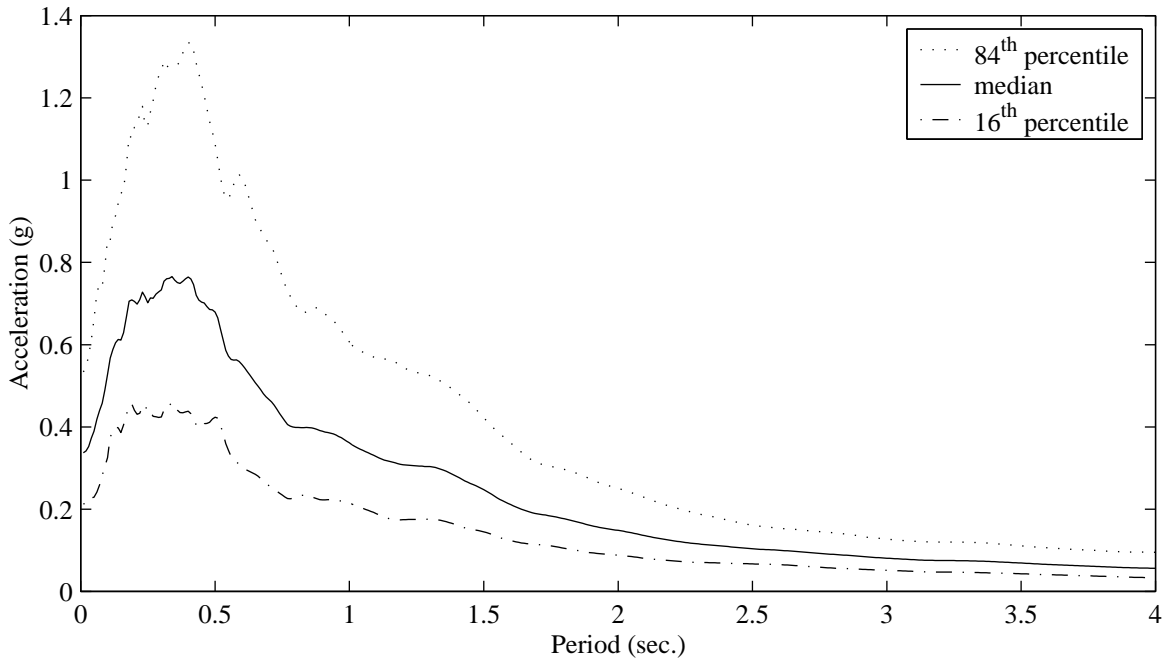


a. acceleration response spectra

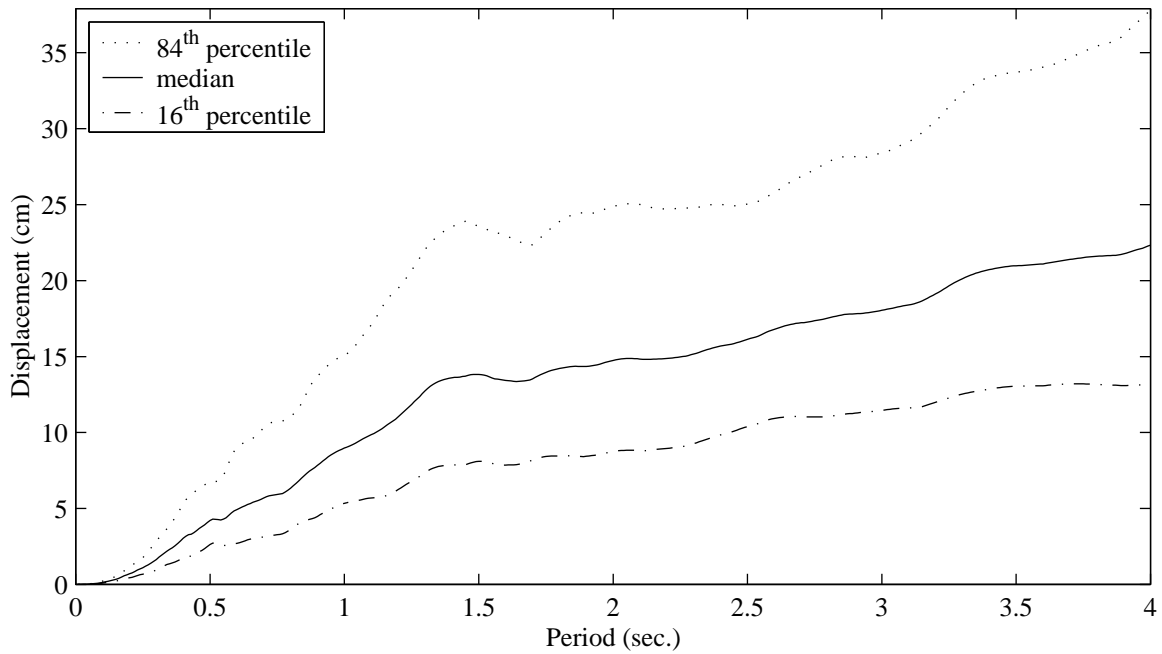


b. displacement response spectra

Figure 3.12. Elastic response spectra for Bin 2 ground motions and 5% critical damping using a lognormal characterization.

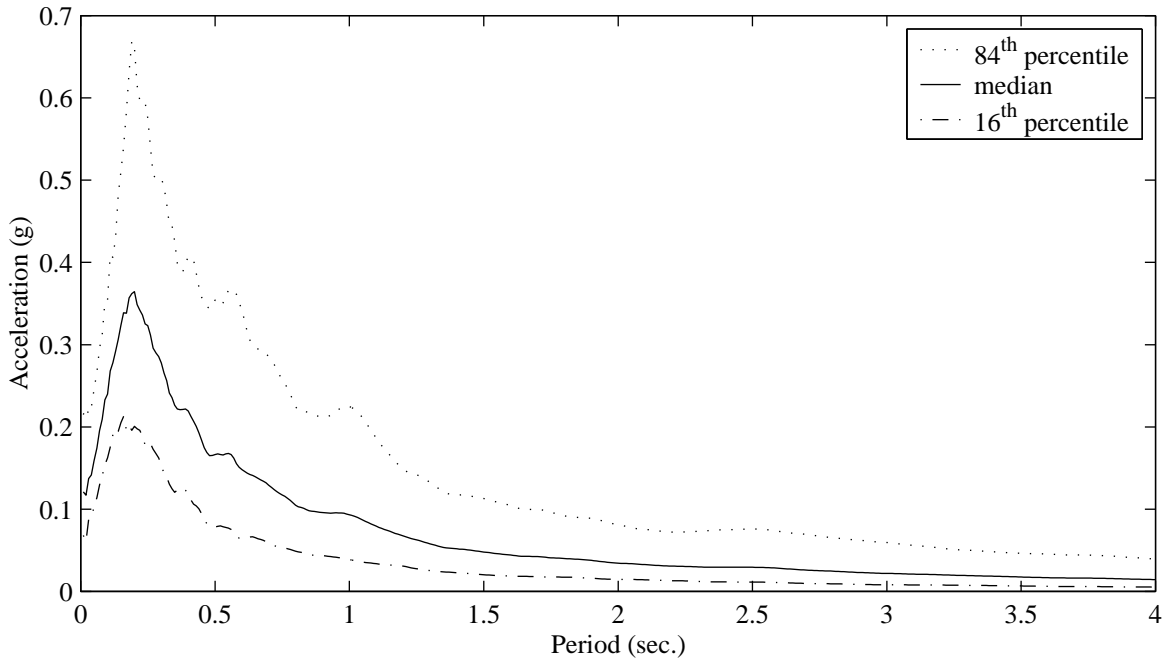


a. acceleration response spectra

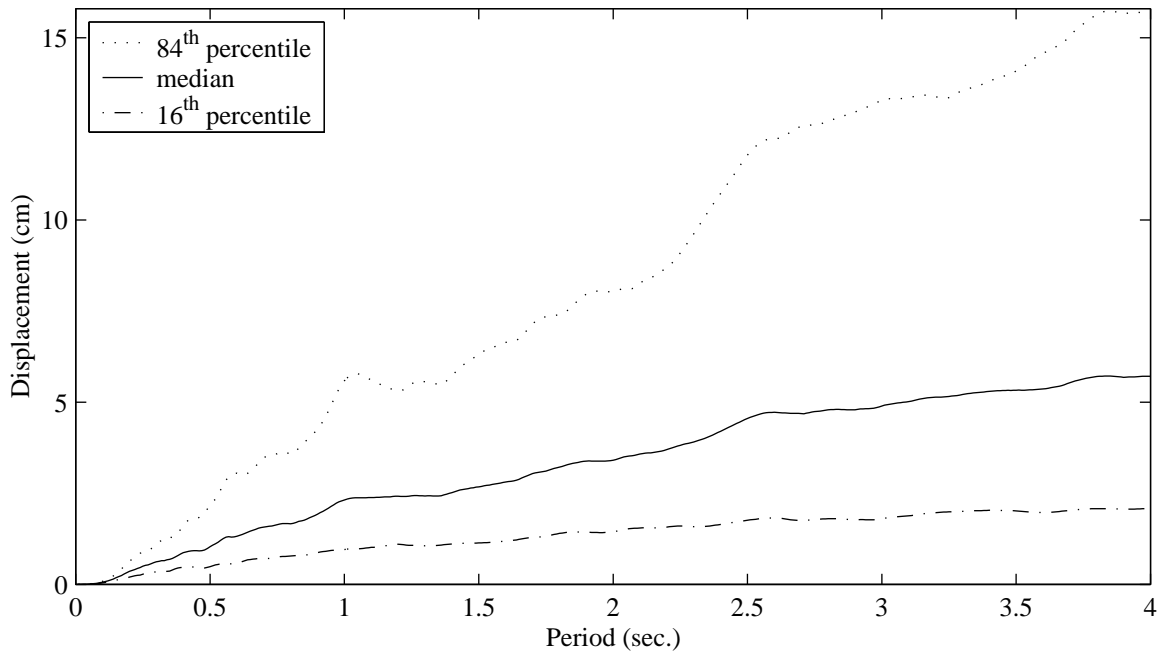


b. displacement response spectra

Figure 3.13. Elastic response spectra for Bin 2M ground motions and 5% critical damping using a lognormal characterization.

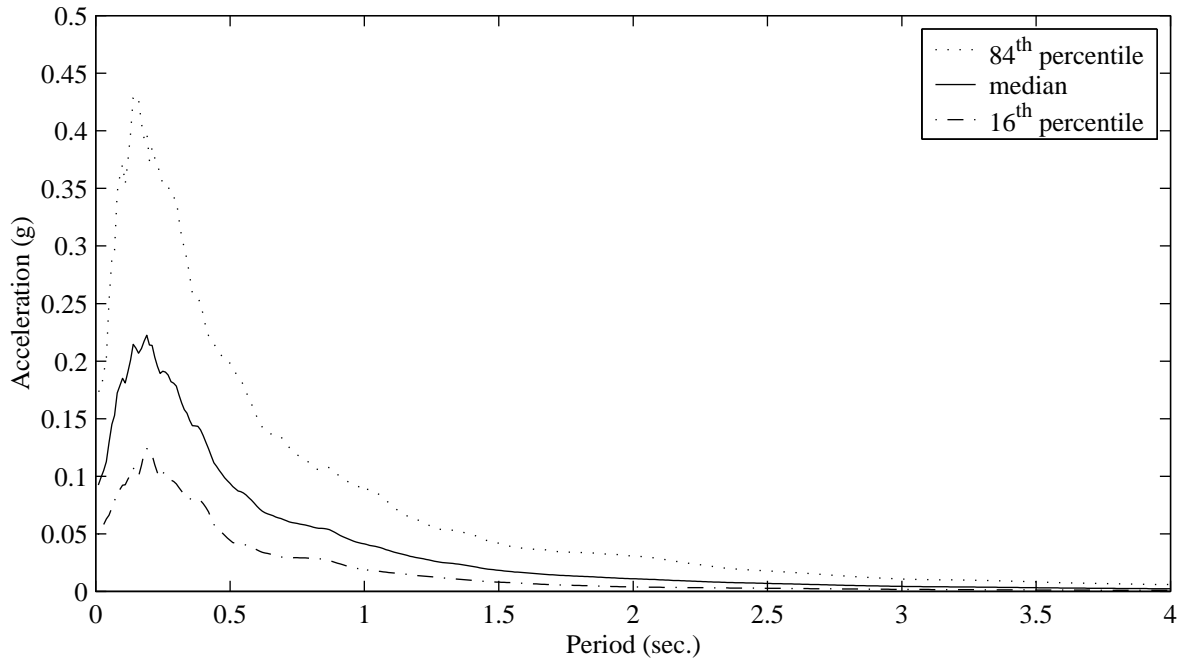


a. acceleration response spectra

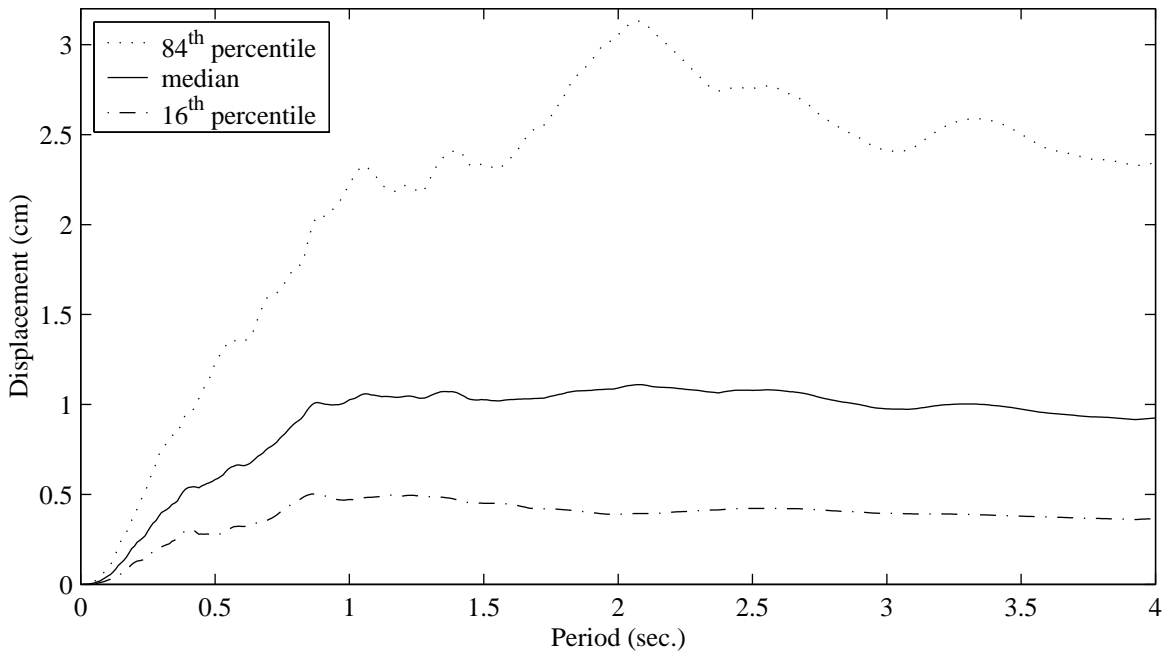


b. displacement response spectra

Figure 3.14. Elastic response spectra for Bin 3 ground motions and 5% critical damping using a lognormal characterization.

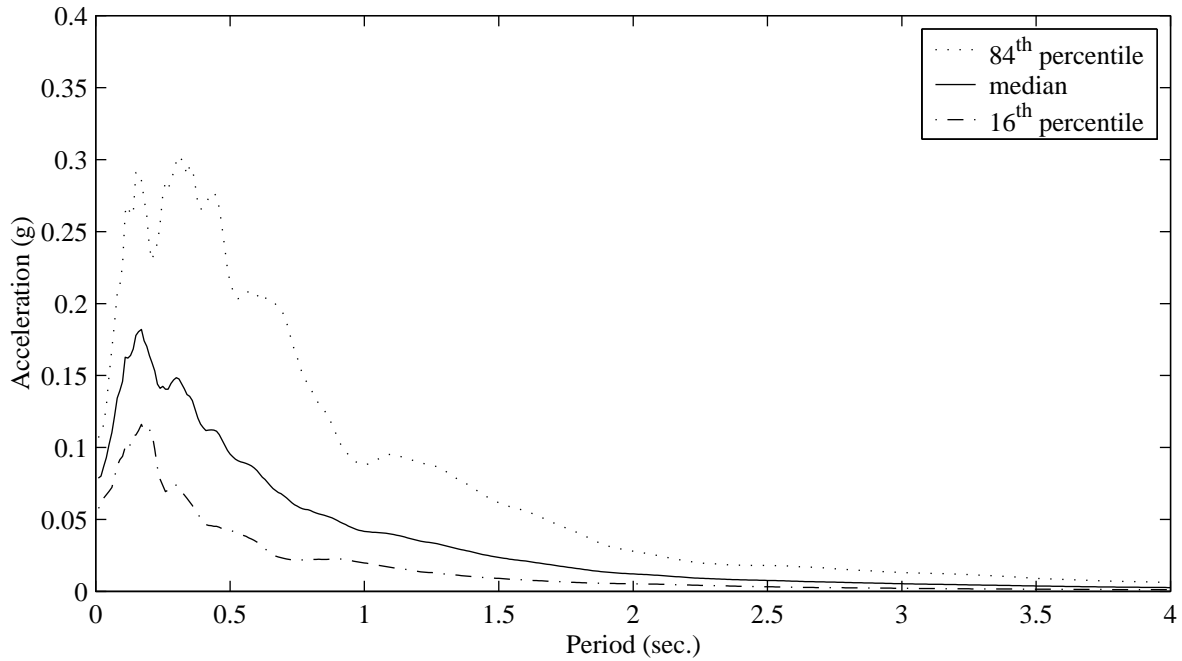


a. acceleration response spectra

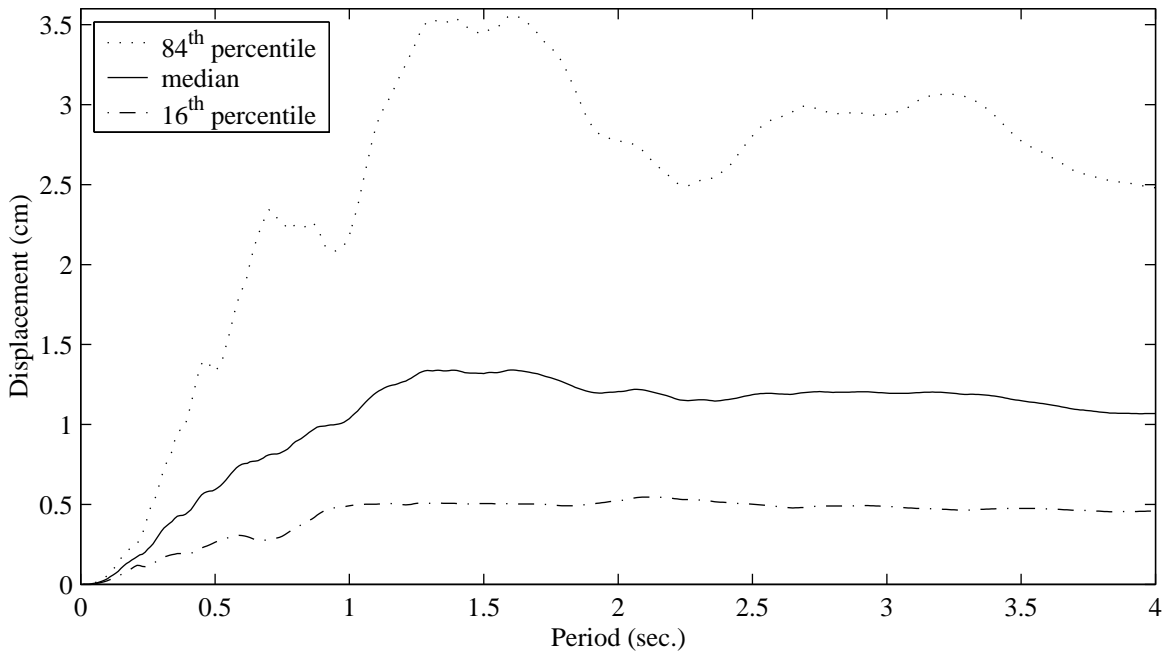


b. displacement response spectra

Figure 3.15. Elastic response spectra for Bin 4 ground motions and 5% critical damping using a lognormal characterization.

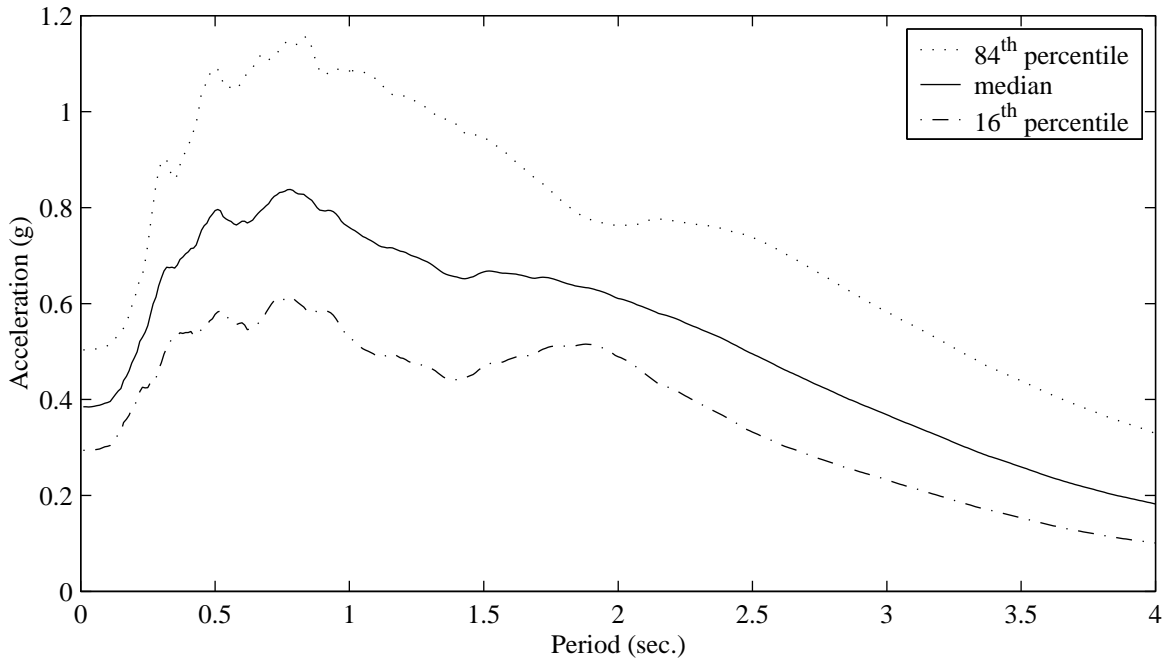


a. acceleration response spectra

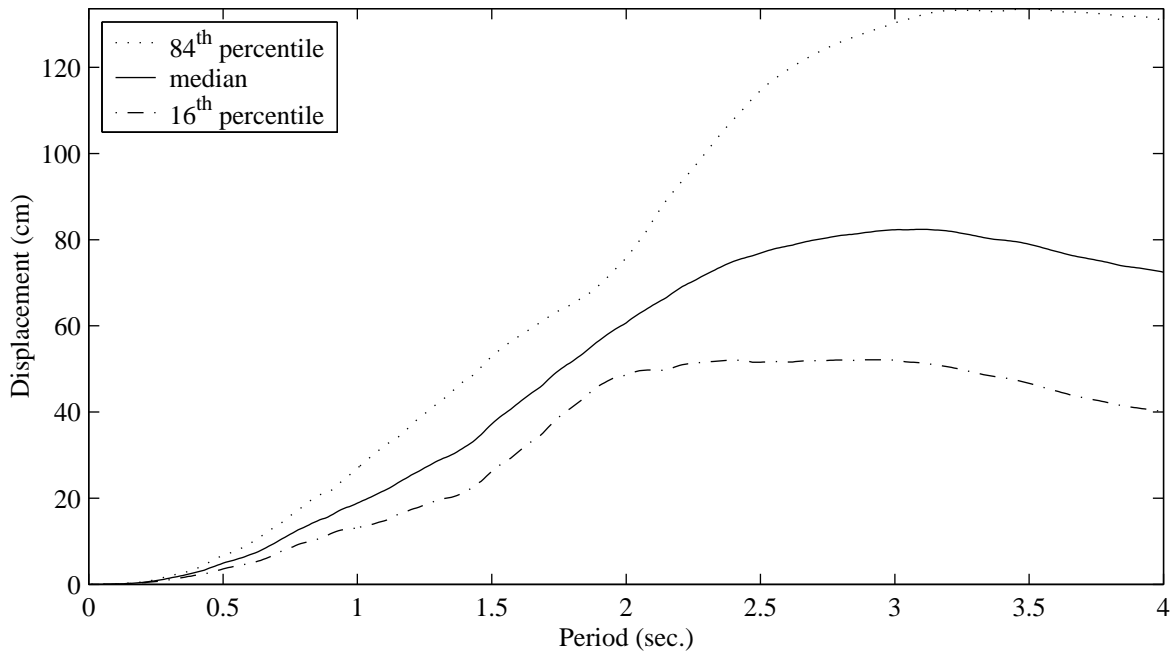


b. displacement response spectra

Figure 3.16. Elastic response spectra for Bin 5 ground motions and 5% critical damping using a lognormal characterization.

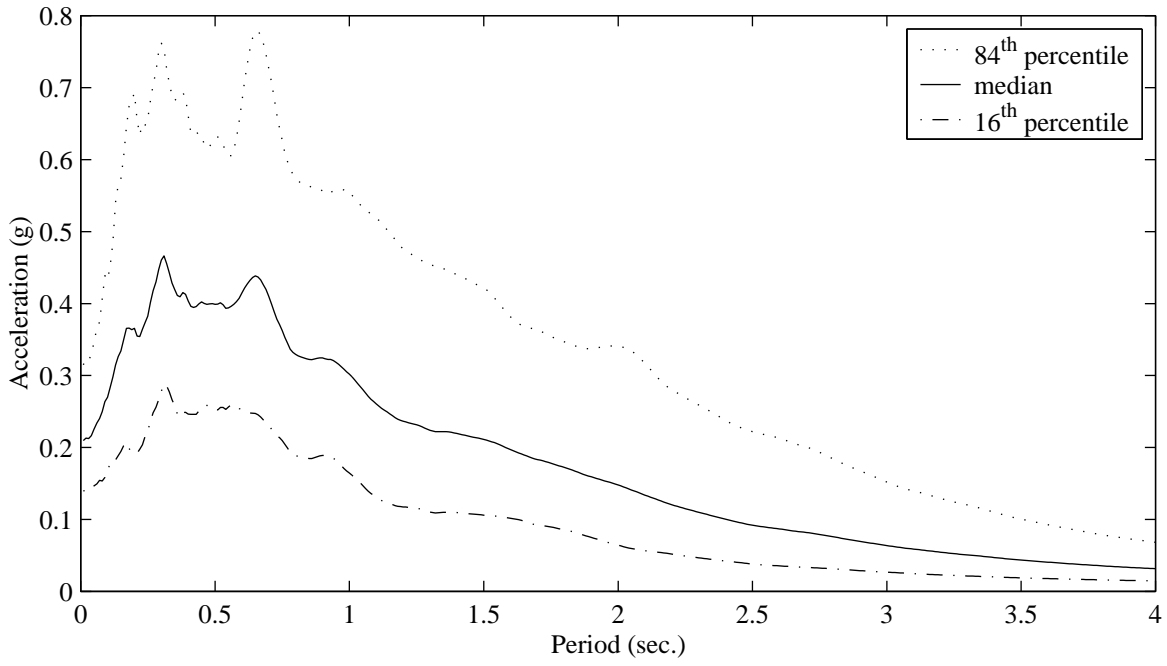


a. acceleration response spectra

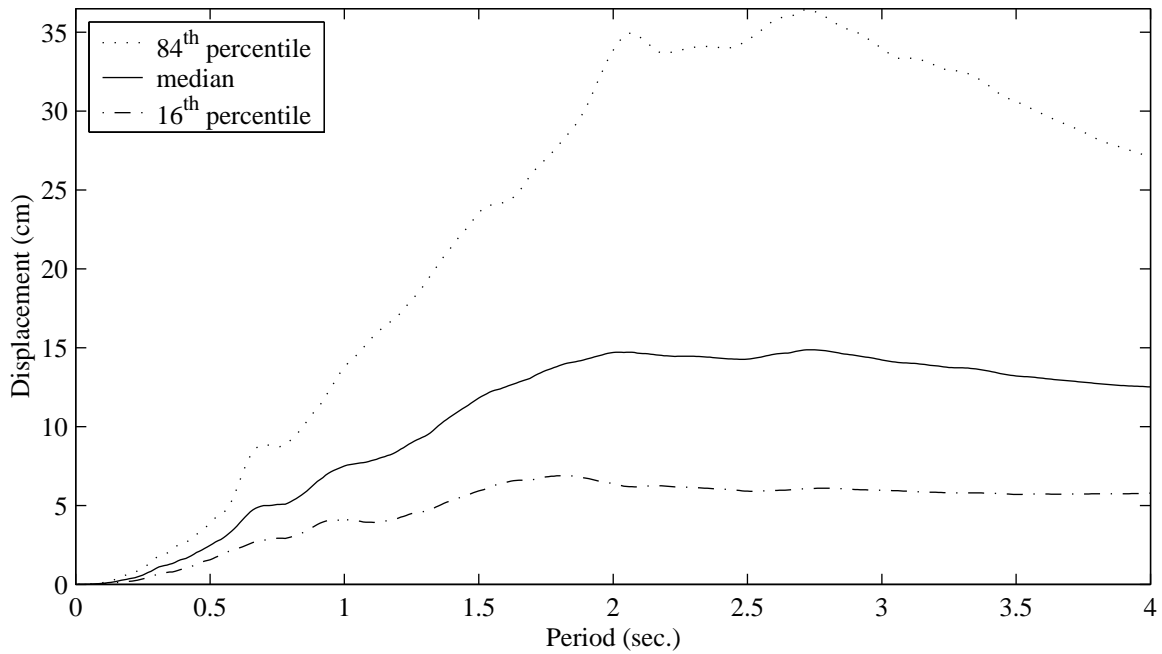


b. displacement response spectra

Figure 3.17. Elastic response spectra for Bin 6 ground motions and 5% critical damping using a lognormal characterization.

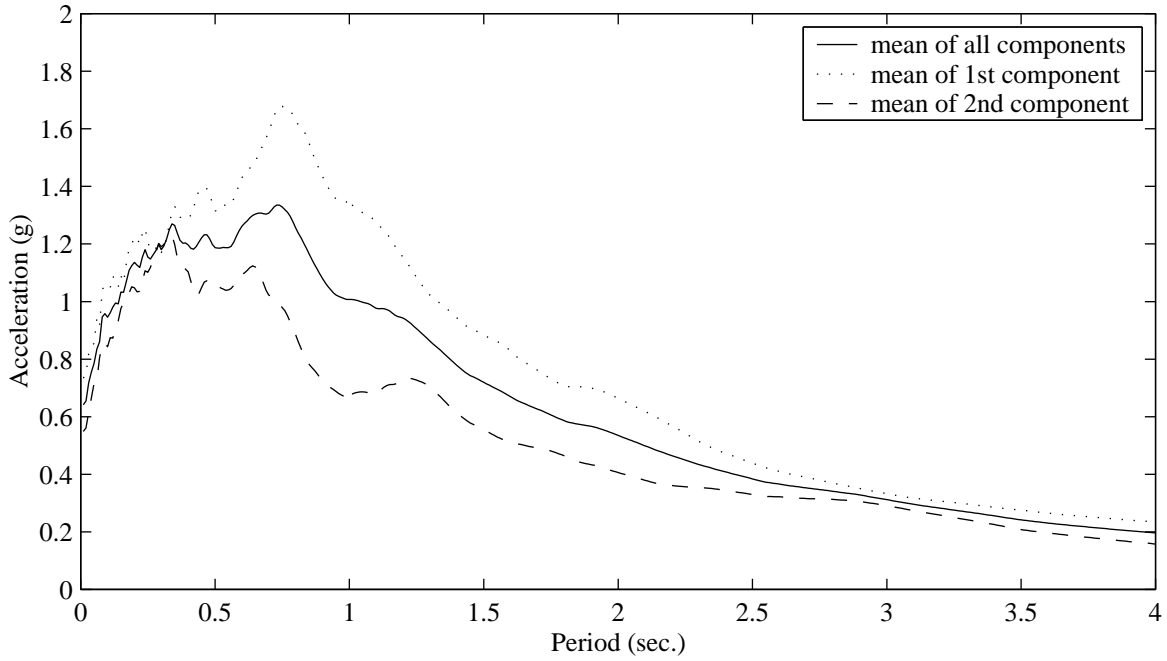


a. acceleration response spectra

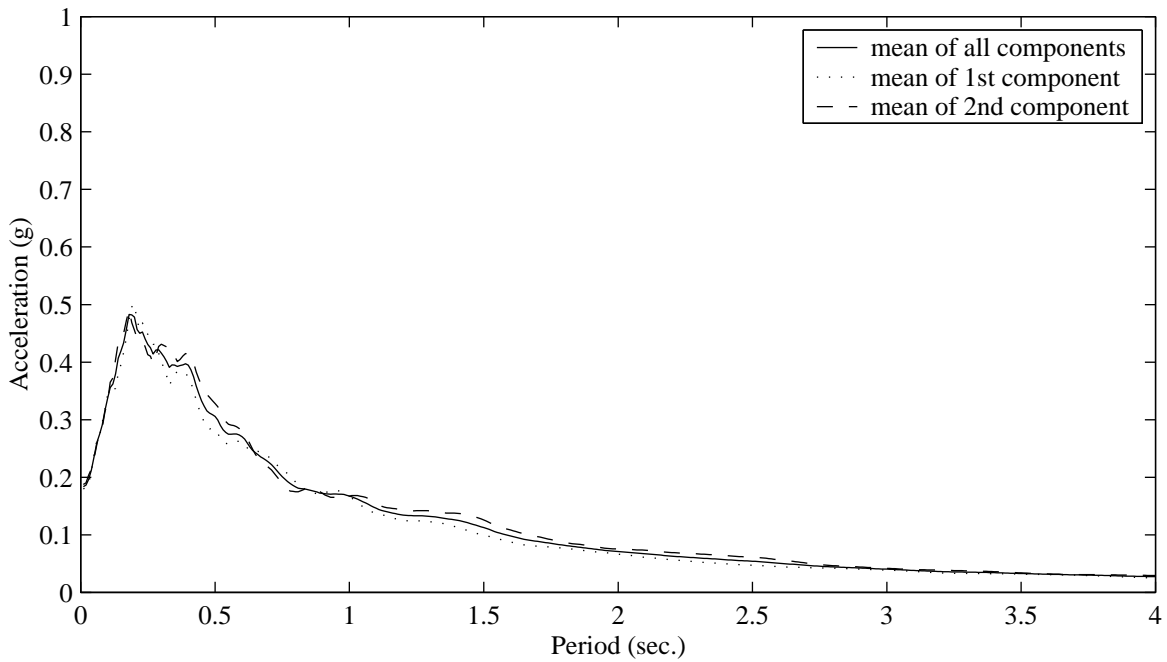


b. displacement response spectra

Figure 3.18. Elastic response spectra for Bin 7 ground motions and 5% critical damping using a lognormal characterization.

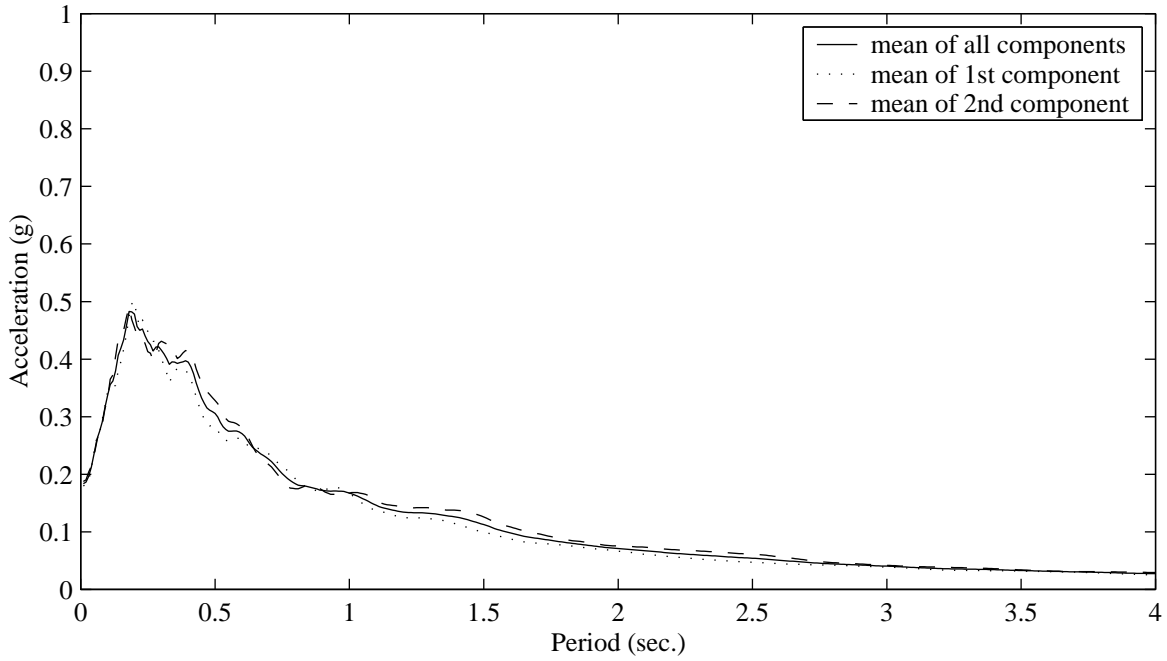


a. acceleration spectra for Bin 1.

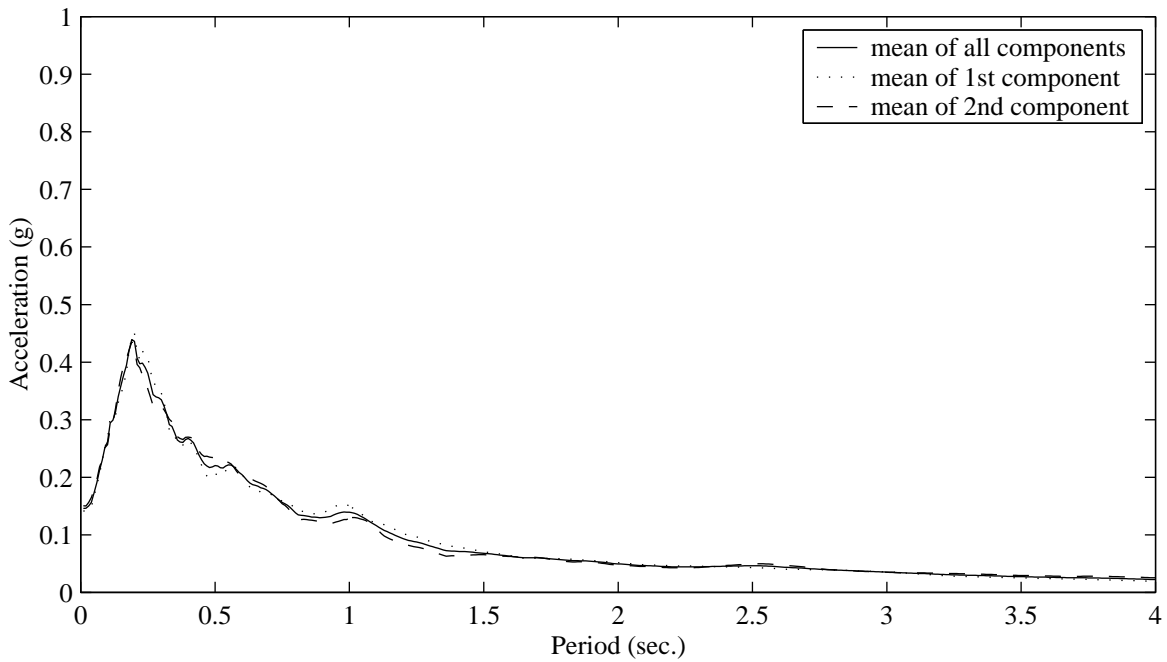


b. acceleration spectra for Bin 2.

Figure 3.19. Mean elastic response spectra for 1st, 2nd, and all, ground motion components and 5% critical damping for Bins 1 and 2.

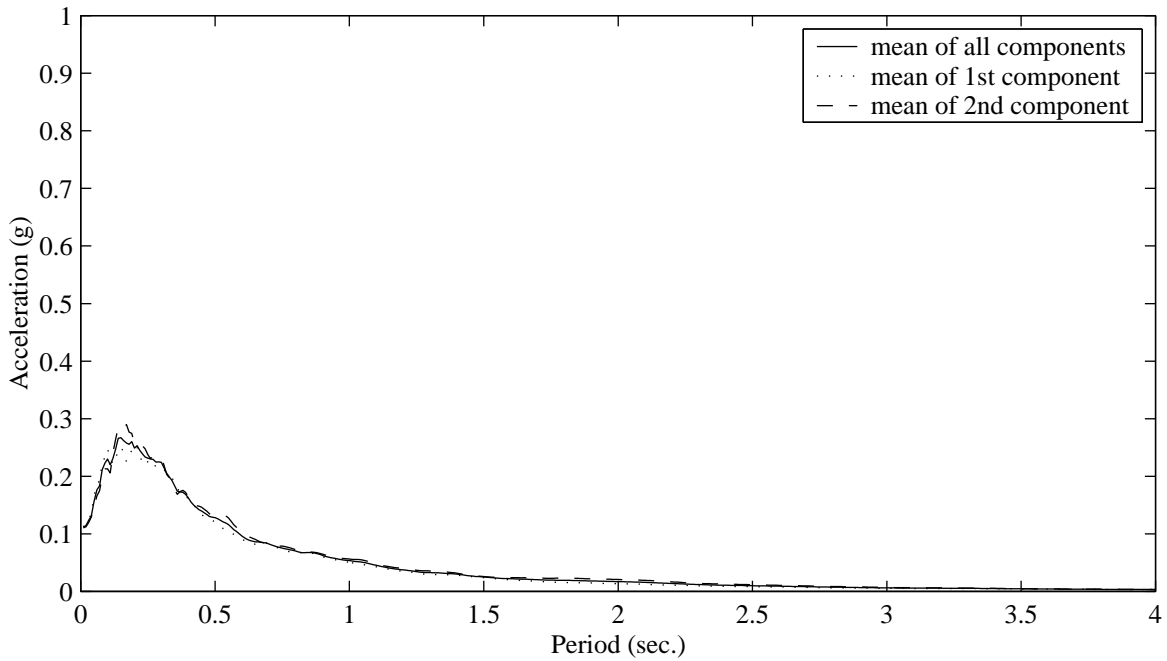


a. acceleration spectra for Bin 2M.

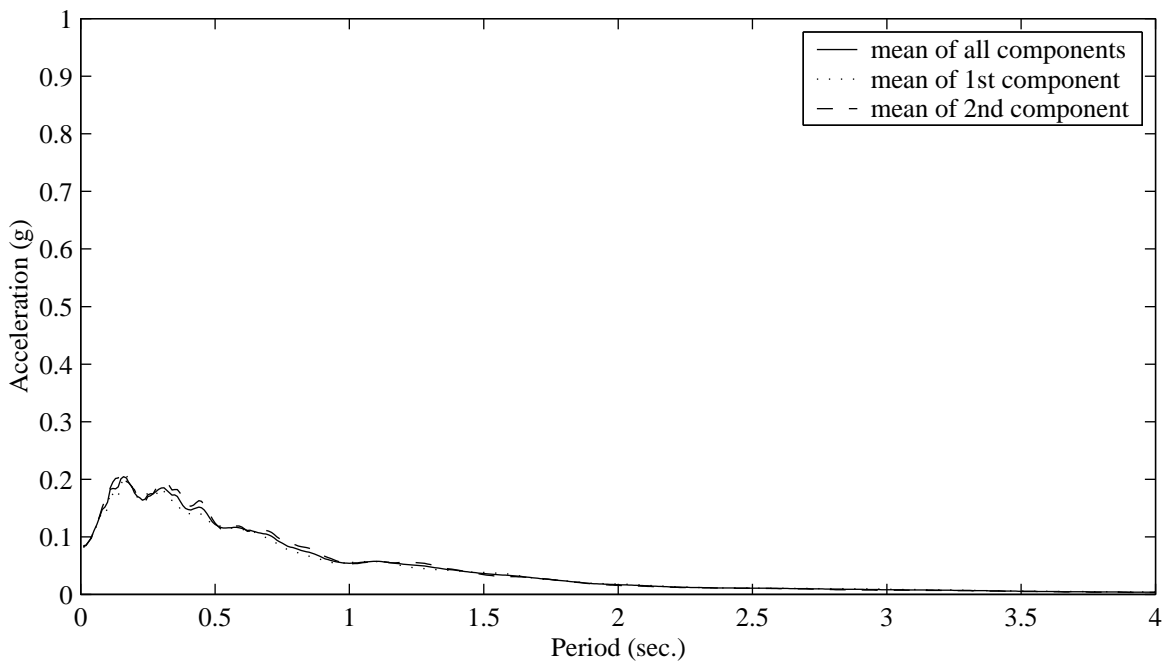


b. acceleration spectra for Bin 3.

Figure 3.20. Mean elastic response spectra for 1st, 2nd, and all, ground motion components and 5% critical damping for Bins 2M and 3.

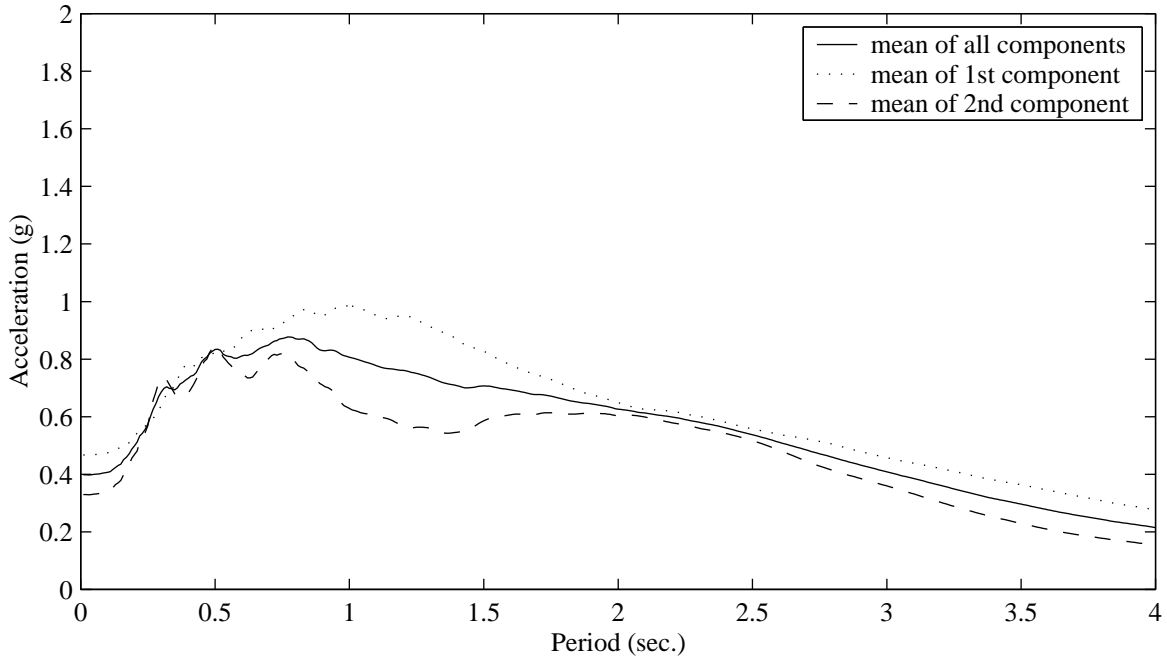


a. acceleration spectra for Bin 4.

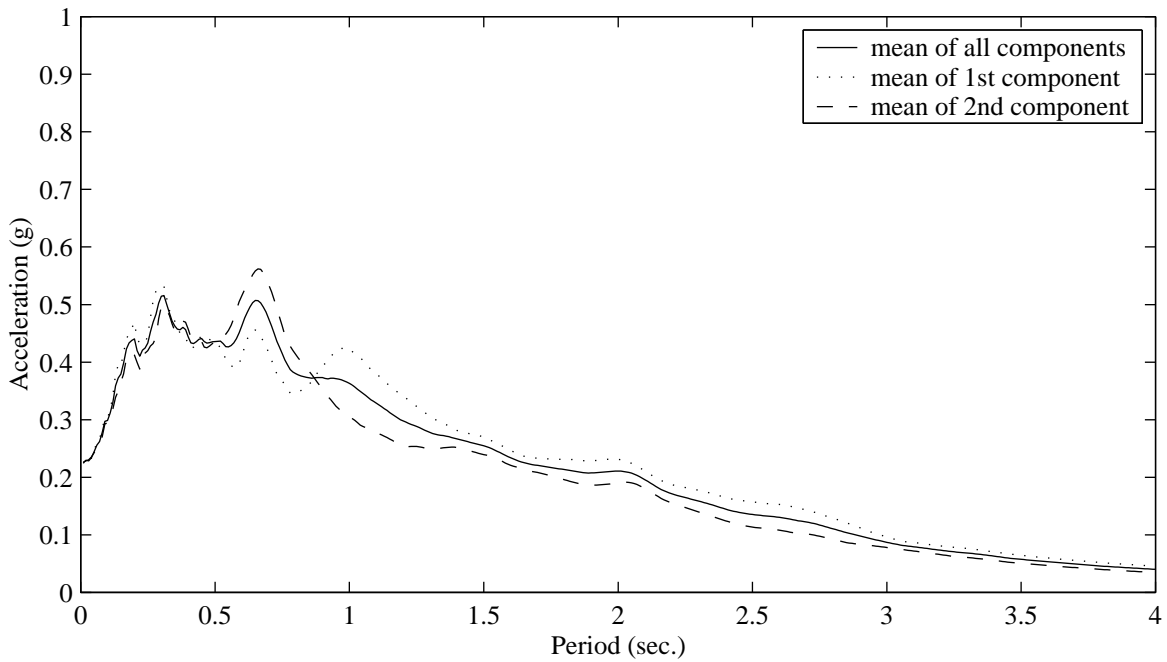


b. acceleration spectra for Bin 5.

Figure 3.21. Mean elastic response spectra for 1st, 2nd, and all, ground motion components and 5% critical damping for Bins 4 and 5.

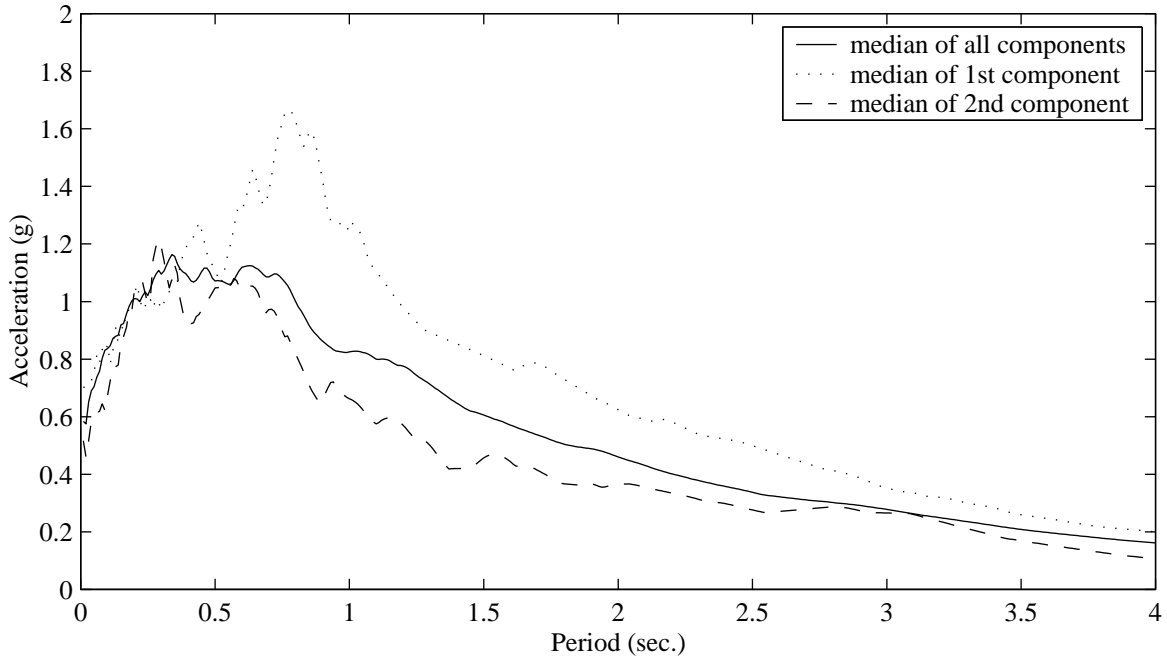


a. acceleration spectra for Bin 6.

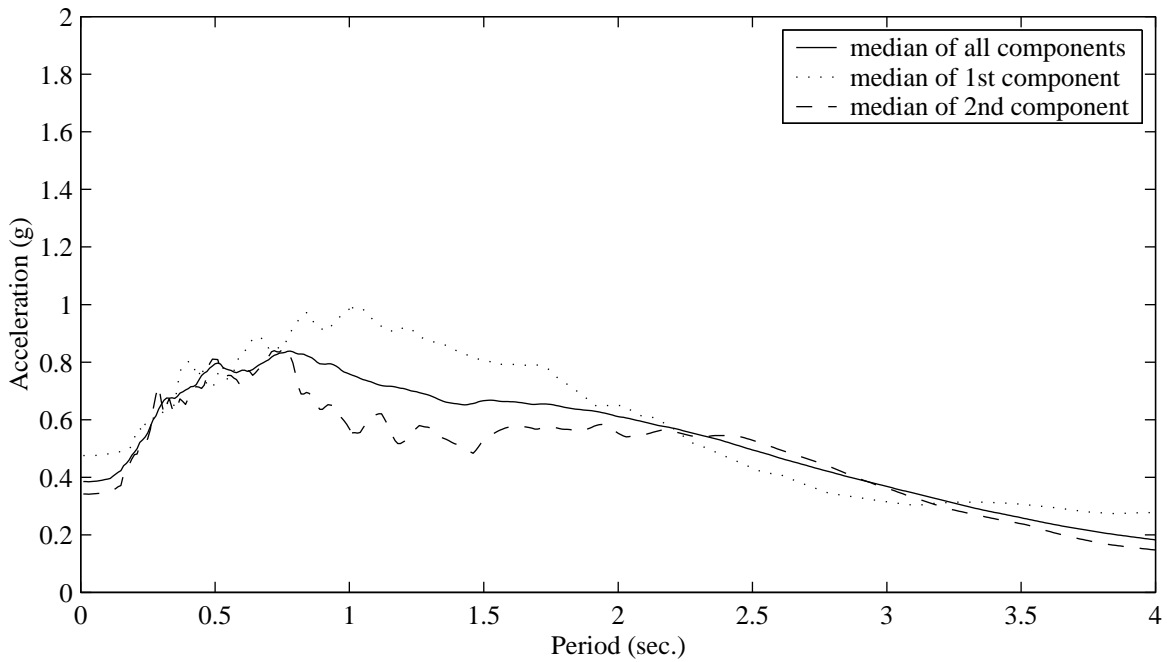


b. acceleration spectra for Bin 7.

Figure 3.22. Mean elastic response spectra for 1st, 2nd, and all, ground motion components and 5% critical damping for Bins 6 and 7.



a. acceleration spectra for Bin 1.



b. acceleration spectra for Bin 6.

Figure 3.23. Median elastic response spectra for 1st, 2nd, and all, ground motion components and 5% critical damping for Bins 1 and 6.

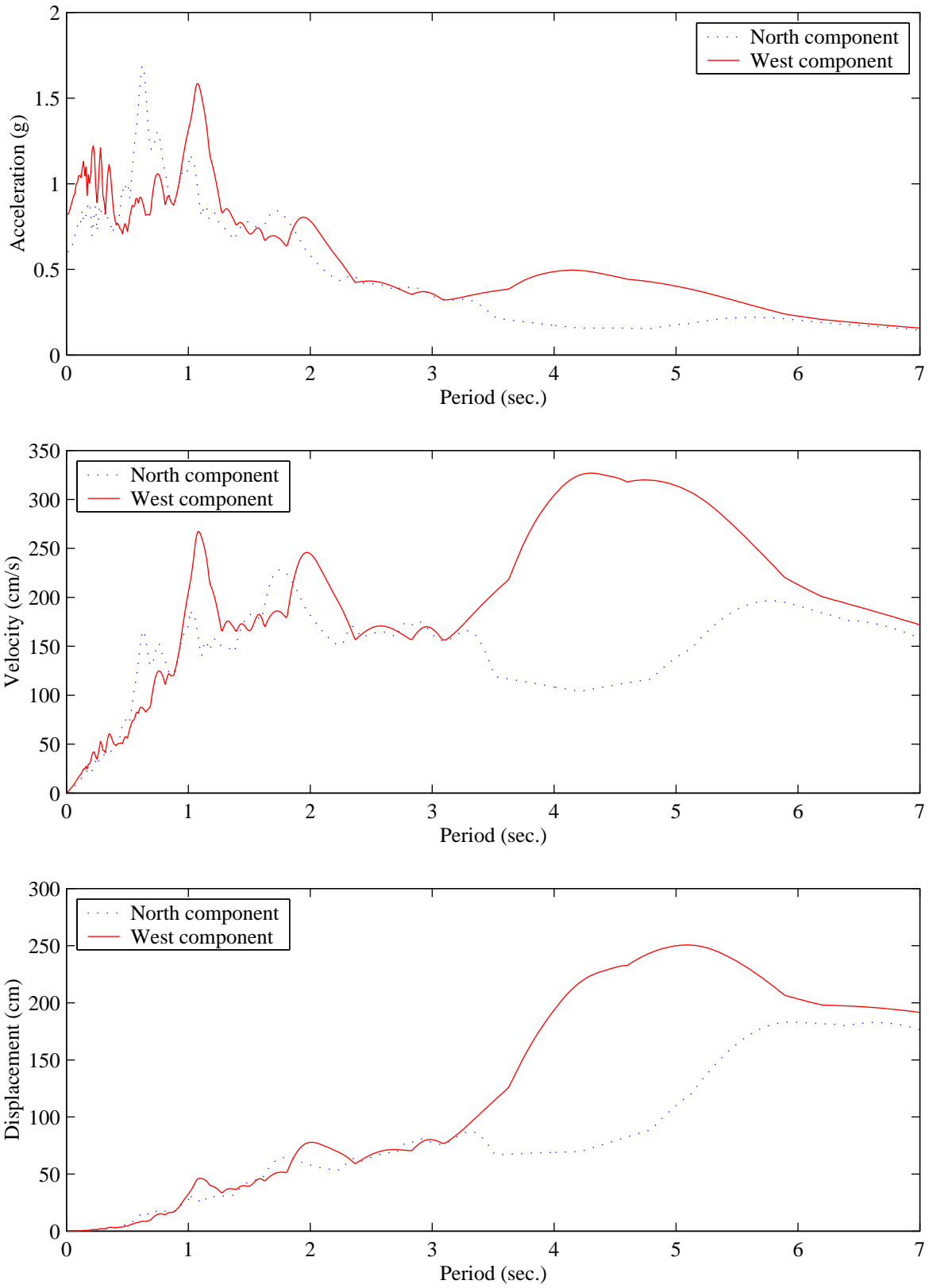


Figure 3.24. Elastic response spectra for record TCU065 and 5% critical damping.

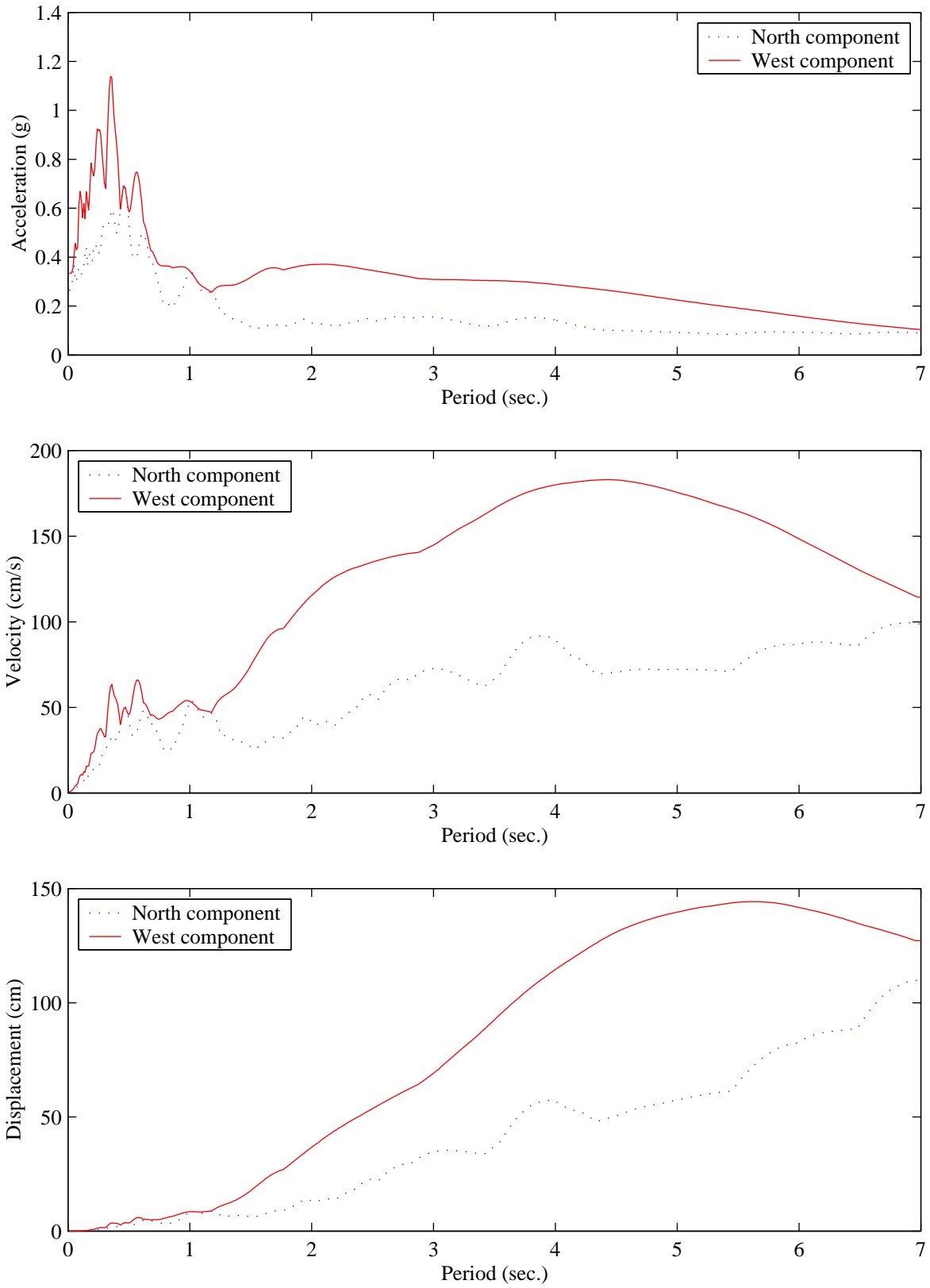
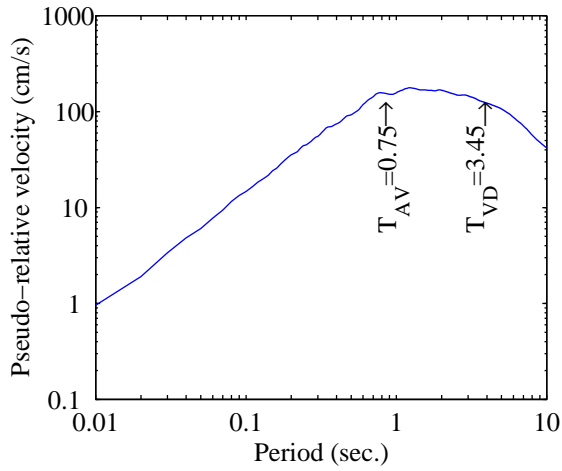
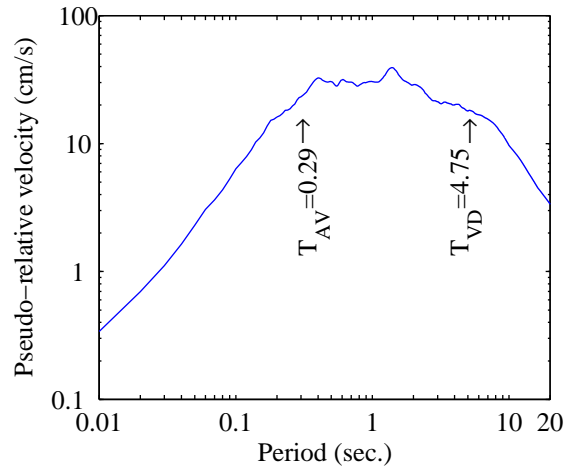


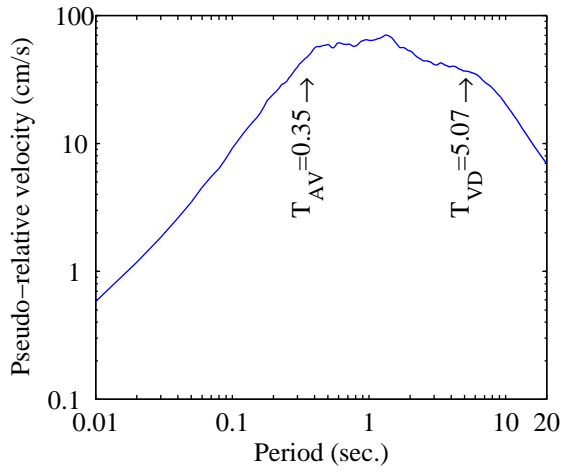
Figure 3.25. Elastic response spectra for record TCU075 and 5% critical damping.



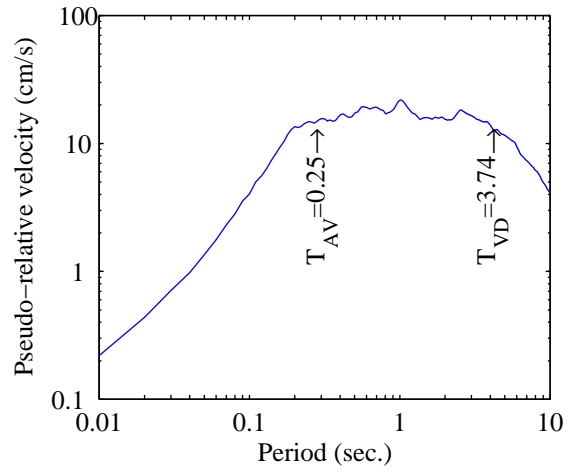
a. mean of Bin 1 and 5% damping



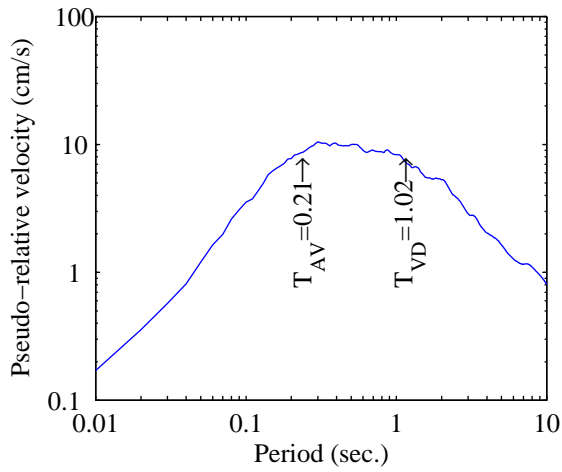
b. mean of Bin 2 and 5% damping



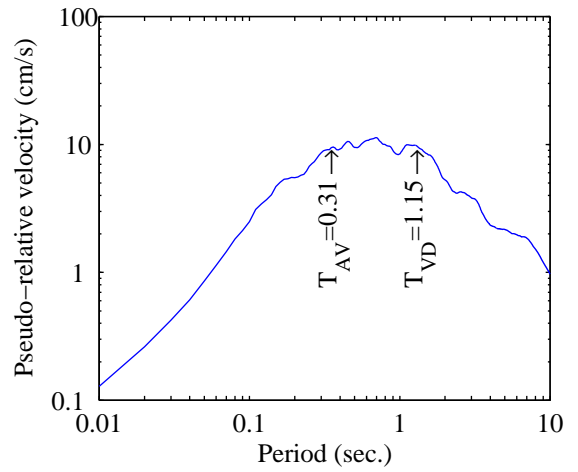
c. mean of Bin 2M and 5% damping



d. mean of Bin 3 and 5% damping



e. mean of Bin 4 and 5% damping



f. mean of Bin 5 and 5% damping

Figure 3.26. Estimated periods for the transition of spectral regions.

SECTION 4

RESPONSE-HISTORY ANALYSIS

4.1 General

Presented in this section is a discussion of the response-history analysis performed using earthquake ground motion records from Section 3. Both unidirectional and bi-directional nonlinear response-history analyses were performed. The nonlinear system consisted of a simple rigid bridge structure supported by four isolator elements. Parameters of each system were varied widely to ensure that the results of analyses performed for this study would be broadly applicable to the design of seismic isolation systems in the United States.

4.2 Nonlinear Response-History Analysis

4.2.1 General

A mathematical model of a simple isolated bridge structure was used for the nonlinear response-history analysis. This model represents the simplest of isolated bridge structures and assumes both the superstructure and substructure to be rigid. The simplicity of this bridge model enables a clear understanding of the effect of bi-directional excitation on the response of isolation systems.

4.2.2 Simple Bridge Model

A schematic representation of the mathematical model used for the isolated bridge structure is shown in Figure 4.1. This schematic shows a single span, assumed rigid, supported by four isolators resting on gravity abutments, also assumed to be rigid. Properties used for the mathematical model of the bridge structure (i.e., dimensions and mass) have been adopted from an example bridge set forth by the Applied Technology Council (ATC, 1986). The single span in the schematic is based on the middle span of the three span bridge structure proposed in the ATC report. The bridge superstructure has been assumed to be concrete with density: $\gamma_c = 2403 \text{ kg/m}^3$. The weight of the bridge deck was determined to be approximately 9900 kN using the following equation

$$W_{deck} = \gamma_c \cdot g \cdot A_{deck} \cdot L_{span} \quad (4.1)$$

where γ_c is the density of the concrete; g is the gravitational acceleration constant; A_{deck} is the cross-sectional area of the deck; and L_{span} is the length of the span supported by the isolators. Values of the geometric parameters are shown in Figure 4.1. The weight (or vertical load) acting on each seismic isolator was determined to be

$$W = \frac{W_{deck}}{4} \quad (4.2)$$

The center of mass (denoted *C.M.*) is assumed to coincide with the center of rigidity of the isolation system in plan as indicated by Figure 4.1. In elevation the *C.M.* is shown to be vertically offset from the center of rigidity of the isolations system by a distance, h . However, for the purpose of response-history analysis, the value of h was assumed to be zero. Therefore, the center of mass in both the horizontal and vertical plane coincide with the center of rigidity, eliminating any torsion or overturning moment due inertial forces assumed to develop at the center of mass as a result of earthquake excitation.

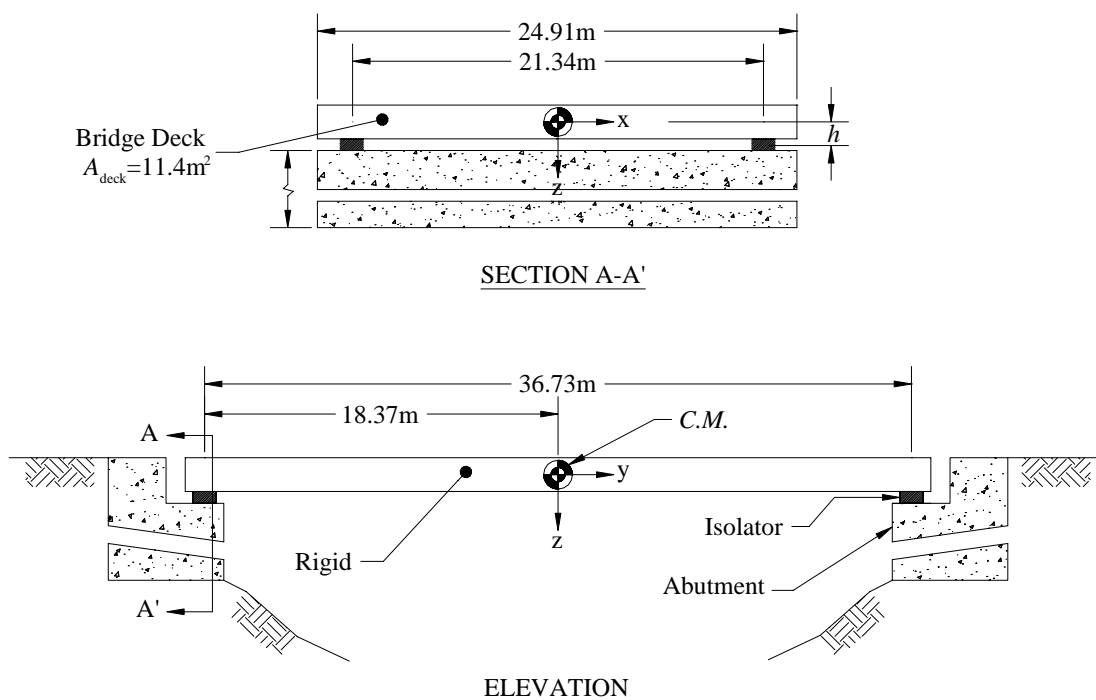


Figure 4.1. Simple bridge model based on: ATC example bridge.

4.2.3 Isolation Parameters

The parameters used for the coupled plasticity model are based on a bilinear characterization of the isolators. This bilinear characterization and defining parameters are shown in Figure 4.2. Here Q_d is the zero-displacement force; F_y is the yield force; K_u is the elastic stiffness; K_d is the second-slope stiffness; d_{yield} is the yield displacement assumed to be 0.025cm for all isolation systems considered; d_{max} is the maximum displacement; and EDC is the energy dissipated in one fully reversed cycle to the maximum displacement. Note this characterization is the same as that assumed by AASHTO in the Guide Specification for Seismic Isolation Design (AASHTO, 1999).

To ensure the results of this study were broadly applicable to the design of seismically isolated bridge structures, isolator parameters were varied, specifically Q_d and T_d the zero-displacement force and second-slope period, respectively. The second slope period can be determined from the second-slope stiffness using the following equation

$$T_d = 2\pi \cdot \sqrt{\frac{W}{K_d \cdot g}} \quad (4.3)$$

where W is the weight acting on an individual isolator defined previously; and g is the gravitational acceleration constant. Table 4.1 shows the range of values used for T_d and Q_d representing twenty different isolation systems. Note the zero-displacement force shown in Table 4.1 has been normalized by W , the weight acting on the isolator.

Table 4.1. Isolator parameter matrix

		T_d (seconds)				
		1.5	2.0	2.5	3.0	4.0
Q_d/W	0.03	A11	A12	A13	A14	A15
	0.06	A21	A22	A23	A24	A25
	0.09	A31	A32	A33	A34	A35
	0.12	A41	A42	A43	A44	A45

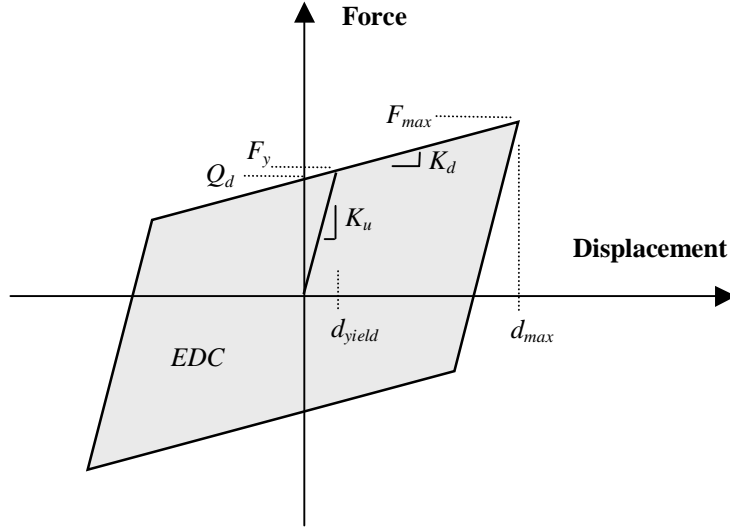


Figure 4.2. Bilinear characterization of an isolation bearing.

4.2.4 Mathematical Model for Isolator Elements

The isolators were modeled using a coupled plasticity formulation. The restoring force of the seismic isolator subjected to lateral displacements is give by

$$F = F_p + K_d \cdot d \quad (4.4)$$

where F_p is the plastic force; d is the isolator displacement; and K_d is the second-slope stiffness previously defined. For the case of bi-directional loading, Equation (4.4) is expressed in terms of vector components

$$\begin{bmatrix} F_x \\ F_y \end{bmatrix} = \begin{bmatrix} F_{px} \\ F_{py} \end{bmatrix} + K_d \cdot \begin{bmatrix} d_x \\ d_y \end{bmatrix} \quad (4.5)$$

where F_{px} is the component of the plastic force acting in the x -direction (which may vary from 0 to F_p due to the coupled behavior of the isolator); F_{py} is the component of the plastic force acting in the y -direction; d_x is the isolator displacement in the x -direction; d_y is the isolator displacement in the y -direction and K_d is the second-slope stiffness (or post elastic stiffness). The components of the plastic force, F_{px} and F_{py} , are determined based on the direction of the full plastic force and an assumed circular yield surface

(Huang, 2000; Mosqueda, 2003). The relationship between the components of the plastic force in each direction and the magnitude of the plastic force must satisfy the following equation

$$F_p = \sqrt{(F_{px}^2 + F_{py}^2)} \quad (4.6)$$

where F_p is the magnitude of the plastic force corresponding to the radius of the assumed circular yield surface. For example, with a lead-rubber bearing, the magnitude of the plastic force is assumed to be equal to the yield strength of the lead core material multiplied by the cross-sectional area of the lead core, $\sigma_L A_L$, or with friction pendulum bearings the plastic force is approximated assuming Coulomb friction, μW , where μ is the dynamic coefficient of friction; and W is the weight acting on the isolator. Contribution of the plastic force in each horizontal direction depends on the phasing of the demand placed on the isolator in the x - and y - directions. This is discussed in the following paragraphs.

Two simple displacement orbits have been selected to demonstrate the response of the coupled plasticity model. The displacement orbits (Mosqueda, 2003) shown in Figures 4.3a and 4.4a are a *box* and a *hourglass* shape, respectively. Force orbits (restoring force) and force-displacement hysteresis for both the x - and y -directions are also plotted in Figures 4.3 and 4.4. In both of these figures the displacement orbits have been annotated with small arrows to indicate the direction of displacement. Also plotted on the displacement orbits are symbols (referred to in the text using italic font) at various points in the displacement orbits. These symbols are also plotted on the force orbits and the x - and y - direction force-displacement hysteresis at coincidental points during the displacement orbit to facilitate a clear understanding of the coupled response and the affect on unidirectional isolator properties. The response of the isolator assuming uncoupled behavior, shown by a dashed-dot line, is also plotted in Figures 4.3 and 4.4.

Presented in Figure 4.3 is the response of the coupled plasticity model subjected to a box displacement orbit from which two important observations can be ascertained. First, referring to Figure 4.3b (force orbit) the force response for the coupled and uncoupled

plasticity models are observed to be significantly different. Focusing on the coupled response, when the isolator is located at the *square* the plastic force is aligned in the y -direction, as the isolator moves from the *square* to the *diamond* the plastic force rotates until it is aligned in the x -direction and remains in this alignment while the isolator moves to the position denoted by the *asterisk*. This drop in force in the y -direction is equal to the magnitude of the plastic force due to the re-alignment of the plastic force from the y -direction to the x -direction. Referring to Figures 4.3c and 4.3d (x - and y - direction hysteresis) the unidirectional properties, i.e., Q_d and β_{eff} (the effective damping) are relatively unaffected due to the box shaped displacement orbit. Since the displacement demand in the x - and y - directions do not occur simultaneously (or are out of phase) the full magnitude of the plastic force is always aligned in one or the other direction. This leads to the second key observation, namely, that the affect of bi-directional displacement demands on unidirectional isolator properties depends on the phasing of the x - and y -displacement components. This observation is further verified by investigation of the response of the isolator subjected to the hourglass displacement orbit.

Referring to Figure 4.4, the hourglass shaped displacement orbit, the affect of bi-directional displacement demands on unidirectional properties is investigated. Two important observations are noted. The first observation is shown by Figures 4.4c and 4.4d where the restoring force from the coupled plasticity model is significantly less than the restoring force from the uncoupled plasticity model as the isolator is displaced from the *circle* to the *square*. The force response in each direction determined from the coupled plasticity model is only a portion of the full plastic force magnitude because the full plastic force is aligned in the direction of incremental displacement. The uncoupled plasticity model significantly overestimates the force response in each of the x - and y -directions. For this displacement orbit, the uncoupled plasticity model over estimates the total plastic force by a factor of $\sqrt{2}$ along the displacement path from the *circle* to the *square*. One consequence of the reduction of restoring force in a particular direction is a reduction in the area of the hysteresis loop, which corresponds to a reduction in the effective damping when the effective damping is defined (AASHTO, 1999) to be

$$\beta_{\text{eff}} = \frac{\text{Area of Hysteresis Loop}}{2\pi \cdot K_{\text{eff}} \cdot d^2} \quad (4.7)$$

where K_{eff} is the effective stiffness of the isolator defined as the peak-to-peak stiffness; and d is the isolator displacement. The second point regarding the response of the coupled plasticity model subjected to the hourglass displacement orbit becomes apparent as the isolator is displaced from the *asterisk* to the *cross*. From Figure 4.4d (y-direction hysteresis), an increase (or spike) in the force response of the coupled model is observed as the isolator moves from the *asterisk* to the *cross*. This brief increase in the force response of the coupled model is a result of the re-alignment of the plastic force. As the isolator move from the *diamond* to the *asterisk* the plastic force is aligned in the x -direction. This observation is supported by the force-displacement response of the isolator in the x -direction of Figure 4.4c, noting the force response from the *diamond* to the *asterisk* is the same as the uncoupled model. As the isolator is displaced from the *asterisk* toward the *cross* the plastic force rotates from the x -direction to the direction of incremental displacement. Briefly during this rotation the plastic force is aligned in the y -direction, and hence the increase in the response of the force in the y -direction shown in Figure 4.4d. The response of the coupled model to the hourglass orbit clearly shows that the restoring force in a particular direction depends the alignment of the plastic force, which depends on the displacement demands in each of the horizontal directions.

When the isolators are represented using a coupled plasticity model, the resulting reduction in restoring force due to bi-directional input translates to an increase in horizontal displacements during nonlinear response-history analysis. The magnitude of the increase in the horizontal displacement of an isolated bridge subjected to bi-directional seismic excitation depends on the phasing of the horizontal ground motions components. For ground motion components that are strongly out-of-phase (as with the box orbit) the increase in displacement may be modest, however, for ground motion components that are strongly in-phase (as with the hourglass orbit) the resulting increase in displacement may be substantial.

4.2.5 The Equation of Motion

The equation of motion for the simple bridge model with two degrees of freedom, namely, translation in the X - and Y - directions (here capital variables will refer to the global degrees of freedom and lowercase to the individual isolator degrees of freedom) at the center of mass can be expressed as

$$\begin{bmatrix} m_{deck} & 0 \\ 0 & m_{deck} \end{bmatrix} \cdot \begin{bmatrix} \ddot{u}_X(t) \\ \ddot{u}_Y(t) \end{bmatrix} + \begin{bmatrix} c & 0 \\ 0 & c \end{bmatrix} \cdot \begin{bmatrix} \dot{u}_X(t) \\ \dot{u}_Y(t) \end{bmatrix} + \begin{bmatrix} F_X(t) \\ F_Y(t) \end{bmatrix} = -1 \cdot \begin{bmatrix} m_{deck} & 0 \\ 0 & m_{deck} \end{bmatrix} \cdot \begin{bmatrix} \ddot{u}_{gX}(t) \\ \ddot{u}_{gY}(t) \end{bmatrix} \quad (4.8)$$

where m_{deck} is the mass of the deck defined to be W_{deck} / g ; c is the viscous damping constant defined below; $\ddot{u}_{X,Y}(t)$ is the acceleration response of the center of the rigid deck in the X - and Y - direction, respectively (note, u is used to denote displacement response while d is used to denote a single displacement value); $\dot{u}_{X,Y}(t)$ is the velocity response of the center of the rigid deck in the X - and Y - direction, respectively; $F_X(t)$ and $F_Y(t)$ are the restoring forces of the isolation system in the X - and Y - direction determined to be the sum of the individual isolator restoring force; and $\ddot{u}_{gX}(t)$ and $\ddot{u}_{gY}(t)$ are the earthquake ground acceleration in the X - and Y - directions, respectively. The superstructure is assumed to have viscous damping, c , calculated using the following expression

$$c = 2 \cdot \zeta \sqrt{(m_{deck} \cdot K_U)} \quad (4.9)$$

where ζ is the critical damping ratio of the superstructure assumed to be 0.01; and K_U is the elastic stiffness of the bridge system which was calculated as the sum of the elastic stiffness of each of the four isolators.

The equation of motion given by Equation (4.8) was integrated numerically using Newmark's Method to obtain the horizontal displacement response of the isolated bridge structure subjected to the earthquake ground motion. A more detailed discussion of this procedure is presented in Appendix C.

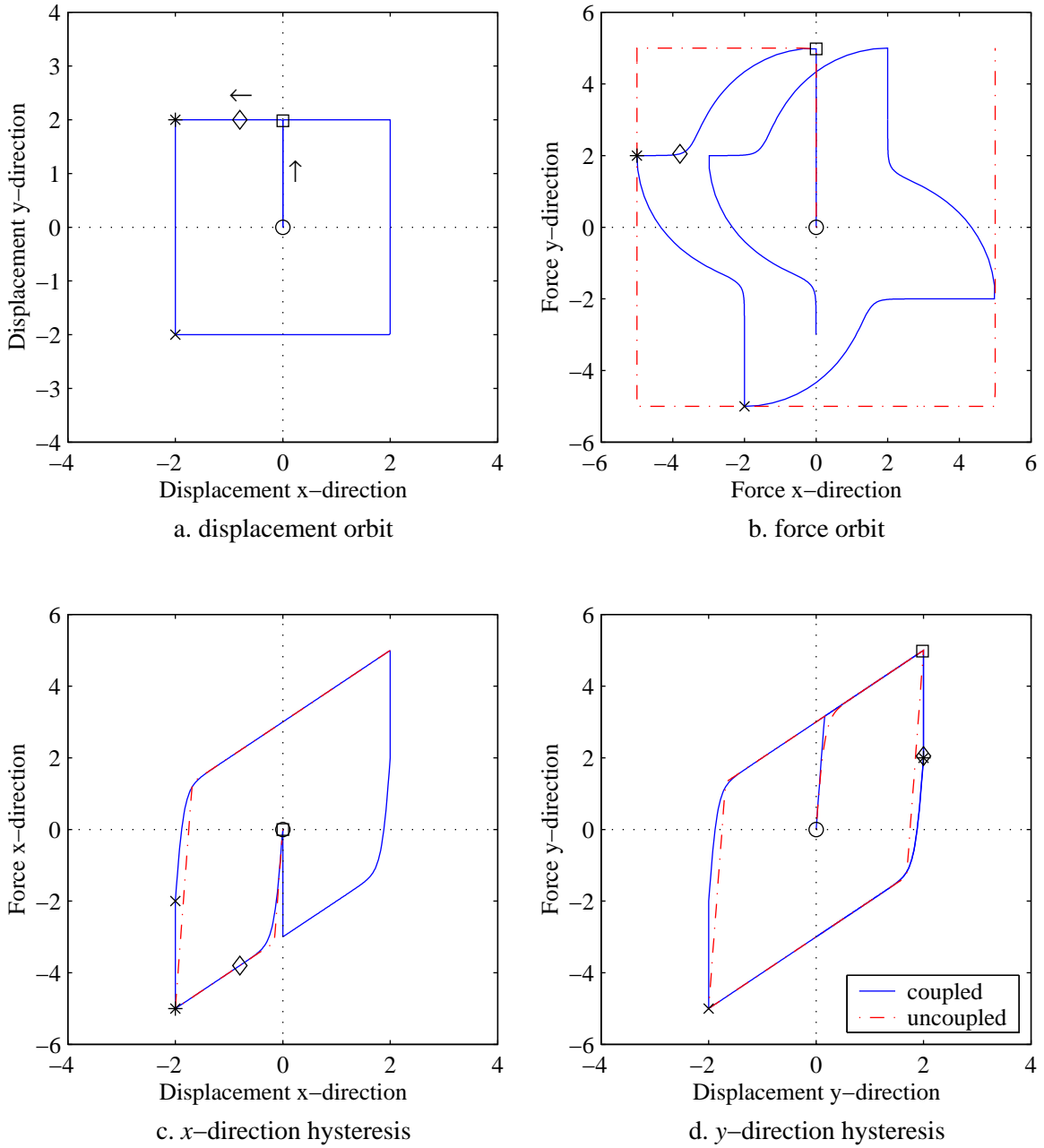


Figure 4.3. Comparison of the response of an isolator using coupled and uncoupled plasticity models for box shape displacement orbit.

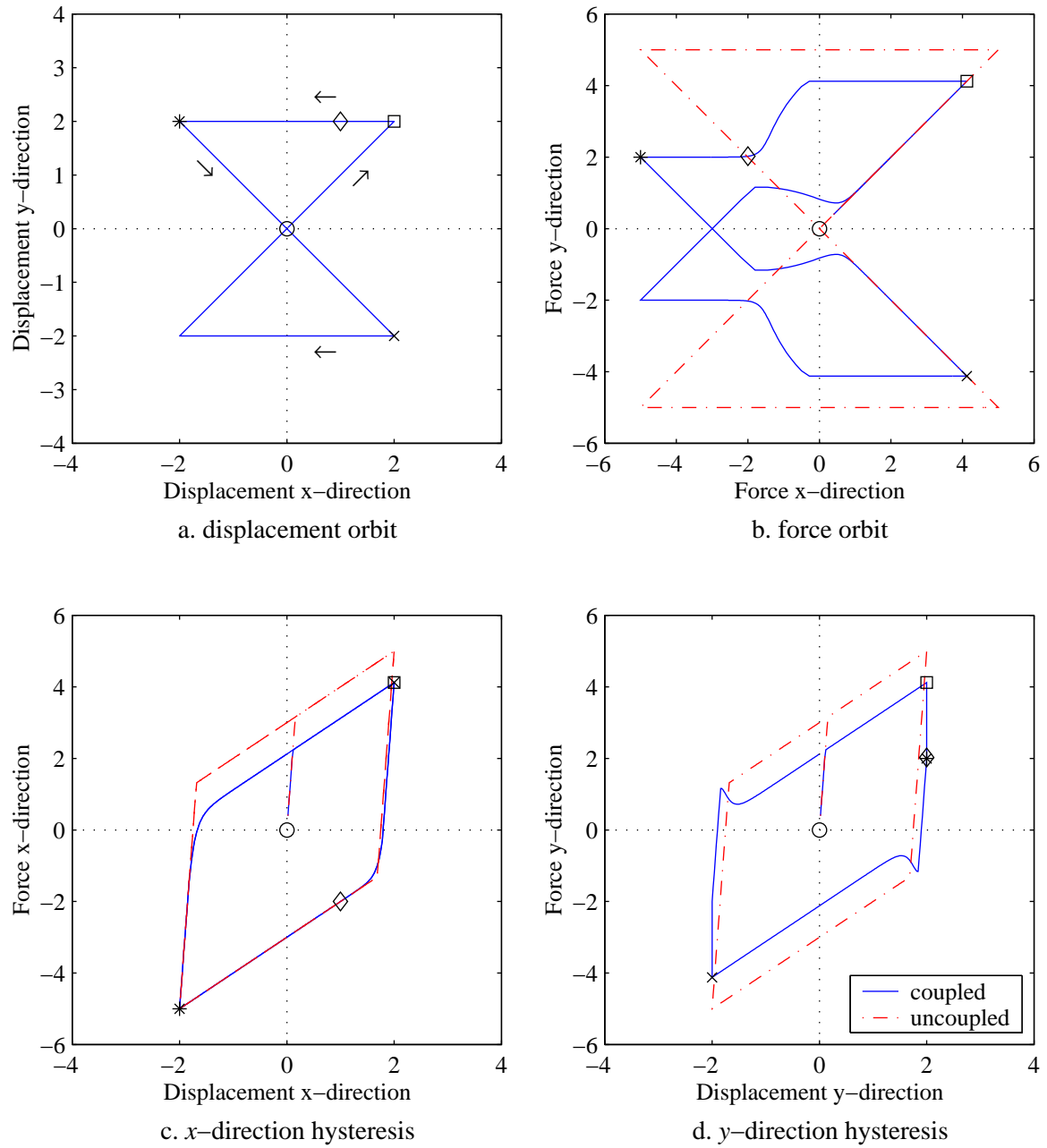


Figure 4.4. Comparison of the response of an isolator using coupled and uncoupled plasticity models for hourglass shape displacement orbit.

SECTION 5

DISPLACEMENT ESTIMATES IN SEISMICALLY ISOLATED BRIDGES

5.1 General

Results of the nonlinear response-history analyses were mined to determine the maximum displacement of a simple isolated bridge system. Maximum displacement data is being used to: (1) evaluate the current AASHTO equation for calculating displacements of the center of rigidity considering unidirectional seismic excitation; (2) compare the calculated AASHTO displacements with the maximum *horizontal* displacements determined from the results of bi-directional nonlinear response-history analysis; and (3) determine the increase in maximum isolator displacement due to bi-directional seismic excitation over those calculated considering unidirectional seismic excitation.

To facilitate comparison between the results of response-history analysis and the maximum displacement using the static analysis procedures of AASHTO, the 1-second spectral acceleration from each bin of ground motions was used. Details of this calculation are presented in the next section.

5.2 Static Analysis Procedure

5.2.1 General

Maximum isolator displacements were calculated using the procedure set forth by the AASHTO Guide Specifications for Seismic Isolation Design, Uniform Load Method (AASHTO, 1999). Equation 3b from the Guide Specifications has been reproduced here

$$d = \frac{250S_i A T_{eff}}{B} \quad (5.1)$$

where d is the design displacement in mm; S_i is a site-soil coefficient; A is an acceleration coefficient; T_{eff} is the effective period of the isolation system at the design

displacement in seconds; and B is a numerical coefficient related to the effective damping of the isolation system determined using Table 7.1-1 from the AASHTO Guide Specifications. To facilitate calculation of the design displacement, the 1-second spectral acceleration determined from either the *mean* or *median* acceleration response spectrum denoted, S_1 , was utilized. The 1-second spectral acceleration calculated for each ground motion bin was assumed to be equal to the product $S_i A$ in the AASHTO equation.

5.2.2 Results of the Static Analysis Procedure

Results of the AASHTO procedure, namely, displacement (d), effective period (T_{eff}), and effective damping (β_{eff}), considering all twenty isolation systems and the mean spectrum from six bins of ground motions are given in Table 5.1. These results are also presented in graphical format shown in Figure 5.1. In this figure the resulting displacements, denoted d , are plotted against the calculated effective period of the isolation system, T_{eff} . Because the effective period is a function of the design displacement the procedure is iterative. Sample calculations and the iterative procedure for two isolation systems are given in Appendix D. These isolation systems are shown in Figures 5.1c and 5.1f with vertical and horizontal lines centered behind the corresponding symbol. The first, an isolation system with $Q_d / W = 0.06$ and $T_d = 4.0$ seconds using the mean 1-second spectral acceleration from ground motion bin 2M and the second, an isolation system with $Q_d / W = 0.03$ and $T_d = 3.0$ seconds using the mean seismic hazard from ground motion bin 7.

The AASHTO procedure was repeated for the same isolation systems using a median characterization of the seismic hazard and the same six ground motion bins. These results are shown graphically in Figure 5.2. Resulting design parameters using the median characterization of the hazard for ground motion bins 1, 2, 2M, 3, 6, and 7 are presented in Table 5.2.

5.2.3 Design Displacement Considering Directivity of Ground Motion Components

In Section 3 the ground motion components of Bin 1 and Bin 6 were shown to exhibit directivity effects, namely, the response spectrum generate using the 1st component of

the ground motion pair is significantly larger than the response spectrum generated using the 2nd component of the ground motion pair. Therefore, to indirectly account for such directivity effects, design displacements were calculated using the AASHTO procedure using the 1-second spectral acceleration determined from the mean (or median) of the 1st component spectrum from Bins 1 and 6, denoted S_1^{1st} . Resulting displacements from these calculations are shown in Figure 5.3. For example, Figures 5.3a and 5.3b show the results of the AASHTO calculation using the 1-second spectral acceleration determined from the mean and median of the 1st component spectra from ground motion bin 1, respectively. Similarly, Figures 5.3c and 5.3d show the resulting displacements using the 1-second spectral acceleration determined from the mean and median of the 1st component spectra from ground motion bin 6, respectively. Numerical values of the resulting AASHTO calculation for Bin 1 and 6 using the mean and median characterizations are given in Tables 5.3 and 5.4.

5.3 Results of Unidirectional Nonlinear Response-History Analysis (URHA)

5.3.1 General

Maximum isolator displacements were tabulated from the results of unidirectional response-history analysis. Mean and median statistics were calculated using the maximum isolator displacements data to facilitate comparison with the results of the static analysis procedure described previously. For a particular ground motion bin containing N components, N maximum isolator displacements were obtained for each isolation system. Median values were calculated assuming the logarithm of the maximum isolator displacement data follow a normal distribution. Parameters of this distribution were estimated using the sample mean and sample standard deviation of the transformed data.

Maximum isolator displacements determined from the results of unidirectional nonlinear response-history analysis for each isolation system and ground motion are presented in Appendix E. Also given in Appendix E are sample statistics calculated for each isolation system. Mean and mean+ 1σ maximum isolator displacements are reproduced and presented in Table 5.5 for all twenty isolation systems and ground motion bins 1, 2, 2M,

3, 6 and 7. Median and 84th percentile displacements calculated assuming a lognormal distribution are presented in Table 5.6.

5.3.2 Comparison of Displacement Results Determined from URHA and Static Analysis Procedure

A comparison of maximum isolator displacements obtained from unidirectional response-history analysis, denoted d_x , with maximum isolator displacements calculated using the static analysis procedure of AASHTO, denoted d , for six bins of ground motions are presented in Figures 5.4 and 5.5 using mean and median statistics respectively. In each of these figures a line with slope 1.0 is plotted for reference. Data points that lie above the line indicate that the AASHTO calculated displacement underestimate the mean (or median) maximum displacement determined from response-history analysis. This discussion will focus on the results obtained using median statistics and ground motion bins 1, 2M, 6, and 7, shown by Figures 5.5a, 5.5c, 5.5e, and 5.5f, respectively. Displacement results obtained from unidirectional response-history analysis using ground motions from Bin 3 are modest. Seismic isolation would not typically be considered a viable alternative for such modest displacement demand.

As shown in Figure 5.5a, Bin 1, the results of the AASHTO calculation are observed to agree well with the results obtained from unidirectional response history analysis. Although the agreement is good, the results of the AASHTO calculation are observed to underestimate the maximum displacements (lie above the line), specifically for isolation systems with $Q_d/W = 0.03$ and $Q_d/W = 0.06$, shown by a circle and diamond respectively. From Figure 5.5c, Bin 2M, the results of the AASHTO calculation are observed to be conservative (lie below the line) for all twenty isolation systems considered when compared to the median maximum isolator displacement determined from unidirectional response-history analysis.

From Figure 5.5e, Bin 6, the AASHTO calculation is observed to underestimate the maximum displacement for almost all isolation systems. Results shown in Figure 5.5f, Bin 7, indicate that the AASHTO calculation is observed to underestimated the maximum displacement for isolation systems with $Q_d/W = 0.03$ and $Q_d/W = 0.06$. Response

spectra generated from the soft-soil ground motions components contained in Bins 6 and 7 exhibited amplification in the long period range. This amplification for periods coincidental with the effective period of the isolation system could explain the large displacements obtained from response-history analysis for systems with $Q_d/W = 0.03$ and $Q_d/W = 0.06$, and the corresponding underestimation of the AASHTO calculated displacements.

Presented in Figure 5.6 is a comparison of the mean and median maximum isolator displacements obtained from unidirectional response-history analysis with the calculated maximum displacements using the AASHTO procedure considering only the first components of the ground motion pairs from Bins 1 and 6. From Figure 5.6b, Bin 1, the AASHTO calculated maximum displacements are observed to conservatively estimate the median maximum isolator displacement determined from unidirectional response-history analysis for all isolation systems considered. From Figure 5.6d, Bin 6, the AASHTO calculated maximum isolator displacements agree well with the median maximum isolator displacements determined from unidirectional response-history analysis. Although the agreement is good, the maximum displacement calculated using the AASHTO procedure slightly underestimated the maximum displacement for several of the isolation systems considered.

5.4 Results of Bi-directional Nonlinear Response-History Analysis (BRHA)

5.4.1 General

Results of bi-directional nonlinear response-history analysis were mined to determine the maximum *horizontal* isolator displacement. Maximum horizontal displacements were determined from the square-root-sum-of-squares response calculated at each time-step during the response-history analysis using the displacement components in each orthogonal direction. Maximum horizontal displacements were determined for each isolation system and each *pair* of ground motions considering bins 1, 2, 2M, 3, 6, and 7. Sample mean and median statistics were calculated from the maximum isolator displacements data to facilitate comparison with the results of the static analysis procedure described previously. For a particular ground motion bin containing N

components, $N/2$ maximum isolator displacements were obtained for each isolation system. Median values were calculated assuming the logarithm of the maximum isolator displacement data follow a normal distribution. Parameters of this distribution were estimated using the sample mean and sample standard deviation of the transformed data.

Maximum horizontal isolator displacements determined for each isolation system and ground motion pair using bi-directional response-history analysis are presented in Appendix E. Mean and median maximum horizontal displacements for the six bins of ground motions and twenty isolation systems considered were reproduced and presented in Tables 5.7 and 5.8, respectively.

5.4.2 Comparison of Displacement Results Determined from BRHA and Static Analysis Procedure

A comparison between maximum horizontal isolator displacements obtained from bi-directional response-history analysis and maximum isolator displacements calculated using the Uniform Load Procedure from the AASHTO Guide Specifications for Seismic Isolation Design is presented. The AASHTO Guide Specifications state that the displacement obtained using Equation 3 is the “Design Displacement at the center of rigidity of the isolation system in the direction under consideration”. However no commentary is provided regarding the combination of displacements obtained from analysis in each orthogonal direction. If one assumes that the resulting displacements should be combine using the recommendations for the combination of elastic forces provided in the AASHTO Standard Specifications For Highway Bridges (1996), Division IA-Seismic Design, Section 3.8, titled “Determination of Elastic Forces and Displacements” and calculates the vector sum assuming 100 percent of the design displacement in one direction and 30 percent of the design displacement in the orthogonal direction, the result is an increase in the design displacement of approximately 4.4 percent. For comparison of the results in this section, this increase was neglected and the results of the bi-directional response-history analysis were compared directly with the design displacements obtained from the procedure discussed in Section 5.2.

Presented in Figures 5.7 and 5.8 is a comparison of maximum *horizontal* isolator displacements calculated from the results of bi-directional response-history analysis, denoted d_{xy} , with maximum isolator displacements calculated using the static analysis procedure of AASHTO, denoted d , for six bins of ground motions using mean and median statistics respectively. Referring to Figure 5.8, a comparison of the median maximum horizontal isolator displacements and displacements calculated using the AASHTO procedure and a median characterization of the hazard, it is observed that the AASHTO calculation (represented by the horizontal axis) underestimate the maximum bi-directional displacement for Bins 1, 2M, 6, and 7, shown by Figures 5.8a, 5.8c, 5.8e, and 5.8f, respectively. From these figures it is clear that the maximum displacements obtained from bi-directional response-history analysis are significantly larger than those calculated using the AASHTO procedure. To quantify the increase in displacement due to bi-directional seismic excitation, the ratio of the maximum displacement determined from bi-directional response-history analysis to the maximum displacement determined from unidirectional response-history analysis was calculated for each isolation system and ground motion pair. The details and results of this calculation are presented in the next section.

5.5 Unidirectional Displacement Multiplier

5.5.1 General

The increase in displacement due to bi-directional excitation was quantified as the ratio of the maximum isolator displacement determined from bi-directional response-history analysis to the maximum displacement determined from unidirectional response-history analysis for each isolation system and ground motion pair. Two factors contribute to the increase in maximum isolator displacement: (1) the contribution of earthquake demand in the orthogonal direction which varies depending on the phasing of the two orthogonal ground motion components and (2) the affect of bi-directional demand on the unidirectional response of the isolator, namely, the characteristic strength (Q_d) and effective damping (β_{eff}), which is a result of the coupled behavior of the isolator and varies depending on the phasing of the two orthogonal ground motion components. This effect was demonstrated in Section 4.

The unidirectional displacement multiplier, α_{xy} , was defined as the median of the ratios of maximum horizontal and maximum unidirectional displacement calculated for a given isolation system and each pair of ground motions in a given bin. This definition is shown by

$$\alpha_{xy} = \text{median} \left\{ \frac{d_{xy}^1}{d_x^1}, \frac{d_{xy}^i}{d_x^i}, \dots, \frac{d_{xy}^{N/2}}{d_x^{N/2}} \right\} \quad (5.2)$$

where d_{xy}^i is maximum *horizontal* isolator displacement determined from bi-directional response-history analysis using the i^{th} ground motion pair; and d_x^i is the maximum isolator displacement determined from unidirectional response-history analysis using the 1st component of the i^{th} ground motion pair. For ground motion bins 1 and 6, where directivity effects are significant, the unidirectional displacement multiplier using the definition above represents the increase in displacement over the larger of the two components. However, this definition must be modified to represent the increase in displacement for the case of average directivity. To account for this, an alternative definition of the displacement multiplier was employed, namely

$$\alpha'_{xy} = \text{median} \left\{ \frac{d_{xy}^1}{(d_x^1 + d_y^1)/2}, \frac{d_{xy}^i}{(d_x^i + d_y^i)/2}, \dots, \frac{d_{xy}^{N/2}}{(d_x^{N/2} + d_y^{N/2})/2} \right\} \quad (5.3)$$

where d_{xy}^i is maximum *horizontal* isolator displacement determined from bi-directional response-history analysis using the i^{th} ground motion pair; d_x^i is the maximum isolator displacement determined from unidirectional displacement using the 1st component of the i^{th} ground motion pair; and d_y^i is the maximum isolator displacement determined from unidirectional displacement using the 2nd component of the i^{th} ground motion pair. This alternative definition uses an average of the maximum isolator displacements obtained from independent unidirectional response-history analysis using the 1st and 2nd components of a ground motion pair.

Results for the unidirectional displacement multiplier (α_{xy}) for each isolation system and ground motion bins 1, 2, 2M, 3, 6, and 7 are presented in Table 5.9. These results are also

plotted in Figure 5.9 where the unidirectional displacement multiplier has been plotted for each value of Q_d/W and as a function of the second-slope stiffness (T_d). Results of the modified unidirectional displacement multiplier (α'_{xy}) for each isolation system considering and ground motion bins 1 and 6 are presented in Table 5.10. These results are also plotted in Figure 5.10 using the same format as α_{xy} . Values of the unidirectional displacement multiplier and modified unidirectional displacement multiplier shown in Figures 5.9c, 5.10a, and 5.10b, corresponding to Bins 2M, 1, and 6, represent an increase in displacement assuming average (Bins 1 and 6) or null (Bin 2M) directivity of the ground motion components respectively. Values of α_{xy} and α'_{xy} are observed to range from approximately 1.5 to 2.0 for these cases. These results suggest that the median maximum displacement of an isolation systems subjected to bi-directional seismic excitation could be up to two times larger than the calculated design displacement based on unidirectional excitation.

The values of the unidirectional displacement multiplier calculated considering the first ground motion components from Bins 1 and 6 are shown in Figures 5.9a and 5.9e, with maximum values of 1.17 and 1.36 respectively. Values of α_{xy} calculated in this manner are smaller because the first ground motion component is significantly larger than the second and result in a displacement that is close to the maximum horizontal displacement. Therefore, for the design of an isolation system in close proximity to a fault, the increase in displacement due to bi-directional seismic excitation may not be significant, if the fault normal spectrum is used as the design spectrum.

5.5.2 Estimates of the Maximum Horizontal Displacement

Maximum isolator displacements obtained using the AASHTO procedure described in Section 5.2 were multiplied by the corresponding unidirectional displacement multiplier and compared to the maximum horizontal displacements determined from bi-directional response-history analysis.

This comparison is presented in Figure 5.11 for ground motion bins 1, 2, 2M, 3, 6, and 7. For Figures 5.11d, 5.11c, 5.11d, and 5.11f, the x -axes are the multiplied AASHTO

displacement, $\alpha_{xy} \cdot d$, and the y-axes are the median maximum displacement determined from bi-directional response-history analysis, d_{xy} . For Figures 5.11a and 5.11e, Bins 1 and 6, the x-axes represent the modified unidirectional displacement multiplier times the AASHTO displacement, $\alpha'_{xy} \cdot d$, the y-axes are the same as the other plots. From these figures it is observed that the modified AASHTO displacement (multiplied by the unidirectional displacement multiplier) still underestimate the median maximum displacements obtained from bi-directional response-history analysis. However the resulting displacements, although unconservative, lead to improved estimates of the maximum horizontal displacement of an isolated bridge structure subjected to bi-directional seismic excitation. This improvement is realized when the results shown in Figure 5.11 are contrasted with the results shown in Figure 5.8.

Figure 5.12 shows the results of the AASHTO displacement determined assuming a lognormal characterization of the hazard considering the first components of the ground motion pairs multiplied by the unidirectional displacement multiplier $\alpha_{xy} \cdot d$ compared with the median maximum displacements obtained from bi-directional response-history analysis. From Figure 5.12a, Bin 1, the modified AASHTO displacements are observed to conservatively estimate the maximum horizontal displacement for all but one isolations system. For Bin 6, Figure 5.12b, the modified AASHTO displacements underestimate the maximum horizontal displacement for all isolation system.

5.6 Conclusions

Based on the results of this investigation the following conclusions are made.

- (1) The maximum isolator displacements calculated using the AASHTO procedure estimated the mean or median maximum displacement determined from unidirectional response-history analysis reasonably well for the case of stiff-soil site conditions, namely, Bin 1 and Bin 2M. The AASHTO displacements underestimated the maximum displacement determined from unidirectional response-history analysis for most isolation systems for soft-soil site conditions, Bin 6 and Bin 7. This underestimation is likely due to the frequency content of the

ground motion components with periods similar to the effective periods of many of the isolated bridge structures considered for this study.

- (2) The maximum isolator displacements calculated using the AASHTO procedure underestimate median maximum horizontal displacements obtained from bi-directional response-history analysis. Two factors contribute to this underestimation, the first, the addition of a second ground motion component and the second, the coupled behavior of the isolator elements.
- (3) Values of the unidirectional displacement multiplier calculated for Bins 1, 2M, and 6 considering average or null directivity range from 1.5 to 2.0. If directivity of the ground motion components is considered and the larger component is used to calculate the maximum displacements, the value of the unidirectional displacement multiplier is observed to be smaller. Use of the unidirectional displacement multiplier lead to improved estimates of the maximum displacement although in many cases the modified AASHTO displacement underestimated the median maximum horizontal isolator displacement.

Table 5.1. Results of the AASHTO design calculation using a mean characterization of the seismic hazard.

Bin	Parameter	Isolation System																			
		$Q_d/W=0.03$				$Q_d/W=0.06$				$Q_d/W=0.09$				$Q_d/W=0.12$							
		T_d (sec.)				T_d (sec.)				T_d (sec.)				T_d (sec.)							
		1.5	2.0	2.5	3.0	4.0	1.5	2.0	2.5	3.0	4.0	1.5	2.0	2.5	3.0	4.0	1.5	2.0	2.5	3.0	4.0
1	d (cm)	44.6	54.6	62.2	69.5	83.0	34.8	41.4	46.5	51.1	57.0	29.5	34.1	37.2	39.7	44.2	25.7	28.4	31.1	33.1	39.3
	T_{eff} (sec.)	1.47	1.95	2.41	2.86	3.74	1.43	1.87	2.28	2.67	3.36	1.39	1.78	2.13	2.44	2.97	1.34	1.68	1.98	2.23	2.69
	β_{eff}	0.02	0.03	0.04	0.06	0.08	0.06	0.08	0.11	0.13	0.19	0.09	0.13	0.17	0.22	0.29	0.13	0.19	0.24	0.29	0.35
2	d (cm)	4.31	4.81	5.19	5.86	6.94	2.93	3.47	3.87	4.18	4.60	2.46	2.79	3.01	3.16	3.34	2.09	2.30	2.43	2.51	2.60
	T_{eff} (sec.)	1.27	1.57	1.81	2.05	2.43	1.02	1.21	1.35	1.46	1.61	0.86	0.97	1.05	1.10	1.17	0.73	0.80	0.85	0.88	0.91
	β_{eff}	0.18	0.24	0.30	0.34	0.40	0.34	0.40	0.45	0.49	0.53	0.43	0.49	0.52	0.55	0.58	0.49	0.53	0.56	0.58	0.60
2M	d (cm)	13.3	15.4	17.3	18.6	20.8	9.3	10.4	11.2	12.5	14.8	7.2	8.3	9.5	10.5	12.0	6.3	7.4	8.3	9.0	10.0
	T_{eff} (sec.)	1.41	1.83	2.22	2.57	3.19	1.29	1.59	1.85	2.08	2.48	1.15	1.39	1.59	1.76	2.00	1.04	1.24	1.39	1.50	1.66
	β_{eff}	0.07	0.10	0.14	0.17	0.23	0.17	0.23	0.29	0.33	0.39	0.26	0.33	0.38	0.42	0.48	0.33	0.39	0.44	0.48	0.53
3	d (cm)	2.49	2.85	3.27	3.62	4.14	1.81	2.07	2.25	2.37	2.52	1.44	1.58	1.66	1.71	1.77	1.18	1.26	1.30	1.33	1.35
	T_{eff} (sec.)	1.16	1.40	1.61	1.78	2.03	0.89	1.01	1.10	1.16	1.24	0.71	0.77	0.81	0.84	0.87	0.58	0.62	0.64	0.65	0.66
	β_{eff}	0.26	0.33	0.37	0.41	0.47	0.41	0.47	0.51	0.54	0.58	0.49	0.54	0.57	0.59	0.61	0.54	0.58	0.60	0.61	0.62
6	d (cm)	33.9	40.4	46.3	51.9	60.3	25.9	30.2	33.8	36.3	40.5	21.4	24.2	26.3	28.2	32.6	18.2	20.2	21.8	24.4	29.0
	T_{eff} (sec.)	1.46	1.93	2.38	2.82	3.65	1.41	1.83	2.21	2.56	3.17	1.35	1.71	2.02	2.29	2.76	1.28	1.59	1.84	2.07	2.46
	β_{eff}	0.03	0.04	0.06	0.07	0.11	0.07	0.11	0.14	0.17	0.24	0.12	0.17	0.22	0.27	0.33	0.17	0.24	0.29	0.33	0.40
7	d (cm)	11.1	12.9	14.3	15.2	17.1	7.6	8.5	9.4	10.6	12.4	5.9	7.0	8.0	8.8	9.9	5.3	6.2	6.9	7.4	8.1
	T_{eff} (sec.)	1.40	1.80	2.17	2.50	3.07	1.25	1.53	1.77	1.99	2.34	1.10	1.33	1.51	1.65	1.86	1.00	1.17	1.30	1.39	1.52
	β_{eff}	0.08	0.12	0.16	0.20	0.26	0.19	0.26	0.32	0.36	0.42	0.29	0.36	0.41	0.44	0.50	0.36	0.42	0.47	0.50	0.54

Table 5.2. Results of the AASHTO design calculation using a median characterization of the seismic hazard.

Bin	Parameter	Isolation System																			
		$Q_d/W=0.03$				$Q_d/W=0.06$				$Q_d/W=0.09$				$Q_d/W=0.12$							
		T_d (sec.)				T_d (sec.)				T_d (sec.)				T_d (sec.)							
		1.5	2.0	2.5	3.0	4.0	1.5	2.0	2.5	3.0	4.0	1.5	2.0	2.5	3.0	4.0	1.5	2.0	2.5	3.0	4.0
1	d (cm)	34.9	41.7	47.7	53.6	62.3	26.8	31.2	35.0	37.7	42.0	22.2	25.1	27.2	29.3	33.6	18.9	21.0	22.7	25.2	30.0
	T_{eff} (sec.)	1.47	1.93	2.39	2.83	3.66	1.41	1.83	2.22	2.58	3.19	1.35	1.72	2.03	2.31	2.78	1.29	1.60	1.85	2.09	2.48
	β_{eff}	0.03	0.04	0.06	0.07	0.10	0.07	0.10	0.13	0.17	0.23	0.12	0.17	0.22	0.26	0.33	0.17	0.23	0.29	0.33	0.39
2	d (cm)	1.94	2.30	2.61	2.86	3.22	1.44	1.60	1.72	1.79	1.89	1.13	1.19	1.24	1.26	1.31	0.92	0.93	0.95	0.97	0.99
	T_{eff} (sec.)	1.10	1.32	1.49	1.64	1.84	0.82	0.92	0.98	1.02	1.08	0.65	0.68	0.71	0.72	0.75	0.52	0.53	0.55	0.56	0.57
	β_{eff}	0.29	0.36	0.41	0.45	0.50	0.44	0.50	0.54	0.56	0.59	0.52	0.56	0.59	0.60	0.61	0.56	0.59	0.61	0.61	0.62
2M	d (cm)	11.0	12.8	14.2	15.0	16.9	7.5	8.4	9.3	10.5	12.3	5.9	7.0	7.9	8.7	9.8	5.3	6.2	6.8	7.3	8.0
	T_{eff} (sec.)	1.40	1.80	2.17	2.49	3.06	1.25	1.53	1.77	1.99	2.33	1.10	1.32	1.50	1.65	1.85	0.99	1.17	1.29	1.39	1.51
	β_{eff}	0.08	0.12	0.16	0.20	0.26	0.20	0.26	0.32	0.36	0.42	0.29	0.36	0.41	0.44	0.50	0.36	0.42	0.47	0.50	0.55
3	d (cm)	1.37	1.61	1.80	1.93	2.11	0.97	1.06	1.11	1.15	1.18	0.73	0.76	0.78	0.80	0.81	0.58	0.59	0.60	0.61	0.61
	T_{eff} (sec.)	1.01	1.18	1.32	1.42	1.55	0.71	0.78	0.82	0.84	0.87	0.53	0.56	0.58	0.58	0.59	0.42	0.43	0.44	0.45	0.45
	β_{eff}	0.35	0.41	0.46	0.49	0.54	0.49	0.54	0.57	0.59	0.61	0.56	0.59	0.60	0.61	0.62	0.59	0.61	0.62	0.62	0.63
6	d (cm)	31.2	36.9	42.6	47.5	55.2	23.7	27.6	30.7	32.7	36.6	19.5	21.8	23.8	25.4	30.0	16.4	18.3	19.9	22.5	26.5
	T_{eff} (sec.)	1.46	1.92	2.37	2.81	3.63	1.40	1.81	2.19	2.53	3.11	1.34	1.68	1.98	2.24	2.70	1.26	1.56	1.80	2.02	2.39
	β_{eff}	0.03	0.05	0.06	0.08	0.11	0.08	0.11	0.15	0.19	0.25	0.13	0.19	0.24	0.28	0.35	0.19	0.25	0.31	0.35	0.41
7	d (cm)	8.5	9.7	10.5	11.3	12.7	5.7	6.3	7.3	8.1	9.4	4.6	5.4	6.1	6.6	7.2	4.1	4.7	5.1	5.4	5.8
	T_{eff} (sec.)	1.37	1.75	2.08	2.38	2.87	1.19	1.43	1.66	1.84	2.12	1.04	1.23	1.37	1.49	1.64	0.92	1.06	1.16	1.23	1.32
	β_{eff}	0.11	0.15	0.20	0.24	0.31	0.24	0.31	0.36	0.40	0.46	0.33	0.40	0.44	0.48	0.53	0.40	0.46	0.50	0.53	0.57

Table 5.3. Results of the AASHTO design calculation using a mean characterization of the seismic hazard considering directivity of the ground motion components.

Bin	Parameter	Isolation System																			
		$Q_d/W=0.03$				$Q_d/W=0.06$				$Q_d/W=0.09$				$Q_d/W=0.12$							
		T_d (sec.)				T_d (sec.)				T_d (sec.)				T_d (sec.)							
		1.5	2.0	2.5	3.0	4.0	1.5	2.0	2.5	3.0	4.0	1.5	2.0	2.5	3.0	4.0	1.5	2.0	2.5	3.0	4.0
1	d (cm)	61.6	79.8	93.6	105.1	124.4	52.6	62.2	71.6	78.9	91.6	44.9	52.5	59.1	64.3	71.1	39.6	45.7	50.0	53.4	59.5
	T_{eff} (sec.)	1.48	1.96	2.44	2.91	3.82	1.45	1.91	2.35	2.77	3.56	1.42	1.85	2.25	2.62	3.26	1.39	1.78	2.13	2.45	2.98
	β_{eff}	0.02	0.02	0.03	0.04	0.06	0.04	0.06	0.07	0.09	0.13	0.06	0.09	0.12	0.15	0.21	0.09	0.13	0.17	0.21	0.28
6	d (cm)	43.8	53.5	60.9	68.2	81.2	34.1	40.6	45.6	50.0	55.6	28.7	33.3	36.4	38.8	43.2	25.0	27.8	30.4	32.4	38.5
	T_{eff} (sec.)	1.47	1.95	2.41	2.86	3.73	1.43	1.87	2.28	2.66	3.35	1.38	1.78	2.12	2.43	2.96	1.33	1.67	1.97	2.22	2.67
	β_{eff}	0.02	0.03	0.05	0.06	0.08	0.06	0.08	0.11	0.13	0.19	0.09	0.13	0.18	0.22	0.29	0.13	0.19	0.24	0.29	0.35

Table 5.4. Results of the AASHTO design calculation using a median characterization of the seismic hazard considering directivity of the ground motion components.

Bin	Parameter	Isolation System																			
		$Q_d/W=0.03$				$Q_d/W=0.06$				$Q_d/W=0.09$				$Q_d/W=0.12$							
		T_d (sec.)				T_d (sec.)				T_d (sec.)				T_d (sec.)							
		1.5	2.0	2.5	3.0	4.0	1.5	2.0	2.5	3.0	4.0	1.5	2.0	2.5	3.0	4.0	1.5	2.0	2.5	3.0	4.0
1	d (cm)	58.0	74.1	86.5	96.7	115.0	48.3	57.5	65.8	72.1	83.7	41.3	48.1	54.2	58.5	65.0	36.1	41.8	45.4	48.7	53.8
	T_{eff} (sec.)	1.48	1.96	2.44	2.90	3.81	1.45	1.90	2.34	2.75	3.53	1.42	1.84	2.23	2.59	3.21	1.38	1.76	2.10	2.41	2.91
	β_{eff}	0.02	0.02	0.03	0.04	0.06	0.04	0.06	0.08	0.10	0.14	0.07	0.10	0.13	0.16	0.23	0.10	0.14	0.19	0.23	0.30
6	d (cm)	43.7	53.4	60.8	68.1	81.1	34.0	40.5	45.5	49.9	55.5	28.7	33.3	36.3	38.8	43.1	25.0	27.7	30.4	32.3	38.4
	T_{eff} (sec.)	1.47	1.95	2.41	2.86	3.73	1.43	1.87	2.28	2.66	3.34	1.38	1.78	2.12	2.43	2.96	1.33	1.67	1.97	2.22	2.67
	β_{eff}	0.02	0.03	0.05	0.06	0.08	0.06	0.08	0.11	0.13	0.19	0.10	0.13	0.18	0.22	0.29	0.13	0.19	0.24	0.29	0.35

Table 5.5. Mean and mean+1 σ maximum isolator displacements determined from unidirectional response-history analysis.

Bin / Statistic	d_x (cm)																																										
	$Q_d/W=0.03$						$Q_d/W=0.06$						$Q_d/W=0.09$						$Q_d/W=0.12$																								
	2.0		2.5		3.0		4.0		1.5		2.0		2.5		3.0		4.0		1.5		2.0		2.5		3.0		4.0																
1	mean	45.0	54.3	56.0	61.4	65.3	37.8	41.8	42.2	44.3	47.2	31.3	33.3	33.6	33.9	36.5	26.0	27.4	27.4	27.3	26.9	29.1	mean + 1 σ	76.5	93.8	90.7	101.2	109.6	66.6	74.9	71.5	74.5	80.1	57.8	62.1	59.3	56.7	62.3	49.8	52.1	50.2	45.9	50.8
2	mean	6.69	6.28	5.91	5.73	5.63	3.67	3.77	3.89	4.05	4.18	2.31	2.49	2.53	2.56	2.69	1.63	1.75	1.85	1.93	2.01	mean + 1 σ	15.9	14.3	13.2	12.6	12.4	8.7	8.8	9.0	9.4	9.8	5.4	5.7	5.7	5.8	6.1	3.8	4.0	4.2	4.4	4.6	4.6
2M	mean	12.7	11.8	11.6	11.7	12.1	8.1	8.0	8.0	8.2	8.5	5.6	5.9	5.9	6.0	6.1	4.0	4.4	4.6	4.8	5.0	mean + 1 σ	21.0	18.9	18.1	17.8	18.6	13.9	13.2	13.1	13.3	13.7	10.2	10.5	10.3	10.2	10.4	8.0	8.6	9.0	9.2	9.5	9.5
3	mean	1.81	1.90	1.94	1.94	1.91	0.96	1.08	1.15	1.15	1.14	0.61	0.64	0.67	0.69	0.73	0.44	0.48	0.50	0.52	0.55	mean + 1 σ	4.75	4.88	4.87	4.71	4.40	2.34	2.74	2.92	2.87	2.81	1.42	1.50	1.60	1.70	1.82	1.07	1.19	1.28	1.33	1.46	1.46
6	mean	43.1	67.5	85.6	87.4	74.6	32.0	47.2	59.7	60.7	55.5	25.6	34.9	42.9	43.4	41.2	19.3	25.8	31.4	32.2	30.7	mean + 1 σ	62.5	91.6	134.5	146.0	124.0	47.4	67.1	100.8	105.1	95.2	38.1	53.2	76.4	78.2	72.2	30.2	41.9	57.2	58.3	52.8	52.8
7	mean	15.6	22.6	20.1	18.2	19.5	9.5	11.0	11.5	10.7	10.3	5.7	6.2	6.5	6.4	6.4	3.0	3.1	3.2	3.3	3.5	mean + 1 σ	25.2	57.2	47.1	36.1	40.7	16.1	24.6	26.8	21.4	18.6	10.8	13.4	13.9	12.6	11.9	6.0	6.2	6.3	6.6	7.0	7.0

Table 5.6. Median and 84th percentile maximum isolator displacements determined from unidirectional response-history analysis.

Bin / Statistic		d_x (cm)																			
		$Q_d/W=0.03$					$Q_d/W=0.06$					$Q_d/W=0.09$					$Q_d/W=0.12$				
		T_d (sec.)					T_d (sec.)					T_d (sec.)					T_d (sec.)				
		1.5	2.0	2.5	3.0	4.0	1.5	2.0	2.5	3.0	4.0	1.5	2.0	2.5	3.0	4.0	1.5	2.0	2.5	3.0	4.0
1	median	40.4	51.4	51.3	58.0	58.8	31.2	37.9	39.2	40.9	49.1	21.9	26.4	28.2	31.2	37.6	18.0	20.7	20.8	23.7	26.7
	84th percentile	77.4	87.0	95.5	105.9	105.1	67.9	71.9	73.4	76.1	79.7	59.7	60.9	60.6	61.0	65.9	51.0	53.4	53.3	51.8	56.1
2	median	3.02	3.41	3.70	3.85	4.06	1.57	1.70	1.70	1.71	1.75	0.86	0.94	0.99	1.01	1.03	0.54	0.55	0.55	0.56	0.57
	84th percentile	13.5	13.2	12.7	12.5	12.4	7.2	7.6	7.9	8.1	8.3	4.4	4.8	5.0	5.1	5.3	3.0	3.3	3.4	3.6	3.7
2M	median	9.9	8.8	10.9	10.8	9.3	6.6	6.4	6.3	6.5	6.7	5.1	5.6	5.9	5.7	5.7	3.3	3.7	4.0	4.2	4.4
	84th percentile	20.6	18.4	17.6	17.7	18.2	13.7	13.6	13.5	13.7	14.2	9.9	10.4	10.4	10.5	10.7	7.2	7.9	8.4	8.7	9.2
3	median	0.70	0.74	0.77	0.82	0.94	0.33	0.34	0.35	0.35	0.38	0.23	0.23	0.24	0.24	0.24	0.18	0.18	0.19	0.19	0.19
	84th percentile	2.71	2.88	2.98	3.05	3.09	1.50	1.66	1.75	1.77	1.80	0.95	0.99	1.03	1.06	1.10	0.67	0.71	0.75	0.76	0.79
6	median	37.5	60.6	69.7	66.3	53.7	27.2	47.2	48.0	43.7	43.7	22.2	34.0	37.7	37.2	35.5	17.6	23.7	24.4	26.3	25.9
	84th percentile	60.9	87.1	122.4	131.2	114.1	46.1	67.2	89.4	92.7	85.6	38.6	54.2	68.1	69.4	65.6	31.9	45.3	55.8	57.6	53.9
7	median	13.3	13.4	11.9	10.2	10.2	8.0	9.5	8.3	8.4	8.4	3.9	4.7	5.1	5.4	5.8	2.2	2.4	2.4	2.5	2.5
	84th percentile	25.3	33.2	30.9	29.3	30.8	17.1	18.4	18.9	18.4	18.3	13.9	14.5	15.3	15.5	15.9	8.1	8.6	9.0	9.3	9.9

Table 5.7. Mean and mean+ 1 σ maximum isolator displacements determined from bi-directional response-history analysis.

Bin / Statistic	d_{xy} (cm)																				
	$Q_d/W=0.03$				$Q_d/W=0.06$				$Q_d/W=0.09$				$Q_d/W=0.12$								
	T_d (sec.)				T_d (sec.)				T_d (sec.)				T_d (sec.)								
1	mean	67.4	86.7	87.1	91.6	103.7	57.7	69.5	68.9	72.0	76.8	50.6	57.3	56.1	57.8	62.7	44.6	48.5	47.6	47.7	51.1
	mean + 1 σ	103.5	131.3	118.0	140.8	152.6	90.8	106.6	96.8	106.7	110.8	81.3	90.4	82.4	82.0	91.4	72.5	77.9	72.0	68.6	75.5
2	mean	11.01	9.72	8.69	8.24	8.33	6.18	6.05	6.12	6.37	6.47	4.10	4.21	4.36	4.56	4.83	2.81	2.84	3.02	3.13	3.26
	mean + 1 σ	24.8	21.3	18.8	17.5	17.5	14.2	13.4	13.3	13.9	14.2	9.2	9.2	9.5	10.0	10.6	6.2	6.1	6.5	6.8	7.2
2M	mean	19.0	18.3	17.1	17.5	18.5	12.5	12.5	12.6	12.7	12.6	9.0	9.2	9.4	9.6	9.7	6.5	6.6	6.9	7.0	7.1
	mean + 1 σ	29.2	27.6	25.2	25.0	27.0	19.4	18.7	19.1	19.3	18.9	14.6	14.4	14.9	15.0	14.8	11.5	11.5	11.8	11.8	11.6
3	mean	2.76	2.96	3.07	2.92	2.58	1.76	1.99	2.04	1.99	1.84	1.08	1.21	1.24	1.25	1.25	0.68	0.75	0.81	0.89	0.98
	mean + 1 σ	7.23	7.69	7.99	7.34	6.01	4.60	5.25	5.31	5.03	4.36	2.74	3.16	3.31	3.33	3.27	1.55	1.77	2.01	2.30	2.68
6	mean	62.9	97.0	132.0	137.2	115.3	50.4	74.5	98.7	101.2	90.0	40.7	59.4	76.4	77.9	72.5	33.7	48.7	61.0	61.9	58.1
	mean + 1 σ	88.5	127.9	187.1	205.4	168.1	70.5	97.2	147.0	156.1	137.2	55.0	76.4	115.7	121.3	111.3	44.0	61.3	89.4	92.8	86.6
7	mean	23.9	37.5	30.2	25.8	28.1	15.6	20.7	20.7	18.4	18.2	10.3	12.6	13.2	12.7	12.2	6.8	7.4	7.5	7.4	7.6
	mean + 1 σ	34.9	98.8	69.2	50.0	61.7	22.9	47.9	46.0	34.3	34.2	16.2	24.9	26.3	22.7	20.0	11.5	12.7	12.8	12.5	13.1

Table 5.8. Median and 84th percentile maximum isolator displacements determined from bi-directional response-history analysis.

Bin / Statistic	d_{xy} (cm)																			
	$Q_d/W=0.03$				$Q_d/W=0.06$				$Q_d/W=0.09$				$Q_d/W=0.12$							
	T_d (sec.)				T_d (sec.)				T_d (sec.)				T_d (sec.)							
	1.5	2.0	2.5	3.0	4.0	1.5	2.0	2.5	3.0	4.0	1.5	2.0	2.5	3.0	4.0	1.5	2.0	2.5	3.0	4.0
1	67.3	72.1	79.6	83.7	90.7	45.5	58.4	64.5	65.6	68.1	39.4	48.6	47.1	57.0	58.9	35.0	42.8	42.7	47.8	49.5
84th percentile	110.1	125.5	120.9	131.6	134.4	96.6	104.3	97.7	101.6	101.8	87.1	90.7	83.0	80.7	85.6	78.1	80.0	73.4	68.9	73.6
2	4.85	4.75	5.08	5.23	5.37	2.23	2.67	2.89	3.00	3.12	1.46	1.62	1.72	1.78	1.86	0.77	0.84	0.88	0.91	0.94
84th percentile	21.9	19.7	17.6	16.8	17.2	13.2	13.4	13.8	14.3	14.5	9.0	9.5	9.9	10.3	10.9	5.9	6.1	6.5	6.7	7.0
2M	19.9	17.5	14.6	18.1	18.8	12.5	12.5	12.6	12.8	13.5	8.6	9.2	9.0	8.6	9.0	5.2	6.2	6.6	6.6	6.5
84th percentile	30.4	28.6	25.3	25.9	27.9	21.1	20.1	20.1	20.3	20.1	15.6	15.5	15.9	16.1	16.1	11.5	11.5	11.9	12.1	12.4
3	1.09	1.14	1.15	1.18	1.24	0.76	0.79	0.80	0.81	0.86	0.42	0.44	0.45	0.45	0.46	0.38	0.39	0.40	0.40	0.41
84th percentile	4.39	4.73	4.91	4.77	4.40	2.87	3.19	3.30	3.28	3.14	1.70	1.83	1.87	1.86	1.88	1.13	1.21	1.28	1.36	1.46
6	60.3	86.8	121.6	103.3	100.5	49.8	69.4	87.7	80.7	71.5	42.2	57.5	67.8	67.8	56.3	35.1	48.1	54.7	53.0	48.8
84th percentile	87.2	126.2	185.4	199.4	161.4	69.1	97.2	143.1	150.7	129.7	54.7	78.9	115.1	121.0	106.9	44.2	63.2	88.5	92.7	86.3
7	24.4	19.0	16.8	18.0	16.0	17.3	12.8	13.1	14.4	13.8	9.9	10.5	10.8	11.0	11.1	6.0	6.7	7.2	7.8	7.4
84th percentile	38.2	54.6	47.2	42.4	44.6	27.3	34.1	34.7	32.4	31.8	21.9	25.1	26.1	25.7	24.9	21.0	23.0	23.8	23.6	24.2

Table 5.9. Unidirectional displacement multiplier.

Bin	α_{xy}																			
	$Q_d/W=0.03$				$Q_d/W=0.06$				$Q_d/W=0.09$				$Q_d/W=0.12$							
	T_d (sec.)				T_d (sec.)				T_d (sec.)				T_d (sec.)							
	1.5	2.0	2.5	3.0	4.0	1.5	2.0	2.5	3.0	4.0	1.5	2.0	2.5	3.0	4.0	1.5	2.0	2.5	3.0	4.0
1	1.08	1.09	1.06	1.04	1.04	1.07	1.08	1.07	1.07	1.08	1.12	1.12	1.15	1.11	1.12	1.11	1.16	1.17	1.16	1.10
2	1.93	1.78	1.80	1.81	1.83	1.60	1.70	1.72	1.71	1.71	1.70	1.62	1.60	1.65	1.77	1.55	1.67	1.71	1.64	1.63
2M	1.54	1.65	1.59	1.55	1.75	1.47	1.53	1.45	1.39	1.50	1.64	1.58	1.50	1.54	1.50	1.55	1.52	1.65	1.59	1.52
3	1.40	1.43	1.39	1.30	1.44	1.66	1.77	1.73	1.75	1.82	1.94	2.14	2.20	2.09	1.96	1.57	1.72	1.77	1.89	1.93
6	1.14	1.21	1.36	1.33	1.17	1.31	1.22	1.26	1.26	1.15	1.23	1.22	1.22	1.20	1.21	1.35	1.28	1.24	1.23	1.25
7	2.12	1.52	1.50	1.35	1.20	1.59	1.54	1.61	1.48	1.46	2.39	2.39	2.08	2.10	2.37	2.12	2.14	2.15	1.93	1.93

Table 5.10. Modified definition of the unidirectional displacement multiplier.

Bin	α'_{xy}																			
	$Q_d/W=0.03$				$Q_d/W=0.06$				$Q_d/W=0.09$				$Q_d/W=0.12$							
	T_d (sec.)				T_d (sec.)				T_d (sec.)				T_d (sec.)							
	1.5	2.0	2.5	3.0	4.0	1.5	2.0	2.5	3.0	4.0	1.5	2.0	2.5	3.0	4.0	1.5	2.0	2.5	3.0	4.0
1	1.53	1.59	1.58	1.58	1.61	1.52	1.68	1.64	1.65	1.60	1.60	1.72	1.69	1.66	1.73	1.65	1.80	1.75	1.76	1.69
6	1.50	1.50	1.59	1.50	1.63	1.58	1.67	1.71	1.68	1.63	1.63	1.66	1.81	1.75	1.72	1.68	1.86	1.87	1.82	1.83

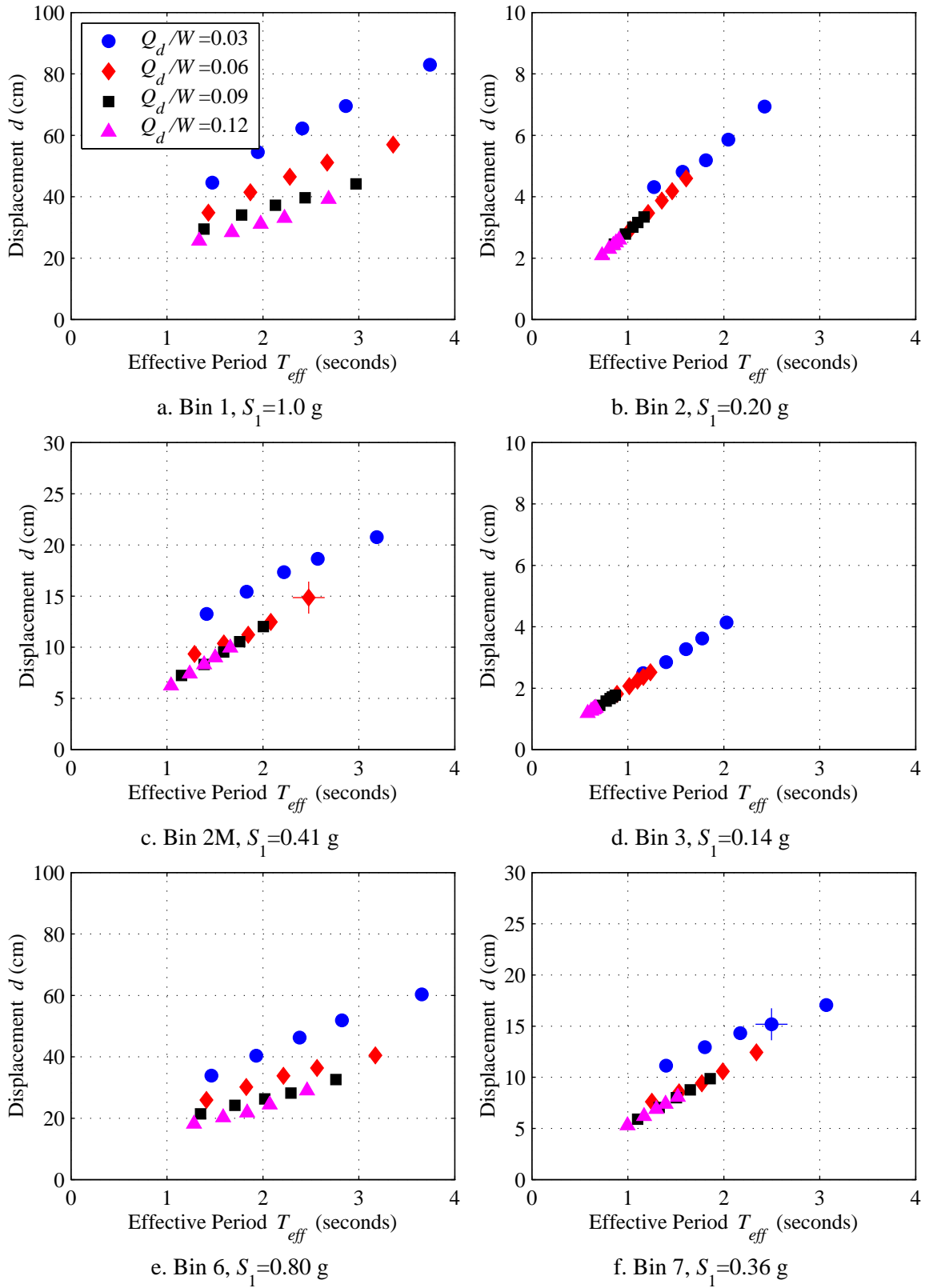


Figure 5.1. Maximum isolator displacements calculated using Equation 3b from the AASHTO Guide Specifications and the *mean* 1-second spectral acceleration.

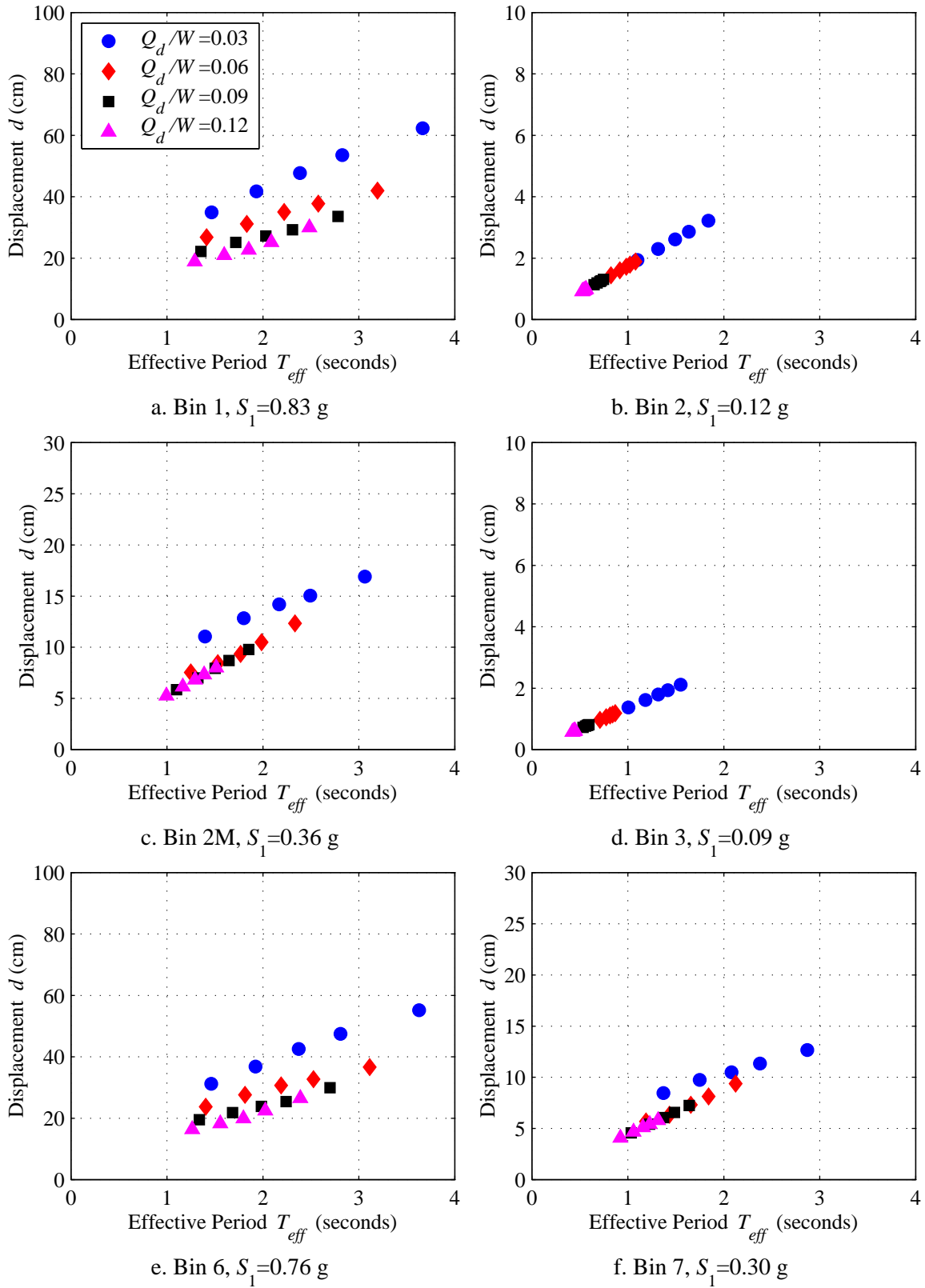


Figure 5.2. Maximum isolator displacements calculated using Equation 3b from the AASHTO Guide Specifications and the *median* 1-second spectral acceleration.

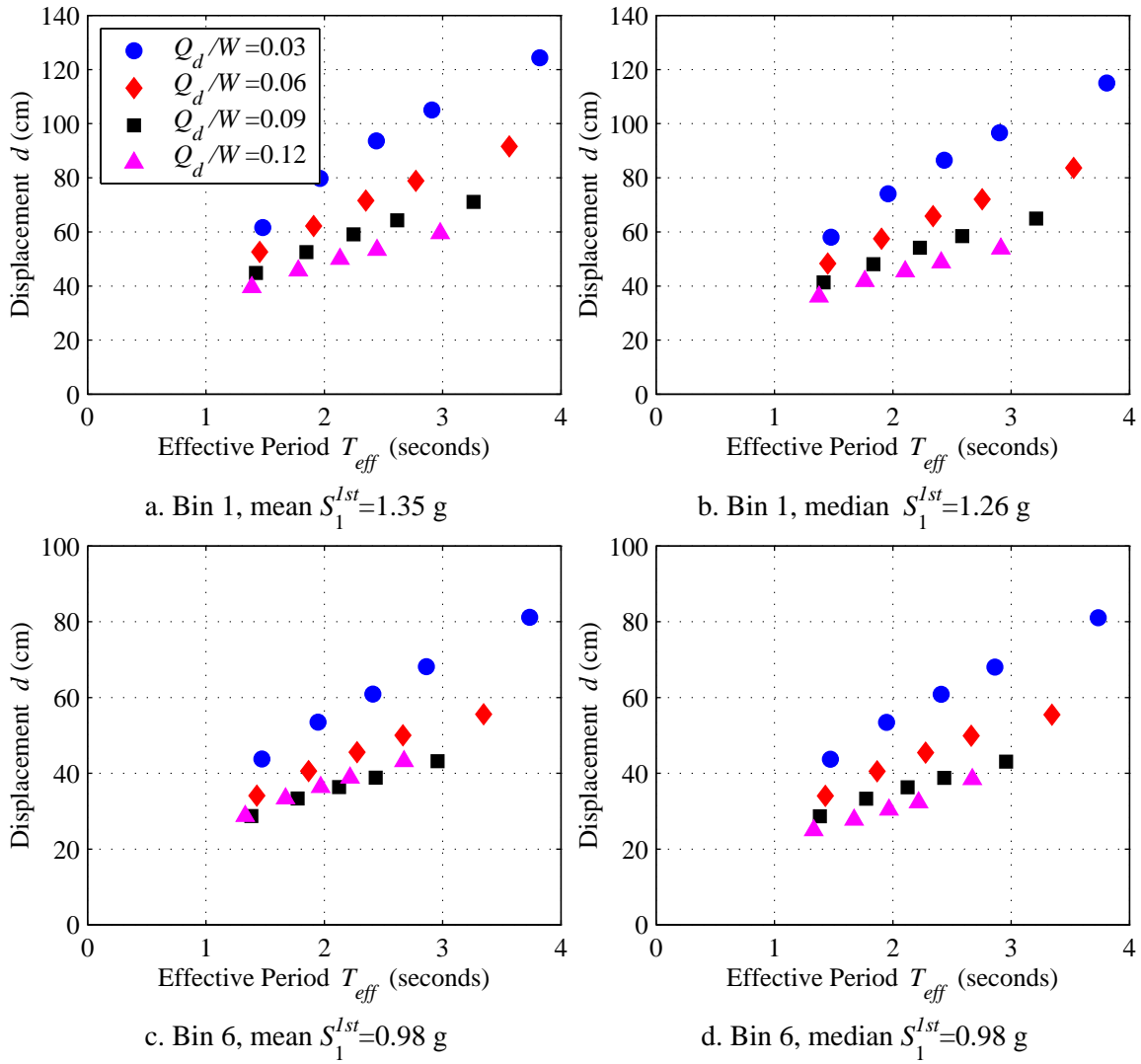


Figure 5.3. Maximum isolator displacements calculated using Equation 3b from the AASHTO Guide Specifications using the 1-second spectral acceleration from the *mean* and *median* first component spectrum for Bins 1 and 6.

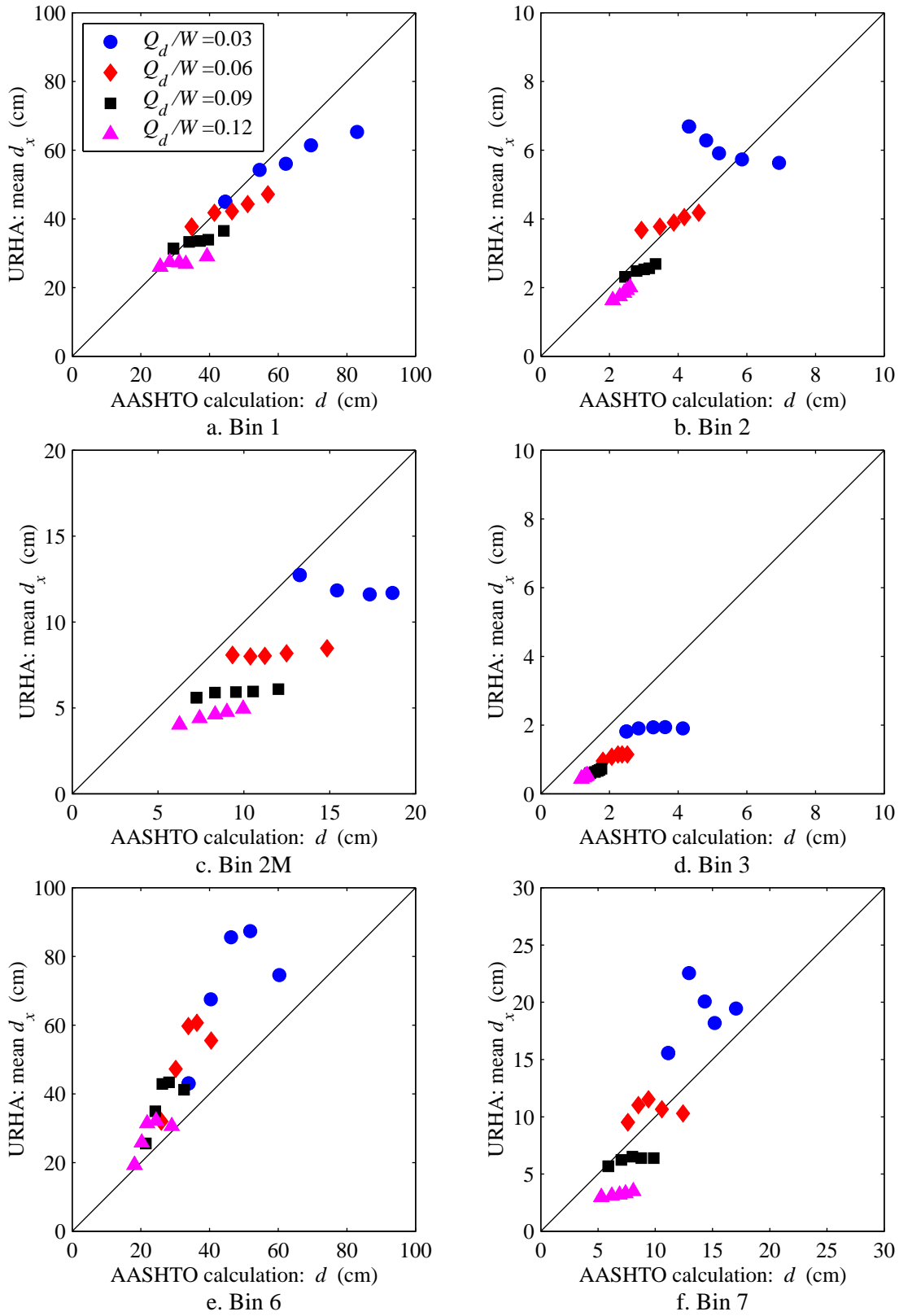


Figure 5.4. Comparison of maximum isolator displacements determined from unidirectional response-history analysis with the results of the AASHTO procedure using a mean characterization of the hazard and six bins of ground motions.

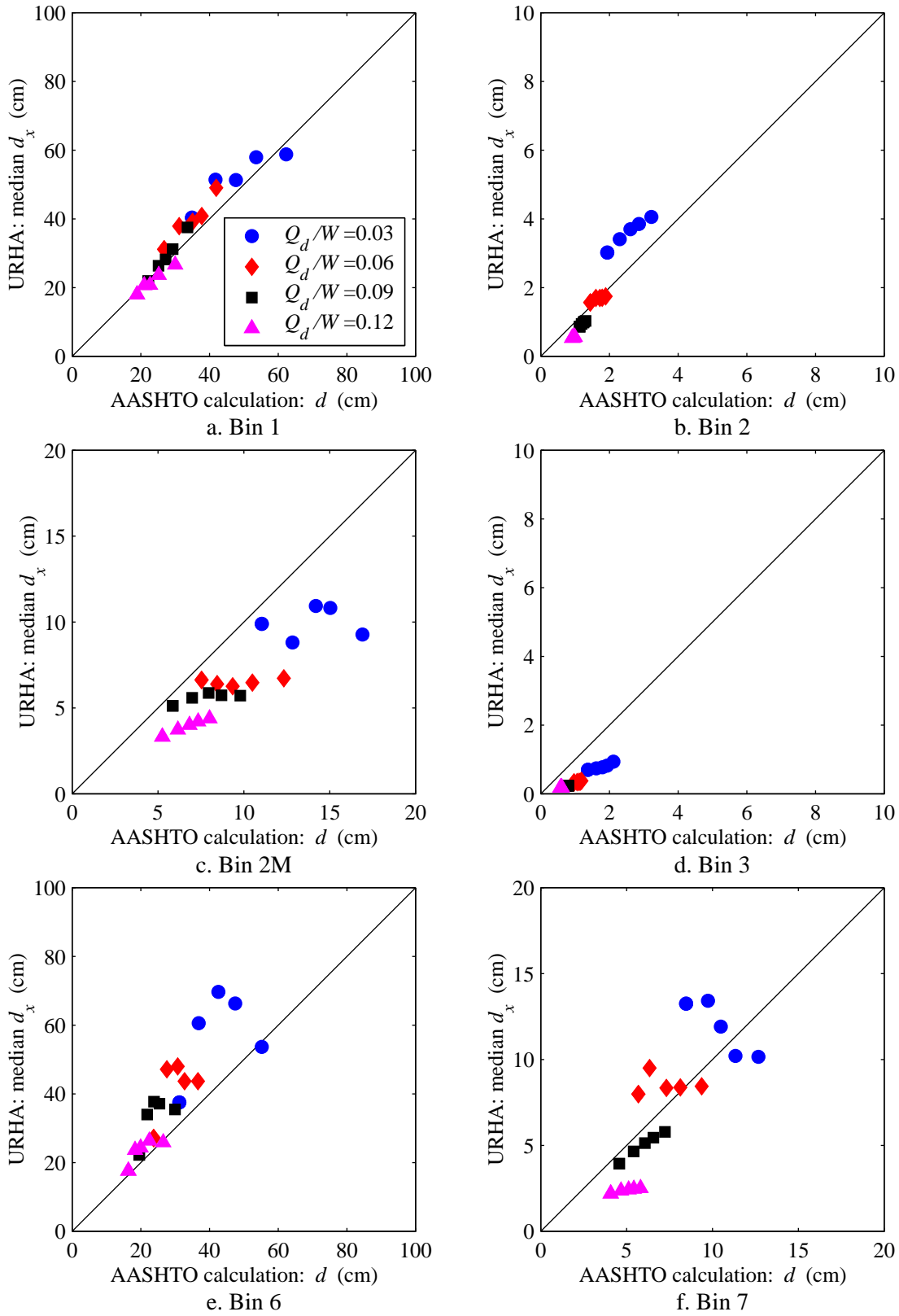


Figure 5.5. Comparison of maximum isolator displacements determined from unidirectional response-history analysis with the results of the AASHTO procedure using a median characterization of the hazard and six bins of ground motions.

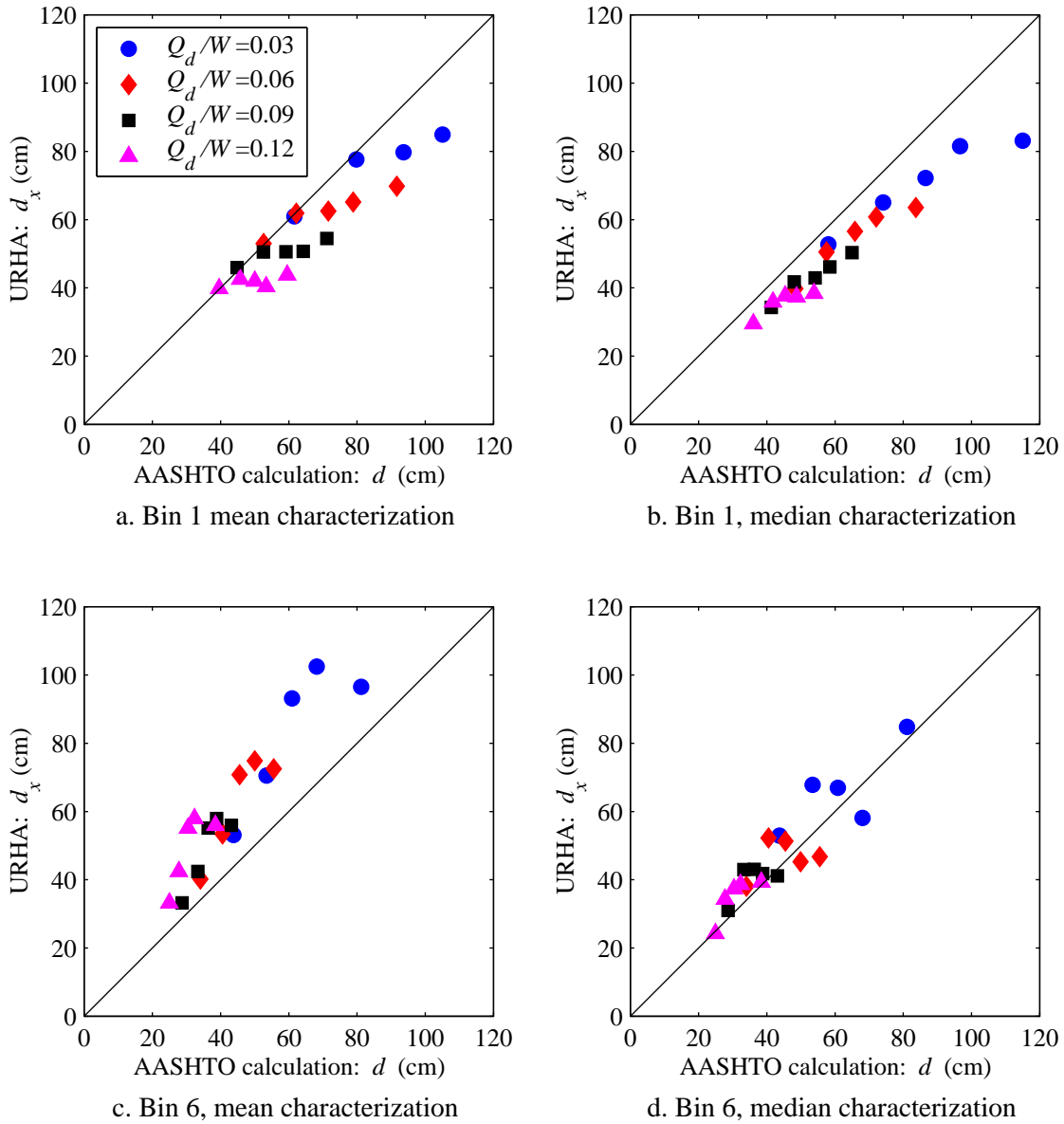


Figure 5.6. Comparison of maximum isolator displacements calculated using the AASHTO procedure and the results of nonlinear response-history analysis using a *mean* and *median* characterization of the hazard considering the first ground motion components contained in Bins 1 and 6.

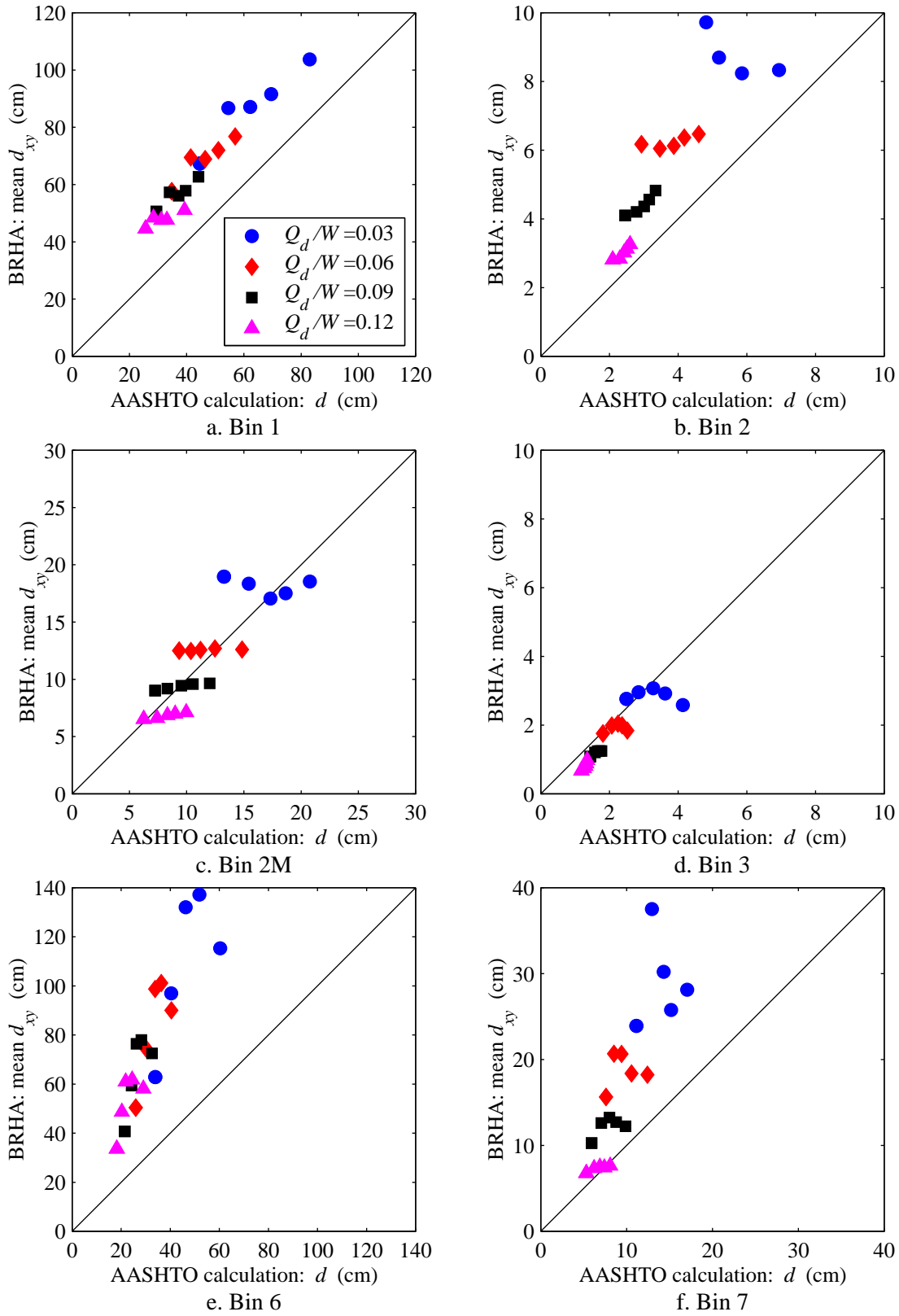


Figure 5.7. Comparison of maximum isolator displacements determined from bi-directional response-history analysis with the results of the AASHTO procedure using a mean characterization of the hazard and six bins of ground motions.

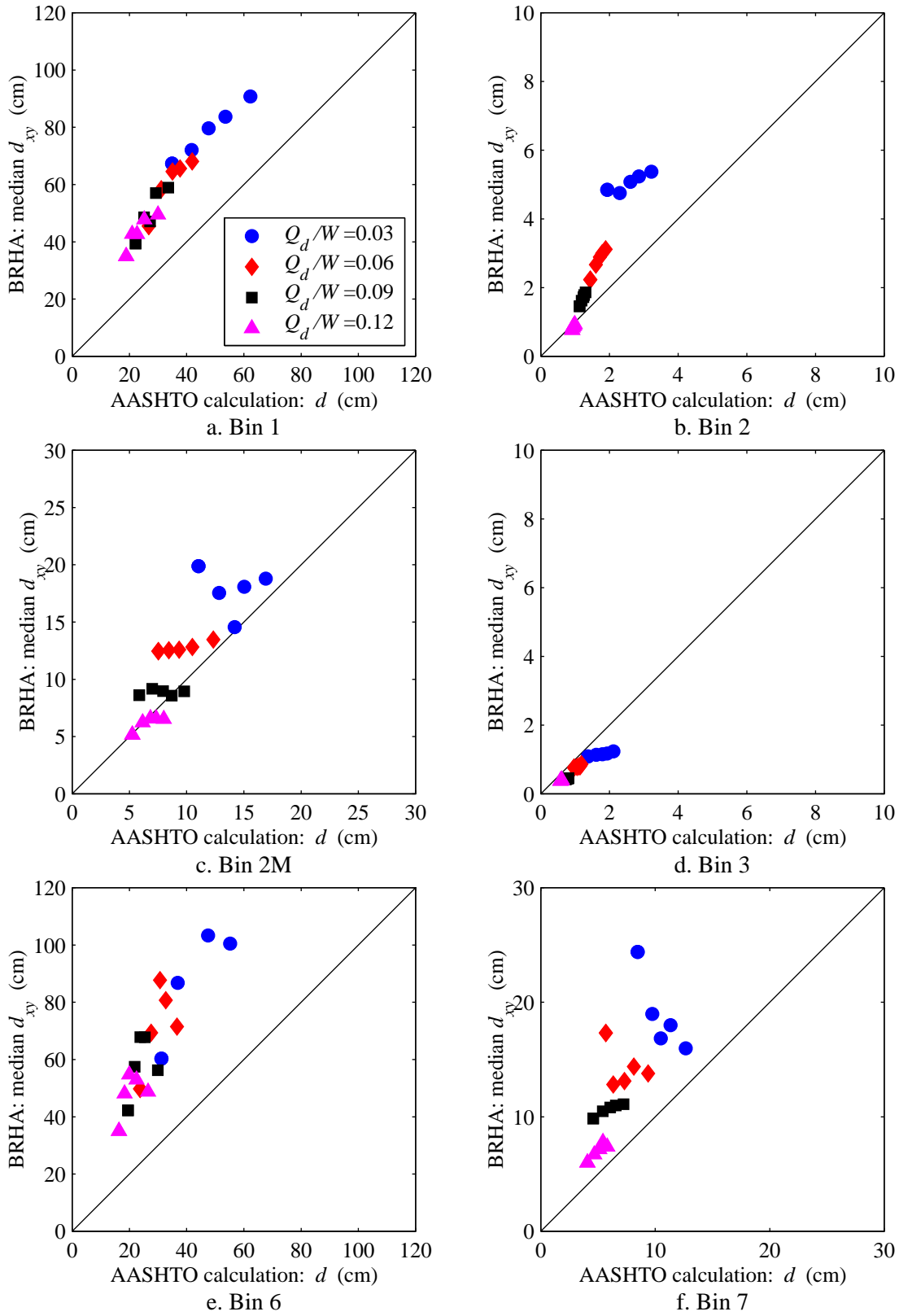


Figure 5.8. Comparison of maximum isolator displacements determined from bi-directional response-history analysis with the results of the AASHTO procedure using a median characterization of the hazard and six bins of ground motions.

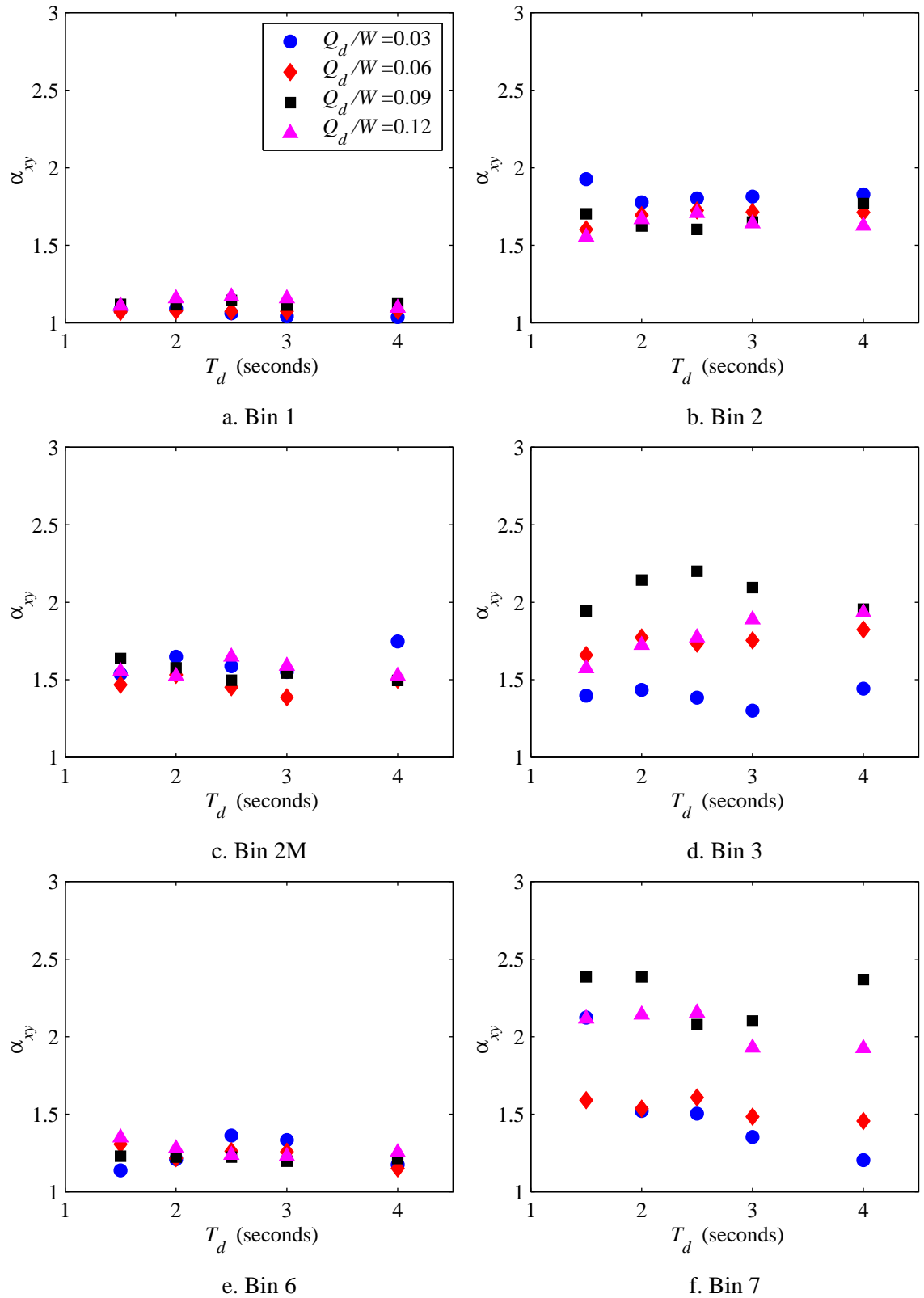


Figure 5.9. Unidirectional displacement multiplier calculated for each isolation system and six bins of ground motions.

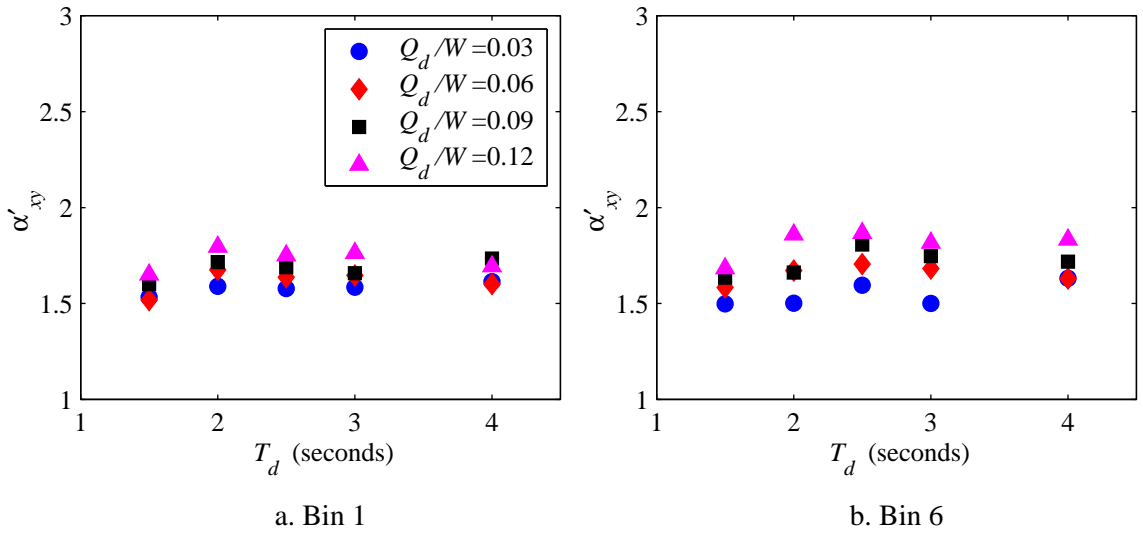


Figure 5.10. Modified unidirectional displacement multiplier calculated for each isolation system and ground motion bins 1 and 6.

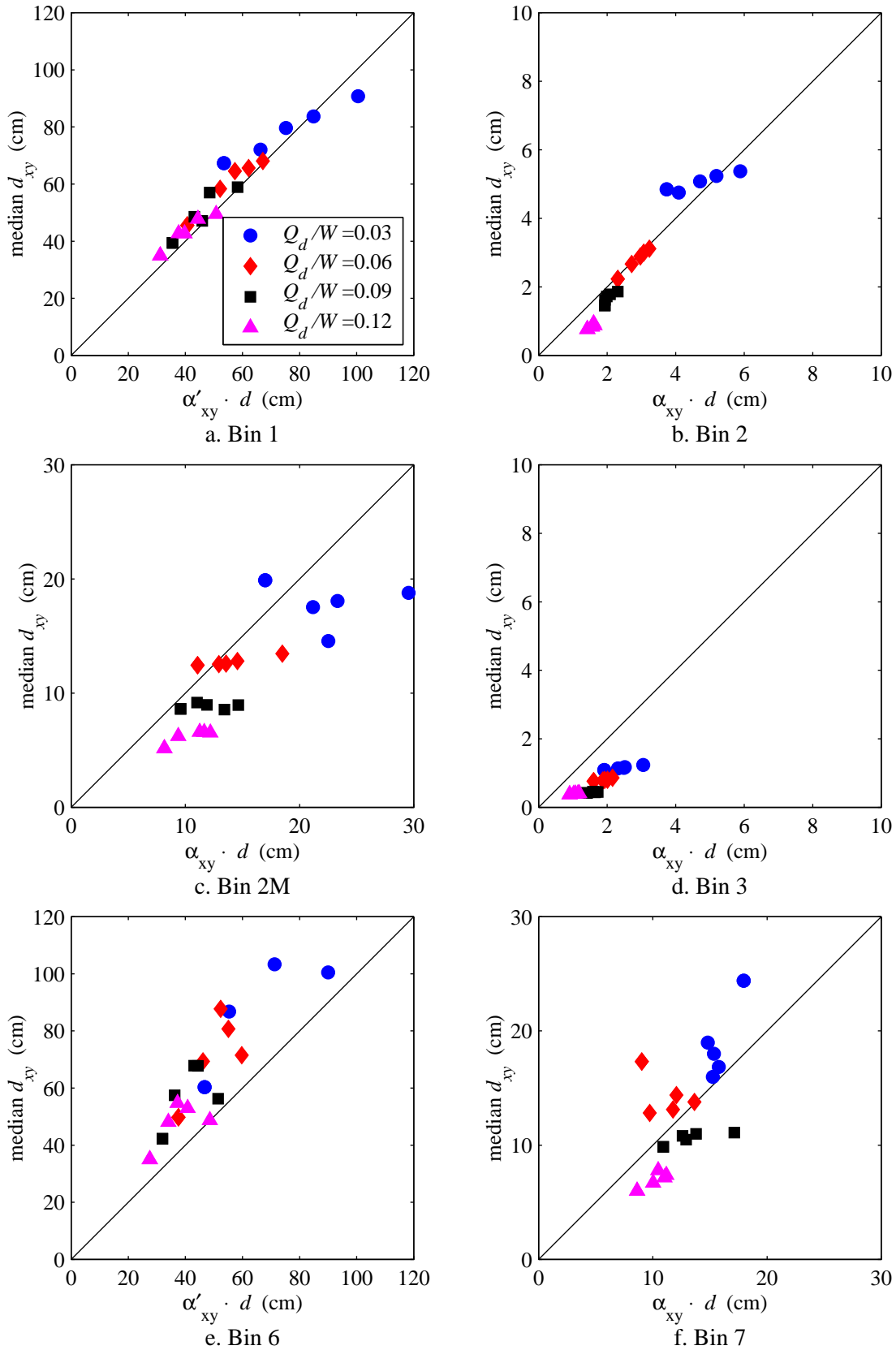


Figure 5.11. Comparison of maximum isolator displacements using median statistics considering six bins of ground motions.

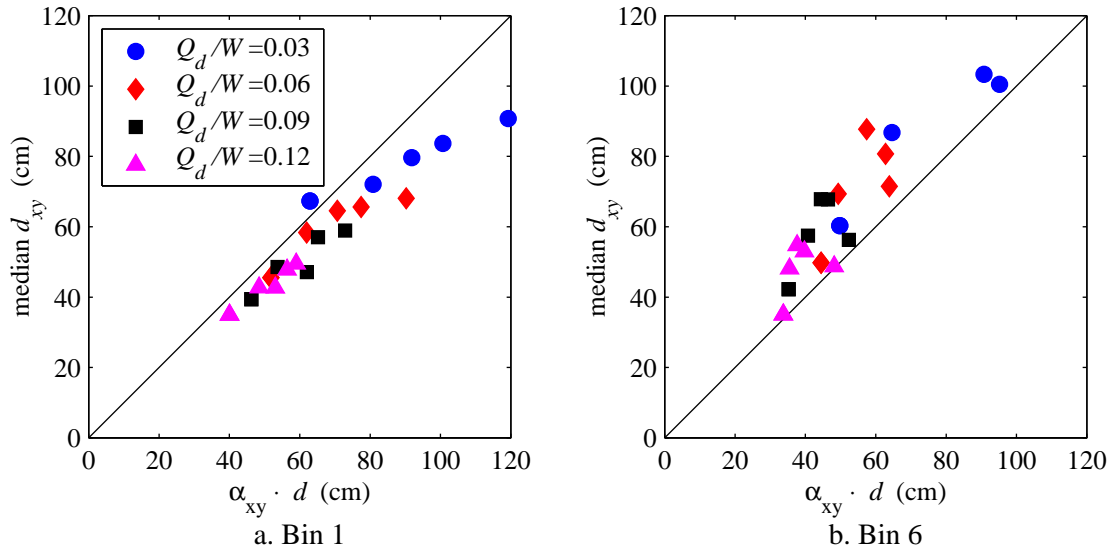


Figure 5.12. Comparison of maximum isolator displacements using median statistics considering the first ground motion components from Bins 1 and 6.

SECTION 6

ENERGY DEMANDS IMPOSED ON SEISMIC ISOLATORS SUBJECTED TO EARTHQUAKE EXCITATION

6.1 General

This section presents the results of an investigation of the energy demands imposed on individual isolators and isolation systems subjected to severe earthquake shaking. Two metrics have been employed to characterize the energy demands imposed on seismic isolators: (1) the total cumulative hysteretic energy dissipated by an individual seismic isolator and (2) the rate-of-energy dissipated by an isolator during earthquake excitation. Data from nonlinear dynamic response-history analysis have been mined to quantify the energy-related demands on seismic isolators during earthquake shaking. Results for the total energy dissipated and rate-of-energy dissipated are presented for six of the eight bins of ground motions used in this research program. Results of the total energy dissipated and rate-of-energy dissipated were used to evaluate current prototype testing requirements for seismic isolators. Finally conclusion and recommendations regarding the prototype testing of seismic isolators is presented.

6.2 Energy Demands on Seismic Isolators

6.2.1 General

Force-displacement response data determined from unidirectional and bi-directional nonlinear response-history analysis considering a simple isolated bridge model was mined to determine the energy dissipated by an individual seismic isolator and the rate-of-energy dissipated when subjected to earthquake excitation. The cumulative energy absorbed was determined by numerically integrating the force-displacement response of an individual seismic isolator. An expression for the cumulative energy absorbed is given by

$$E_T = \int F \cdot dU \quad (6.1)$$

where F is the restoring force of the seismic isolator and dU is an incremental displacement. Plotted in Figure 6.1 are two sample cumulative energy histories calculated from the results of unidirectional response-history analysis using a ground motion record from the 1992 Cape Mendocino Earthquake, Petrolia Station, considering two different sets of isolator parameters. Ground motion record, nf08, is part of ground motion bin 1. Figure 6.1a presents both the *absorbed energy* history (shown by a solid line) calculated using Equation (6.1) and the *dissipated energy* history (shown by the dashed line) for an isolation system with isolator properties $Q_d/W = 0.03$ and $T_d = 2.5$ seconds. The difference between the *absorbed* and *dissipated* energy is the energy recovered due to the un-loading of the isolator. However, the *absorbed* and *dissipated* energies converge as the displacement response of the isolation system diminished. This is shown in Figure 6.1a where the *absorbed* and *dissipated* energy histories between approximately 12 seconds and 60 seconds (corresponding to the end of the energy history) coincide. Therefore, the total energy dissipated was taken to be the final value of the absorbed energy history calculated using Equation (6.1). For isolators with larger characteristic strengths (i.e., $Q_d/W = 0.12$) and moderate displacement demands, the difference between the *absorbed* and *dissipated* energy is insignificant. This is shown by Figure 6.1b for the energy history calculated using ground motion record nf08 and isolator properties: $Q_d/W = 0.12$ and $T_d = 4.0$ seconds. Again the *absorbed* and *dissipated* energies are shown by a solid and dashed line, respectively. Noting that the *dissipated*, and not the *absorbed* energy histories were used for the calculation of the rate-of-energy dissipated.

6.2.2 Normalized Energy Dissipated

6.2.2.1 General

The total cumulative energy dissipated by an individual seismic isolator, determined from response-history analysis, was normalized by the energy dissipated in one fully reversed cycle to the maximum displacement, where the maximum displacement was calculated by response-history analysis.

The energy dissipated in one fully reversed cycle to the maximum displacement, denoted EDC , by a bilinear isolator (see Figure 4.2) was calculated using Equation (6.2) and has been adopted from the AASHTO Guide Specifications (1999).

$$EDC = 4Q_d(d_{max} - d_{yield}) \quad (6.2)$$

where Q_d is the characteristic strength of the isolator; d_{max} is the maximum displacement of the isolator determined from response-history analysis; and d_{yield} is the yield displacement that is assumed herein to be negligible. An expression for the normalized energy dissipated, abbreviated NED , is presented in Equation (6.3).

$$NED = \frac{\int F \cdot du}{EDC} \quad (6.3)$$

Normalizing the total energy dissipated by the EDC allows the results of this study to be generally applicable to isolators and isolation systems idealized using a bilinear force-displacement characteristics and represents the number of harmonic cycles to the maximum displacement to dissipate an amount of energy equivalent to the energy dissipated in a severe earthquake.

6.2.2.2 Unidirectional Seismic Excitation

Normalized energy dissipated (NED) data determined from the results of unidirectional response-history analysis has been presented for ground motion bins 1, 2, 2M, 3, 6, and 7. The NED was calculated for each isolation system and each ground motion record within a particular bin. This data is presented in Appendix F, including sample mean, sample standard deviation, mean plus one standard deviation, and coefficient of variation information calculated for each isolation system, denoted mean, σ , mean + 1σ and COV, respectively. Mean and mean + 1σ NED statistics for the six bins of ground motions and twenty isolation systems considered are presented in Table 6.1. Mean NED information is plotted for each isolation system and bin of ground motions in Figures 6.2a through 6.7a. For example, shown in Figure 6.2a is mean NED data calculated from the results of unidirectional response-history analysis using Bin 1 ground motions plotted as

a function of the normalized strength of the isolator, Q_d/W , for each of the five values of the second slope-period, T_d , considered for this study. This figure indicates a decreasing trend in NED with increasing isolator strength Q_d/W suggesting that isolators with larger characteristic strengths require fewer harmonic cycles to dissipate an equivalent amount of energy. Figure 6.2a also shows a decreasing trend in NED with increasing second-slope period, T_d , (or decreasing second-slope stiffness). For typical isolator properties, $Q_d/W = 0.06$ and $T_d = 2.5$ seconds, the mean value for NED is approximately 2.5. Similar trends were observed for Bins 2, 2M, 3, 6 and 7 and are shown in Figures 6.3a, 6.4a, 6.5a, 6.6a and 6.7a, respectively. Mean NED including standard deviation information is also presented in Figures 6.2 through 6.7 for each isolation system considered. Sample standard deviation information has been included to indicate the dispersion of NED data about the mean.

6.2.2.3 Bi-directional Seismic Excitation

The cumulative energy dissipated by an individual seismic isolator due to bi-directional excitation was calculated as the sum of the energy dissipated in the x - and y - directions at each time step during the response-history analysis. The equation for the cumulative energy dissipated for bi-directional excitation is the same as that for unidirectional excitation, namely Equation (6.1), however the restoring force F has been re-defined as

$$F = [F_x \quad F_y] \quad (6.4)$$

where F_x and F_y are components of the restoring force in the x - and y - direction respectively. Similarly the incremental displacement dU has been re-expressed as

$$dU = [dU_x \quad dU_y] \quad (6.5)$$

where dU_x and dU_y are the components of the incremental displacement in the x - and y - direction respectively. Substituting Equations (6.4) and (6.5) into Equation (6.1) and performing the dot product, the following expression is obtained

$$E_T = \int F_x \cdot dU_x + \int F_y \cdot dU_y \quad (6.6)$$

showing that the total energy dissipated due to bi-directional seismic excitation can be determined as the sum of the energy dissipated in the x - and y - directions.

The total cumulative energy dissipated by an individual seismic isolator due to bi-directional seismic excitation was calculated for each isolation system and normalized by the EDC , shown by Equation (6.2). However, for the case of bi-directional excitation, the maximum displacement, d_{max} , used to calculate the EDC was determined as the maximum of the square-root-sum-of-squares response calculated from the displacement response in the x - and y - directions for each time step of the response-history analysis.

Normalized energy dissipated data calculated from the results of bi-directional nonlinear response-history analysis for each set of isolation parameters and each ground motion *pair* is presented in Appendix F, including sample mean, sample standard deviation, mean plus one standard deviation, and coefficient of variation information. Mean and mean + 1σ NED statistics calculated from the results of bi-directional response-history analysis for the six bins of ground motions and twenty isolation systems considered are presented in Table 6.2. Mean NED information is plotted, including standard deviation information, in Figures 6.8 through 6.13. This presentation is the same as that utilized for NED calculated from the results of unidirectional nonlinear response-history analysis. Mean NED calculated using the results of bi-directional nonlinear response-history analysis show similar trends to those observed considering unidirectional response-history analysis data.

A comparison of the mean NED calculated from the results of unidirectional and bi-directional nonlinear response-history analysis for each ground motion bin and set of isolator parameters is presented in Figures 6.14a through 6.16a. These figures show the mean NED calculated from bi-directional response-history analysis is greater than the mean NED calculated from unidirectional response-history analysis. However, the difference between NED calculated from bi-directional and unidirectional excitation tends to decrease with increasing strength (Q_d/W) and increasing second-slope period (T_d). This trend is observed for all six bins of ground motions. Mean plus one standard deviation NED data are plotted using the same format in Figures 6.17 through 6.19.

6.2.3 Rate-of-Energy Dissipated

6.2.3.1 General

The rate-of-energy dissipated by an individual seismic isolator during seismic excitation was investigated utilizing the force-displacement data determined from unidirectional and bi-directional response-history analysis.

Shown in Figure 6.20 are sample energy histories calculated for each of the twenty isolation systems using a ground motion record from the 1992, Cape Mendocino earthquake, Rio Dell Over Pass station (RIO360), which is included in ground motion bin 2M. The total energy dissipated (E_T) is observed to increase with increasing isolator strength (Q_d/W) and decrease with increasing second-slope period (T_d) for this particular ground motion record. Figure 6.20 also suggests that the rate of energy dissipated varies for different isolator properties. For this ground motion record, systems with large Q_d/W (see Figure 6.20d) dissipate the total energy in less time than systems with small Q_d/W (see Figure 6.20a).

Two definitions to quantify the rate-of-energy dissipated by isolators (or power demands placed on seismic isolators) during seismic excitation have been employed. The first, referred to herein as *Definition 1*, is similar to a definition utilized by Mosqueda (2002) and is given by

$$R_E^{90} = \frac{0.95E_T - 0.05E_T}{t_{95} - t_5} \quad (6.7)$$

where $0.95E_T$ represents ninety-five percent of the total energy dissipated; $0.05E_T$ represents five percent of the total energy dissipated; t_5 is the time instant during the response-history coinciding with five percent of the total energy dissipated; and t_{95} is the time coinciding with ninety-five percent of the total energy dissipated. The second definition employed, referred to herein as *Definition 2*, is given by

$$R_E^{50} = \frac{0.75E_T - 0.25E_T}{t_{75} - t_{25}} \quad (6.8)$$

where $0.75E_T$ represents seventy-five percent of the total energy dissipated; $0.25E_T$ represents twenty-five percent of the total energy dissipated; t_{25} is the time instant during the response-history coinciding with twenty-five percent of the total energy dissipated; and t_{75} is the time coinciding with seventy-five percent of the total energy dissipated.

The energy history calculated using ground motion RIO360 and isolation parameters $Q_d/W = 0.03$ and $T_d = 2.5$ seconds shown in Figure 6.20b has been reproduced in Figure 6.21 to graphically depict the two definitions of the rate-of-energy dissipated employed for this study. Figure 6.21a shows *Definition 1* (R_E^{90}) which is observed to significantly underestimate the maximum rate-of-energy dissipated for this ground motion record. This underestimation was greater in isolation systems with low characteristic strengths (Q_d/W). Because of this underestimation, a second definition was employed, namely, *Definition 2* (R_E^{50}) shown by Figure 6.21b. This figure shows the second definition better estimates the maximum rate-of-energy dissipated for the given system and ground motion. This observation holds for all isolation systems considered in this study.

6.2.3.2 Unidirectional Seismic Excitation

Rate-of-energy dissipated data calculated from the results of unidirectional response-history analysis using *Definition 1* and *Definition 2*, normalized by T_d , is presented in Appendix F. Also presented in Appendix F are the sample mean, sample standard deviation, mean plus one standard deviation, and coefficient of variation information, denoted mean, σ , mean + 1σ and COV, respectively. Mean and mean + 1σ normalized rate-of-energy dissipated statistics using *Definition 1* and *Definition 2* are presented in Tables 6.3 and 6.4, respectively.

Plotted in Figure 6.22 is mean R_E/T_d data calculated using *Definition 1* for each isolation system and each ground motion bin considering unidirectional excitation. Similarly, mean R_E/T_d data calculated for each isolation system and each ground motion bin using *Definition 2* is plotted in Figure 6.23. The mean rate-of-energy dissipated is observed to increase with increasing characteristic strength for ground motion bins 1 and 2M,

corresponding to near-field and large-magnitude small-distance earthquake events, respectively with stiff-soil site conditions. However this trend was not observed for bins 6 and 7, corresponding to near-field, soft-soil and large-magnitude, soft-soil events, respectively. The difference in the results of stiff- and soft-soil conditions may be attributed to the shift of the peak response into the longer period range for the soft-soil ground motions components.

6.2.3.3 Bi-directional Seismic Excitation

The rate-of-energy dissipated considering bi-directional seismic excitation was calculated in a similar fashion as previously described for the case of unidirectional response-history analysis. However, the total cumulative energy due to bi-directional excitation was calculated as the sum of the cumulative energy in x - and y -directions at every time step as described previously using Equation (6.6). The rate-of-energy dissipated was then calculated using this total cumulative energy dissipated and the two definitions previously described. Rate-of-energy dissipated data calculated using *Definition 1* and *Definition 2* normalized by T_d is presented in Appendix F including sample mean, sample standard deviation, mean plus one standard deviation, and coefficient of variation information calculated for each isolation system, denoted mean, σ , mean + 1σ and COV, respectively. Mean and mean + 1σ statistics for the normalized rate-of-energy dissipated using *Definition 1* and *Definition 2* are presented in Tables 6.5 and 6.6, respectively.

Rate-of-energy dissipated data determined using *Definition 1* and *Definition 2* for each of the six bins of ground motions are plotted in Figures 6.24 and 6.25, respectively. Note this presentation is identical to that utilized for unidirectional R_E (see Figure 6.22 and 6.23). Again an increasing trend in R_E is observed with increasing Q_d/W for ground motion bins 1 and 2M for both *Definition 1* and *Definition 2*.

A comparison of the mean R_E/T_d calculated from the results of unidirectional and bi-directional nonlinear response-history analysis using *Definition 1* (R_E^{90}) and *Definition 2* (R_E^{50}) is presented in Figures 6.26, 6.27, and 6.28 for each of the six bins of

ground motions. For example, Figure 6.26a compares the rate-of-energy dissipated for ground motion bin 1 considering each definition and both unidirectional and bi-directional seismic excitation. From Figure 6.26a, it is observed that for both definitions the rate-of-energy dissipated is larger for bi-directional excitation. Also, in an average sense, R_E^{50} is observed to be larger than R_E^{90} , which is consistent with the results shown in Figure 6.21. Similar trends were observed for the remaining five ground motion bins shown by Figure 6.26b through 6.28b. Mean + 1σ normalized rate-of-energy dissipated information is presented in Figures 6.29 through 6.31. This format is the same as for the mean normalized rate-of-energy dissipated information.

6.2.3.4 Equivalent Harmonic Frequency

A procedure for calculating an equivalent harmonic frequency (f_{eq}) for the prototype testing of seismic isolators is presented. This equivalent frequency is intended capture the energy and power demands on an isolator and isolation system subjected to earthquake excitation. Results of this calculation were used to evaluate the power demands placed on isolators using the current prototype testing requirements. Considering the NED as an equivalent number of harmonic cycles to dissipate the total energy, E_T , an equivalent period of the harmonic cycles can be calculated using

$$T_{eq} = \frac{t_{100}}{NED} \quad (6.9)$$

where t_{100} is defined as the time required to dissipate the total energy which can be approximated (assuming the rate-of-energy dissipated is constant) by

$$t_{100} = \frac{E_T}{R_E} \quad (6.10)$$

where E_T is the total hysteretic energy dissipated and R_E is the previously defined rate-of-energy dissipated (or power) calculated using Equation (6.7) or Equation (6.8). Further, the total energy dissipated can be expressed as a function of the energy dissipated per cycle, EDC , and normalized energy dissipated, NED . Substituting this expression and Equation (6.10) into Equation (6.9) yields

$$T_{eq} = \frac{4Q_d d_{max}}{R_E} \quad (6.11)$$

noting, that the NED in the expression for the total energy dissipated cancels with the NED in the denominator of Equation (6.9). Inverting the expression shown in Equation (6.11) results in an equation to calculate an equivalent harmonic frequency as a function of the observed rate-of-energy dissipated and known isolator design parameters

$$f_{eq} = \frac{R_E}{4Q_d d_{max}} \quad (6.12)$$

where f_{eq} is the equivalent harmonic frequency; R_E is the rate-of-energy dissipated determined using either of the two definitions employed here; Q_d is the characteristic strength of the isolator; and d_{max} is the maximum displacement of the isolation system determined either from the AASHTO Guide Specification for Seismic Isolation Design (1999) or, as with this study, using nonlinear response-history analysis.

A graphical presentation of the calculated equivalent harmonic frequency using the two definitions for R_E and an energy history calculated for $Q_d/W = 0.06$ and $T_d = 4.0$ seconds using ground motion record RIO360 is shown in Figure 6.32. From Figure 6.32a it is observed that R_E^{90} underestimates the maximum power demands placed on the isolator but provides a reasonable estimate of the duration of time to dissipate the total energy (t_{100}). The total energy dissipated is equivalent to 2 fully reversed cycles to the maximum displacement (i.e., $NED \approx 2.0$) therefore the equivalent harmonic frequency is determined using the EDC and the assumed linear R_E . Figure 6.32b shows R_E^{50} better estimates the maximum power demand placed on the isolator. However, assuming the rate-of-energy dissipated is equal to the maximum power over the duration of the energy history underestimated the time duration to dissipate the total energy (t_{100}) resulting in a conservative (higher) equivalent harmonic frequency.

An equivalent harmonic frequency (f_{eq}) was calculated for several isolation systems using Equation (6.12) and the results of unidirectional response-history analysis

considering two ground motion records; RIO360 and CNP196 incorporated into Bin 2M, are presented in Tables 6.7 and 6.8 respectively. Three values of an equivalent frequency calculated using two different methods are presented in these tables. The first, f^1_{eq} , was calculated using Equation (6.12) and R_E^{90}/T_d data, the second, f^2_{eq} , was calculated using Equation (6.12) and R_E^{50}/T_d data, and the third equivalent frequency, f^3_{eq} , calculated using $1/T_{eff}$. Where T_{eff} is the effective period of the isolation system at the maximum displacement, determined from response-history analysis.

From Table 6.7 the calculated equivalent frequency using *Definition 1* for the rate-of-energy dissipated, f^1_{eq} , is observed to be approximately one half the equivalent frequency calculated using *Definition 2* for the rate-of-energy dissipated, namely, f^2_{eq} . This is consistent with the observations from Figure 6.32. The equivalent harmonic frequency, f^2_{eq} , better estimates the maximum power demands placed on the isolator because the total energy (NED) is input to the isolator over a shorter period of time. Values of the equivalent harmonic frequency calculated using the effective period, f^3_{eq} , yield similar results to f^2_{eq} for this ground motion record. This observation suggests the calculation of an equivalent harmonic frequency using the effective period conservatively estimates the maximum power demands placed on the isolator. In some instances, f^2_{eq} is observed to be greater than f^3_{eq} . This is a consequence of the assumed constant rate-of-energy dissipated being equal to the maximum for the entire energy history. In these instances the difference is observed to be small.

6.3 Conclusions

6.3.1 General

A brief discussion regarding the current prototype testing requirements for seismic isolation bearings set forth by the American Association of State Highway and Transportations Officials (AASHTO, 1999) and the Highway Innovative Technology Evaluation Center (HITEC, 2002) is presented. This discussion is followed by conclusions regarding current prototype testing requirements for seismic isolators

subjected to seismic loading based on the results of this investigation. Recommendations for prototype testing requirements based on the results of this investigation are presented by specifying a *number of harmonic cycles* to the maximum displacement and an *equivalent harmonic frequency* of the displacement cycles in Hertz.

6.3.2 Current Prototype Testing Requirements

The current prototype testing requirements for seismic isolators subjected to earthquake loading specified by the AASHTO Guide Specifications for Seismic Isolation Design (1999) are:

- (1) with a vertical load similar to the typical or average dead load the isolator shall be subjected to *three* fully reversed cycles of loading at each of the following multiples of the total design displacement: 1.0, 0.25, 0.50, 0.75, 1.0 and 1.25 in the respective sequence.
- (2) with a vertical load similar to the typical or average dead load the isolator shall be subjected to $15 S_i / B$ cycles not to exceed 25 but not less than 10 fully reversed cycles to the design displacement as calculated using the AASHTO Guide Specifications for Seismic Isolation Design Equation 3 started from a displacement equal to the offset displacement. Here S_i is a numerical coefficient for site-soil profiles determined from Table 5-1; and B is a numerical coefficient related to the effective damping of the isolation system determined from Table 7.1-1.
- (3) 3 fully reversed cycles of loading at the total design displacement.

Prototype testing requirements for seismic isolators subjected to earthquake loading specified by the *Velocity Characterization Test* of HITEC (2002) are:

- (1) 3 fully reversed cycles of sinusoidal loading to the maximum displacement at 0.1 Hz with a vertical load equal to the rated compressive load (denoted, RCL).

- (2) 3 fully reversed cycles of sinusoidal loading to the maximum displacement at the expected fundamental frequency of the isolated bridge or 0.5 Hz if the fundamental frequency has not been determined at the time of testing with a vertical load equal to the RCL.

6.3.3 Conclusions Regarding the Current Prototype Testing Requirements

Results of the investigation of the energy demands imposed on seismic isolators subjected to earthquake excitation were used to evaluate the current prototype testing requirements for seismic isolators. The two metrics used to assess the current requirements are the total energy dissipated by the isolator during maximum earthquake shaking (NED) and the rate-of-energy dissipated (R_E).

Normalized energy dissipated data represents the number of harmonic cycles to the maximum displacement to dissipate an equivalent amount of energy as observed from numerical simulation of maximum earthquake excitation. Therefore, NED determined in this study can be directly compared to the number of harmonic cycles specified by code requirements for the prototype testing. Rate-of-energy dissipated data determined in this study was used to calculate an equivalent harmonic frequency (see Equation (6.12), Tables 6.7 and 6.8). This equivalent harmonic frequency was then used to evaluate the power demands placed on prototype seismic isolators by the code specified prototype testing requirements.

Based on the results of *unidirectional* nonlinear response-history analysis using six bins of ground motions and twenty isolation systems the following conclusions were drawn.

- (1) The prototype testing requirements specified by the AASHTO Guide Specifications for Seismic Isolation Design (1999):
 - (i) significantly over estimate the total energy demands placed on seismic isolators during maximum earthquake excitation in terms of the number of required harmonic displacement cycles. The three seismic loading tests specified results in 31 cycles of displacement to various amplitudes with a minimum of 22 cycles of displacement with amplitude greater than or equal to the design

displacement. If an isolator with 20 percent critical damping (corresponding to a damping coefficient of 1.5) and a site-soil coefficient of 1.0 (corresponding to site profile type I) is assumed, the resulting number of cycles for the second load test specified by the AASHTO procedures is determined to be 10. For typical application of seismic isolation, namely, large-magnitude, small-distance (Bin 2M), the mean *NED* observed for isolation systems with $Q_d / W \geq 0.06$ and $T_d \geq 2.0$ seconds is 2 or less.

(ii) do not specify any criteria regarding a required harmonic frequency for the displacement cycles. The absence of a specified frequency will likely result in power demands placed on the isolator during prototype testing that are inconsistent with the demands observed from numerical simulation of maximum earthquake excitation. Results of such a prototype test could lead to erroneous conclusions regarding the performance of the isolator (or isolation system) during a design or maximum earthquake event.

(2) The prototype testing requirements specified by the Highway Innovative Technology Evaluation Center (2002):

(i) result in total energy demands (3 fully reversed cycles to the maximum displacement at each frequency) that are consistent with the results of this study when considering the mean *NED* from Bin 1 and Bin 2M, near-field and large-magnitude, small-distance events respectively, and isolators with $Q_d / W \geq 0.06$ and $T_d \geq 2.0$ seconds .

Based on the results of *bi-directional* nonlinear response-history analysis using six bins of ground motions and twenty isolation systems the following conclusions were drawn.

(1) The prototype testing requirements specified by the AASHTO Guide Specifications for Seismic Isolation Design (1999):

(ii) over estimate the total energy demands placed on seismic isolators during maximum earthquake excitation in terms of the number of required harmonic

cycles; for a seismic hazard represented by the large-magnitude, small-distance ground motion bin (Bin 2M), the mean *NED* observed for isolation systems with $Q_d/W \geq 0.06$ and $T_d \geq 2.0$ seconds is approximately 3 or less.

(iii) do not specify any a required harmonic frequency for the displacement cycles.

(2) The prototype testing requirements specified by the Highway Innovative Technology Evaluation Center (2002) do not specify any requirements for an equivalent number of cycles due to bi-directional excitation under the *Velocity Characterization Test*.

6.3.4 Recommendations for the Prototype Testing of Seismic Isolators

Based on the results of this investigation the following recommendations for the prototype testing requirements of seismic isolators subjected to seismic loading are presented.

(1) for *unidirectional* seismic excitation:

3 fully reversed cycles of displacement to an amplitude equal to the maximum design displacement. Note the mean *NED* for Bins 1 and 6 and mean + 1σ *NED* for Bins 2M and 7 considering an isolation system with $Q_d/W = 0.06$ and $T_d = 2.0$ seconds (which represent upper bound values of *NED* for plausible isolation systems) were determined to be 2.7, 3.0, 2.8 and 3.3, respectively.

at a frequency corresponding to the effective (or fundamental) frequency of the isolated structure. Although $1/T_{eff}$ leads to a conservative estimate of the power demand placed on the isolator, demands of this magnitude can be realized as suggested from the results of numerical simulation of maximum earthquake excitation. This conservatism is justified given the simplicity of the calculation and the uncertainty in the magnitude and intensity of ground motion shaking.

(2) for *bi-directional* seismic excitation:

4 fully reversed cycles of displacement to an amplitude equal to the maximum design displacement. Note the mean *NED* for Bins 1 and 6 and mean + 1σ *NED* for Bins 2M and 7 considering an isolation system with $Q_d / W = 0.06$ and $T_d = 2.0$ seconds (which represent upper bound values of *NED* for plausible isolation systems) were determined to be 3.4, 4.6, 3.7 and 4.96, respectively.

at a frequency corresponding to the effective (or fundamental) frequency of the isolated structure calculated using the maximum horizontal displacement of the isolation system.

Given that isolated structures are always subjected to bi-directional excitation, the rules given in part (2) above [for bi-directional seismic excitation] could replace the AASHTO Guide Specifications test (1), (2), and (3) given in Section 6.3.2.

Table 6.1. Mean and mean + 1σ normalized energy dissipated (*NED*) determined from the results of unidirectional response-history analysis for six bins of ground motions.

Bin	Statistic	<i>NED</i>																							
		$Q_d/W=0.03$						$Q_d/W=0.06$						$Q_d/W=0.09$						$Q_d/W=0.12$					
		T_d (sec.)						T_d (sec.)						T_d (sec.)						T_d (sec.)					
		1.5	2.0	2.5	3.0	4.0	1.5	2.0	2.5	3.0	4.0	1.5	2.0	2.5	3.0	4.0	1.5	2.0	2.5	3.0	4.0				
1	mean	5.58	4.20	3.38	2.99	2.16	3.44	2.68	2.41	2.12	1.77	2.67	2.14	1.88	1.75	1.50	2.16	1.82	1.66	1.53	1.35				
	mean + 1σ	8.44	6.47	4.86	4.16	2.94	5.29	4.02	3.45	2.98	2.57	4.21	3.20	2.63	2.44	2.12	3.17	2.64	2.42	2.20	1.98				
2	mean	2.61	2.06	1.86	1.76	1.70	1.76	1.58	1.47	1.41	1.35	1.50	1.38	1.33	1.30	1.26	1.28	1.21	1.16	1.14	1.12				
	mean + 1σ	3.89	2.98	2.65	2.49	2.44	2.53	2.33	2.16	2.07	1.99	2.19	2.03	2.00	1.96	1.89	1.96	1.88	1.83	1.81	1.78				
2M	mean	3.50	2.79	2.35	2.18	1.98	2.21	1.92	1.74	1.63	1.49	1.72	1.50	1.42	1.37	1.30	1.41	1.25	1.16	1.12	1.08				
	mean + 1σ	5.40	4.30	3.69	3.46	3.07	3.10	2.82	2.51	2.31	2.03	2.22	2.00	1.95	1.87	1.77	1.93	1.73	1.62	1.58	1.53				
3	mean	3.63	3.33	3.15	3.03	2.88	2.68	2.51	2.40	2.34	2.29	2.15	2.04	1.99	1.95	1.91	1.65	1.60	1.56	1.54	1.52				
	mean + 1σ	4.89	4.49	4.25	4.11	3.98	3.63	3.47	3.33	3.28	3.23	2.87	2.74	2.68	2.64	2.59	2.36	2.31	2.25	2.23	2.21				
6	mean	5.08	5.43	4.52	3.44	2.32	3.19	3.02	2.65	2.22	1.67	2.24	2.02	1.80	1.61	1.31	1.69	1.45	1.30	1.18	1.05				
	mean + 1σ	7.61	7.39	6.33	4.61	3.08	4.65	4.19	3.53	2.90	2.16	3.11	2.77	2.40	2.08	1.62	2.32	1.92	1.73	1.54	1.39				
7	mean	3.89	3.70	2.90	2.61	2.31	2.17	2.01	1.71	1.56	1.42	1.32	1.26	1.11	1.02	0.93	0.94	0.86	0.78	0.73	0.68				
	mean + 1σ	5.75	6.57	4.43	3.81	3.41	3.12	3.26	2.52	2.30	2.08	1.95	2.01	1.69	1.51	1.35	1.54	1.40	1.27	1.18	1.06				

Table 6.2. Mean and mean + 1 σ normalized energy dissipated (*NED*) determined from the results of bi-directional response-history analysis for six bins of ground motions.

Bin	Statistic	<i>NED</i>																							
		$Q_d/W=0.03$						$Q_d/W=0.06$						$Q_d/W=0.09$						$Q_d/W=0.12$					
		T_d (sec.)						T_d (sec.)						T_d (sec.)						T_d (sec.)					
		1.5	2.0	2.5	3.0	4.0	1.5	2.0	2.5	3.0	4.0	1.5	2.0	2.5	3.0	4.0	1.5	2.0	2.5	3.0	4.0				
1	mean	7.92	5.76	4.49	4.21	2.56	4.93	3.41	2.96	2.59	1.92	3.77	2.74	2.42	2.07	1.64	2.97	2.37	2.03	1.79	1.49				
	mean + 1 σ	11.51	9.42	6.42	6.10	3.38	7.84	5.42	4.39	3.81	2.66	6.54	4.56	3.85	3.02	2.32	4.93	4.05	3.14	2.58	2.08				
2	mean	3.41	2.59	2.28	2.10	1.95	2.42	2.00	1.80	1.68	1.61	1.90	1.75	1.65	1.59	1.51	1.65	1.59	1.52	1.49	1.46				
	mean + 1 σ	5.30	4.05	3.38	3.00	2.72	3.45	2.94	2.60	2.38	2.25	2.78	2.70	2.58	2.50	2.36	2.59	2.60	2.53	2.50	2.47				
2M	mean	4.97	3.62	3.09	2.71	2.43	3.18	2.50	2.24	2.15	2.04	2.40	2.07	1.90	1.83	1.75	2.05	1.86	1.73	1.66	1.57				
	mean + 1 σ	7.44	5.48	5.05	4.07	3.55	4.63	3.68	3.42	3.41	3.09	3.36	3.01	2.85	2.79	2.68	2.89	2.73	2.59	2.52	2.38				
3	mean	5.05	4.74	4.58	4.44	4.32	3.41	3.00	2.81	2.73	2.65	2.69	2.50	2.43	2.41	2.34	2.39	2.27	2.21	2.15	2.10				
	mean + 1 σ	6.90	6.74	6.68	6.46	6.23	5.01	4.36	4.07	3.92	3.80	3.40	3.22	3.19	3.24	3.11	3.19	3.08	3.01	2.96	2.92				
6	mean	7.51	8.58	6.66	4.84	2.86	4.45	4.63	4.10	3.20	2.12	3.25	3.05	2.73	2.34	1.72	2.48	2.11	1.87	1.68	1.40				
	mean + 1 σ	11.14	12.08	8.61	6.07	3.75	6.31	6.22	5.29	4.12	2.84	4.59	4.01	3.14	2.86	2.14	3.50	2.78	2.27	1.99	1.71				
7	mean	5.29	5.26	3.86	3.59	3.24	3.30	3.22	2.54	2.27	2.10	2.21	2.00	1.74	1.58	1.43	1.58	1.43	1.27	1.19	1.10				
	mean + 1 σ	7.69	9.75	5.96	5.23	4.95	4.57	4.96	3.56	3.22	3.01	3.10	2.98	2.58	2.34	2.12	2.33	2.14	1.88	1.77	1.64				

Table 6.3. Mean and mean+ 1 σ normalized rate-of-energy dissipated data calculated using Definition 1 and the results of unidirectional response-history analysis for six bins of ground motions.

Bin	Statistic	R_E^{90} / T_d (kN-m / second / second)																			
		$Q_d/W=0.03$			$Q_d/W=0.06$			$Q_d/W=0.09$			$Q_d/W=0.12$										
		T_d (sec.)			T_d (sec.)			T_d (sec.)			T_d (sec.)										
		1.5	2.0	2.5	3.0	4.0	1.5	2.0	2.5	3.0	4.0	1.5	2.0	2.5	3.0	4.0	1.5	2.0	2.5	3.0	4.0
1	mean	34.1	23.6	15.7	13.1	7.6	52.3	32.1	22.8	17.5	10.9	62.4	37.3	26.9	20.6	13.0	68.1	42.9	29.6	22.5	14.8
	mean + 1 σ	63.4	43.4	28.6	24.6	12.7	104.5	65.1	43.3	33.3	20.1	130.7	78.7	53.6	39.7	25.8	149.7	92.6	61.4	45.6	30.5
2	mean	5.11	2.40	1.34	0.90	0.61	5.06	3.05	1.99	1.45	1.01	4.68	3.20	2.36	1.79	1.29	4.06	2.86	2.21	1.82	1.35
	mean + 1 σ	14.17	6.68	3.38	2.03	1.31	14.65	8.28	4.99	3.48	2.36	11.94	7.98	5.80	4.34	3.13	10.27	7.17	5.51	4.52	3.35
2M	mean	8.28	4.51	2.56	1.85	1.25	11.05	6.03	3.97	2.96	2.01	11.52	7.17	5.08	3.91	2.75	11.73	7.19	6.04	4.91	3.24
	mean + 1 σ	16.08	8.80	4.51	2.96	1.91	23.97	11.61	7.07	5.03	3.30	26.36	14.45	9.71	7.28	5.02	29.43	16.07	14.57	11.46	6.74
3	mean	3.63	3.33	3.15	3.03	2.88	2.68	2.51	2.40	2.34	2.29	2.15	2.04	1.99	1.95	1.91	1.65	1.60	1.56	1.54	1.52
	mean + 1 σ	4.89	4.49	4.25	4.11	3.98	3.63	3.47	3.33	3.28	3.23	2.87	2.74	2.68	2.64	2.59	2.36	2.31	2.25	2.23	2.21
6	mean	29.6	29.7	26.5	18.7	8.7	46.0	40.9	35.6	27.9	15.5	46.6	40.8	37.7	29.3	18.4	48.5	39.5	34.0	27.2	18.1
	mean + 1 σ	51.1	43.5	44.1	33.1	15.0	82.9	66.8	65.0	52.3	28.0	83.8	70.5	73.5	57.2	35.2	86.1	71.3	70.0	55.8	36.1
7	mean	10.1	9.7	4.8	3.4	2.4	14.1	10.4	7.2	4.8	3.2	12.6	10.3	7.4	5.2	3.6	10.1	7.3	5.5	4.3	3.1
	mean + 1 σ	19.2	26.6	11.0	6.7	5.1	27.2	22.7	15.2	8.7	5.6	26.8	22.7	15.9	10.3	6.9	21.6	15.1	10.9	8.5	6.0

Table 6.4. Mean and mean+ 1 σ normalized rate-of-energy dissipated data calculated using Definition 2 and the results of unidirectional response-history analysis for six bins of ground motions.

Bin	Statistic	R_E^{50} / T_d (kN-m / second / second)																			
		$Q_d/W=0.03$				$Q_d/W=0.06$				$Q_d/W=0.09$				$Q_d/W=0.12$							
		T_d (sec.)				T_d (sec.)				T_d (sec.)				T_d (sec.)							
		1.5	2.0	2.5	3.0	4.0	1.5	2.0	2.5	3.0	4.0	1.5	2.0	2.5	3.0	4.0	1.5	2.0	2.5	3.0	4.0
1	mean	40.7	29.4	20.5	16.9	11.3	66.6	42.9	30.1	24.0	18.7	89.2	52.4	49.5	35.0	21.3	101.3	108.4	53.0	37.9	23.3
	mean + 1 σ	73.6	52.6	35.5	30.7	19.2	128.3	83.6	54.9	44.1	33.6	177.3	109.2	106.0	70.9	40.4	213.4	276.7	117.3	78.9	45.3
2	mean	6.98	3.80	2.41	1.58	1.05	7.34	5.13	3.78	2.98	2.13	6.82	5.02	4.11	3.36	2.51	7.14	5.55	4.33	3.60	2.69
	mean + 1 σ	17.43	9.02	5.62	3.36	2.12	18.54	12.40	8.99	6.99	4.99	16.69	12.15	10.04	8.17	6.14	17.45	13.70	10.74	8.97	6.71
2M	mean	12.31	6.32	4.08	2.84	1.91	15.56	9.95	7.21	5.38	3.80	16.35	11.19	10.72	7.90	5.57	17.26	13.29	13.47	10.67	7.42
	mean + 1 σ	22.80	11.22	6.94	4.36	2.84	31.32	18.62	13.17	9.49	6.65	35.11	23.25	27.92	18.58	12.57	38.86	30.46	39.51	30.43	20.14
3	mean	1.59	1.10	0.73	0.58	0.40	1.61	1.22	0.91	0.71	0.49	1.39	0.95	0.76	0.64	0.48	1.18	0.89	0.71	0.59	0.43
	mean + 1 σ	4.95	3.31	1.98	1.54	1.02	5.14	3.96	2.80	2.09	1.37	4.04	2.68	2.12	1.78	1.34	3.62	2.77	2.22	1.82	1.34
6	mean	37.5	37.6	32.6	23.4	11.5	54.9	51.4	45.7	34.5	28.0	62.4	54.7	91.9	54.9	29.2	62.8	80.6	67.0	47.1	27.6
	mean + 1 σ	63.6	54.4	54.0	40.2	19.1	94.7	80.6	83.1	63.6	58.9	105.0	89.9	193.9	110.2	56.7	112.8	201.3	149.3	100.5	53.9
7	mean	15.9	14.6	7.6	5.1	3.8	18.6	14.8	10.6	7.3	4.8	18.8	14.6	12.1	8.9	5.9	16.0	12.0	8.6	6.7	4.8
	mean + 1 σ	27.9	38.6	17.0	9.2	7.4	35.4	33.8	24.1	13.8	8.3	36.5	29.8	25.7	17.3	11.0	32.5	24.5	16.9	12.9	9.1

Table 6.5. Mean and mean+ 1 σ normalized rate-of-energy dissipated data calculated using Definition 1 and the results of bi-directional response-history analysis for six bins of ground motions.

Bin	Statistic	R_E^{90} / T_d (kN-m / second / second)																			
		$Q_d/W=0.03$				$Q_d/W=0.06$				$Q_d/W=0.09$				$Q_d/W=0.12$							
		T_d (sec.)				T_d (sec.)				T_d (sec.)				T_d (sec.)							
		1.5	2.0	2.5	3.0	4.0	1.5	2.0	2.5	3.0	4.0	1.5	2.0	2.5	3.0	4.0	1.5	2.0	2.5	3.0	4.0
1	mean	58.8	41.3	28.0	23.0	13.0	93.7	60.4	42.5	31.5	19.1	118.4	70.5	47.5	36.1	22.3	131.6	79.6	52.9	39.3	26.1
	mean + 1 σ	97.3	66.2	44.7	39.9	18.7	163.7	105.3	68.9	54.3	31.5	213.8	126.8	79.2	60.1	37.4	243.9	146.2	90.2	66.9	45.2
2	mean	10.00	3.97	2.10	1.38	0.96	10.54	5.24	3.31	2.44	1.66	9.26	6.21	4.26	3.29	2.36	8.55	5.66	4.39	3.51	2.55
	mean + 1 σ	25.11	9.99	4.98	2.91	1.94	27.84	12.63	7.73	5.55	3.66	23.55	15.69	10.37	7.94	5.65	22.48	14.49	11.21	8.86	6.40
2M	mean	16.58	8.26	4.42	3.27	2.29	19.21	10.19	6.54	4.88	3.38	19.95	12.82	8.80	6.75	4.81	22.01	13.60	9.97	7.92	5.70
	mean + 1 σ	29.08	15.12	7.31	5.04	3.40	34.51	16.97	10.55	7.64	5.15	35.58	22.45	14.99	11.33	8.01	45.47	26.52	19.18	15.09	10.79
3	mean	5.05	4.74	4.58	4.44	4.32	3.41	3.00	2.81	2.73	2.65	2.69	2.50	2.43	2.41	2.34	2.39	2.27	2.21	2.15	2.10
	mean + 1 σ	6.90	6.74	6.68	6.46	6.23	5.01	4.36	4.07	3.92	3.80	3.40	3.22	3.19	3.24	3.11	3.19	3.08	3.01	2.96	2.92
6	mean	50.8	51.8	42.5	31.1	13.8	79.4	76.2	64.5	49.3	24.5	86.5	82.8	73.1	55.7	31.6	90.1	83.0	71.5	56.2	35.4
	mean + 1 σ	81.5	68.9	61.3	46.0	20.8	126.8	107.2	98.2	78.0	39.5	137.5	125.4	117.2	91.8	52.0	137.1	129.2	118.7	93.8	59.3
7	mean	18.2	21.7	8.9	6.0	4.0	25.7	22.1	12.9	9.2	6.4	26.0	19.7	15.3	11.4	7.6	25.5	17.9	12.8	9.9	6.6
	mean + 1 σ	32.4	60.4	20.0	11.7	8.2	42.2	46.9	23.5	15.3	11.7	44.5	33.9	25.4	17.8	11.5	46.5	31.2	21.4	16.6	11.4

Table 6.6. Mean and mean+ 1 σ normalized rate-of-energy dissipated data calculated using Definition 2 and the results of bi-directional response-history analysis for six bins of ground motions.

Bin	Statistic	R_E^{30} / T_d (kN-m / second / second)																							
		$Q_d/W=0.03$						$Q_d/W=0.06$						$Q_d/W=0.09$						$Q_d/W=0.12$					
		T_d (sec.)						T_d (sec.)						T_d (sec.)						T_d (sec.)					
		1.5	2.0	2.5	3.0	4.0	1.5	2.0	2.5	3.0	4.0	1.5	2.0	2.5	3.0	4.0	1.5	2.0	2.5	3.0	4.0				
1	mean	67.3	49.6	34.6	26.5	17.4	115.5	79.6	56.1	42.0	30.9	154.2	99.3	91.8	62.1	35.5	177.3	140.8	95.4	63.6	40.3				
	mean + 1 σ	110	79.0	53.3	44.4	22.5	197	130.5	84.8	68.2	45.2	275	167.5	163.7	101.7	55.3	321	269.8	175.8	107.6	65.7				
2	mean	12.71	6.46	3.59	2.18	1.45	14.79	8.12	5.87	3.85	3.03	14.25	9.89	8.08	6.33	4.42	12.56	9.63	7.83	6.43	4.74				
	mean + 1 σ	29.27	14.79	8.12	4.65	2.82	34.38	18.54	12.96	7.81	6.19	32.62	22.37	18.26	14.08	9.63	27.99	21.04	17.21	14.10	10.35				
2M	mean	21.36	11.34	6.34	4.37	2.97	29.37	15.65	11.13	7.41	5.67	31.28	20.13	16.27	12.36	8.46	30.60	22.86	18.39	15.08	10.73				
	mean + 1 σ	35.38	19.06	10.20	6.60	4.19	49.76	26.11	18.25	11.28	8.40	57.57	35.33	28.66	21.40	14.45	63.68	45.69	37.42	30.99	21.73				
3	mean	2.33	1.49	1.12	0.88	0.59	3.35	2.01	1.47	1.27	0.90	2.93	2.09	1.71	1.41	1.04	2.71	1.72	1.37	1.14	0.85				
	mean + 1 σ	6.24	3.75	2.77	2.11	1.34	10.01	5.52	3.87	3.38	2.35	8.65	6.11	5.01	4.11	3.01	7.85	4.65	3.70	3.08	2.31				
6	mean	60.3	61.5	52.6	39.1	19.0	95.1	89.4	79.0	59.9	32.6	114.4	97.8	95.1	67.8	39.9	130.7	107.4	97.3	71.7	43.9				
	mean + 1 σ	93.6	86.6	74.2	57.0	26.5	151.7	125.3	123.2	97.4	53.3	177.1	146.7	158.7	113.6	65.9	205.3	153.4	158.6	117.5	70.7				
7	mean	26.1	27.9	11.7	8.3	5.4	34.2	28.6	16.9	10.9	9.2	34.6	25.5	25.3	17.1	11.6	30.0	27.0	19.7	15.7	10.8				
	mean + 1 σ	40.1	72.9	24.2	16.0	11.4	53.5	64.0	32.9	18.5	16.7	60.8	49.7	49.8	28.1	18.0	53.4	47.4	33.9	26.9	18.8				

Table 6.7. Sample calculation for the equivalent frequency (f_{eq}) using results of unidirectional response-history analysis and ground motion RIO360 from Bin 2M.

Q_d/W	W (kN)	g (m/sec./sec.)	T_d (sec.)	K_d kN/m	R_E^{90} / T_d	R_E^{90} (kN-m / sec.)	R_E^{50} / T_d	R_E^{50} (kN-m / sec.)	d_{max} (cm)	K_{eff} (kN/m)	T_{eff} (sec.)	f_{eq}^1 (Hz)	f_{eq}^2 (Hz)	f_{eq}^3 (Hz)
0.06	2473	9.81	2.0	2488	3.81	7.6	11.14	22.3	6.43	4795	1.44	0.20	0.58	0.69
			2.5	1592	2.81	7.0	7.92	19.8	5.30	4393	1.51	0.22	0.63	0.66
			3.0	1106	2.22	6.7	6.34	19.0	4.70	4261	1.53	0.24	0.68	0.65
			4.0	622	1.62	6.5	4.94	19.8	5.17	3492	1.69	0.21	0.64	0.59
0.09			2.0	2488	9.87	19.7	14.99	30.0	6.58	5871	1.30	0.34	0.51	0.77
			2.5	1592	7.70	19.3	11.59	29.0	5.84	5400	1.36	0.37	0.56	0.74
			3.0	1106	6.32	19.0	9.42	28.3	5.21	5381	1.36	0.41	0.61	0.74
			4.0	622	4.69	18.7	6.93	27.7	4.64	5419	1.36	0.45	0.67	0.74
0.12			2.0	2488	17.64	35.3	31.30	62.6	6.44	7099	1.18	0.46	0.82	0.84
			2.5	1592	13.72	34.3	23.76	59.4	6.08	6474	1.24	0.48	0.82	0.81
			3.0	1106	11.27	33.8	19.52	58.6	5.71	6304	1.26	0.50	0.86	0.80
			4.0	622	8.35	33.4	14.29	57.1	5.30	6218	1.27	0.53	0.91	0.79

Notes:

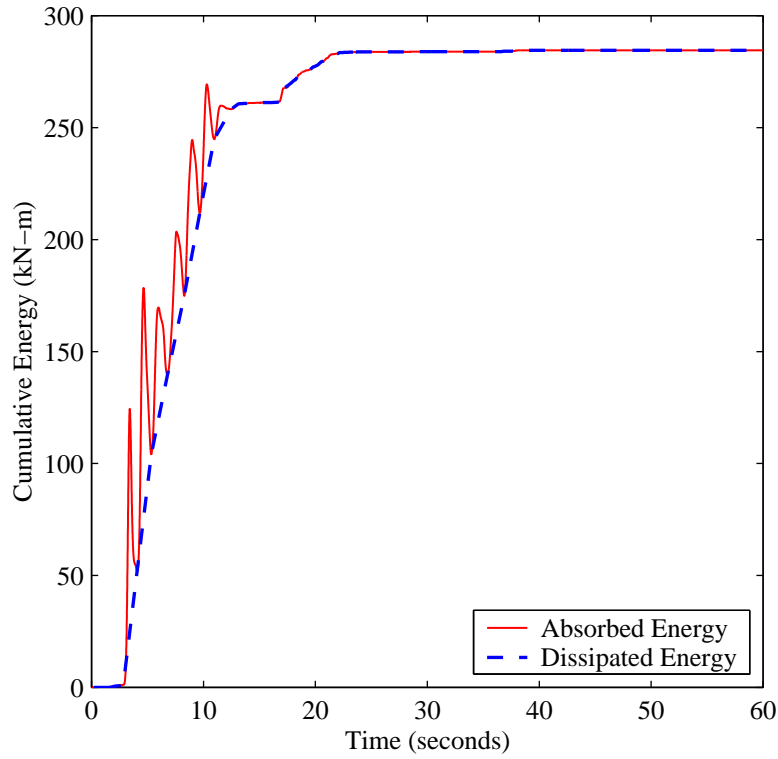
- 1 equivalent frequency calculated using Equation 6-12 and R_E , Definition 1
- 2 equivalent frequency calculated using Equation 6-12 and R_E , Definition 2
- 3 equivalent frequency calculated using $1 / T_{eff}$

Table 6.8. Sample calculation for the equivalent frequency (f_{eq}) using results of unidirectional response-history analysis and ground motion CNP196 from Bin 2M.

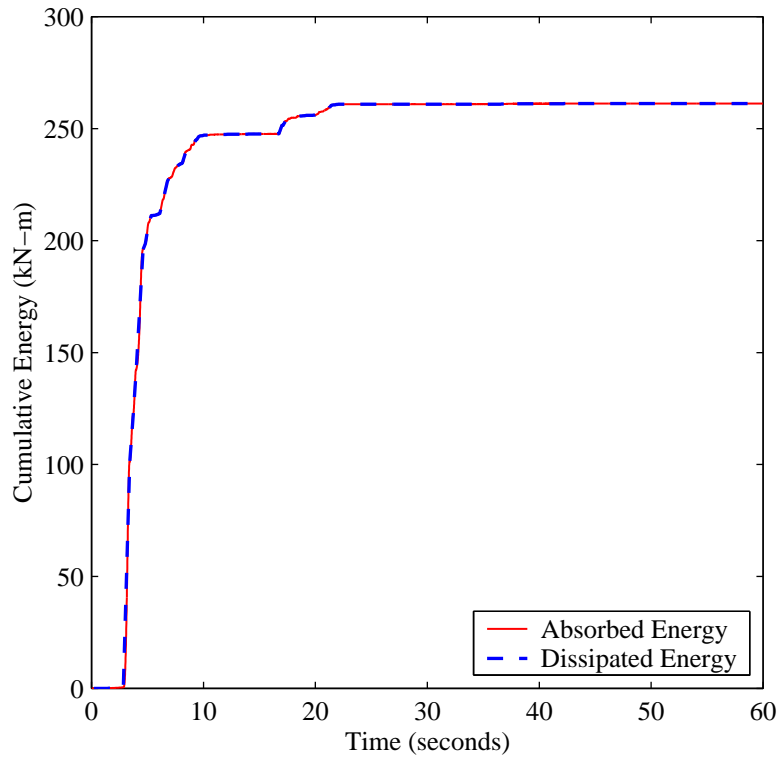
Q_d / W	W (kN)	g (m/sec./sec.)	T_d (sec.)	K_d (kN/m)	R_E^{90} / T_d	R_E^{90} (kN-m / sec.)	R_E^{50} / T_d	R_E^{50} (kN-m / sec.)	d_{max} (cm)	K_{eff} (kN/m)	T_{eff} (sec.)	f_{eq}^1 (Hz)	f_{eq}^2 (Hz)	f_{eq}^3 (Hz)
0.06	2473	9.81	2.0	2488	12.98	25.96	14.06	28.11	12.77	3649.8	1.65	0.34	0.37	0.61
			2.5	1592	9.58	23.95	10.71	26.78	15.06	2577.5	1.96	0.27	0.30	0.51
			3.0	1106	6.64	19.91	7.50	22.51	16.27	2017.5	2.22	0.21	0.23	0.45
			4.0	622	4.29	17.17	4.65	18.61	17.28	1480.9	2.59	0.17	0.18	0.39
0.09			2.0	2488	10.54	21.08	11.14	22.28	9.13	4927.0	1.42	0.26	0.27	0.70
			2.5	1592	8.15	20.38	8.70	21.75	8.24	4293.1	1.52	0.28	0.30	0.66
			3.0	1106	6.62	19.85	7.06	21.17	8.25	3803.8	1.62	0.27	0.29	0.62
			4.0	622	4.84	19.38	5.14	20.57	9.13	3058.7	1.80	0.24	0.25	0.55
0.12			2.0	2488	8.66	17.32	12.45	24.90	7.52	6431.8	1.24	0.19	0.28	0.80
			2.5	1592	6.65	16.62	9.63	24.08	7.91	5344.6	1.36	0.18	0.26	0.73
			3.0	1106	5.43	16.29	7.77	23.30	8.30	4682.9	1.46	0.17	0.24	0.69
			4.0	622	4.11	16.44	5.82	23.28	8.75	4014.3	1.57	0.16	0.22	0.64

Notes:

- 1 equivalent frequency calculated using Equation 6-12 and R_E , Definition 1
- 2 equivalent frequency calculated using Equation 6-12 and R_E , Definition 2
- 3 equivalent frequency calculated using $1 / T_{eff}$



a. isolator properties: $Q_d/W=0.03$ and $T_d=2.5$ seconds.



b. isolator properties: $Q_d/W=0.12$ and $T_d=4.0$ seconds.

Figure 6.1. Cumulative energy histories calculated from the results of unidirectional response-history analysis considering two sets of isolator properties and a ground motion record from the 1992 Cape Mendocino Earthquake, Petrolia Station, (nf08) and included in Bin 1.

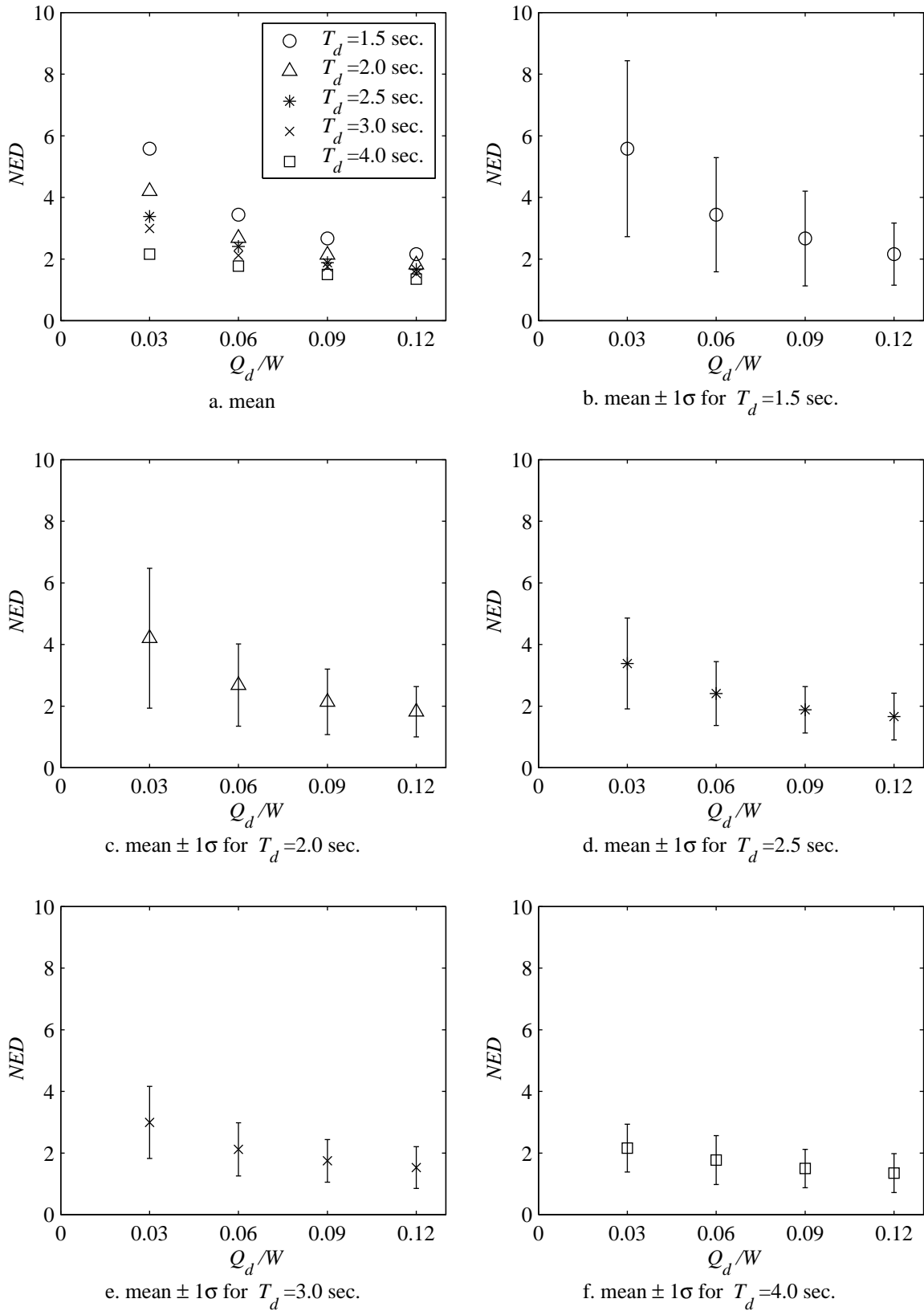


Figure 6.2. Normalized energy dissipated (NED) based on the results of unidirectional response-history analysis and Bin 1 ground motions.

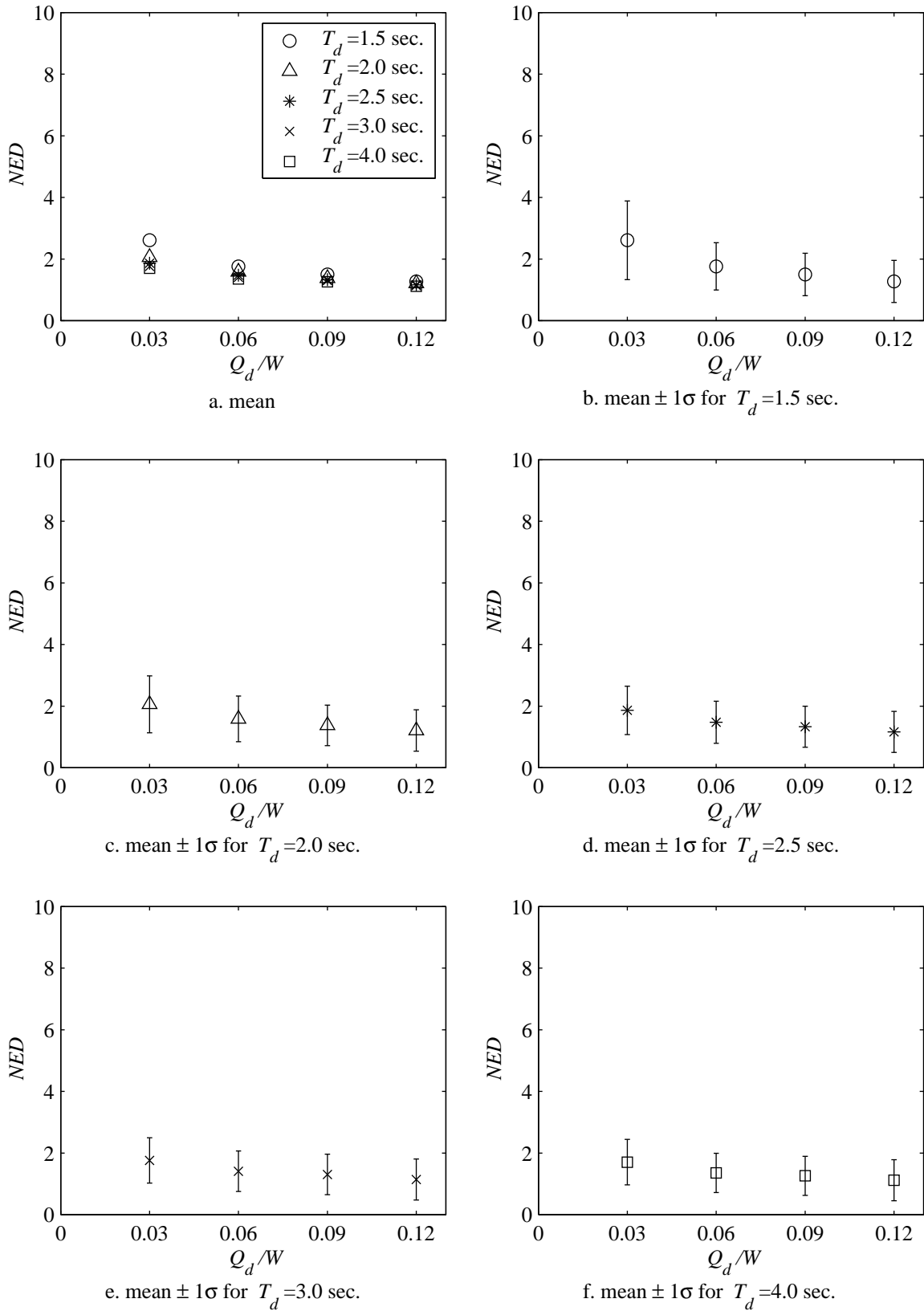


Figure 6.3. Normalized energy dissipated (*NED*) based on the results of unidirectional response–history analysis and Bin 2 ground motions.

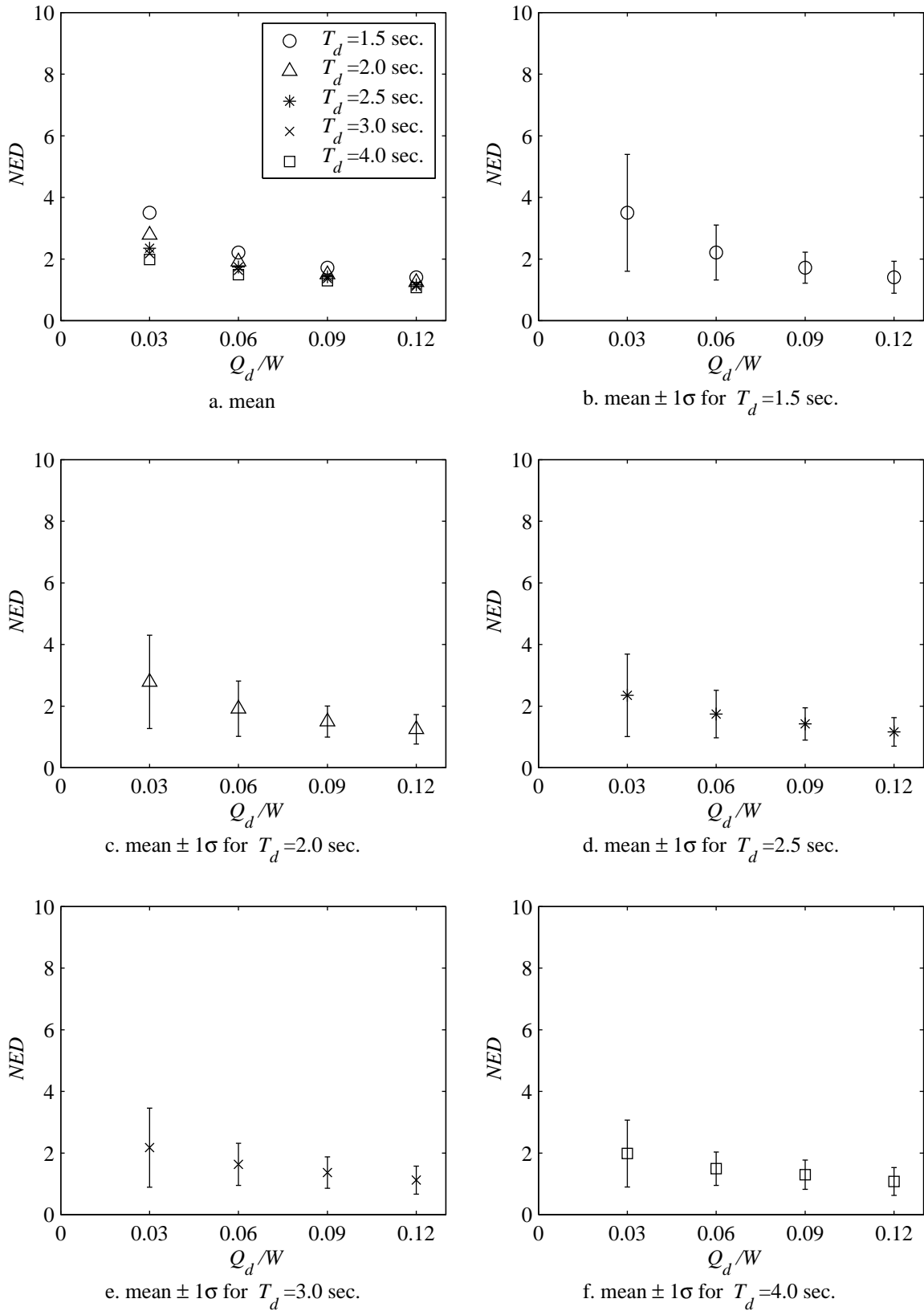


Figure 6.4. Normalized energy dissipated (*NED*) based on the results of unidirectional response–history analysis and Bin 2M ground motions.

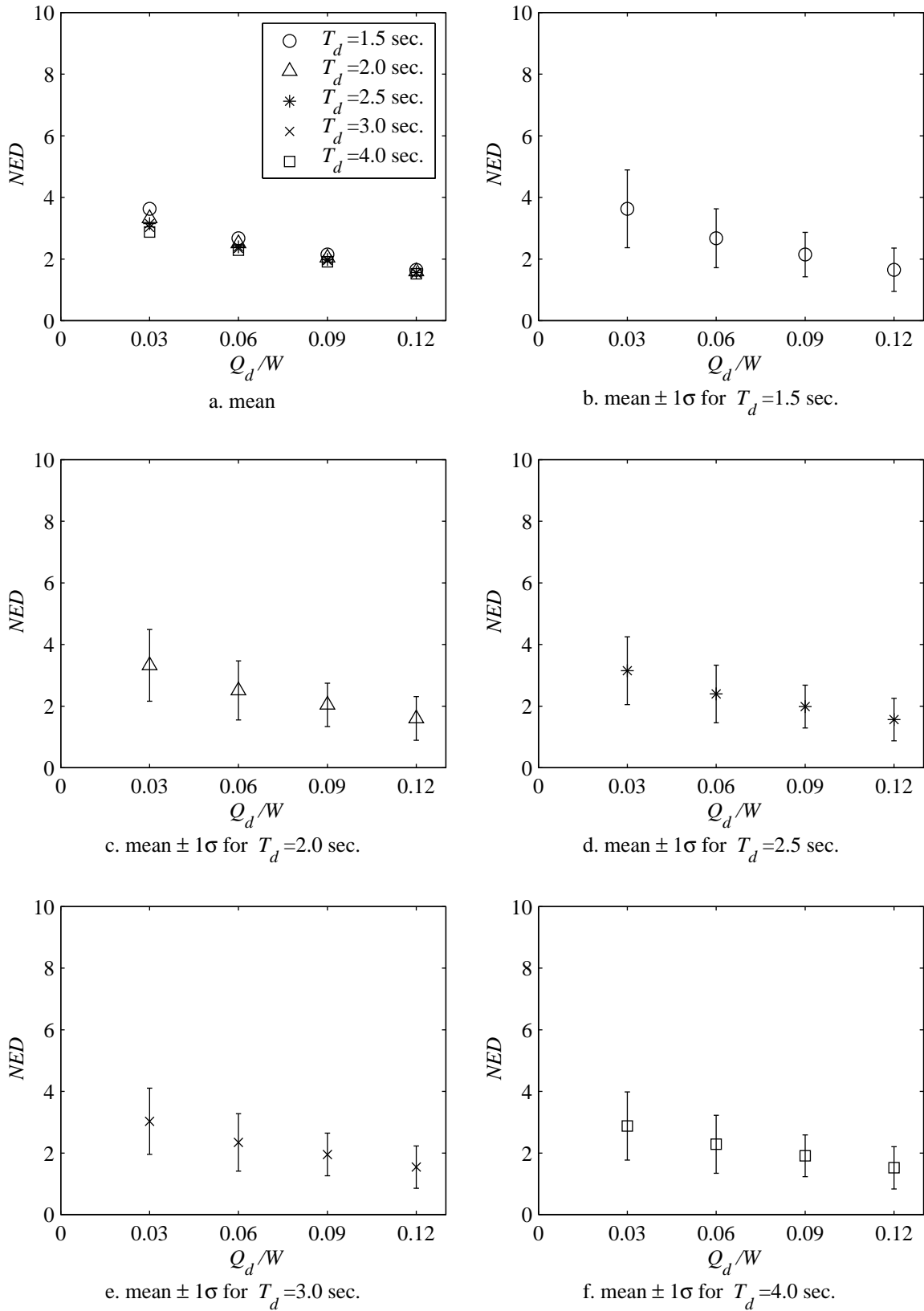


Figure 6.5. Normalized energy dissipated (NED) based on the results of unidirectional response–history analysis and Bin 3 ground motions.

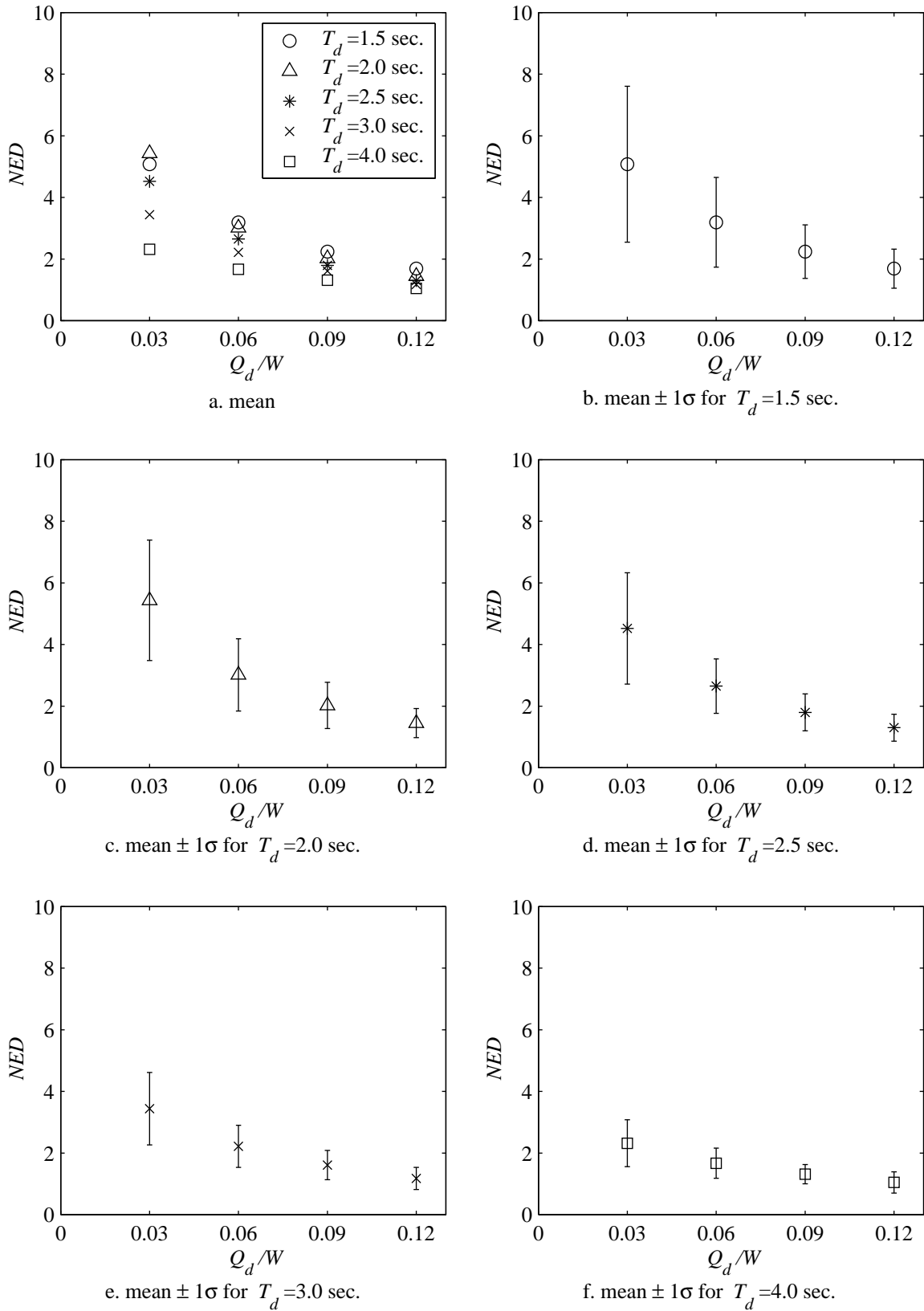


Figure 6.6. Normalized energy dissipated (NED) based on the results of unidirectional response-history analysis and Bin 6 ground motions.

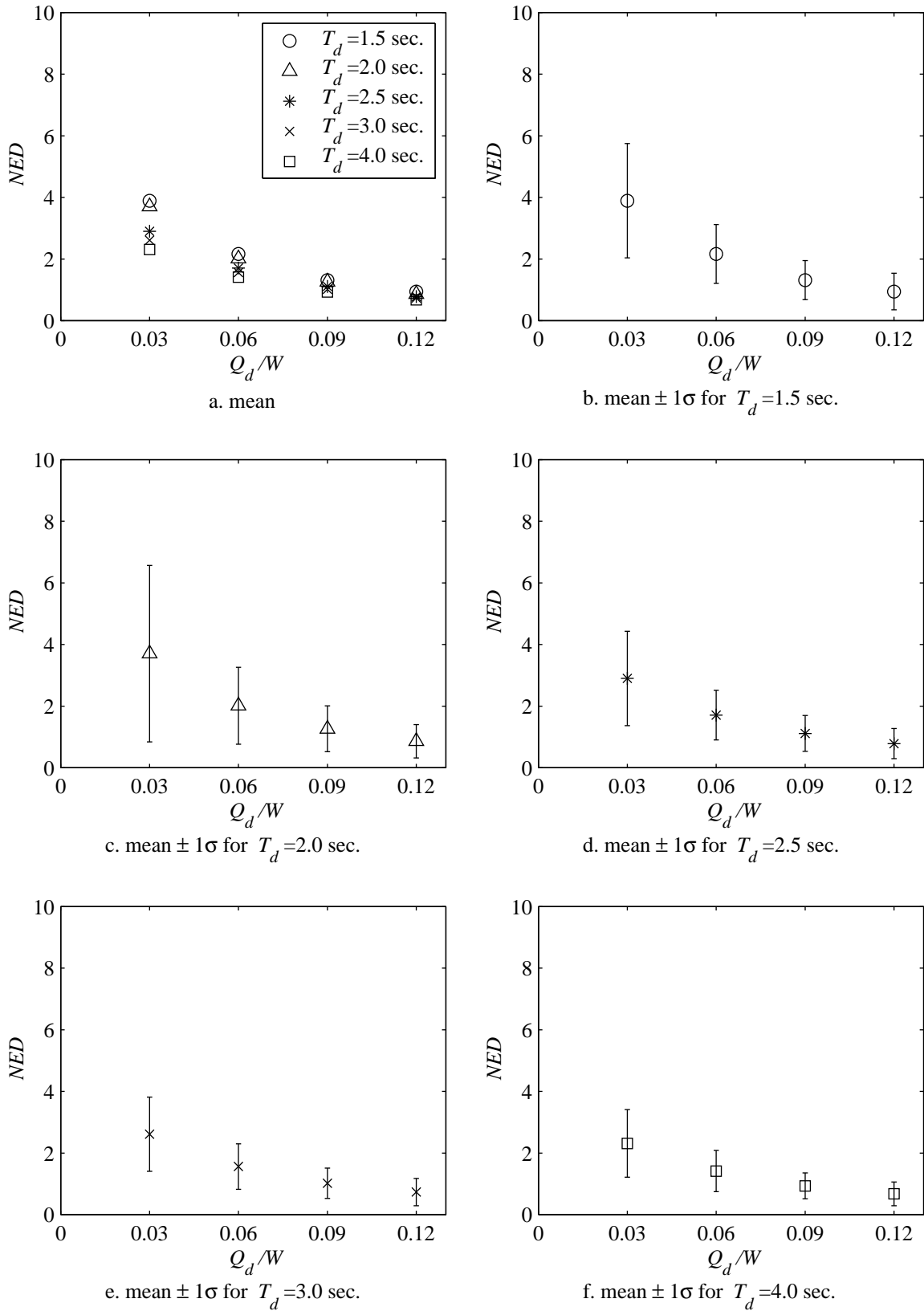


Figure 6.7. Normalized energy dissipated (NED) based on the results of unidirectional response–history analysis and Bin 7 ground motions.

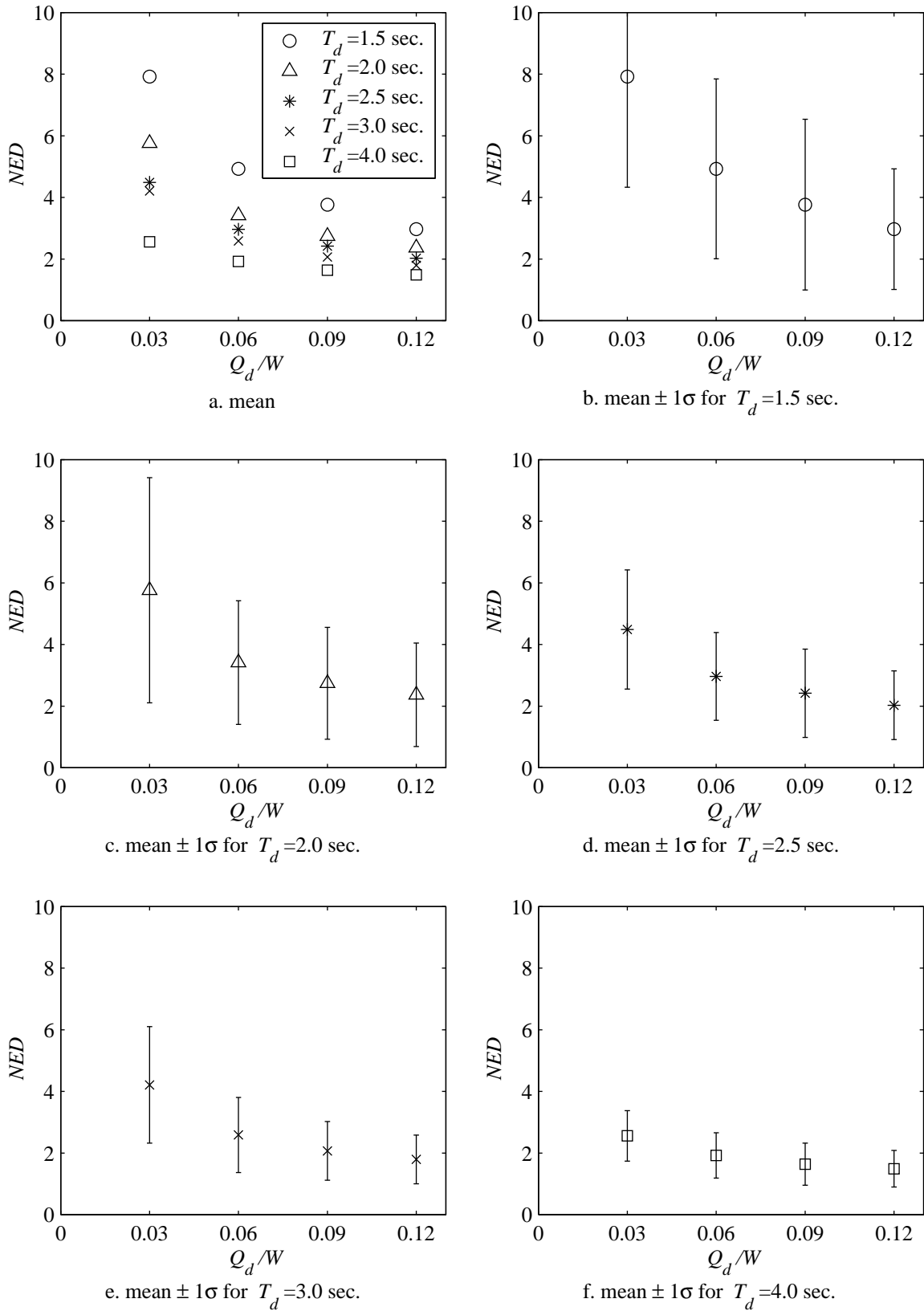


Figure 6.8. Normalized energy dissipated (NED) based on the results of bi-directional response-history analysis and Bin 1 ground motions.

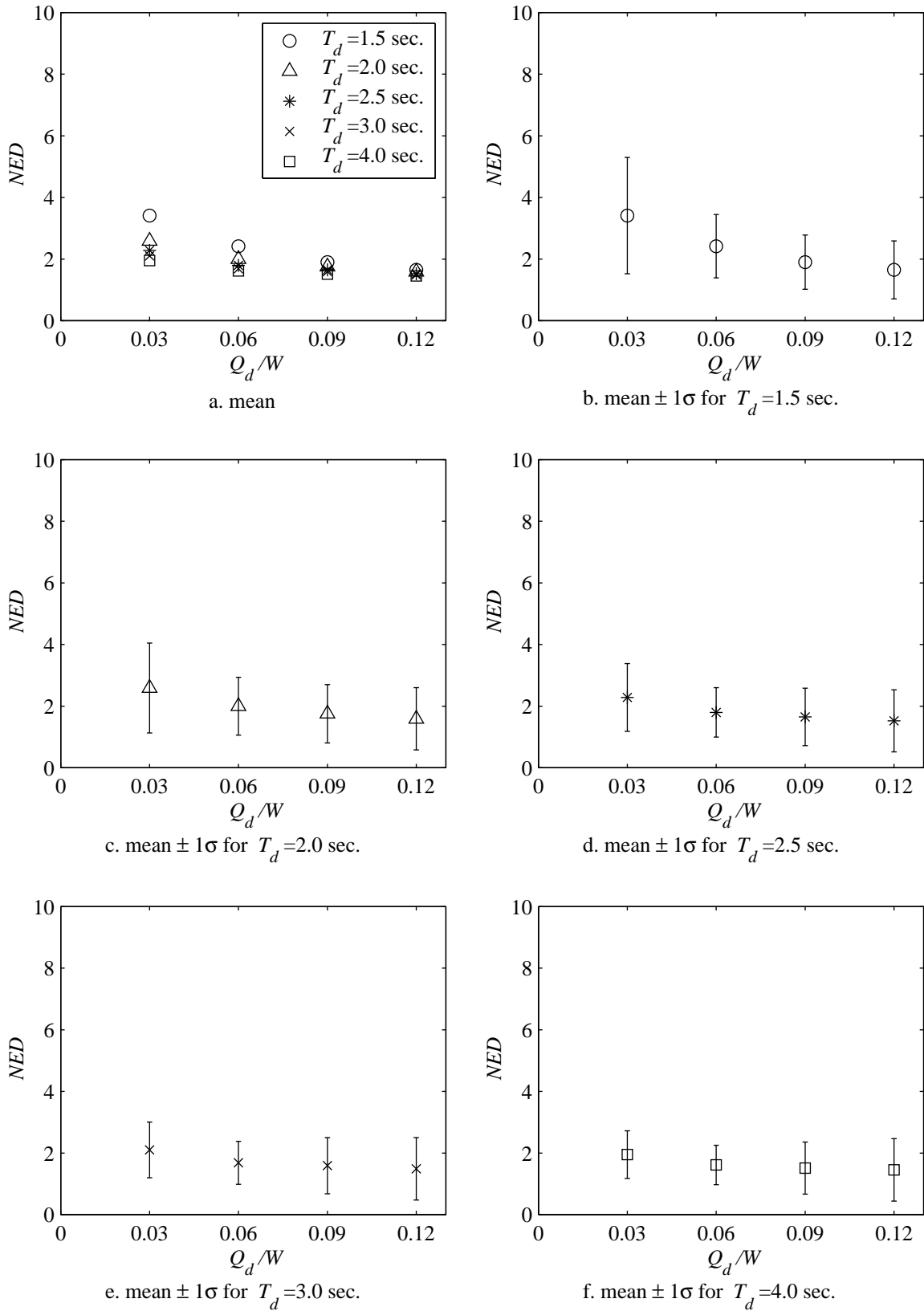


Figure 6.9. Normalized energy dissipated (*NED*) based on the results of bi-directional response-history analysis and Bin 2 ground motions.

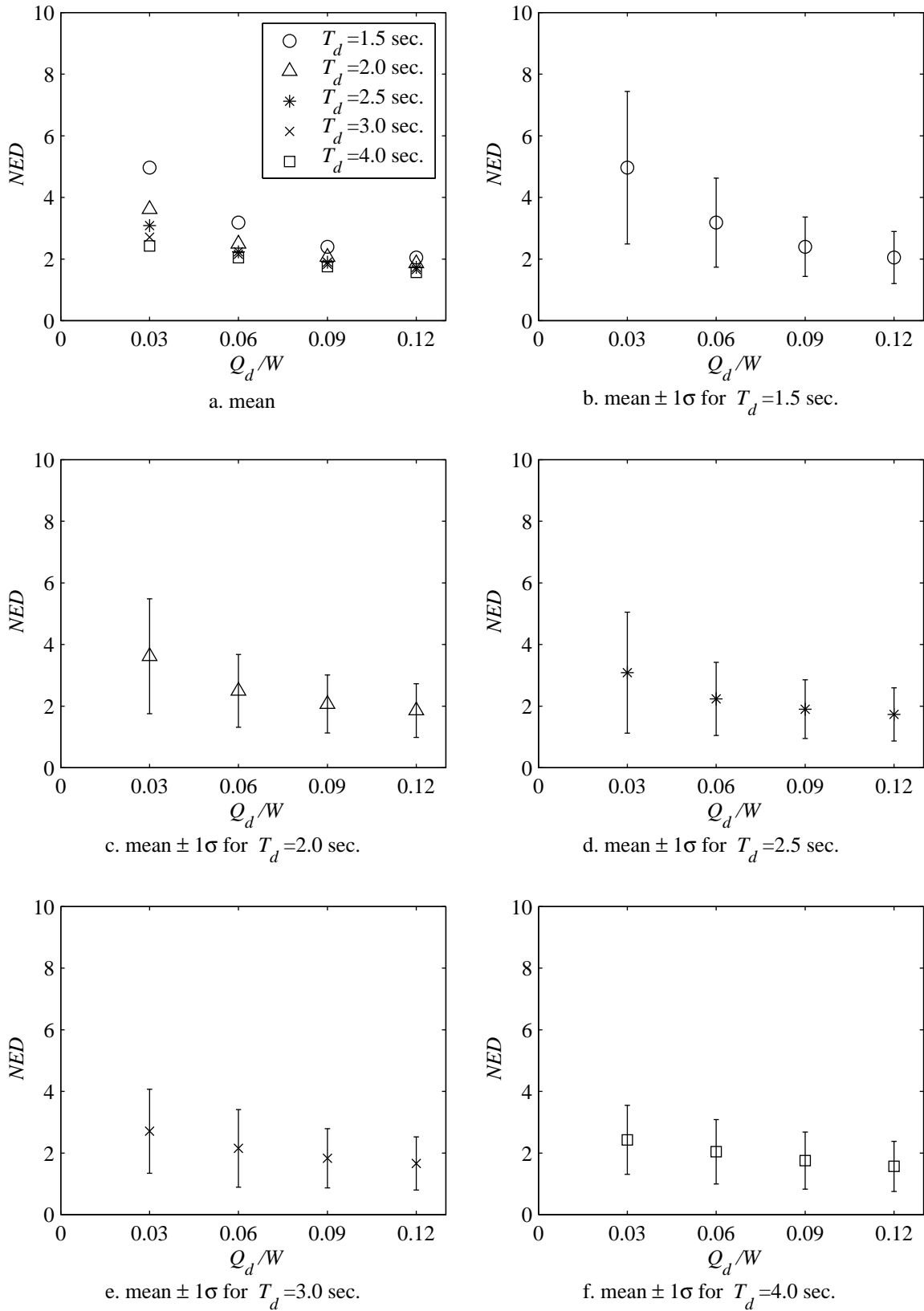


Figure 6.10. Normalized energy dissipated (NED) based on the results of bi-directional response-history analysis and Bin 2M ground motions.

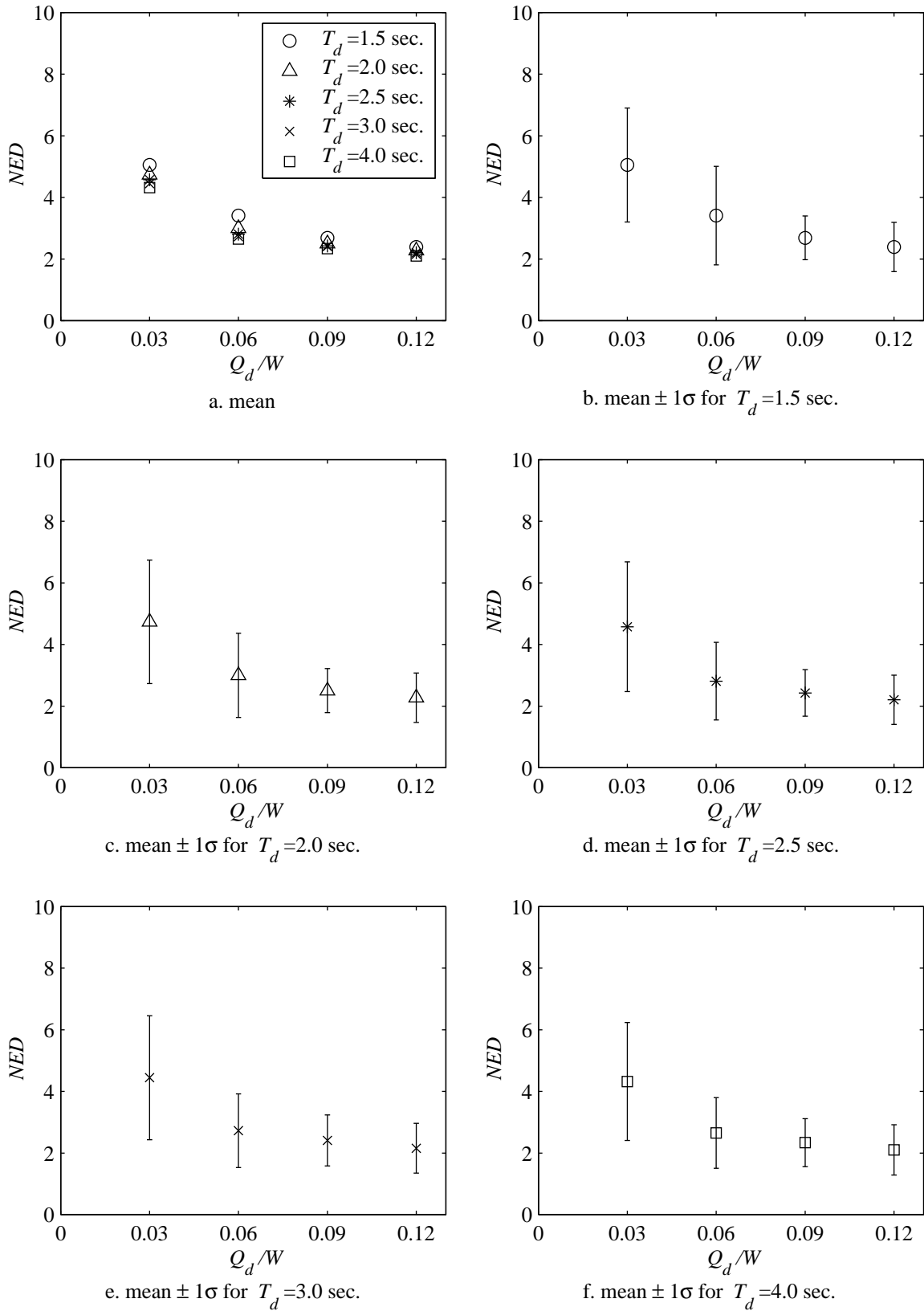


Figure 6.11. Normalized energy dissipated (NED) based on the results of bi-directional response-history analysis and Bin 3 ground motions.

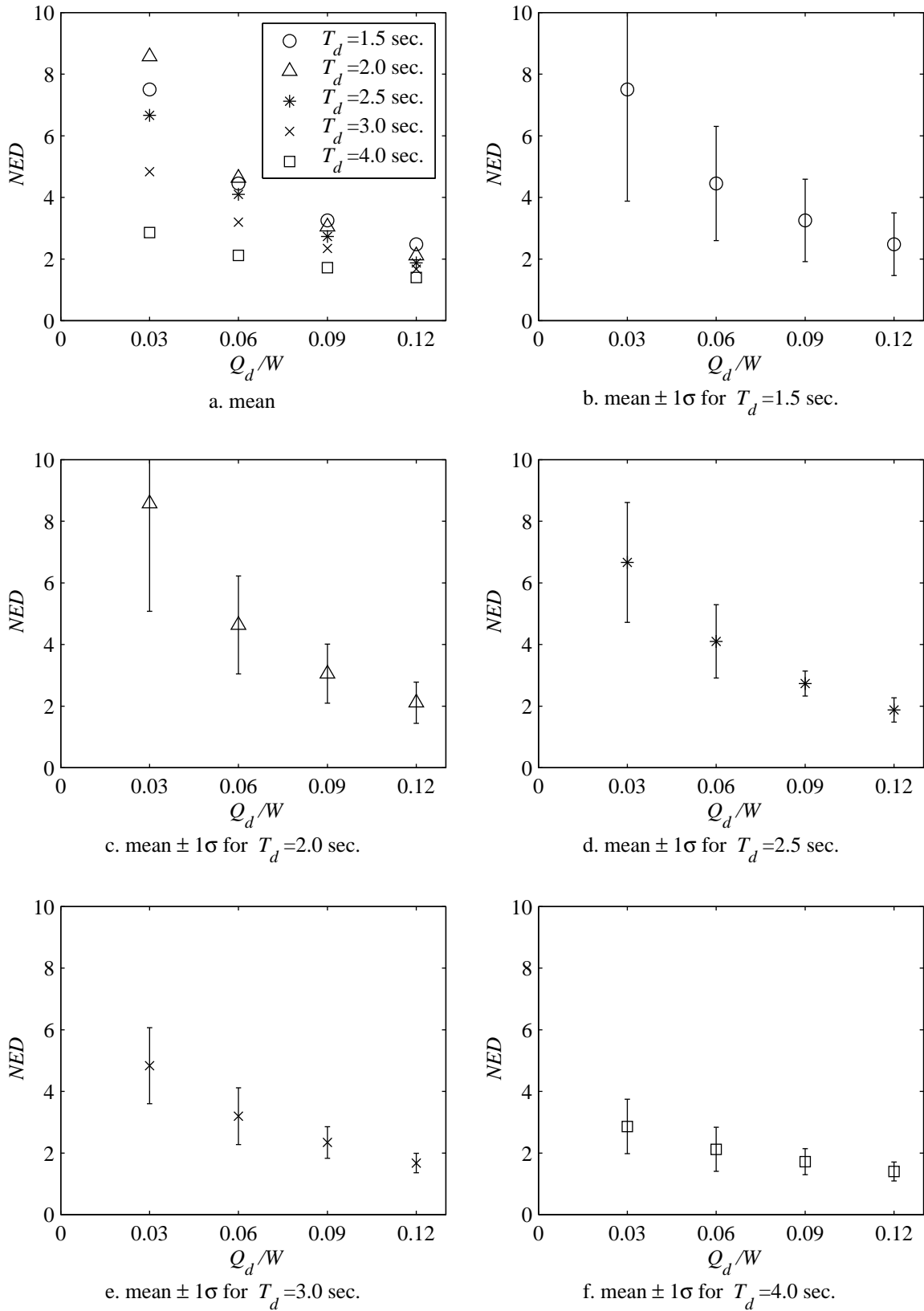


Figure 6.12. Normalized energy dissipated (NED) based on the results of bi-directional response-history analysis and Bin 6 ground motions.

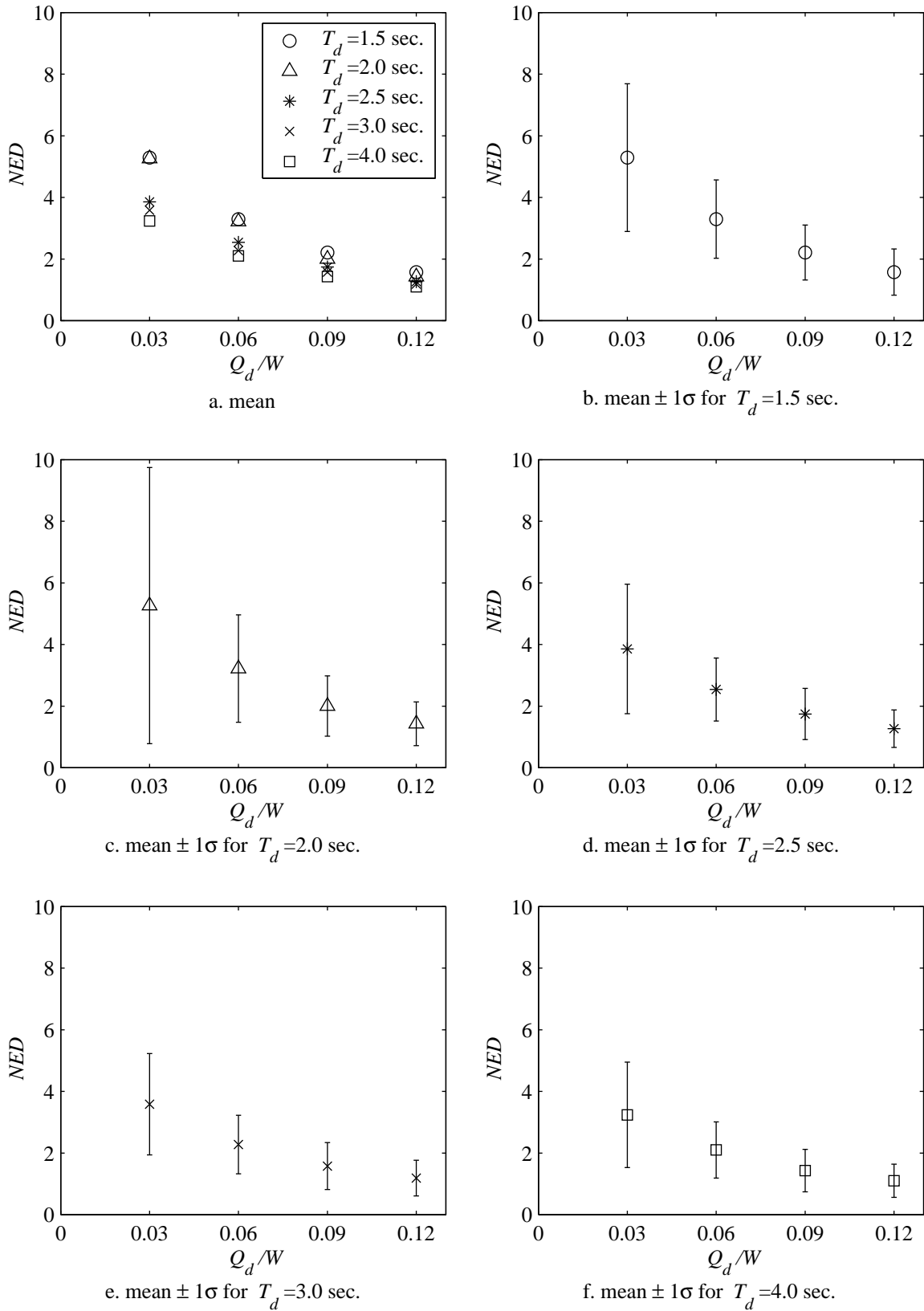
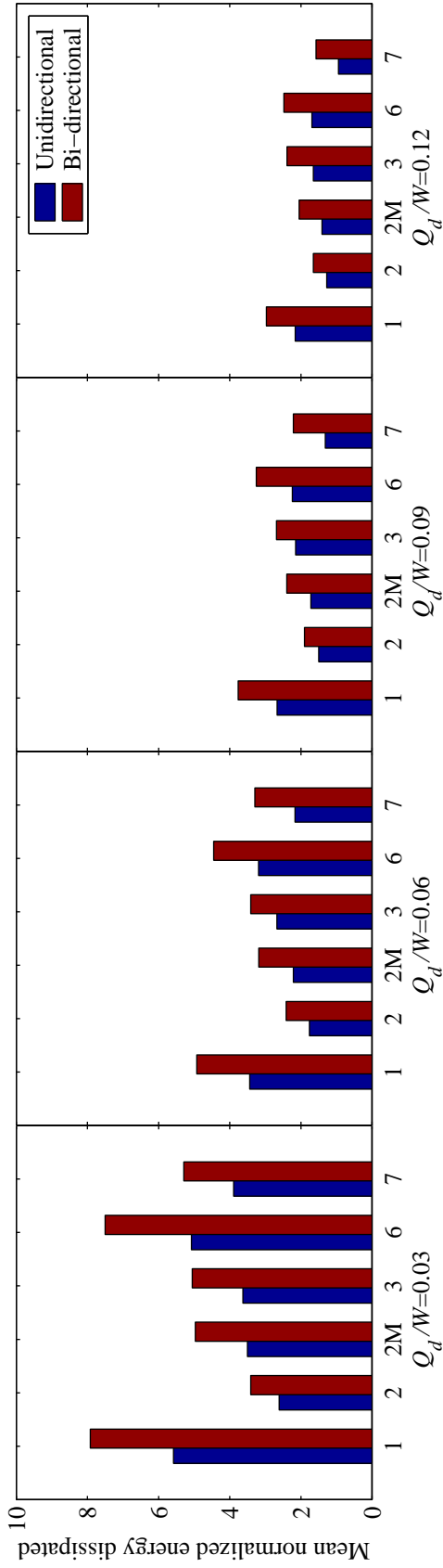
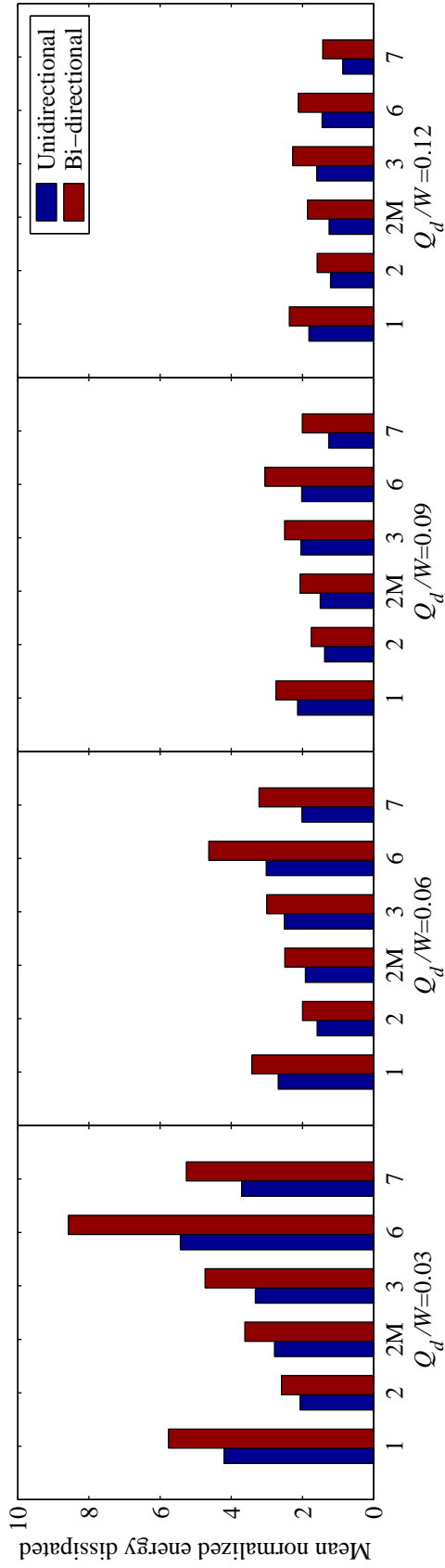


Figure 6.13. Normalized energy dissipated (NED) based on the results of bi-directional response-history analysis and Bin 7 ground motions.



a. $T_d = 1.5$ seconds



b. $T_d = 2.0$ seconds

Figure 6.14. Comparison of the mean normalized energy dissipated (NED) calculated for unidirectional and bi-directional excitation considering all values of Q_d/W , $T_d = 1.5$ seconds and $T_d = 2.0$ seconds, for ground motion bins 1, 2, 2M, 3, 6, and 7.

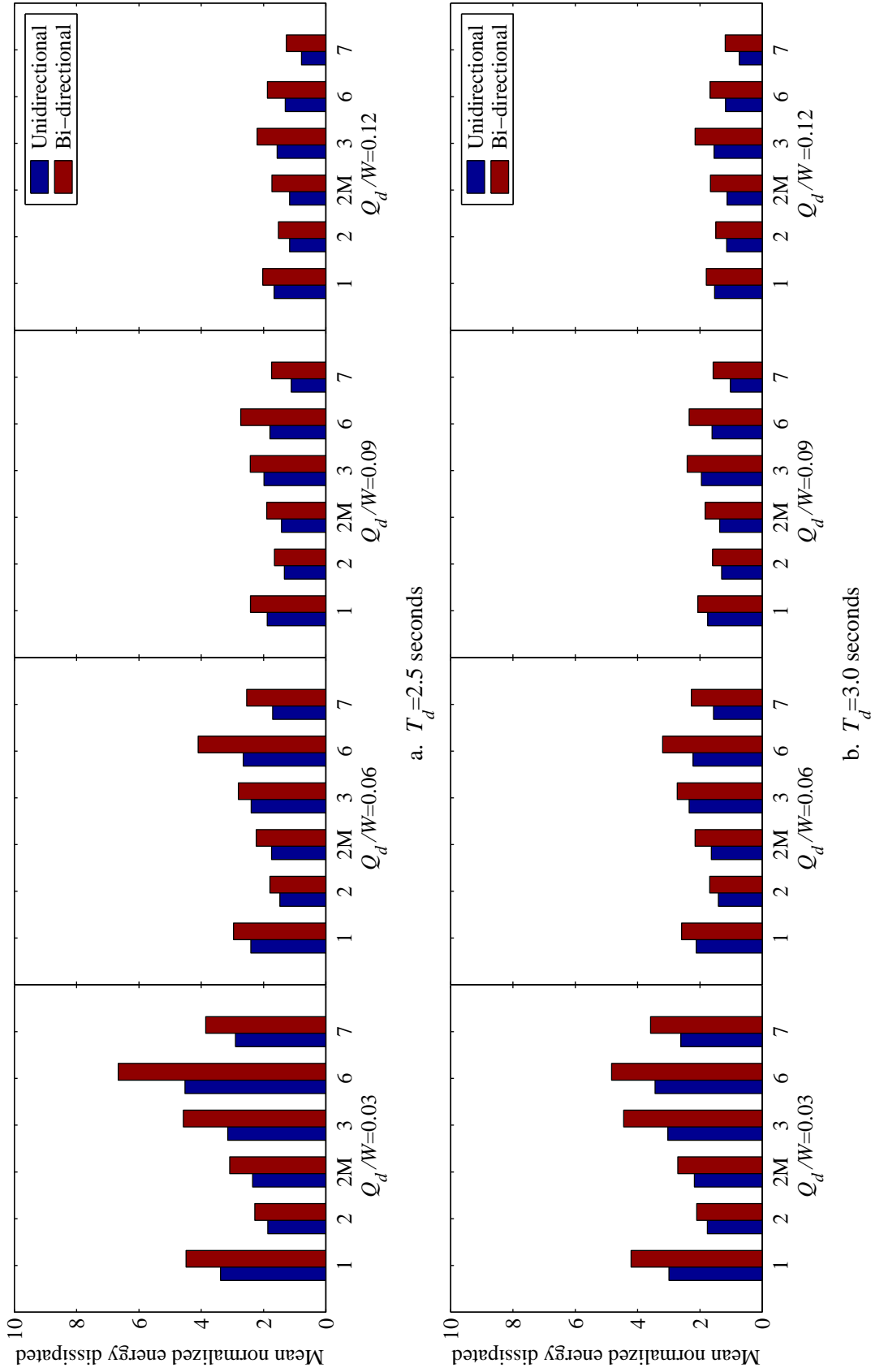
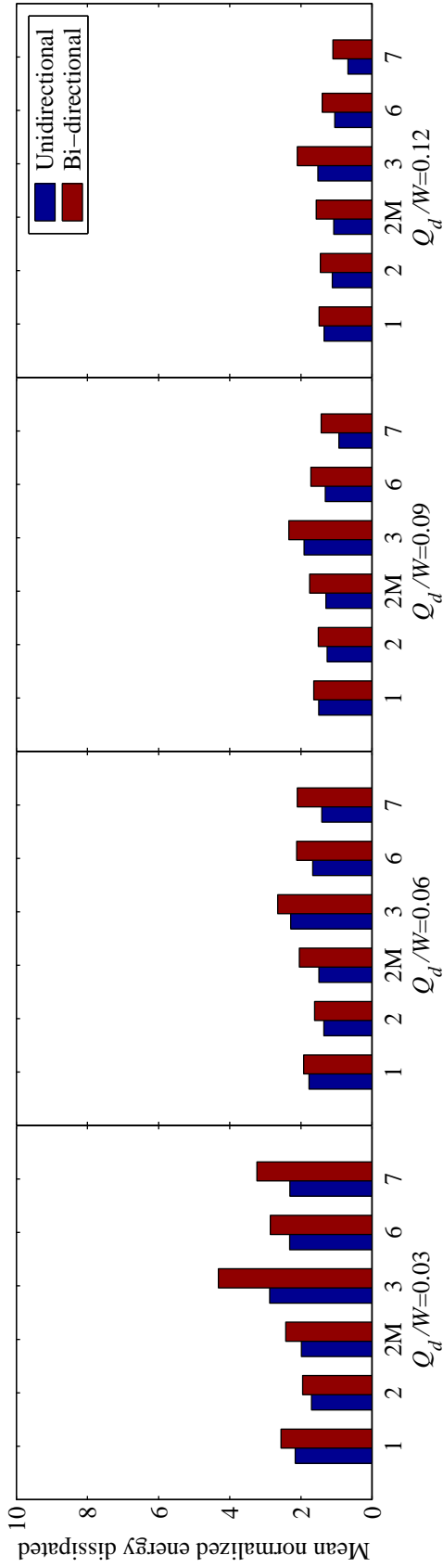
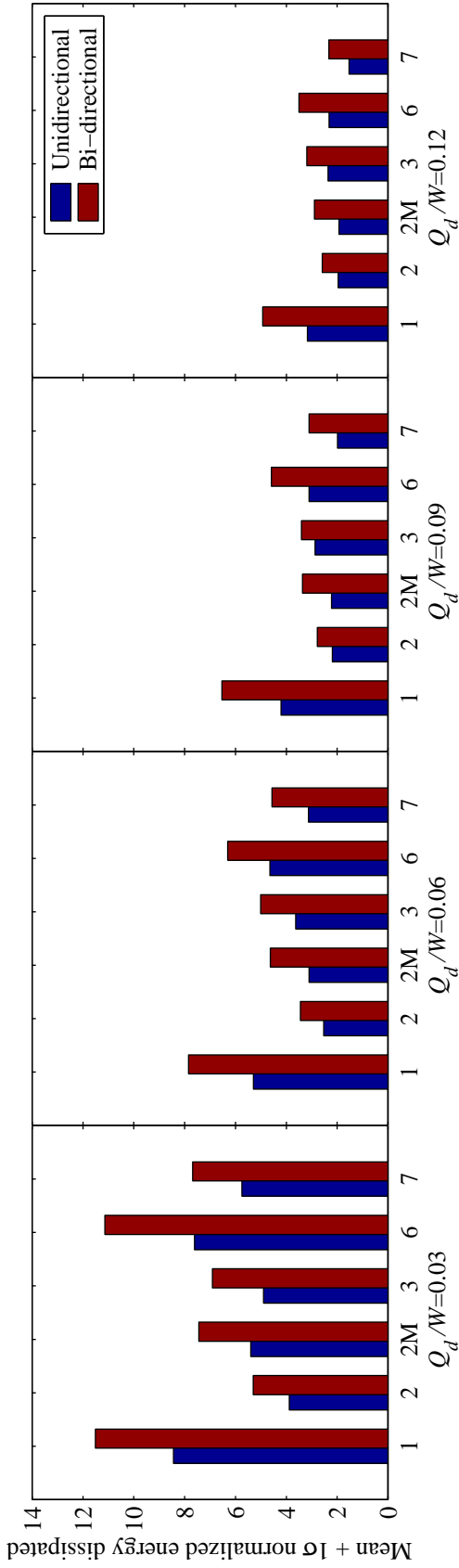


Figure 6.15. Comparison of the mean normalized energy dissipated (NED) calculated for unidirectional and bi-directional excitation considering all values of Q_d/W , $T_d = 2.5$ seconds and $T_d = 3.0$ seconds, for ground motion bins 1, 2, 2M, 3, 6, and 7.

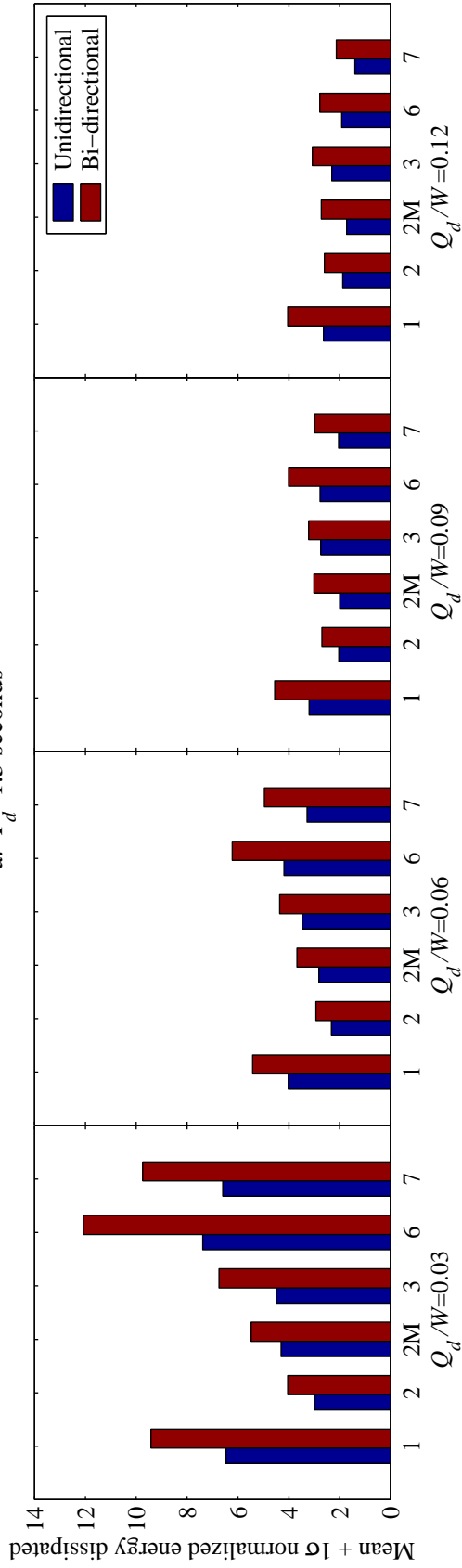


a. $T_d=4.0$ seconds

Figure 6.16. Comparison of the mean normalized energy dissipated (NED) calculated for unidirectional and bi-directional excitation considering all values of Q_d/W , and $T_d=4.0$ seconds, for ground motion bins 1, 2, 2M, 3, 6, and 7.



a. $T_d = 1.5$ seconds



b. $T_d = 2.0$ seconds

Figure 6.17. Comparison of the mean + 1σ normalized energy dissipated (NED) calculated for unidirectional and bi-directional excitation considering all values of Q_d/W , $T_d = 1.5$ seconds and $T_d = 2.0$ seconds, for ground motion bins 1, 2, 2M, 3, 6, and 7.

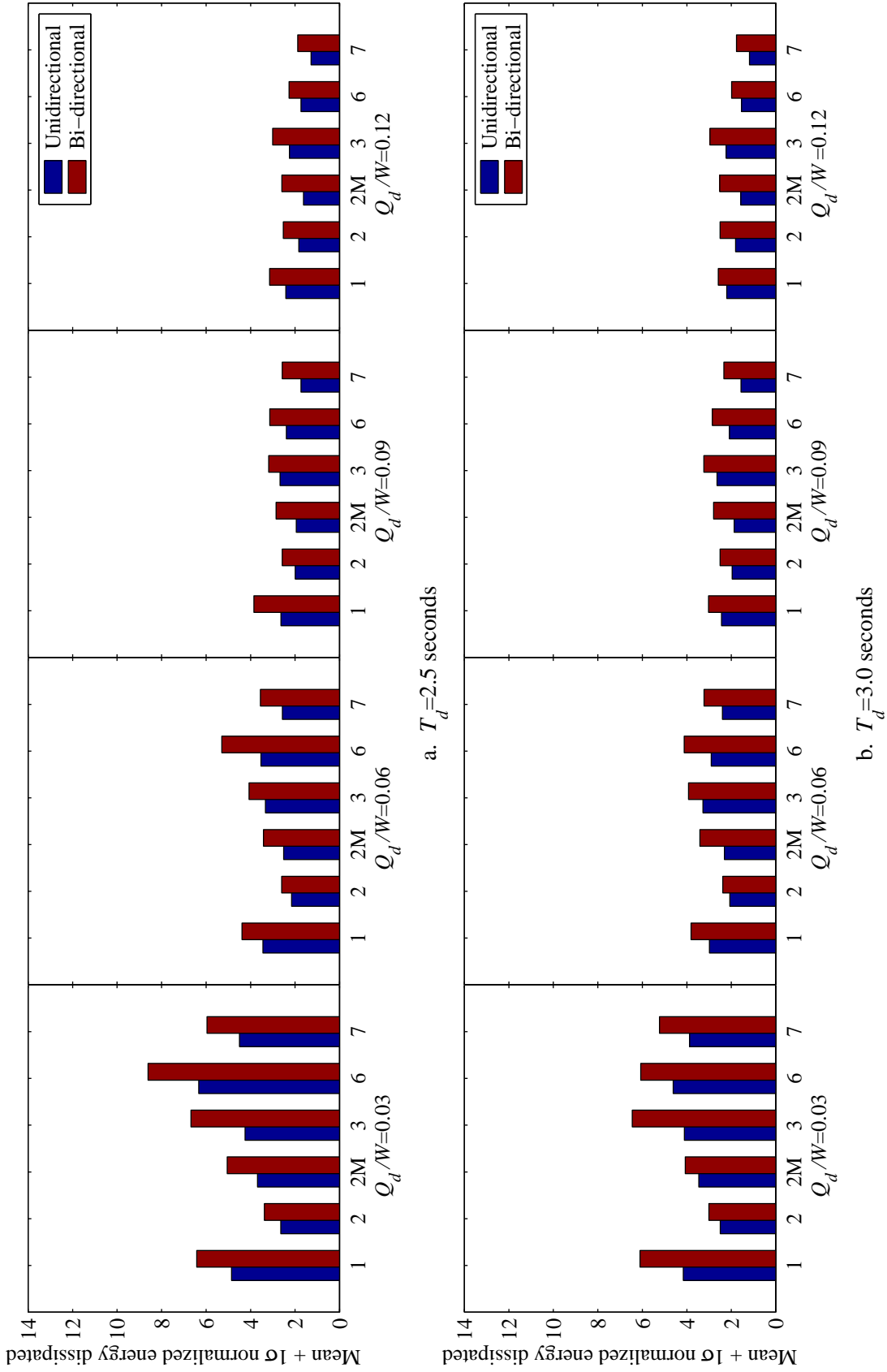
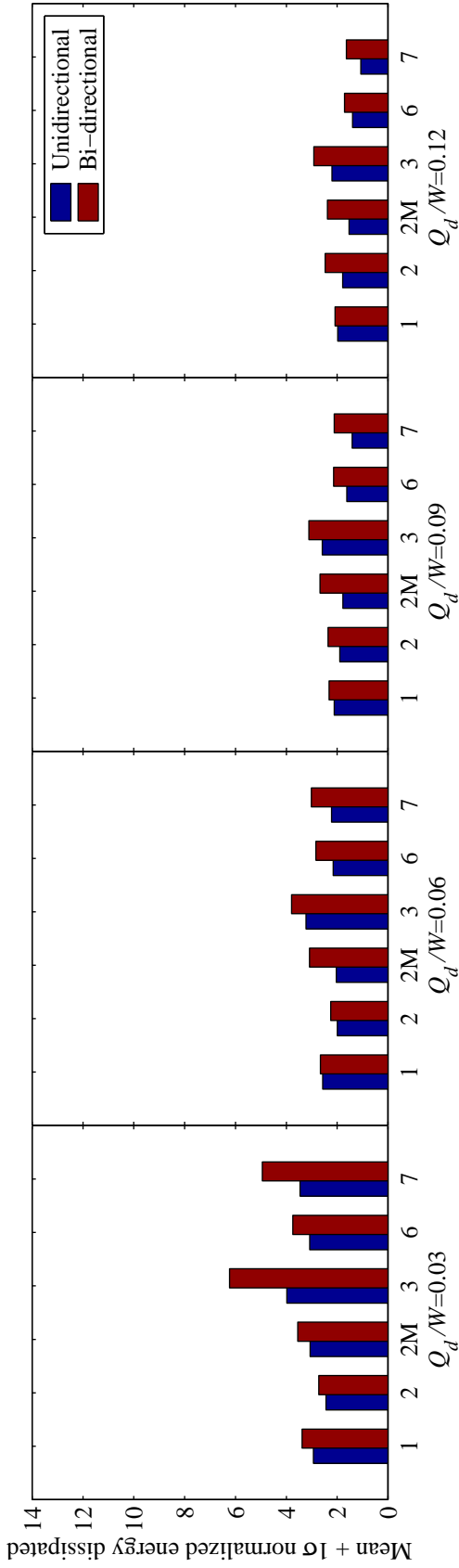


Figure 6.18. Comparison of the mean + 1σ normalized energy dissipated (NED) calculated for unidirectional and bi-directional excitation considering all values of Q_d/W , $T_d=2.5$ seconds and $T_d=3.0$ seconds, for ground motion bins 1, 2, 2M, 3, 6, and 7.



a. $T_d=4.0$ seconds

Figure 6.19. Comparison of the mean + 1σ normalized energy dissipated (NED) calculated for unidirectional and bi-directional excitation considering all values of Q_d/W , $T_d=4.0$ seconds, for ground motion bins 1, 2, 2M, 3, 6, and 7.

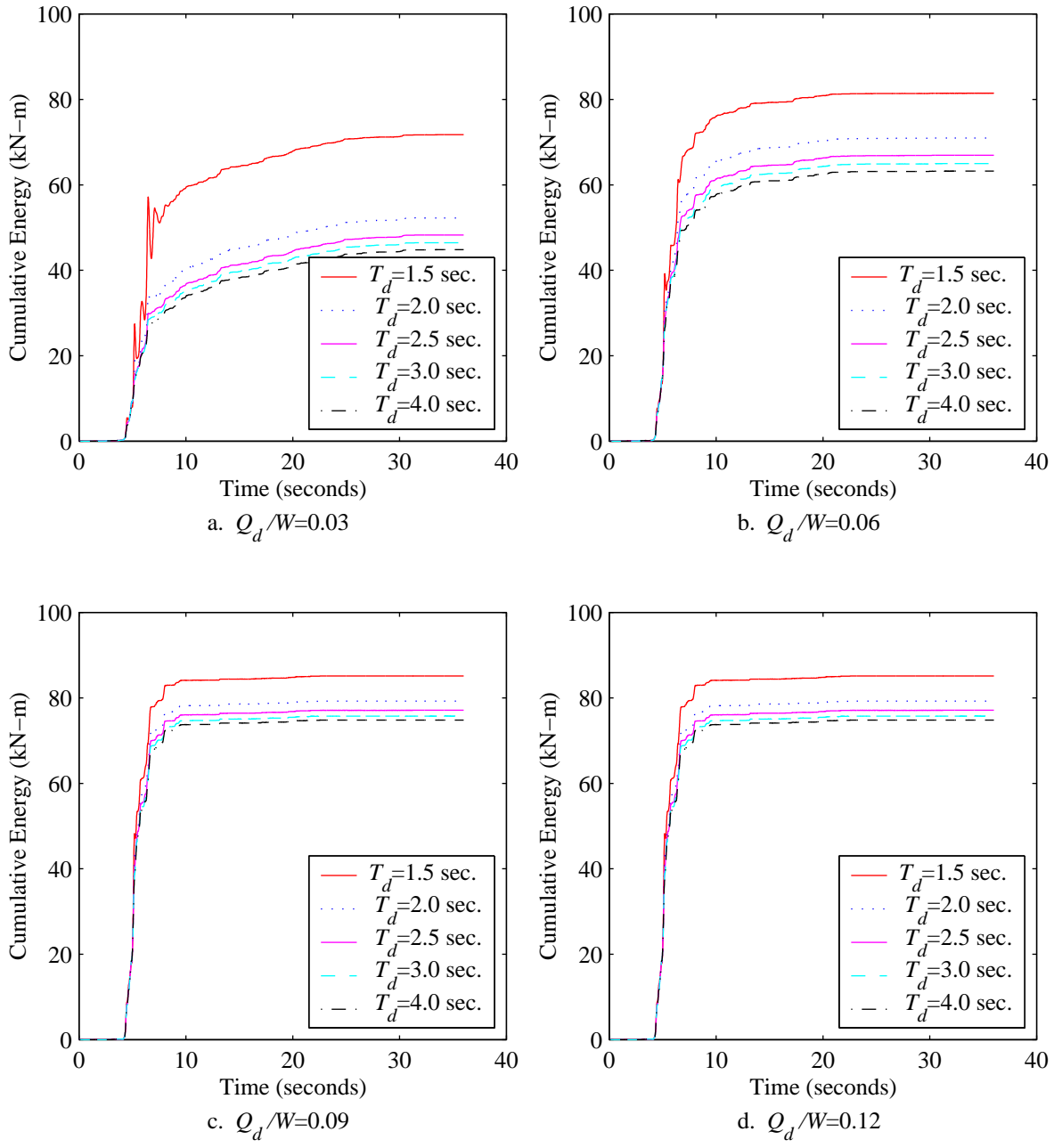
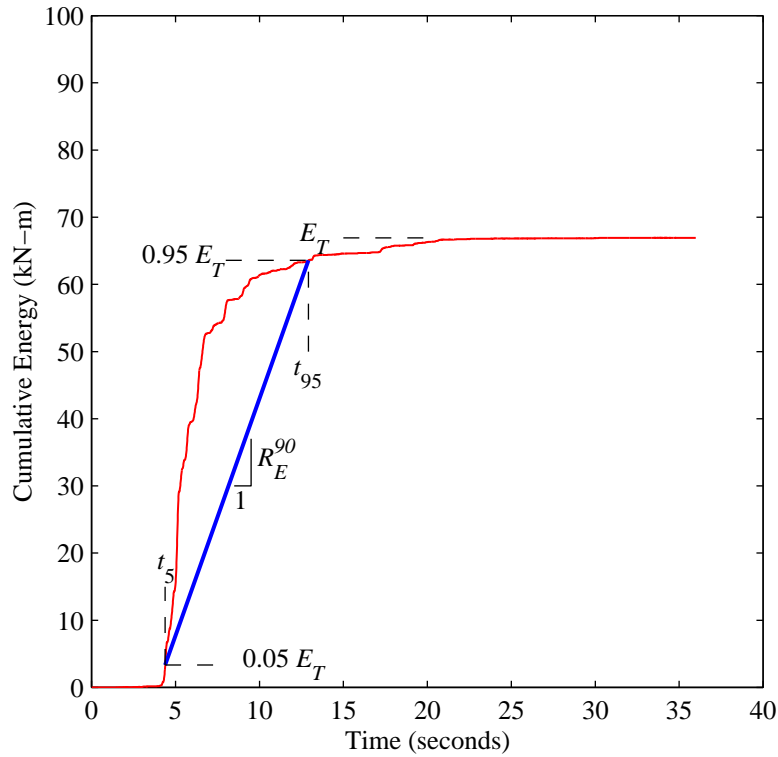
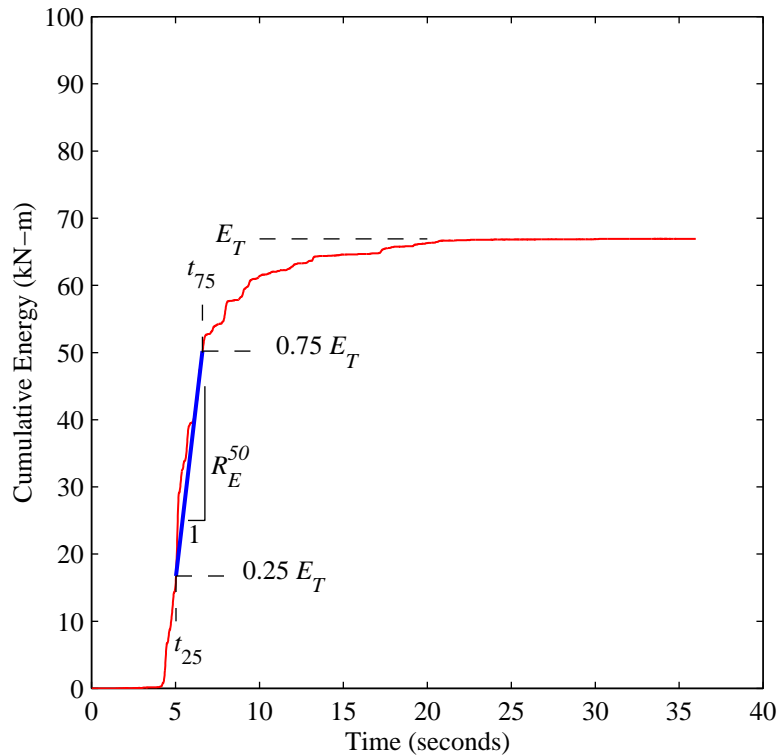


Figure 6.20. Sample energy history results from unidirectional response-history analysis performed using a ground motion record from the Cape Mendocino earthquake, Rio Dell Over Pass station (RIO360), incorporated into Bin 2M.



a. rate-of-energy dissipated, *Definition 1* (R_E^{90})



b. rate-of-energy dissipated, *Definition 2* (R_E^{50})

Figure 6.21. Two definitions for the rate-of-energy dissipated by a seismic isolator (R_E) using a sample energy history calculated considering isolator properties: $Q_d/W=0.06$ and $T_d=2.5$ sec., and ground motion RIO360 from Bin 2M.

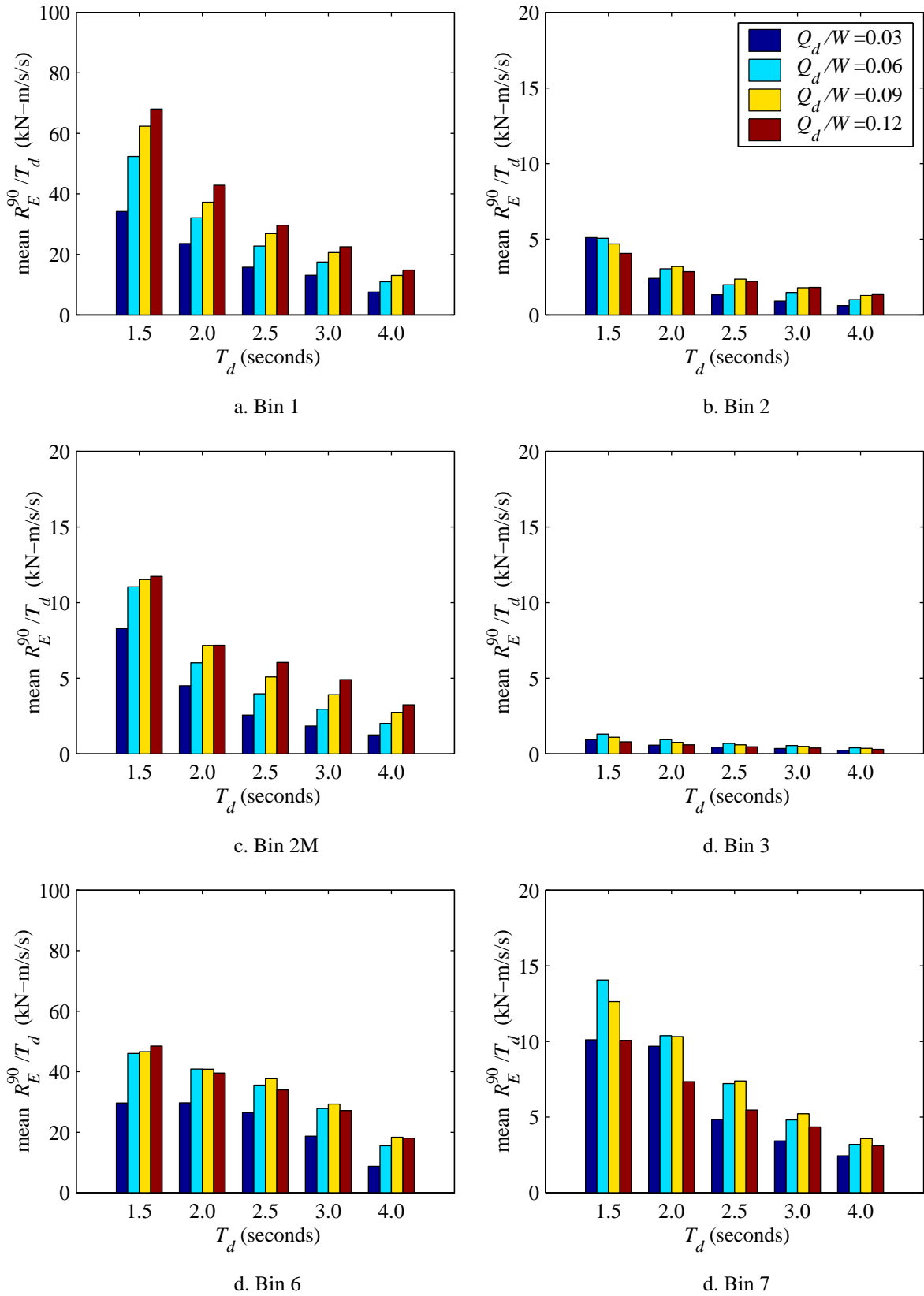


Figure 6.22. Normalized rate-of-energy dissipated calculated using *Definition 1* (R_E^{90}) and the results of unidirectional response-history analysis.

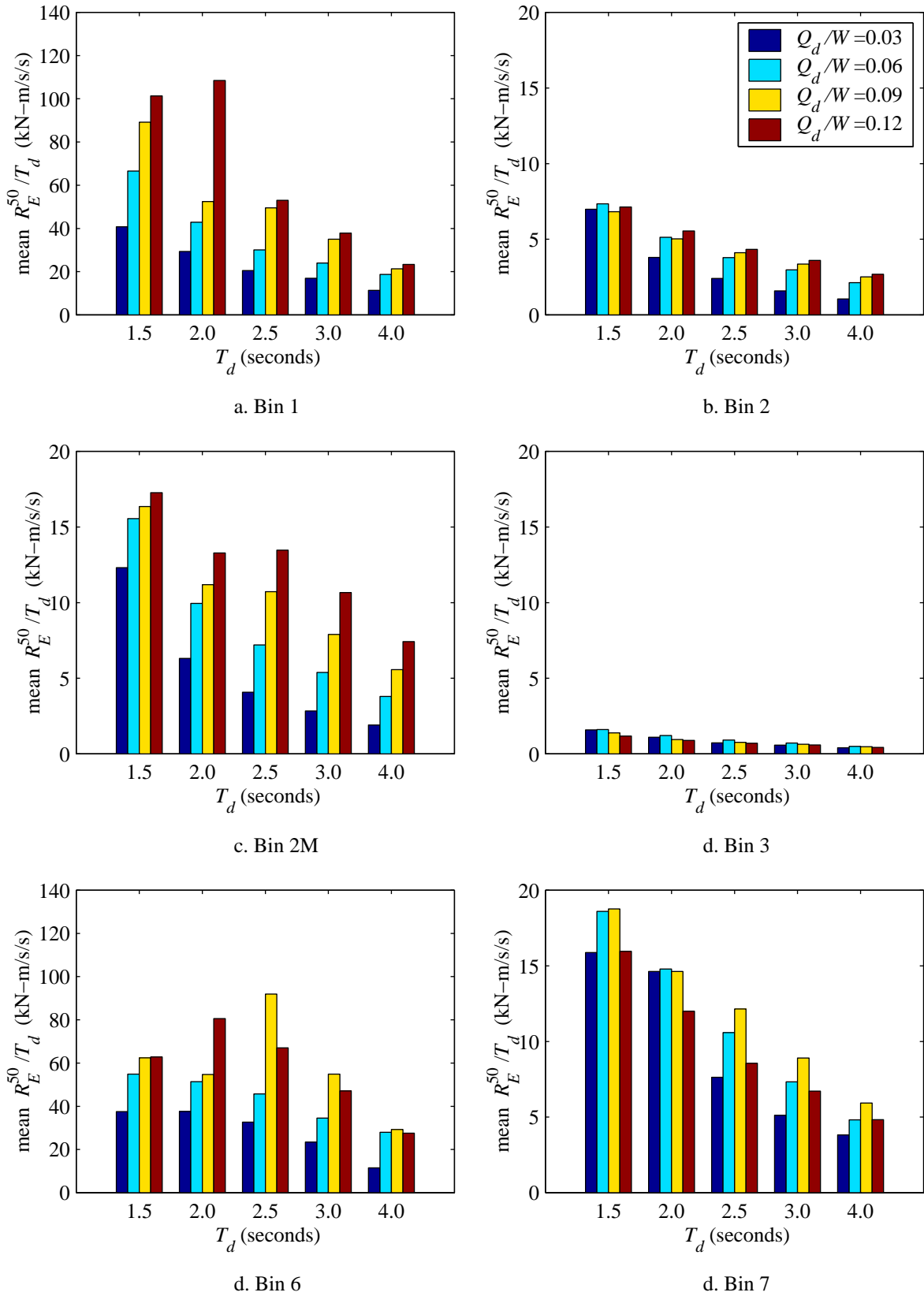


Figure 6.23. Normalized rate-of-energy dissipated calculated using *Definition 2* (R_E^{50}) and the results of unidirectional response-history analysis.

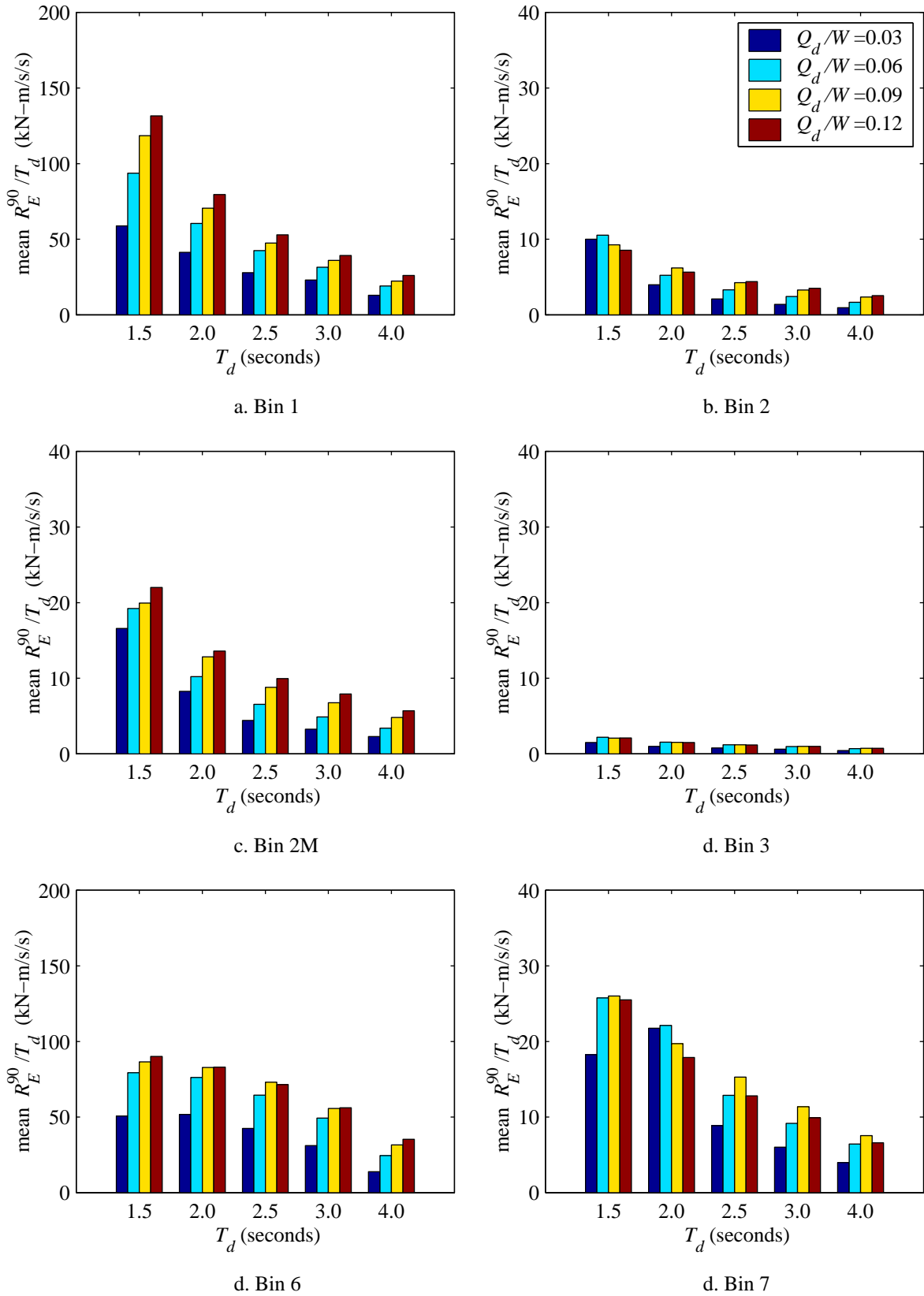


Figure 6.24. Normalized rate-of-energy dissipated calculated using *Definition 1* (R_E^{90}) and the results of bi-directional response-history analysis.

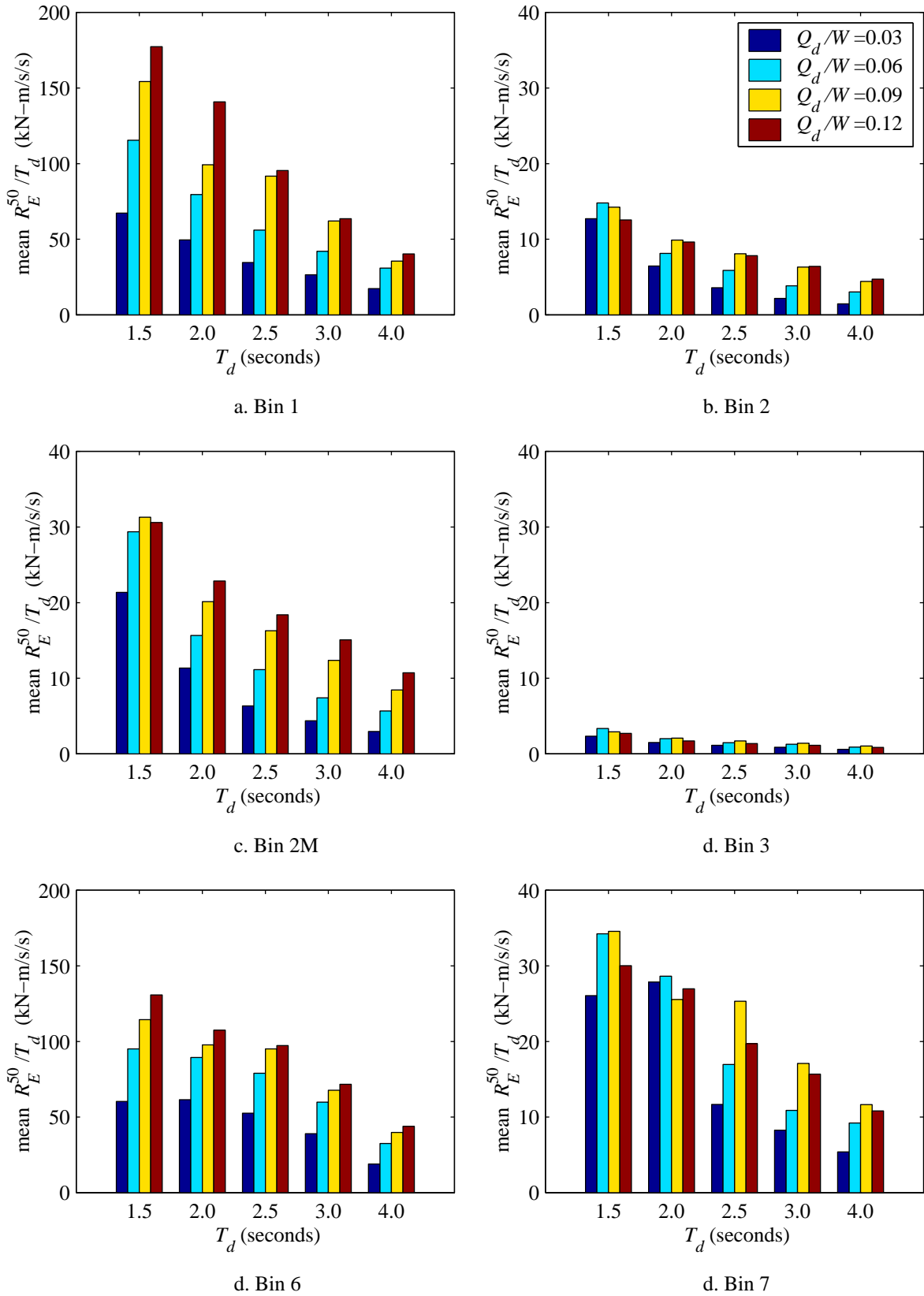


Figure 6.25. Normalized rate-of-energy dissipated calculated using *Definition 2* (R_E^{50}) and the results of bi-directional response-history analysis.

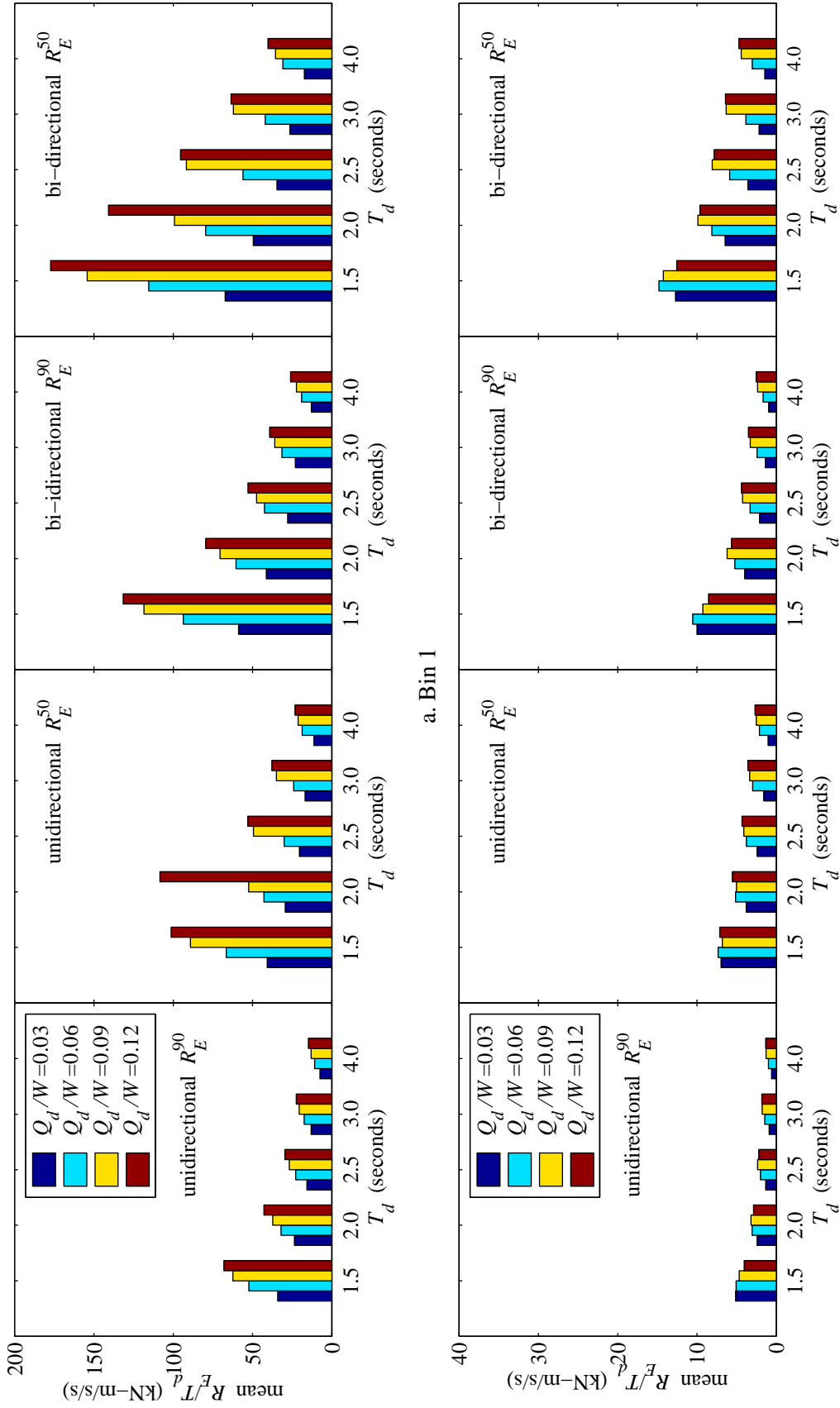


Figure 6.26. Comparison of mean normalized rate-of-energy dissipated (R_E^{90} and R_E^{50}) data calculated using two definitions (R_E^{90} and R_E^{50}) and the results of unidirectional and bi-directional response-history analysis considering ground motion bins 1 and 2.

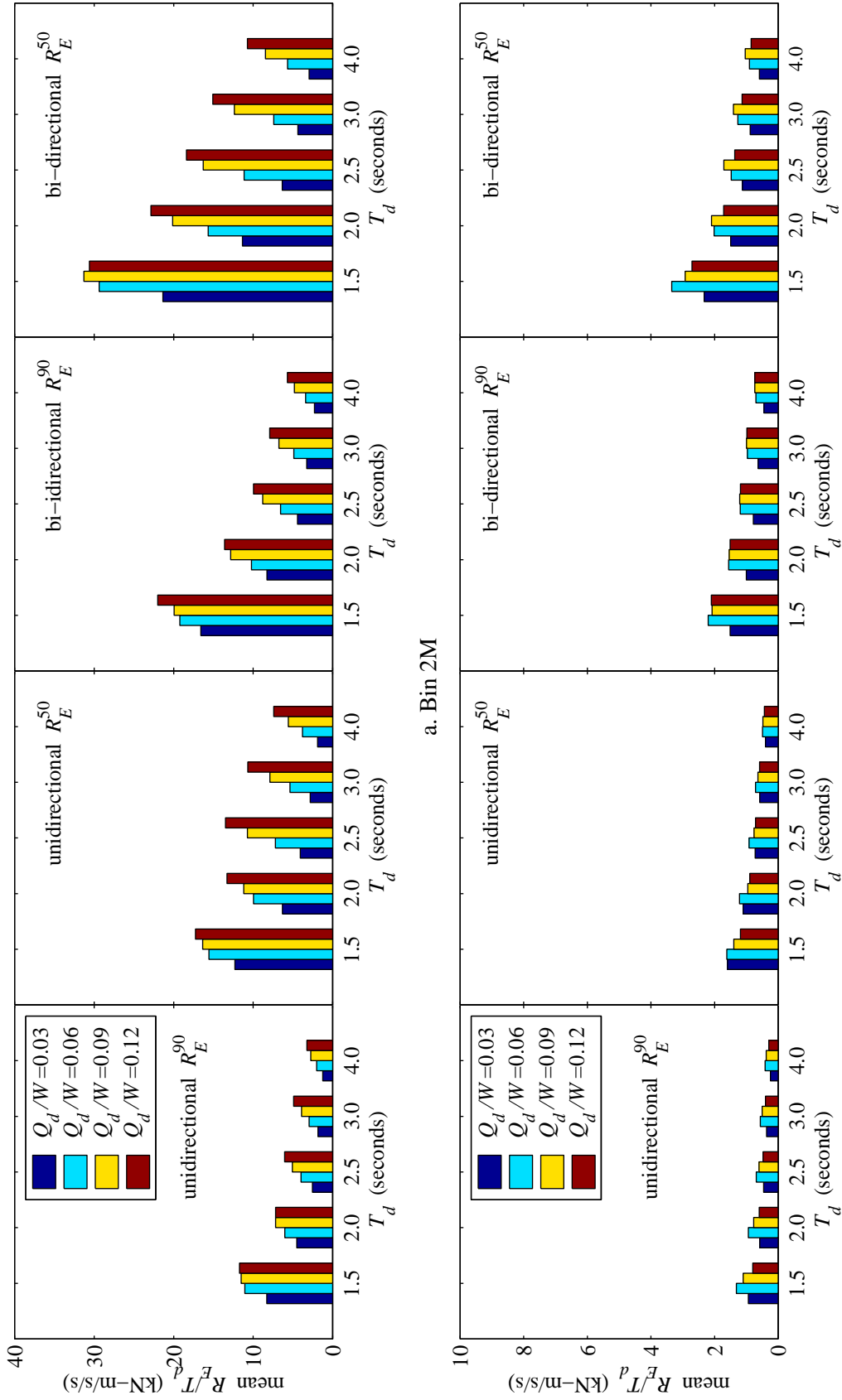
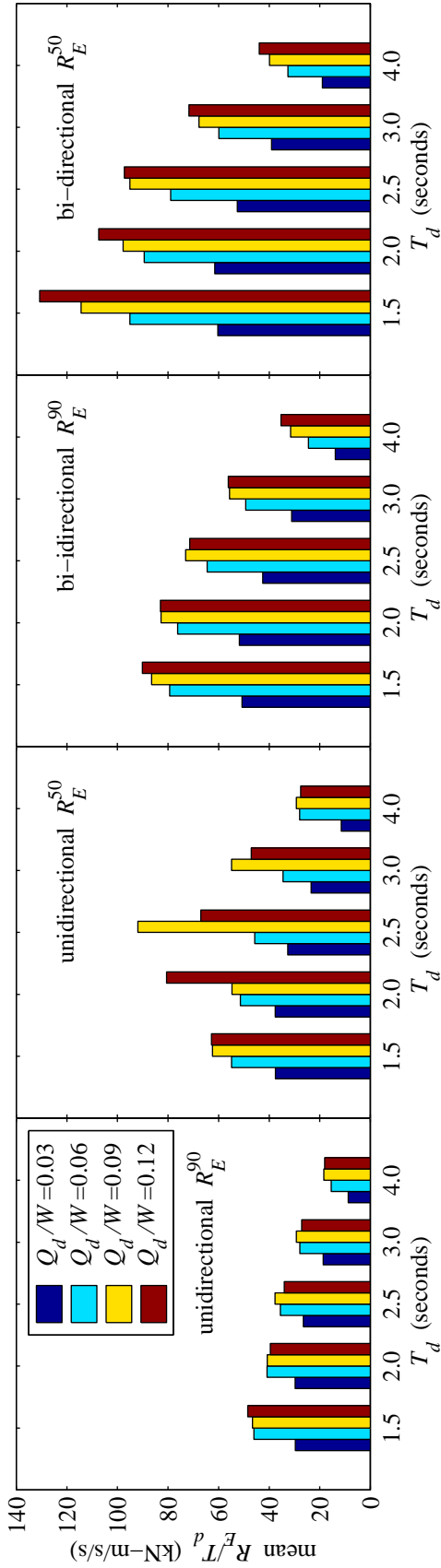
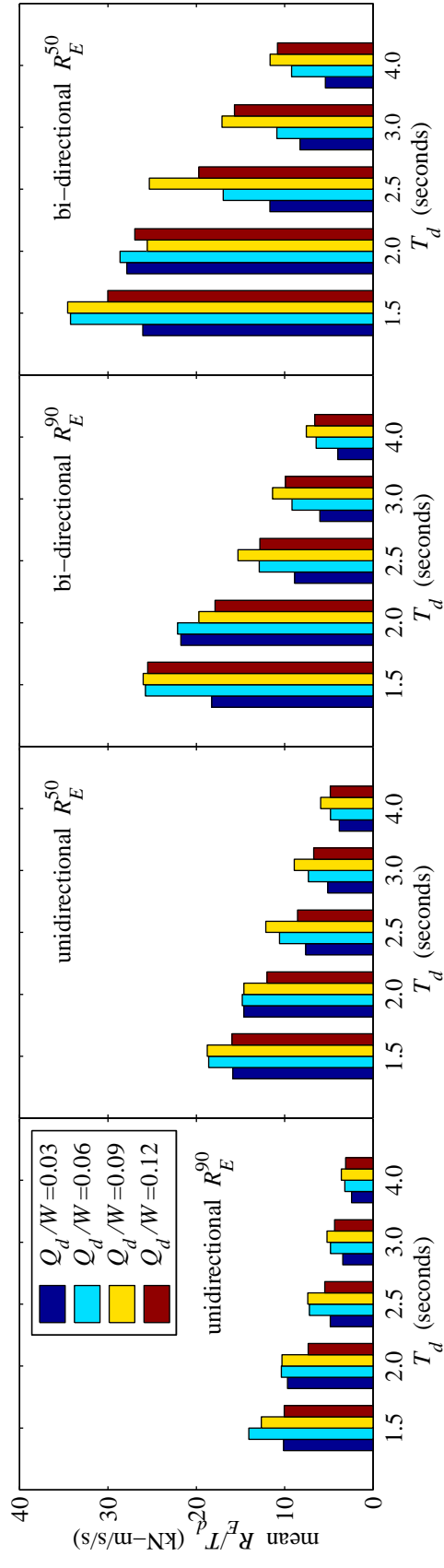


Figure 6.27. Comparison of mean normalized rate-of-energy dissipated (R_E^{90} and R_E^{50}) data calculated using two definitions (R_E^{90} and R_E^{50}) and the results of unidirectional and bi-directional response-history analysis considering ground motion bins 2M and 3.



a. Bin 6



b. Bin 7

Figure 6.28. Comparison of mean normalized rate-of-energy dissipated (R_E^{90} and R_E^{50}) and the results of unidirectional and bi-directional response-history analysis considering ground motion bins 6 and 7.

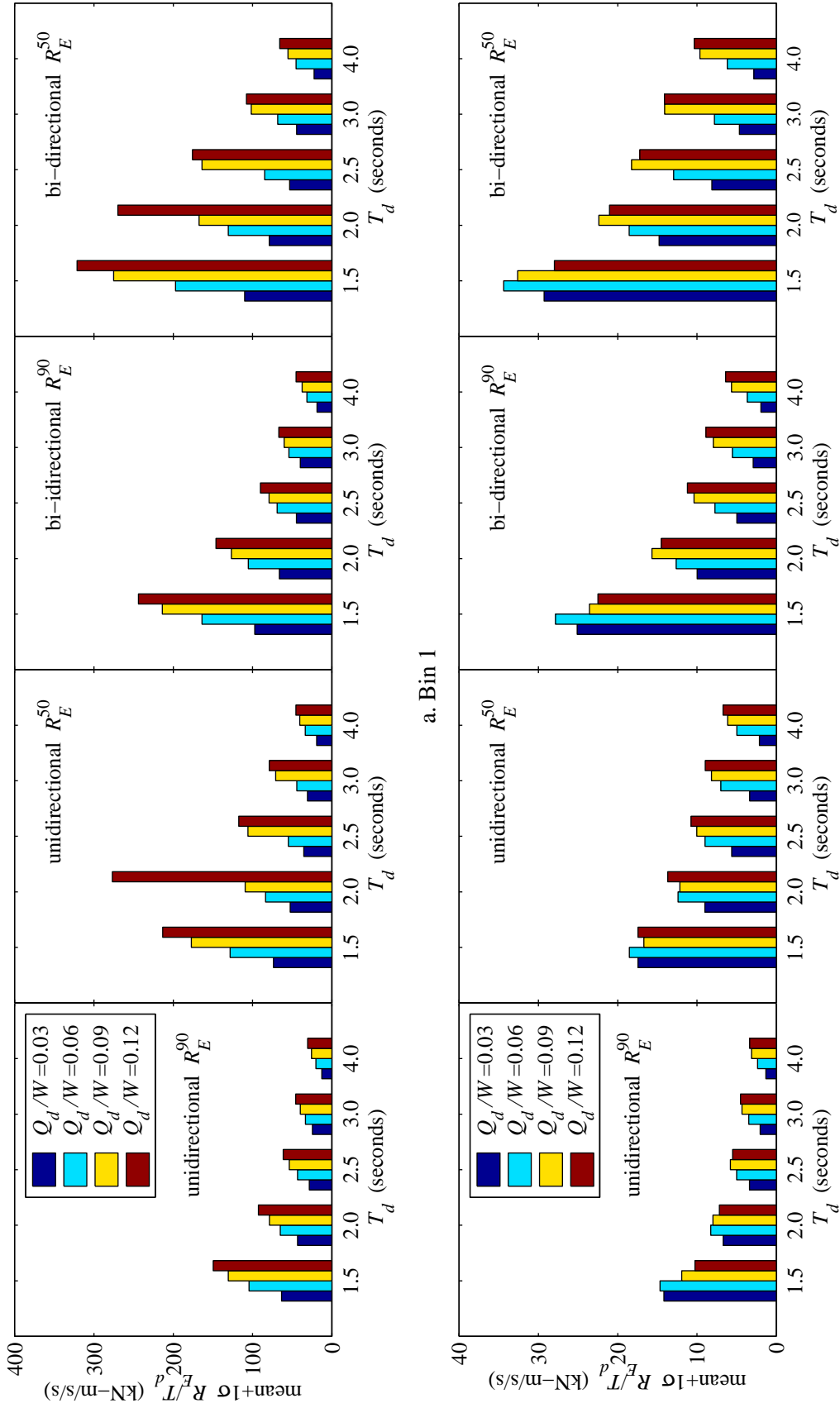


Figure 6.29. Comparison of mean+1σ normalized rate-of-energy dissipated (R_E^{90} and R_E^{50}) data calculated using two definitions (R_E^{90} and R_E^{50}) and the results of unidirectional and bi-directional analysis considering ground motion bins 1 and 2.

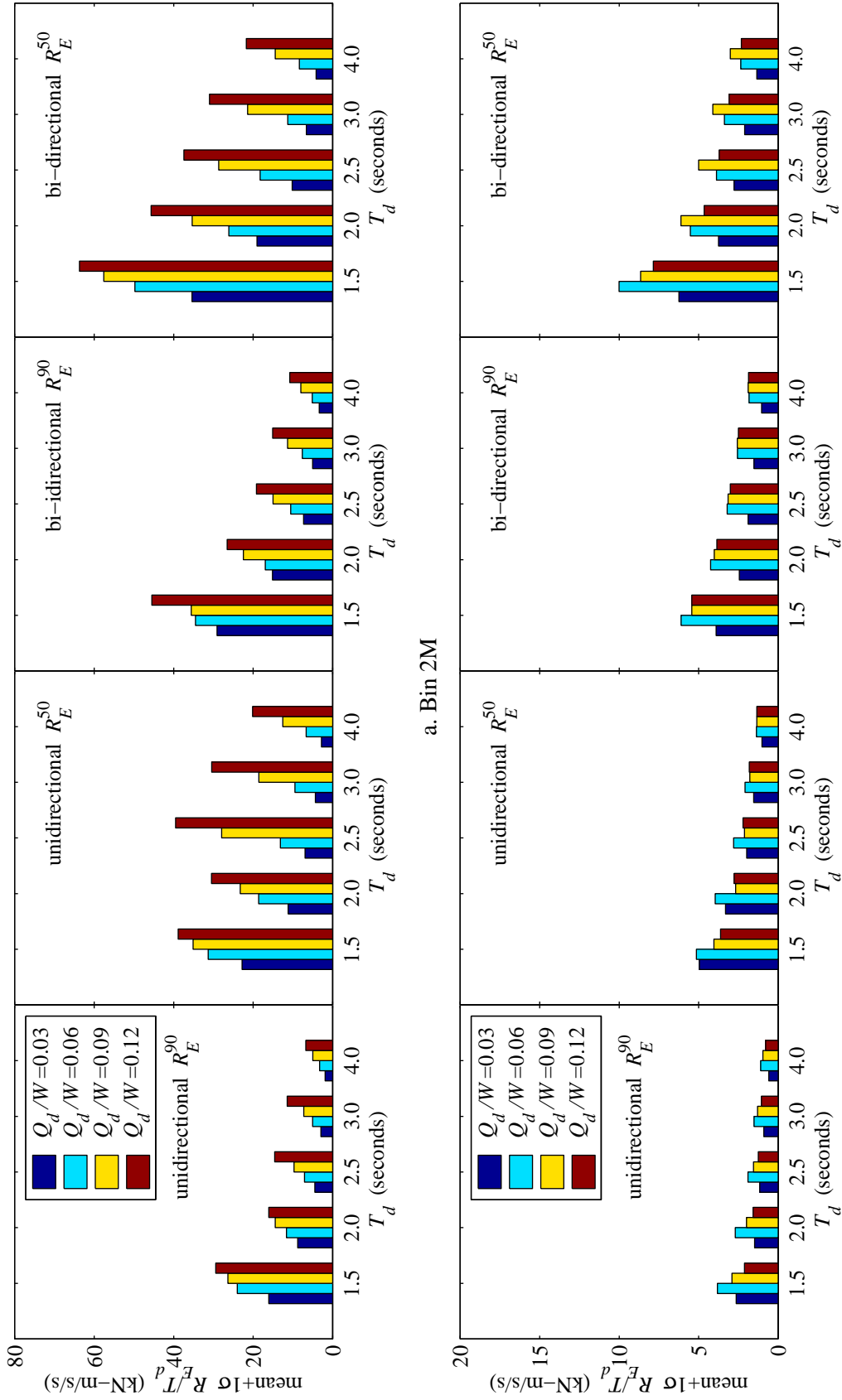
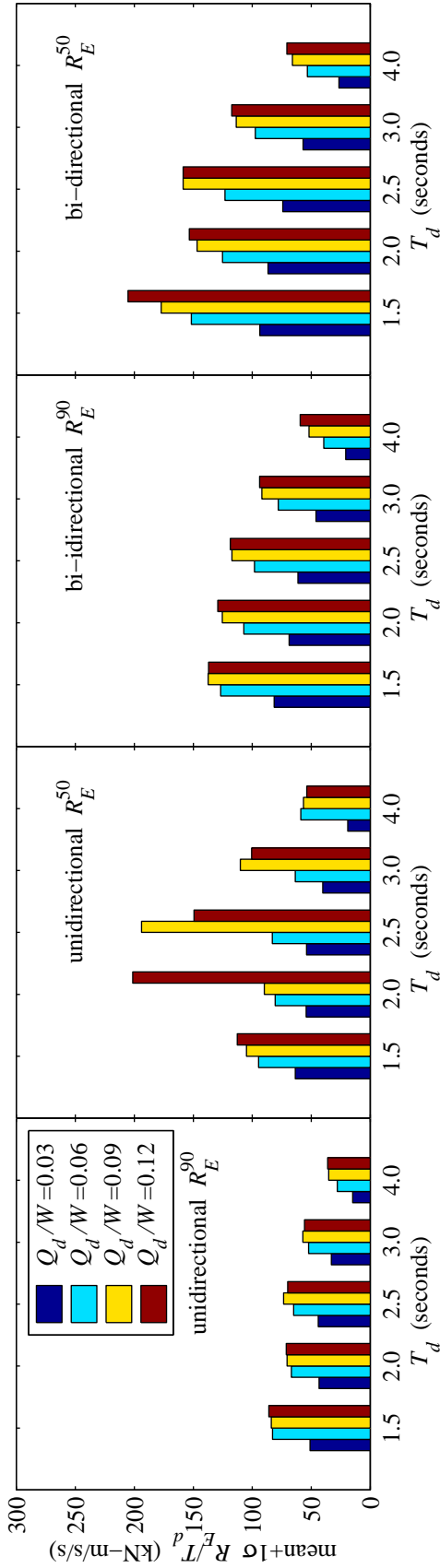
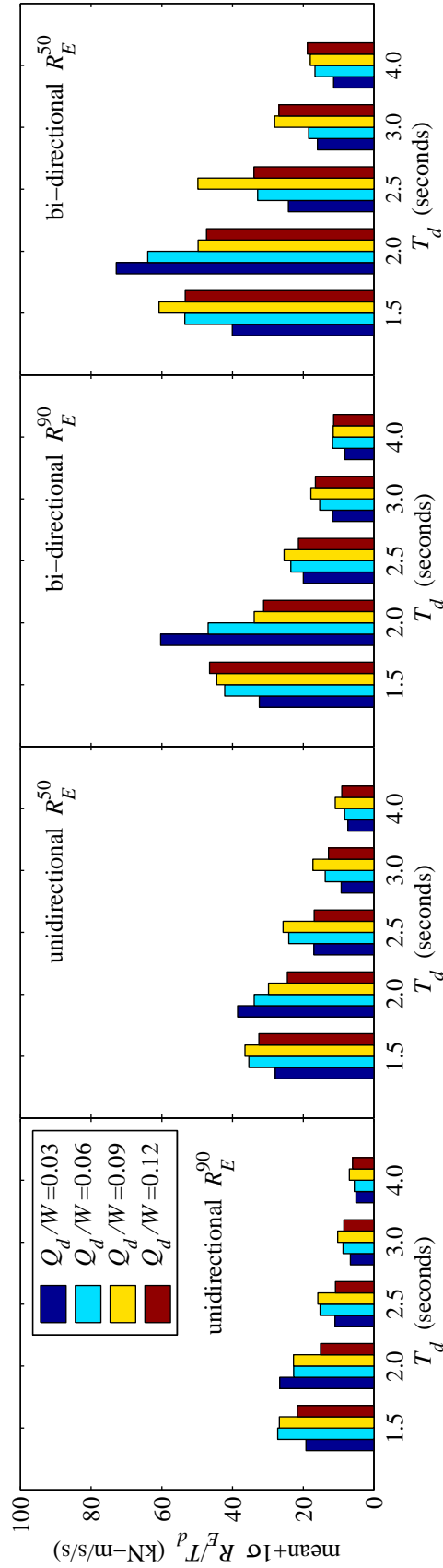


Figure 6.30. Comparison of mean+1σ normalized rate-of-energy dissipated (R_E^{90} and R_E^{50}) data calculated using two definitions (R_E^{90} and R_E^{50}) and the results of unidirectional and bi-directional response-history analysis considering ground motion bins 2M and 3.

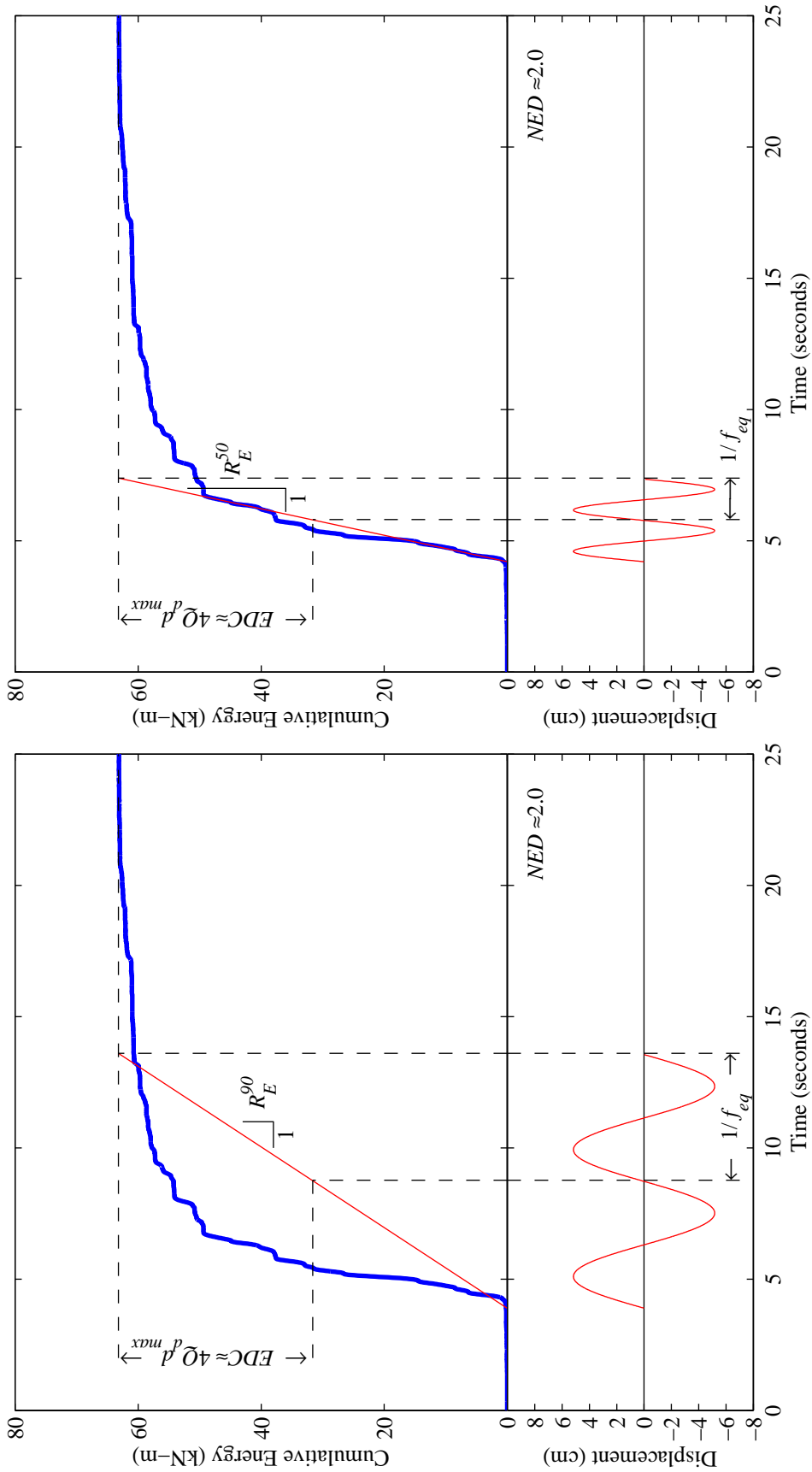


a. Bin 6



b. Bin 7

Figure 6.31. Comparison of mean+1 σ normalized rate-of-energy dissipated (R_E^{90} and R_E^{50}) and the results of unidirectional and bi-directional response-history analysis considering ground motion bins 6 and 7.



a. f_{eq} using R_E^{90}

b. f_{eq} using R_E^{50}

Figure 6.32. Schematic of the equivalent frequency (f_{eq}) determined using two definitions of the rate-of-energy (R_E) dissipated for isolator properties: $Q_d/W=0.06$ and $T_d=4.0$ seconds and ground motion record RIO360 from Bin 2M.

SECTION 7

SUMMARY, CONCLUSIONS, AND RECOMMENDATIONS

7.1 Summary

The design of seismic isolation systems for bridge structures in the United States is governed by the American Association of State Highway and Transportation Officials (AASHTO) Guide Specification for Seismic Isolation Design (AASHTO, 1999). The Guide Specifications provide procedures for the design of individual seismic isolators and isolation systems, and full-scale testing of seismic isolators. This study investigated key assumptions inherent in the equation for calculation displacements in seismically isolated bridges (Equation 3 of the Guide Specifications). Further, the validity of the current testing protocol for full-scale prototype seismic isolators for seismic loading as specified by the Guide Specifications was investigated.

To facilitate response-history analysis, earthquake ground motions were collected and organized into eight bins: Near-Field (Bin 1); Large Magnitude Small Distance (Bin 2); Modified Large-Magnitude Small Distance (Bin 2M); Large-Magnitude Large Distance (Bin 3); Small-Magnitude Small-Distance (Bin 4); Small-Magnitude Large-Distance (Bin 5); Near-Field Soft-Soil (Bin 6); and Large-Magnitude Soft-Soil (Bin 7). For each bin of ground motions, the seismic hazard was characterized using the mean and median spectrum. Mean and median spectra were utilized for the calculation of the maximum design displacement using the static analysis procedures given by AASHTO (1999). Nonlinear response-history analysis was performed considering a simple isolated bridge model and twenty combinations of isolator properties subjected to unidirectional and bi-directional seismic excitation using 77 pairs of earthquake ground motion records. These properties of the seismic isolators, namely, the characteristic strength normalized by the weight acting on the isolator ($0.03 < Q_d/W < 0.12$) and the second slope-period ($1.5 \text{ seconds} < T_d < 4.0 \text{ seconds}$) were varied widely to represent most bridge isolation systems. The results of the response-history analyses were mined to determine maximum isolator displacements and energy demands imposed on seismic isolators during

maximum earthquake shaking. Energy demands were quantified using two metrics: (1) the total energy dissipated by the seismic isolator normalized by the energy dissipated by one fully reversed cycle to the maximum displacement and (2) the rate-of-energy dissipated.

7.2 Conclusions

The key conclusion of this study are:

- (1) The mean spectrum used to characterized the seismic hazard for ground motion bins 1 through 5 shows that displacements increase linearly over the period range of interest for the design of seismic isolation systems for bridges.
- (2) Maximum displacements calculated using the AASHTO procedure match well the median maximum displacements observed from unidirectional response-history analysis considering ground motion bins representing rock or stiff-soil site conditions, namely, Bin 1 and Bin 2M.
- (3) As expected, maximum displacements calculated using the AASHTO procedure underestimate the median maximum displacements observed from unidirectional response-history analysis considering ground motion bins with soft-soil characteristics, namely, Bin 6 and Bin 7. This underestimation was more prevalent in isolation systems with $Q_d / W \leq 0.06$.
- (4) Maximum displacements calculated using the AASHTO procedure underestimate the median maximum horizontal displacements observed from bi-directional response-history analysis for all isolation systems considered by a factor of 2, 1.8, and 3 for ground motion bins 1, 2M, and 7 respectively.
- (5) Values of the unidirectional displacement multiplier, α_{xy} , indicated that bi-directional seismic excitation results in maximum horizontal displacements that are 1.5 to 2 times larger than those calculated considering unidirectional seismic excitation only. This increase in displacement is a result of two factors,

namely, displacement demand from the orthogonal component and the coupled behavior of the isolator element.

(6) The AASHTO procedure for the prototype testing of seismic isolators for seismic testing impose far greater demands on isolators (in terms of the number of cycles to the maximum displacement) than were observed from numerical simulation of maximum earthquake excitation (i.e, *NED*) considering both unidirectional and bi-directional earthquake excitation.

(7) The use of $1/T_{eff}$ to determine the testing frequency for prototype testing of seismic isolators for seismic loading results in conservative, yet appropriate, power demands on the seismic isolators.

7.3 Recommendations

This sections presents recommendations for future research and recommendations for a testing protocol for prototype seismic isolators.

7.3.1 Future Research

Results of this study suggest that bi-directional seismic excitation increases maximum isolator displacements over those calculated assuming unidirectional excitation. It is therefore important that the displacement calculated using the static analysis procedure presented in the AASHTO Guide Specifications be sufficiently accurate (conservative). One possibility is to modify the current displacement equation (Equation 3) as follows

$$d = \alpha_{xy} \frac{250AS_i T_{eff}}{B} \quad (7.1)$$

where α_{xy} is a displacement multiplier that accounts for: (1) the displacement demand due to the orthogonal component, (2) the coupled behavior of the isolators, and (3) the changes in unidirectional properties, namely, B and T_{eff} ; and $(250AS_i)$ is the hazard representation at 1-second.

In this research study, a modest number of ground motion pairs were included in each ground motion bin. Therefore results are based on sample statistics with a sample set containing 10 or 12 data points. It would be of value to increase the number of ground motion pairs in the ground motion bins, for instance, the Large-Magnitude Small-Distance (Bin 2M) to 20 or 30 such that a thorough statistical analysis could be conducted to determine appropriate values of α_{xy} for each set of isolator parameters (Q_d and T_d).

7.3.2 Prototype Testing Protocol

Based on the results of the investigation of the energy demands imposed on seismic isolators the following *seismic* load testing protocol is recommended. The proposed seismic testing protocol would replace, not supplement, Prototype Tests: 13.2 (b) (3), 13.2 (b) (4), 13.2 (b) (5), and 13.2 (b) (6) of the AASHTO Guide Specifications (1999):

Four (4) fully reversed cycles of sinusoidal loading to the total maximum displacement at a frequency equal to $1/T^*$, where T^* is the effective period of the isolation system at the total design displacement.

SECTION 8

REFERENCES

- AASHTO. (1999). *Guide Specifications for Seismic Isolation Design*. American Association of State Highway and Transportation Officials, Washington, D.C.
- AASHTO. (1996). *Standard Specifications for Highway Bridges*. American Association of State Highway and Transportation Officials, 16th Edition, Washington, D.C.
- AASHTO. (1991). *Guide Specifications for Seismic Isolation Design*. American Association of State Highway and Transportation Officials, Washington, D.C.
- ATC. (1986). *Seismic Design Guidelines for Highway Bridges*. Applied Technology Council, Report 6, Redwood City, CA.
- Benuska, L. (1990). "Loma Prieta Earthquake Reconnaissance Report." *Earthquake Spectra*, EERI, Sup. Volume 6, Chapter 3; Ground motions: 25 – 80.
- Chopra, A. K. (1995). *Dynamics of Structures: Theory and Application to Earthquake Engineering*, Prentice Hall, Upper Saddle River, NJ.
- Chopra, A. K., Chintanapakdee, C. (2001). "Comparing response of SDF systems to near-fault and far-fault earthquake motions in context of spectra region." *Earthquake Engineering and Structural Dynamics*. 30:1769-1789.
- Constantinou, M., Mokha, A., and Reinhorn, A.M. (1990). "Teflon Bearing in Base Isolation II: Modeling." *Journal of Structural Engineering*, ASCE 116(2), 455–474.
- CSI. (2000). *SAP2000 Nonlinear Version 7.4: Structural Analysis Program*. Computers and Structures, Inc., Berkeley, CA.
- CSI. (1997). *SAP2000 Reference Manual*. Computers and Structures, Inc., Berkeley, CA.

- FEMA (2001). *FEMA 368 NEHRP Recommended Provisions for Seismic Regulations for New Buildings and Other Structures, Part 1-Provisions*, Building Seismic Safety Council for the Federal Emergency Management Agency, Washington, D.C.
- Heath, M. T. (2002). *Scientific Computing: An Introductory Survey, (Second Ed.)*, McGraw Hill, New York, NY.
- HITEC. (2002). *Guidelines for Testing Large Seismic Isolators and Energy Dissipation Devices*, Highway Innovative Technology Evaluation Center, CERF Report: #40600.
- Huang, W.H., Fenves, G.L., Whittaker, A.S., and Mahin, S.A. (2000). “Characterization of seismic isolation bearings for bridges from bi-directional testing.” *Proceedings, 12th World Conference on Earthquake Engineering*, New Zealand.
- ICBO. (1997). *Uniform Building Code*, International Conference of Building Officials, Whittier, California.
- Krawinkler, H. (2001). Personal Communication.
- MathWorks (1999). *MatLab Function Reference*. The MathWorks, Inc. Natick, MA.
- Miranda, E. (2002). Personal Communication.
- Miranda, E. (1991) “Seismic evaluation and upgrading of existing buildings.” *Ph.D. Thesis*, University of California, Berkeley, CA.
- Mokha, A.S., Constantionu, M.C., and Reinhorn, A.M. (1993). “Verification of Friction Model of Teflon Bearings Under Triaxial Load.” *Journal of Structural Engineering*, ASCE 119(1), 240–261.
- Mosqueda G., Whittaker, A.S., and Fenves, G.L. (2003). “Characterization and Modeling of Friction Pendulum Bearings Subjected to Multiple Components of Excitation.” *Journal of Structural Engineering*, ASCE, accepted for publication.

- Mosqueda, G., Whittaker, A.S., Fenves, G.L., and Mellon, D. (2002). "Performance characterization of fluid viscous dampers." *Seventh U.S. National Conference on Earthquake Engineering*, Earthquake Engineering Research Institute, Boston, MA.
- Nagarajaiah S., Reinhorn, A. M., and Constantinou, M.C. (1989). "Nonlinear dynamic analysis of three-dimensional base isolated structures-program 3D-BASIS." *Report No. NCEER-89-0019*, Nat. Center for Earthquake Engineering Research, State University of New York, Buffalo, N.Y.
- Newmark, N.M. (1959). "A method of computation for structural dynamics." *Journal of the Engineering Mechanics Division*, ASCE 85(3), 67-94.
- PEER. (2000). *Strong Motion Database*. <<http://peer.berkeley.edu/smcat/>>
- SAC. (1997). *Suites of Earthquake Ground Motions for Analysis of Steel Moment Frame Structure*, Report SAC/BD-97/03, Woodward-Clyde Federal Services, SAC Steel Project.
- Somerville, P. (2000). "Characterization of Near-Fault Ground motions." *U.S. – Japan Workshop on the Effects of Near-Field Earthquake Shaking*, Pacific Earthquake Engineering Research Center, San Francisco, CA.
- Soong, T.T. (1981). *Probabilistic Modeling and Analysis in Science and Engineering*, John Wiley & Sons, New York, NY.

APPENDIX A

EARTHQUAKE GROUND MOTION RECORDS

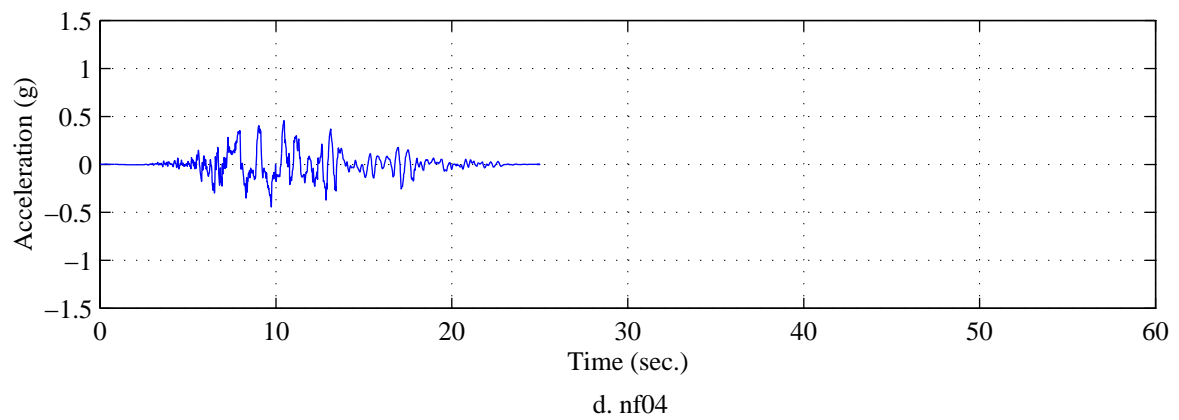
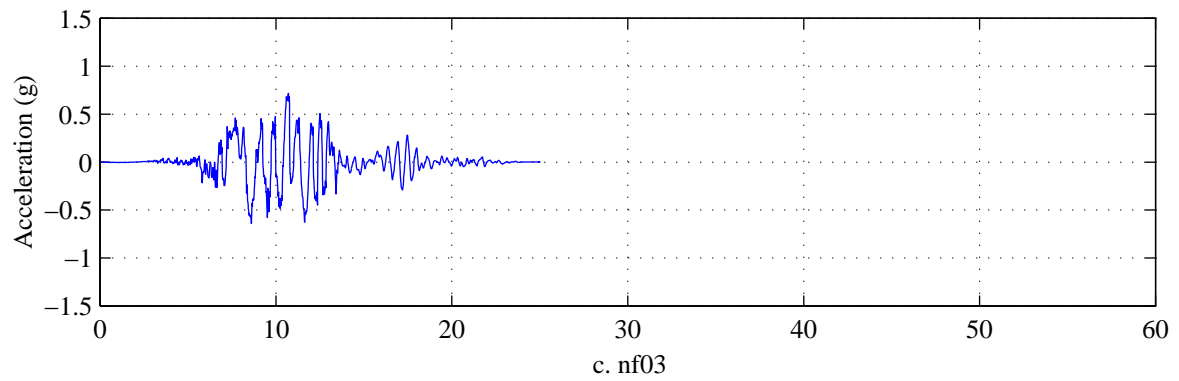
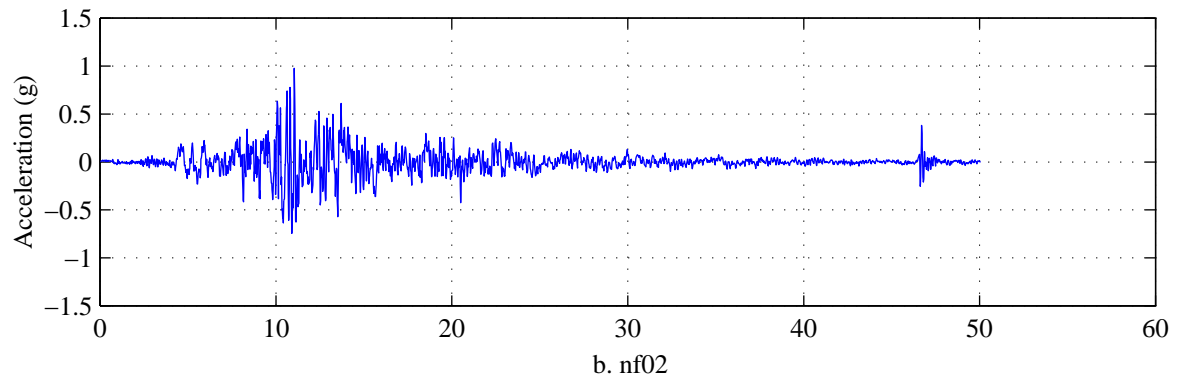
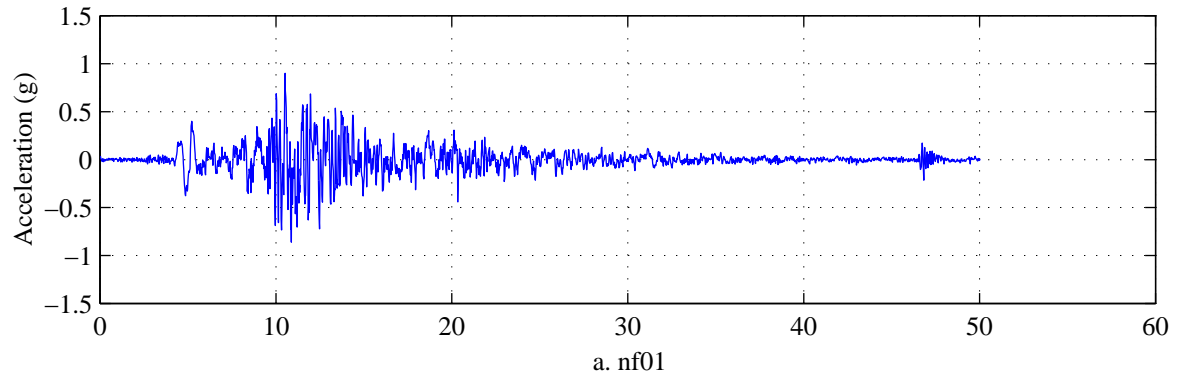


Figure A.1. Ground acceleration time histories from Bin 1.

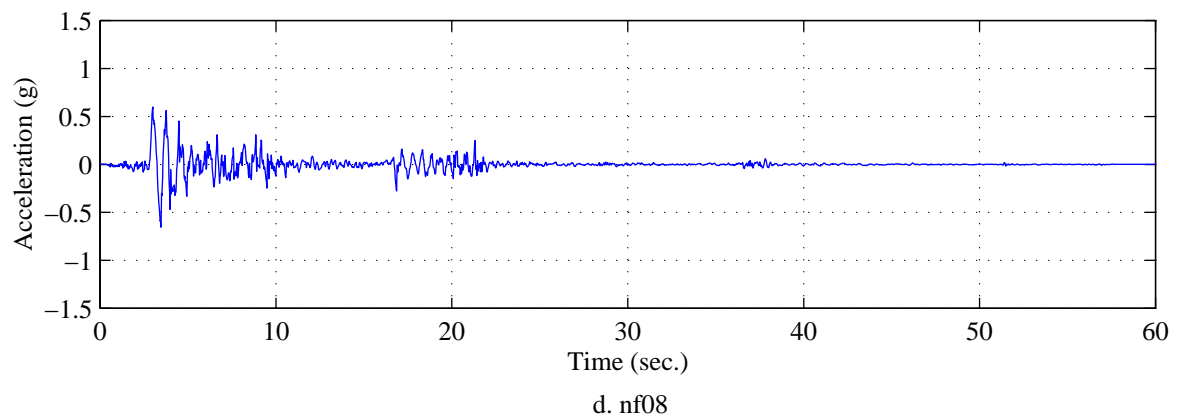
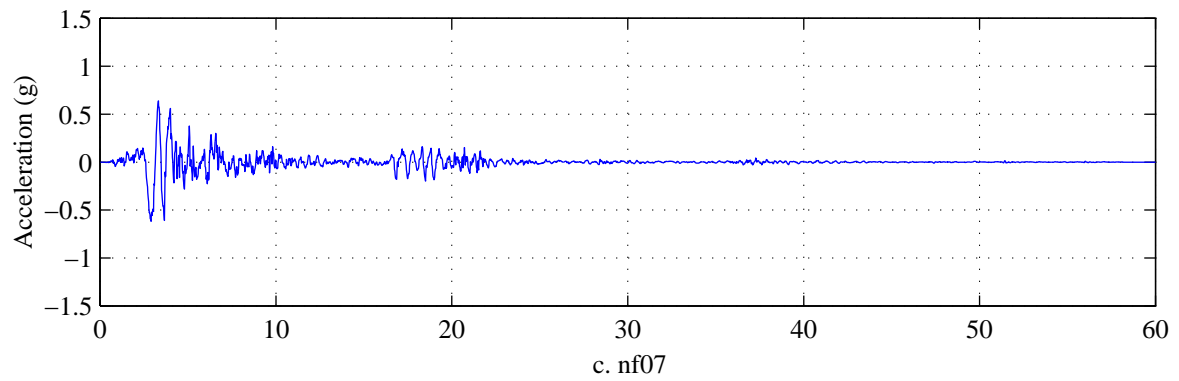
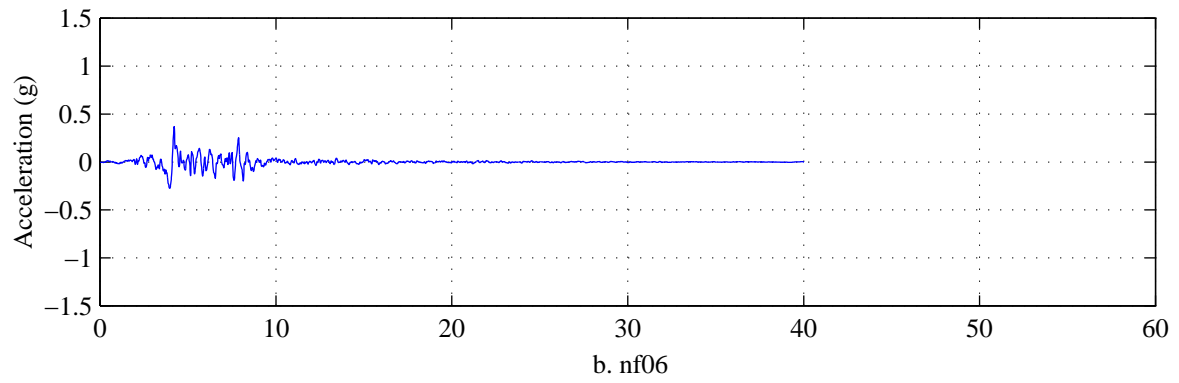
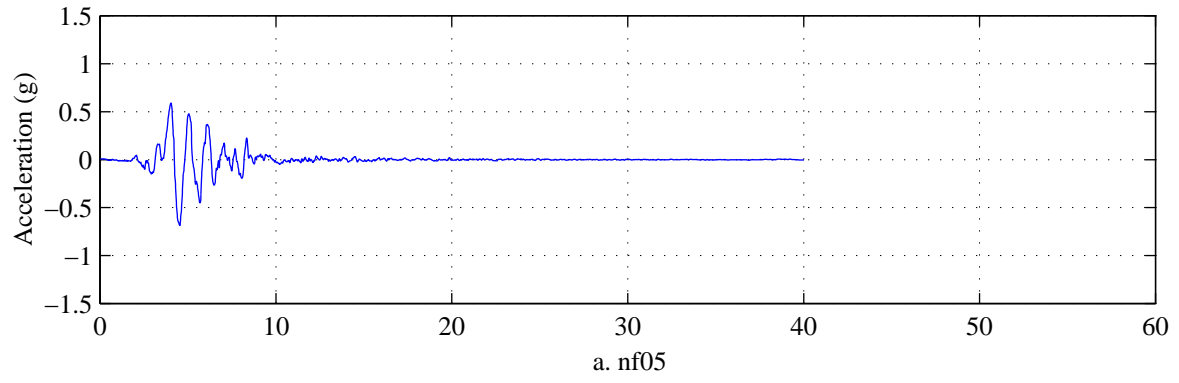


Figure A.2. Ground acceleration time histories from Bin 1.

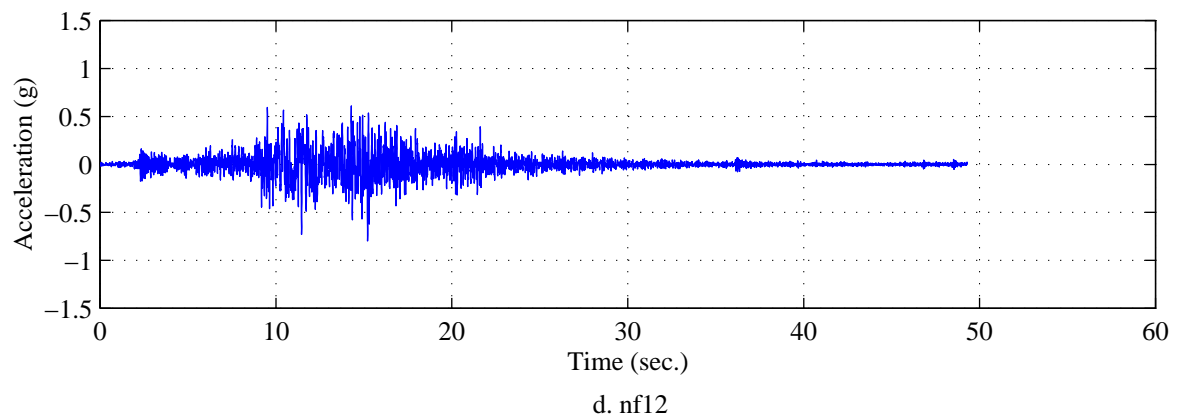
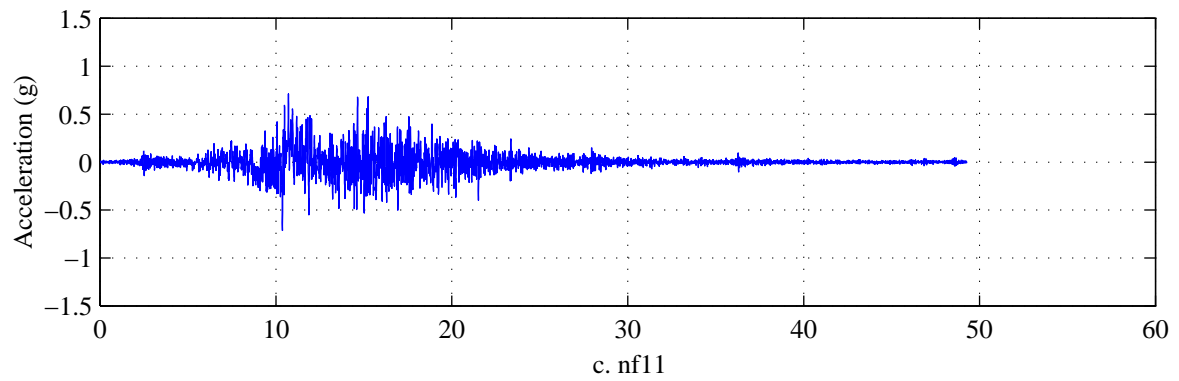
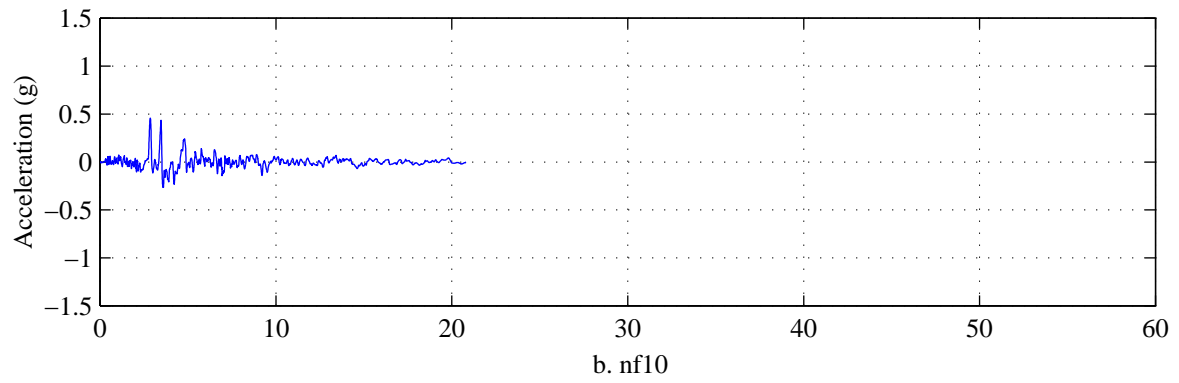
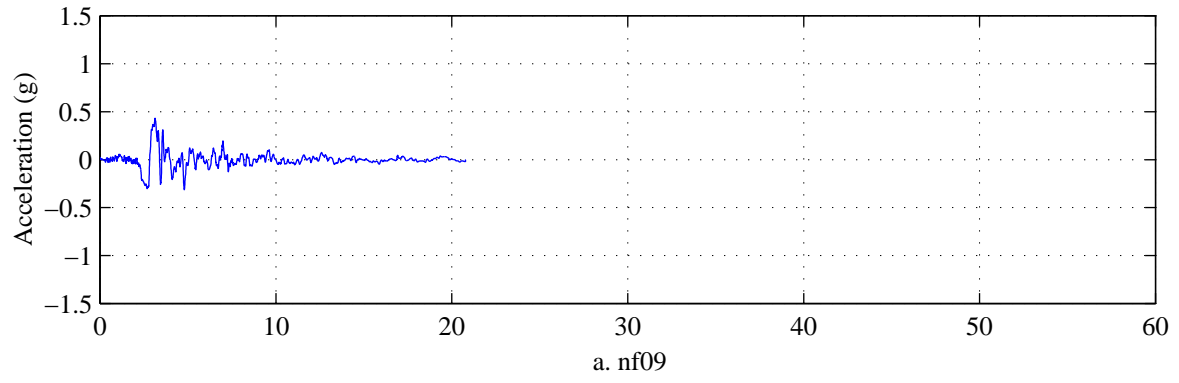


Figure A.3. Ground acceleration time histories from Bin 1.

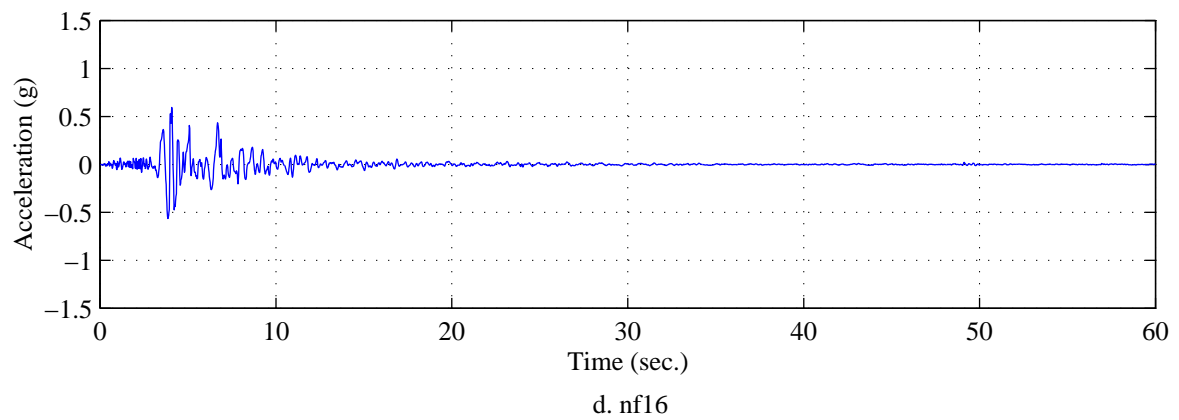
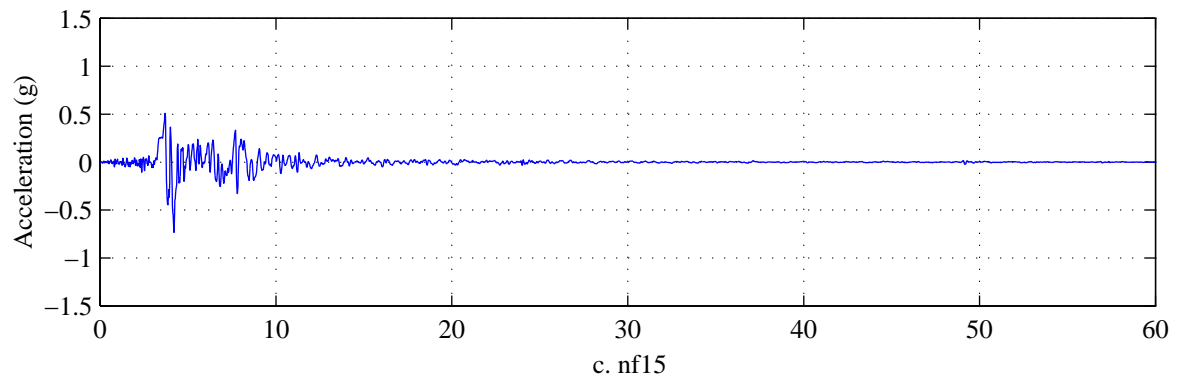
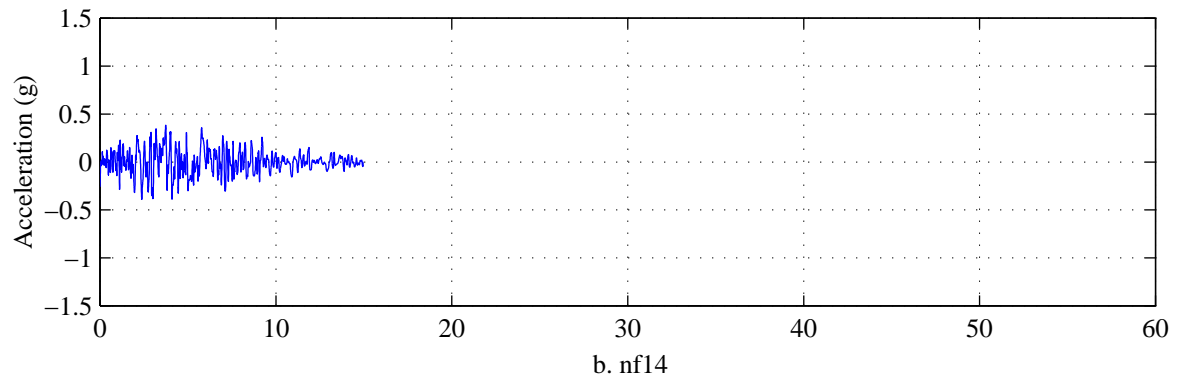
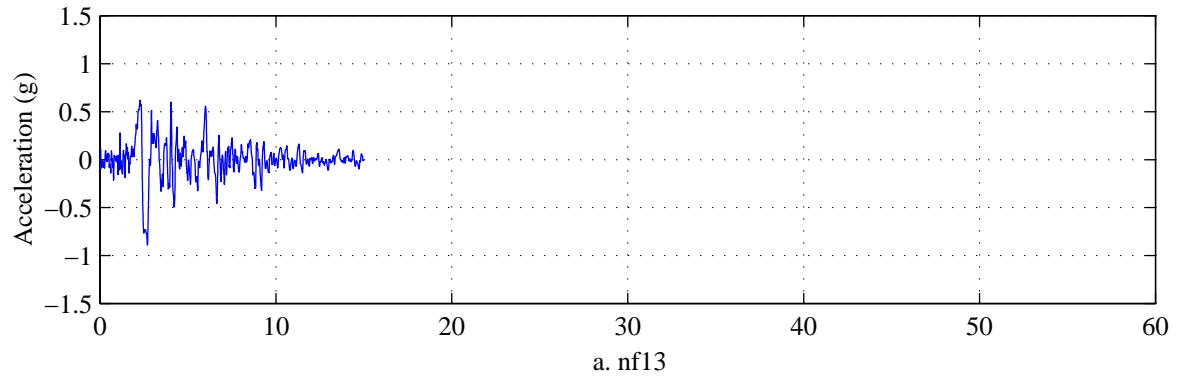


Figure A.4. Ground acceleration time histories from Bin 1.

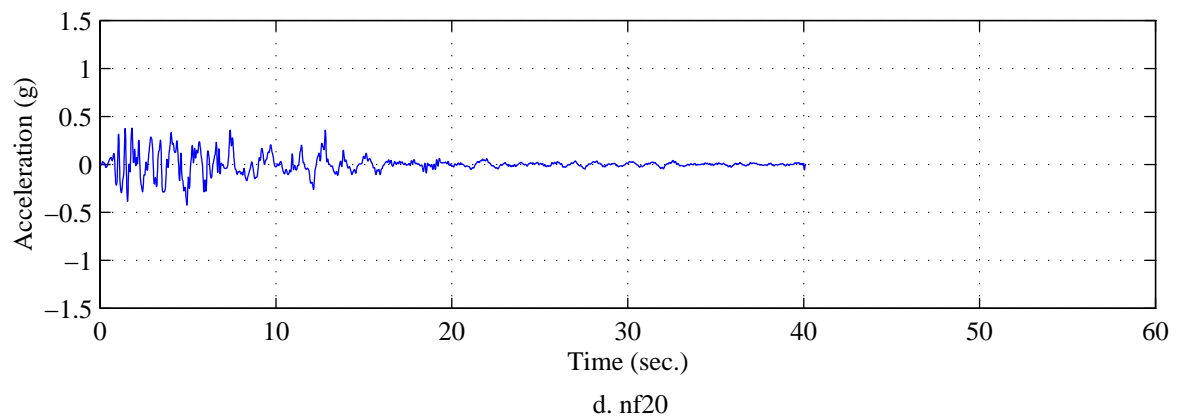
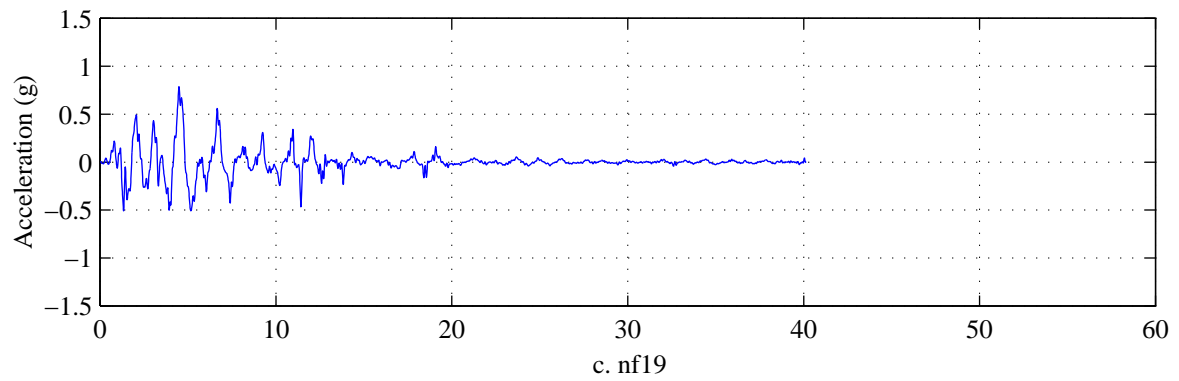
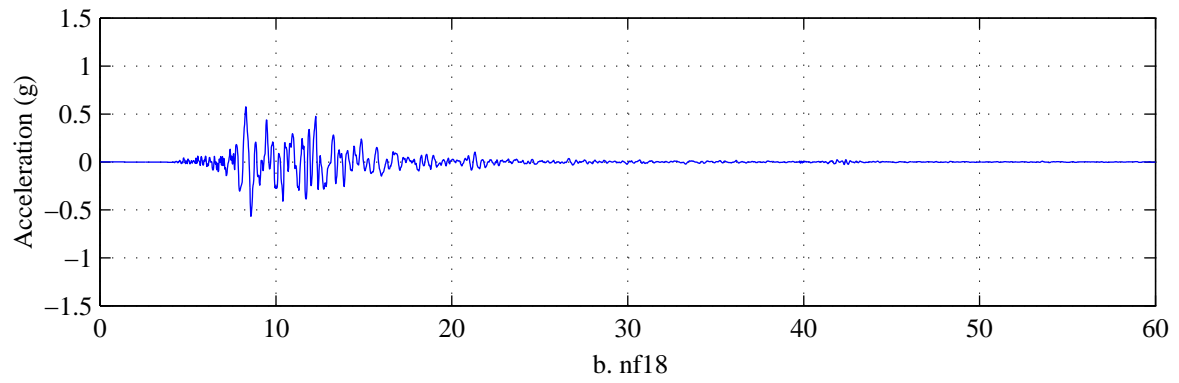
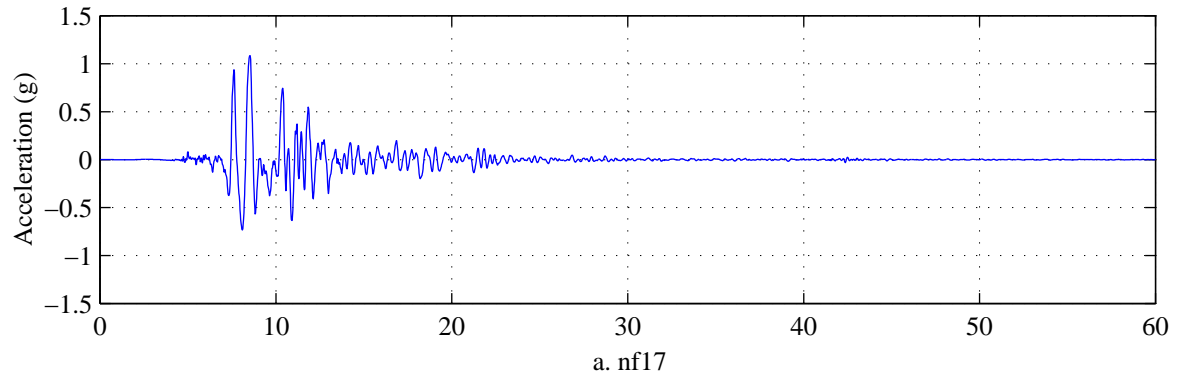


Figure A.5. Ground acceleration time histories from Bin 1.

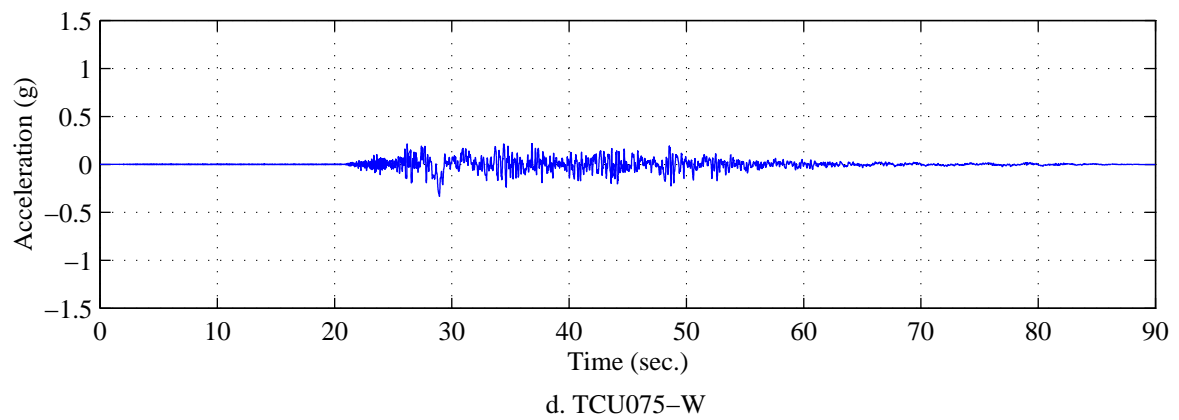
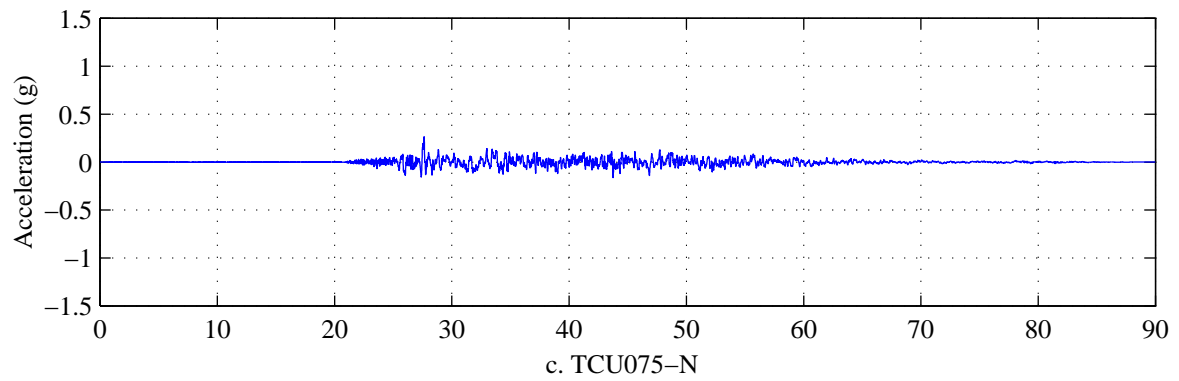
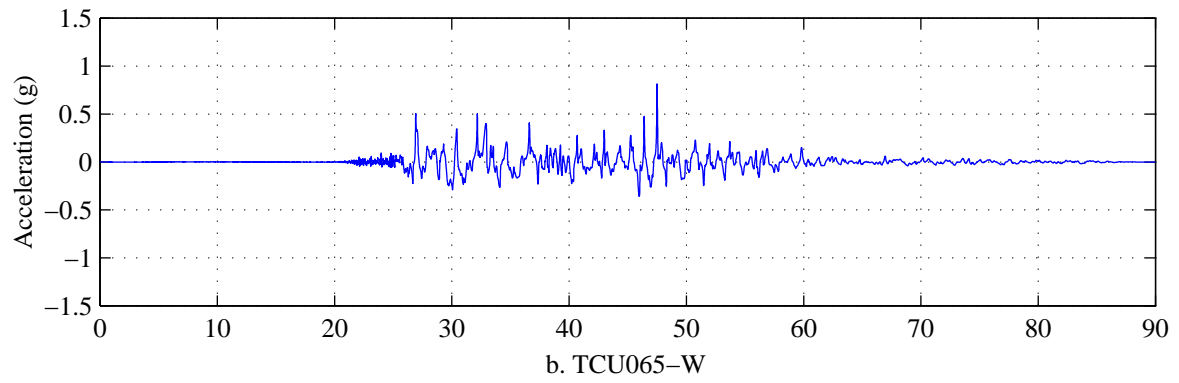
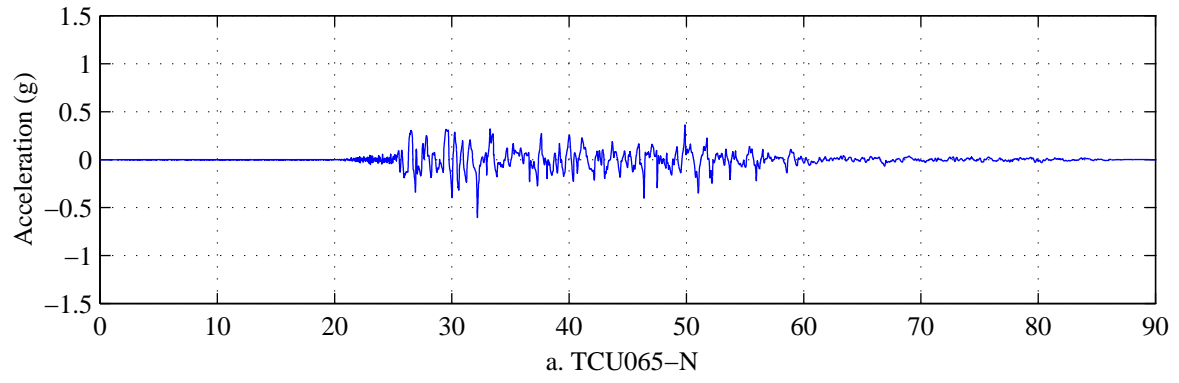


Figure A.6. Ground acceleration time histories from Bin 1.

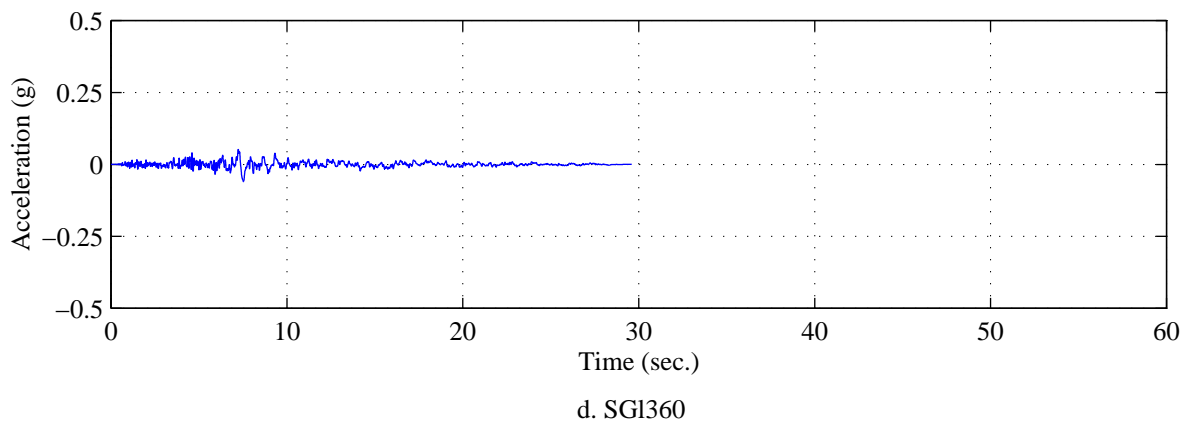
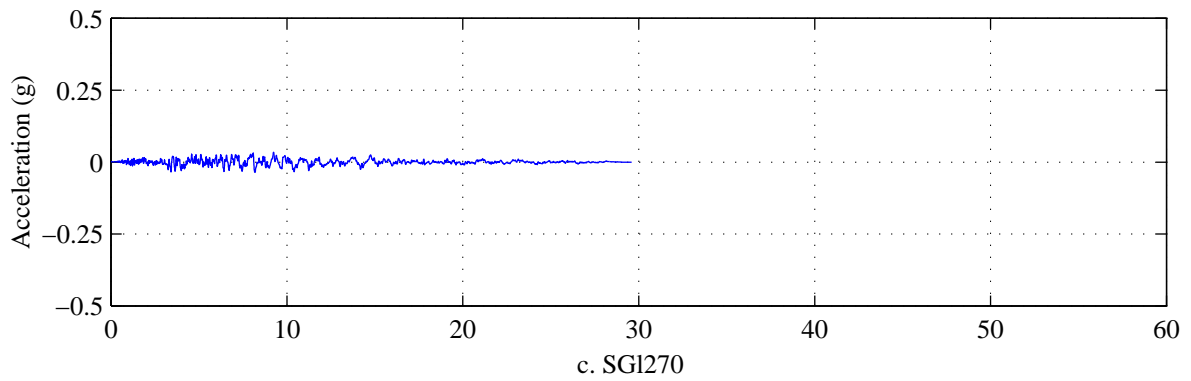
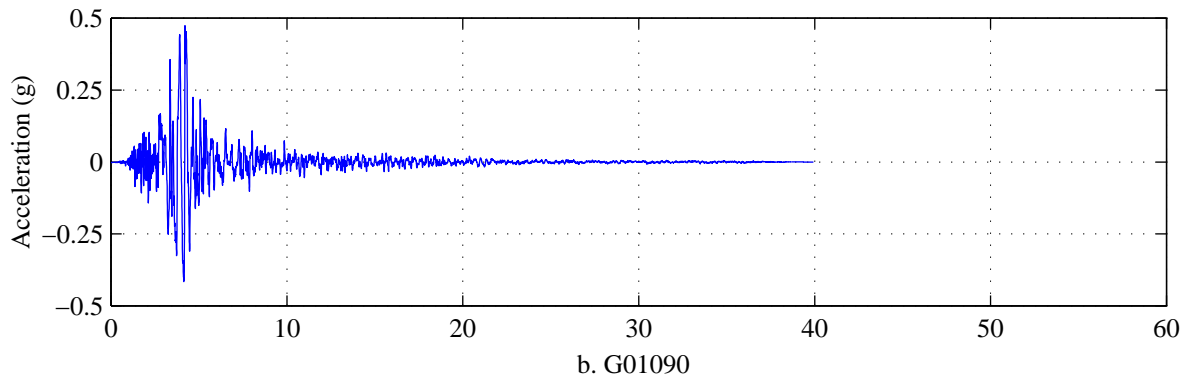
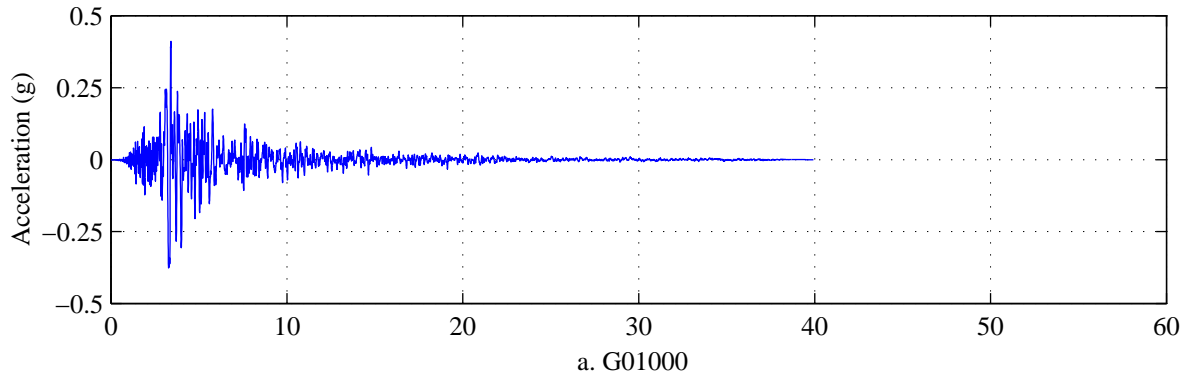


Figure A.7. Ground acceleration time histories from Bin 2.

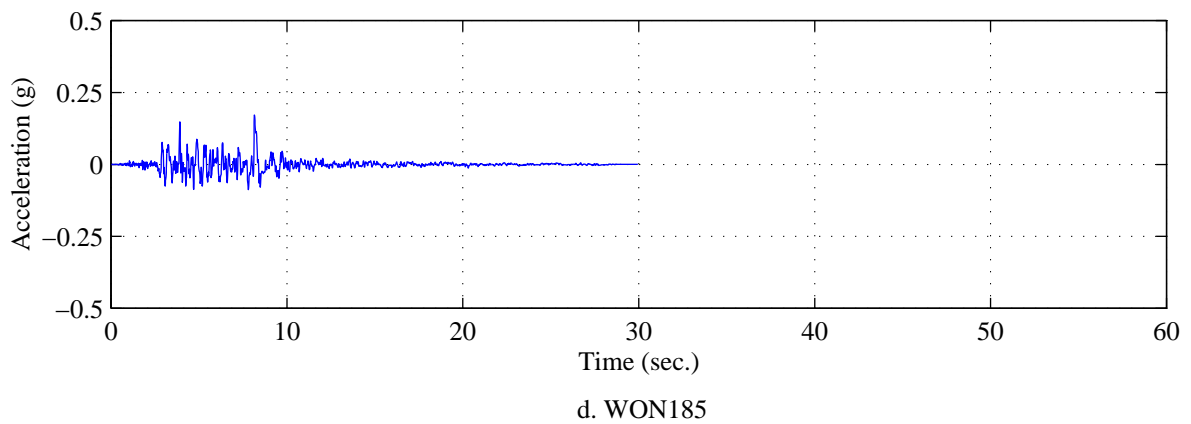
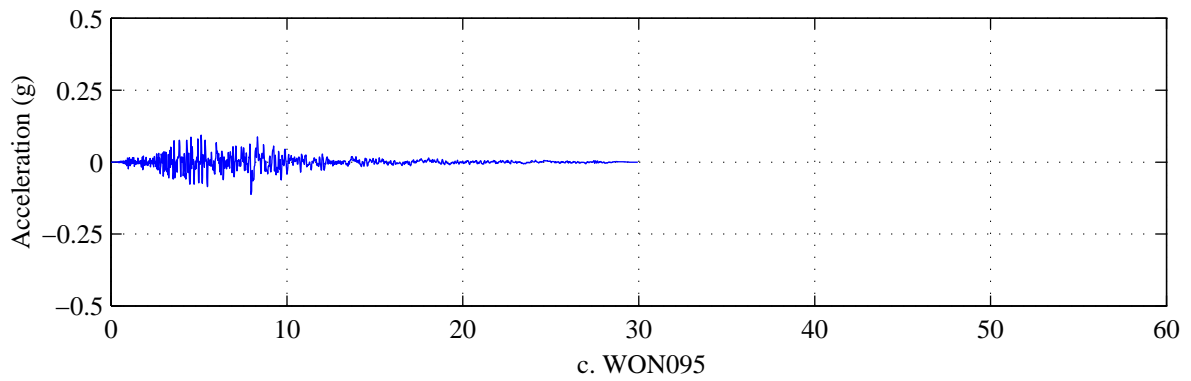
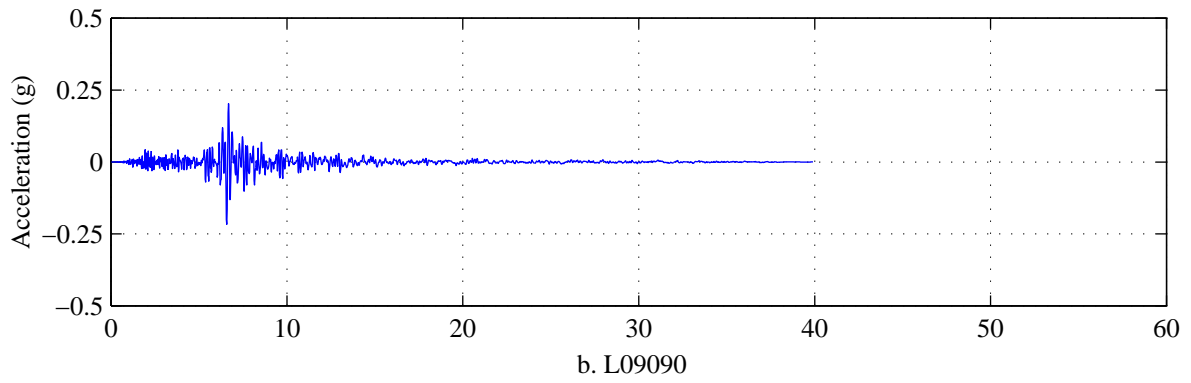
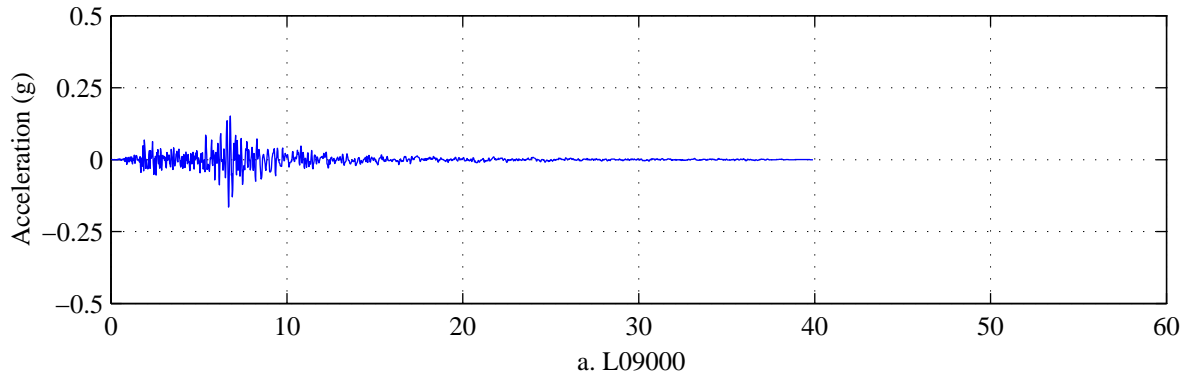


Figure A.8. Ground acceleration time histories from Bin 2.

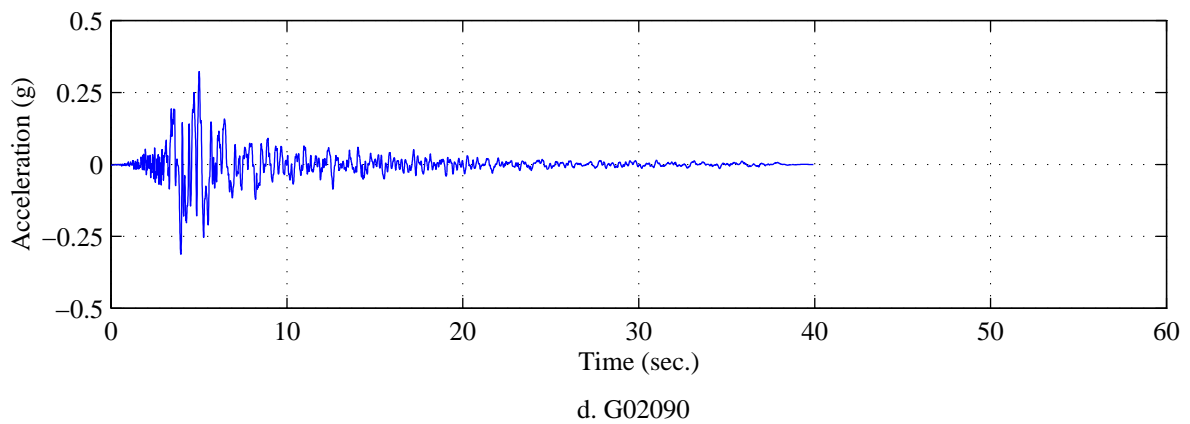
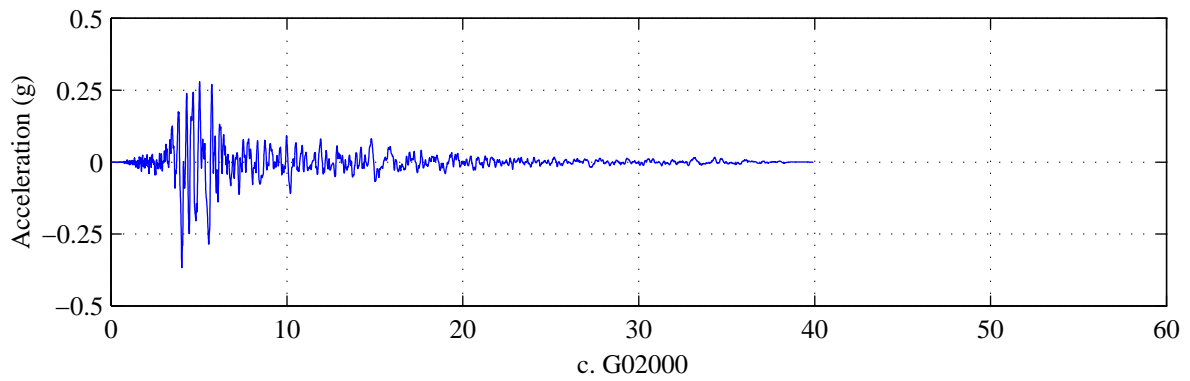
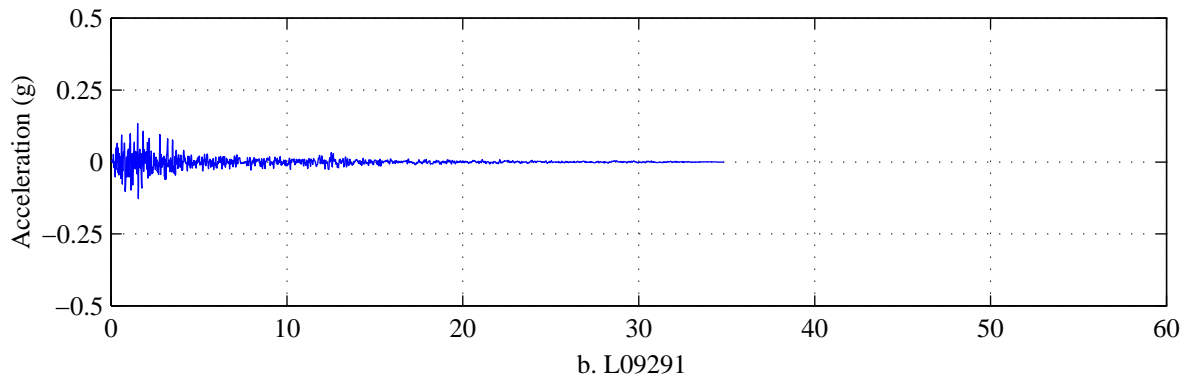
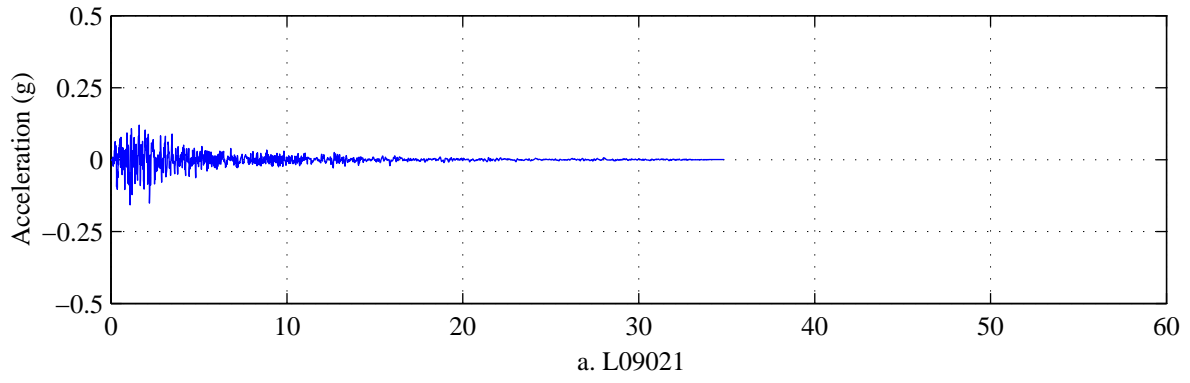


Figure A.9. Ground acceleration time histories from Bin 2.

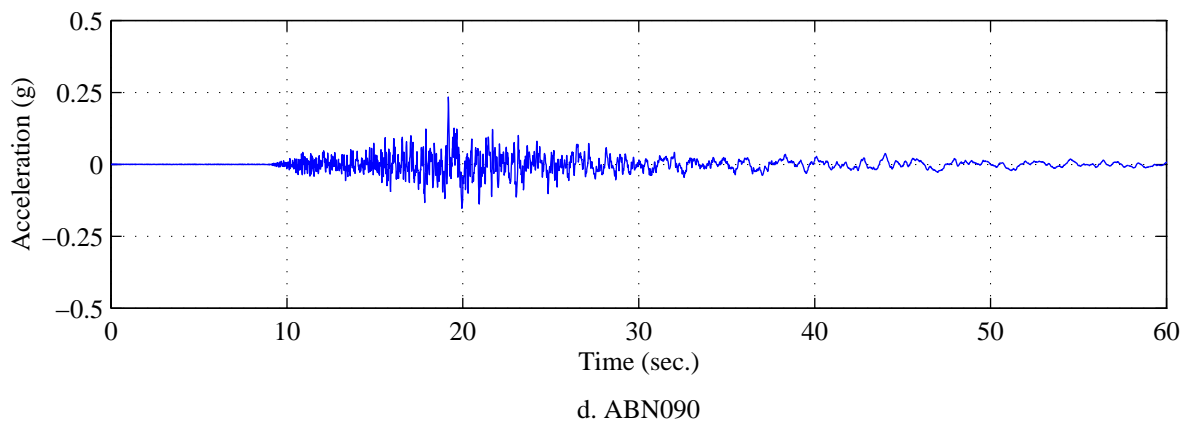
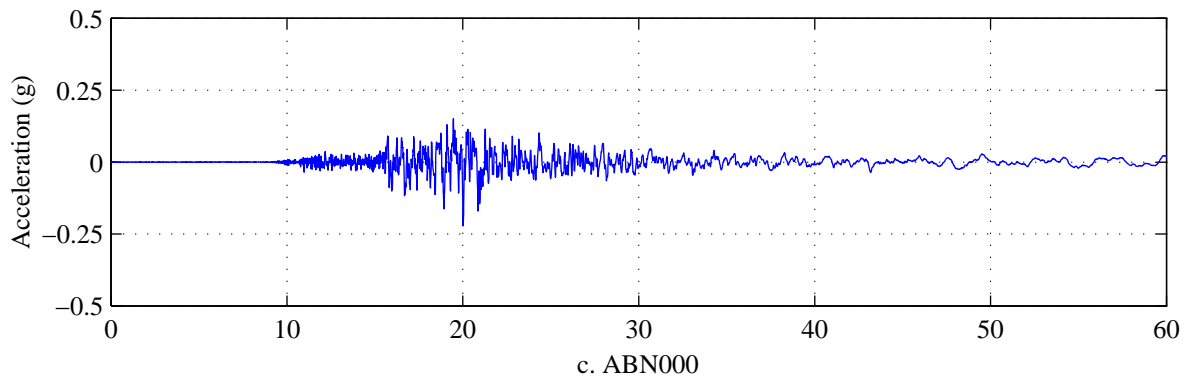
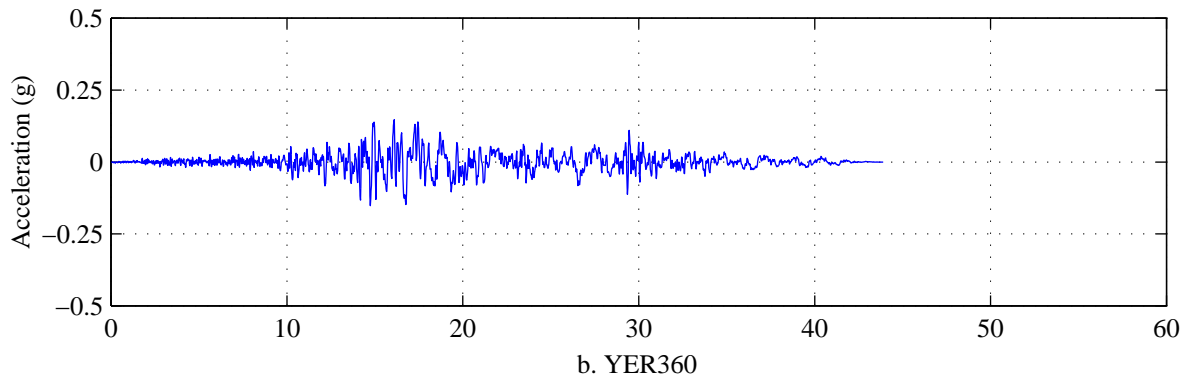
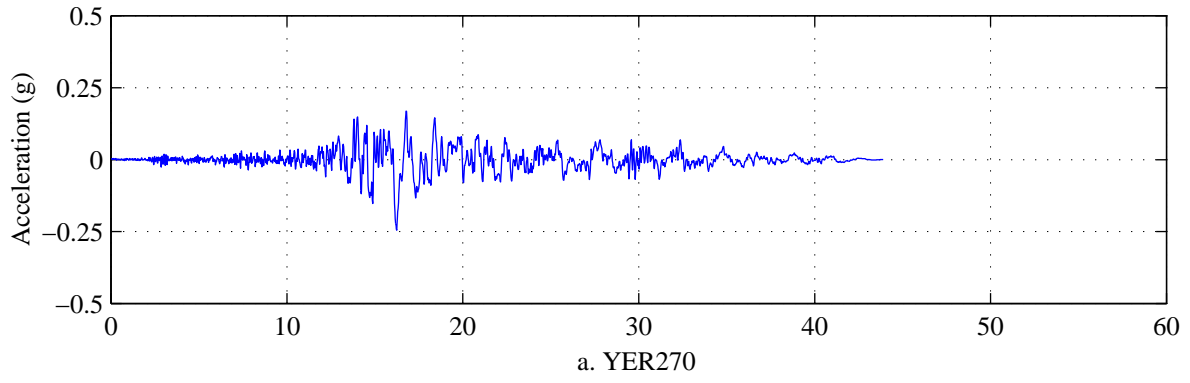
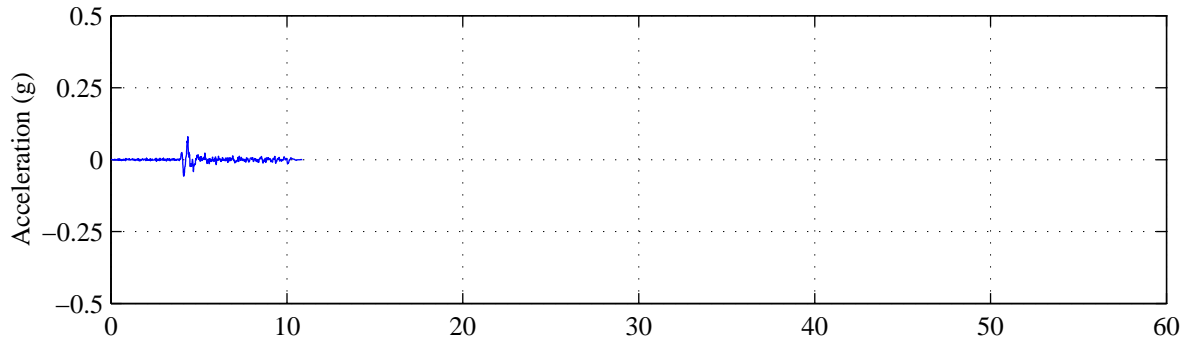
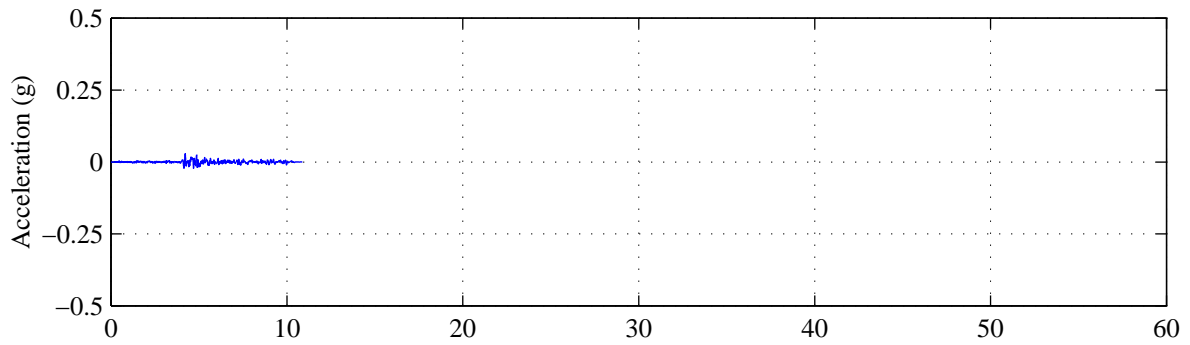


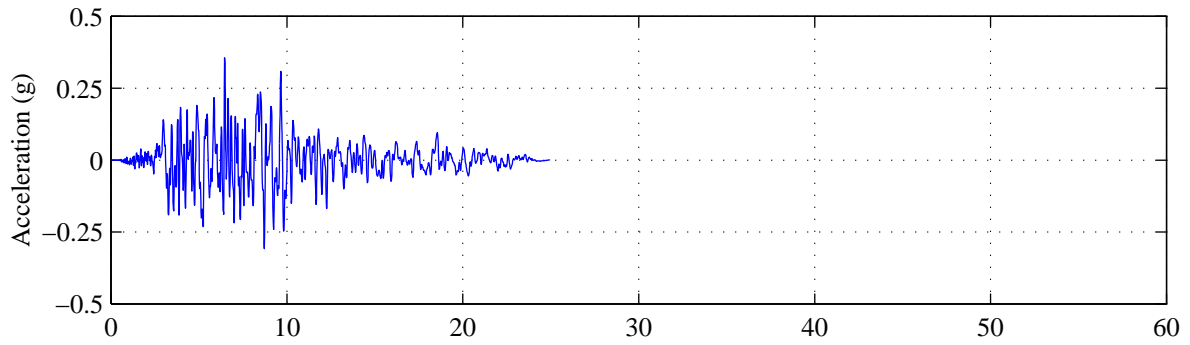
Figure A.10. Ground acceleration time histories from Bin 2.



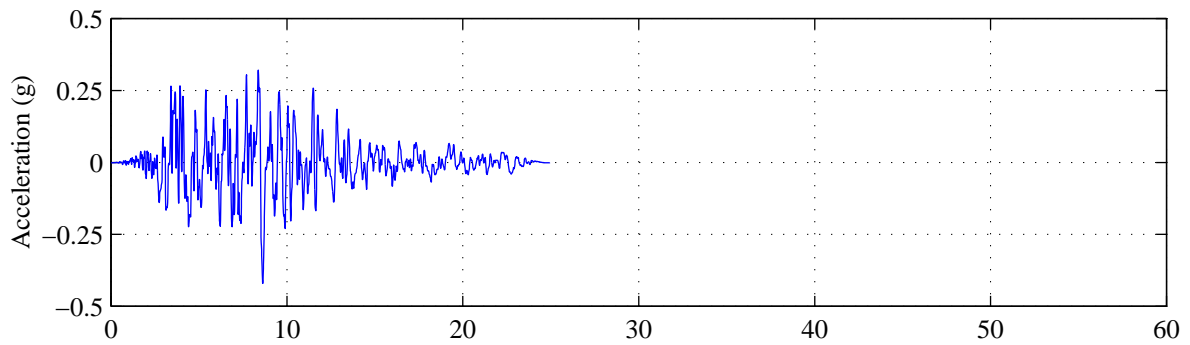
a. A-E01140



b. A-E01230



c. CNP106



d. CNP196

Figure A.11. Ground acceleration time histories from Bin 2.

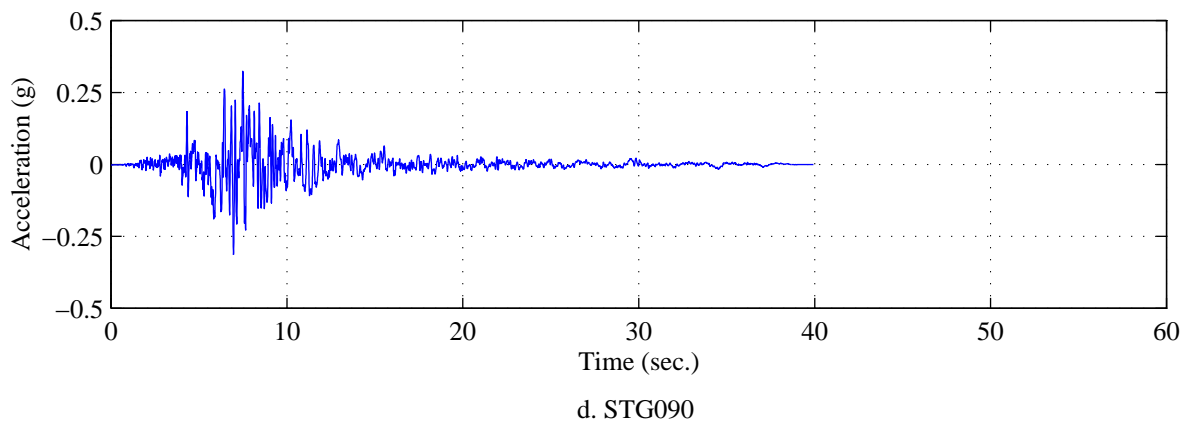
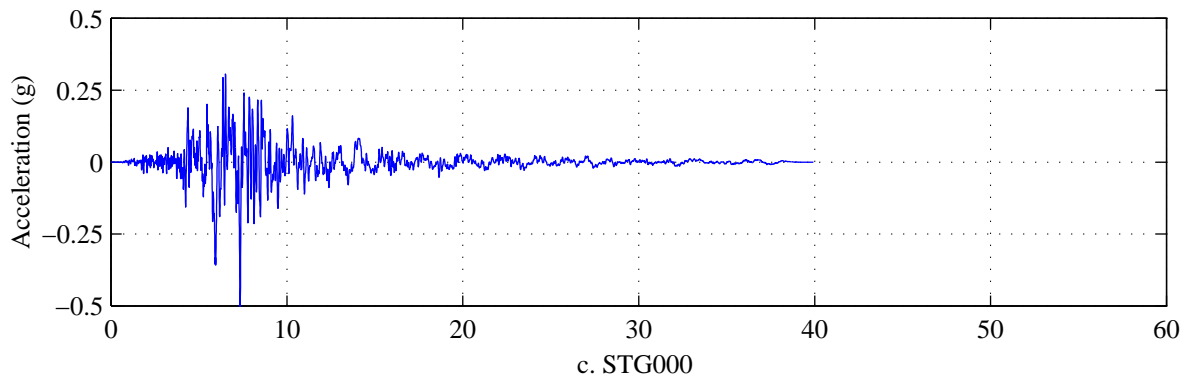
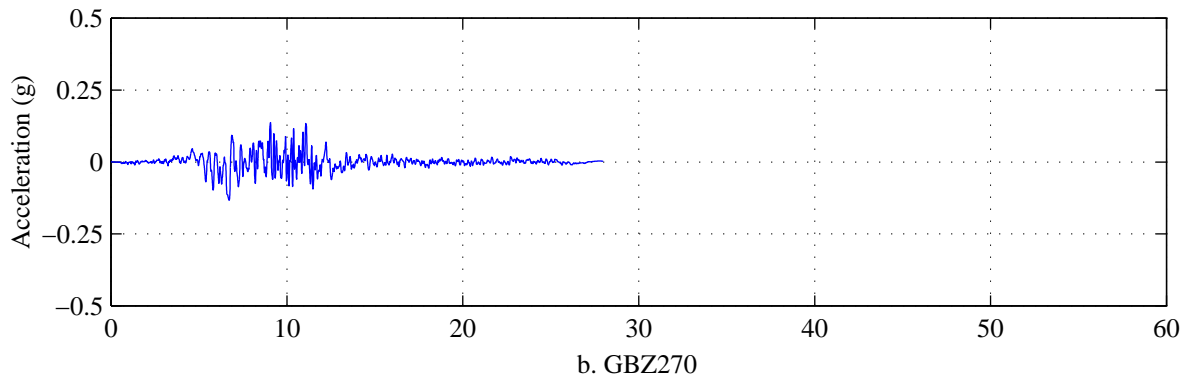
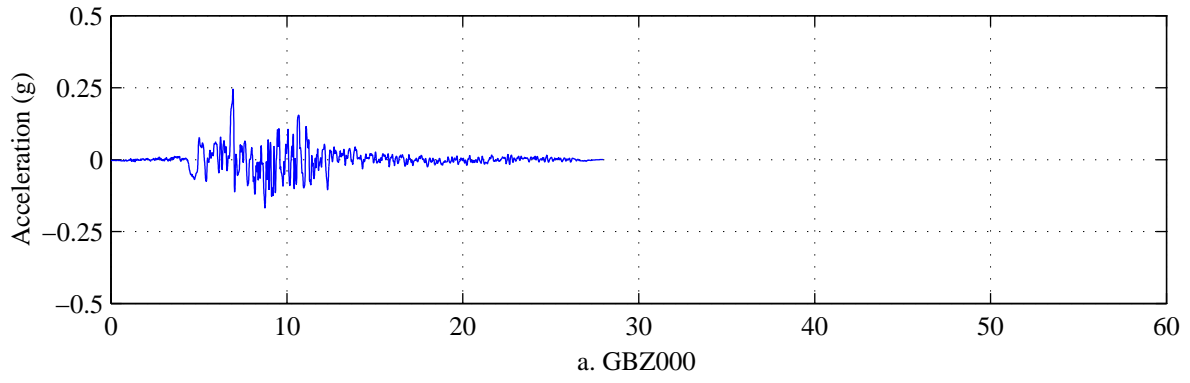
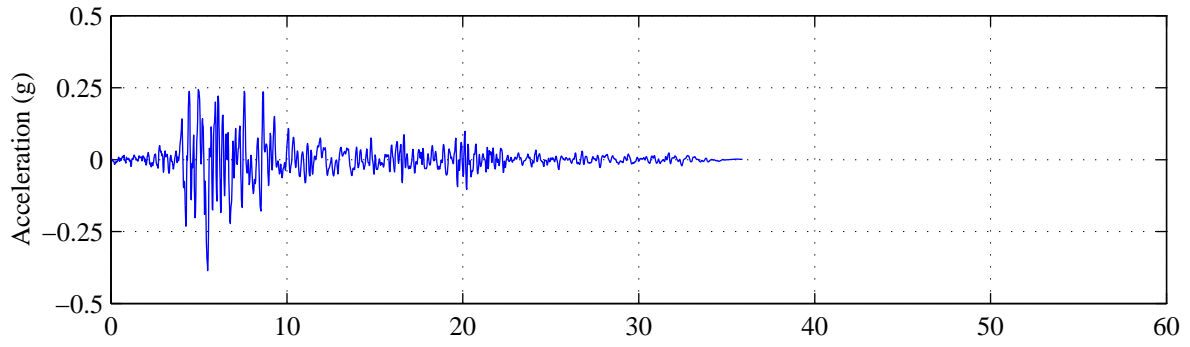
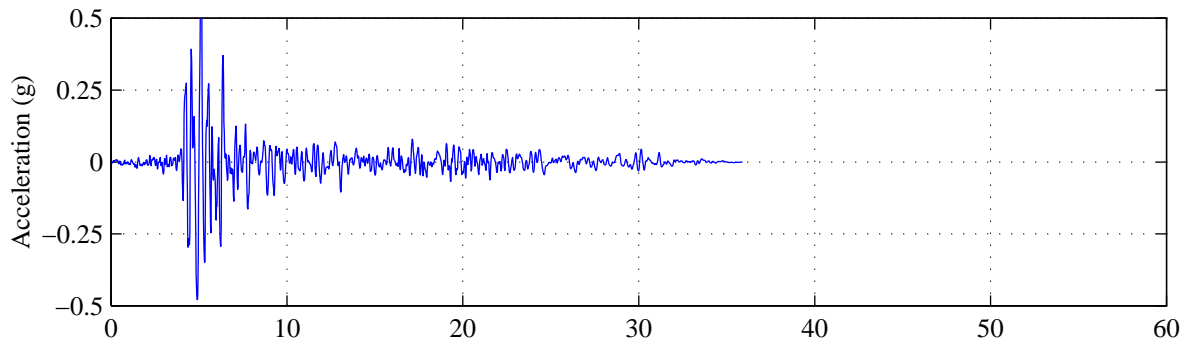


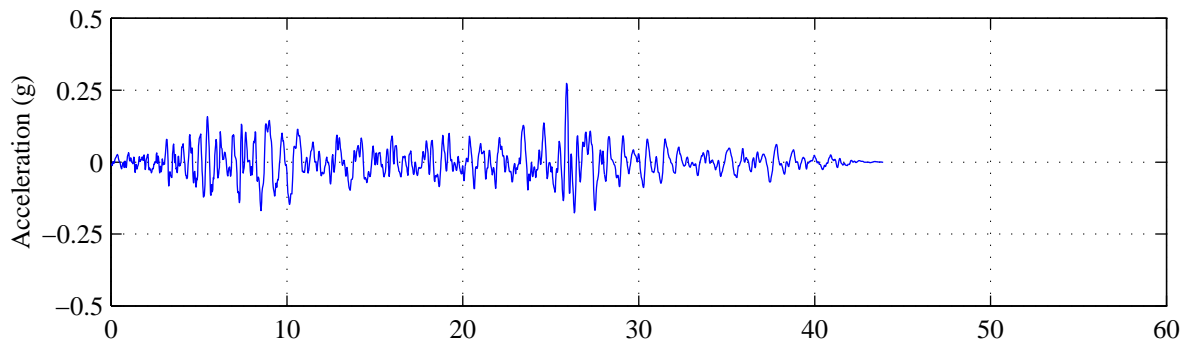
Figure A.12. Ground acceleration time histories from Bin 2M.



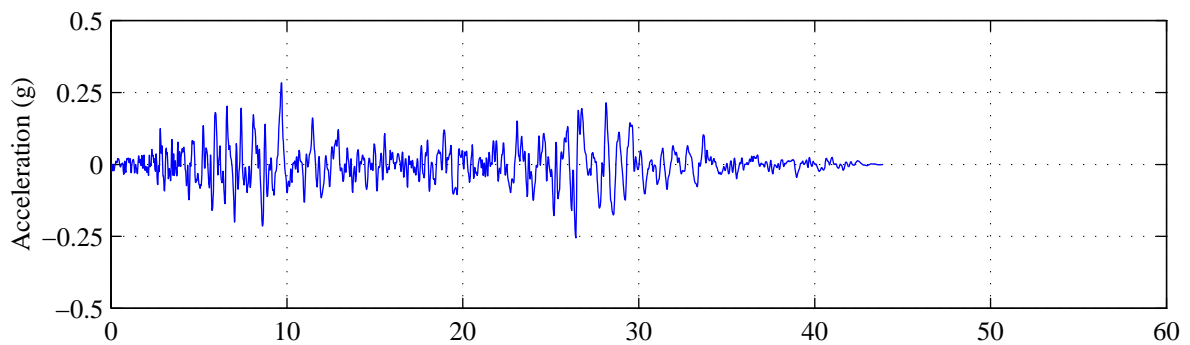
a. RIO270



b. RIO360

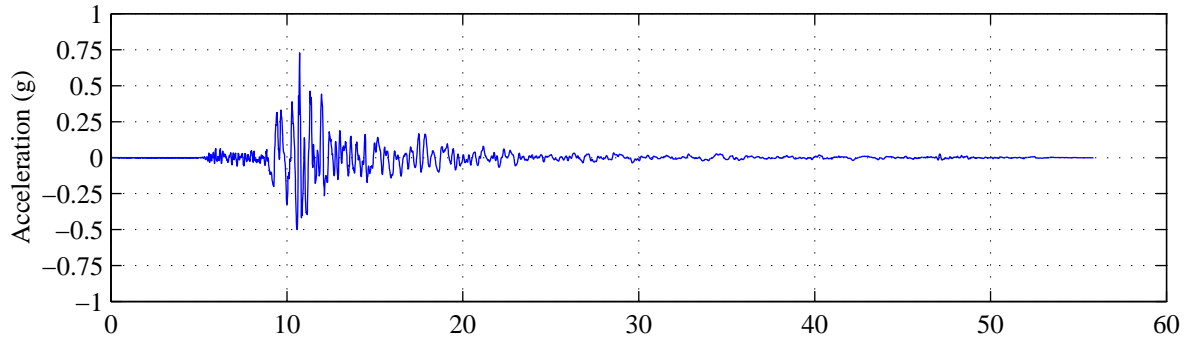


c. JOS000

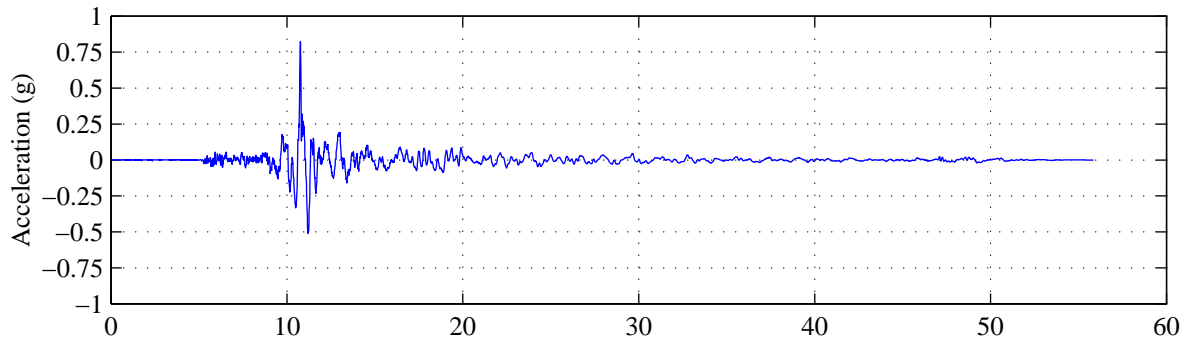


d. JOS090

Figure A.13. Ground acceleration time histories from Bin 2M.



a. BOL000



b. BOL090

Figure A.14. Ground acceleration time histories from Bin 2M.

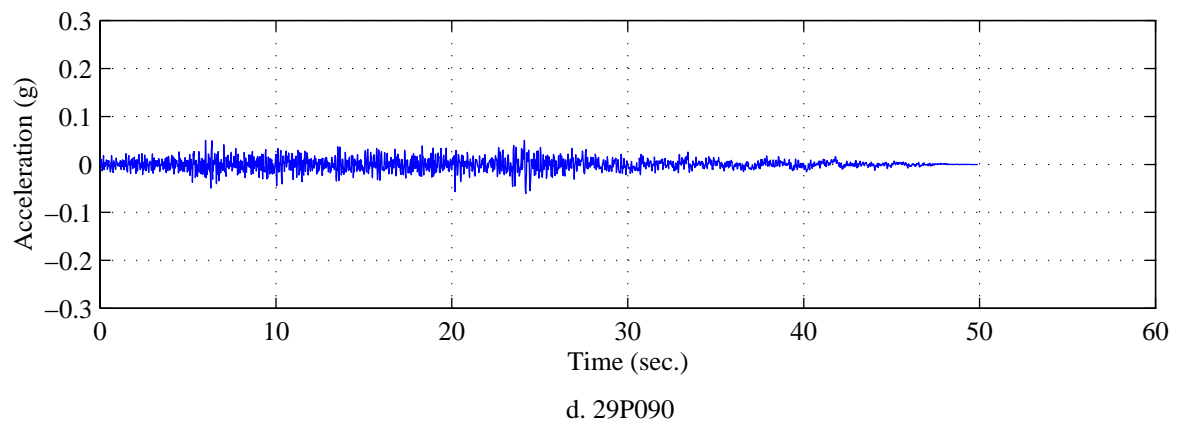
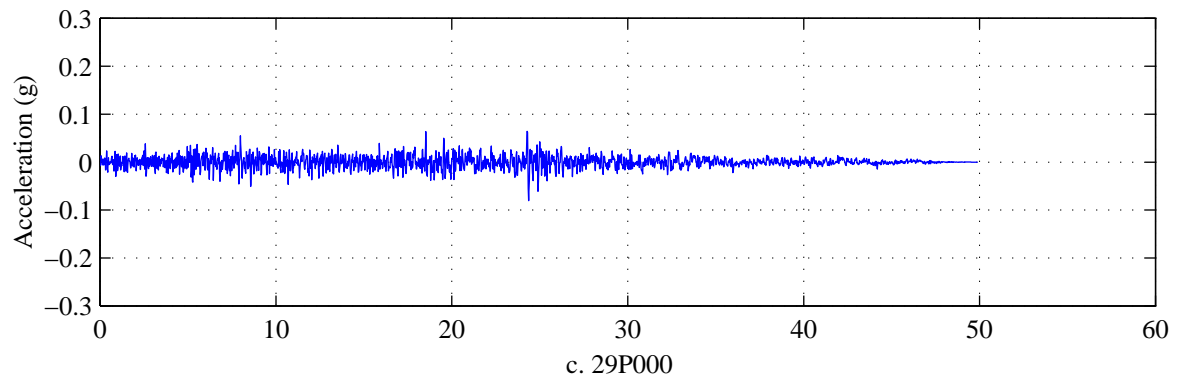
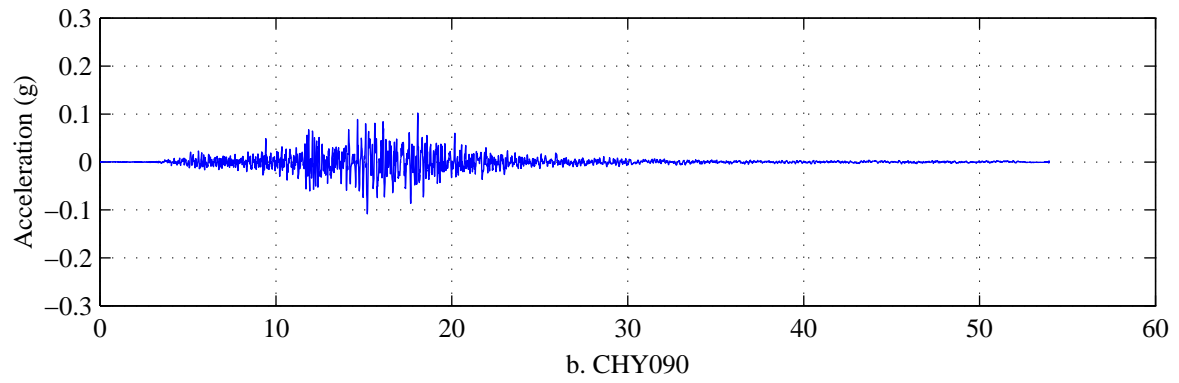
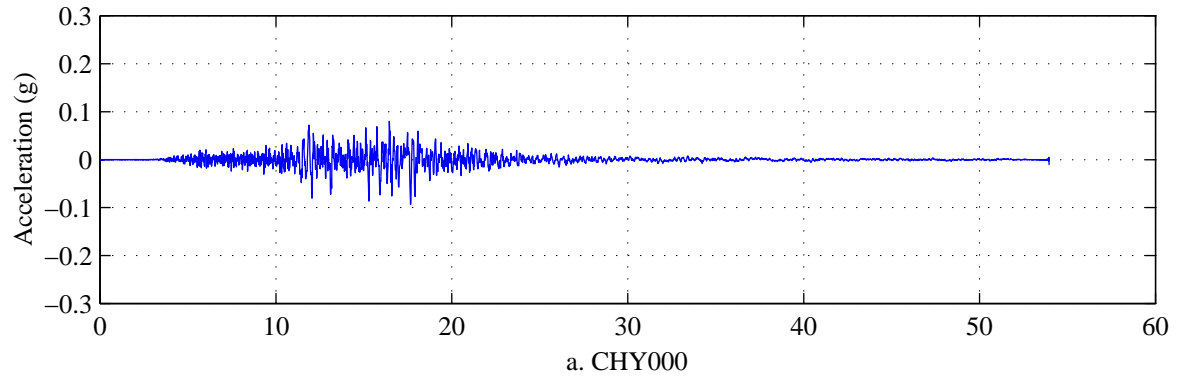


Figure A.15. Ground acceleration time histories from Bin 3.

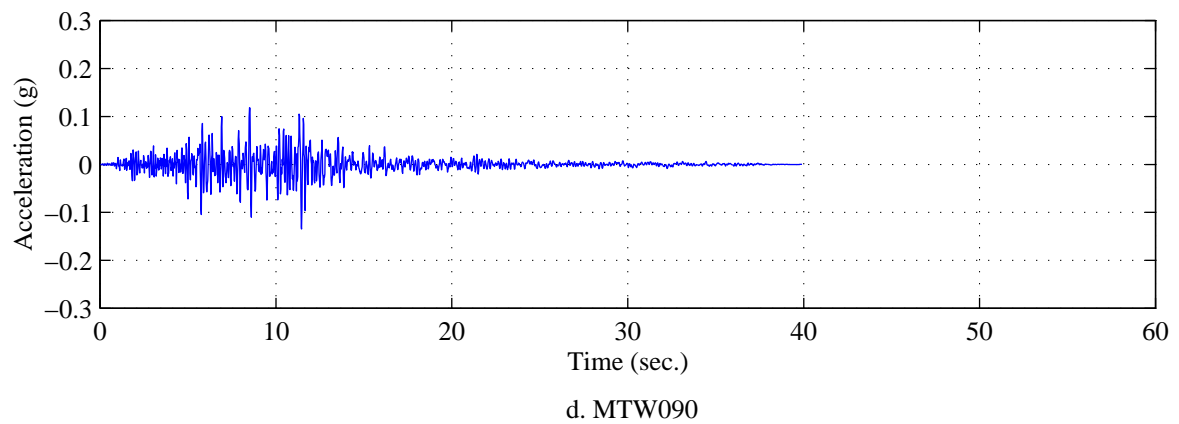
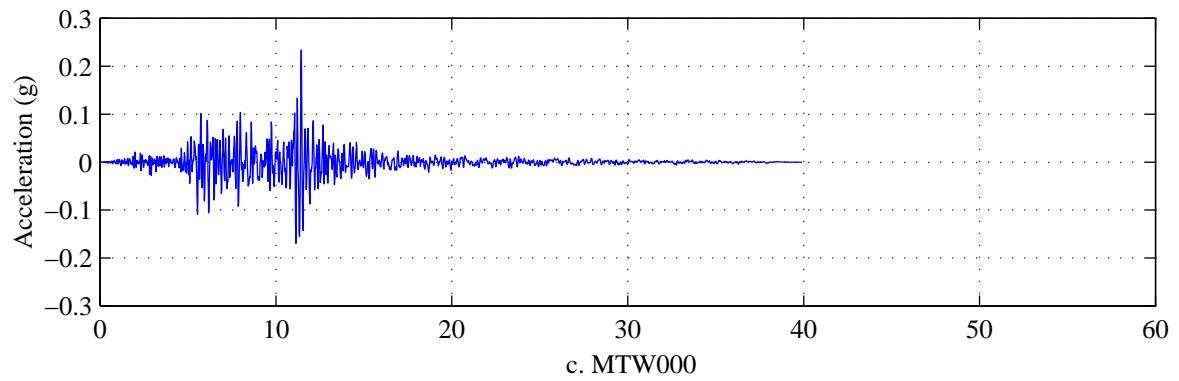
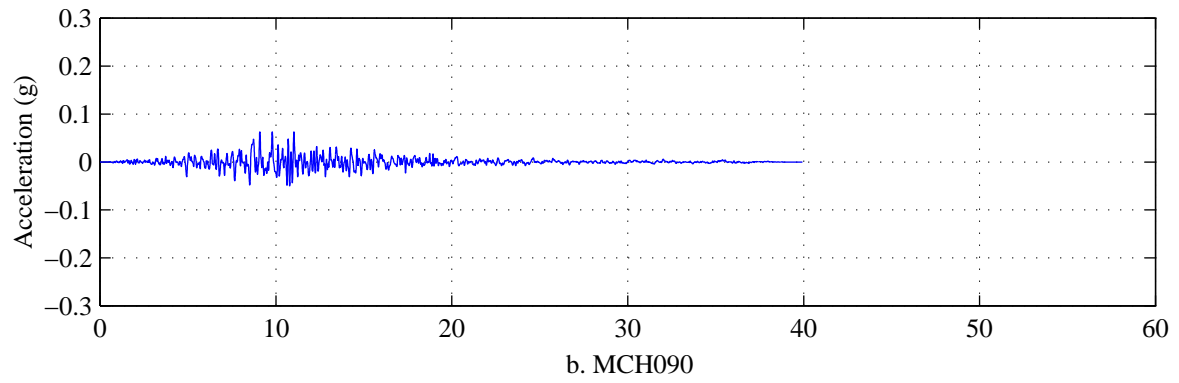
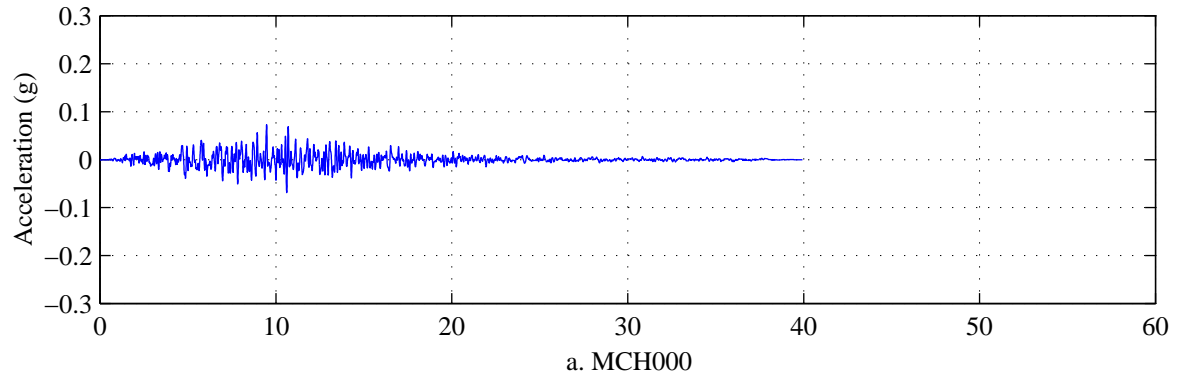


Figure A.16. Ground acceleration time histories from Bin 3.

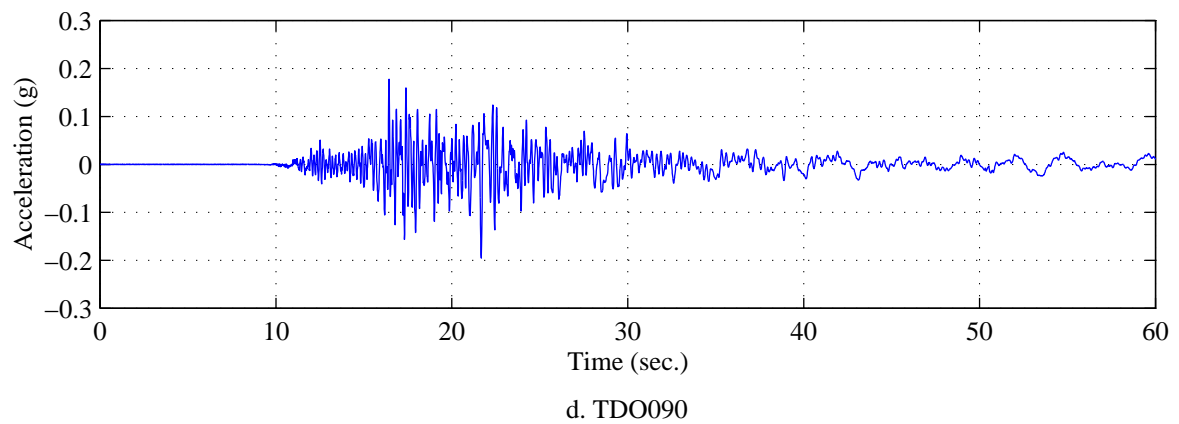
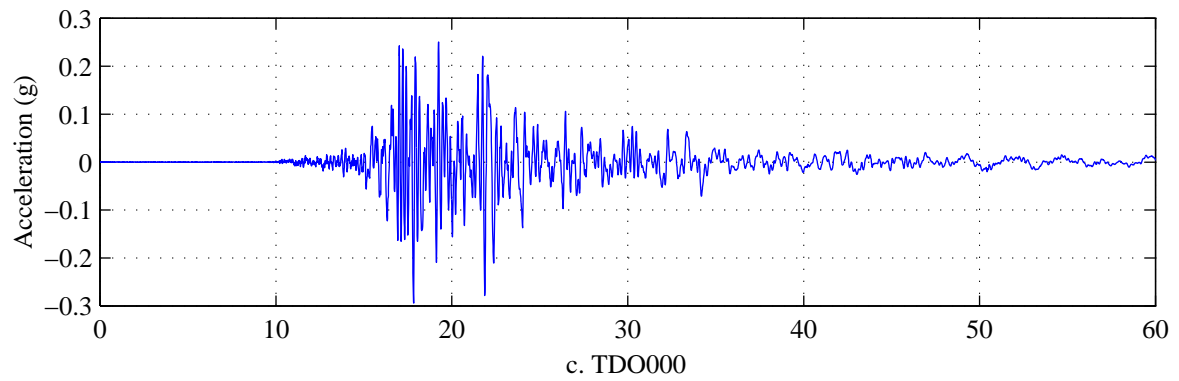
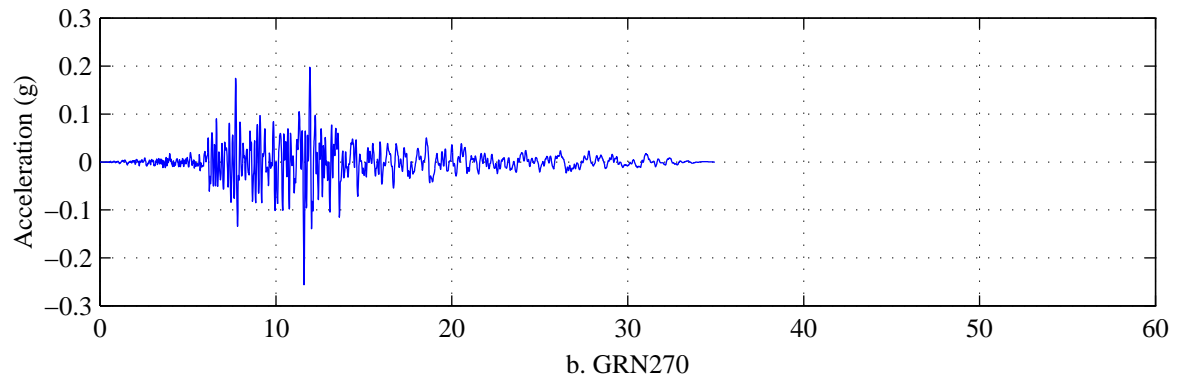
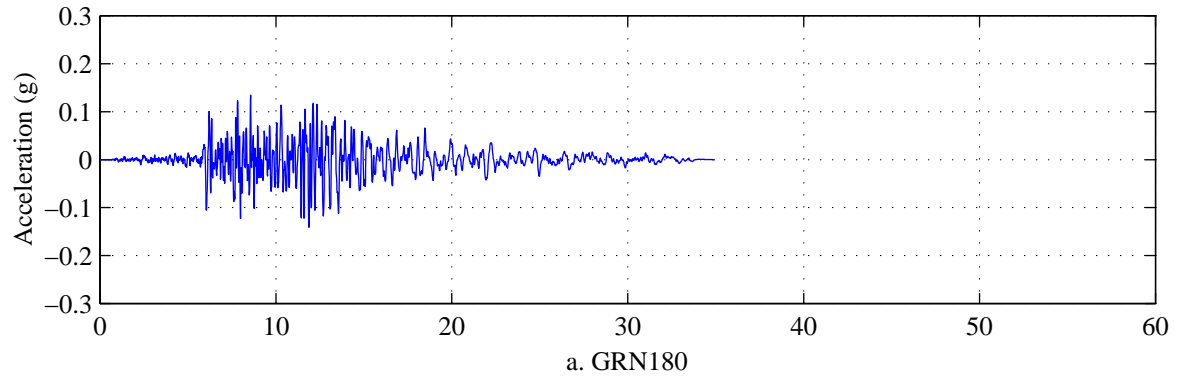


Figure A.17. Ground acceleration time histories from Bin 3.

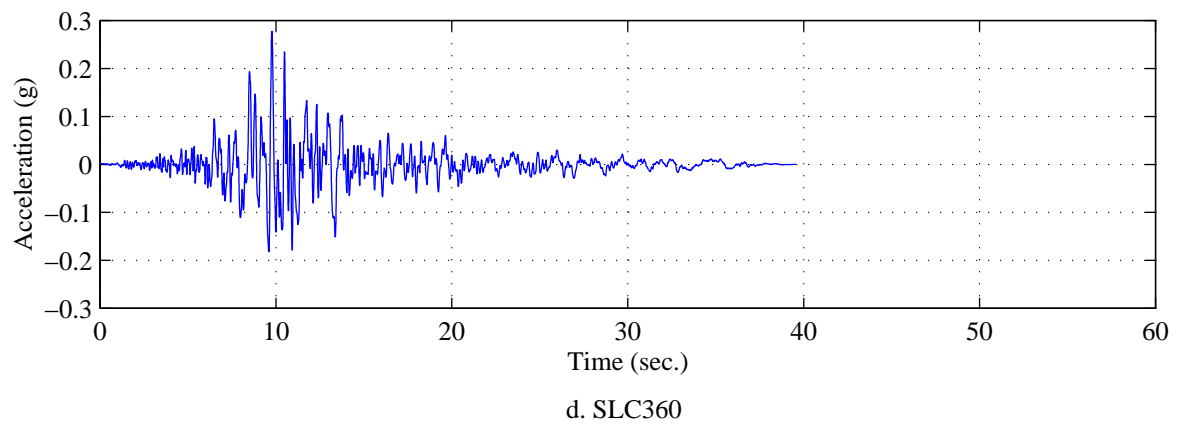
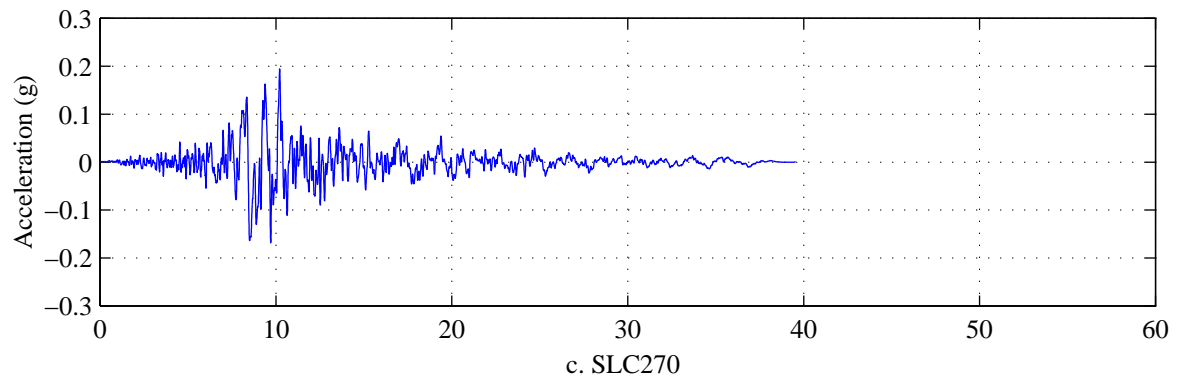
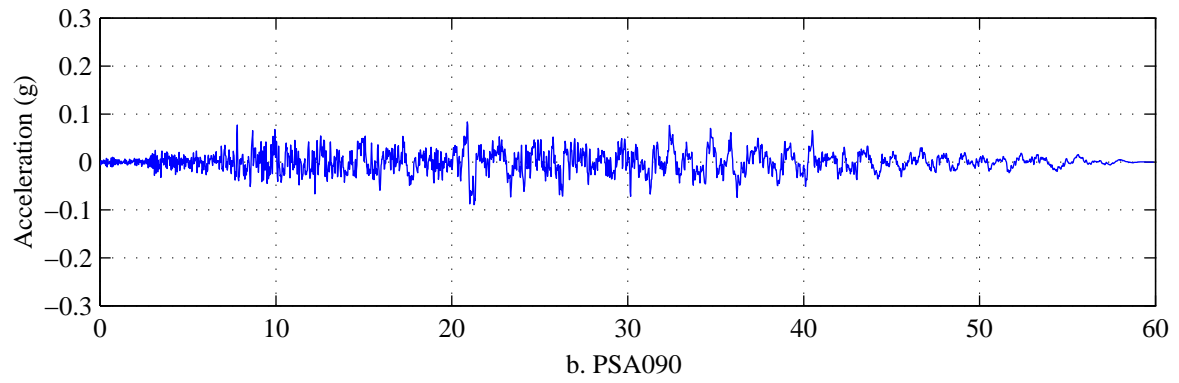
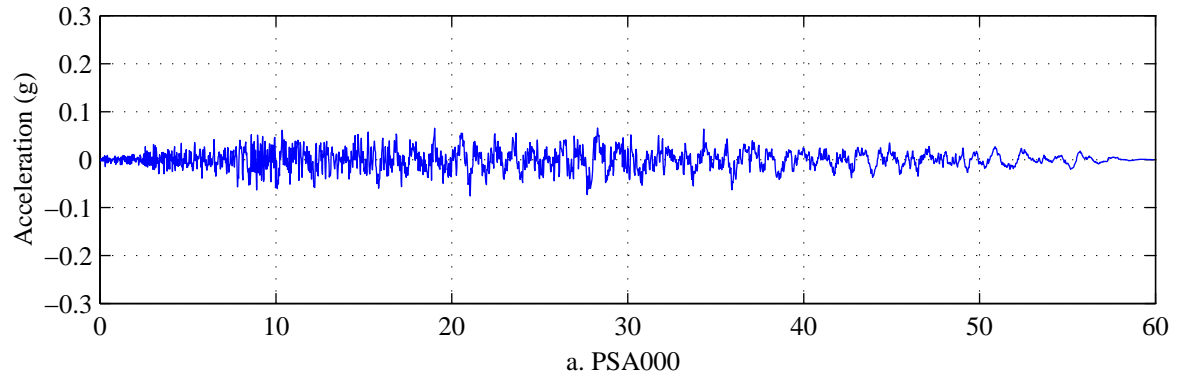


Figure A.18. Ground acceleration time histories from Bin 3.

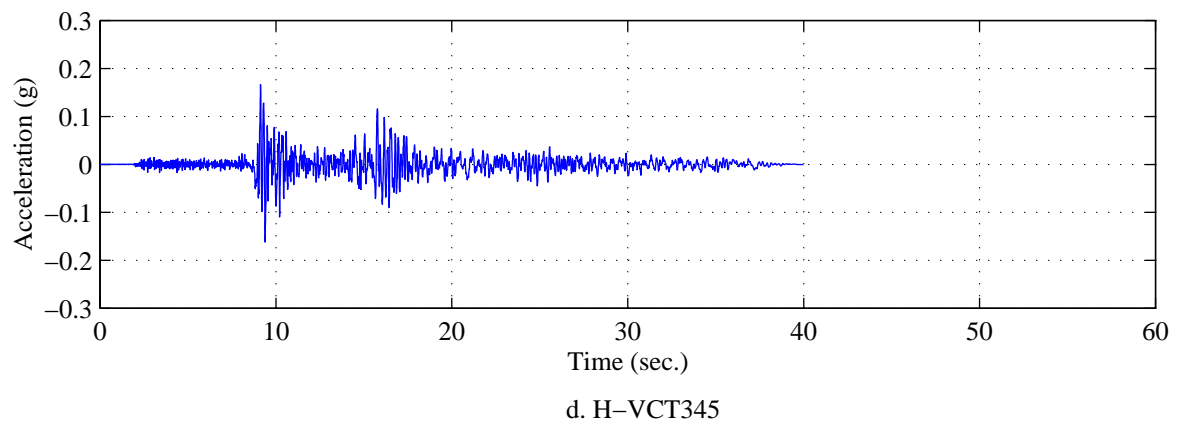
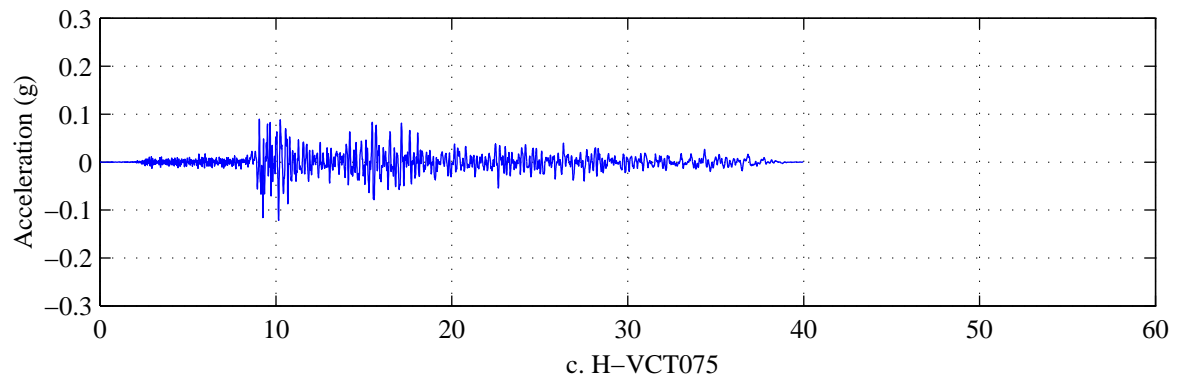
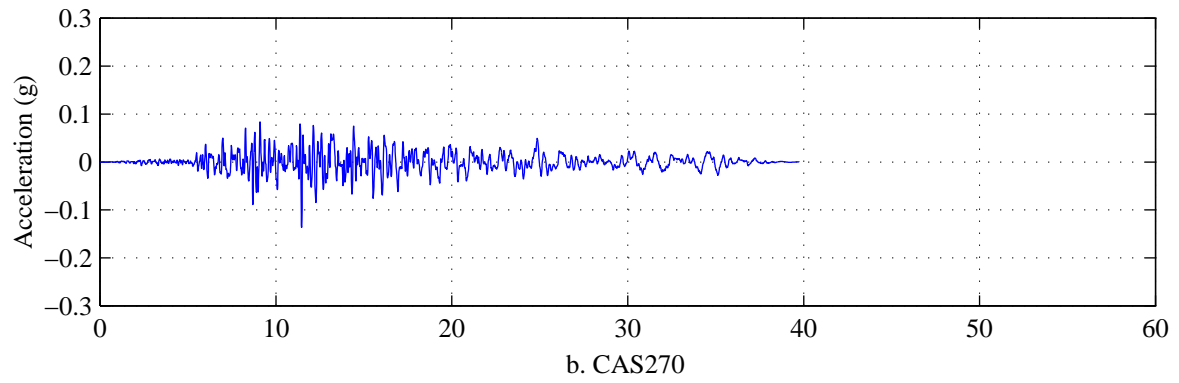
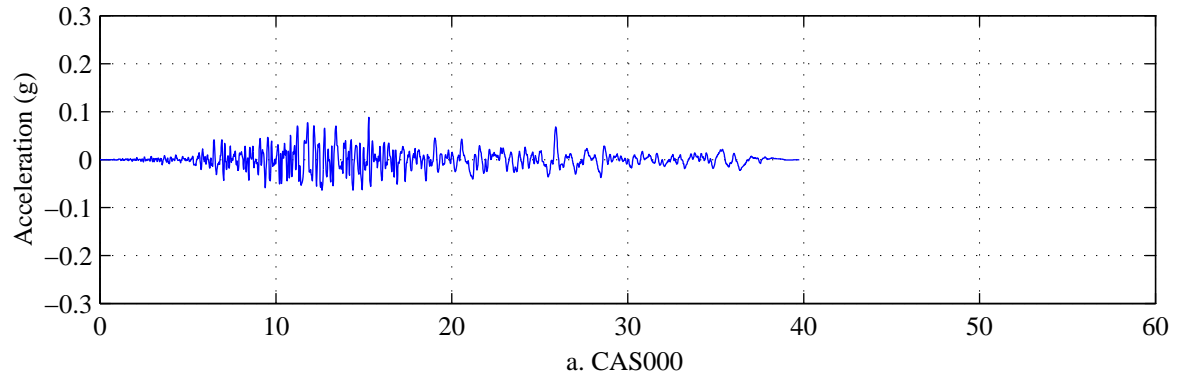


Figure A.19. Ground acceleration time histories from Bin 3.

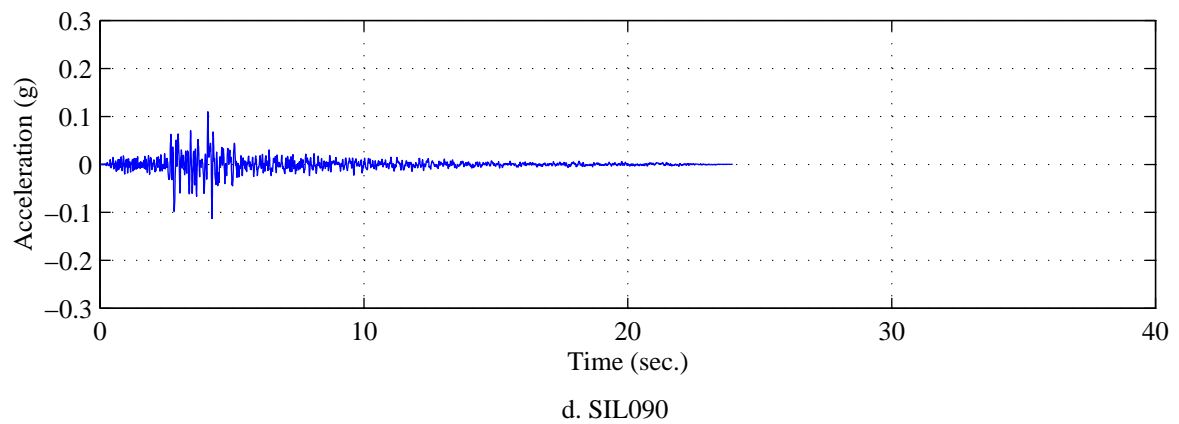
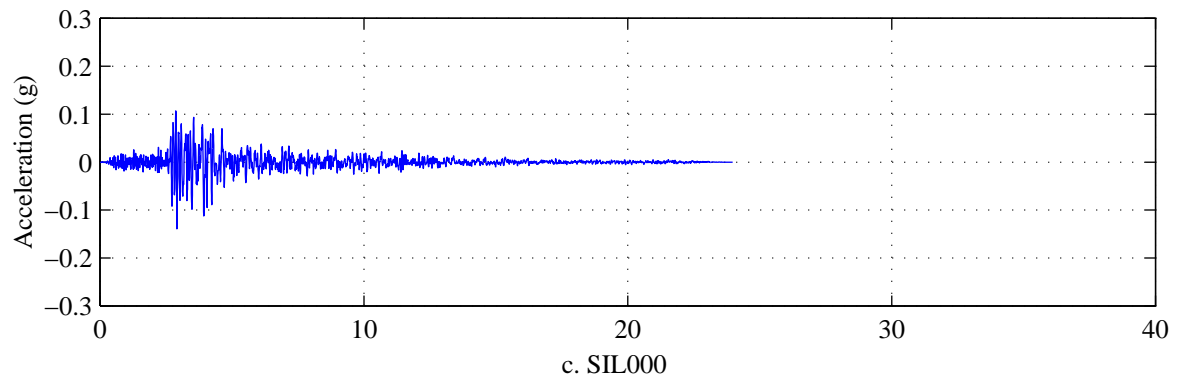
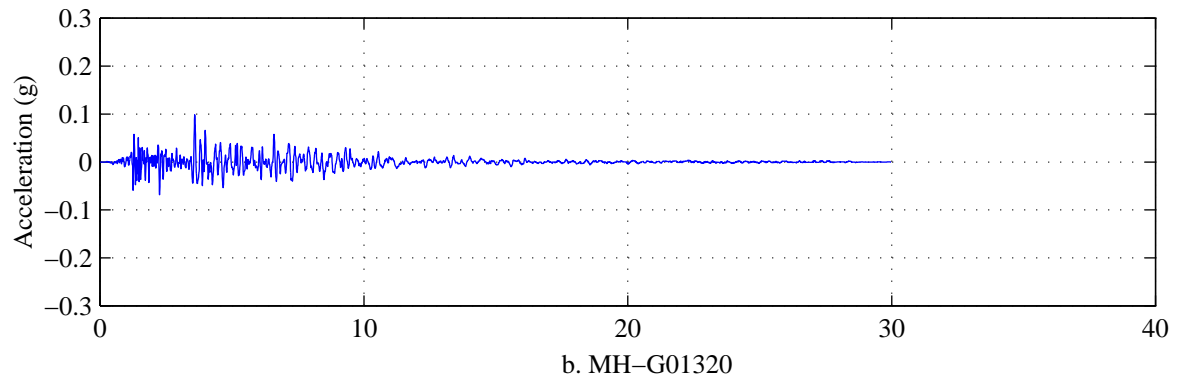
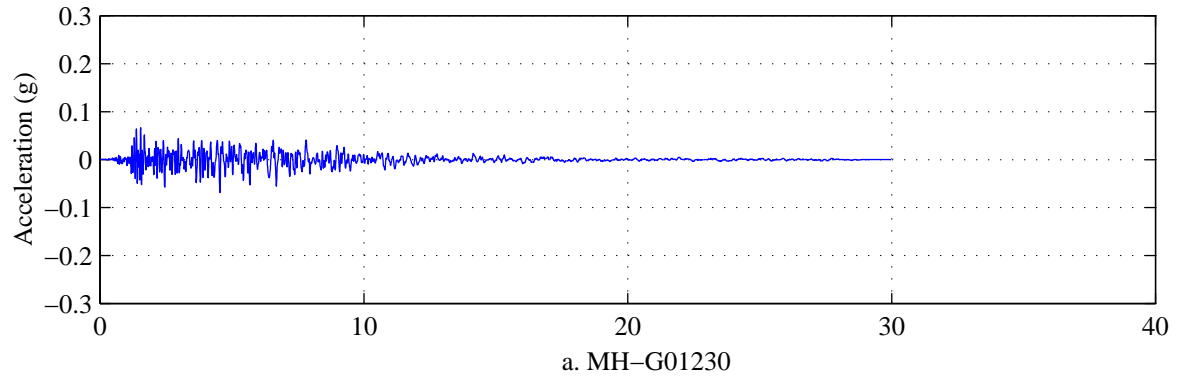
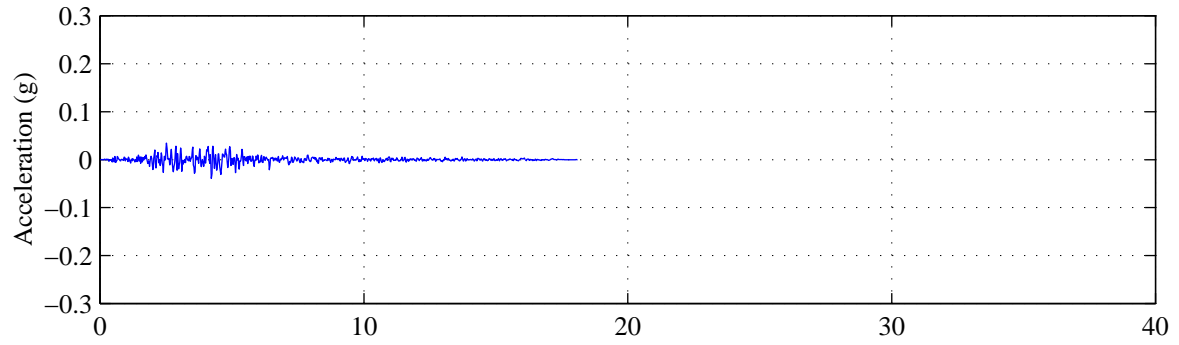
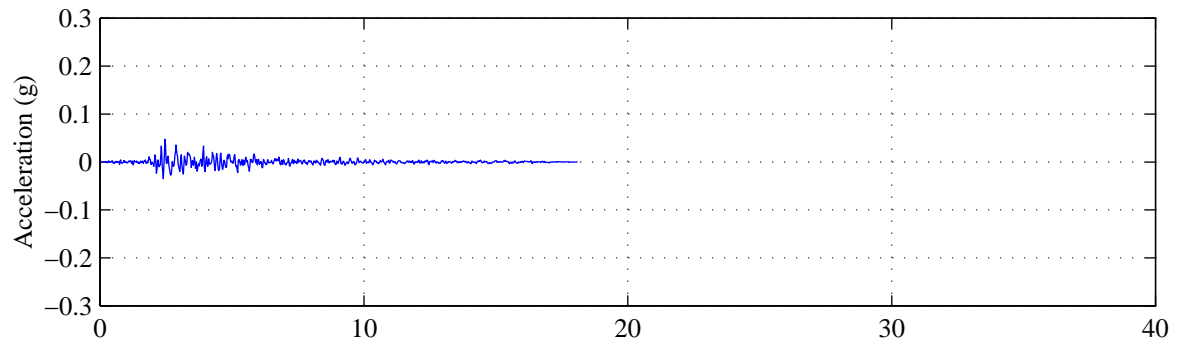


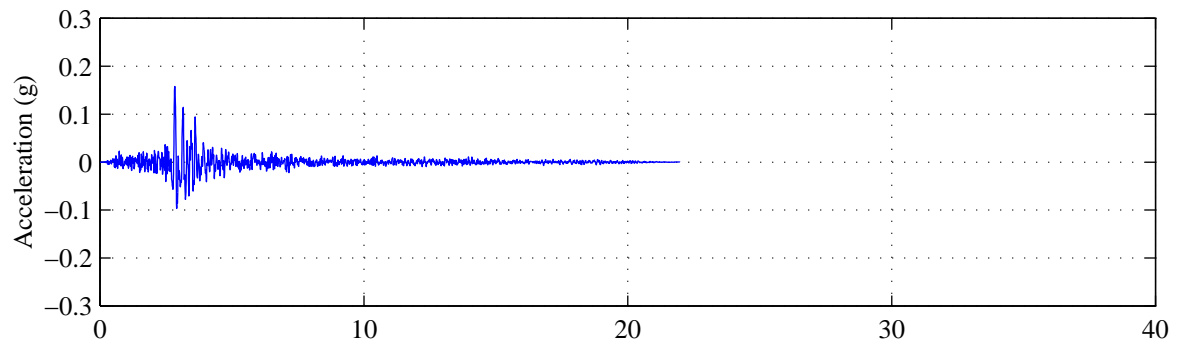
Figure A.20. Ground acceleration time histories from Bin 4.



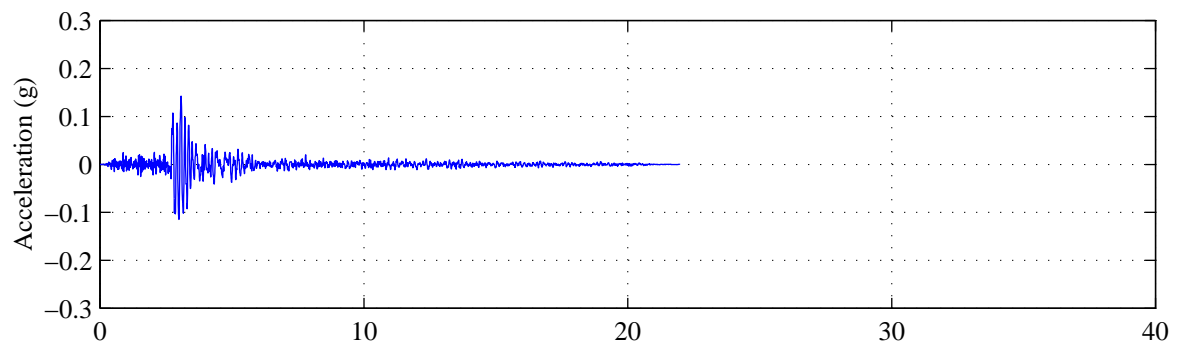
a. A-WON075



b. A-WON165



c. B-MTW000



d. B-MTW090

Figure A.21. Ground acceleration time histories from Bin 4.

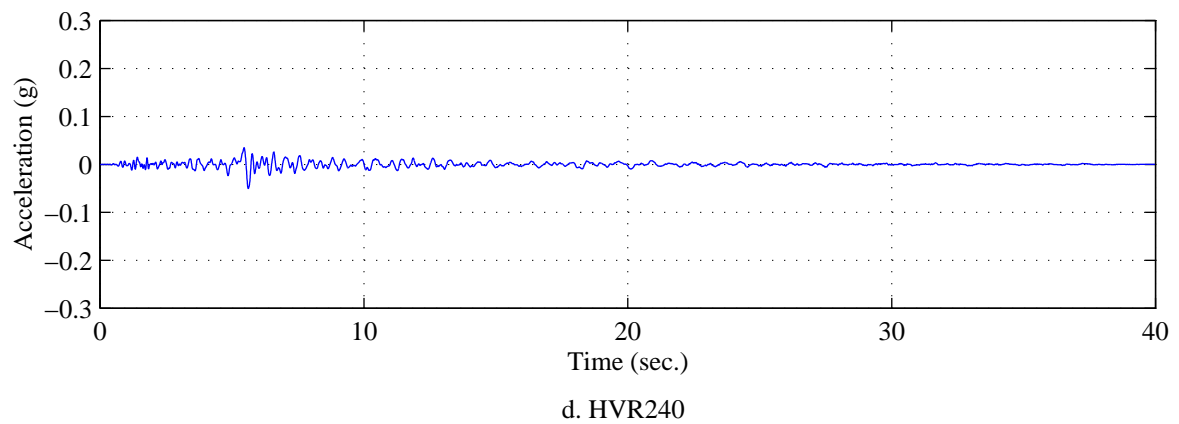
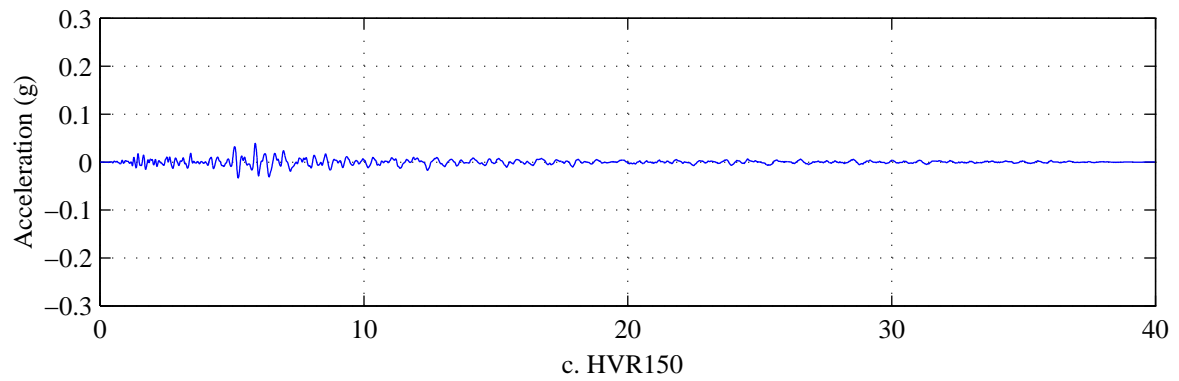
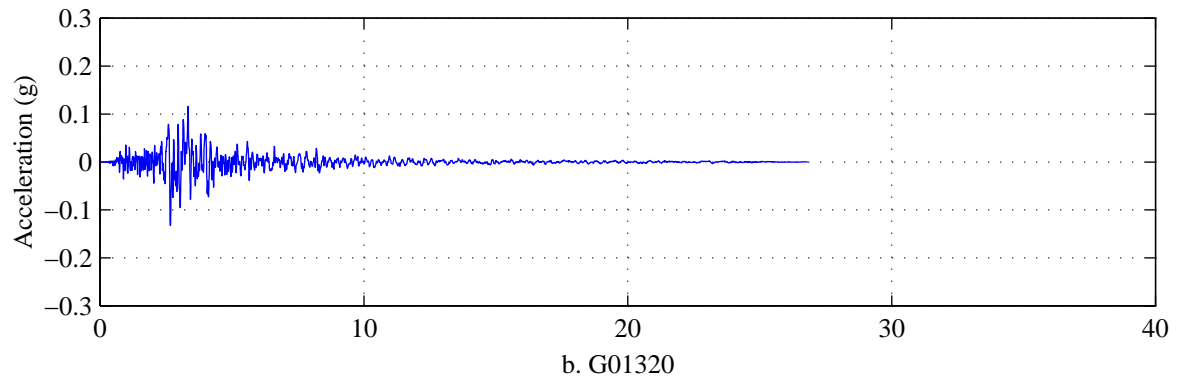
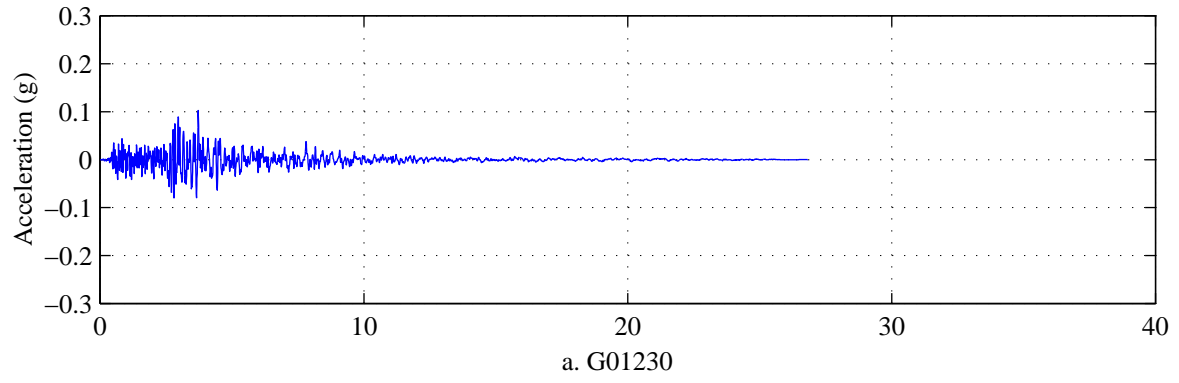
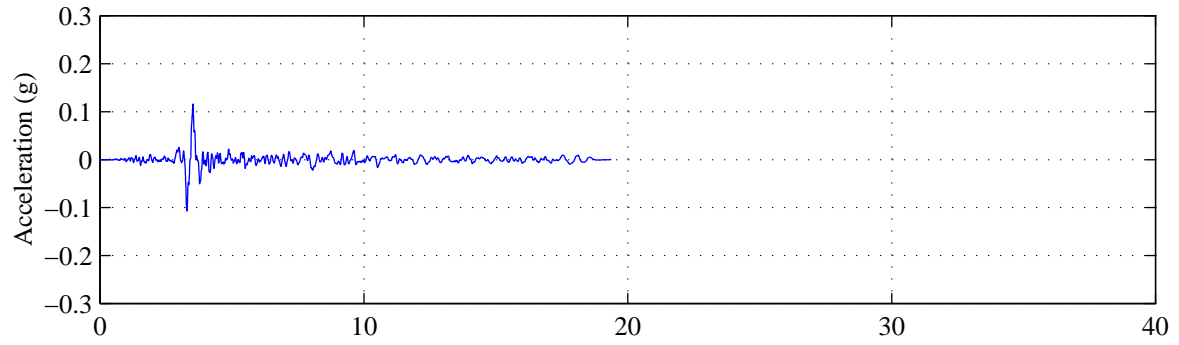
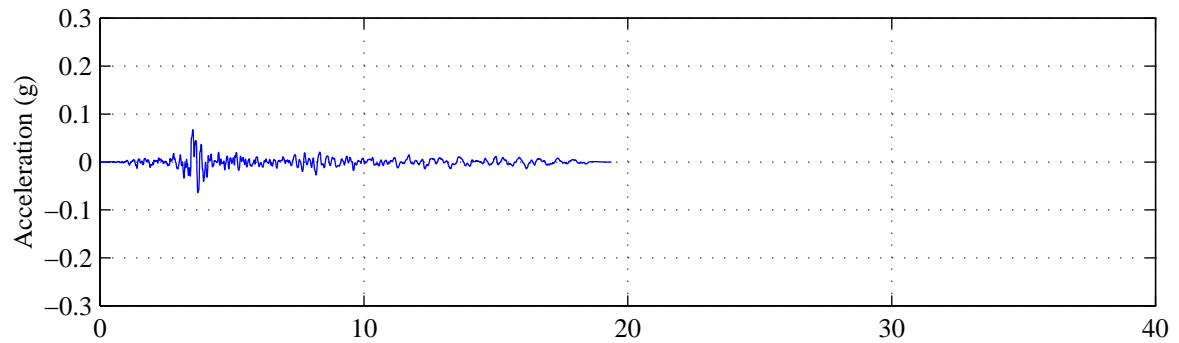


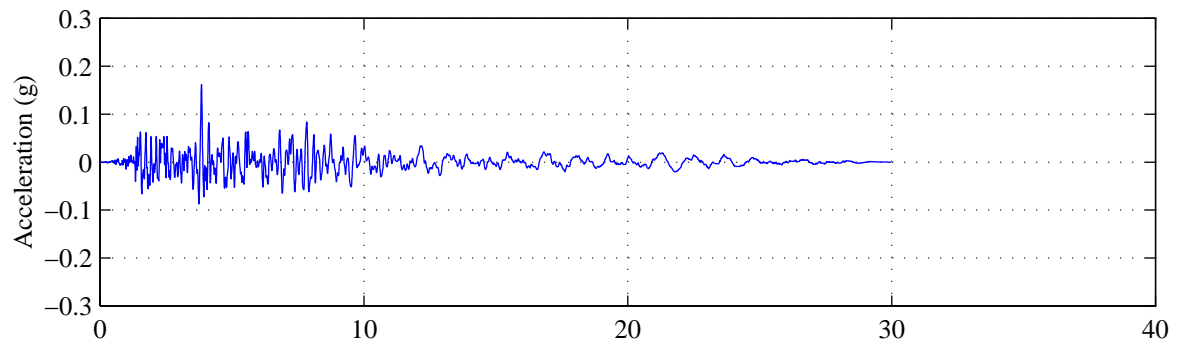
Figure A.22. Ground acceleration time histories from Bin 4.



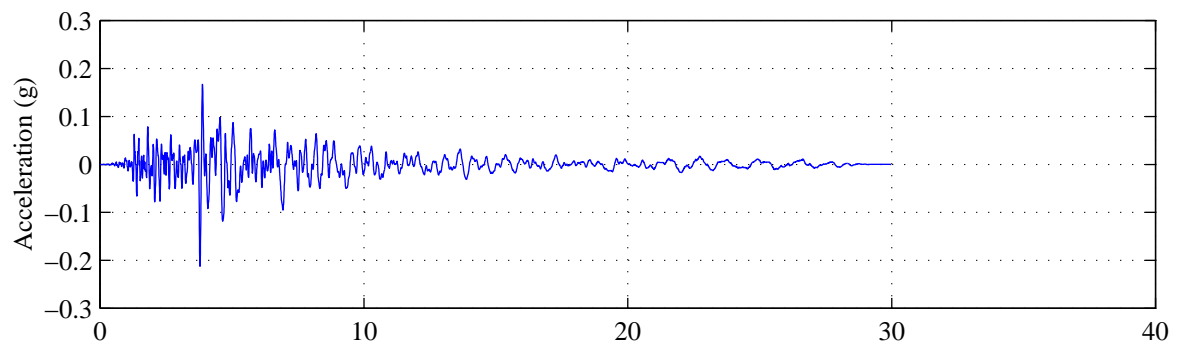
a. A-CXO225



b. A-CXO315

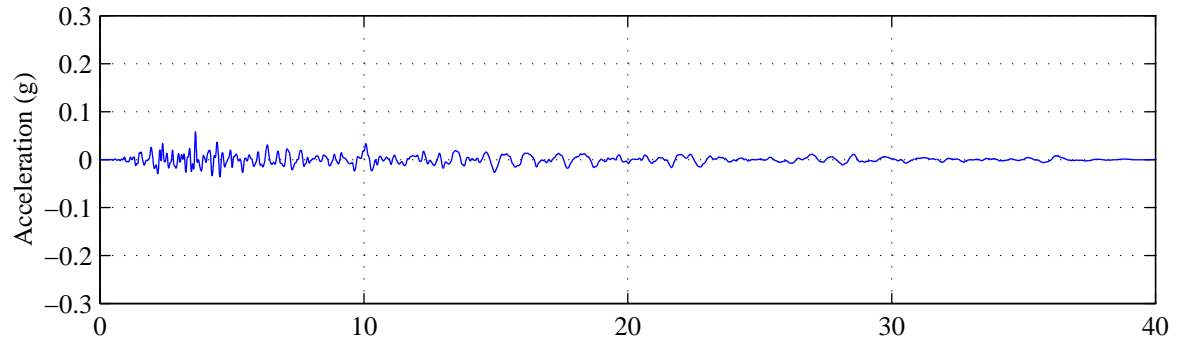


c. G02000

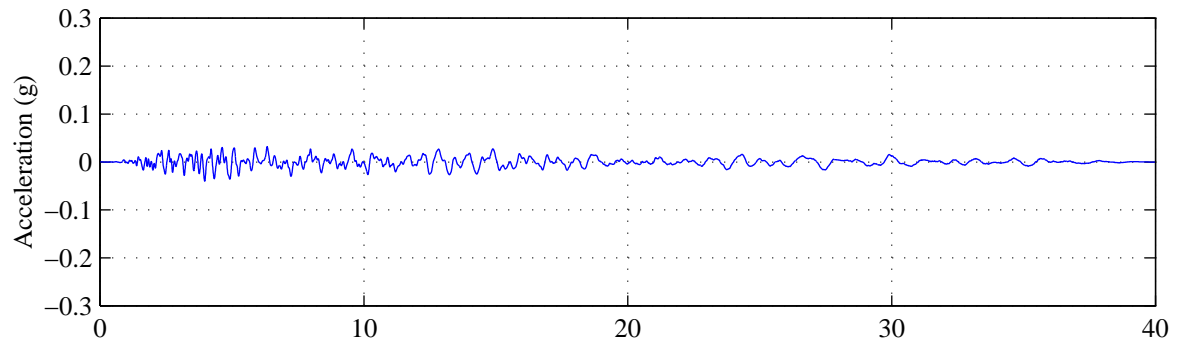


d. G02090

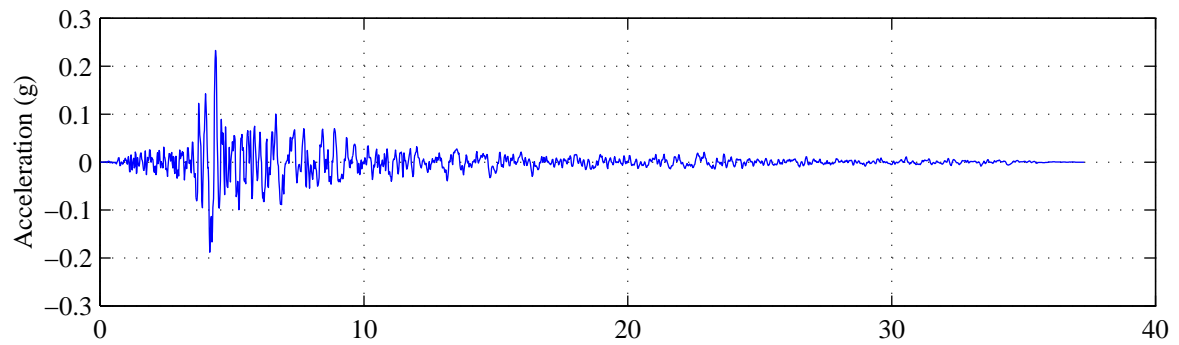
Figure A.23. Ground acceleration time histories from Bin 4.



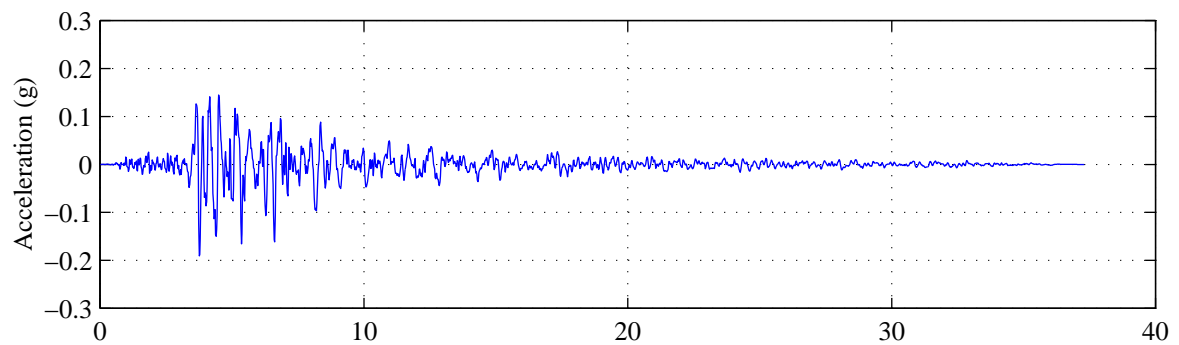
a. A-SRM070



b. A-SRM340

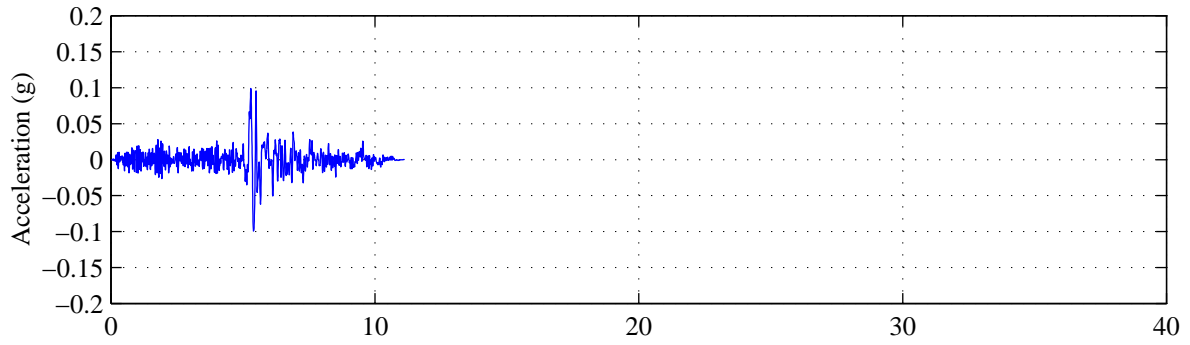


c. A-BUE250

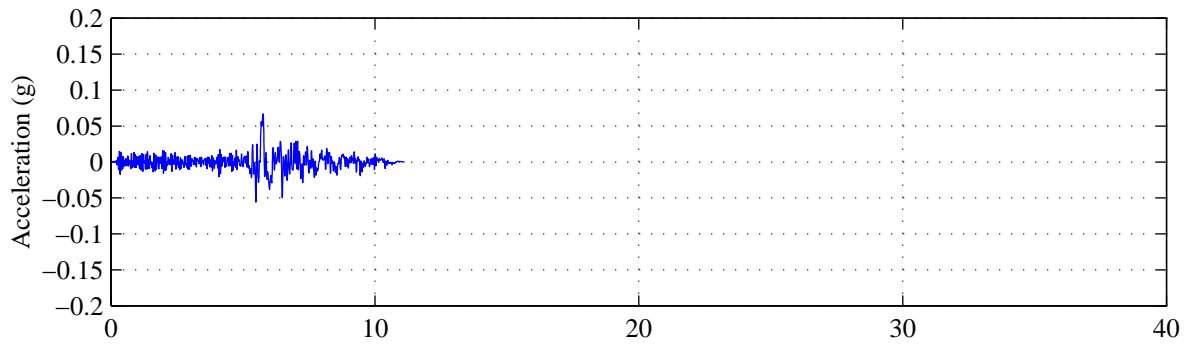


d. A-BUE340

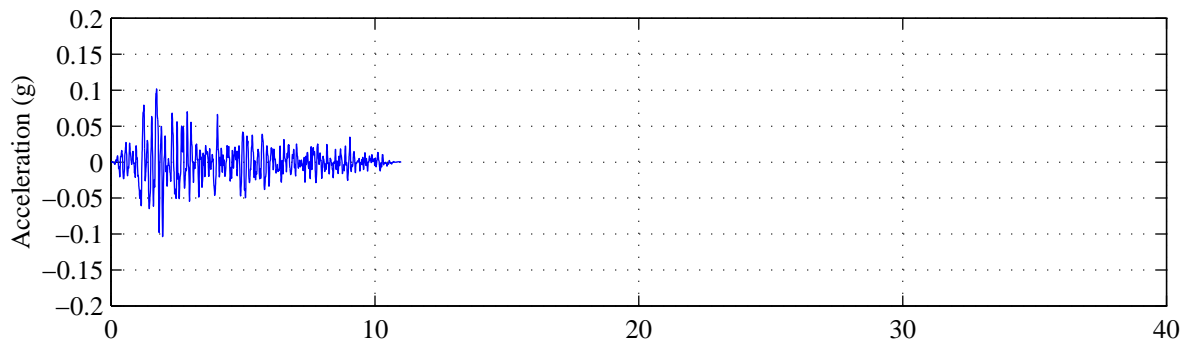
Figure A.24. Ground acceleration time histories from Bin 4.



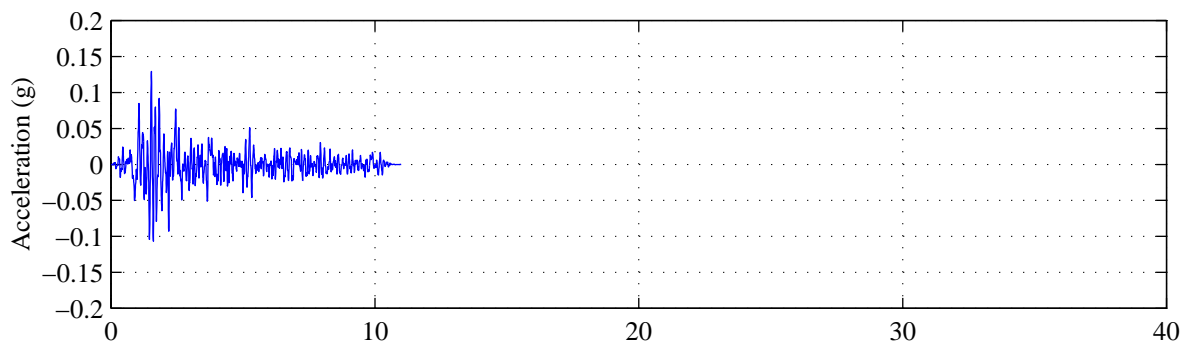
a. AZF225



b. AZF315



c. ARM270



d. ARM360

Figure A.25. Ground acceleration time histories from Bin 5.

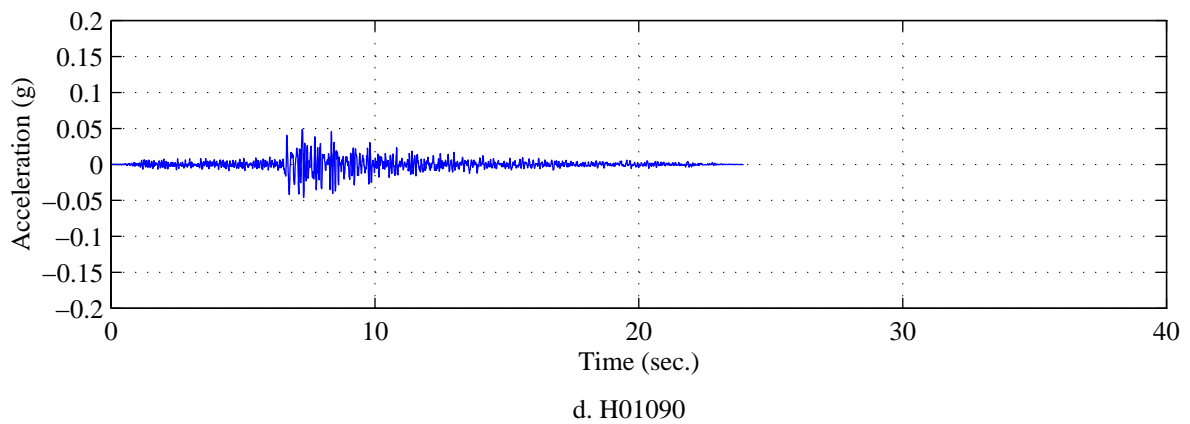
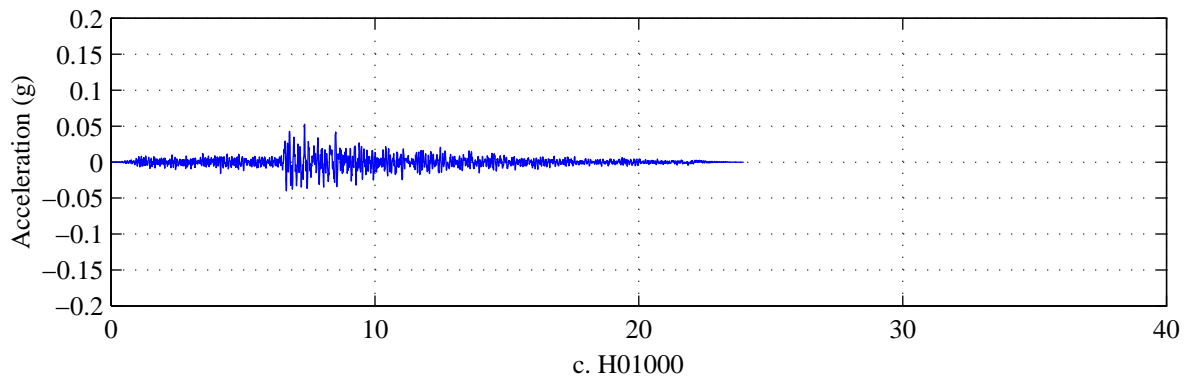
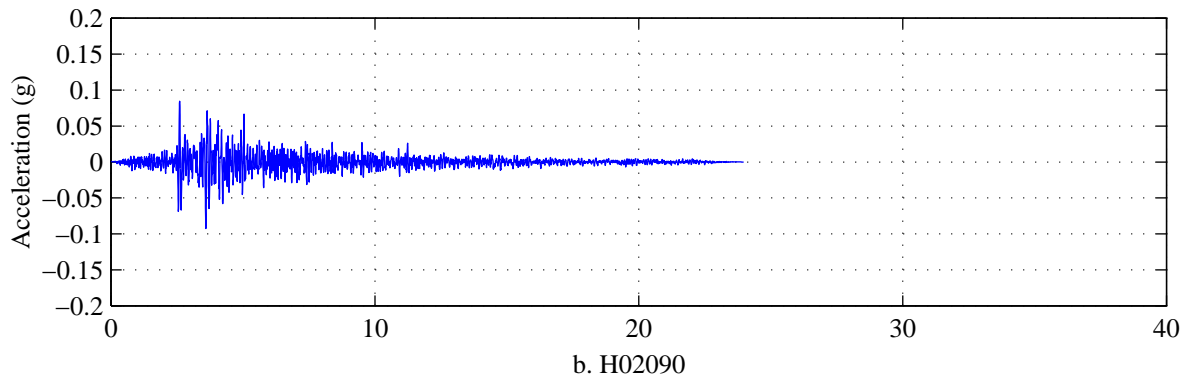
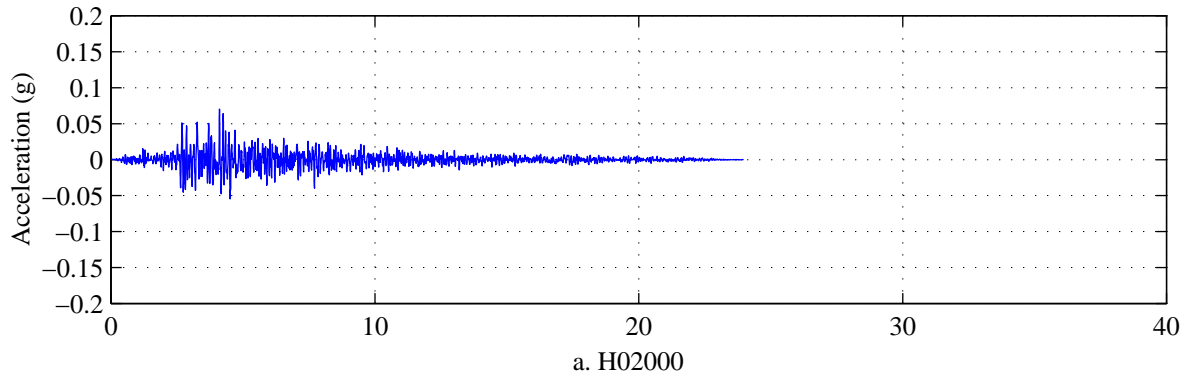


Figure A.26. Ground acceleration time histories from Bin 5.

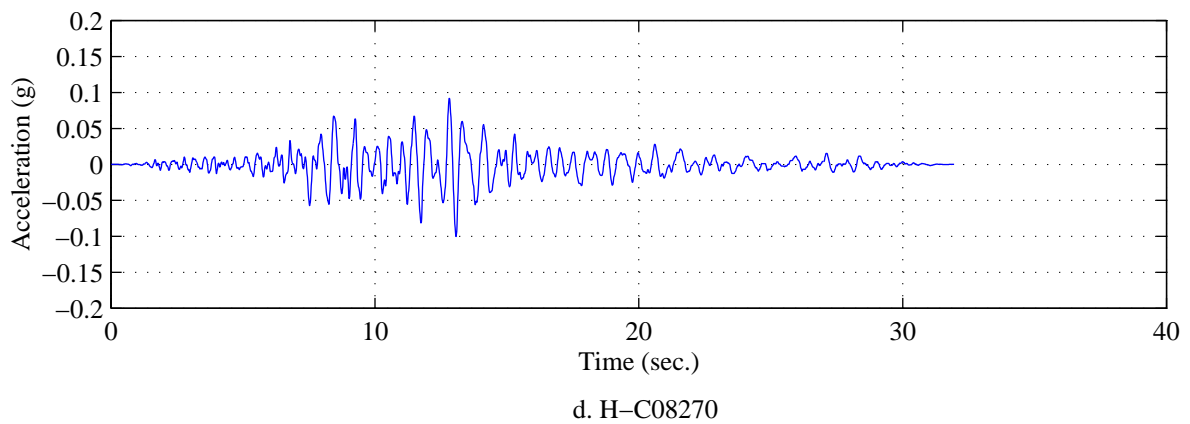
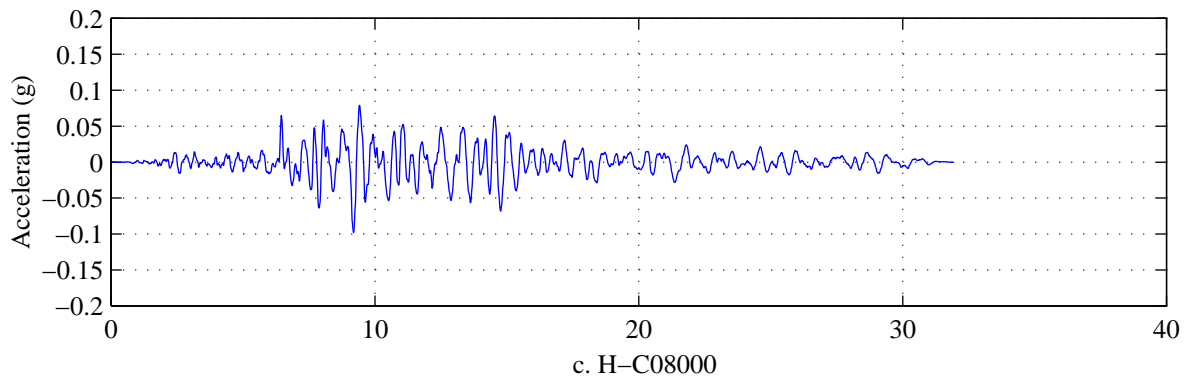
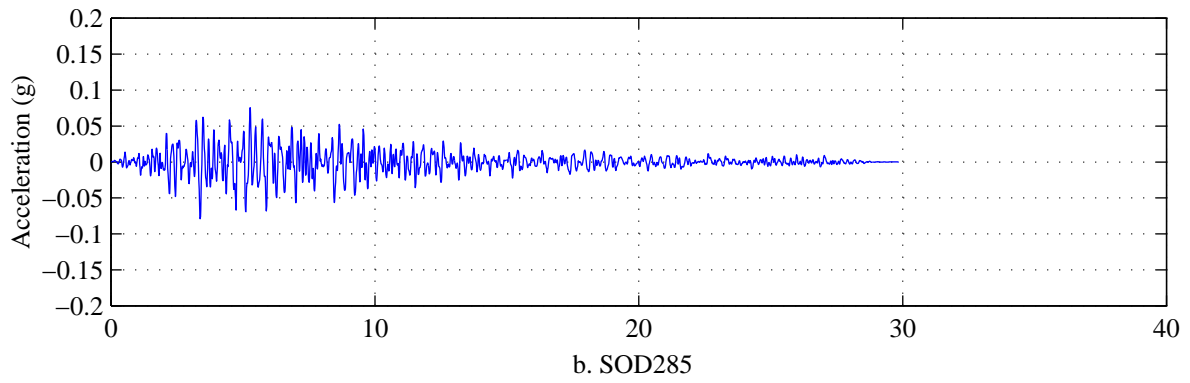
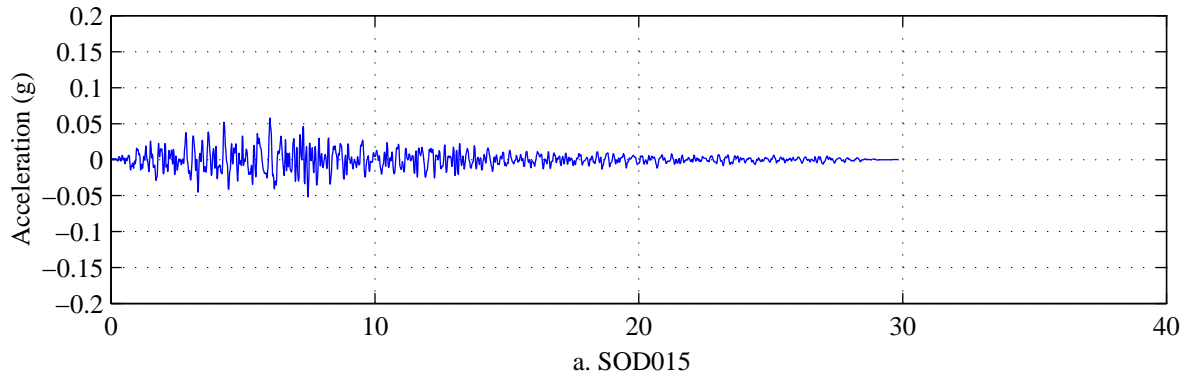
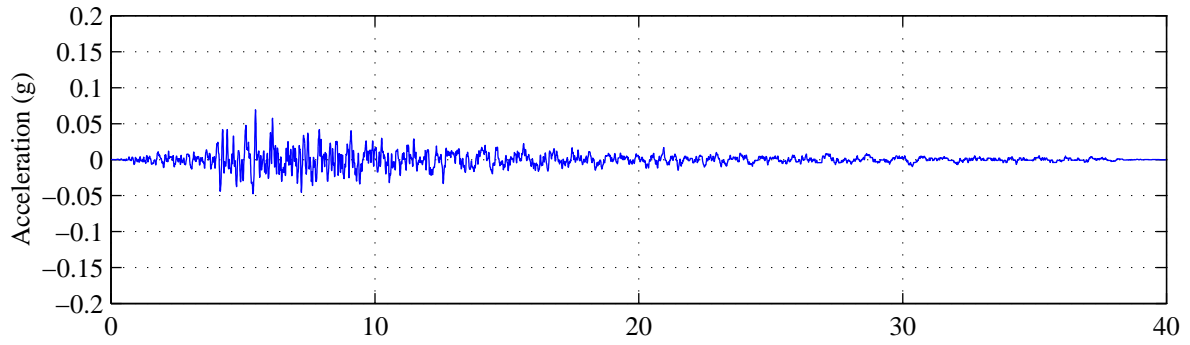
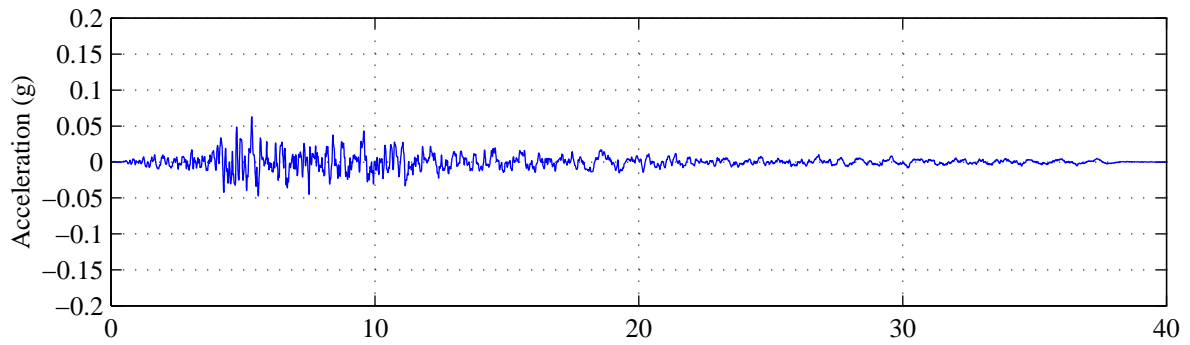


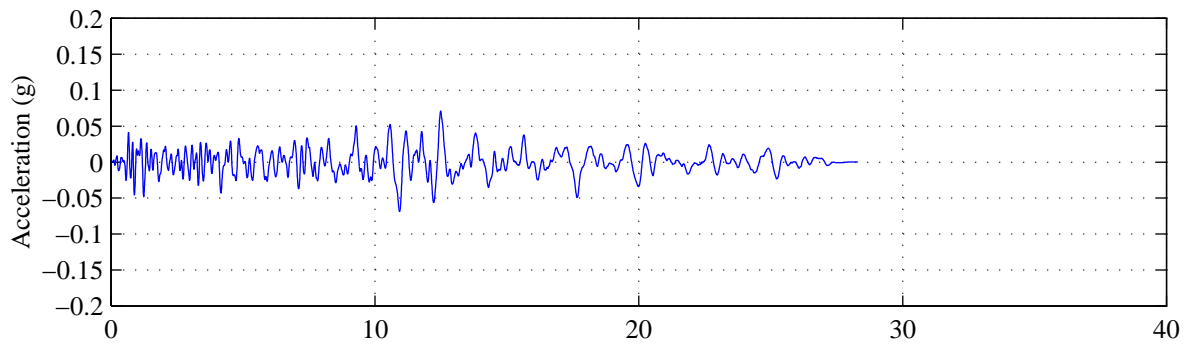
Figure A.27. Ground acceleration time histories from Bin 5.



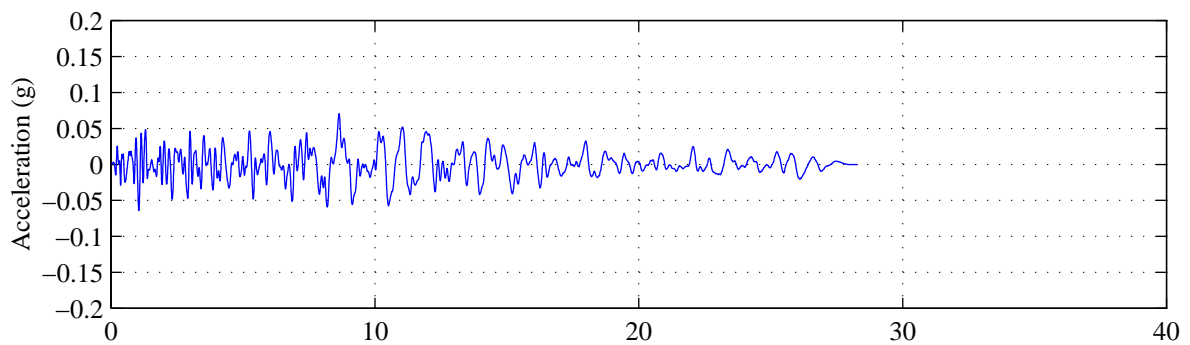
a. H06270



b. H06360

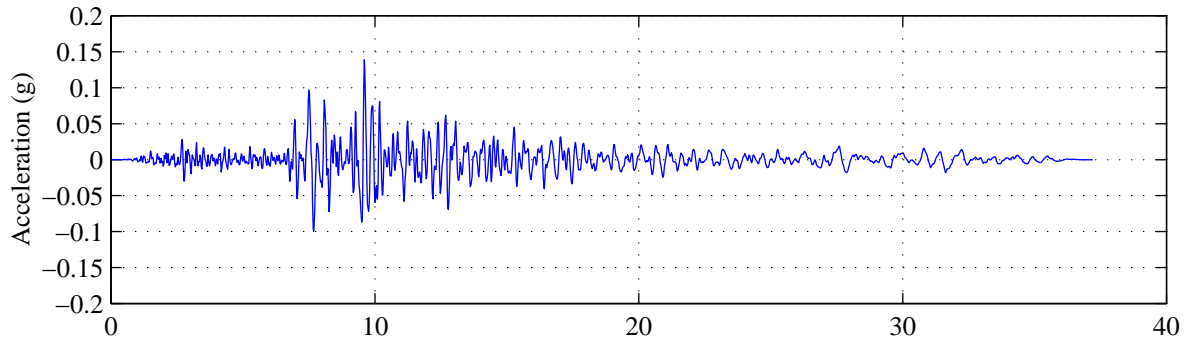


c. HCH001

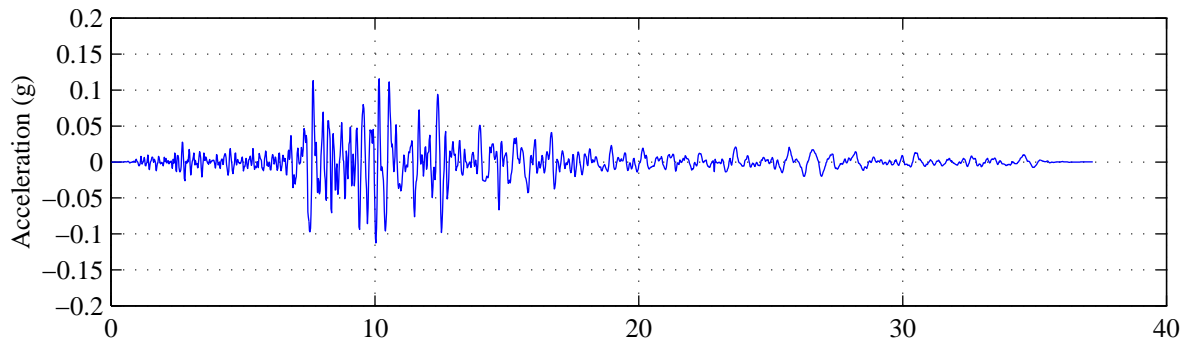


d. HCH271

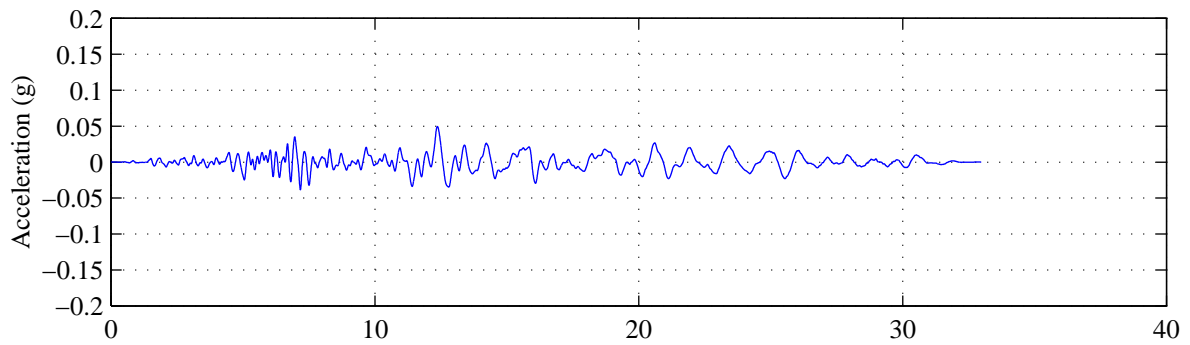
Figure A.28. Ground acceleration time histories from Bin 5.



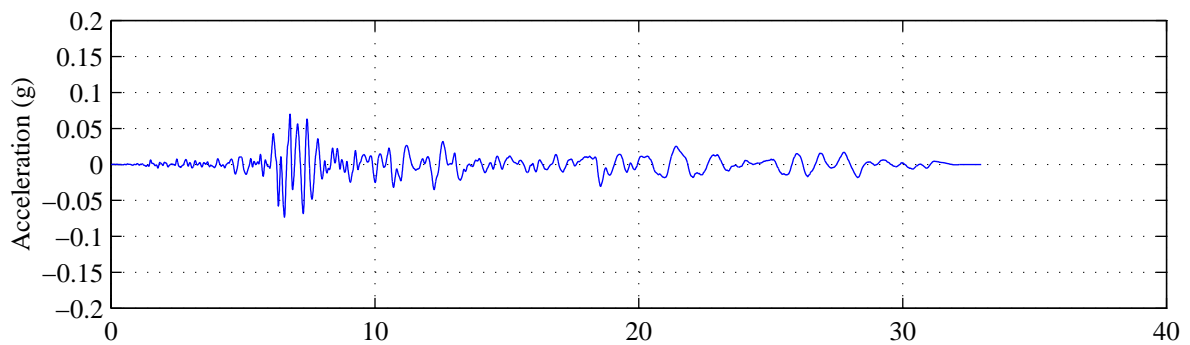
a. A-CNP106



b. A-CNP196



c. A-STP093



d. A-STP183

Figure A.29. Ground acceleration time histories from Bin 5.

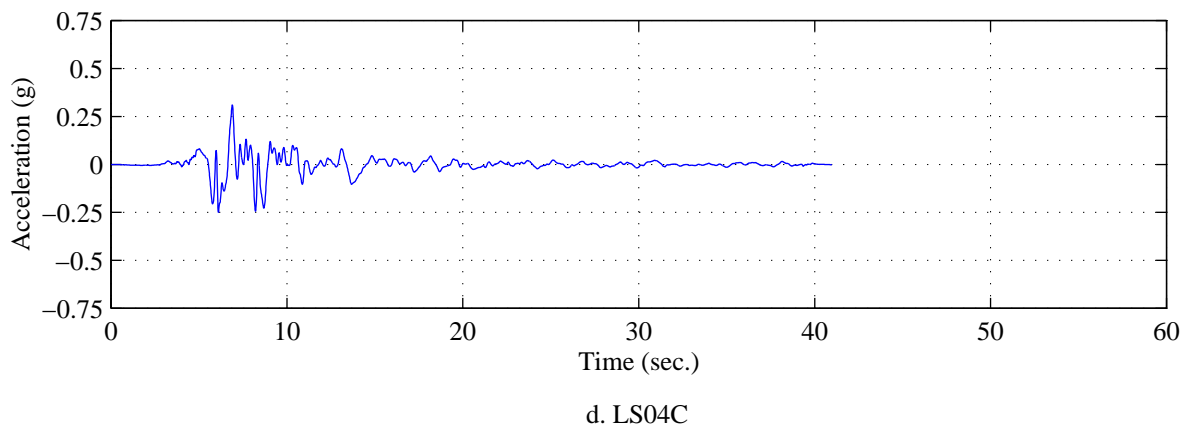
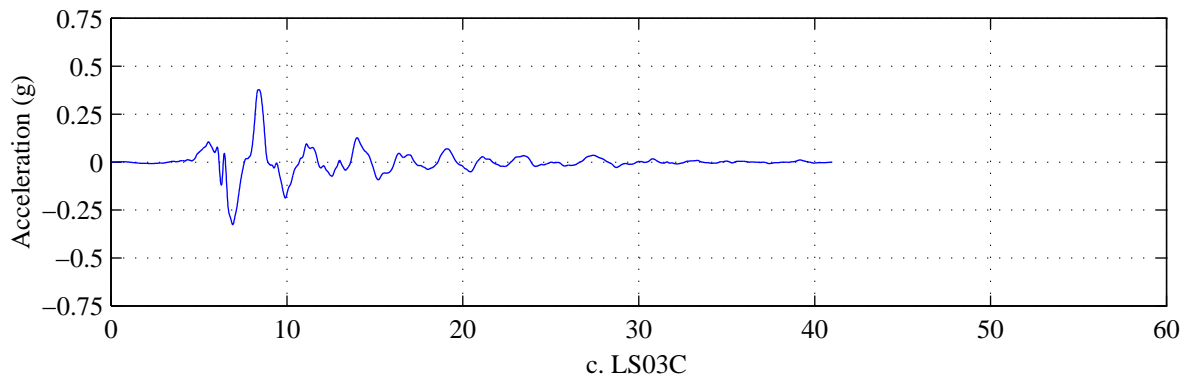
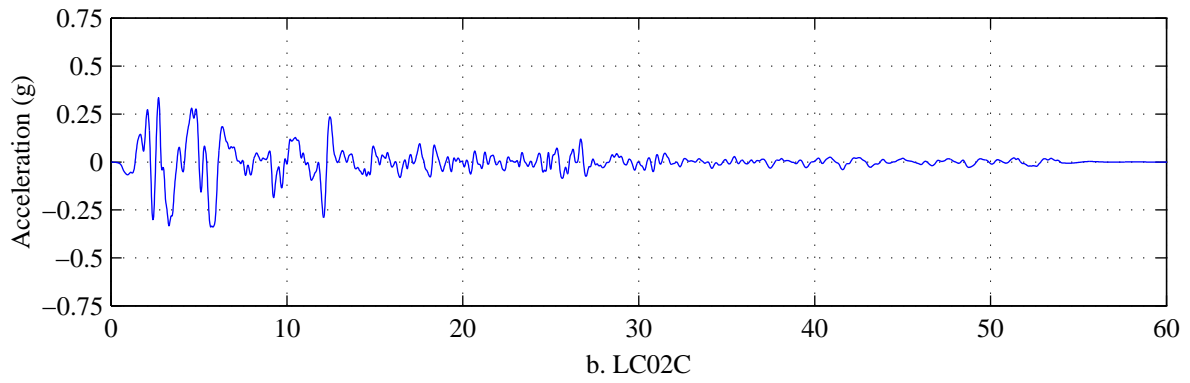
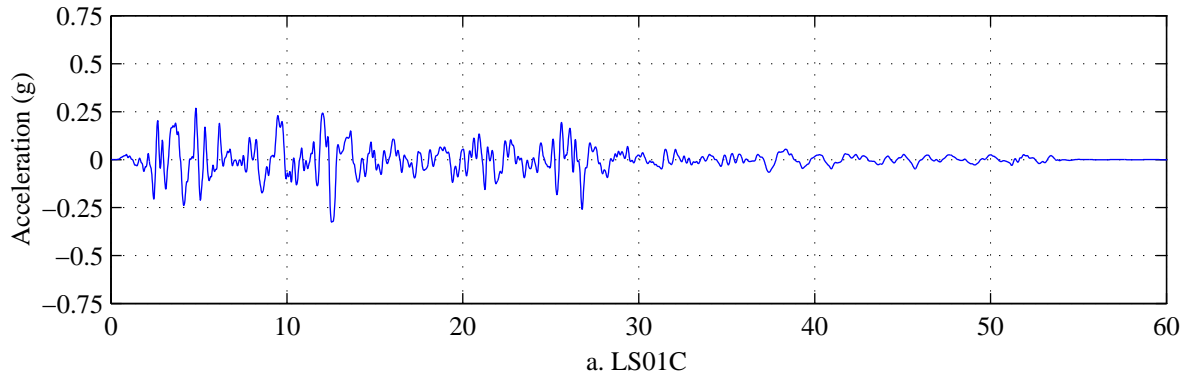


Figure A.30. Ground acceleration time histories from Bin 6.

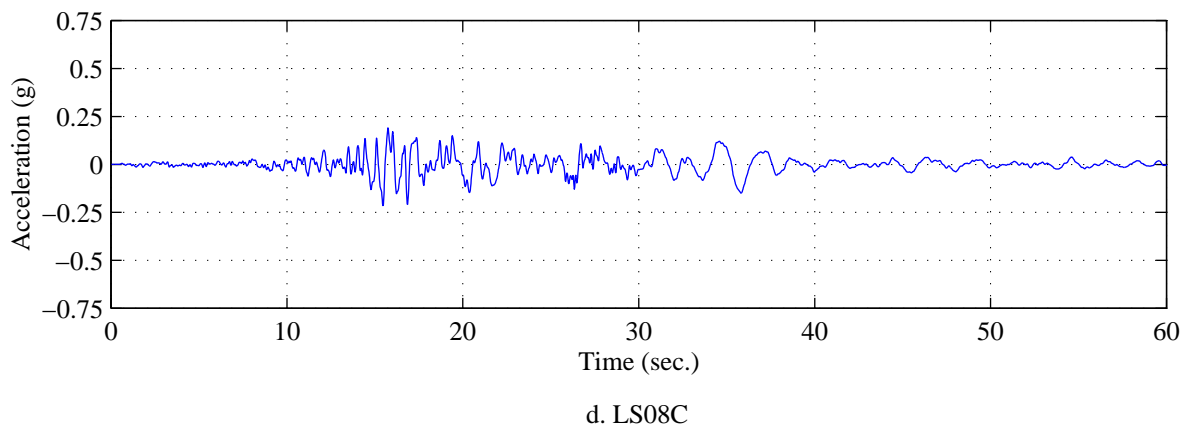
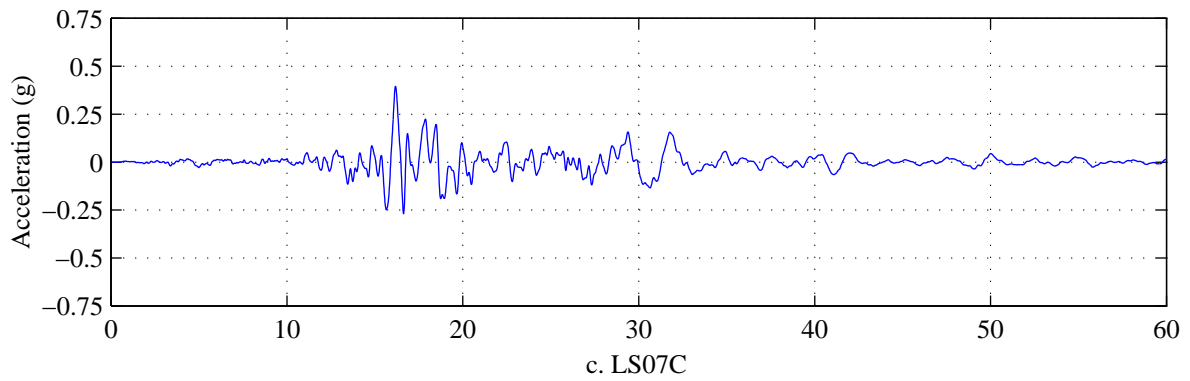
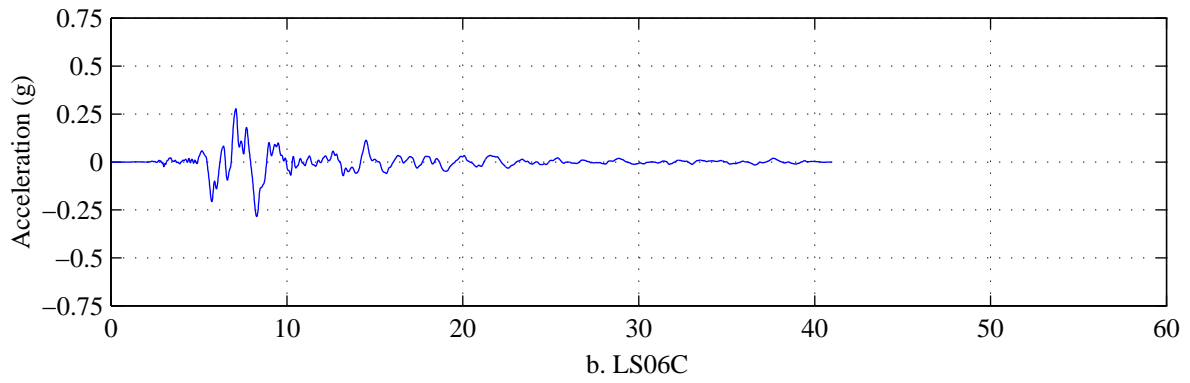
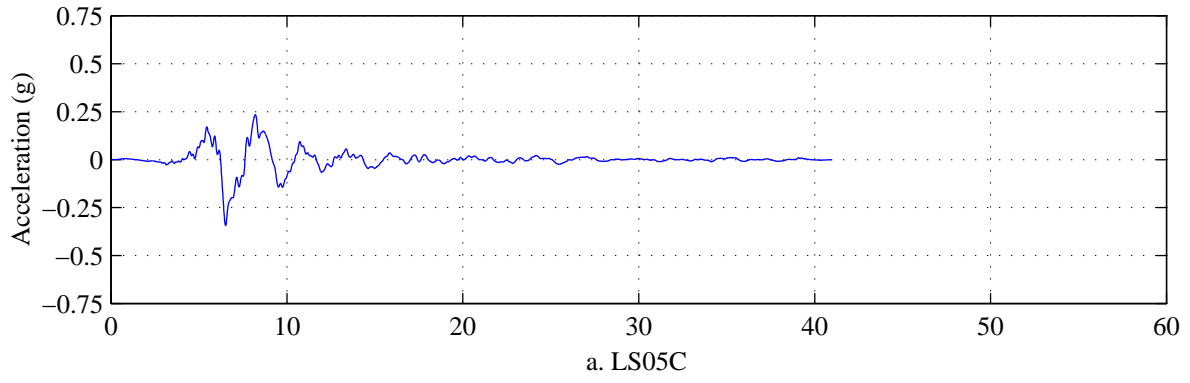


Figure A.31. Ground acceleration time histories from Bin 6.

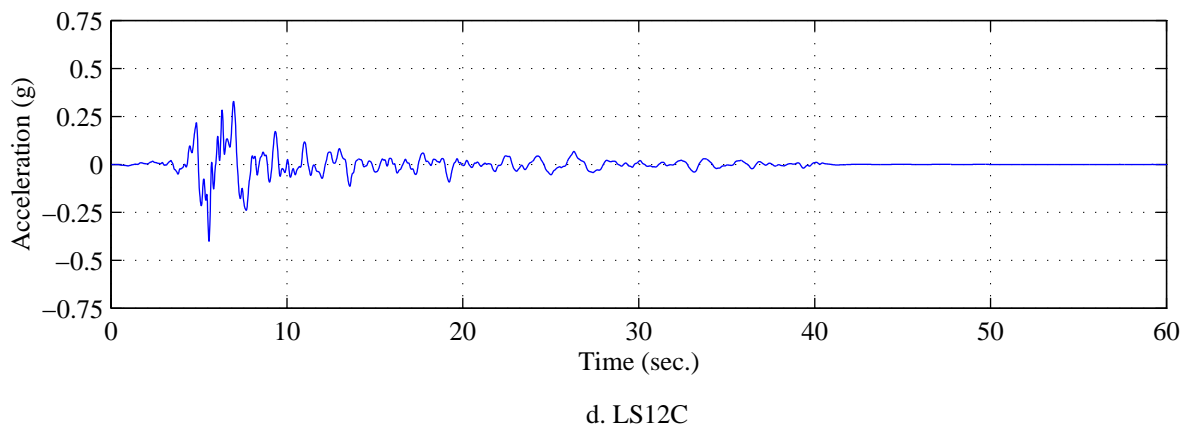
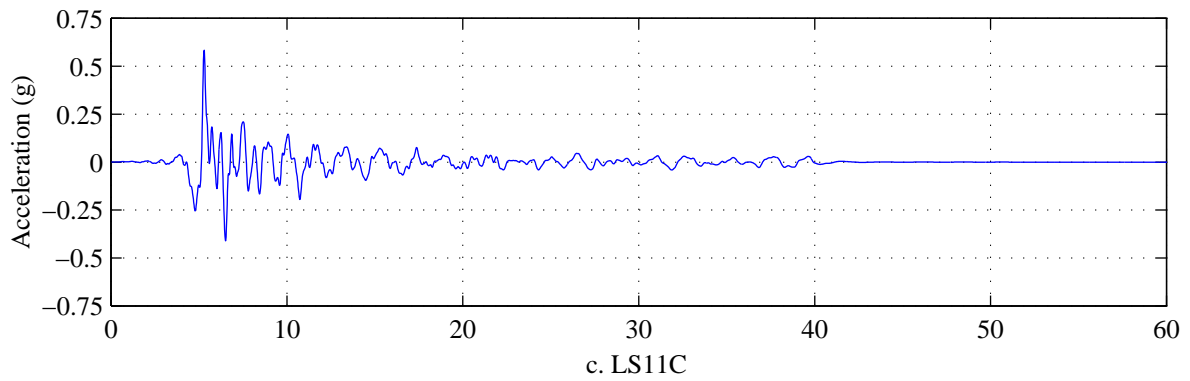
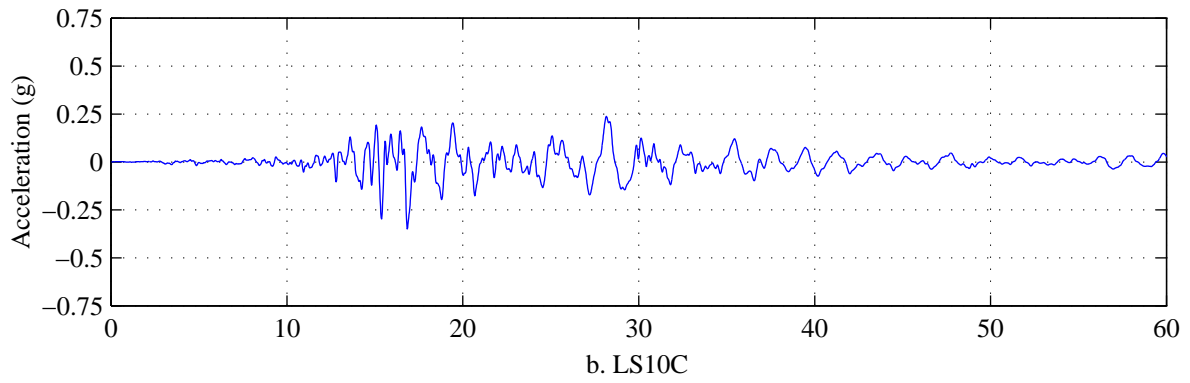
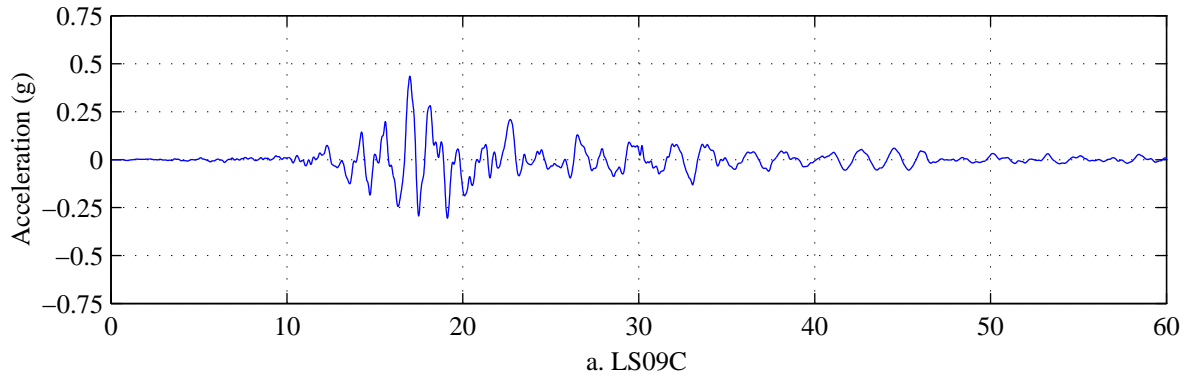


Figure A.32. Ground acceleration time histories from Bin 6.

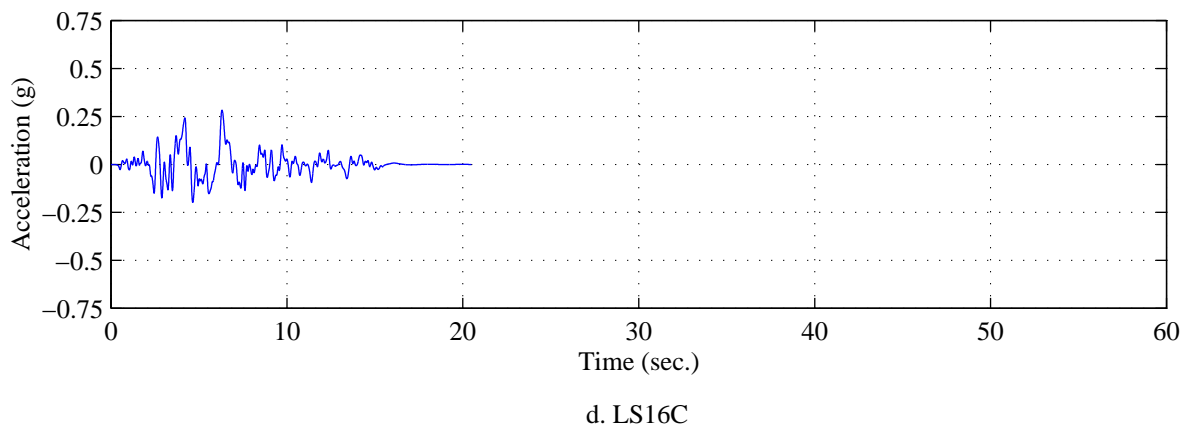
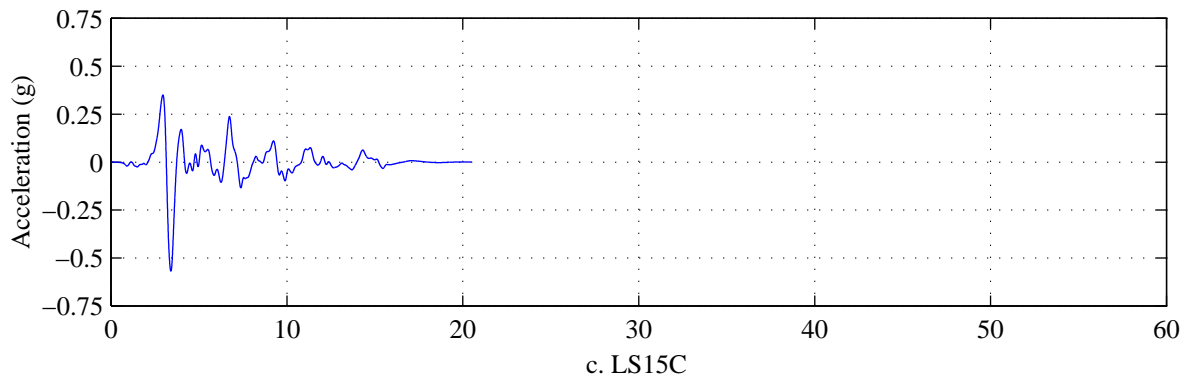
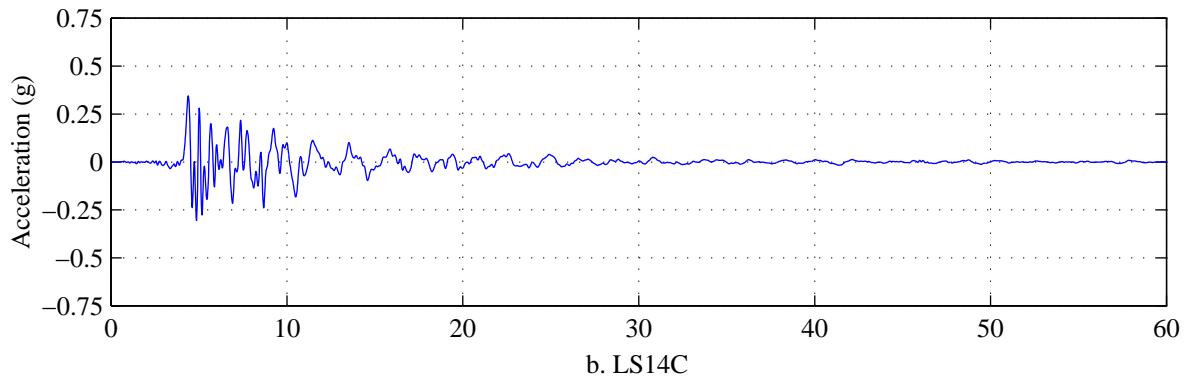
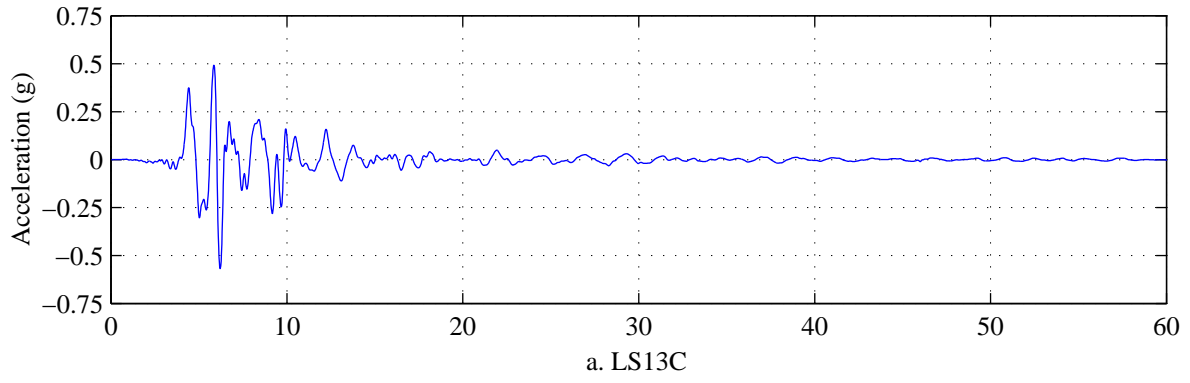


Figure A.33. Ground acceleration time histories from Bin 6.

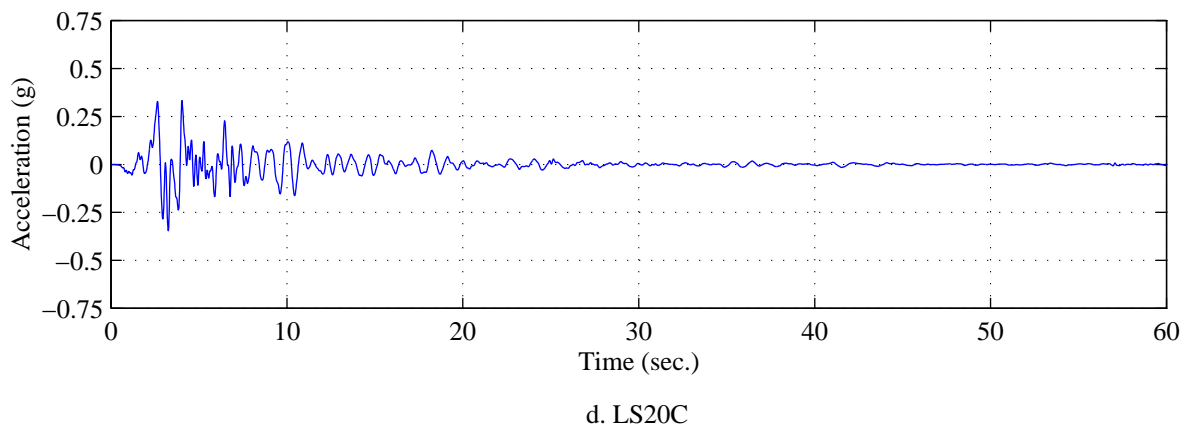
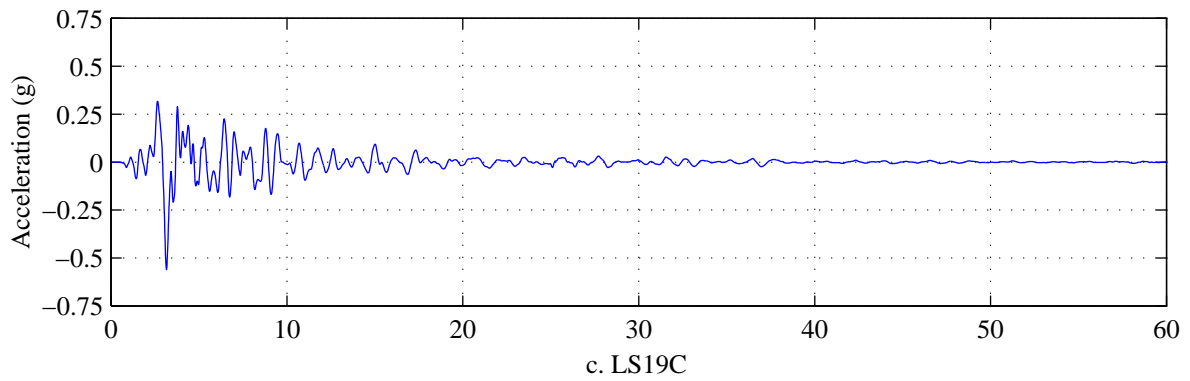
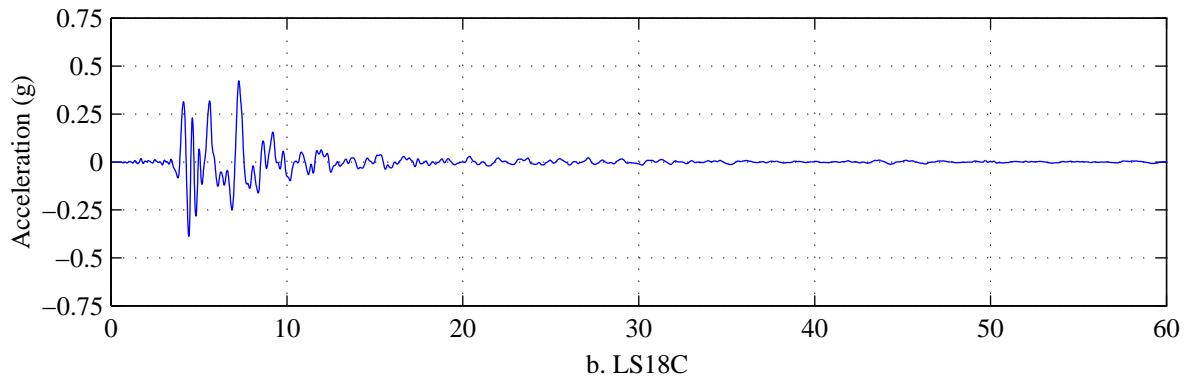
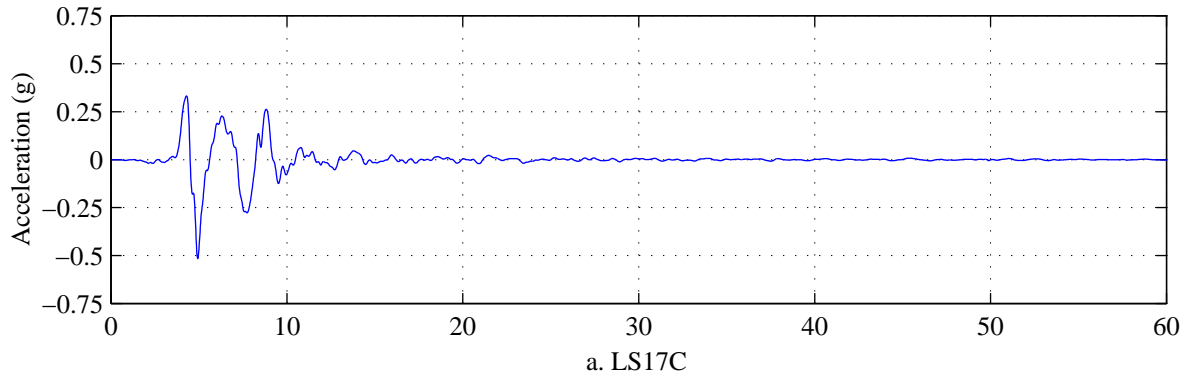
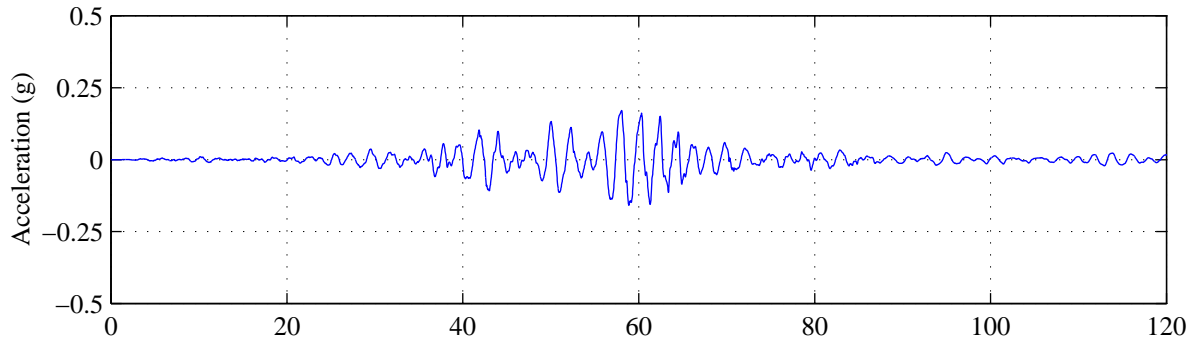
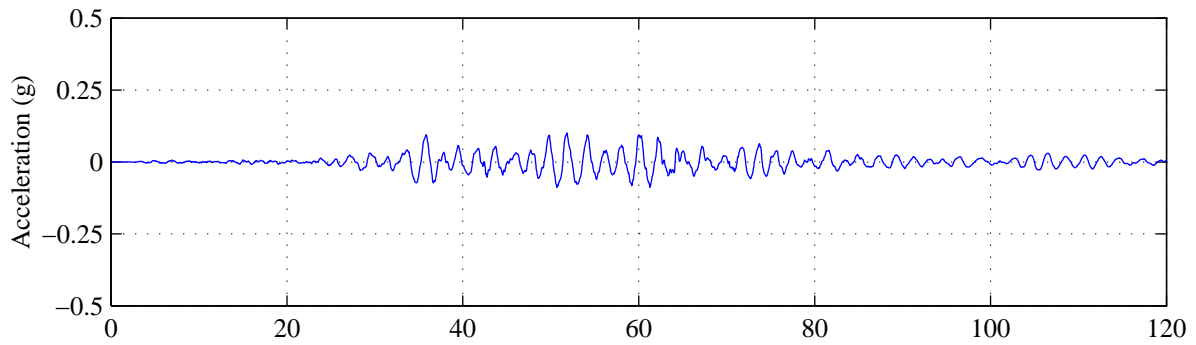


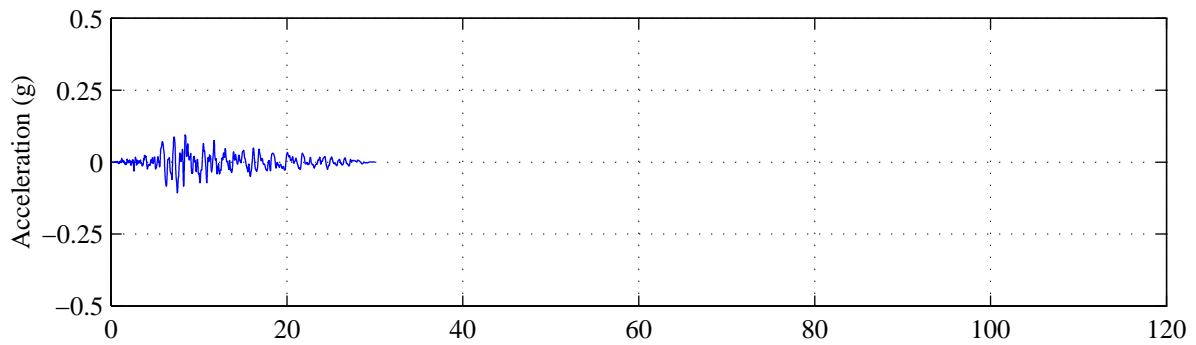
Figure A.34. Ground acceleration time histories from Bin 6.



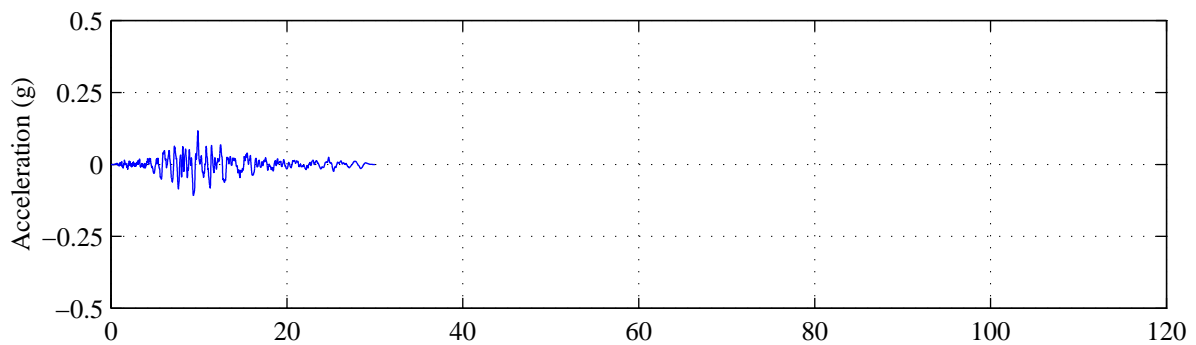
a. SCTEW



b. SCTNS



c. MEN270



d. MEN360

Figure A.35. Ground acceleration time histories from Bin 7.

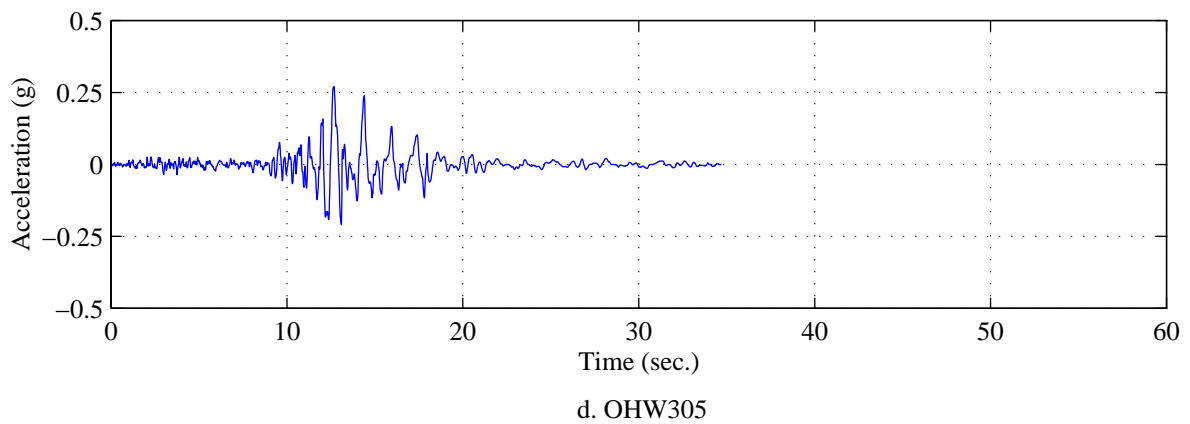
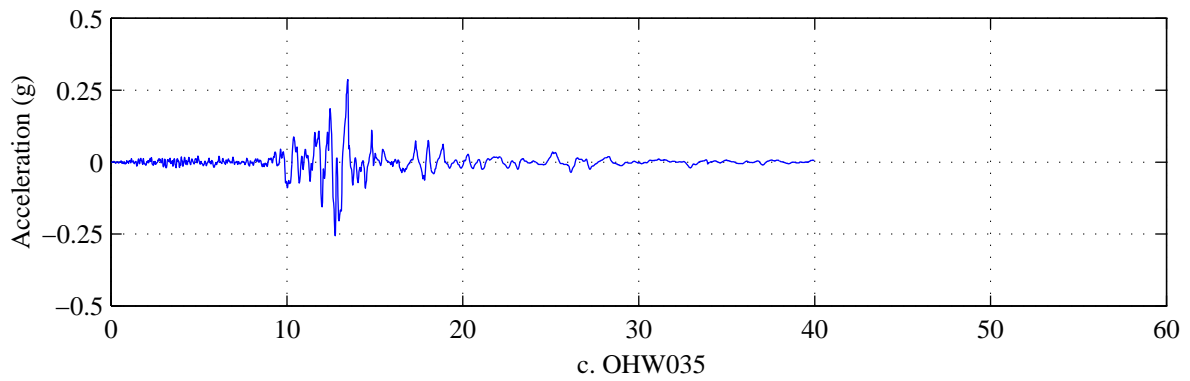
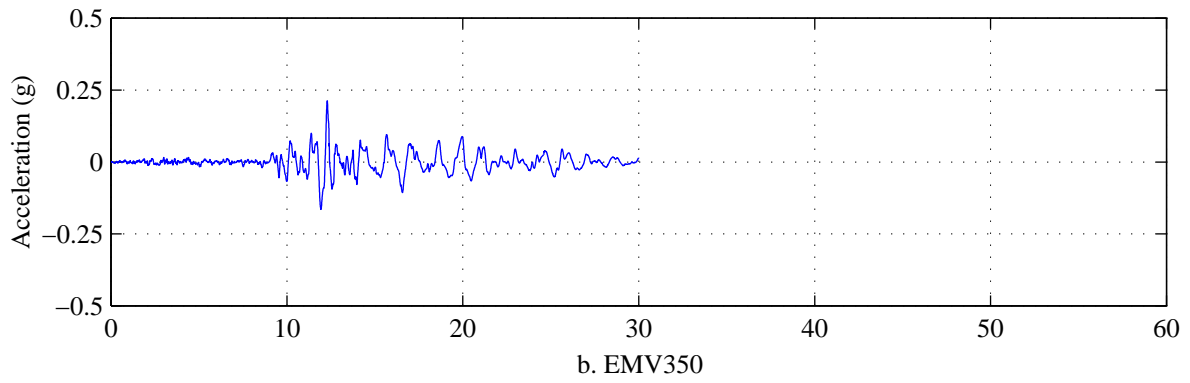
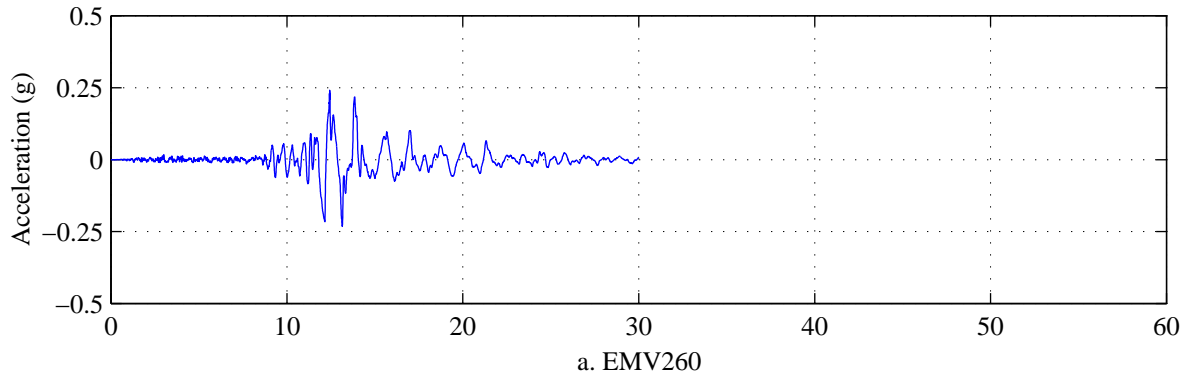


Figure A.36. Ground acceleration time histories from Bin 7.

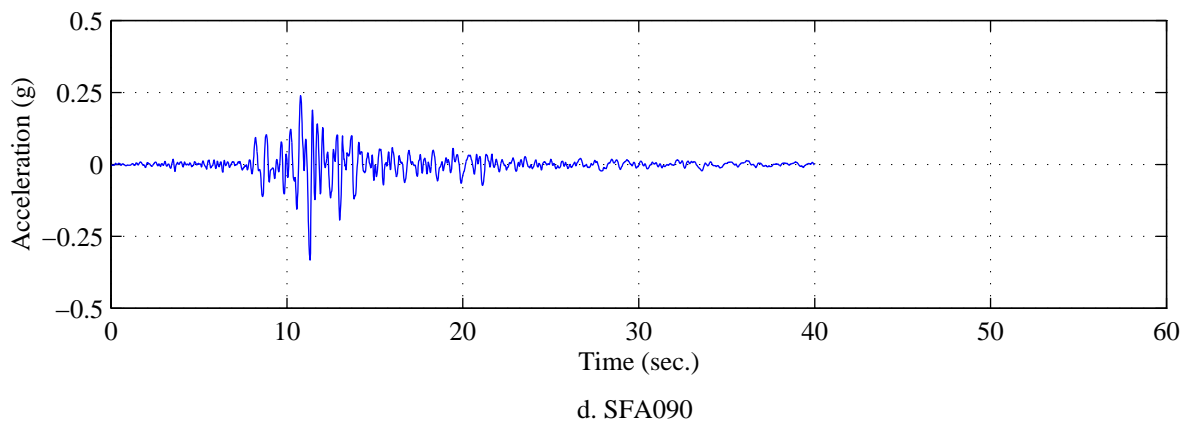
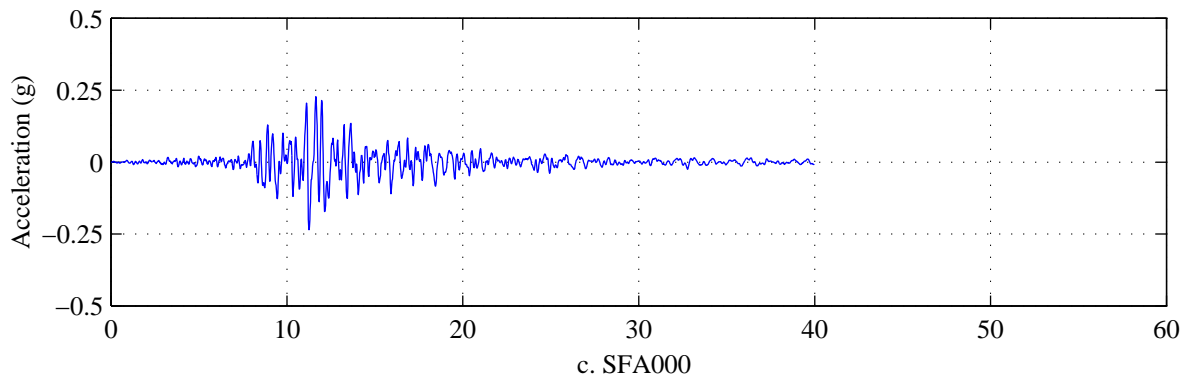
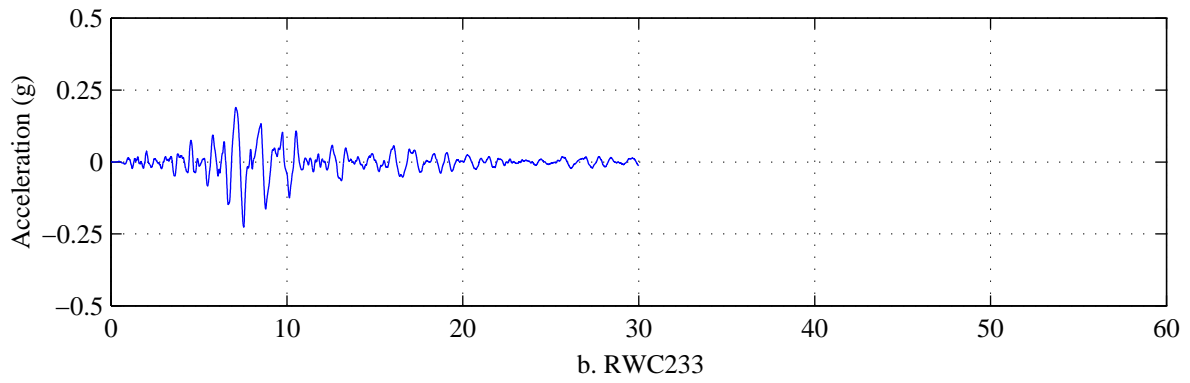
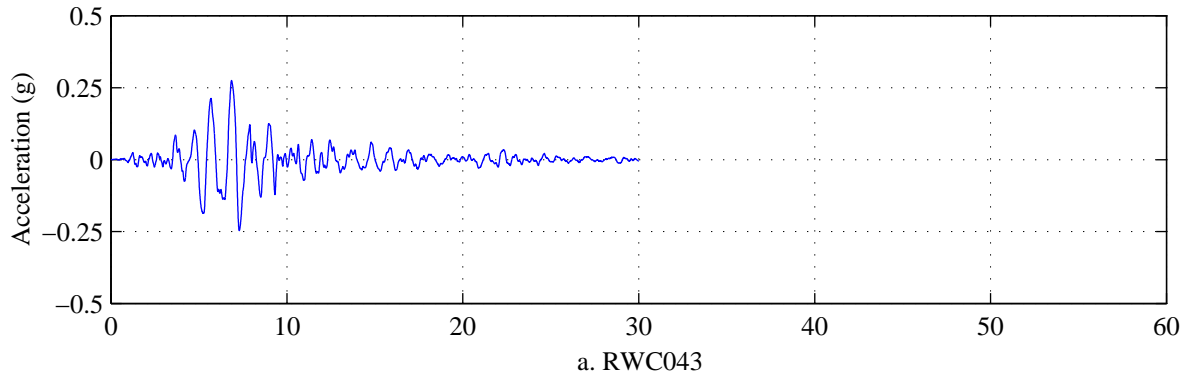


Figure A.37. Ground acceleration time histories from Bin 7.

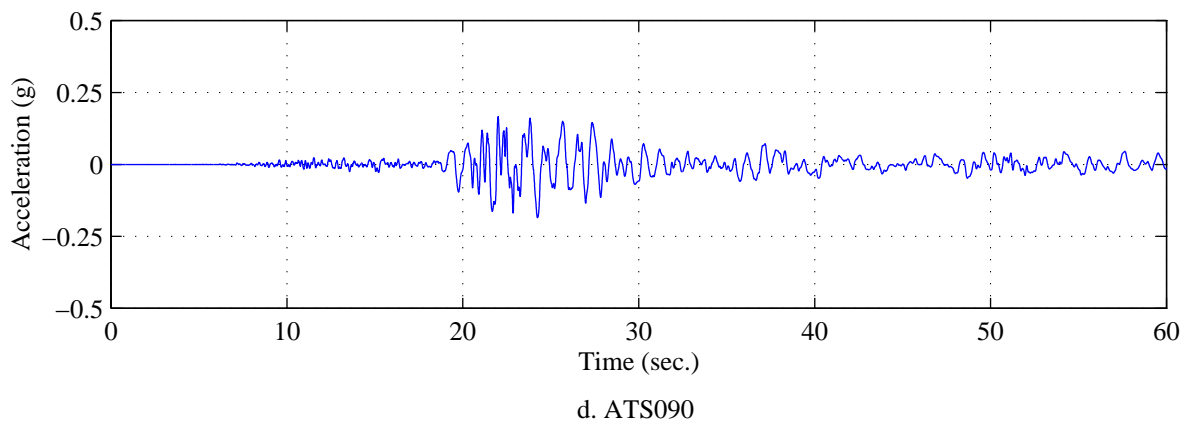
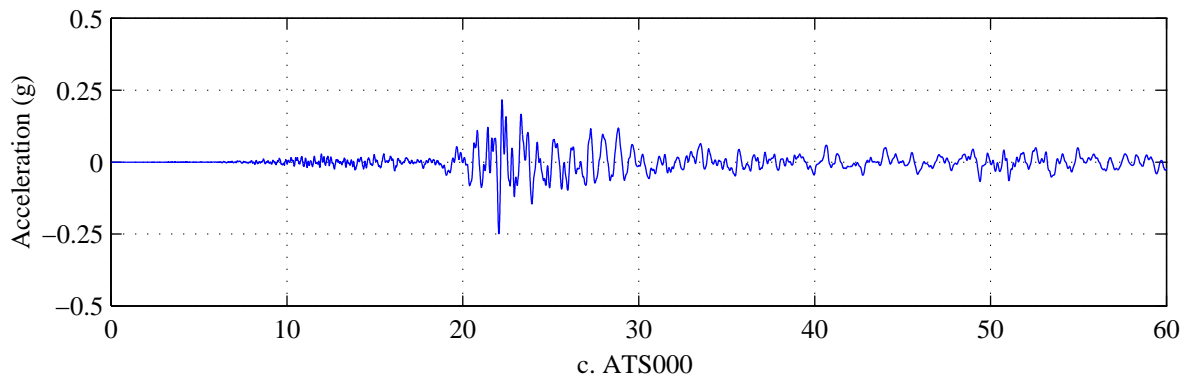
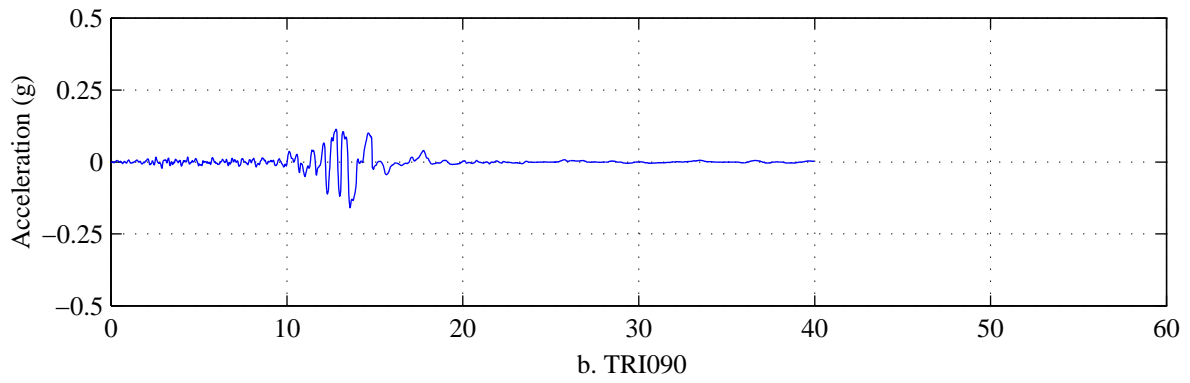
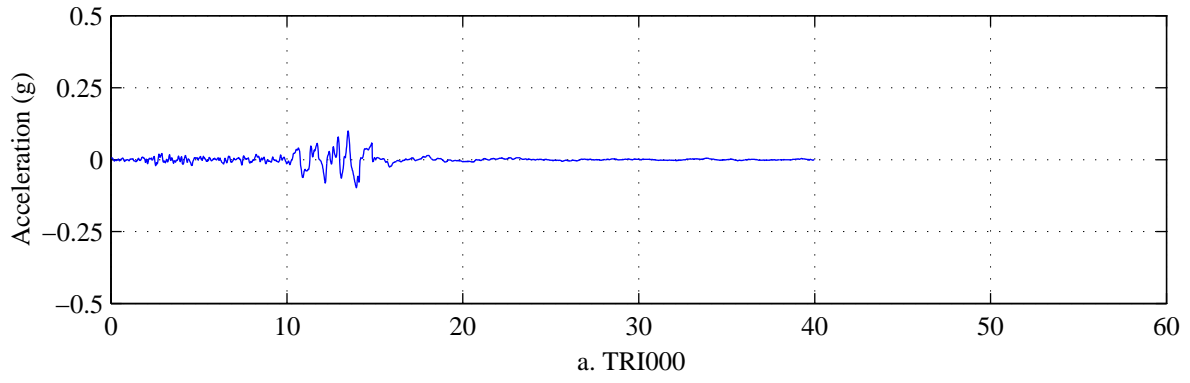


Figure A.38. Ground acceleration time histories from Bin 7.

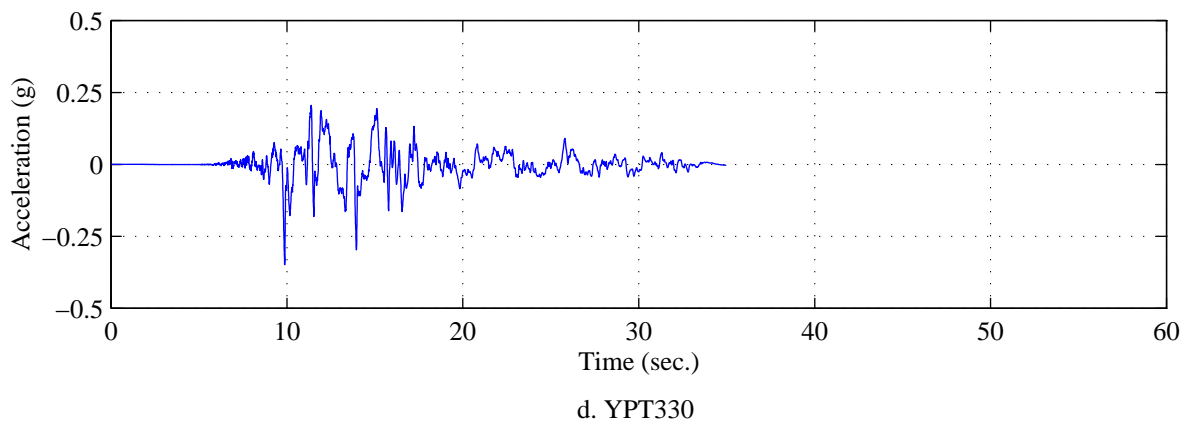
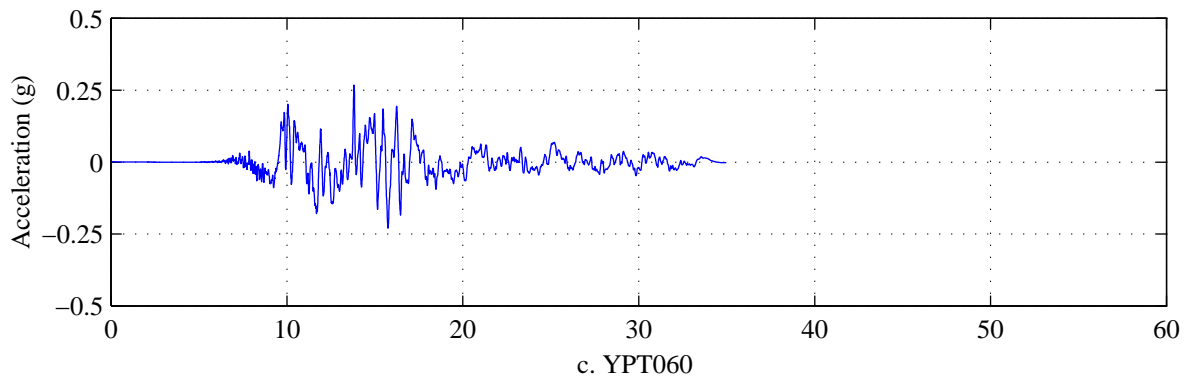
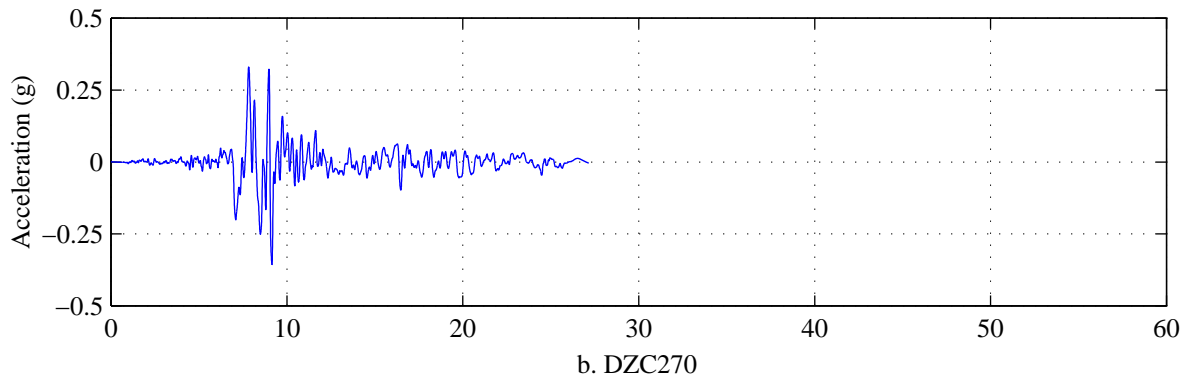
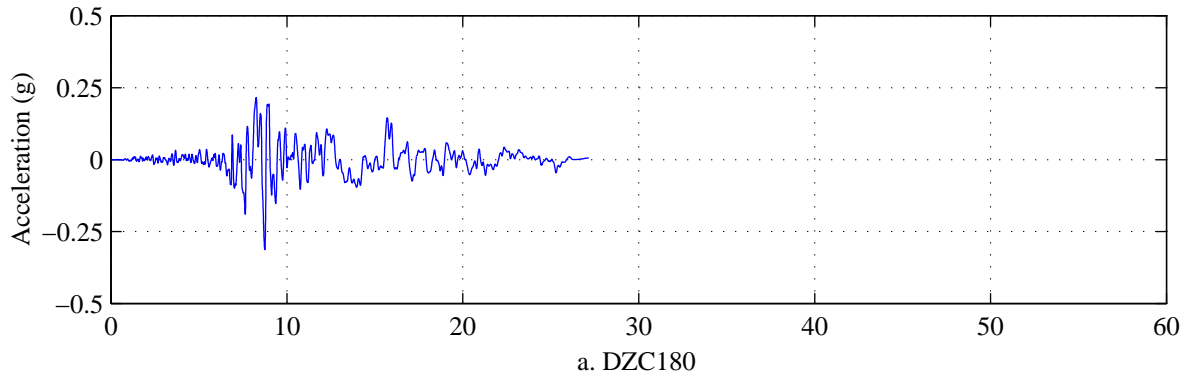


Figure A.39. Ground acceleration time histories from Bin 7.

APPENDIX B

INVESTIGATION OF THE DISTRIBUTION OF SPECTRAL ACCELERATION DATA

B.1 General

This section presents an investigation of the distribution of four samples of spectral acceleration data corresponding to four natural periods of vibration. The data samples were selected from two sets of elastic response spectra generated using ground motions from Bin 1 and Bin 2: the Near-Field and Large-Magnitude, Small-Distance bins, respectively. The motivation for the work described in this section is to determine whether the observed spectral acceleration data follow either of two proposed continuous probability distribution functions. First, a qualitative comparison is made between the observed data and two continuous distribution functions to assess which distribution best characterized the sample data. To facilitate this qualitative analysis, the observed data was organized into equally spaced intervals from which a frequency diagram was constructed. Parameters for the two distributions were estimated from the data samples. The normal and lognormal distributions are plotted with the corresponding frequency diagrams. Cumulative frequency and cumulative distribution functions were also calculated and are presented in a graphical format. Finally, a goodness-of-fit test was conducted on one sample set of spectral acceleration data to quantitatively determine which distribution is best for the spectral acceleration data. Results of the quantitative analysis are presented in tabular and graphical format.

B.2 Organization of Spectral Acceleration Data

Four spectral acceleration data sets were selected. The first and second data sets were taken from the Near-Field (Bin 1) elastic response spectra, the first at a period of 2.0 seconds (constant velocity region) and the second sample at a period of 4.0 seconds (constant displacement region). These period represent a typical lower and upper bound for the period of isolated bridge structures. The third and fourth data sets were taken from the Large-Magnitude, Small-Distance (Bin 2) elastic response spectra at periods of

0.5 seconds and 2.0 seconds, representing the constant acceleration and constant velocity regions, respectively. The elastic response spectra for Bin 1 and Bin 2 are plotted in Figures B.1a and B.2.a respectively. To construct the frequency diagrams the data samples were then organized into k equally spaced intervals where the number of intervals were determined using the following formula

$$k = 1 + 3.3 \cdot \log_{10}(n) \quad (\text{B.1})$$

where n is the sample size (Soong, 1981). The sample sizes are 24 and 20 for Bin 1 and Bin 2 respectively. Equation (B.1) yields the same number of intervals for each sample when the results obtained from (B.1) are rounded to the next largest integer. Frequency diagrams for each data sample are shown in Figures B.1b, B.1.c, B.2b, and B.2c.

B.3 Continuous Distribution Functions

The *Normal* (or Gaussian) and the *Lognormal* distributions were selected as possible models for the distribution of spectral acceleration data. Based on the observation that the lognormal distribution is bounded on one side by zero, makes it a good choice for characterizing spectral acceleration data. The normal distribution may extend into the negative range, which is inconsistent with the observed data. Despite this possibility, the normal distribution has been investigated because it is a popular choice when describing the distribution of continuous random variables and its parameters are well understood by engineers.

The parameters for the normal distributions, namely, mean and variance, were estimated from the data sample and calculated using the following formula

$$m_x = \left[\frac{1}{n} \cdot \sum_{i=1}^n x_i \right] \quad (\text{B.2})$$

$$\sigma_x^2 = \left[\frac{1}{n-1} \cdot \sum_{i=1}^n (x_i - m)^2 \right] \quad (\text{B.3})$$

where m_x is the sample mean; n is the sample number; x_i are the sample values taken to be the spectral data and σ_x^2 is sample variance.

The parameters of the lognormal distributions were determined by taking the natural logarithm of the data samples and then calculating the sample mean and sample variance of each using the previously described equations (B.2) and (B.3). For instance, if x is defined to be

$$x = \ln(y) \quad (B.4)$$

where y is the spectral acceleration data assumed to be lognormally distributed, then x can be assumed to be random variable that follows a normal distribution. The parameters of the lognormal distribution were then estimated using the following formula

$$\theta_y = \exp(m_x) \quad (B.5)$$

$$\sigma_{\ln y} = \sigma_x \quad (B.6)$$

where θ_y and $\sigma_{\ln y}$ are the estimated parameters of the lognormal distributions; m_x is the sample mean of x calculated using Equation (B.2) and σ_x is the standard deviation of x calculated as the square-root of the result of Equation (B.3). It is important to note that θ_y and $\sigma_{\ln y}$ are not the mean and standard deviation of the lognormal random variable, y , rather parameters of the distribution that are related to the mean and variance of y . These estimated parameters were then used to calculate the normal and lognormal distribution functions plotted in Figures B.1b, B.1c, B.2b and B.2c.

B.4 Qualitative Assessment of the Distribution of Spectral Acceleration Data

To gain an idea of the distribution of the spectral acceleration data, the frequency diagrams constructed from the binned spectral acceleration data were plotted with both the normal and lognormal distribution functions whose parameters were established as described previously.

Referring to Figures B.2b and B.2c it appears that the lognormal distribution is a reasonable model for the distribution of the spectral acceleration data for both periods, 0.5 and 2.0 seconds, respectively. The lognormal model has the added benefit of being bounded by zero, which is characteristic of the spectral acceleration data. A significant portion of the normal distribution is observed to lie in the negative region as a result of the small sample means and large sample variances, which makes the normal distribution assumption less reasonable. Both the lognormal and normal distribution functions were numerically integrated to determine the cumulative distribution functions and are plotted in Figures B.2d and B.2e. Also plotted are the cumulative frequency diagrams for each of the data samples. Again, the assumed lognormal distribution results in a cumulative distribution function that better characterizes the observed spectral data shown by the cumulative frequency diagram. Similar trends are observed from the data samples from Bin 1 spectra, see Figures B.1b, B.1c, B.1d and B.1e.

Although this analysis provides a qualitative assessment of the lognormal and normal distributions, a quantitative measure of the appropriateness of each of the assumed models is necessary. This quantitative analysis is presented in the next section.

B.5 Quantitative Analysis of Spectral Acceleration Data

A goodness-of-fit test was conducted to quantitatively determine which distribution better characterizes the spectral acceleration data. For the goodness-of-fit tests, one spectral acceleration data sample was selected and tested for the normal and lognormal distribution. This sample was selected from the spectra of Bin 2 and for a period of 0.5 seconds, see Figures B.2a and B.2b. The *Kolmogorov-Smirnov* test (or K-S) was selected to determine the goodness-of-fit of the acceleration data to the normal and lognormal distributions. The K-S test was selected for three reasons: first the sample size, n , is small (20) and therefore makes a Chi-squared test an inappropriate choice; second the K-S test is for use with continuous distribution functions; and third, the results of the test are not sensitive to the selection of interval number and size as is the case with the Chi-squared test (Soong, 1981).

The K-S test is a statistical measure of the difference between the observed cumulative distribution function and the theoretical cumulative distribution function, either the normal or the lognormal for this investigation. The significance level of the test, α , is related to the deviation parameter, D_2 by the following formula

$$P(D_2 > c_{n,\alpha}) = \alpha \quad (\text{B.7})$$

where $c_{n,\alpha}$ is the threshold value associated with the given significance level, α . The distribution is accepted if the sample deviation parameter d_2 , determined by means of the K-S test, is less than the tabled threshold value $c_{n,\alpha}$ for the given level of significance. It should be noted that no special consideration is made by the K-S test for estimated parameters. Rather it is recommended that the value of the sample deviation parameter, d_2 , should be significantly lower than the tabled threshold value $c_{n,\alpha}$ when the parameters of the theoretical distribution are estimated from the sample (Soong, 1981).

B.6 Results of the Goodness-of-Fit Test

Results of the two tests performed using the same spectral acceleration data sample (Bin 2 spectra at a period of 0.5 seconds) are presented in Tables B.1 and B.2. Table B.1 presents the results of a K-S test for normal distribution and Table B.2 presents the results of a K-S test for lognormal distribution. The value of, $c_{n,\alpha}$, was determined from standard tables using a sample size of 20 and a significance level of 5%, resulting in a value of 0.29, see Tables B.1 and B.2. From Table B.1 the result of the K-S test yields a sample deviation value of 0.182, which is less than the 0.29 and therefore the hypothesis that the spectral acceleration data follow a normal distribution is accepted at the 5% significance level. This sample deviation d_2 can be seen graphically from Figure B.3a indicated by an arrow and annotation. However, because the parameters of the theoretical distributions were estimated from the sample, it is questionable whether the observed value of d_2 is significantly below $c_{20,5\%}$ as recommended.

From the second K-S test a sample deviation value of 0.074 was determined, which is significantly less than 0.29, see Table B.2. Therefore the hypothesis is again accepted and the data is assumed to follow a lognormal distribution at the 5% significance level. Note, the value of d_2 obtained from the lognormal test is significantly lower than that obtained from the test for the normal distribution. This implies that the lognormal distribution is a better model for the spectral acceleration data than the normal distribution. Again the sample deviation value can be seen graphically from Figure B.3b where the maximum deviation is indicated by the arrow and the annotation.

B.7 Conclusions

The two K-S tests determined both distributions were accepted at the 5% significance level. However, the lognormal distribution appears to be a better choice for the following reasons:

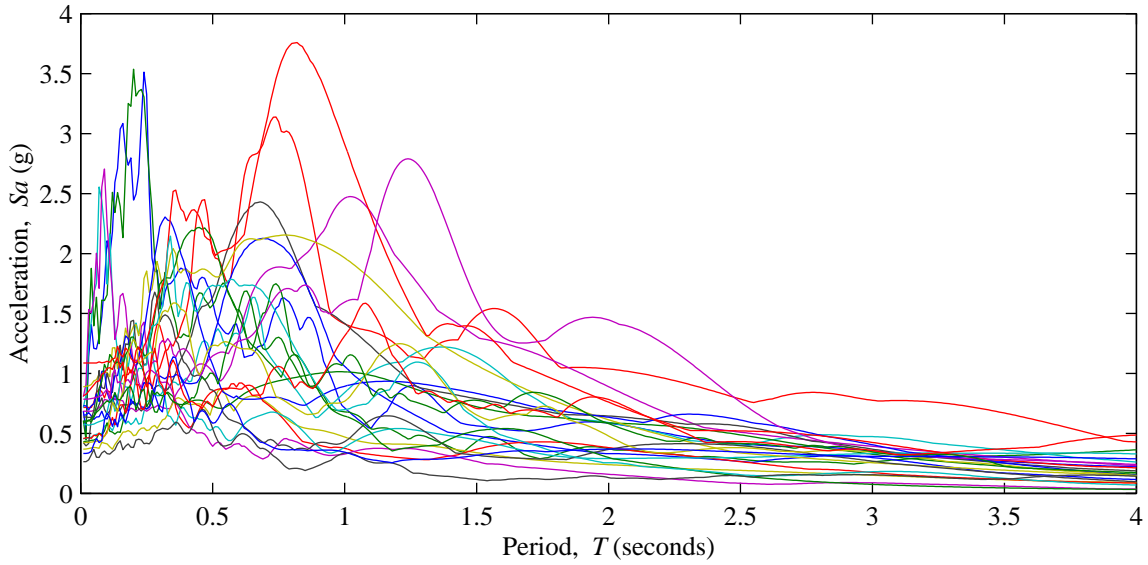
1. Qualitatively the cumulative lognormal distribution matches well the cumulative observed distribution shown in Figure B.3 with the added benefit that neither the observed data nor the lognormal distribution take on negative values.
2. The sample deviation, d_2 , is significantly lower than the sample deviation value obtained from the K-S test for normal distribution as well as the threshold value $c_{n,\alpha}$.

Table B.1. K-S test for Bin 2 spectra acceleration data assuming a normal distribution

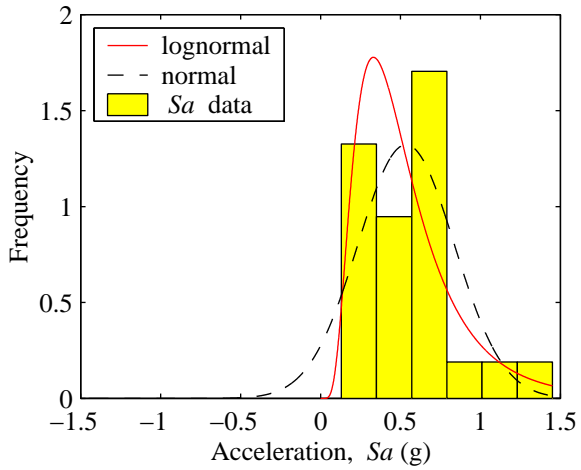
i	Sa ($T=0.5$)	x	Observed Cumulative Distribution $F(x)$	Theoretical Cumulative Distribution $F_t(x)$	$F(x)-F_t(x)$	Abs[$F(x)$ $-F_t(x)$]	d_2	$c_{20,5\%}$
1	0.349	0.020	0.05	0.131	-0.081	0.081	0.182	0.29
2	0.356	0.059	0.1	0.158	-0.058	0.058		
3	0.931	0.069	0.15	0.165	-0.015	0.015		
4	0.738	0.074	0.2	0.168	0.031	0.031		
5	0.136	0.128	0.25	0.213	0.036	0.036		
6	0.020	0.136	0.3	0.220	0.079	0.079		
7	0.556	0.154	0.35	0.237	0.112	0.112		
8	1.200	0.154	0.4	0.237	0.162	0.162		
9	0.677	0.186	0.45	0.267	0.182	0.182		
10	0.750	0.297	0.5	0.388	0.111	0.111		
11	0.128	0.349	0.55	0.449	0.100	0.100		
12	0.186	0.357	0.6	0.458	0.141	0.141		
13	0.074	0.439	0.65	0.557	0.092	0.092		
14	0.069	0.547	0.7	0.681	0.018	0.018		
15	0.059	0.556	0.75	0.690	0.059	0.059		
16	0.154	0.677	0.8	0.806	-0.006	0.006		
17	0.154	0.738	0.85	0.852	-0.002	0.002		
18	0.297	0.750	0.9	0.860	0.039	0.039		
19	0.547	0.931	0.95	0.9485	0.001	0.001		
20	0.439	1.200	1	0.992	0.007	0.007		

Table B.2. K-S test for Bin 2 spectra acceleration data assuming a lognormal distribution

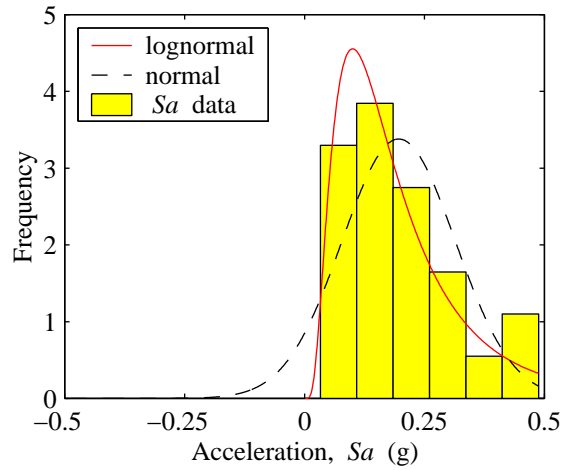
i	Sa ($T=0.5$)	$x=$ $\ln(Sa)$	y	Observed Cumulative Distribution $F(y)$	Theoretical Cumulative Distribution $F_i(y)$	$F(y)-$ $F_i(y)$	Abs[$F(y)$ $-F_i(y)$]	d_2	$c_{20,5\%}$
1	0.349	-1.051	0.20	0.05	0.0102	0.0397	0.0397	0.074	0.29
2	0.357	-1.030	0.059	0.1	0.0911	0.008	0.008		
3	0.931	-0.071	0.069	0.15	0.116	0.033	0.033		
4	0.738	-0.304	0.074	0.2	0.129	0.071	0.071		
5	0.136	-1.994	0.128	0.25	0.266	-0.016	0.016		
6	0.020	-3.887	0.136	0.3	0.285	0.014	0.014		
7	0.556	-0.587	0.154	0.35	0.325	0.024	0.024		
8	1.200	0.182	0.154	0.4	0.325	0.074	0.074		
9	0.677	-0.390	0.186	0.45	0.390	0.059	0.059		
10	0.750	-0.287	0.297	0.5	0.562	-0.062	0.062		
11	0.128	-2.054	0.349	0.55	0.620	-0.070	0.070		
12	0.186	-1.683	0.357	0.6	0.627	-0.027	0.027		
13	0.074	-2.604	0.439	0.65	0.697	-0.047	0.047		
14	0.069	-2.671	0.547	0.7	0.764	-0.064	0.064		
15	0.059	-2.824	0.556	0.75	0.768	-0.018	0.018		
16	0.154	-1.868	0.677	0.8	0.820	-0.020	0.020		
17	0.154	-1.869	0.738	0.85	0.840	0.009	0.009		
18	0.297	-1.213	0.750	0.9	0.844	0.055	0.055		
19	0.547	-0.603	0.931	0.95	0.887	0.062	0.062		
20	0.439	-0.823	1.20	1.0	0.925	0.074	0.074		



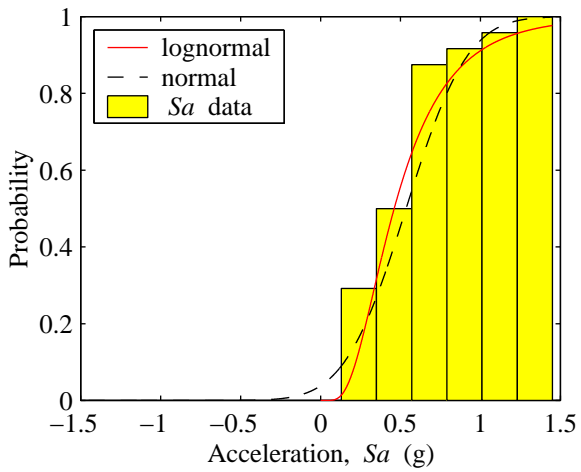
a. acceleration response spectra for Bin 1 ground motions and 5% critical damping



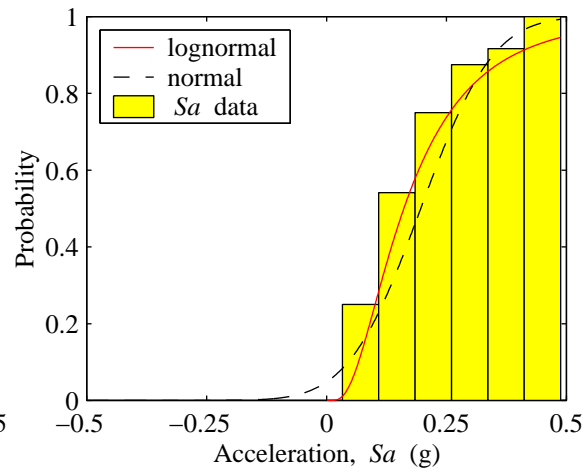
b. distribution for $T=2$ seconds



c. distribution for $T=4$ seconds

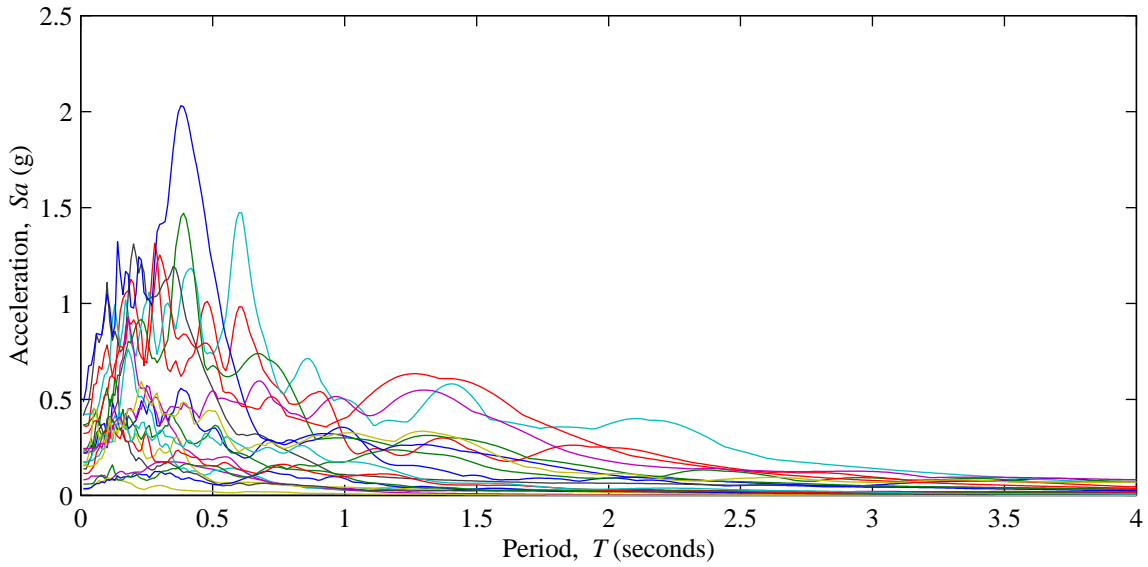


d. cumulative distribution for $T=2$ seconds

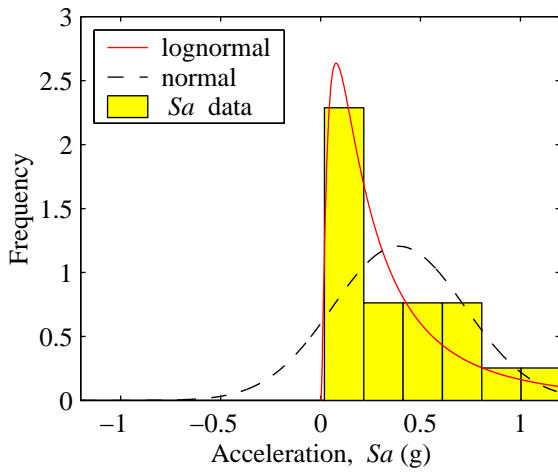


e. cumulative distribution for $T=4$ seconds

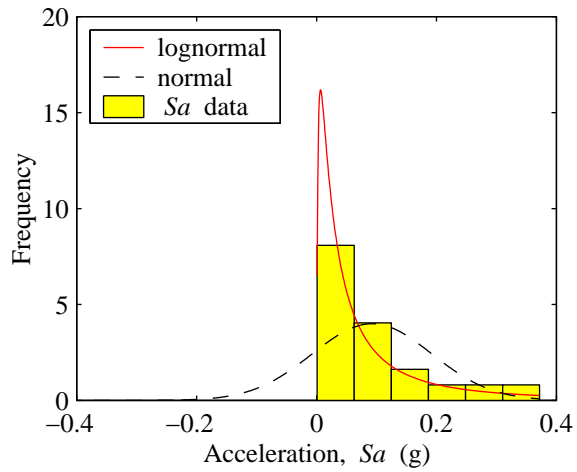
Figure B.1. Distribution of spectral acceleration data for Bin 1 spectra



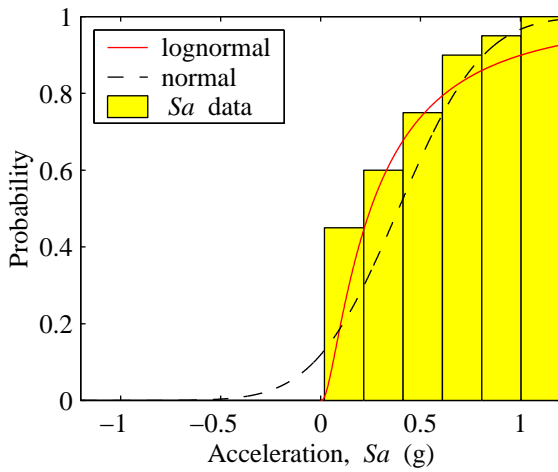
a. acceleration response spectra for Bin 2 ground motions and 5% critical damping



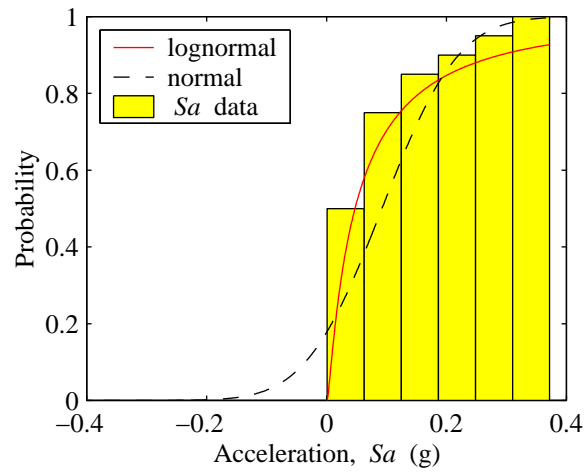
b. distribution for $T=0.5$ seconds



c. distribution for $T=2$ seconds

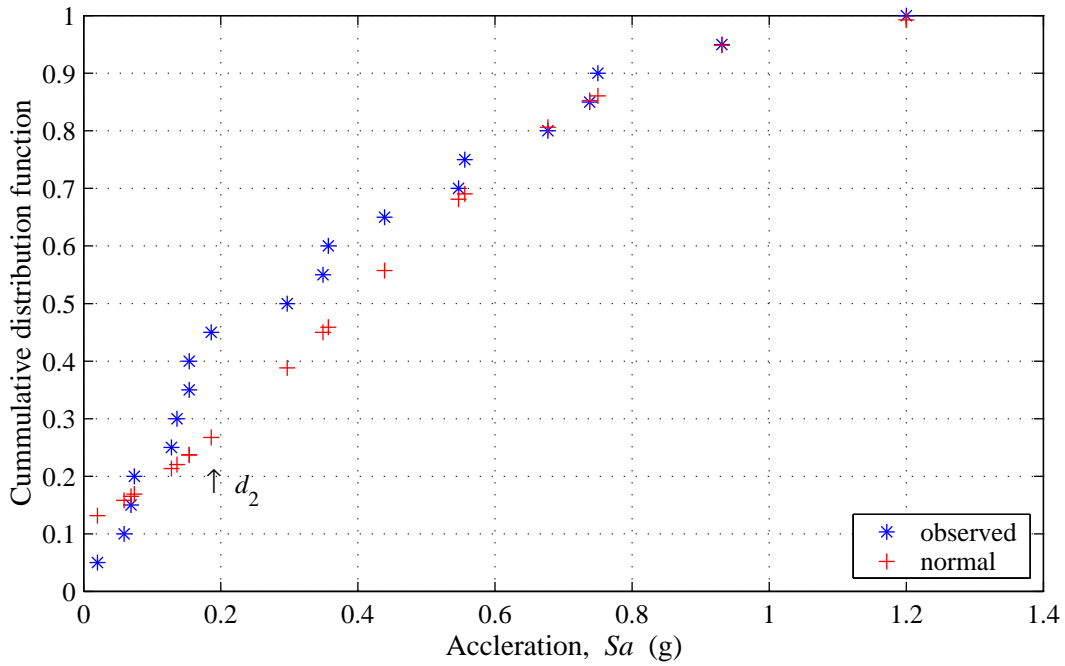


d. cumulative distribution for $T=0.5$ seconds

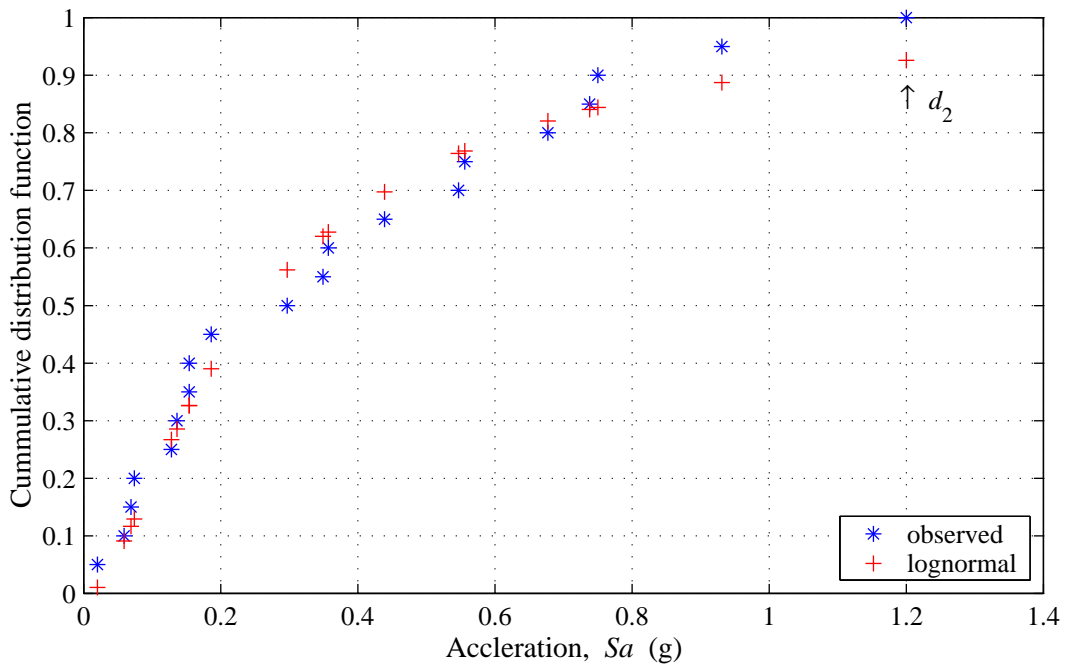


e. cumulative distribution for $T=2$ seconds

Figure B.2. Distribution of spectral acceleration data for Bin 2 spectra.



a. theoretical and observed cumulative distribution functions



b. theoretical and observed cumulative distribution functions

Figure B.3. Results of the Kolmogorov–Smirnov goodness-of-fit test performed on spectral acceleration data from Bin 2 at $T=0.5$ seconds.

APPENDIX C

NUMERICAL PROCEDURE FOR NONLINEAR RESPONSE-HISTORY ANALYSIS AND VERIFICATION USING SAP2000

C.1 General

Presented in this appendix is a discussion of the numerical procedures used to solve the nonlinear equation of motion and verification of the solution using the structural analysis software package, SAP2000 (CSI, 2000).

C.2 Numerical Procedure

C.2.1 General

A generalized form of the equation of motion is given in Equation (C.1). The simple bridge model assumed for this study has three degrees-of-freedom: translation in the x - and y - directions and rotation about the vertical axis, resulting in an equation of motion with matrix and vector quantities. For simplicity of explanation all quantities shown in this appendix are presented in scalar form. The scalar equation of motion is

$$m\ddot{u} + c\dot{u} + f_s = -m\ddot{u}_g \quad (\text{C.1})$$

where m is the system mass; c is the damping coefficient; f_s is the nonlinear force-displacement response; \dot{u} and \ddot{u} are the relative velocity and relative acceleration respectively; and \ddot{u}_g is the ground acceleration.

C.2.2 Newmark's Method

To solve the equation of motion, *Newmark's* step-by-step integration procedure was employed (Newmark, 1959). This procedure is based on the following equations

$$\dot{u}_{i+1} = \dot{u}_i + [(1-\gamma)\Delta t] \ddot{u}_i + (\gamma\Delta t) \ddot{u}_{i+1} \quad (\text{C.2})$$

$$u_{i+1} = u_i + (\Delta t)\dot{u}_i + [(0.5-\beta)(\Delta t)^2] \ddot{u}_i + [\beta(\Delta t)^2] \ddot{u}_{i+1} \quad (\text{C.3})$$

where u_{i+1} , \dot{u}_{i+1} , and \ddot{u}_{i+1} are the relative displacement, velocity, and acceleration at time-step $i+1$; u_i , \dot{u}_i , and \ddot{u}_i are the relative displacement, velocity, and acceleration at time-step i ; Δt is the incremental time-step size; and γ and β are parameters chosen to be $1/2$ and $1/4$, respectively. This choice of γ and β correspond to an assumed average acceleration response over the incremental displacement Δt . Because Equations (C.2) and (C.3) include information from the current time step, i , and the future time step, $i+1$, the procedure is implicit and therefore has a larger stability region than an explicit method (Heath, 2002). Choosing γ and β to be $1/2$ and $1/4$, respectively, yields a stability limit of infinity, implying the solution procedure is unconditionally stable for all Δt (Newmark, 1959). Although the procedure is unconditionally stable, Δt must be chosen sufficiently small to yield an accurate solution. A discussion regarding solution accuracy and time-step size is presented in a subsequent section of this appendix. For linear systems, the incremental displacement, Δu_i , and incremental velocity, $\Delta \dot{u}_i$, can be determined directly at each time step. However, for nonlinear systems an iterative procedure is required at each time step.

C.2.3 Coupled-Plasticity Model

The seismic isolator elements were characterized using a rate-independent plasticity model utilized by Huang et al. (2000). The rate-independent plasticity model is composed of an assumed yield function, a flow rule, and a hardening rule. The yield function is given by

$$F = f_p - (1-\alpha)f_y \quad (\text{C.4})$$

where α is the ratio of the post-elastic stiffness to the elastic stiffness; f_y is the assumed yield force; $(1-\alpha)f_y$ is the plastic force (equivalent to the characteristic strength of an isolator denoted Q_d); and f_p represents the hysteretic force. For 2-dimensional analysis, the yield surface is circular and f_p is determined as the Euclidean norm (or 2-norm) of the two Cartesian components of hysteretic force. The expression shown in Equation (C.4) determines the state of the restoring force with respect to the yield surface. This is shown by the logical expression in Equation (C.5).

$$\begin{aligned} F < 0 & \quad \text{elastic} \\ F = 0 & \quad \text{yielding} \end{aligned} \tag{C.5}$$

The incremental plastic deformation is governed by an associative plastic flow rule shown in Equation (C.6)

$$\dot{u}_p = \dot{\gamma} \frac{\partial F}{\partial f_p} \tag{C.6}$$

where \dot{u}_p is the incremental plastic deformation rate and $\dot{\gamma}$ is a proportionality factor. Equation (C.6) was solved incrementally using the *Backward Euler Method* which is implicit and unconditionally stable (Heath, 2002).

The restoring force (f_s), assuming the system is yielding, is determined from the following equation

$$f_s = \alpha k_u u + f_p \tag{C.7}$$

where α has been defined previously as the ratio of the post-elastic stiffness to the elastic stiffness; k_u is the elastic stiffness; u is the displacement composed of an elastic displacement and plastic displacement; and f_p is the plastic force, equal to $(1-\alpha)f_y$ for unidirectional excitation.

Two schematics of the numerical procedure implemented in Matlab are shown in Figure C.1 and Figure C.2. The step-by-step integration scheme (*Newmark's Method*) utilized to solve the equation of motion with nonlinear restoring force is shown by Figure C.1. This figure is based on the *Newmark* procedure found in Chopra (1995). The basic logic and flow of information (variables) for the numerical procedure is shown. Because the force-displacement relationship (f_s) is nonlinear, an iterative procedure is required for every time step. *Newton-Raphson* was selected for the iterative procedure and is shown in Figure C.1 by the operation box labeled *Newton-Raphson Iteration*. Within the *Newton-Raphson Iteration* box is a nested operation box labeled *Coupled-Plasticity Model*. The transfer of information between these two operations is detailed in Figure C.2. During the

Newton-Raphson iterations, an updated value of the displacement, u_{i+1}^j , is passed to the *Coupled-Plasticity* model which returns a value for the restoring force, $f_{s_i}^j$, and tangent stiffness, k_T^j , the *Newton-Raphson* iteration then continues until the estimated error is less than some pre-defined error tolerance, tol . Details of the *Coupled-Plasticity Model* have not been presented here, however, information regarding this characterization of seismic isolators can be found in Huang et al. (2000).

C.2.4 Stability and Accuracy of Solution

Two parameters of the numerical method affect the stability and accuracy of the solution. As previously mentioned both *Newmark's Method* and *Backward Euler's Method* are implicit and unconditionally stable. Therefore only the accuracy of the solution need be investigated for various values of the solution time-step size, Δt , and the relative error tolerance, tol . To facilitate this investigation, nonlinear response-history analysis was performed to investigate the stability and accuracy of the numerical method utilized for this study. To facilitate this investigation an isolation system with $Q_d/W = 0.12$ and $T_d = 4.0$ seconds was selected. The ground motion record used for analyses discussed here is from the 1992, Northridge Earthquake, Canoga Park Station (denoted, CNP196) and has been incorporated into ground motion bin 2M. Two values of the yield displacement, d_{yield} , were assumed for this investigation, 0.01 and 0.1 inches. A yield displacement of 0.01 inches is typical of friction pendulum isolators (FPS), which exhibit large initial stiffness (or "elastic" stiffness).

Figure C.3 shows the solution obtained from response-history analysis performed considering four values of the time-step size, Δt , using an error tolerance of $1e-8$ and an assumed yield displacement of 0.01 inches. From the top plot of Figure C.3 it appears that the solution is indeed stable for each value of the time-step considered. The top plot of Figure C.3 suggest that the solution obtained for each time-step yield are identical. Referring to the bottom plot of Figure C.3, the changed scale of the vertical axis shows discrepancies in the solution for each time-step from approximately 13 seconds to 25 seconds, corresponding to the elastic response of the isolator. These differences are

observed for time-steps: 0.01, 0.004 and 0.003. However, solutions obtained for time-steps 0.003 and 0.001 are identical, suggesting a time-step of 0.003 is a threshold for accuracy. Time-step values of 0.004 and 0.003 corresponds to $T_u/20$ and $T_u/30$, respectively, where T_u is the period calculated from the “elastic” stiffness. A time-step of 0.01 corresponds to the input time-step. For each of the four time-step sizes considered here, the difference in the maximum displacement and the energy dissipated by the isolators (two parameters of interest in this study) calculated from each of the solutions is negligibly small. For the stiffest system considered here, a time step of $T_u/20$ is sufficient without requiring excessive computation.

For comparative purposes the previous system ($Q_d/W = 0.12$ and $T_d = 4.0$ seconds) was analyzed assuming a yield displacement of 0.1 inches for three values of Δt . The resulting “elastic” stiffness is ten times less than that calculated assuming $d_{yield} = 0.01$ inches. Results of analyses performed for this system are shown in Figure C.4. From this figure, it is clear that there is no difference between the solutions obtained considering time-steps of 0.01, 0.004 and 0.003. Therefore, for systems with moderate initial stiffness (i.e, lead-rubber bearings) stable and accurate solutions using this numerical procedure can be obtained even for reasonably large time-steps.

Shown in Figure C.5 are solutions obtained considering various error tolerances, tol , and a time-step of 0.004. A yield displacement of 0.01 inches and isolator parameters $Q_d/W = 0.12$ and $T_d = 4.0$ seconds were assumed. The *Newton-Raphson* iterations are terminated when the change in the calculated incremental plastic displacement is sufficiently small compared to the specified error tolerance, see Figure C2. From Figure C.5, the solutions obtained for each of the three values of the error tolerance are identical. Therefore, an error tolerance of $1e-4$, is sufficiently small without requiring excessive computation.

C.3 Verification using SAP2000

Displacement and force results obtained from unidirectional response-history analysis performed using the previously mentioned numerical procedure implemented in Matlab

(MathWorks, 1999) were compared with results obtained from a commercially available structural analysis software package, SAP2000 Nonlinear (CSI, 2000). Two different isolation systems were considered for the comparison, the first system with: $Q_d / W = 0.06$ and $T_d = 3.0$ seconds, and the second system with: $Q_d / W = 0.09$ and $T_d = 3.0$ seconds. A yield displacement of 0.01 inches was assumed for both systems.

An identical model of the simple isolated bridge structure assumed in this study was generated in SAP2000. For the SAP analyses, a rigid superstructure was modeled using *Body* constraints. This constraint holds the relative deformations of the assigned nodes to zero. A lumped mass was placed at the center of rigidity of the superstructure and included in the *Body* constraints. The superstructure was supported by four *Plastic1* elements. Although this version of SAP2000 offers two elements specific for modeling seismic isolators; *Isolator1* and *Isolator2*, the *Plastic1* element was chosen. The *Plastic1* element is based on a hysteretic behavior proposed by Wen (CSI, 1997). Using this element, in SAP2000, the transition between the elastic and plastic regions can be modified by specifying the value of the parameter, *exp*. In this case, a value of 20 was assigned and corresponds to a sharp transition between the elastic stiffness and the post-elastic stiffness. This sharp transition is in agreement with the *coupled-plasticity model* utilized in the Matlab code. Isolator properties used for the Matlab and SAP2000 analyses are presented in Table C.1.

Presented in Figure C.6 is a comparison of displacement and force response results obtained using the Matlab code and SAP2000 for an isolation system with properties: $Q_d / W = 0.06$ and $T_d = 3.0$ seconds. In this figure results obtained using Matlab code and SAP2000 are shown by a solid gray line and a dotted black line, respectively. The force and displacement results obtained using Matlab and SAP2000 are in excellent agreement. Similarly a comparison of the force and displacement results for an isolation system with parameters $Q_d / W = 0.09$ and $T_d = 3.0$ seconds are presented in Figure C.7. Again the results agree exceptionally well.

C.4 Conclusion

The numerical procedure implement in Matlab is unconditionally stable and sufficiently accurate given that (1) the time-step size, Δt , is taken to be approximately equal to $T_u / 20$ and (2) the relative error tolerance for the *Newton-Raphson* Iteration is specified to be $1e-4$ or smaller. Results obtained from the numerical routine implemented in Matlab were verified using SAP2000.

Table C.1. Isolator Parameters for Verification Analyses.

		<i>Newmark's Method</i> implement in Matlab				SAP2000 Nonlinear ver7.4			
		<i>Coupled-Plasticity Model</i>				<i>Plastic1</i>			
Q_d / W	T_d	d_{yield}	Q_d	K_u	K_d	Stiffness	Yield Strength	Post Yield Ratio	Yield Exponent
	(sec.)	(cm)	(kN)	(kN/cm)	(kN/cm)	k	yield	ratio	exp
						(kN/cm)	(kN)		
0.06	3.0	0.0254	148.4	5842.5	11.1	5842.5	148.4	1.89e-3	20
0.09	3.0	0.0254	222.6	8763.8	11.1	8763.8	222.6	1.26e-3	20
0.09	4.0	0.0254	222.6	8763.8	6.22	-	-	-	-
0.12	4.0	0.0254	296.8	11685	6.22	-	-	-	-
0.12	4.0	0.254	296.8	1168.5	6.22	-	-	-	-

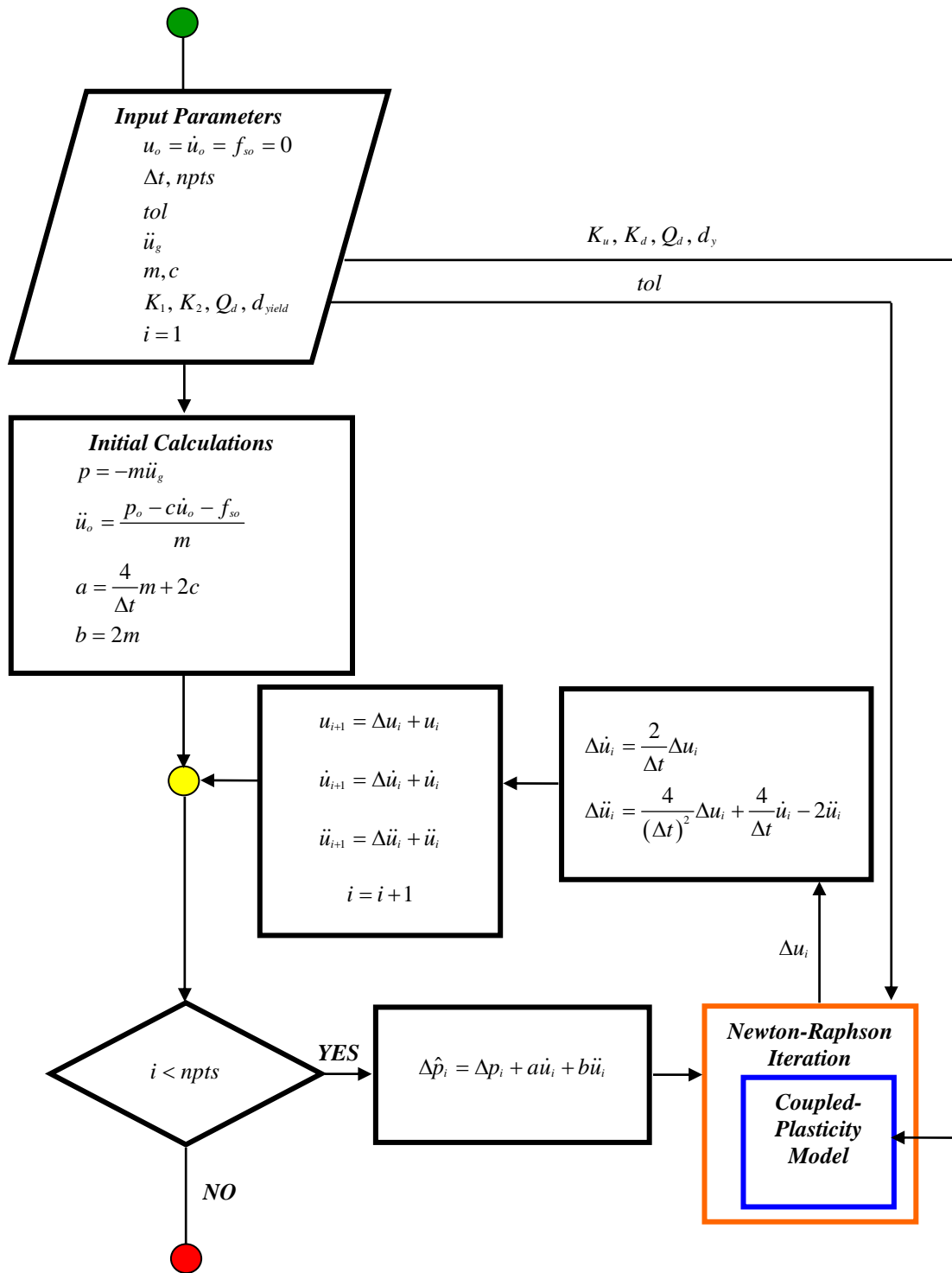


Figure C.1. Flow chart for numerical solution procedure using *Newmark's Method*.

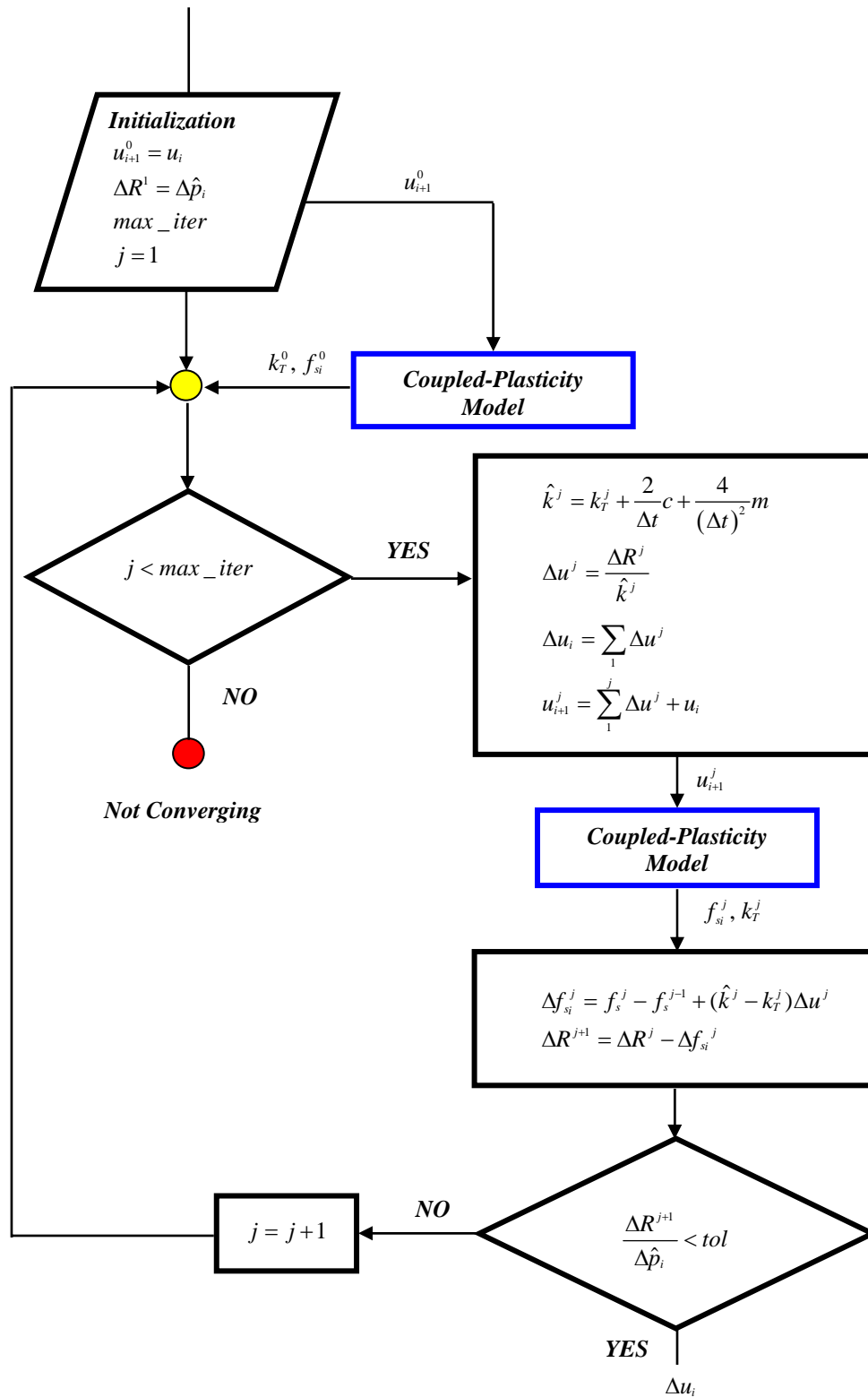


Figure C.2. Flow chart for *Newton-Raphson* Iteration procedure.

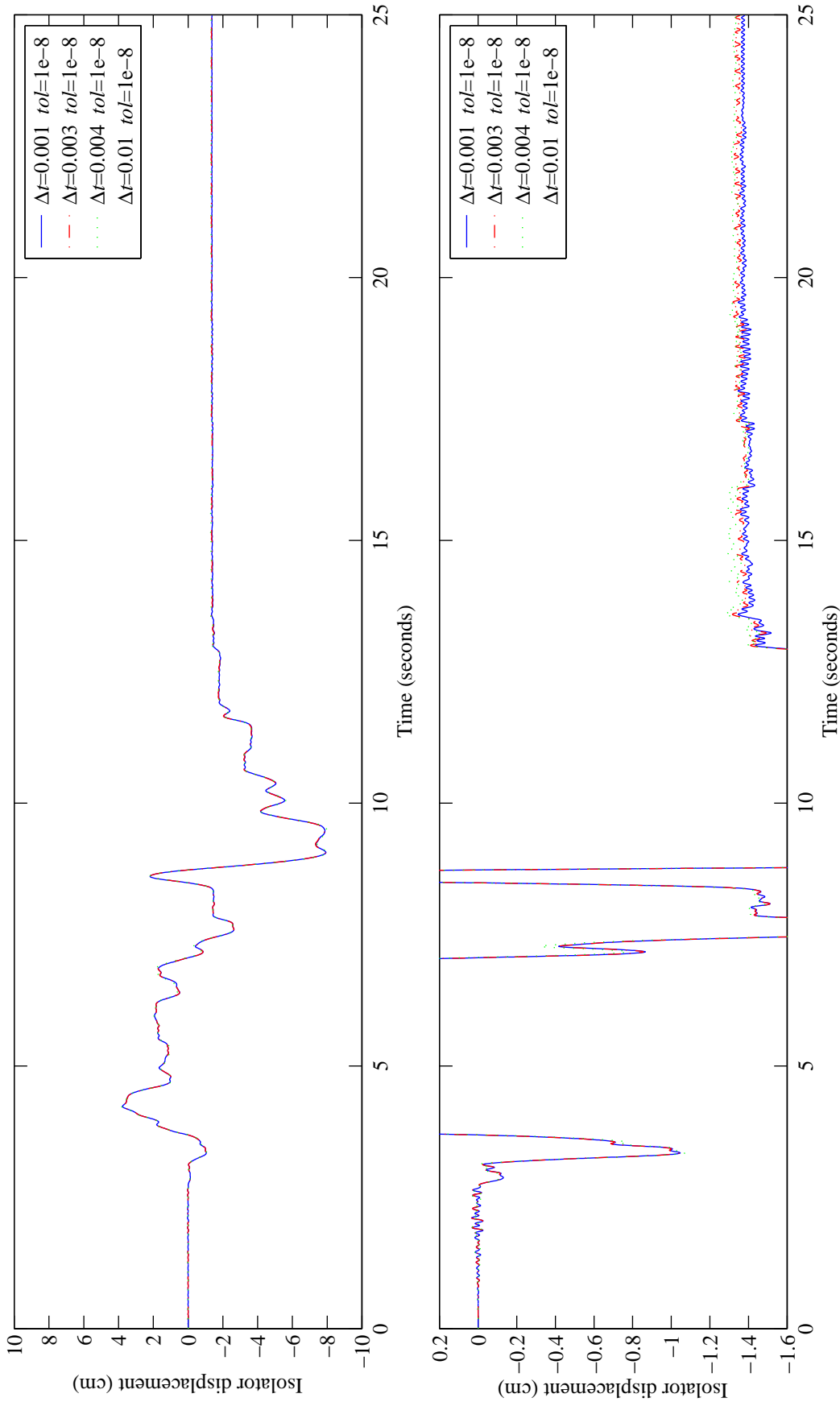


Figure C.3. Comparison of displacement response calculated using Newmark's Average Acceleration Method (coded in MatLab) for various time-step sizes (Δt) and convergence tolerance, $tol=1e-8$, considering isolator properties: $Q_d/W=0.12$, $T_d=4.0$ sec., and $d_{yield}=0.01$ inches and ground motion; CNP196, from Bin2M.

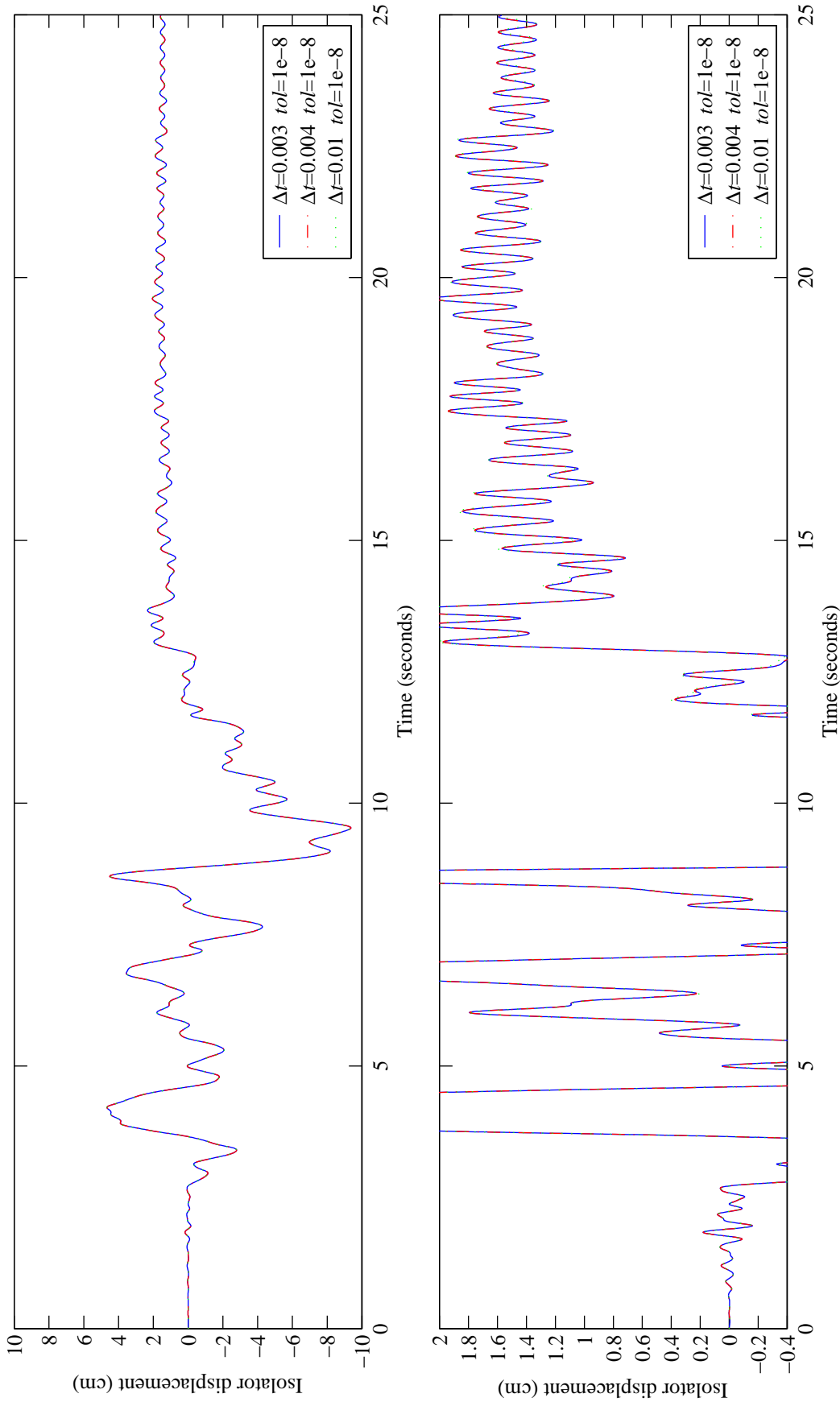


Figure C.4. Comparison of displacement response calculated using Newmark's Average Acceleration Method (coded in MatLab) for various time-step sizes (Δt) and convergence tolerance, $tol=1e-8$, considering isolator properties: $Q_d/W=0.12$, $T_d=4.0$ sec., and $d_{yield}=0.1$ inches and ground motion; CNP196, from Bin2M.

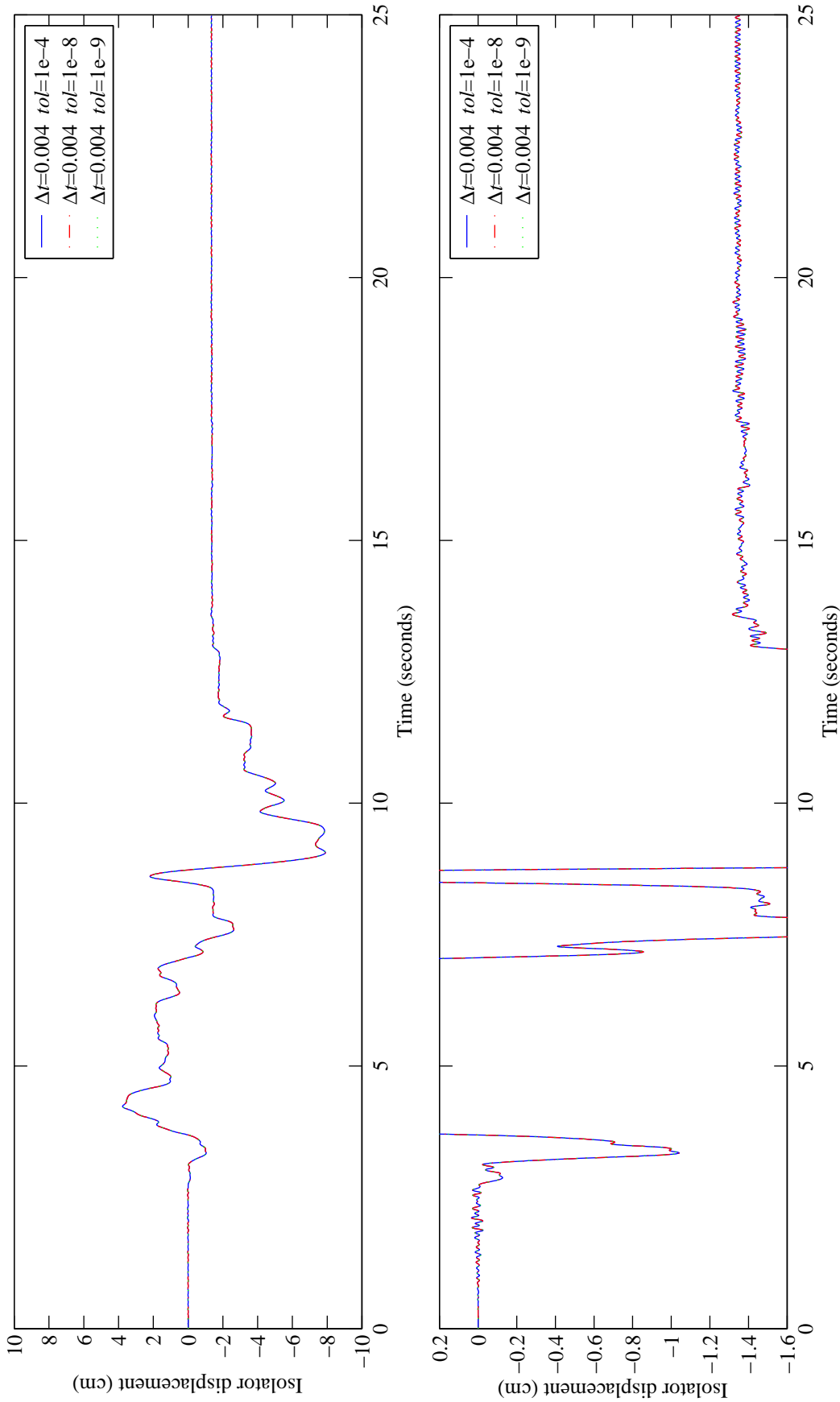


Figure C.5. Comparison of displacement response calculated using Newmark's Average Acceleration Method (coded in MatLab) for and various convergence tolerance (tol) and time-step, $\Delta t=0.004$, considering isolator properties: $Q_d/W=0.12$, $T_d=4.0$ sec., and $d_{yield}=0.01$ inches and ground motion; CNP196, from Bin2M.

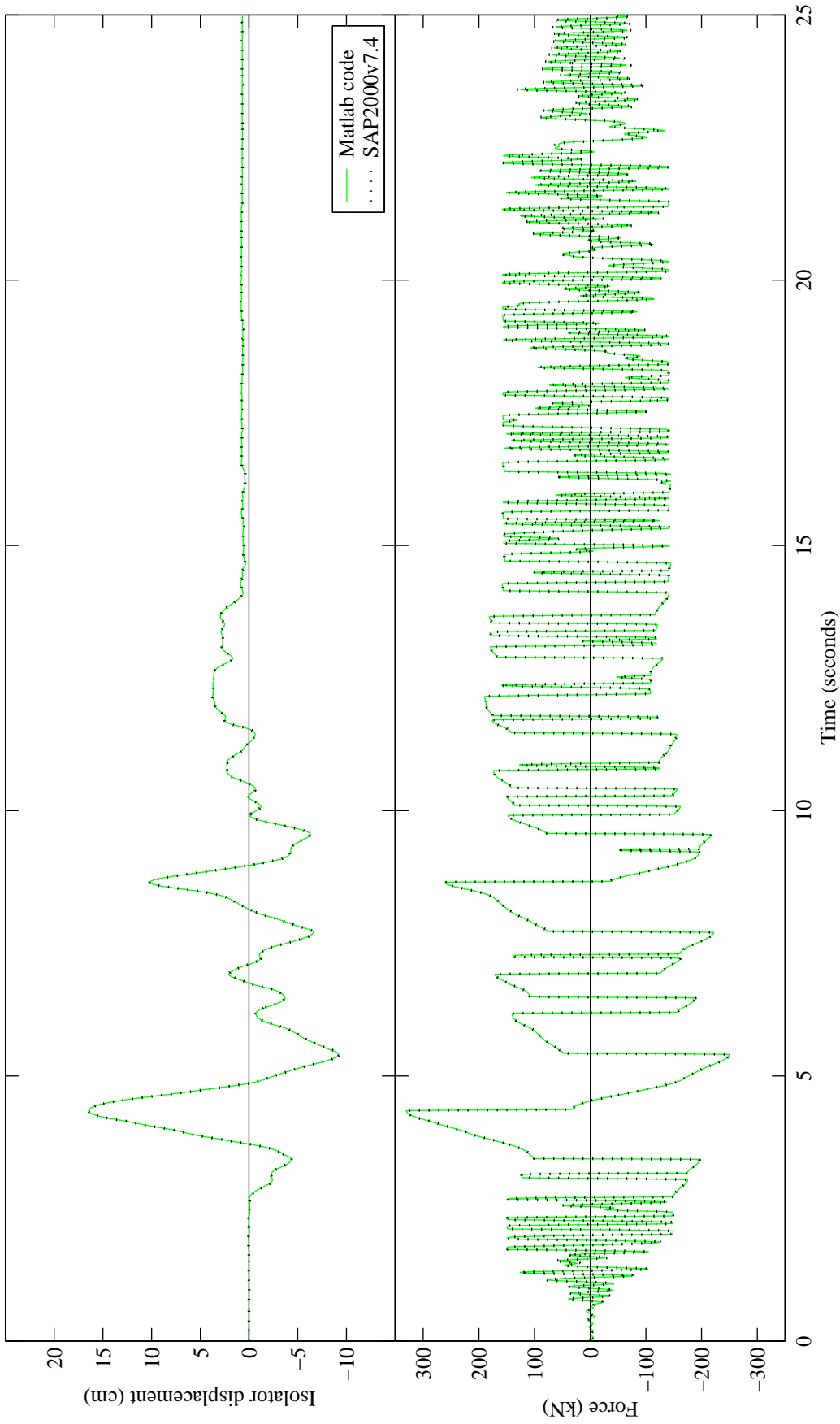


Figure C.6. Comparison between isolator response calculated using Newmark's Average Acceleration Method (coded in Matlab) and SAP2000 Nonlinear (version 7.4) for $Q_d/W=0.06$ and $T_d=3.0$ sec. using ground motion CNP196 from Bin2M.

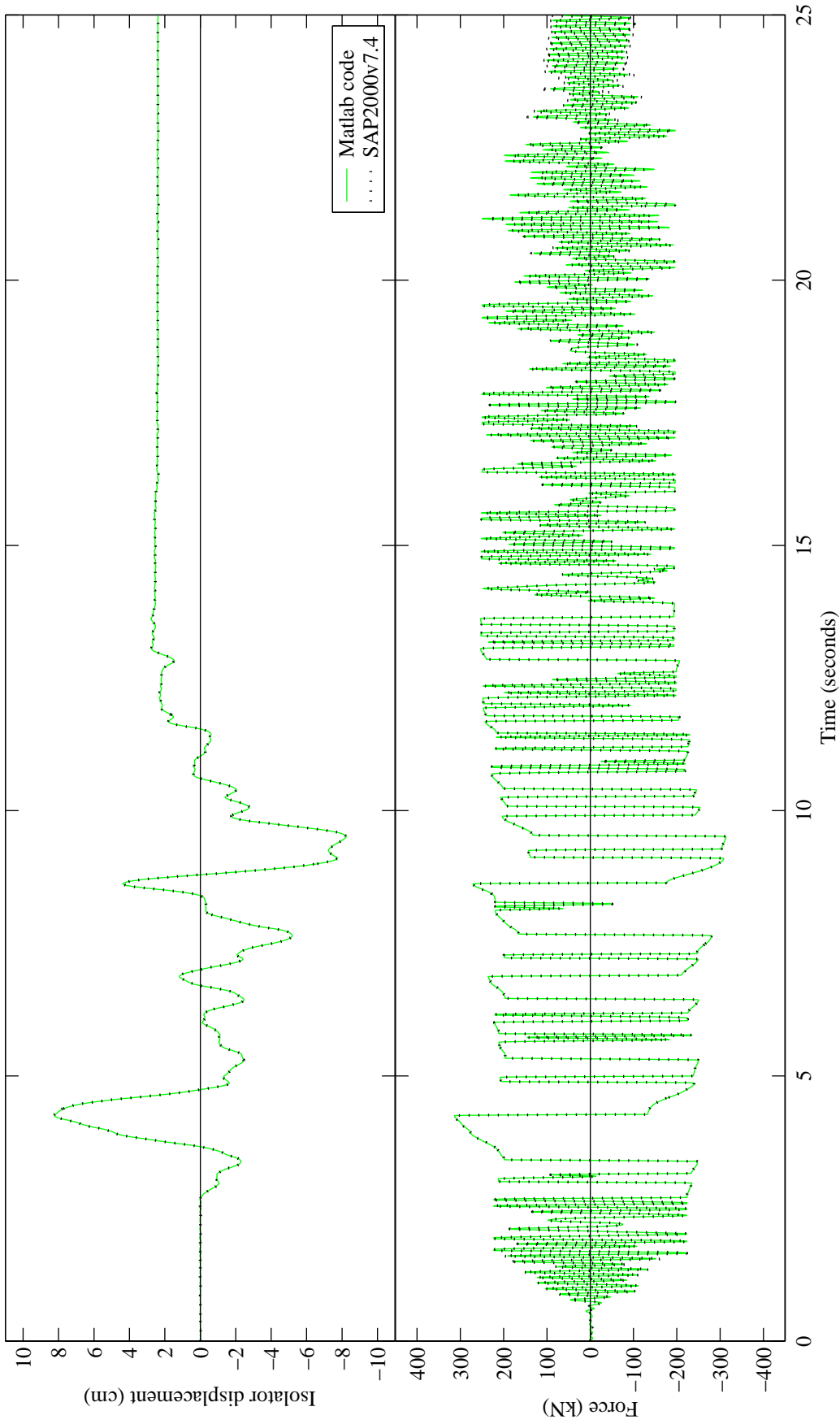


Figure C.7. Comparison between isolator response calculated using Newmark's Average Acceleration Method (coded in Matlab) and SAP2000 Nonlinear (version 7.4) for $Q_d/W=0.09$ and $T_d=3.0$ sec. using ground motion CNP196 from Bin2M.

APPENDIX D

SAMPLE CALCULATIONS TO DETERMINE ISOLATOR DISPLACEMENTS USING THE AASHTO PROCEDURE AND EQUATION 3B FROM THE GUIDE SPECIFICATIONS.

D.1 Sample calculations considering the 1-second mean spectral acceleration from Bin 2M and isolator properties: $Q_d / W = 0.06$ and $T_d = 4.0$ sec. Values of B determined using Table 7.1-1 of the AASHTO Guide Specifications.

Initial Parameters:

Gravitational Acceleration	$g = 981 \text{ cm/sec.}^2$	
Weight Acting on Isolator	$W = 2473 \text{ kN}$	
1-Second Spectral Acceleration	$S_1 = 0.41 \text{ g}$	
Site Coefficient times Acceleration Coefficient		$S_i \cdot A = 0.41 \text{ g}$
Second-Slope Period	$T_d = 4.0 \text{ sec.}$	

Initial Calculations:

Characteristic Strength	$Q_d = 0.06 \cdot W$	$Q_d = 148.4 \text{ kN}$
Second-Slope Stiffness	$K_d = \frac{4\pi^2}{T_d^2} \cdot \frac{W}{g}$	$K_d = 622 \text{ kN/m}$
Initial Estimated Displacement	$d = 10 \text{ cm}$	

Iteration 1:

Effective Stiffness	$K_{eff} = \frac{Q_d}{d} + K_d$	$K_{eff} = 2105.8 \text{ kN/m}$
Effective Period	$T_{eff} = 2\pi \sqrt{\frac{W}{K_{eff} \cdot g}}$	$T_{eff} = 2.17 \text{ sec.}$
Effective Damping	$\beta_{eff} = \frac{2Q_d}{\pi \cdot K_{eff} \cdot d}$	$\beta_{eff} = 0.449$
Damping Coefficient	$B = 1.7$	
Displacement	$d = \frac{25 \cdot S_i \cdot A \cdot T_{eff}}{B}$	$d = 13.11 \text{ cm}$

Relative Error	$\text{Error} = 100 \cdot \frac{ d^{old} - d^{new} }{d^{new}}$	Error=23.7%
----------------	--	-------------

Iteration 2:

Trial Displacement	$d^{old} = 13.11 \text{ cm}$	
Effective Stiffness	$K_{eff} = \frac{Q_d}{d} + K_d$	$K_{eff} = 1754.0 \text{ kN/m}$
Effective Period	$T_{eff} = 2\pi \sqrt{\frac{W}{K_{eff} \cdot g}}$	$T_{eff} = 2.38 \text{ sec.}$
Effective Damping	$\beta_{eff} = \frac{2Q_d}{\pi \cdot K_{eff} \cdot d}$	$\beta_{eff} = 0.41$
Damping Coefficient	$B = 1.7$	
Displacement	$d = \frac{25 \cdot S_i \cdot A \cdot T_{eff}}{B}$	$d = 14.36 \text{ cm}$
Relative Error	$\text{Error} = 100 \cdot \frac{ d^{old} - d^{new} }{d^{new}}$	Error=8.7%

Iteration 3:

Trial Displacement	$d^{old} = 14.36 \text{ cm}$	
Effective Stiffness	$K_{eff} = \frac{Q_d}{d} + K_d$	$K_{eff} = 1655.1 \text{ kN/m}$
Effective Period	$T_{eff} = 2\pi \sqrt{\frac{W}{K_{eff} \cdot g}}$	$T_{eff} = 2.45 \text{ sec.}$
Effective Damping	$\beta_{eff} = \frac{2Q_d}{\pi \cdot K_{eff} \cdot d}$	$\beta_{eff} = 0.397$
Damping Coefficient	$B = 1.7$	
Displacement	$d = \frac{25 \cdot S_i \cdot A \cdot T_{eff}}{B}$	$d = 14.78 \text{ cm}$
Relative Error	$\text{Error} = 100 \cdot \frac{ d^{old} - d^{new} }{d^{new}}$	Error=2.8%

Iteration 4:

Trial Displacement	$d^{old} = 14.78 \text{ cm}$	
Effective Stiffness	$K_{eff} = \frac{Q_d}{d} + K_d$	$K_{eff} = 1625.7 \text{ kN/m}$

Effective Period	$T_{eff} = 2\pi \sqrt{\frac{W}{K_{eff} \cdot g}}$	$T_{eff} = 2.47 \text{ sec.}$
Effective Damping	$\beta_{eff} = \frac{2Q_d}{\pi \cdot K_{eff} \cdot d}$	$\beta_{eff} = 0.39$
Damping Coefficient	$B = 1.7$	
Displacement	$d = \frac{25 \cdot S_i \cdot A \cdot T_{eff}}{B}$	$d = 14.92 \text{ cm}$
Relative Error	$\text{Error} = 100 \cdot \frac{ d^{old} - d^{new} }{d^{new}}$	$\text{Error} = 0.94\%$

Final Values:

Effective Damping	<u>$\beta_{eff} = 0.39$</u>
Effective Period	<u>$T_{eff} = 2.47 \text{ sec.}$</u>
Displacement	<u>$d = 14.92 \text{ cm}$</u>

D.2 Sample calculations considering the 1-second mean spectral acceleration from Bin 7 and isolator properties: $Q_d / W = 0.03$ and $T_d = 3.0 \text{ sec.}$ Values of B determined using Table 7.1-1 of the AASHTO Guide Specifications.

Initial Parameters:

Gravitational Acceleration	$g = 981 \text{ cm / sec.}^2$
Weight Acting on Isolator	$W = 2473 \text{ kN}$
1-Second Spectral Acceleration	$S_1 = 0.36 \text{ g}$
Site Coefficient times Acceleration Coefficient	$S_i \cdot A = 0.36 \text{ g}$
Second-Slope Period	$T_d = 3.0 \text{ sec.}$

Initial Calculations:

Characteristic Strength	$Q_d = 0.03 \cdot W$	$Q_d = 74.2 \text{ kN}$
Second-Slope Stiffness	$K_d = \frac{4\pi^2}{T_d^2} \cdot \frac{W}{g}$	$K_d = 1105.8 \text{ kN/m}$
Initial Estimated Displacement		$d = 17 \text{ cm}$

Iteration 1:

Effective Stiffness	$K_{eff} = \frac{Q_d}{d} + K_d$	$K_{eff} = 1542.2 \text{ kN/m}$
Effective Period	$T_{eff} = 2\pi \sqrt{\frac{W}{K_{eff} \cdot g}}$	$T_{eff} = 2.54 \text{ sec.}$
Effective Damping	$\beta_{eff} = \frac{2Q_d}{\pi \cdot K_{eff} \cdot d}$	$\beta_{eff} = 0.18$
Damping Coefficient	$B = 1.44$	

Iteration 1 Continued:

Displacement	$d = \frac{25 \cdot S_i \cdot A \cdot T_{eff}}{B}$	$d = 15.88 \text{ cm}$
Relative Error Estimate	$E^{est} = 100 \cdot \frac{ d^{old} - d^{new} }{d^{new}}$	$E^{est} = 7.0\%$

Iteration 2:

Trial Displacement	$d^{old} = 15.88 \text{ cm}$	
Effective Stiffness	$K_{eff} = \frac{Q_d}{d} + K_d$	$K_{eff} = 1573.1 \text{ kN/m}$
Effective Period	$T_{eff} = 2\pi \sqrt{\frac{W}{K_{eff} \cdot g}}$	$T_{eff} = 2.51 \text{ sec.}$
Effective Damping	$\beta_{eff} = \frac{2Q_d}{\pi \cdot K_{eff} \cdot d}$	$\beta_{eff} = 0.189$
Damping Coefficient	$B = 1.47$	
Displacement	$d = \frac{25 \cdot S_i \cdot A \cdot T_{eff}}{B}$	$d = 15.43 \text{ cm}$
Relative Error Estimate	$E^{est} = 100 \cdot \frac{ d^{old} - d^{new} }{d^{new}}$	$E^{est} = 2.9\%$

Iteration 3:

Trial Displacement	$d^{old} = 15.43 \text{ cm}$	
Effective Stiffness	$K_{eff} = \frac{Q_d}{d} + K_d$	$K_{eff} = 1586.6 \text{ kN/m}$

Effective Period	$T_{eff} = 2\pi\sqrt{\frac{W}{K_{eff} \cdot g}}$	$T_{eff} = 2.5 \text{ sec.}$
Effective Damping	$\beta_{eff} = \frac{2Q_d}{\pi \cdot K_{eff} \cdot d}$	$\beta_{eff} = 0.193$
Damping Coefficient	$B = 1.48$	
Displacement	$d = \frac{25 \cdot S_i \cdot A \cdot T_{eff}}{B}$	$d = 15.24 \text{ cm}$
Relative Error Estimate	$E^{est} = 100 \cdot \frac{ d^{old} - d^{new} }{d^{new}}$	$E^{est} = 1.2\%$

Iteration 4:

Trial Displacement	$d^{old} = 15.24 \text{ cm}$	
Effective Stiffness	$K_{eff} = \frac{Q_d}{d} + K_d$	$K_{eff} = 1592.7 \text{ kN/m}$
Effective Period	$T_{eff} = 2\pi\sqrt{\frac{W}{K_{eff} \cdot g}}$	$T_{eff} = 2.5 \text{ sec.}$
Effective Damping	$\beta_{eff} = \frac{2Q_d}{\pi \cdot K_{eff} \cdot d}$	$\beta_{eff} = 0.195$
Damping Coefficient	$B = 1.485$	
Displacement	$d = \frac{25 \cdot S_i \cdot A \cdot T_{eff}}{B}$	$d = 15.16 \text{ cm}$
Relative Error Estimate	$E^{est} = 100 \cdot \frac{ d^{old} - d^{new} }{d^{new}}$	$E^{est} = 0.53\%$

Final Values:

Effective Damping	<u>$\beta_{eff} = 0.195$</u>
Effective Period	<u>$T_{eff} = 2.5 \text{ sec.}$</u>
Displacement	<u>$d = 15.16 \text{ cm}$</u>

APPENDIX E

MAXIMUM ISOLATOR DISPLACEMENT DATA

Table E.1. Maximum isolator displacements determined from the results of unidirectional response-history analysis using Bin 1 ground motions.

Record	d_x (cm)																			
	$Q_d/W=0.03$				$Q_d/W=0.06$				$Q_d/W=0.09$				$Q_d/W=0.12$							
	T_d (seconds)				T_d (seconds)				T_d (seconds)				T_d (seconds)							
	1.5	2.0	2.5	3.0	4.0	1.5	2.0	2.5	3.0	4.0	1.5	2.0	2.5	3.0	4.0	1.5	2.0	2.5	3.0	4.0
nf01	34.0	57.0	63.2	74.2	80.9	29.0	46.5	47.9	53.6	66.0	26.6	36.3	40.6	44.7	53.5	23.1	29.8	34.7	37.3	43.1
nf02	21.7	26.1	31.3	50.8	117.0	16.2	19.0	24.2	36.0	55.1	13.5	16.4	22.4	28.4	38.9	11.6	15.2	19.3	23.5	28.7
nf03	109.4	105.1	130.0	199.6	176.2	94.3	92.5	104.9	142.5	150.7	77.8	79.8	89.3	94.9	117.5	61.7	68.8	76.3	70.6	90.1
nf04	78.4	54.1	54.3	95.2	84.5	62.5	39.9	38.3	51.8	54.0	47.2	27.7	27.7	34.8	38.5	31.3	22.5	21.1	23.9	26.9
nf05	83.2	90.1	73.7	81.4	85.4	73.4	77.1	64.0	66.0	73.2	65.8	66.6	56.6	52.7	58.6	60.0	61.5	52.2	46.7	51.5
nf06	16.0	16.5	19.1	20.9	22.7	11.2	11.3	12.4	13.2	14.0	7.3	7.3	7.8	8.2	8.5	5.0	4.8	5.0	5.1	5.3
nf07	43.4	63.8	93.1	82.4	71.3	39.0	50.4	62.4	64.4	65.6	34.0	42.8	49.0	53.4	58.8	30.5	38.8	44.3	48.0	52.5
nf08	25.9	31.4	35.2	44.4	39.7	22.8	27.8	30.9	33.0	35.5	20.1	24.2	26.7	28.4	30.3	18.1	21.5	23.6	25.0	26.5
nf09	42.4	58.1	70.6	65.8	58.7	36.4	42.7	50.7	50.9	48.5	31.3	35.5	38.2	40.5	40.3	26.7	29.1	30.6	31.4	32.4
nf10	18.7	30.3	34.1	35.6	30.1	12.2	16.9	21.6	22.7	20.5	7.9	10.6	11.9	11.5	10.4	6.0	6.8	7.2	7.5	7.9
nf11	21.0	32.1	48.9	64.1	95.5	18.7	29.9	40.0	48.2	61.1	15.6	22.3	28.6	34.0	40.8	11.2	15.4	19.0	22.1	25.9
nf12	11.9	11.6	11.2	10.4	11.5	7.5	7.7	7.6	7.4	7.0	4.7	5.0	4.8	4.5	3.9	3.2	3.0	2.6	2.8	2.9
nf13	65.4	60.5	51.2	48.2	52.2	57.3	55.2	47.6	41.2	44.2	52.8	50.4	44.6	38.2	36.6	49.4	47.5	42.6	37.5	32.3
nf14	15.2	32.2	48.9	45.6	33.7	12.4	18.4	23.1	18.6	16.3	9.4	12.3	13.2	12.0	10.1	6.2	6.8	7.3	7.1	6.6
nf15	58.5	66.2	102.8	91.6	58.9	40.6	50.7	63.8	59.0	51.6	34.6	40.7	41.2	43.3	42.5	28.5	33.0	31.5	33.5	33.7
nf16	28.5	28.3	18.5	13.1	11.7	19.5	18.6	12.1	12.5	12.8	14.9	13.0	13.0	13.6	14.8	11.2	11.6	12.1	12.4	13.1
nf17	107.8	81.0	78.7	88.1	73.1	94.2	70.0	65.0	72.0	61.5	80.1	58.9	52.6	57.0	47.2	66.0	48.0	40.7	42.5	45.4
nf18	39.0	21.4	17.5	18.5	14.6	30.2	17.4	16.1	15.0	13.3	20.8	13.8	13.3	13.0	16.0	14.0	13.4	13.0	12.7	12.4
nf19	104.7	190.7	140.7	83.9	88.1	103.3	156.8	127.1	81.3	70.6	100.0	131.3	112.1	76.5	66.8	94.5	106.9	95.9	70.6	71.0
nf20	41.7	48.8	51.5	57.8	39.7	40.2	35.9	32.0	27.3	20.1	31.9	29.3	25.0	22.0	18.0	23.5	21.5	20.5	18.4	15.6
TCU065W	47.0	93.8	56.7	81.7	165.0	35.2	45.4	42.6	62.5	94.8	23.0	25.0	32.5	47.6	60.8	17.9	19.9	22.0	28.2	29.4
TCU065N	46.6	64.9	58.6	53.2	53.6	32.1	43.2	41.1	40.2	42.3	20.2	30.5	29.7	27.0	31.3	14.6	18.1	17.6	19.9	24.9
TCU075W	14.5	32.9	47.2	58.1	91.7	14.2	25.7	34.2	40.5	49.6	10.1	16.9	21.9	25.5	30.4	8.4	11.9	14.4	16.2	18.4
TCU075N	4.7	5.5	7.8	10.3	11.9	3.8	3.6	3.4	3.4	3.4	2.9	2.8	2.7	2.6	2.5	2.1	2.2	2.2	2.2	2.2
median	40.4	51.4	51.3	58.0	58.8	31.2	37.9	39.2	40.9	49.1	21.9	26.4	28.2	31.2	37.6	18.0	20.7	20.8	23.7	26.7
84th per.	77.4	87.0	95.5	105.9	105.1	67.9	71.9	73.4	76.1	79.7	59.7	60.9	60.6	61.0	65.9	51.0	53.4	53.3	51.8	56.1
mean	45.0	54.3	56.0	61.4	65.3	37.8	41.8	42.2	44.3	47.2	31.3	33.3	33.6	33.9	36.5	26.0	27.4	27.3	26.9	29.1
σ	31.5	39.5	34.7	39.8	44.3	28.8	33.1	29.3	30.2	32.9	26.4	28.8	25.8	22.8	25.8	23.8	24.7	22.8	19.0	21.7
mean + σ	76.5	93.8	90.7	101.2	109.6	66.6	74.9	71.5	74.5	80.1	57.8	62.1	59.3	56.7	62.3	49.8	52.1	50.2	45.9	50.8
COV	0.70	0.73	0.62	0.65	0.68	0.76	0.79	0.69	0.68	0.70	0.84	0.86	0.77	0.67	0.71	0.91	0.90	0.84	0.71	0.75

Table E.2. Maximum isolator displacements determined from the results of unidirectional response-history analysis using Bin 2 ground motions.

	d_x (cm)																			
	$Q_d/W=0.03$				$Q_d/W=0.06$				$Q_d/W=0.09$				$Q_d/W=0.12$							
	T_d (seconds)				T_d (seconds)				T_d (seconds)				T_d (seconds)							
Record	1.5	2.0	2.5	3.0	4.0	1.5	2.0	2.5	3.0	4.0	1.5	2.0	2.5	3.0	4.0	1.5	2.0	2.5	3.0	4.0
G01000	3.4	3.7	3.9	4.0	4.1	2.8	3.0	3.1	3.1	3.1	1.8	2.1	2.3	2.5	2.8	2.0	2.5	2.9	3.1	3.4
G01090	8.7	8.9	7.0	6.4	6.8	5.2	5.7	5.5	5.1	4.5	4.1	4.3	4.4	4.4	4.5	3.3	3.4	3.4	3.4	3.4
SGI270	0.12	0.14	0.14	0.15	0.16	0.05	0.05	0.05	0.06	0.06	0.05	0.05	0.05	0.05	0.05	0.05	0.05	0.05	0.05	0.05
SGI360	0.74	0.77	0.79	0.78	0.77	0.10	0.11	0.11	0.12	0.12	0.05	0.05	0.05	0.05	0.05	0.06	0.06	0.06	0.06	0.06
L09000	0.46	0.52	0.57	0.58	0.59	0.38	0.39	0.39	0.39	0.39	0.28	0.31	0.32	0.33	0.33	0.22	0.21	0.21	0.21	0.20
L09090	0.5	0.5	0.5	0.5	0.5	0.7	0.7	0.8	0.8	0.8	0.6	0.5	0.5	0.5	0.5	0.6	0.6	0.6	0.6	0.6
WON095	1.29	1.35	1.37	1.38	1.38	0.73	0.80	0.84	0.87	0.89	0.27	0.28	0.28	0.28	0.29	0.14	0.14	0.14	0.14	0.14
WON185	3.2	3.4	3.6	3.8	4.1	2.0	2.3	2.5	2.6	2.7	1.2	1.4	1.4	1.5	1.5	0.4	0.4	0.5	0.5	0.5
SFL09021	0.37	0.44	0.49	0.52	0.54	0.19	0.21	0.22	0.23	0.24	0.12	0.13	0.13	0.14	0.14	0.10	0.10	0.10	0.10	0.10
SFL09291	0.24	0.23	0.23	0.23	0.22	0.15	0.15	0.15	0.15	0.15	0.13	0.13	0.13	0.13	0.13	0.11	0.11	0.11	0.11	0.11
G02000	10.0	8.7	9.4	9.0	8.0	5.8	6.3	6.7	6.8	6.8	4.9	5.3	5.9	6.3	6.7	3.8	4.1	4.2	4.5	4.8
G02090	32.4	23.4	19.1	17.7	14.4	17.6	17.0	14.1	14.1	13.1	8.8	9.2	8.2	6.9	6.6	4.6	4.8	5.0	5.2	5.3
YER270	20.6	18.2	15.7	15.4	17.2	9.5	11.2	13.2	14.8	16.9	5.8	7.8	9.1	10.0	11.1	4.1	5.0	5.5	5.8	6.2
YER360	8.0	7.4	7.5	7.7	8.3	2.6	2.0	2.0	2.0	2.0	0.8	0.9	0.9	0.9	1.0	0.5	0.5	0.5	0.5	0.6
ABN000	2.9	3.4	3.8	3.9	4.0	1.7	2.2	2.4	2.7	3.0	1.1	1.3	1.4	1.4	1.5	0.9	1.0	1.0	1.0	1.1
ABN090	4.8	5.4	5.7	6.2	6.7	1.4	1.4	1.4	1.4	1.5	0.9	1.0	1.1	1.1	1.1	0.8	0.8	0.8	0.8	0.9
A-E01140	0.32	0.30	0.29	0.30	0.30	0.09	0.09	0.09	0.09	0.10	0.04	0.04	0.04	0.04	0.04	0.04	0.04	0.04	0.04	0.04
A-E01230	0.02	0.02	0.02	0.02	0.02	0.03	0.03	0.03	0.03	0.03	0.04	0.04	0.04	0.04	0.04	0.05	0.05	0.05	0.05	0.05
CNPI06	11.2	12.2	11.9	11.1	9.6	8.3	9.1	9.3	9.5	10.0	5.3	5.9	6.2	6.3	6.4	3.3	3.6	3.8	3.9	4.0
CNPI96	24.5	26.6	26.2	25.0	25.0	14.0	12.8	15.1	16.3	17.3	9.9	9.1	8.2	8.2	9.1	7.7	7.5	7.9	8.3	8.7
median	3.02	3.41	3.70	3.85	4.06	1.57	1.70	1.70	1.71	1.75	0.86	0.94	0.99	1.01	1.03	0.54	0.55	0.55	0.56	0.57
84th per.	13.50	13.23	12.75	12.52	12.42	7.24	7.55	7.85	8.11	8.32	4.39	4.80	4.96	5.06	5.29	3.00	3.25	3.43	3.57	3.71
mean	6.69	6.28	5.91	5.73	5.63	3.67	3.77	3.89	4.05	4.18	2.31	2.49	2.53	2.56	2.69	1.63	1.75	1.85	1.93	2.01
σ	9.19	8.04	7.30	6.92	6.73	5.03	5.00	5.07	5.37	5.65	3.08	3.21	3.19	3.22	3.44	2.13	2.21	2.35	2.47	2.59
mean + σ	15.88	14.32	13.21	12.65	12.36	8.70	8.77	8.96	9.43	9.83	5.39	5.69	5.72	5.78	6.13	3.76	3.96	4.20	4.39	4.60
COV	1.37	1.28	1.24	1.21	1.19	1.37	1.32	1.30	1.33	1.35	1.33	1.29	1.26	1.26	1.28	1.31	1.27	1.27	1.28	1.29

Table E.3. Maximum isolator displacements determined from the results of unidirectional response-history analysis using Bin 2M ground motions.

	d_x (cm)																			
	$Q_d/W=0.03$				$Q_d/W=0.06$				$Q_d/W=0.09$				$Q_d/W=0.12$							
	T_d (seconds)				T_d (seconds)				T_d (seconds)				T_d (seconds)							
Record	1.5	2.0	2.5	3.0	4.0	1.5	2.0	2.5	3.0	4.0	1.5	2.0	2.5	3.0	4.0	1.5	2.0	2.5	3.0	4.0
G01000	3.4	3.7	3.9	4.0	4.1	2.8	3.0	3.1	3.1	3.1	1.8	2.1	2.3	2.5	2.8	2.0	2.5	2.9	3.1	3.4
G01090	8.7	8.9	7.0	6.4	6.8	5.2	5.7	5.5	5.1	4.5	4.1	4.3	4.4	4.4	4.5	3.3	3.4	3.4	3.4	3.4
GBZ000	6.0	7.7	11.5	14.8	20.2	4.5	5.3	5.8	6.1	6.5	3.1	3.4	3.6	3.7	3.9	1.7	1.8	1.8	1.8	1.8
GBZZ70	3.6	4.6	5.3	5.5	6.7	1.9	2.1	2.2	2.3	2.3	0.9	0.9	1.0	1.0	1.0	0.3	0.3	0.3	0.3	0.3
STG000	21.6	21.9	19.8	19.4	20.6	14.4	14.4	13.1	13.9	14.7	6.4	7.6	8.5	9.1	9.7	4.0	5.2	5.8	6.3	6.9
STG090	8.7	7.8	10.4	16.6	23.6	3.9	4.8	5.1	5.8	6.7	2.3	2.5	2.5	2.6	2.6	1.1	1.1	1.1	1.2	1.2
RIO270	14.3	12.5	11.6	10.6	8.9	11.3	11.1	10.3	9.5	8.8	8.8	8.9	8.3	8.0	7.4	5.7	5.9	6.1	6.0	5.8
RIO360	9.7	6.0	5.6	5.9	6.5	7.5	6.4	5.3	4.7	5.2	7.1	6.6	5.8	5.2	4.6	6.6	6.4	6.1	5.7	5.3
JOS000	8.7	6.9	7.2	7.0	7.6	5.3	4.4	4.8	5.5	6.6	3.7	4.1	4.4	4.7	5.1	2.4	2.5	2.6	2.7	2.7
JOS090	15.0	15.7	12.4	12.5	13.7	8.7	8.9	9.2	9.5	10.8	6.0	5.9	6.0	6.5	7.2	3.4	3.8	4.3	4.6	5.8
G02000	10.0	8.7	9.4	9.0	8.0	5.8	6.3	6.7	6.8	6.8	4.9	5.3	5.9	6.3	6.7	3.8	4.1	4.2	4.5	4.8
G02090	32.4	23.4	19.1	17.7	14.4	17.6	17.0	14.1	14.1	13.1	8.8	9.2	8.2	6.9	6.6	4.6	4.8	5.0	5.2	5.3
YER270	20.6	18.2	15.7	15.4	17.2	9.5	11.2	13.2	14.8	16.9	5.8	7.8	9.1	10.0	11.1	4.1	5.0	5.5	5.8	6.2
YER360	8.0	7.4	7.5	7.7	8.3	2.6	2.0	2.0	2.0	2.0	0.8	0.9	0.9	0.9	1.0	0.5	0.5	0.5	0.5	0.6
ABN000	2.9	3.4	3.8	3.9	4.0	1.7	2.2	2.4	2.7	3.0	1.1	1.3	1.4	1.4	1.5	0.9	1.0	1.0	1.0	1.1
ABN090	4.8	5.4	5.7	6.2	6.7	1.4	1.4	1.4	1.4	1.5	0.9	1.0	1.1	1.1	1.1	0.8	0.8	0.8	0.8	0.9
BOL000	16.4	19.4	23.4	21.3	16.8	12.6	14.3	16.7	16.2	15.4	9.6	11.5	12.3	12.8	13.3	6.4	8.1	9.2	10.0	10.8
BOL090	24.2	16.2	14.6	13.9	12.6	22.5	17.7	15.3	14.4	14.1	20.6	19.7	18.4	17.6	16.6	18.1	19.5	19.9	20.1	20.1
CNPI06	11.2	12.2	11.9	11.1	9.6	8.3	9.1	9.3	9.5	10.0	5.3	5.9	6.2	6.3	6.4	3.3	3.6	3.8	3.9	4.0
CNPI96	24.5	26.6	26.2	25.0	25.0	14.0	12.8	15.1	16.3	17.3	9.9	9.1	8.2	8.2	9.1	7.7	7.5	7.9	8.3	8.7
median	9.9	8.8	10.9	10.8	9.3	6.6	6.4	6.3	6.5	6.7	5.1	5.6	5.9	5.7	5.7	3.3	3.7	4.0	4.2	4.4
84th per.	20.6	18.4	17.6	17.7	18.2	13.7	13.6	13.5	13.7	14.2	9.9	10.4	10.4	10.5	10.7	7.2	7.9	8.4	8.7	9.2
mean	12.7	11.8	11.6	11.7	12.1	8.1	8.0	8.0	8.2	8.5	5.6	5.9	5.9	6.0	6.1	4.0	4.4	4.6	4.8	5.0
σ	8.2	7.1	6.5	6.1	6.5	5.8	5.2	5.1	5.1	5.3	4.6	4.6	4.3	4.3	4.3	4.0	4.2	4.4	4.5	4.5
mean + σ	21.0	18.9	18.1	17.8	18.6	13.9	13.2	13.1	13.3	13.7	10.2	10.5	10.3	10.2	10.4	8.0	8.6	9.0	9.2	9.5
COV	0.65	0.60	0.56	0.52	0.54	0.72	0.65	0.63	0.63	0.62	0.83	0.77	0.73	0.72	0.70	0.98	0.97	0.95	0.94	0.92

Table E.4. Maximum isolator displacements determined from the results of unidirectional response-history analysis using Bin 3 ground motions.

Record	d_x (cm)																			
	$Q_d/W=0.03$				$Q_d/W=0.06$				$Q_d/W=0.09$				$Q_d/W=0.12$							
	T_d (seconds)				T_d (seconds)				T_d (seconds)				T_d (seconds)							
	1.5	2.0	2.5	3.0	4.0	1.5	2.0	2.5	3.0	4.0	1.5	2.0	2.5	3.0	4.0	1.5	2.0	2.5	3.0	4.0
CHY000	0.50	0.60	0.65	0.68	0.71	0.20	0.19	0.18	0.18	0.18	0.12	0.12	0.12	0.12	0.12	0.13	0.13	0.13	0.13	0.13
CHY090	0.33	0.35	0.37	0.38	0.39	0.31	0.32	0.33	0.34	0.35	0.23	0.23	0.23	0.23	0.24	0.16	0.16	0.16	0.16	0.16
29P000	0.15	0.17	0.18	0.19	0.22	0.14	0.15	0.16	0.16	0.16	0.08	0.09	0.10	0.10	0.11	0.11	0.12	0.13	0.13	0.14
29P090	0.19	0.18	0.17	0.16	0.15	0.10	0.09	0.11	0.11	0.12	0.09	0.10	0.10	0.11	0.11	0.11	0.11	0.12	0.12	0.13
MCH000	0.25	0.28	0.29	0.30	0.31	0.13	0.15	0.16	0.17	0.18	0.10	0.10	0.11	0.11	0.11	0.09	0.09	0.09	0.09	0.09
MCH090	0.44	0.47	0.48	0.48	0.53	0.11	0.11	0.12	0.12	0.13	0.10	0.10	0.10	0.10	0.10	0.10	0.10	0.10	0.10	0.10
MTW000	0.65	0.69	0.76	0.84	0.96	0.62	0.65	0.67	0.69	0.71	0.49	0.52	0.53	0.54	0.55	0.39	0.39	0.38	0.38	0.38
MTW090	0.49	0.50	0.50	0.49	0.46	0.35	0.35	0.34	0.33	0.32	0.23	0.24	0.24	0.24	0.24	0.20	0.21	0.21	0.22	0.22
GRN180	0.73	0.77	0.84	0.91	0.98	0.54	0.60	0.65	0.69	0.71	0.33	0.34	0.35	0.36	0.37	0.28	0.29	0.30	0.30	0.30
GRN270	1.66	1.28	1.22	1.20	1.18	1.61	1.77	1.86	1.91	1.95	0.99	1.04	1.06	1.06	1.07	0.64	0.65	0.66	0.67	0.67
TDO000	2.89	3.83	4.22	4.55	4.48	2.46	2.82	3.00	2.97	2.65	2.02	2.05	1.97	1.94	2.09	1.29	1.30	1.40	1.44	1.50
TDO090	1.69	1.98	2.22	2.41	2.64	1.31	1.44	1.52	1.56	1.62	0.90	0.89	0.85	0.82	0.78	0.56	0.60	0.62	0.63	0.64
PSA000	1.29	1.40	1.54	1.63	1.73	0.13	0.13	0.13	0.13	0.13	0.10	0.10	0.10	0.10	0.10	0.10	0.09	0.09	0.09	0.09
PSA090	2.67	2.92	3.07	3.12	3.06	0.63	0.76	0.84	0.90	0.99	0.12	0.13	0.14	0.15	0.16	0.15	0.15	0.16	0.16	0.16
SLC270	12.12	12.15	12.05	10.96	8.29	5.46	6.82	7.24	6.99	6.43	2.58	2.67	2.98	3.31	3.66	1.01	1.18	1.25	1.31	1.39
SLC360	7.50	7.63	7.23	7.47	8.69	3.54	3.67	3.98	4.01	4.54	2.53	2.82	3.14	3.34	3.55	2.71	3.12	3.40	3.57	3.99
CAS000	0.69	0.72	0.74	0.76	0.82	0.21	0.22	0.23	0.23	0.23	0.11	0.11	0.11	0.11	0.11	0.13	0.13	0.13	0.13	0.13
CAS270	0.72	0.76	0.79	0.80	0.92	0.31	0.34	0.36	0.37	0.41	0.25	0.27	0.28	0.28	0.29	0.21	0.21	0.22	0.22	0.22
H-VCT075	0.50	0.54	0.57	0.58	0.60	0.25	0.27	0.27	0.27	0.27	0.19	0.20	0.20	0.21	0.21	0.14	0.14	0.14	0.14	0.14
H-VCT345	0.83	0.85	0.86	0.89	1.04	0.72	0.75	0.77	0.78	0.81	0.56	0.59	0.60	0.61	0.62	0.38	0.39	0.40	0.41	0.41
median	0.70	0.74	0.77	0.82	0.94	0.33	0.34	0.35	0.35	0.38	0.23	0.23	0.24	0.24	0.24	0.18	0.18	0.19	0.19	0.19
84th per.	2.71	2.88	2.98	3.05	3.09	1.50	1.66	1.75	1.77	1.80	0.95	0.99	1.03	1.06	1.10	0.67	0.71	0.75	0.76	0.79
mean	1.81	1.90	1.94	1.94	1.91	0.96	1.08	1.15	1.15	1.14	0.61	0.64	0.67	0.69	0.73	0.44	0.48	0.50	0.52	0.55
σ	2.94	2.98	2.93	2.77	2.50	1.39	1.66	1.77	1.73	1.66	0.81	0.86	0.94	1.01	1.09	0.63	0.71	0.78	0.81	0.91
mean + σ	4.75	4.88	4.87	4.71	4.40	2.34	2.74	2.92	2.87	2.81	1.42	1.50	1.60	1.70	1.82	1.07	1.19	1.28	1.33	1.46
COV	1.62	1.56	1.51	1.43	1.31	1.45	1.54	1.55	1.51	1.45	1.34	1.36	1.41	1.45	1.50	1.41	1.49	1.54	1.57	1.65

Table E.5. Maximum isolator displacements determined from the results of unidirectional response-history analysis using Bin 6 ground motions.

	d_x (cm)																			
	$Q_d/W=0.03$					$Q_d/W=0.06$					$Q_d/W=0.09$					$Q_d/W=0.12$				
	T_d (seconds)					T_d (seconds)					T_d (seconds)					T_d (seconds)				
Record	1.5	2.0	2.5	3.0	4.0	1.5	2.0	2.5	3.0	4.0	1.5	2.0	2.5	3.0	4.0	1.5	2.0	2.5	3.0	4.0
LS01C	47.4	55.8	43.7	33.0	27.4	21.1	28.7	23.6	22.6	21.0	19.3	16.4	16.3	16.7	18.2	14.2	15.2	15.2	14.5	14.1
LS02C	32.0	138.3	155.7	149.6	97.9	27.8	86.4	113.0	101.8	82.2	26.4	66.2	85.1	73.6	61.7	21.2	49.0	58.9	47.7	35.3
LS03C	25.1	68.3	145.9	232.2	203.6	24.3	61.7	112.4	153.0	153.9	21.3	52.6	84.5	111.0	118.6	18.2	45.2	67.5	79.7	84.6
LS04C	24.9	42.6	72.2	72.8	48.5	17.0	23.6	39.0	39.9	31.9	12.2	17.6	18.8	16.6	16.6	8.5	8.3	7.9	9.2	10.7
LS05C	29.6	58.4	127.1	181.7	182.3	27.3	47.4	90.0	130.1	141.4	21.9	35.8	60.0	80.3	98.0	16.2	29.1	41.8	50.4	57.1
LS06C	26.4	59.7	87.2	89.5	75.0	23.3	43.7	57.3	60.1	50.0	21.1	31.8	38.6	40.4	34.4	16.9	20.8	21.6	21.9	19.8
LS07C	38.2	54.1	67.2	94.4	94.6	27.0	36.8	38.6	43.3	40.6	22.6	24.6	24.2	23.1	24.9	18.3	20.4	21.0	21.0	21.5
LS08C	18.6	44.5	53.7	53.5	43.2	12.9	20.4	25.3	27.4	26.5	6.5	8.7	9.3	9.0	8.3	2.3	2.2	2.0	1.9	2.2
LS09C	93.3	54.8	46.1	55.2	97.1	69.6	50.6	43.9	39.4	67.5	49.2	42.6	41.8	41.0	41.3	32.6	34.6	37.2	38.3	38.9
LS10C	55.3	61.4	97.7	78.4	52.8	35.4	39.8	46.5	42.4	39.2	21.0	25.5	25.9	23.5	27.7	10.2	12.3	14.9	16.8	20.9
LS11C	52.5	69.3	66.8	56.4	51.8	32.6	49.9	49.5	44.1	43.8	26.8	36.2	36.9	37.2	36.6	21.5	27.1	30.7	32.7	34.4
LS12C	36.8	84.4	99.5	87.0	70.5	26.7	62.2	74.3	68.8	62.4	22.9	41.9	49.5	49.6	44.4	17.0	24.8	26.5	29.0	24.1
LS13C	67.3	95.8	61.2	51.5	75.0	52.9	54.0	52.4	42.8	49.2	44.2	44.8	44.0	37.1	37.2	35.7	35.8	35.8	31.3	28.0
LS14C	24.8	44.8	42.8	37.9	21.7	14.6	16.5	17.2	15.3	15.7	8.4	9.6	10.3	10.7	11.2	6.5	7.2	7.7	7.9	8.2
LS15C	55.8	67.7	62.4	59.9	54.5	49.4	55.3	54.2	50.5	43.6	43.7	48.9	48.7	46.4	41.0	38.5	43.4	44.3	43.6	41.1
LS16C	22.1	51.7	81.4	75.5	52.6	14.6	34.2	46.2	47.9	32.2	15.2	19.4	20.2	20.8	20.8	7.8	9.4	10.8	12.3	14.3
LS17C	68.8	112.9	237.9	207.6	134.0	54.4	95.9	193.2	176.2	119.5	47.7	79.4	152.8	144.0	101.6	41.2	63.3	112.8	110.8	79.5
LS18C	55.3	65.9	38.2	28.9	24.6	41.0	46.9	30.6	24.9	17.4	28.7	32.2	25.6	20.2	20.5	20.1	22.6	22.2	23.7	27.7
LS19C	53.3	67.9	72.9	52.7	44.9	43.5	54.3	50.3	46.5	44.3	35.1	43.4	42.2	42.7	42.0	27.0	34.0	37.6	39.1	39.9
LS20C	33.4	52.1	51.9	49.8	40.0	24.4	36.6	36.7	36.2	27.9	17.2	21.4	23.7	23.6	18.9	12.0	11.6	11.9	12.1	10.8
median	37.5	60.6	69.7	66.3	53.7	27.2	47.2	48.0	43.7	43.7	22.2	34.0	37.7	37.2	35.5	17.6	23.7	24.4	26.3	25.9
84th per.	60.9	87.1	122.4	131.2	114.1	46.1	67.2	89.4	92.7	85.6	38.6	54.2	68.1	69.4	65.6	31.9	45.3	55.8	57.6	53.9
mean	43.1	67.5	85.6	87.4	74.6	32.0	47.2	59.7	60.7	55.5	25.6	34.9	42.9	43.4	41.2	19.3	25.8	31.4	32.2	30.7
σ	19.5	24.0	49.0	58.6	49.4	15.4	19.9	41.0	44.4	39.7	12.5	18.3	33.5	34.8	31.0	10.9	16.1	25.8	26.1	22.1
mean + σ	62.5	91.6	134.5	146.0	124.0	47.4	67.1	100.8	105.1	95.2	38.1	53.2	76.4	78.2	72.2	30.2	41.9	57.2	58.3	52.8
COV	0.45	0.36	0.57	0.67	0.66	0.48	0.42	0.69	0.73	0.72	0.49	0.52	0.78	0.80	0.75	0.56	0.62	0.82	0.81	0.72

Table E.6. Maximum isolator displacements determined from the results of unidirectional response-history analysis using Bin 7 ground motions.

	d_x (cm)																									
	$Q_d/W=0.03$						$Q_d/W=0.06$						$Q_d/W=0.09$						$Q_d/W=0.12$							
	T_d (seconds)						T_d (seconds)						T_d (seconds)						T_d (seconds)							
Record	1.5	2.0	2.5	3.0	4.0	1.5	2.0	2.5	3.0	4.0	1.5	2.0	2.5	3.0	4.0	1.5	2.0	2.5	3.0	4.0	1.5	2.0	2.5	3.0	4.0	
SCTEW	23.0	155.2	125.0	73.5	43.4	19.9	64.9	72.7	50.2	35.5	14.6	31.9	33.0	26.2	20.3	8.0	8.8	7.2	7.2	7.2	7.4	8.0	8.8	7.2	7.2	7.4
SCTNS	11.82	70.38	45.74	29.25	20.78	6.44	9.71	8.18	7.06	7.02	0.24	0.31	0.38	0.43	0.48	0.02	0.02	0.02	0.02	0.02	0.02	0.02	0.02	0.02	0.02	0.02
MEN270	2.87	3.85	4.26	4.31	3.97	1.41	1.50	1.66	1.77	1.86	0.11	0.11	0.11	0.12	0.12	0.03	0.03	0.03	0.03	0.03	0.03	0.03	0.03	0.03	0.03	0.03
MEN360	5.35	5.05	4.98	5.36	5.75	1.53	1.73	1.83	1.90	1.97	0.49	0.52	0.54	0.55	0.56	0.05	0.05	0.05	0.05	0.05	0.05	0.05	0.05	0.05	0.05	0.05
EMV260	35.6	17.3	12.4	10.5	10.8	18.2	13.3	10.3	8.5	8.8	8.9	7.6	7.2	6.6	5.9	3.7	3.7	3.5	3.3	3.2	3.2	3.7	3.7	3.5	3.3	3.2
EMV360	8.9	6.4	5.3	4.8	4.7	3.9	4.2	4.4	4.5	4.6	2.0	2.0	2.1	2.2	2.2	0.8	0.8	0.9	0.9	0.9	0.9	0.8	0.8	0.9	0.9	0.9
OHW035	15.7	14.9	16.4	15.7	13.3	12.6	10.9	11.7	12.1	12.3	8.3	7.3	8.4	9.1	9.8	3.9	3.8	4.2	4.5	4.9	4.9	3.9	3.8	4.2	4.5	4.9
OHW305	25.7	14.8	10.8	9.4	9.5	11.1	9.6	8.4	10.4	13.1	9.7	8.9	8.3	8.8	10.0	7.1	7.0	6.9	7.0	7.6	7.6	7.1	7.0	6.9	7.0	7.6
RWC043	23.5	11.9	12.7	15.3	14.4	22.0	11.2	12.6	14.7	15.0	17.2	12.1	12.4	13.7	15.2	10.7	10.5	11.3	12.1	13.1	13.1	10.7	10.5	11.3	12.1	13.1
RWC233	16.0	9.4	8.5	7.9	7.3	10.4	8.4	8.3	8.2	8.0	6.2	5.7	5.8	5.9	6.0	3.0	2.7	2.8	2.8	2.9	2.9	3.0	2.7	2.8	2.8	2.9
SFA000	6.9	4.9	4.2	4.5	4.9	4.8	4.0	3.5	3.0	2.8	2.8	2.6	2.5	2.5	2.5	2.1	2.2	2.2	2.2	2.3	2.3	2.1	2.2	2.2	2.2	2.3
SFA090	8.0	7.1	7.1	7.8	8.6	6.8	5.9	6.3	6.8	7.3	3.8	4.5	5.0	5.3	5.6	2.3	2.6	2.6	2.7	2.8	2.8	2.3	2.6	2.6	2.7	2.8
TRI000	5.41	5.16	5.24	5.23	5.42	1.16	1.07	1.01	0.96	0.90	0.06	0.06	0.06	0.06	0.06	0.03	0.03	0.03	0.03	0.03	0.03	0.03	0.03	0.03	0.03	0.03
TRI090	14.69	18.82	17.19	16.73	15.87	7.53	9.38	10.13	10.39	10.46	4.04	4.82	5.31	5.62	6.00	1.07	1.28	1.39	1.46	1.53	1.53	1.07	1.28	1.39	1.46	1.53
ATS000	5.8	5.6	5.5	6.6	8.6	3.1	3.7	4.3	4.6	4.6	2.0	1.9	2.2	2.3	2.2	1.5	1.5	1.5	1.5	1.6	1.6	1.5	1.5	1.5	1.5	1.6
ATS090	19.8	12.5	11.4	9.9	8.3	10.4	7.0	5.9	5.8	6.0	3.6	3.9	4.1	4.4	4.8	1.6	1.7	1.9	1.9	2.0	2.0	1.6	1.7	1.9	1.9	2.0
DZC180	11.5	14.4	19.4	26.2	35.1	8.4	10.2	10.3	10.2	10.0	5.0	6.0	6.2	6.3	6.3	2.3	2.9	3.2	3.4	3.7	3.7	2.3	2.9	3.2	3.4	3.7
DZC270	31.2	35.1	29.1	23.8	21.3	22.0	20.6	21.9	21.0	17.6	14.2	13.3	14.1	13.6	13.3	6.9	7.5	8.1	8.4	8.6	8.6	6.9	7.5	8.1	8.4	8.6
YPT060	10.3	19.2	29.4	39.1	80.0	7.3	10.4	11.0	13.3	15.2	3.5	3.4	4.0	4.5	5.2	1.5	1.5	1.5	1.6	1.8	1.8	1.5	1.5	1.5	1.6	1.8
YPT330	29.1	19.3	26.8	48.0	67.2	11.6	12.6	16.2	17.9	22.8	6.9	7.9	8.7	9.9	11.3	3.3	3.8	4.6	5.2	5.9	5.9	3.3	3.8	4.6	5.2	5.9
median	13.3	13.4	11.9	10.2	10.2	8.0	9.5	8.3	8.4	8.4	3.9	4.7	5.1	5.4	5.8	2.2	2.4	2.4	2.5	2.5	2.5	2.2	2.4	2.4	2.5	2.5
84th per.	25.3	33.2	30.9	29.3	30.8	17.1	18.4	18.9	18.4	18.3	13.9	14.5	15.3	15.5	15.9	8.1	8.6	9.0	9.3	9.9	9.9	8.1	8.6	9.0	9.3	9.9
mean	15.6	22.6	20.1	18.2	19.5	9.5	11.0	11.5	10.7	10.3	5.7	6.2	6.5	6.4	6.4	3.0	3.1	3.2	3.3	3.5	3.5	3.0	3.1	3.2	3.3	3.5
σ	9.7	34.6	27.0	17.9	21.3	6.6	13.5	15.3	10.7	8.3	5.1	7.1	7.4	6.2	5.5	3.0	3.0	3.1	3.2	3.5	3.5	3.0	3.0	3.1	3.2	3.5
mean + σ	25.2	57.2	47.1	36.1	40.7	16.1	24.6	26.8	21.4	18.6	10.8	13.4	13.9	12.6	11.9	6.0	6.2	6.3	6.6	7.0	7.0	6.0	6.2	6.3	6.6	7.0
COV	0.62	1.53	1.35	0.98	1.09	0.70	1.23	1.33	1.01	0.80	0.89	1.14	1.13	0.97	0.86	1.00	0.98	0.96	0.97	0.99	0.99	1.00	0.98	0.96	0.97	0.99

Table E.7. Maximum isolator displacements determined from the results of bi-directional response-history analysis using Bin 1 ground motions.

Ground motion pair	d_{xy} (cm)																			
	$Q_d/W=0.03$					$Q_d/W=0.06$					$Q_d/W=0.09$					$Q_d/W=0.12$				
	T_d (seconds)					T_d (seconds)					T_d (seconds)					T_d (seconds)				
	1.5	2.0	2.5	3.0	4.0	1.5	2.0	2.5	3.0	4.0	1.5	2.0	2.5	3.0	4.0	1.5	2.0	2.5	3.0	4.0
nf01/nf02	33.1	70.3	68.9	85.2	150.2	29.8	48.2	53.3	63.6	88.0	27.4	38.8	46.9	55.3	70.1	24.7	34.3	41.8	47.7	58.0
nf03/nf04	121.7	123.9	144.2	241.4	202.9	108.2	109.9	119.1	175.0	167.2	92.6	97.4	103.0	122.1	139.6	76.7	85.7	90.1	96.4	111.7
nf05/nf06	85.7	94.7	79.0	87.5	91.4	76.4	81.1	67.7	71.3	79.3	67.9	70.8	59.5	58.8	65.6	61.8	63.3	53.5	49.3	54.5
nf07/nf08	49.8	73.2	102.0	97.1	85.1	45.0	59.3	75.1	76.2	76.1	40.5	51.5	60.2	64.2	70.6	37.2	47.1	53.7	58.2	63.7
nf09/nf10	43.3	63.0	73.4	69.1	60.5	37.6	48.6	54.6	52.6	49.4	32.5	37.2	40.0	42.3	41.3	28.2	31.3	32.9	33.9	34.0
nf11/nf12	25.7	35.3	51.4	66.0	99.0	21.8	32.4	42.9	51.2	64.6	18.7	26.3	32.7	37.9	45.0	15.1	20.2	23.7	26.7	30.2
nf13/nf14	68.1	70.9	68.6	50.6	54.1	59.3	57.4	49.5	44.2	47.5	55.2	53.1	46.4	38.7	41.2	51.3	49.2	43.6	37.6	35.7
nf15/nf16	66.6	70.4	106.4	92.4	59.0	44.7	56.3	70.5	63.5	50.8	38.2	45.6	47.3	48.0	43.1	32.8	38.5	38.6	38.3	36.5
nf17/nf18	118.1	84.7	80.3	89.5	74.5	104.6	75.0	68.5	75.2	62.5	90.8	65.5	57.2	62.1	53.9	76.6	55.9	47.1	49.9	44.5
nf19/nf20	112.4	196.5	140.8	82.2	90.1	104.4	163.4	127.4	80.2	71.6	101.7	139.0	112.6	75.1	63.9	97.0	117.0	97.3	70.1	65.6
TCU065	68.5	124.1	81.3	78.2	183.5	46.0	74.9	61.4	67.7	111.3	30.2	42.5	41.5	60.4	84.7	25.3	26.4	34.2	48.0	61.1
TCU075	15.5	33.3	48.8	60.0	94.0	14.1	27.2	36.6	43.5	53.6	11.5	19.8	25.5	29.2	33.6	8.2	12.6	15.1	16.4	17.5
median	67.3	72.1	79.6	83.7	90.7	45.5	58.4	64.5	65.6	68.1	39.4	48.6	47.1	57.0	58.9	35.0	42.8	42.7	47.8	49.5
84th per.	110.1	125.5	120.9	131.6	134.4	96.6	104.3	97.7	101.6	101.8	87.1	90.7	83.0	80.7	85.6	78.1	80.0	73.4	68.9	73.6
mean	67.4	86.7	87.1	91.6	103.7	57.7	69.5	68.9	72.0	76.8	50.6	57.3	56.1	57.8	62.7	44.6	48.5	47.6	47.7	51.1
σ	36.2	44.6	30.9	49.2	48.9	33.2	37.1	27.9	34.7	34.0	30.7	33.1	26.3	24.2	28.7	27.9	29.4	24.3	20.9	24.4
mean + σ	103.5	131.3	118.0	140.8	152.6	90.8	106.6	96.8	106.7	110.8	81.3	90.4	82.4	82.0	91.4	72.5	77.9	72.0	68.6	75.5
COV	0.54	0.51	0.35	0.54	0.47	0.58	0.53	0.41	0.48	0.44	0.61	0.58	0.47	0.42	0.46	0.63	0.61	0.51	0.44	0.48

Table E.8. Maximum isolator displacements determined from the results of bi-directional response-history analysis using Bin 2 ground motions.

Ground motion	d_{xy} (cm)																			
	$Q_d/W=0.03$					$Q_d/W=0.06$					$Q_d/W=0.09$					$Q_d/W=0.12$				
	T_d (seconds)					T_d (seconds)					T_d (seconds)					T_d (seconds)				
pair	1.5	2.0	2.5	3.0	4.0	1.5	2.0	2.5	3.0	4.0	1.5	2.0	2.5	3.0	4.0	1.5	2.0	2.5	3.0	4.0
G01	9.21	9.03	7.68	7.75	8.23	5.99	5.99	5.49	5.22	4.96	4.96	5.40	5.51	5.51	5.45	4.42	4.75	4.83	4.87	4.89
SGI	0.84	0.87	0.87	0.87	0.86	0.09	0.09	0.09	0.10	0.10	0.08	0.08	0.08	0.08	0.08	0.08	0.08	0.08	0.08	0.08
L09	0.65	0.70	0.71	0.76	0.81	0.85	0.87	0.88	0.89	0.90	0.66	0.65	0.64	0.63	0.63	0.65	0.65	0.65	0.65	0.65
WON	3.22	3.22	3.19	3.19	3.32	2.10	2.32	2.48	2.60	2.77	1.53	1.69	1.79	1.84	1.90	0.72	0.77	0.79	0.81	0.82
SFL09	0.44	0.50	0.55	0.58	0.61	0.29	0.33	0.36	0.38	0.39	0.19	0.20	0.20	0.21	0.21	0.13	0.13	0.13	0.13	0.13
G02	39.24	26.99	22.01	19.95	15.99	24.02	20.70	18.15	17.66	15.94	14.35	14.10	13.84	14.51	14.81	8.68	8.60	9.49	10.07	10.73
YER	23.80	18.95	16.16	15.35	20.02	11.82	12.95	14.39	15.82	17.49	6.91	8.85	10.34	11.47	12.91	4.57	5.72	6.53	7.07	7.69
ABN	6.47	6.28	6.97	7.28	7.43	2.36	3.02	3.30	3.40	3.47	1.39	1.55	1.66	1.73	1.83	0.82	0.91	0.97	1.01	1.06
A-E01	0.33	0.30	0.30	0.31	0.31	0.11	0.11	0.11	0.11	0.11	0.05	0.05	0.05	0.05	0.05	0.06	0.06	0.06	0.06	0.06
CNP	25.91	30.39	28.51	26.31	25.72	14.13	14.11	15.98	17.49	18.56	10.89	9.50	9.52	9.59	10.42	8.01	6.75	6.69	6.60	6.52
median	4.85	4.75	5.08	5.23	5.37	2.23	2.67	2.89	3.00	3.12	1.46	1.62	1.72	1.78	1.86	0.77	0.84	0.88	0.91	0.94
84th per.	21.87	19.65	17.62	16.84	17.16	13.17	13.45	13.76	14.25	14.46	9.02	9.50	9.93	10.35	10.93	5.92	6.12	6.50	6.72	6.97
mean	11.01	9.72	8.69	8.24	8.33	6.18	6.05	6.12	6.37	6.47	4.10	4.21	4.36	4.56	4.83	2.81	2.84	3.02	3.13	3.26
σ	13.76	11.54	10.12	9.27	9.19	8.04	7.31	7.19	7.52	7.68	5.09	5.00	5.12	5.41	5.76	3.37	3.27	3.52	3.69	3.89
mean + σ	24.77	21.26	18.81	17.50	17.52	14.22	13.36	13.31	13.89	14.15	9.19	9.21	9.48	9.97	10.59	6.19	6.11	6.54	6.82	7.16
COV	1.25	1.19	1.16	1.13	1.10	1.30	1.21	1.17	1.18	1.19	1.24	1.19	1.17	1.19	1.19	1.20	1.15	1.16	1.18	1.19

Table E.9. Maximum isolator displacements determined from the results of bi-directional response-history analysis using Bin 2M ground motions.

Ground motion	d_{xy} (cm)																			
	$Q_d/W=0.03$				$Q_d/W=0.06$				$Q_d/W=0.09$				$Q_d/W=0.12$							
	T_d (seconds)				T_d (seconds)				T_d (seconds)				T_d (seconds)							
pair	1.5	2.0	2.5	3.0	4.0	1.5	2.0	2.5	3.0	4.0	1.5	2.0	2.5	3.0	4.0	1.5	2.0	2.5	3.0	4.0
G01	9.2	9.0	7.7	7.7	8.2	6.0	6.0	5.5	5.2	5.0	5.0	5.4	5.5	5.5	5.5	4.4	4.7	4.8	4.9	4.9
GBZ	5.7	7.5	13.0	20.0	31.5	4.9	5.9	6.5	7.0	7.7	3.6	4.1	4.3	4.5	4.7	2.4	2.5	2.6	2.7	2.7
STG	22.8	23.8	22.7	25.5	28.3	16.4	16.6	17.1	18.8	21.0	9.7	10.7	12.3	13.4	14.6	5.8	6.8	7.7	8.4	9.1
RIO	16.7	13.9	11.4	10.0	9.4	13.1	12.1	10.0	8.7	8.0	10.3	9.8	8.4	7.4	6.9	7.9	7.4	6.7	6.6	6.6
JOS	16.9	16.1	12.7	16.2	17.6	11.3	11.8	10.8	9.8	11.0	7.6	7.8	7.6	7.5	7.5	4.0	4.1	4.2	4.3	5.1
G02	39.2	27.0	22.0	19.9	16.0	24.0	20.7	18.2	17.7	15.9	14.3	14.1	13.8	14.5	14.8	8.7	8.6	9.5	10.1	10.7
YER	23.8	19.0	16.2	15.4	20.0	11.8	13.0	14.4	15.8	17.5	6.9	8.8	10.3	11.5	12.9	4.6	5.7	6.5	7.1	7.7
ABN	6.5	6.3	7.0	7.3	7.4	2.4	3.0	3.3	3.4	3.5	1.4	1.5	1.7	1.7	1.8	0.8	0.9	1.0	1.0	1.1
BOL	22.8	30.4	29.4	26.8	21.2	21.0	21.5	24.0	23.0	17.9	20.5	20.1	20.8	20.1	17.4	18.9	18.7	18.9	18.4	16.9
CNP	25.9	30.4	28.5	26.3	25.7	14.1	14.1	16.0	17.5	18.6	10.9	9.5	9.5	9.6	10.4	8.0	6.8	6.7	6.6	6.5
median	19.9	17.5	14.6	18.1	18.8	12.5	12.5	12.6	12.8	13.5	8.6	9.2	9.0	8.6	9.0	5.2	6.2	6.6	6.6	6.5
84th per.	30.4	28.6	25.3	25.9	27.9	21.1	20.1	20.1	20.3	20.1	15.6	15.5	15.9	16.1	16.1	11.5	11.5	11.9	12.1	12.4
mean	19.0	18.3	17.1	17.5	18.5	12.5	12.5	12.6	12.7	12.6	9.0	9.2	9.4	9.6	9.7	6.5	6.6	6.9	7.0	7.1
σ	10.3	9.3	8.1	7.5	8.5	6.9	6.2	6.5	6.7	6.3	5.5	5.2	5.4	5.4	5.1	5.0	4.8	4.9	4.8	4.5
mean + σ	29.2	27.6	25.2	25.0	27.0	19.4	18.7	19.1	19.3	18.9	14.6	14.4	14.9	15.0	14.8	11.5	11.5	11.8	11.8	11.6
COV	0.54	0.50	0.48	0.43	0.46	0.55	0.50	0.52	0.52	0.50	0.61	0.57	0.57	0.57	0.53	0.77	0.73	0.71	0.69	0.63

Table E.10. Maximum isolator displacements determined from the results of bi-directional response-history analysis using Bin 3 ground motions.

Ground motion pair	d_{xy} (cm)																			
	$Q_d/W=0.03$				$Q_d/W=0.06$				$Q_d/W=0.09$				$Q_d/W=0.12$							
	T_d (seconds)				T_d (seconds)				T_d (seconds)				T_d (seconds)							
	1.5	2.0	2.5	3.0	4.0	1.5	2.0	2.5	3.0	4.0	1.5	2.0	2.5	3.0	4.0	1.5	2.0	2.5	3.0	4.0
CHY	0.61	0.72	0.78	0.82	0.87	0.54	0.63	0.69	0.72	0.76	0.30	0.34	0.37	0.38	0.39	0.26	0.27	0.28	0.28	0.28
29P	0.19	0.18	0.18	0.19	0.19	0.11	0.13	0.14	0.15	0.16	0.16	0.16	0.17	0.17	0.17	0.13	0.14	0.14	0.15	0.15
MCH	0.48	0.55	0.61	0.64	0.68	0.20	0.23	0.25	0.26	0.28	0.16	0.17	0.17	0.17	0.17	0.10	0.11	0.11	0.11	0.11
MTW	0.72	0.69	0.68	0.69	0.72	0.77	0.78	0.79	0.79	0.80	0.54	0.53	0.53	0.53	0.53	0.50	0.52	0.52	0.53	0.54
GRN	1.74	1.47	1.42	1.46	1.48	1.62	1.78	1.88	1.94	2.01	1.10	1.18	1.21	1.23	1.25	0.74	0.75	0.75	0.75	0.74
TDO	3.36	4.57	5.17	5.19	5.03	2.60	2.91	3.03	3.00	2.81	1.95	1.93	1.81	1.67	1.76	1.23	1.25	1.28	1.30	1.31
PSA	3.23	3.25	3.19	3.12	2.94	1.07	1.26	1.39	1.47	1.57	0.19	0.22	0.25	0.27	0.30	0.17	0.18	0.18	0.19	0.20
SLC	15.09	15.85	16.39	14.76	11.46	9.55	10.95	11.00	10.28	8.62	5.53	6.54	6.93	7.01	6.84	2.93	3.48	4.06	4.77	5.71
CAS	0.91	0.94	0.93	0.95	1.03	0.39	0.44	0.47	0.49	0.51	0.31	0.34	0.36	0.37	0.39	0.21	0.22	0.22	0.23	0.23
H-VCT	1.27	1.34	1.38	1.40	1.44	0.75	0.79	0.81	0.82	0.93	0.61	0.64	0.65	0.66	0.66	0.52	0.54	0.55	0.56	0.56
median	1.09	1.14	1.15	1.18	1.24	0.76	0.79	0.80	0.81	0.86	0.42	0.44	0.45	0.45	0.46	0.38	0.39	0.40	0.40	0.41
84th per.	4.39	4.73	4.91	4.77	4.40	2.87	3.19	3.30	3.28	3.14	1.70	1.83	1.87	1.86	1.88	1.13	1.21	1.28	1.36	1.46
mean	2.76	2.96	3.07	2.92	2.58	1.76	1.99	2.04	1.99	1.84	1.08	1.21	1.24	1.25	1.25	0.68	0.75	0.81	0.89	0.98
σ	4.47	4.73	4.91	4.42	3.42	2.84	3.26	3.26	3.04	2.52	1.66	1.95	2.06	2.08	2.03	0.87	1.02	1.20	1.41	1.70
mean + σ	7.23	7.69	7.99	7.34	6.01	4.60	5.25	5.31	5.03	4.36	2.74	3.16	3.31	3.33	3.27	1.55	1.77	2.01	2.30	2.68
COV	1.62	1.60	1.60	1.51	1.32	1.61	1.64	1.60	1.52	1.37	1.53	1.62	1.66	1.67	1.63	1.27	1.38	1.48	1.60	1.73

Table E.1.1. Maximum isolator displacements determined from the results of bi-directional response-history analysis using Bin 6 ground motions.

Ground motion pair	d_{xy} (cm)																			
	$Q_d/W=0.03$					$Q_d/W=0.06$					$Q_d/W=0.09$					$Q_d/W=0.12$				
	T_d (seconds)					T_d (seconds)					T_d (seconds)					T_d (seconds)				
	1.5	2.0	2.5	3.0	4.0	1.5	2.0	2.5	3.0	4.0	1.5	2.0	2.5	3.0	4.0	1.5	2.0	2.5	3.0	4.0
LS01C/LS02C	52.2	156.2	159.2	159.0	99.1	33.5	108.5	117.6	104.8	84.4	28.0	71.0	91.1	79.2	66.9	23.0	54.6	68.1	57.4	49.5
LS03C/LS04C	35.9	82.1	175.0	261.0	214.0	32.3	70.6	138.4	184.6	176.8	28.3	60.2	104.9	137.3	142.4	24.1	51.9	82.2	99.0	107.5
LS05C/LS06C	31.9	71.1	173.0	209.6	198.7	28.5	59.5	128.6	163.1	163.0	24.5	51.4	95.6	118.0	128.9	22.3	44.1	69.3	86.3	95.7
LS07C/LS08C	42.4	59.5	67.2	98.8	116.1	32.4	40.6	44.3	51.2	46.1	25.6	26.1	23.9	23.2	28.7	21.7	22.7	21.6	20.2	19.7
LS09C/LS10C	114.8	70.2	119.1	97.8	101.8	91.1	59.6	56.7	53.1	76.6	68.0	54.7	50.4	47.4	52.5	49.0	46.6	46.8	46.6	48.1
LS11C/LS12C	61.3	118.1	124.2	107.9	72.7	48.4	96.1	101.4	94.8	66.4	39.1	75.7	79.0	78.6	60.1	31.4	56.0	62.2	62.1	52.8
LS13C/LS14C	71.0	107.6	69.0	62.6	84.1	57.7	68.2	59.6	49.4	54.1	49.2	52.0	50.6	41.6	43.7	41.0	43.4	42.1	35.0	35.7
LS15C/LS16C	59.3	81.2	92.8	89.0	70.8	51.2	57.8	66.6	63.8	55.9	45.3	51.0	50.3	47.1	45.5	40.1	45.1	45.2	43.3	39.1
LS17C/LS18C	93.3	132.3	241.6	210.0	134.1	71.8	107.3	199.9	180.1	120.3	51.8	88.8	162.0	150.0	104.5	45.2	73.0	125.4	120.2	86.2
LS19C/LS20C	66.7	91.4	99.4	76.6	61.4	56.8	76.9	74.0	66.7	56.6	47.7	62.9	56.6	56.9	51.6	38.7	49.6	47.3	48.5	47.2
median	60.3	86.8	121.6	103.3	100.5	49.8	69.4	87.7	80.7	71.5	42.2	57.5	67.8	67.8	56.3	35.1	48.1	54.7	53.0	48.8
84th per.	87.2	126.2	185.4	199.4	161.4	69.1	97.2	143.1	150.7	129.7	54.7	78.9	115.1	121.0	106.9	44.2	63.2	88.5	92.7	86.3
mean	62.9	97.0	132.0	137.2	115.3	50.4	74.5	98.7	101.2	90.0	40.7	59.4	76.4	77.9	72.5	33.7	48.7	61.0	61.9	58.1
σ	25.7	30.9	55.0	68.1	52.9	20.1	22.7	48.3	54.9	47.2	14.2	17.0	39.3	43.4	38.9	10.4	12.6	28.4	30.9	28.5
mean + σ	88.5	127.9	187.1	205.4	168.1	70.5	97.2	147.0	156.1	137.2	55.0	76.4	115.7	121.3	111.3	44.0	61.3	89.4	92.8	86.6
COV	0.41	0.32	0.42	0.50	0.46	0.40	0.30	0.49	0.54	0.52	0.35	0.29	0.51	0.56	0.54	0.31	0.26	0.47	0.50	0.49

Table E.12. Maximum isolator displacements determined from the results of bi-directional response-history analysis using Bin 7 ground motions.

Ground motion pair	d_{xy} (cm)																								
	$Q_d/W=0.03$						$Q_d/W=0.06$						$Q_d/W=0.09$						$Q_d/W=0.12$						
	T_d (seconds)						T_d (seconds)						T_d (seconds)						T_d (seconds)						
	1.5	2.0	2.5	3.0	4.0	1.5	2.0	2.5	3.0	4.0	1.5	2.0	2.5	3.0	4.0	1.5	2.0	2.5	3.0	4.0	1.5	2.0	2.5	3.0	4.0
SCT	23.9	209.9	136.6	77.8	39.4	21.5	96.2	90.2	56.2	36.9	16.2	45.0	47.2	36.1	24.5	11.7	17.0	14.9	10.9	8.9	0.04	0.04	0.04	0.04	0.04
MEN	6.42	6.97	6.90	6.05	6.22	2.18	2.08	2.16	2.21	2.25	0.49	0.60	0.66	0.69	0.73	0.04	0.04	0.04	0.04	0.04	0.04	0.04	0.04	0.04	0.04
EMV	41.0	16.4	11.3	10.2	9.8	19.6	13.0	10.7	10.9	11.0	11.3	9.2	8.2	8.6	8.9	6.3	5.9	5.4	5.6	5.9	6.3	5.9	5.4	5.6	5.9
OHW	31.6	22.7	21.7	20.5	15.7	19.7	16.1	16.5	16.0	14.7	13.0	13.1	13.4	13.4	13.3	10.2	11.0	11.5	11.6	11.7	10.2	11.0	11.5	11.6	11.7
RWC	24.9	12.1	13.6	16.6	16.3	23.2	12.6	14.0	16.2	17.1	18.7	13.6	14.1	15.7	17.8	14.3	12.8	14.1	15.5	17.5	14.3	12.8	14.1	15.5	17.5
SFA	8.4	7.4	7.6	8.2	8.6	7.7	6.4	6.5	6.9	7.4	6.5	5.7	5.2	5.5	5.9	5.2	5.1	5.0	4.8	4.6	5.2	5.1	5.0	4.8	4.6
TRI	17.2	21.6	20.1	19.4	17.7	10.0	11.2	12.2	12.7	12.9	5.1	6.3	7.1	7.7	8.4	1.7	2.1	2.3	2.5	2.6	1.7	2.1	2.3	2.5	2.6
ATS	21.6	14.2	11.3	9.5	10.5	13.4	8.5	7.8	7.5	7.8	6.2	4.8	4.6	4.6	5.3	2.2	2.1	2.2	2.3	2.3	2.2	2.1	2.2	2.3	2.3
DZC	32.0	38.7	32.3	29.0	39.6	23.9	23.2	24.0	22.1	17.2	16.7	16.1	17.4	17.3	15.7	10.4	10.0	10.9	11.2	11.3	10.4	10.0	10.9	11.2	11.3
YPT	32.2	25.2	40.8	60.4	117.4	15.0	17.3	22.5	33.1	55.2	8.4	11.7	14.5	17.4	21.9	5.6	7.5	8.9	10.0	11.4	5.6	7.5	8.9	10.0	11.4
median	24.4	19.0	16.8	18.0	16.0	17.3	12.8	13.1	14.4	13.8	9.9	10.5	10.8	11.0	11.1	6.0	6.7	7.2	7.8	7.4	6.0	6.7	7.2	7.8	7.4
84th per.	38.2	54.6	47.2	42.4	44.6	27.3	34.1	34.7	32.4	31.8	21.9	25.1	26.1	25.7	24.9	21.0	23.0	23.8	23.6	24.2	21.0	23.0	23.8	23.6	24.2
mean	23.9	37.5	30.2	25.8	28.1	15.6	20.7	20.7	18.4	18.2	10.3	12.6	13.2	12.7	12.2	6.8	7.4	7.5	7.4	7.6	6.8	7.4	7.5	7.4	7.6
σ	11.0	61.3	38.9	24.2	33.6	7.3	27.2	25.4	15.9	16.0	5.9	12.3	13.1	10.0	7.7	4.7	5.4	5.3	5.1	5.4	4.7	5.4	5.3	5.1	5.4
mean + σ	34.9	98.8	69.2	50.0	61.7	22.9	47.9	46.0	34.3	34.2	16.2	24.9	26.3	22.7	20.0	11.5	12.7	12.8	12.5	13.1	11.5	12.7	12.8	12.5	13.1
COV	0.46	1.63	1.29	0.94	1.19	0.46	1.32	1.23	0.86	0.87	0.58	0.98	0.99	0.79	0.63	0.70	0.73	0.70	0.68	0.71	0.70	0.73	0.70	0.68	0.71

APPENDIX F

**NORMALIZED ENERGY DISSIPATED AND RATE-OF-ENERGY
DISSIPATED DATA**

Table F1. Normalized energy dissipated data from unidirectional response-history analysis using Bin 1 ground motions.

Record	NED																			
	$Q_d/W=0.03$				$Q_d/W=0.06$				$Q_d/W=0.09$				$Q_d/W=0.12$							
	T_d				T_d				T_d				T_d							
	1.5	2	2.5	3	4	1.5	2	2.5	3	4	1.5	2	2.5	3	4	1.5	2	2.5	3	4
nf01	5.60	5.64	3.12	2.39	2.11	3.80	3.11	2.46	2.00	1.62	2.93	2.37	1.92	1.67	1.40	2.53	2.03	1.66	1.48	1.27
nf02	5.14	4.68	4.47	3.31	2.80	4.17	3.66	3.01	2.33	1.93	3.74	2.96	2.35	2.07	1.60	3.09	2.41	1.96	1.67	1.44
nf03	7.08	3.40	5.70	5.75	2.42	4.39	2.35	3.13	3.43	1.58	3.29	2.05	2.27	2.53	1.43	2.72	1.97	1.90	2.09	1.42
nf04	5.49	3.63	4.77	4.32	1.78	3.02	2.79	2.77	2.64	1.63	2.16	2.69	2.39	2.01	1.51	1.91	2.40	2.12	1.82	1.49
nf05	5.00	2.52	3.35	2.79	1.25	2.67	1.40	1.65	1.37	0.91	2.08	1.20	1.17	1.16	0.88	1.84	1.09	1.09	1.10	0.87
nf06	2.02	1.53	1.26	1.06	0.86	1.49	1.19	0.98	0.85	0.72	1.24	1.10	0.95	0.88	0.79	1.10	1.06	0.93	0.89	0.83
nf07	5.10	3.12	4.65	3.38	1.52	2.08	1.99	2.71	1.95	1.18	1.35	1.41	1.58	1.31	0.93	1.07	1.03	0.97	0.90	0.76
nf08	2.52	2.28	2.72	3.09	1.84	1.87	1.48	1.40	1.40	1.11	1.53	1.18	1.09	1.03	0.91	1.41	1.07	0.97	0.91	0.83
nf09	2.49	4.26	2.30	3.07	1.42	1.50	2.17	1.63	1.36	0.98	1.13	1.39	1.27	1.07	0.81	0.95	1.00	0.95	0.85	0.71
nf10	2.86	2.10	1.85	1.86	1.44	1.57	1.35	1.11	0.94	0.85	1.45	1.16	1.04	1.01	0.98	1.31	0.98	0.89	0.76	0.64
nf11	2.57	1.52	1.21	1.68	2.11	1.37	1.07	0.95	1.02	1.03	1.09	0.90	0.83	0.83	0.72	1.04	0.89	0.80	0.72	0.63
nf12	3.09	2.01	1.88	1.96	1.71	2.26	1.98	1.97	2.01	2.08	2.42	2.29	2.35	2.51	2.90	2.84	3.04	3.43	3.28	3.07
nf13	7.39	4.88	2.69	1.79	1.47	4.29	2.33	1.73	1.63	1.29	3.12	1.67	1.39	1.45	1.30	2.33	1.32	1.15	1.20	1.25
nf14	2.91	2.80	2.56	2.39	1.52	2.24	1.87	1.77	1.94	1.74	1.92	1.67	1.61	1.73	1.93	2.07	1.97	1.90	1.95	2.06
nf15	6.76	3.87	4.68	2.39	1.60	3.65	2.36	2.75	1.99	1.39	1.91	1.64	1.99	1.60	1.19	1.29	1.44	1.30	1.12	0.90
nf16	4.59	3.05	2.27	2.67	2.57	2.69	2.35	2.51	2.17	1.93	2.10	1.97	1.72	1.55	1.34	1.83	1.58	1.42	1.32	1.18
nf17	8.38	5.20	2.03	2.13	2.63	4.86	3.03	1.83	1.56	1.84	3.84	2.32	1.90	1.61	1.77	3.45	2.27	2.12	1.85	1.59
nf18	5.04	3.42	3.57	3.57	3.64	3.88	3.28	2.95	2.98	3.11	3.54	3.23	2.86	2.76	2.10	3.15	2.40	2.20	2.10	2.07
nf19	10.47	8.95	5.76	2.88	2.32	5.74	5.16	3.57	2.57	2.19	3.66	3.86	2.77	2.33	2.01	2.54	3.19	2.43	2.13	1.64
nf20	6.07	5.44	3.37	3.46	2.79	4.03	3.67	3.34	3.63	3.73	3.17	2.66	2.50	2.54	2.66	2.66	2.11	1.94	1.96	2.15
TCU065W	13.74	9.73	5.60	4.71	3.44	8.28	6.22	4.69	3.24	2.55	6.99	5.03	3.50	2.71	1.93	4.20	3.24	3.00	2.43	2.22
TCU065N	9.73	8.85	5.74	5.63	3.92	7.84	5.25	4.65	3.83	3.08	6.43	3.98	3.22	3.19	2.49	4.33	3.26	2.89	2.40	1.79
TCU075W	4.32	3.01	1.89	2.65	2.22	2.29	1.60	1.38	1.29	1.30	1.61	1.21	1.01	0.91	0.85	1.22	1.00	0.92	0.83	0.68
TCU075N	5.62	5.04	3.77	2.91	2.45	2.54	2.73	2.90	2.80	2.75	1.37	1.39	1.43	1.47	1.49	0.95	0.91	0.90	0.89	0.89
mean	5.58	4.20	3.38	2.99	2.16	3.44	2.68	2.41	2.12	1.77	2.67	2.14	1.88	1.75	1.50	2.16	1.82	1.66	1.53	1.35
σ	2.86	2.27	1.47	1.17	0.78	1.85	1.34	1.04	0.86	0.80	1.54	1.06	0.75	0.69	0.62	1.01	0.82	0.76	0.68	0.63
mean + σ	8.44	6.47	4.86	4.16	2.94	5.29	4.02	3.45	2.98	2.57	4.21	3.20	2.63	2.44	2.12	3.17	2.64	2.42	2.20	1.98
COV	0.51	0.54	0.44	0.39	0.36	0.54	0.50	0.43	0.41	0.45	0.58	0.50	0.40	0.40	0.41	0.47	0.45	0.46	0.44	0.47

Table F.2. Normalized energy dissipated data from unidirectional response-history analysis using Bin 2 ground motions.

Record	NED																			
	$Q_d/W=0.03$				$Q_d/W=0.06$				$Q_d/W=0.09$				$Q_d/W=0.12$							
	T_d				T_d				T_d				T_d							
	1.5	2	2.5	3	4	1.5	2	2.5	3	4	1.5	2	2.5	3	4	1.5	2	2.5	3	4
G01000	1.71	1.56	1.47	1.42	1.36	1.44	1.37	1.34	1.32	1.29	1.79	1.56	1.43	1.29	1.16	1.33	1.03	0.90	0.82	0.75
G01090	2.21	1.35	1.40	1.43	1.29	1.55	1.32	1.30	1.35	1.51	1.45	1.31	1.25	1.23	1.21	1.56	1.46	1.41	1.39	1.38
SGI270	1.62	1.45	1.37	1.31	1.27	1.08	1.05	1.04	1.03	1.02	0.57	0.57	0.57	0.57	0.57	0.35	0.35	0.35	0.35	0.35
SGI360	0.79	0.76	0.74	0.74	0.73	1.24	1.14	1.10	1.08	1.06	1.13	1.13	1.13	1.13	1.13	0.70	0.70	0.70	0.70	0.70
L09000	3.52	3.06	2.80	2.73	2.66	2.35	2.32	2.31	2.31	2.31	2.15	1.99	1.90	1.86	1.82	2.29	2.35	2.38	2.41	2.43
L09090	3.17	3.25	3.22	3.17	3.20	1.63	1.57	1.53	1.51	1.49	1.46	1.46	1.46	1.47	1.47	0.97	0.96	0.95	0.94	0.94
WON095	1.31	1.18	1.12	1.11	1.10	0.93	0.85	0.81	0.79	0.76	1.45	1.40	1.38	1.36	1.35	1.75	1.70	1.67	1.66	1.64
WON185	1.40	1.12	1.00	0.92	0.81	0.72	0.61	0.55	0.52	0.49	0.46	0.43	0.42	0.41	0.40	0.59	0.56	0.55	0.54	0.54
SFL09021	2.76	2.32	2.09	1.98	1.87	2.74	2.51	2.37	2.29	2.21	2.32	2.14	2.06	2.02	1.98	1.55	1.53	1.52	1.52	1.51
SFL09291	3.13	3.15	3.18	3.20	3.23	2.71	2.69	2.68	2.68	2.68	2.34	2.35	2.36	2.37	2.37	2.30	2.29	2.28	2.28	2.27
G02000	3.67	2.23	1.64	1.62	1.75	1.85	1.60	1.38	1.32	1.29	1.38	1.26	1.09	1.01	0.92	1.33	1.18	1.10	1.02	0.95
G02090	5.59	1.90	1.47	1.34	1.51	2.94	1.55	1.32	1.14	1.06	1.80	1.26	1.24	1.34	1.32	1.36	1.21	1.05	0.99	0.94
YER270	4.29	1.94	1.68	1.62	1.60	2.11	1.27	0.93	0.79	0.71	1.16	0.81	0.67	0.60	0.52	0.64	0.56	0.50	0.47	0.44
YER360	3.49	2.50	2.17	1.98	1.83	2.18	2.31	2.28	2.24	2.12	2.49	2.29	2.21	2.17	2.13	2.08	2.04	2.02	2.01	1.96
ABN000	3.00	2.40	2.14	2.07	1.98	2.08	1.67	1.46	1.32	1.16	1.23	1.09	1.02	0.98	0.95	0.93	0.86	0.83	0.82	0.80
ABN090	1.70	1.67	1.55	1.35	1.15	1.89	1.85	1.77	1.72	1.66	1.71	1.56	1.47	1.43	1.39	1.42	1.34	1.29	1.26	1.24
A-E01140	0.82	0.87	0.88	0.87	0.85	0.276	0.273	0.272	0.271	0.271	0.186	0.188	0.189	0.190	0.191	0.023	0.024	0.024	0.024	0.025
A-E01230	1.45	1.43	1.42	1.42	1.41	0.73	0.73	0.73	0.73	0.73	0.50	0.50	0.50	0.50	0.50	0.36	0.36	0.36	0.36	0.36
CNP106	2.56	2.68	2.81	2.72	2.70	1.92	1.85	1.79	1.69	1.54	2.07	1.86	1.74	1.66	1.63	2.19	1.97	1.85	1.78	1.73
CNP196	4.01	4.37	3.07	2.23	1.79	2.85	3.17	2.51	2.08	1.72	2.33	2.35	2.54	2.48	2.20	1.78	1.71	1.56	1.46	1.40
mean	2.61	2.06	1.86	1.76	1.70	1.76	1.58	1.47	1.41	1.35	1.50	1.38	1.33	1.30	1.26	1.28	1.21	1.16	1.14	1.12
σ	1.28	0.92	0.78	0.73	0.74	0.77	0.74	0.68	0.66	0.64	0.69	0.66	0.67	0.66	0.63	0.68	0.67	0.67	0.67	0.67
mean + σ	3.89	2.98	2.65	2.49	2.44	2.53	2.33	2.16	2.07	1.99	2.19	2.03	2.00	1.96	1.89	1.96	1.88	1.83	1.81	1.78
COV	0.49	0.45	0.42	0.42	0.43	0.44	0.47	0.46	0.47	0.47	0.46	0.48	0.50	0.50	0.50	0.54	0.56	0.57	0.58	0.60

Table F.3. Normalized energy dissipated data from unidirectional response-history analysis using Bin 2M ground motions.

Record	NED																			
	$Q_d/W=0.03$				$Q_d/W=0.06$				$Q_d/W=0.09$				$Q_d/W=0.12$							
	T_d				T_d				T_d				T_d							
	1.5	2	2.5	3	4	1.5	2	2.5	3	4	1.5	2	2.5	3	4	1.5	2	2.5	3	4
G01000	1.71	1.56	1.47	1.42	1.36	1.44	1.37	1.34	1.32	1.29	1.79	1.56	1.43	1.29	1.16	1.33	1.03	0.90	0.82	0.75
G01090	2.21	1.35	1.40	1.43	1.29	1.55	1.32	1.30	1.35	1.51	1.45	1.31	1.25	1.23	1.21	1.56	1.46	1.41	1.39	1.38
GBZ000	1.70	1.53	1.29	1.14	0.92	1.15	1.03	0.99	0.93	0.86	0.88	0.75	0.70	0.66	0.63	0.72	0.67	0.64	0.62	0.61
GBZ270	1.67	1.32	1.19	1.14	0.94	1.07	0.96	0.92	0.90	0.87	1.19	1.11	1.07	1.04	1.02	0.87	0.88	0.88	0.88	0.89
STG000	2.58	2.77	1.60	1.46	1.15	1.80	1.44	1.26	1.05	0.96	1.70	1.39	1.14	0.98	0.83	1.25	0.88	0.80	0.75	0.68
STG090	2.62	2.23	1.88	1.45	1.02	2.41	1.81	1.63	1.48	1.31	1.85	1.64	1.61	1.59	1.57	2.13	2.07	2.02	1.99	1.96
RIO270	5.43	2.20	2.03	2.00	2.27	2.03	1.49	1.41	1.47	1.51	1.43	1.20	1.18	1.20	1.26	1.08	0.99	0.96	0.98	1.01
RIO360	2.48	2.95	2.88	2.66	2.31	1.83	1.86	2.13	2.33	2.06	1.34	1.35	1.48	1.63	1.81	1.21	1.20	1.23	1.30	1.38
JOS000	7.93	7.42	6.21	5.98	5.19	4.40	4.47	3.78	3.21	2.56	2.04	1.69	1.53	1.40	1.26	0.75	0.68	0.64	0.62	0.59
JOS090	7.96	5.21	5.58	5.31	4.26	4.48	3.80	3.48	3.23	2.71	2.93	2.70	2.56	2.29	1.97	2.09	1.68	1.43	1.31	1.02
G02000	3.67	2.23	1.64	1.62	1.75	1.85	1.60	1.38	1.32	1.29	1.38	1.26	1.09	1.01	0.92	1.33	1.18	1.10	1.02	0.95
G02090	5.59	1.90	1.47	1.34	1.51	2.94	1.55	1.32	1.14	1.06	1.80	1.26	1.24	1.34	1.32	1.36	1.21	1.05	0.99	0.94
YER270	4.29	1.94	1.68	1.62	1.60	2.11	1.27	0.93	0.79	0.71	1.16	0.81	0.67	0.60	0.52	0.64	0.56	0.50	0.47	0.44
YER360	3.49	2.50	2.17	1.98	1.83	2.18	2.31	2.28	2.24	2.12	2.49	2.29	2.21	2.17	2.13	2.08	2.04	2.02	2.01	1.96
ABN000	3.00	2.40	2.14	2.07	1.98	2.08	1.67	1.46	1.32	1.16	1.23	1.09	1.02	0.98	0.95	0.93	0.86	0.83	0.82	0.80
ABN090	1.70	1.67	1.55	1.35	1.15	1.89	1.85	1.77	1.72	1.66	1.71	1.56	1.47	1.43	1.39	1.42	1.34	1.29	1.26	1.24
BOL000	2.67	3.23	2.14	2.12	2.26	2.274	1.917	1.626	1.591	1.595	2.080	1.674	1.559	1.469	1.367	2.233	1.703	1.479	1.353	1.240
BOL090	2.78	4.31	2.81	2.47	2.38	1.96	1.66	1.54	1.45	1.33	1.53	1.12	0.94	0.87	0.84	1.23	0.86	0.68	0.61	0.56
CNP106	2.56	2.68	2.81	2.72	2.70	1.92	1.85	1.79	1.69	1.54	2.07	1.86	1.74	1.66	1.63	2.19	1.97	1.85	1.78	1.73
CNP196	4.01	4.37	3.07	2.23	1.79	2.85	3.17	2.51	2.08	1.72	2.33	2.35	2.54	2.48	2.20	1.78	1.71	1.56	1.46	1.40
mean	3.50	2.79	2.35	2.18	1.98	2.21	1.92	1.74	1.63	1.49	1.72	1.50	1.42	1.37	1.30	1.41	1.25	1.16	1.12	1.08
σ	1.90	1.52	1.34	1.28	1.08	0.89	0.90	0.77	0.68	0.54	0.50	0.50	0.53	0.51	0.47	0.52	0.48	0.46	0.45	0.45
mean + σ	5.40	4.30	3.69	3.46	3.07	3.10	2.82	2.51	2.31	2.03	2.22	2.00	1.95	1.87	1.77	1.93	1.73	1.62	1.58	1.53
COV	0.54	0.54	0.57	0.59	0.55	0.40	0.47	0.44	0.42	0.36	0.29	0.34	0.37	0.37	0.37	0.37	0.38	0.40	0.41	0.42

Table F.4. Normalized energy dissipated data from unidirectional response-history analysis using Bin 3 ground motions.

Record	NED																			
	$Q_d/W=0.03$				$Q_d/W=0.06$				$Q_d/W=0.09$				$Q_d/W=0.12$							
	T_d				T_d				T_d				T_d							
	1.5	2	2.5	3	4	1.5	2	2.5	3	4	1.5	2	2.5	3	4	1.5	2	2.5	3	4
CHY000	2.52	2.09	1.91	1.83	1.76	1.83	1.94	2.03	2.06	2.09	1.53	1.56	1.57	1.58	1.58	0.95	0.93	0.92	0.91	0.90
CHY090	4.22	3.90	3.73	3.65	3.56	2.39	2.34	2.28	2.21	2.10	2.05	2.02	2.01	2.00	1.99	2.46	2.48	2.48	2.49	2.49
29P000	5.68	5.29	4.84	4.49	4.05	2.53	2.41	2.35	2.31	2.26	2.69	2.40	2.27	2.19	2.11	1.49	1.35	1.27	1.24	1.20
29P090	4.35	4.50	4.78	5.07	5.36	3.67	3.98	3.55	3.31	3.06	2.72	2.46	2.30	2.21	2.11	1.56	1.44	1.38	1.35	1.32
MCH000	3.42	3.07	2.94	2.86	2.77	2.94	2.50	2.29	2.19	2.08	1.75	1.72	1.71	1.70	1.69	1.14	1.14	1.13	1.13	1.13
MCH090	1.39	1.28	1.24	1.22	1.10	1.54	1.48	1.40	1.35	1.31	0.90	0.88	0.87	0.87	0.87	0.55	0.55	0.54	0.54	0.54
MTW000	3.54	3.31	2.97	2.70	2.36	2.29	2.20	2.11	2.05	1.98	2.15	2.05	1.99	1.95	1.90	2.06	2.08	2.09	2.09	2.10
MTW090	4.05	3.96	3.92	3.96	4.18	3.19	3.20	3.26	3.32	3.40	2.70	2.65	2.63	2.62	2.61	1.78	1.70	1.66	1.64	1.62
GRN180	6.51	5.94	5.38	4.96	4.54	4.19	3.70	3.39	3.22	3.11	3.56	3.47	3.34	3.25	3.15	3.07	2.98	2.90	2.86	2.81
GRN270	2.84	3.49	3.56	3.59	3.61	1.50	1.37	1.31	1.28	1.25	1.58	1.51	1.48	1.47	1.47	1.62	1.59	1.57	1.56	1.55
TDO000	5.10	3.90	3.34	2.98	2.97	3.24	2.74	2.53	2.55	2.83	2.72	2.62	2.70	2.73	2.52	3.05	2.95	2.71	2.62	2.49
TDO090	4.28	3.52	3.10	2.81	2.54	2.53	2.24	2.10	2.02	1.93	1.86	1.88	1.96	2.02	2.10	1.69	1.57	1.50	1.47	1.45
PSA000	3.29	2.89	2.52	2.32	2.12	4.82	4.78	4.77	4.77	4.77	3.35	3.29	3.26	3.24	3.23	2.49	2.52	2.53	2.54	2.55
PSA090	2.55	2.32	2.19	2.07	1.99	1.32	1.13	1.04	0.97	0.89	2.72	2.48	2.24	2.10	1.97	1.54	1.46	1.42	1.40	1.38
SLC270	1.65	1.36	1.24	1.30	1.44	1.52	1.21	1.06	1.02	1.05	1.31	1.16	1.03	0.93	0.83	1.06	0.94	0.86	0.79	0.73
SLC360	2.86	2.46	2.58	2.46	1.98	2.70	2.41	2.21	2.19	1.90	1.80	1.47	1.29	1.22	1.14	0.87	0.77	0.71	0.67	0.60
CAS000	3.88	3.54	3.42	3.28	3.01	2.802	2.611	2.527	2.484	2.444	1.930	1.919	1.914	1.902	1.889	1.207	1.201	1.199	1.198	1.197
CAS270	3.55	3.29	3.18	3.11	2.71	3.02	2.73	2.60	2.48	2.26	1.77	1.65	1.59	1.56	1.54	1.24	1.23	1.23	1.22	1.22
H-VCT075	4.26	3.87	3.68	3.58	3.48	3.68	3.49	3.46	3.47	3.44	2.72	2.58	2.52	2.49	2.46	2.13	2.14	2.14	2.14	2.14
H-VCT345	2.65	2.54	2.49	2.38	2.03	1.80	1.71	1.66	1.63	1.56	1.12	1.06	1.04	1.03	1.02	1.07	1.03	1.02	1.01	1.00
mean	3.63	3.33	3.15	3.03	2.88	2.68	2.51	2.40	2.34	2.29	2.15	2.04	1.99	1.95	1.91	1.65	1.60	1.56	1.54	1.52
σ	1.26	1.16	1.10	1.08	1.10	0.95	0.96	0.94	0.93	0.94	0.72	0.70	0.69	0.69	0.68	0.70	0.71	0.69	0.69	0.69
mean + σ	4.89	4.49	4.25	4.11	3.98	3.63	3.47	3.33	3.28	3.23	2.87	2.74	2.68	2.64	2.59	2.36	2.31	2.25	2.23	2.21
COV	0.35	0.35	0.35	0.36	0.38	0.36	0.38	0.39	0.40	0.41	0.34	0.34	0.35	0.35	0.35	0.43	0.44	0.44	0.45	0.45

Table F.5. Normalized energy dissipated data from unidirectional response-history analysis using Bin 6 ground motions.

Record	NED																			
	$Q_d/W=0.03$				$Q_d/W=0.06$				$Q_d/W=0.09$				$Q_d/W=0.12$							
	T_d				T_d				T_d				T_d							
	1.5	2	2.5	3	4	1.5	2	2.5	3	4	1.5	2	2.5	3	4	1.5	2	2.5	3	4
LS01C	7.39	5.23	4.13	4.22	4.07	7.16	4.00	3.48	3.15	3.00	3.77	3.39	2.85	2.51	2.09	2.20	1.85	1.64	1.61	1.53
LS02C	4.40	8.04	3.59	5.46	1.96	3.38	5.42	2.56	3.08	1.56	2.72	3.48	1.98	1.77	1.43	2.49	2.19	1.71	1.61	1.71
LS03C	2.33	2.64	6.44	6.31	2.44	1.75	1.80	3.59	3.71	1.58	1.16	1.43	2.35	2.42	1.29	1.17	1.19	1.58	1.51	1.08
LS04C	1.99	2.90	4.53	3.67	1.88	1.35	1.86	1.93	1.76	1.38	1.25	1.42	1.28	1.27	1.09	1.25	1.32	1.15	0.97	0.83
LS05C	1.63	1.74	6.43	5.01	2.85	1.27	1.60	3.38	2.56	1.51	1.15	1.55	2.10	1.83	1.19	1.35	1.39	1.41	1.28	1.04
LS06C	3.21	3.47	5.30	2.35	1.58	2.06	2.17	2.06	1.44	1.16	1.50	1.51	1.25	1.08	1.03	1.12	1.04	0.90	0.84	0.83
LS07C	5.21	5.29	4.62	4.07	3.30	2.90	3.29	2.80	2.53	2.37	2.07	1.99	1.70	1.79	1.58	1.40	0.97	0.90	0.88	0.81
LS08C	6.67	6.36	3.94	3.17	2.93	3.96	2.85	2.34	1.95	1.66	2.44	1.82	1.60	1.53	1.54	1.57	1.59	1.62	1.70	1.44
LS09C	10.24	5.73	4.71	3.22	3.16	5.76	1.94	1.94	2.24	1.73	3.80	1.48	1.23	1.31	1.49	2.52	1.27	0.94	0.91	0.91
LS10C	10.02	8.62	7.24	3.56	3.27	4.14	5.73	4.22	2.96	2.28	3.68	3.71	2.74	2.47	1.71	3.31	2.53	1.86	1.47	1.08
LS11C	7.48	8.47	3.01	2.23	1.63	3.88	2.97	1.86	1.58	1.23	1.58	1.86	1.42	1.15	1.01	1.05	1.28	0.97	0.85	0.74
LS12C	3.56	6.12	3.69	3.52	1.54	1.85	2.53	2.27	1.81	1.13	1.69	1.55	1.65	1.34	1.01	1.27	1.25	1.33	1.12	1.05
LS13C	5.86	7.72	2.49	2.62	2.35	4.32	4.47	2.24	2.30	1.84	3.42	2.42	1.82	1.86	1.69	2.75	1.39	1.24	1.47	1.63
LS14C	3.25	6.33	3.65	2.66	2.95	3.00	3.79	3.04	2.82	2.17	2.64	1.92	1.62	1.47	1.34	1.44	1.24	1.14	1.06	0.98
LS15C	5.95	6.17	3.56	2.75	1.96	3.26	2.66	1.84	1.37	1.35	2.35	1.29	1.14	1.08	0.93	1.46	0.99	0.78	0.77	0.73
LS16C	2.19	5.21	3.45	2.69	1.42	2.19	2.39	1.96	1.57	1.48	1.42	1.45	1.29	1.21	1.06	0.99	0.82	0.68	0.58	0.50
LS17C	6.68	5.83	9.73	4.24	1.88	3.45	3.46	5.00	2.60	1.46	2.06	2.80	3.32	2.12	1.44	1.61	2.47	2.52	1.85	1.49
LS18C	6.31	5.16	2.25	2.10	2.02	3.32	3.11	2.12	1.80	2.06	2.34	2.18	1.62	1.63	1.36	1.78	1.53	1.19	0.96	0.73
LS19C	3.99	3.14	4.86	3.14	1.67	2.54	2.03	2.52	1.76	1.22	1.99	1.64	1.63	1.20	0.90	1.60	1.32	1.16	0.93	0.69
LS20C	3.26	4.51	2.80	1.77	1.49	2.30	2.28	1.84	1.36	1.22	1.80	1.54	1.35	1.11	1.09	1.43	1.39	1.30	1.17	1.11
mean	5.08	5.43	4.52	3.44	2.32	3.19	3.02	2.65	2.22	1.67	2.24	2.02	1.80	1.61	1.31	1.69	1.45	1.30	1.18	1.05
σ	2.53	1.95	1.81	1.18	0.76	1.46	1.17	0.88	0.68	0.49	0.87	0.75	0.60	0.47	0.31	0.63	0.47	0.43	0.36	0.35
mean + σ	7.61	7.39	6.33	4.61	3.08	4.65	4.19	3.53	2.90	2.16	3.11	2.77	2.40	2.08	1.62	2.32	1.92	1.73	1.54	1.39
COV	0.50	0.36	0.40	0.34	0.33	0.46	0.39	0.33	0.31	0.29	0.39	0.37	0.33	0.30	0.24	0.37	0.32	0.33	0.31	0.33

Table F.6. Normalized energy dissipated data from unidirectional response-history analysis using Bin 7 ground motions.

Record	NED																			
	$Q_d/W=0.03$				$Q_d/W=0.06$				$Q_d/W=0.09$				$Q_d/W=0.12$							
	T_d				T_d				T_d				T_d							
	1.5	2	2.5	3	4	1.5	2	2.5	3	4	1.5	2	2.5	3	4	1.5	2	2.5	3	4
SCTEW	6.09	13.75	7.09	4.83	4.28	4.04	6.46	3.48	2.91	2.62	2.68	3.46	2.55	2.11	1.80	1.95	1.80	1.52	1.22	0.99
SCTNS	7.99	9.35	6.45	5.87	5.01	3.70	3.25	3.24	2.93	2.35	0.29	0.28	0.27	0.27	0.27	0.01	0.01	0.01	0.01	0.01
MEN270	3.58	2.50	2.18	2.10	2.17	1.14	0.98	0.87	0.81	0.76	0.46	0.48	0.48	0.49	0.49	0.11	0.12	0.12	0.12	0.12
MEN360	2.10	1.83	1.77	1.55	1.34	1.01	0.79	0.68	0.64	0.58	0.51	0.47	0.46	0.45	0.44	0.24	0.24	0.24	0.24	0.24
EMV260	7.73	2.73	2.53	2.54	2.25	3.43	2.06	1.64	1.68	1.45	1.73	1.45	1.30	1.28	1.29	1.29	1.11	1.05	1.11	1.12
EMV360	5.18	3.80	3.67	3.63	3.43	1.25	0.97	0.89	0.85	0.82	0.95	0.87	0.80	0.77	0.73	0.79	0.67	0.62	0.59	0.59
OHW035	2.81	2.24	1.22	1.09	1.10	1.71	1.38	1.02	0.87	0.77	0.98	0.95	0.76	0.67	0.58	0.83	0.87	0.76	0.71	0.65
OHW305	5.78	2.82	2.62	2.59	2.30	2.84	1.95	1.76	1.30	0.94	1.17	1.07	1.01	0.89	0.76	0.79	0.74	0.72	0.69	0.62
RWC043	2.79	3.04	2.58	2.00	1.88	2.09	2.33	1.76	1.40	1.27	1.87	1.64	1.35	1.13	0.92	1.60	1.22	0.96	0.81	0.68
RWC233	3.35	2.66	2.46	2.43	2.45	2.46	1.61	1.38	1.28	1.23	1.51	1.19	1.03	0.98	0.94	0.96	0.90	0.85	0.82	0.79
SFA000	2.81	3.34	3.55	3.14	2.76	2.01	2.12	2.32	2.57	2.72	1.78	1.69	1.63	1.60	1.58	1.02	0.93	0.90	0.89	0.88
SFA090	2.72	2.28	2.02	1.77	1.54	1.67	1.58	1.38	1.23	1.10	1.29	1.12	1.01	0.94	0.88	1.06	0.88	0.83	0.81	0.77
TRI000	1.79	1.66	1.35	1.20	1.01	0.78	0.80	0.82	0.84	0.88	0.60	0.61	0.62	0.63	0.63	0.11	0.11	0.11	0.11	0.11
TRI090	2.09	1.87	1.86	1.39	0.96	1.36	1.21	0.94	0.83	0.74	0.80	0.63	0.55	0.50	0.45	0.28	0.27	0.27	0.27	0.26
ATS000	5.18	4.46	4.23	3.44	2.69	3.27	2.52	2.06	1.89	1.80	1.57	1.39	1.21	1.13	1.13	0.84	0.78	0.73	0.71	0.68
ATS090	3.30	3.68	3.19	3.40	3.75	2.63	2.98	2.96	2.76	2.47	1.85	1.58	1.43	1.32	1.16	1.08	0.99	0.92	0.87	0.81
DZC180	2.62	2.96	2.04	1.98	1.78	1.58	1.57	1.64	1.60	1.52	1.10	0.87	0.83	0.81	0.80	1.08	0.89	0.80	0.75	0.71
DZC270	1.98	3.51	2.11	1.85	1.31	1.23	1.63	1.35	1.12	1.09	1.08	1.23	1.07	1.01	0.95	1.15	1.11	1.02	0.95	0.89
YPT060	4.37	2.48	2.09	2.48	2.07	2.34	1.83	1.93	1.72	1.60	2.19	2.40	2.06	1.81	1.54	2.03	2.01	2.01	1.87	1.62
YPT330	3.63	3.09	2.97	2.97	2.18	2.79	2.25	2.05	1.99	1.61	1.91	1.91	1.84	1.64	1.35	1.68	1.53	1.26	1.12	0.96
mean	3.89	3.70	2.90	2.61	2.31	2.17	2.01	1.71	1.56	1.42	1.32	1.26	1.11	1.02	0.93	0.94	0.86	0.78	0.73	0.68
σ	1.85	2.86	1.53	1.20	1.10	0.95	1.25	0.81	0.74	0.67	0.63	0.74	0.58	0.49	0.42	0.59	0.54	0.49	0.44	0.39
mean + σ	5.75	6.57	4.43	3.81	3.41	3.12	3.26	2.52	2.30	2.08	1.95	2.01	1.69	1.51	1.35	1.54	1.40	1.27	1.18	1.06
COV	0.48	0.77	0.53	0.46	0.47	0.44	0.62	0.47	0.47	0.47	0.48	0.59	0.52	0.48	0.45	0.63	0.63	0.62	0.60	0.57

Table F.7. Normalized energy dissipated data from bi-directional response-history analysis using Bin 1 ground motions.

Ground motion pair	NED																			
	$Q_d/W=0.03$				$Q_d/W=0.06$				$Q_d/W=0.09$				$Q_d/W=0.12$							
	T_d				T_d				T_d				T_d							
	1.5	2	2.5	3	4	1.5	2	2.5	3	4	1.5	2	2.5	3	4	1.5	2	2.5	3	4
nf01/nf02	8.54	6.19	4.64	3.78	3.09	5.63	4.40	3.28	2.83	2.54	4.39	3.53	2.66	2.30	2.05	3.73	2.84	2.23	1.98	1.74
nf03/nf04	9.08	4.54	6.81	6.79	2.70	5.82	2.79	3.98	4.25	1.90	4.29	2.39	2.75	3.07	1.67	3.56	2.16	2.25	2.38	1.60
nf05/nf06	5.26	2.67	3.84	2.99	1.34	2.83	1.50	1.83	1.47	0.98	2.17	1.26	1.28	1.17	0.88	1.91	1.15	1.16	1.14	0.91
nf07/nf08	5.80	3.66	5.40	4.42	1.80	2.73	2.31	3.01	2.63	1.52	1.87	1.75	2.01	1.70	1.19	1.53	1.39	1.37	1.19	0.96
nf09/nf10	3.68	5.08	3.31	4.15	2.00	2.09	2.65	2.05	1.86	1.35	1.51	1.85	1.68	1.37	1.10	1.23	1.36	1.29	1.15	0.97
nf11/nf12	3.95	1.84	1.37	1.83	2.21	2.12	1.35	1.12	1.17	1.18	1.57	1.18	1.03	1.02	0.91	1.43	1.16	1.07	0.97	0.86
nf13/nf14	7.71	5.52	4.02	3.97	2.18	4.64	3.31	2.90	2.32	1.75	3.43	2.27	2.00	1.98	1.60	2.70	1.79	1.63	1.65	1.54
nf15/nf16	8.44	4.89	4.93	2.54	1.84	5.14	3.00	2.99	2.16	1.66	3.18	2.38	2.41	1.94	1.55	2.18	1.92	1.84	1.61	1.38
nf17/nf18	9.27	5.49	2.48	2.85	3.05	5.40	3.34	2.18	1.90	2.21	4.23	2.66	2.21	1.88	2.02	3.78	2.49	2.33	2.03	2.11
nf19/nf20	11.32	10.01	7.05	5.35	3.39	7.01	5.94	4.12	3.71	2.96	4.79	4.50	3.30	3.15	2.79	3.49	3.76	2.96	2.76	2.25
TCU065	16.58	15.40	7.42	8.52	4.29	12.62	8.38	6.44	5.18	3.42	11.71	7.65	6.43	4.14	2.86	8.39	7.08	5.04	3.56	2.61
TCU075	5.45	3.85	2.55	3.36	2.78	3.07	2.01	1.66	1.57	1.59	2.05	1.49	1.24	1.11	1.04	1.70	1.30	1.19	1.10	0.95
mean	7.92	5.76	4.49	4.21	2.56	4.93	3.41	2.96	2.59	1.92	3.77	2.74	2.42	2.07	1.64	2.97	2.37	2.03	1.79	1.49
σ	3.59	3.65	1.93	1.89	0.82	2.92	2.01	1.43	1.22	0.73	2.77	1.82	1.43	0.95	0.68	1.96	1.68	1.11	0.79	0.59
mean + σ	11.51	9.42	6.42	6.10	3.38	7.84	5.42	4.39	3.81	2.66	6.54	4.56	3.85	3.02	2.32	4.93	4.05	3.14	2.58	2.08
COV	0.45	0.63	0.43	0.45	0.32	0.59	0.59	0.48	0.47	0.38	0.74	0.66	0.59	0.46	0.42	0.66	0.71	0.55	0.44	0.40

Table F.8. Normalized energy dissipated data from bi-directional response-history analysis using Bin 2 ground motions.

Ground motion pair	NED																			
	$Q_d/W=0.03$				$Q_d/W=0.06$				$Q_d/W=0.09$				$Q_d/W=0.12$							
	T_d				T_d				T_d				T_d							
	1.5	2	2.5	3	4	1.5	2	2.5	3	4	1.5	2	2.5	3	4	1.5	2	2.5	3	4
G01	2.50	1.73	1.78	1.68	1.54	1.93	1.75	1.82	1.88	1.94	1.76	1.56	1.50	1.48	1.48	1.67	1.52	1.46	1.43	1.41
SGI	1.07	1.01	1.00	0.99	0.99	2.32	2.17	2.10	2.07	2.04	1.26	1.21	1.18	1.17	1.16	0.78	0.75	0.74	0.73	0.72
L09	4.37	4.02	3.93	3.61	3.37	2.16	2.08	2.04	2.02	1.98	2.02	2.06	2.09	2.10	2.12	1.48	1.47	1.47	1.47	1.47
WON	1.88	1.64	1.55	1.49	1.38	1.15	1.01	0.92	0.86	0.80	0.69	0.63	0.60	0.58	0.56	0.79	0.75	0.73	0.72	0.71
SFL09	3.72	3.19	2.91	2.75	2.58	3.09	2.69	2.48	2.37	2.25	3.01	2.95	2.88	2.80	2.72	3.08	3.07	3.07	3.07	3.07
G02	6.27	2.12	1.71	1.66	1.91	3.41	1.79	1.44	1.31	1.33	2.26	1.61	1.31	1.14	1.04	1.83	1.55	1.29	1.16	1.05
YER	5.76	2.88	2.67	2.70	2.30	2.93	1.77	1.33	1.17	1.11	1.87	1.27	1.01	0.89	0.77	1.13	0.90	0.79	0.72	0.65
ABN	2.77	2.64	2.33	2.16	2.01	2.88	2.26	2.07	1.99	1.93	2.42	2.18	2.05	1.96	1.85	2.39	2.14	2.01	1.93	1.84
A-E01	0.91	0.96	0.93	0.92	0.90	0.48	0.48	0.48	0.48	0.47	0.55	0.55	0.55	0.55	0.55	0.34	0.34	0.34	0.34	0.34
CNP	4.86	5.70	4.02	3.05	2.50	3.82	3.97	3.29	2.68	2.27	3.16	3.50	3.35	3.22	2.85	2.99	3.39	3.33	3.32	3.29
mean	3.41	2.59	2.28	2.10	1.95	2.42	2.00	1.80	1.68	1.61	1.90	1.75	1.65	1.59	1.51	1.65	1.59	1.52	1.49	1.46
σ	1.89	1.46	1.10	0.90	0.77	1.03	0.94	0.80	0.70	0.64	0.88	0.95	0.93	0.91	0.85	0.94	1.01	1.01	1.01	1.01
mean + σ	5.30	4.05	3.38	3.00	2.72	3.45	2.94	2.60	2.38	2.25	2.78	2.70	2.58	2.50	2.36	2.59	2.60	2.53	2.50	2.47
COV	0.55	0.56	0.48	0.43	0.40	0.43	0.47	0.45	0.41	0.40	0.46	0.54	0.56	0.57	0.56	0.57	0.64	0.66	0.68	0.70

Table F.9. Normalized energy dissipated data from bi-directional response-history analysis using Bin 2M ground motions.

Ground motion pair	NED																			
	$Q_d/W=0.03$				$Q_d/W=0.06$				$Q_d/W=0.09$				$Q_d/W=0.12$							
	T_d				T_d				T_d				T_d							
	1.5	2	2.5	3	4	1.5	2	2.5	3	4	1.5	2	2.5	3	4	1.5	2	2.5	3	4
G01	2.50	1.73	1.78	1.68	1.54	1.93	1.75	1.82	1.88	1.94	1.76	1.56	1.50	1.48	1.48	1.67	1.52	1.46	1.43	1.41
GBZ	2.76	2.27	1.66	1.40	1.09	1.62	1.47	1.38	1.32	1.21	1.16	1.03	0.95	0.90	0.85	0.90	0.81	0.77	0.74	0.72
STG	3.47	3.28	2.39	2.12	1.67	2.36	1.90	1.53	1.29	1.14	2.01	1.68	1.31	1.15	1.01	1.78	1.46	1.23	1.10	0.99
RIO	6.33	2.88	3.01	3.15	3.22	2.92	2.14	2.28	2.51	2.62	2.25	1.94	2.09	2.28	2.37	2.08	1.96	2.04	2.04	1.98
JOS	10.67	7.43	8.28	6.14	5.01	6.84	5.18	5.17	5.41	4.58	4.72	3.97	3.75	3.66	3.54	3.78	3.24	2.98	2.80	2.32
G02	6.27	2.12	1.71	1.66	1.91	3.41	1.79	1.44	1.31	1.33	2.26	1.61	1.31	1.14	1.04	1.83	1.55	1.29	1.16	1.05
YER	5.76	2.88	2.67	2.70	2.30	2.93	1.77	1.33	1.17	1.11	1.87	1.27	1.01	0.89	0.77	1.13	0.90	0.79	0.72	0.65
ABN	2.77	2.64	2.33	2.16	2.01	2.88	2.26	2.07	1.99	1.93	2.42	2.18	2.05	1.96	1.85	2.39	2.14	2.01	1.93	1.84
BOL	4.26	5.23	3.04	3.01	3.04	3.11	2.72	2.04	1.96	2.29	2.38	1.95	1.70	1.63	1.77	1.94	1.59	1.42	1.37	1.42
CNP	4.86	5.70	4.02	3.05	2.50	3.82	3.97	3.29	2.68	2.27	3.16	3.50	3.35	3.22	2.85	2.99	3.39	3.33	3.32	3.29
mean	4.97	3.62	3.09	2.71	2.43	3.18	2.50	2.24	2.15	2.04	2.40	2.07	1.90	1.83	1.75	2.05	1.86	1.73	1.66	1.57
σ	2.48	1.86	1.96	1.36	1.12	1.44	1.18	1.18	1.26	1.04	0.96	0.94	0.95	0.96	0.92	0.85	0.87	0.86	0.86	0.81
mean + σ	7.44	5.48	5.05	4.07	3.55	4.63	3.68	3.42	3.41	3.09	3.36	3.01	2.85	2.79	2.68	2.89	2.73	2.59	2.52	2.38
COV	0.50	0.52	0.64	0.50	0.46	0.45	0.47	0.53	0.58	0.51	0.40	0.46	0.50	0.53	0.53	0.41	0.47	0.50	0.52	0.52

Table F.10. Normalized energy dissipated data from bi-directional response-history analysis using Bin 3 ground motions.

Ground motion pair	NED																			
	$Q_d/W=0.03$				$Q_d/W=0.06$				$Q_d/W=0.09$				$Q_d/W=0.12$							
	T_d				T_d				T_d				T_d							
	1.5	2	2.5	3	4	1.5	2	2.5	3	4	1.5	2	2.5	3	4	1.5	2	2.5	3	4
CHY	4.15	3.46	3.18	3.01	2.81	2.25	1.92	1.77	1.69	1.60	2.29	2.01	1.88	1.82	1.76	2.04	1.94	1.89	1.86	1.82
29P	8.89	9.12	9.19	8.87	8.64	7.23	6.15	5.62	5.32	5.02	3.08	2.93	2.86	2.81	2.77	2.64	2.47	2.39	2.34	2.30
MCH	3.35	2.89	2.63	2.48	2.33	2.86	2.50	2.29	2.17	2.05	1.82	1.74	1.70	1.68	1.66	1.68	1.63	1.61	1.60	1.58
MTW	5.19	5.40	5.40	5.30	5.07	3.15	3.08	3.04	3.02	3.00	3.18	3.22	3.23	3.23	3.23	2.59	2.53	2.49	2.47	2.43
GRN	5.37	5.93	5.92	5.72	5.56	2.99	2.66	2.50	2.40	2.30	2.54	2.39	2.33	2.29	2.26	2.59	2.58	2.58	2.59	2.59
TDO	6.59	4.80	4.14	3.97	3.91	4.22	3.67	3.47	3.47	3.68	3.70	3.64	3.85	4.15	3.90	4.21	4.06	3.93	3.87	3.80
PSA	4.97	4.80	4.63	4.47	4.47	1.81	1.56	1.43	1.35	1.27	3.76	3.25	2.88	2.66	2.45	2.91	2.78	2.72	2.60	2.47
SLC	2.64	2.22	2.07	2.27	2.61	2.12	1.66	1.55	1.58	1.78	1.86	1.56	1.43	1.38	1.38	1.81	1.45	1.23	1.04	0.87
CAS	6.07	5.69	5.65	5.47	5.02	4.57	4.01	3.75	3.61	3.47	2.56	2.29	2.17	2.11	2.04	2.01	1.92	1.87	1.85	1.82
H-VCT	3.31	3.05	2.95	2.88	2.78	2.93	2.77	2.70	2.66	2.33	2.09	2.00	1.96	1.93	1.91	1.43	1.37	1.35	1.33	1.32
mean	5.05	4.74	4.58	4.44	4.32	3.41	3.00	2.81	2.73	2.65	2.69	2.50	2.43	2.41	2.34	2.39	2.27	2.21	2.15	2.10
σ	1.85	2.01	2.10	2.01	1.91	1.60	1.37	1.26	1.20	1.15	0.71	0.71	0.76	0.83	0.78	0.80	0.80	0.80	0.81	0.81
mean + σ	6.90	6.74	6.68	6.46	6.23	5.01	4.36	4.07	3.92	3.80	3.40	3.22	3.19	3.24	3.11	3.19	3.08	3.01	2.96	2.92
COV	0.37	0.42	0.46	0.45	0.44	0.47	0.46	0.45	0.44	0.43	0.26	0.29	0.31	0.34	0.33	0.33	0.35	0.36	0.37	0.39

Table F.11. Normalized energy dissipated data from bi-directional response-history analysis using Bin 6 ground motions.

Ground motion pair	NED																			
	$Q_d/W=0.03$				$Q_d/W=0.06$				$Q_d/W=0.09$				$Q_d/W=0.12$							
	T_d				T_d				T_d				T_d							
	1.5	2	2.5	3	4	1.5	2	2.5	3	4	1.5	2	2.5	3	4	1.5	2	2.5	3	4
LS01C/S02C	9.07	8.77	4.53	6.04	2.83	7.32	5.87	3.20	3.75	2.23	5.70	4.81	2.62	2.54	1.98	4.52	3.33	2.22	2.15	1.88
LS03C/LS04C	2.63	3.63	7.65	7.07	2.76	1.88	2.20	4.15	4.25	1.80	1.47	1.68	2.75	2.84	1.46	1.27	1.36	1.94	1.87	1.20
LS05C/LS06C	3.48	4.21	8.07	5.35	3.12	2.37	2.80	4.33	2.88	1.68	1.97	2.20	2.74	2.14	1.30	1.62	1.75	1.82	1.54	1.14
LS07C/LS08C	7.78	12.52	8.13	5.82	4.21	4.69	5.86	4.90	4.10	3.70	3.01	3.45	3.15	3.11	2.32	1.92	1.52	1.35	1.43	1.40
LS09C/LS10C	15.25	13.63	8.09	4.68	4.51	7.36	6.98	6.55	4.58	3.00	4.82	3.73	2.87	2.72	2.36	3.47	2.40	1.78	1.66	1.59
LS11C/LS12C	9.70	11.53	4.87	3.77	2.36	4.24	4.48	2.79	2.03	1.65	2.42	2.53	2.22	1.58	1.36	1.82	1.90	1.75	1.36	1.17
LS13C/LS14C	6.72	10.05	4.49	3.68	2.70	4.70	5.90	3.18	2.98	2.23	3.87	3.63	2.52	2.50	2.00	3.15	2.19	1.90	2.01	1.79
LS15C/LS16C	6.47	9.00	5.76	4.56	2.35	3.75	4.81	3.69	2.72	1.92	2.79	2.75	2.67	2.25	1.67	2.02	1.84	1.61	1.52	1.35
LS17C/LS18C	9.11	7.52	9.99	4.36	2.02	5.21	4.62	5.23	2.71	1.58	4.10	3.65	3.56	2.23	1.55	3.05	3.16	2.78	2.00	1.60
LS19C/LS20C	4.86	4.91	5.06	3.04	1.78	3.00	2.83	2.99	1.97	1.42	2.39	2.10	2.21	1.52	1.19	1.98	1.67	1.59	1.22	0.92
mean	7.51	8.58	6.66	4.84	2.86	4.45	4.63	4.10	3.20	2.12	3.25	3.05	2.73	2.34	1.72	2.48	2.11	1.87	1.68	1.40
σ	3.63	3.50	1.94	1.23	0.88	1.85	1.59	1.19	0.92	0.72	1.34	0.96	0.40	0.51	0.42	1.02	0.67	0.39	0.31	0.31
mean + σ	11.14	12.08	8.61	6.07	3.75	6.31	6.22	5.29	4.12	2.84	4.59	4.01	3.14	2.86	2.14	3.50	2.78	2.27	1.99	1.71
COV	0.48	0.41	0.29	0.26	0.31	0.42	0.34	0.29	0.29	0.34	0.41	0.31	0.15	0.22	0.25	0.41	0.32	0.21	0.19	0.22

Table F.12. Normalized energy dissipated data from bi-directional response-history analysis using Bin 7 ground motions.

Ground motion pair	NED																			
	$Q_d/W=0.03$				$Q_d/W=0.06$				$Q_d/W=0.09$				$Q_d/W=0.12$							
	T_d				T_d				T_d				T_d							
	1.5	2	2.5	3	4	1.5	2	2.5	3	4	1.5	2	2.5	3	4	1.5	2	2.5	3	4
SCT	9.21	17.76	9.21	6.68	7.06	5.49	7.87	4.73	4.10	3.94	3.50	3.86	2.92	2.52	2.51	2.14	2.23	1.85	1.81	1.67
MEN	3.92	3.04	2.78	3.03	2.74	2.73	2.61	2.35	2.20	2.07	1.04	0.87	0.80	0.76	0.73	0.58	0.59	0.59	0.59	0.59
EMV	9.35	4.10	4.14	4.02	3.78	5.08	2.85	2.32	2.03	1.83	2.23	1.68	1.52	1.30	1.12	1.42	1.25	1.21	1.06	0.97
OHW	6.77	3.19	2.01	1.74	2.10	3.65	2.32	1.61	1.47	1.47	2.37	1.62	1.30	1.19	1.08	1.68	1.14	0.96	0.89	0.84
RWC	4.65	4.57	3.53	2.69	2.46	3.12	3.06	2.35	1.85	1.58	2.60	2.12	1.72	1.40	1.16	2.03	1.59	1.20	1.01	0.83
SFA	4.72	3.79	3.23	2.83	2.59	2.65	2.61	2.37	2.16	1.97	1.82	1.78	1.85	1.71	1.57	1.19	1.11	1.11	1.14	1.18
TRI	2.52	2.16	2.14	1.61	1.11	1.48	1.48	1.12	0.94	0.81	0.99	0.78	0.66	0.59	0.51	0.40	0.35	0.31	0.30	0.29
ATS	4.40	5.13	5.25	5.84	5.12	3.30	3.91	3.73	3.68	3.39	3.18	3.33	3.21	3.01	2.53	2.59	2.56	2.37	2.26	2.16
DZC	2.83	4.78	3.20	3.20	2.35	1.81	2.56	2.14	1.92	2.01	1.36	1.58	1.31	1.23	1.24	1.23	1.37	1.25	1.17	1.11
YPT	4.54	4.13	3.07	4.22	3.07	3.65	2.92	2.67	2.39	1.92	3.02	2.38	2.15	2.05	1.86	2.50	2.10	1.82	1.64	1.39
mean	5.29	5.26	3.86	3.59	3.24	3.30	3.22	2.54	2.27	2.10	2.21	2.00	1.74	1.58	1.43	1.58	1.43	1.27	1.19	1.10
σ	2.40	4.48	2.10	1.64	1.71	1.27	1.74	1.02	0.95	0.91	0.89	0.98	0.83	0.76	0.69	0.75	0.71	0.61	0.58	0.54
mean + σ	7.69	9.75	5.96	5.23	4.95	4.57	4.96	3.56	3.22	3.01	3.10	2.98	2.58	2.34	2.12	2.33	2.14	1.88	1.77	1.64
COV	0.45	0.85	0.55	0.46	0.53	0.39	0.54	0.40	0.42	0.44	0.40	0.49	0.48	0.48	0.48	0.48	0.50	0.48	0.49	0.49

Table F.13. Normalized rate-of-energy dissipated data calculated using Definition 1 and the results of unidirectional response-history analysis performed with Bin 1 ground motions.

Record	R_E^{90} / T_d (kN-m / second / second)																			
	$Q_d/W=0.03$				$Q_d/W=0.06$				$Q_d/W=0.09$				$Q_d/W=0.12$							
	T_d				T_d				T_d				T_d							
	1.5	2	2.5	3	4	1.5	2	2.5	3	4	1.5	2	2.5	3	4	1.5	2	2.5	3	4
nf01	14.6	24.4	11.4	8.4	6.1	19.9	20.9	13.3	10.1	7.6	27.2	22.8	16.1	12.7	9.8	28.8	22.6	17.1	13.4	9.8
nf02	9.8	8.0	7.2	7.5	10.2	12.7	9.6	8.1	8.0	9.1	15.7	11.3	10.0	9.5	8.0	16.7	13.1	10.9	9.6	7.6
nf03	95.6	40.9	49.2	57.7	22.3	153.3	73.7	66.8	71.2	43.3	185.8	94.2	76.7	76.4	59.7	203.9	108.8	88.2	83.7	63.4
nf04	59.2	27.5	19.3	25.1	11.0	93.1	39.9	24.9	26.5	14.4	95.9	40.9	26.4	23.9	13.5	74.4	49.0	29.9	24.0	16.2
nf05	59.3	33.9	24.7	19.2	11.2	113.2	63.7	37.7	28.8	20.3	174.2	88.1	53.3	47.2	26.9	238.4	117.1	89.0	64.7	43.4
nf06	11.7	6.1	4.7	3.6	2.3	13.4	8.0	5.7	4.3	2.9	10.9	7.2	5.3	4.3	3.0	9.3	6.4	4.8	3.9	2.8
nf07	33.9	26.5	32.7	20.8	4.8	19.6	19.0	44.4	31.1	7.1	16.5	32.9	46.1	37.9	15.9	50.2	51.0	45.7	40.0	23.1
nf08	7.2	6.1	6.9	8.9	3.1	9.6	7.0	5.9	5.3	3.3	11.6	7.9	6.5	5.4	3.8	26.8	8.9	12.1	9.9	4.2
nf09	25.9	32.9	24.0	15.5	10.1	51.5	47.3	37.9	28.8	18.7	77.5	54.2	44.8	35.0	22.7	82.7	69.4	48.2	36.8	25.6
nf10	13.2	11.3	9.0	8.3	4.2	16.1	15.6	11.8	9.4	5.5	19.3	14.1	14.9	10.0	5.5	18.6	11.4	7.4	5.4	3.5
nf11	9.8	6.5	6.7	10.5	12.2	8.5	8.3	8.2	9.7	11.3	8.1	7.5	7.4	7.5	6.0	7.3	6.8	6.1	5.4	4.2
nf12	6.1	2.3	1.6	1.3	0.9	4.4	2.9	2.3	1.9	1.4	4.3	3.2	2.6	2.1	1.6	4.6	3.5	2.8	2.3	1.7
nf13	71.5	34.3	15.5	8.7	5.9	121.0	43.2	26.5	17.6	10.1	153.7	57.2	30.9	22.4	14.1	162.6	66.5	38.7	29.0	17.3
nf14	8.9	13.7	15.3	10.9	4.5	11.9	12.6	12.4	8.9	4.8	12.6	11.3	9.4	7.7	5.3	12.5	9.9	8.2	6.8	5.0
nf15	52.8	31.6	33.8	22.2	9.8	73.7	46.8	48.8	36.5	20.0	65.9	50.4	49.1	37.9	20.7	54.4	53.4	36.8	27.8	16.6
nf16	23.1	15.9	6.1	4.2	2.7	31.5	21.7	11.5	8.2	5.5	34.9	21.6	14.5	10.9	7.6	32.2	22.0	16.6	13.0	9.0
nf17	83.0	39.5	17.2	16.9	11.2	156.5	64.4	28.1	21.6	16.6	216.9	88.7	55.8	40.7	25.0	277.5	127.3	70.1	52.4	35.5
nf18	36.1	10.7	6.9	6.0	4.1	62.3	19.7	12.7	9.8	6.8	68.8	26.4	17.9	13.9	9.7	59.1	32.2	22.7	16.6	11.8
nf19	95.2	92.8	42.8	17.1	9.4	156.3	152.9	79.9	36.8	19.5	182.7	181.1	108.2	49.0	26.4	187.9	196.4	116.3	63.8	33.0
nf20	35.1	22.5	12.3	12.2	5.6	48.3	31.0	19.8	14.4	8.7	47.8	27.5	17.9	13.2	8.4	40.7	22.0	15.3	11.6	8.0
TCU065W	32.9	43.7	11.9	11.2	16.9	39.1	31.7	17.5	15.0	14.3	35.2	21.7	15.5	14.9	10.1	23.1	15.3	12.5	10.7	7.7
TCU065N	28.3	28.0	13.3	9.7	5.1	33.3	24.1	16.6	10.9	6.8	26.9	19.4	12.4	9.2	6.3	17.8	12.6	8.7	6.8	4.8
TCU075W	4.6	5.7	4.1	6.6	7.1	5.0	5.0	4.7	4.4	4.3	3.9	3.8	3.3	2.9	2.5	3.3	2.9	2.7	2.2	1.6
TCU075N	1.6	1.3	1.1	0.9	0.7	1.4	1.1	0.8	0.7	0.5	0.9	0.6	0.5	0.4	0.3	0.6	0.4	0.3	0.3	0.2
mean	34.1	23.6	15.7	13.1	7.6	52.3	32.1	22.8	17.5	10.9	62.4	37.3	26.9	20.6	13.0	68.1	42.9	29.6	22.5	14.8
σ	29.3	19.8	12.9	11.5	5.1	52.1	33.0	20.5	15.8	9.2	68.3	41.4	26.7	19.1	12.8	81.7	49.7	31.8	23.1	15.6
mean + σ	63.4	43.4	28.6	24.6	12.7	104.5	65.1	43.3	33.3	20.1	130.7	78.7	53.6	39.7	25.8	149.7	92.6	61.4	45.6	30.5
COV	0.86	0.84	0.82	0.88	0.68	1.00	1.03	0.90	0.90	0.84	1.10	1.11	0.99	0.93	0.98	1.20	1.16	1.07	1.03	1.05

Table F.14. Normalized rate-of-energy dissipated data calculated using Definition 1 and the results of unidirectional response-history analysis performed with Bin 2 ground motions.

Record	R_E^{90} / T_d (kN-m / second / second)																			
	$Q_d/W=0.03$				$Q_d/W=0.06$				$Q_d/W=0.09$				$Q_d/W=0.12$							
	T_d				T_d				T_d				T_d							
	1.5	2	2.5	3	4	1.5	2	2.5	3	4	1.5	2	2.5	3	4	1.5	2	2.5	3	4
G01000	1.32	0.99	0.79	0.65	0.48	2.74	2.08	1.66	1.38	1.02	3.57	2.68	2.15	1.80	1.35	3.85	2.87	2.29	1.92	1.45
G01090	9.50	3.62	2.21	1.62	1.17	9.88	6.67	5.01	3.56	2.59	13.46	9.43	7.34	6.04	4.46	17.58	12.03	9.36	7.70	5.71
SGI270	0.028	0.022	0.018	0.015	0.011	0.014	0.011	0.009	0.007	0.005	0.012	0.009	0.007	0.006	0.005	0.009	0.007	0.005	0.005	0.003
SGI360	0.146	0.108	0.083	0.068	0.050	0.031	0.024	0.019	0.016	0.012	0.019	0.014	0.011	0.009	0.007	0.018	0.014	0.011	0.009	0.007
L09000	0.34	0.25	0.20	0.16	0.12	0.37	0.28	0.22	0.19	0.14	0.54	0.41	0.32	0.27	0.20	0.61	0.46	0.36	0.30	0.23
L09090	0.41	0.30	0.24	0.20	0.15	0.94	0.69	0.55	0.45	0.31	0.80	0.60	0.47	0.39	0.29	0.80	0.59	0.47	0.39	0.29
WON095	0.49	0.34	0.25	0.21	0.16	0.38	0.29	0.23	0.19	0.14	0.33	0.25	0.20	0.17	0.13	0.25	0.18	0.15	0.12	0.09
WON185	1.36	0.87	0.66	0.54	0.40	0.95	0.69	0.55	0.45	0.34	0.67	0.52	0.42	0.35	0.27	0.28	0.21	0.17	0.14	0.11
SFL09021	0.20	0.15	0.12	0.10	0.07	0.22	0.17	0.13	0.11	0.08	0.18	0.14	0.11	0.09	0.07	0.10	0.07	0.06	0.05	0.04
SFL09291	0.11	0.08	0.07	0.05	0.04	0.12	0.09	0.07	0.06	0.04	0.13	0.10	0.08	0.07	0.05	0.15	0.11	0.09	0.07	0.05
G02000	6.15	2.29	1.42	1.12	0.81	6.02	4.29	3.13	2.52	1.82	14.87	10.71	7.54	5.21	3.78	16.31	11.54	8.89	7.28	5.40
G02090	35.43	11.48	4.46	2.86	1.93	40.30	20.29	9.37	6.09	3.89	25.56	15.81	10.87	7.47	5.27	15.44	10.53	7.82	6.30	4.58
YER270	3.79	1.71	1.17	0.92	0.69	1.27	0.75	0.58	0.46	0.33	0.61	0.46	0.37	0.31	0.23	0.39	0.29	0.24	0.20	0.15
YER360	16.41	3.39	1.91	1.54	1.31	12.23	4.80	3.25	2.62	2.05	8.07	5.67	3.84	2.68	1.72	4.09	2.90	2.21	2.01	1.57
ABN000	1.14	0.84	0.67	0.55	0.40	1.29	0.95	0.74	0.61	0.44	0.74	0.55	0.44	0.37	0.27	0.58	0.44	0.35	0.30	0.22
ABN090	1.30	1.09	0.85	0.67	0.44	0.85	0.60	0.47	0.39	0.29	0.71	0.53	0.42	0.35	0.26	0.64	0.48	0.38	0.32	0.24
A-E01140	0.76	0.56	0.44	0.37	0.27	0.015	0.011	0.009	0.008	0.006	0.007	0.006	0.004	0.004	0.003	0.004	0.003	0.002	0.002	0.002
A-E01230	0.01	0.01	0.01	0.01	0.00	0.01	0.01	0.01	0.01	0.00	0.02	0.01	0.01	0.01	0.01	0.02	0.02	0.01	0.01	0.01
CNP106	3.39	3.11	2.63	1.93	1.24	6.36	5.06	4.00	3.21	2.30	7.88	5.41	4.28	3.52	2.59	7.76	5.81	4.58	3.78	2.81
CNP196	19.88	16.88	8.59	4.45	2.53	17.27	13.22	9.82	6.64	4.31	15.49	10.74	8.28	6.69	4.91	12.42	8.71	6.68	5.47	4.14
mean	5.11	2.40	1.34	0.90	0.61	5.06	3.05	1.99	1.45	1.01	4.68	3.20	2.36	1.79	1.29	4.06	2.86	2.21	1.82	1.35
σ	9.06	4.28	2.04	1.13	0.70	9.59	5.23	3.00	2.03	1.35	7.25	4.78	3.44	2.55	1.84	6.20	4.31	3.30	2.70	2.00
mean + σ	14.17	6.68	3.38	2.03	1.31	14.65	8.28	4.99	3.48	2.36	11.94	7.98	5.80	4.34	3.13	10.27	7.17	5.51	4.52	3.35
COV	1.77	1.78	1.52	1.25	1.14	1.89	1.71	1.51	1.40	1.34	1.55	1.49	1.46	1.42	1.42	1.53	1.50	1.50	1.48	1.48

Table F.15. Normalized rate-of-energy dissipated data calculated using Definition 1 and the results of unidirectional response-history analysis performed with Bin 2M ground motions.

Record	R_E^{90} / T_d (kN-m / second / second)																			
	$Q_d/W=0.03$				$Q_d/W=0.06$				$Q_d/W=0.09$				$Q_d/W=0.12$							
	T_d				T_d				T_d				T_d							
	1.5	2	2.5	3	4	1.5	2	2.5	3	4	1.5	2	2.5	3	4	1.5	2	2.5	3	4
G01000	1.33	0.99	0.79	0.65	0.48	2.70	2.04	1.63	1.36	1.00	3.50	2.63	2.11	1.76	1.32	3.80	2.83	2.26	1.89	1.42
G01090	8.77	3.56	2.18	1.60	1.15	9.87	6.61	4.92	3.55	2.56	13.43	9.49	7.37	6.06	4.50	17.58	12.01	9.39	7.71	5.71
GBZ000	2.34	2.05	2.13	2.10	1.87	3.88	3.05	2.59	2.19	1.61	3.34	2.35	1.85	1.52	1.12	2.15	1.57	1.24	1.02	0.76
GBZ270	1.49	1.15	0.96	0.77	0.58	1.29	0.95	0.77	0.64	0.48	1.09	0.82	0.65	0.54	0.40	0.45	0.34	0.27	0.23	0.17
STG000	11.86	10.14	3.64	2.66	1.64	20.98	12.49	7.52	5.26	3.69	15.59	11.20	7.73	5.71	3.38	8.41	5.02	4.10	3.44	2.60
STG090	5.42	2.67	2.69	2.85	2.18	5.32	3.73	2.85	2.47	1.93	3.84	2.81	2.27	1.88	1.40	3.77	2.80	2.23	1.85	1.39
RIO270	15.35	2.71	1.73	1.27	0.90	14.86	6.34	3.78	2.97	1.84	15.21	9.20	6.44	5.18	3.79	10.45	7.34	5.82	4.91	3.66
RIO360	2.73	1.32	0.95	0.76	0.55	6.51	3.81	2.81	2.22	1.62	14.37	9.87	7.70	6.32	4.69	24.57	17.64	13.72	11.27	8.35
JOS000	4.84	2.56	1.71	1.32	0.91	3.67	2.32	1.72	1.37	0.99	1.82	1.26	0.98	0.79	0.58	0.59	0.42	0.33	0.27	0.19
JOS090	8.71	4.20	2.82	2.24	1.46	5.84	3.78	2.86	2.28	1.64	3.99	2.76	2.11	1.70	1.21	2.20	1.51	1.15	0.94	0.70
G02000	6.20	2.29	1.43	1.13	0.81	6.06	4.31	3.12	2.50	1.80	14.19	10.30	6.79	5.14	3.74	15.85	11.23	8.63	7.08	5.27
G02090	32.29	11.53	4.48	2.85	1.89	37.83	20.17	9.31	6.09	3.86	26.49	15.72	10.58	7.43	5.22	15.47	10.39	7.92	6.31	4.53
YER270	16.25	3.34	1.92	1.53	1.30	12.26	4.80	3.22	2.58	2.03	8.10	5.67	3.81	2.65	1.71	4.10	2.80	2.18	1.97	1.56
YER360	3.75	1.72	1.17	0.91	0.69	1.28	0.75	0.58	0.46	0.33	0.61	0.46	0.37	0.31	0.23	0.38	0.29	0.24	0.20	0.15
ABN000	1.15	0.83	0.66	0.55	0.40	1.29	0.95	0.74	0.61	0.44	0.74	0.55	0.44	0.36	0.27	0.57	0.43	0.35	0.29	0.22
ABN090	1.30	1.09	0.85	0.67	0.44	0.85	0.60	0.47	0.39	0.29	0.71	0.53	0.42	0.35	0.26	0.64	0.48	0.38	0.32	0.24
BOL000	7.2	8.5	5.4	3.8	2.3	11.9	8.5	6.7	5.3	3.8	13.4	10.7	8.7	7.1	5.2	24.3	14.5	11.6	11.0	7.4
BOL090	13.2	11.1	4.4	2.9	1.7	51.2	17.3	10.2	7.0	3.8	66.9	31.1	18.9	13.3	8.6	79.1	37.6	37.8	28.4	13.6
CNP106	3.43	3.08	2.63	1.92	1.23	6.34	5.09	4.02	3.21	2.30	7.86	5.42	4.27	3.51	2.59	7.76	5.80	4.57	3.77	2.79
CNP196	18.11	15.34	8.56	4.42	2.52	17.04	12.98	9.58	6.64	4.29	15.16	10.54	8.15	6.62	4.84	12.36	8.66	6.65	5.43	4.11
mean	8.28	4.51	2.56	1.85	1.25	11.05	6.03	3.97	2.96	2.01	11.52	7.17	5.08	3.91	2.75	11.73	7.19	6.04	4.91	3.24
σ	7.79	4.29	1.96	1.11	0.66	12.93	5.58	3.10	2.08	1.28	14.85	7.28	4.63	3.37	2.27	17.71	8.89	8.53	6.54	3.50
mean + σ	16.08	8.80	4.51	2.96	1.91	23.97	11.61	7.07	5.03	3.30	26.36	14.45	9.71	7.28	5.02	29.43	16.07	14.57	11.46	6.74
COV	0.94	0.95	0.76	0.60	0.53	1.17	0.93	0.78	0.70	0.64	1.29	1.02	0.91	0.86	0.83	1.51	1.24	1.41	1.33	1.08

Table F.16. Normalized rate-of-energy dissipated data calculated using Definition 1 and the results of unidirectional response-history analysis performed with Bin 3 ground motions.

Record	R_E^{90} / T_d (kN-m / second / second)																			
	$Q_d/W=0.03$				$Q_d/W=0.06$				$Q_d/W=0.09$				$Q_d/W=0.12$							
	T_d				T_d				T_d				T_d							
	1.5	2	2.5	3	4	1.5	2	2.5	3	4	1.5	2	2.5	3	4	1.5	2	2.5	3	4
CHY000	2.52	2.09	1.91	1.83	1.76	1.83	1.94	2.03	2.06	2.09	1.53	1.56	1.57	1.58	1.58	0.95	0.93	0.92	0.91	0.90
CHY090	4.22	3.90	3.73	3.65	3.56	2.39	2.34	2.28	2.21	2.10	2.05	2.02	2.01	2.00	1.99	2.46	2.48	2.48	2.49	2.49
29P000	5.68	5.29	4.84	4.49	4.05	2.53	2.41	2.35	2.31	2.26	2.69	2.40	2.27	2.19	2.11	1.49	1.35	1.27	1.24	1.20
29P090	4.35	4.50	4.78	5.07	5.36	3.67	3.98	3.55	3.31	3.06	2.72	2.46	2.30	2.21	2.11	1.56	1.44	1.38	1.35	1.32
MCH000	3.42	3.07	2.94	2.86	2.77	2.94	2.50	2.29	2.19	2.08	1.75	1.72	1.71	1.70	1.69	1.14	1.14	1.13	1.13	1.13
MCH090	1.39	1.28	1.24	1.22	1.10	1.54	1.48	1.40	1.35	1.31	0.90	0.88	0.87	0.87	0.87	0.55	0.55	0.54	0.54	0.54
MTW000	3.54	3.31	2.97	2.70	2.36	2.29	2.20	2.11	2.05	1.98	2.15	2.05	1.99	1.95	1.90	2.06	2.08	2.09	2.09	2.10
MTW090	4.05	3.96	3.92	3.96	4.18	3.19	3.20	3.26	3.32	3.40	2.70	2.65	2.63	2.62	2.61	1.78	1.70	1.66	1.64	1.62
GRN180	6.51	5.94	5.38	4.96	4.54	4.19	3.70	3.39	3.22	3.11	3.56	3.47	3.34	3.25	3.15	3.07	2.98	2.90	2.86	2.81
GRN270	2.84	3.49	3.56	3.59	3.61	1.50	1.37	1.31	1.28	1.25	1.58	1.51	1.48	1.47	1.47	1.62	1.59	1.57	1.56	1.55
TDO000	5.10	3.90	3.34	2.98	2.97	3.24	2.74	2.53	2.55	2.83	2.72	2.62	2.70	2.73	2.52	3.05	2.95	2.71	2.62	2.49
TDO090	4.28	3.52	3.10	2.81	2.54	2.53	2.24	2.10	2.02	1.93	1.86	1.88	1.96	2.02	2.10	1.69	1.57	1.50	1.47	1.45
PSA000	3.29	2.89	2.52	2.32	2.12	4.82	4.78	4.77	4.77	4.77	3.35	3.29	3.26	3.24	3.23	2.49	2.52	2.53	2.54	2.55
PSA090	2.55	2.32	2.19	2.07	1.99	1.32	1.13	1.04	0.97	0.89	2.72	2.48	2.24	2.10	1.97	1.54	1.46	1.42	1.40	1.38
SLC270	1.65	1.36	1.24	1.30	1.44	1.52	1.21	1.06	1.02	1.05	1.31	1.16	1.03	0.93	0.83	1.06	0.94	0.86	0.79	0.73
SLC360	2.86	2.46	2.58	2.46	1.98	2.70	2.41	2.21	2.19	1.90	1.80	1.47	1.29	1.22	1.14	0.87	0.77	0.71	0.67	0.60
CAS000	3.88	3.54	3.42	3.28	3.01	2.802	2.611	2.527	2.484	2.444	1.930	1.919	1.914	1.902	1.889	1.207	1.201	1.199	1.198	1.197
CAS270	3.55	3.29	3.18	3.11	2.71	3.02	2.73	2.60	2.48	2.26	1.77	1.65	1.59	1.56	1.54	1.24	1.23	1.23	1.22	1.22
H-VCT075	4.26	3.87	3.68	3.58	3.48	3.68	3.49	3.46	3.47	3.44	2.72	2.58	2.52	2.49	2.46	2.13	2.14	2.14	2.14	2.14
H-VCT345	2.65	2.54	2.49	2.38	2.03	1.80	1.71	1.66	1.63	1.56	1.12	1.06	1.04	1.03	1.02	1.07	1.03	1.02	1.01	1.00
mean	3.63	3.33	3.15	3.03	2.88	2.68	2.51	2.40	2.34	2.29	2.15	2.04	1.99	1.95	1.91	1.65	1.60	1.56	1.54	1.52
σ	1.26	1.16	1.10	1.08	1.10	0.95	0.96	0.94	0.93	0.94	0.72	0.70	0.69	0.69	0.68	0.70	0.71	0.69	0.69	0.69
mean + σ	4.89	4.49	4.25	4.11	3.98	3.63	3.47	3.33	3.28	3.23	2.87	2.74	2.68	2.64	2.59	2.36	2.31	2.25	2.23	2.21
COV	0.35	0.35	0.35	0.36	0.38	0.36	0.38	0.39	0.40	0.41	0.34	0.34	0.35	0.35	0.35	0.43	0.44	0.44	0.45	0.45

Table F.17. Normalized rate-of-energy dissipated data calculated using Definition 1 and the results of unidirectional response-history analysis performed with Bin 6 ground motions.

Record	R_E^{90} / T_d (kN-m / second / second)																			
	$Q_d/W=0.03$				$Q_d/W=0.06$				$Q_d/W=0.09$				$Q_d/W=0.12$							
	T_d				T_d				T_d				T_d							
	1.5	2	2.5	3	4	1.5	2	2.5	3	4	1.5	2	2.5	3	4	1.5	2	2.5	3	4
LS01C	22.9	16.1	8.0	4.8	2.9	22.7	13.3	7.5	5.4	3.6	17.1	9.6	6.4	4.8	3.3	10.2	6.7	4.7	3.7	2.5
LS02C	10.6	61.6	40.4	37.9	9.9	30.7	102.4	60.2	48.0	16.9	37.1	93.8	83.9	44.3	18.8	37.4	77.6	56.4	30.4	16.8
LS03C	7.3	17.0	50.1	55.8	25.9	15.4	31.2	68.4	84.5	45.9	23.5	44.4	76.4	80.3	56.4	37.5	65.9	80.3	78.1	55.9
LS04C	9.7	17.6	25.1	19.0	6.1	10.5	24.1	23.6	21.2	11.6	17.0	21.2	19.4	14.9	10.8	22.4	18.0	12.8	10.6	8.0
LS05C	9.2	15.3	46.8	40.7	21.5	22.5	35.8	63.9	63.5	37.1	26.3	42.7	61.0	63.0	46.2	35.2	48.3	54.1	50.7	39.2
LS06C	18.3	28.4	31.6	22.2	9.0	31.0	40.6	31.9	28.2	17.7	37.7	39.3	34.5	28.4	19.6	44.1	39.8	22.7	18.6	14.6
LS07C	21.3	20.0	12.7	14.2	9.6	16.8	18.6	12.2	10.1	7.1	15.3	11.7	8.0	6.7	4.8	37.9	7.7	5.8	4.1	3.1
LS08C	10.6	13.1	8.3	6.2	3.7	8.3	6.7	5.5	4.2	2.7	4.0	2.9	2.2	1.7	1.2	1.3	0.9	0.7	0.6	0.4
LS09C	74.6	13.9	8.3	5.8	10.5	133.4	14.3	9.8	8.7	10.7	127.0	33.3	20.9	18.5	16.5	132.6	35.1	21.9	18.3	14.4
LS10C	47.1	26.9	26.1	11.3	4.8	33.4	35.9	20.9	13.4	6.9	28.1	25.6	15.2	10.6	6.6	16.4	11.7	8.3	6.2	4.3
LS11C	45.6	41.7	17.2	9.6	4.9	50.4	44.4	30.4	18.8	10.5	38.6	60.9	35.4	23.0	13.9	52.3	59.0	43.2	33.7	22.5
LS12C	12.2	34.8	33.8	20.1	4.1	37.8	51.4	53.5	35.8	21.9	51.1	57.2	51.5	40.3	26.3	44.9	45.8	42.4	36.8	22.0
LS13C	63.8	47.7	20.2	13.9	11.2	112.7	60.4	31.9	23.1	15.2	126.5	51.3	37.6	28.8	21.5	123.2	47.7	33.9	29.5	22.3
LS14C	11.4	24.2	14.4	8.5	3.8	19.9	16.2	12.7	9.7	5.9	15.9	10.2	8.1	6.4	4.6	10.7	7.8	6.9	5.0	3.4
LS15C	49.9	37.2	19.1	11.1	8.9	97.4	45.4	31.4	20.5	13.5	98.4	48.2	36.8	26.8	16.2	103.5	54.9	36.8	28.4	17.9
LS16C	11.6	27.2	24.8	18.3	8.5	22.2	34.3	31.8	25.0	14.7	26.2	23.0	18.9	15.6	10.8	14.7	11.0	8.4	7.0	6.0
LS17C	58.5	54.5	80.5	42.9	16.8	88.6	102.2	132.4	86.6	42.9	90.0	125.8	155.6	112.7	59.4	81.7	131.4	156.5	118.4	69.8
LS18C	46.7	35.7	14.2	7.3	4.4	63.2	54.0	25.4	15.9	9.5	62.6	46.1	28.7	20.4	13.1	50.1	37.9	25.7	18.9	12.9
LS19C	41.0	31.5	27.1	15.9	4.9	78.9	55.4	38.2	23.3	10.6	69.3	51.9	40.0	29.3	12.4	82.7	64.9	49.4	32.8	17.5
LS20C	20.5	29.9	21.3	8.2	3.3	25.3	31.5	19.8	11.3	5.6	20.7	17.1	13.4	8.9	5.1	30.8	18.7	9.6	11.6	7.8
mean	29.6	29.7	26.5	18.7	8.7	46.0	40.9	35.6	27.9	15.5	46.6	40.8	37.7	29.3	18.4	48.5	39.5	34.0	27.2	18.1
σ	21.4	13.7	17.6	14.4	6.2	36.9	25.9	29.4	24.4	12.5	37.2	29.7	35.9	27.9	16.8	37.6	31.7	36.0	28.6	18.1
mean + σ	51.1	43.5	44.1	33.1	15.0	82.9	66.8	65.0	52.3	28.0	83.8	70.5	73.5	57.2	35.2	86.1	71.3	70.0	55.8	36.1
COV	0.72	0.46	0.66	0.77	0.71	0.80	0.63	0.83	0.88	0.80	0.80	0.73	0.95	0.95	0.92	0.78	0.80	1.06	1.05	1.00

Table F.18. Normalized rate-of-energy dissipated data calculated using Definition 1 and the results of unidirectional response-history analysis performed with Bin 7 ground motions.

Record	$Q_d/W=0.03$												R_E^{90} / T_d (kN-m / second / second)												$Q_d/W=0.12$											
	T_d												$Q_d/W=0.09$												T_d											
	1.5	2	2.5	3	4	1.5	2	2.5	3	4	1.5	2	2.5	3	4	1.5	2	2.5	3	4																
SCTEW	8.78	95.05	30.55	13.95	4.81	12.99	56.70	38.89	14.22	6.34	17.00	51.89	31.07	12.99	6.68	23.28	17.88	10.60	7.13	4.39																
SCTNS	4.27	23.50	8.74	4.13	1.83	3.20	3.19	2.14	1.41	0.85	0.02	0.01	0.01	0.01	0.01	0.00	0.00	0.00	0.00	0.00																
MEN270	1.77	1.25	0.96	0.78	0.55	1.44	0.86	0.67	0.56	0.41	0.06	0.05	0.04	0.03	0.02	0.01	0.01	0.00	0.00	0.00																
MEN360	2.68	1.65	1.26	1.03	0.73	1.06	0.71	0.55	0.47	0.33	0.27	0.20	0.16	0.14	0.10	0.01	0.01	0.01	0.01	0.01																
EMV260	41.40	8.37	4.04	2.85	1.89	40.30	19.01	10.58	6.83	4.56	29.37	21.70	15.20	11.50	7.85	17.57	11.54	8.36	6.82	4.99																
EMV350	8.54	3.21	1.95	1.42	0.97	3.09	1.52	0.99	0.80	0.59	2.17	1.53	1.19	0.98	0.86	7.24	5.43	4.27	3.51	2.68																
OHW035	15.06	6.24	2.96	2.00	1.27	23.17	11.08	7.44	5.50	3.76	24.68	21.83	15.74	12.41	7.72	19.66	15.01	11.83	9.85	7.21																
OHW305	27.72	8.66	4.33	3.04	2.03	21.33	12.20	7.23	5.16	3.69	21.90	13.38	9.08	7.00	5.08	17.81	12.30	9.34	7.51	5.44																
RWC043	20.16	5.84	4.23	3.27	2.13	58.63	18.18	12.41	9.54	6.59	59.45	30.23	21.18	16.30	11.33	46.87	28.47	19.54	14.85	10.18																
RWC233	10.27	3.05	1.99	1.54	1.07	25.92	10.22	6.77	5.15	3.54	23.85	12.28	8.63	6.86	4.74	11.67	8.38	5.62	4.53	3.26																
SFA000	3.53	2.07	1.49	1.18	0.84	4.81	3.20	2.40	1.85	1.34	7.79	4.33	3.24	2.59	1.89	7.15	5.12	4.05	3.37	2.53																
SFA090	3.43	1.86	1.30	1.03	0.73	8.05	4.86	3.62	2.87	2.08	8.19	6.47	5.13	4.19	3.02	7.69	5.25	4.08	3.37	2.48																
TRI000	4.07	2.35	1.83	1.36	0.91	1.57	1.11	0.86	0.70	0.51	0.04	0.03	0.03	0.02	0.02	0.001	0.001	0.001	0.001	0.000																
TRI090	11.69	12.66	6.93	4.89	3.22	14.12	9.67	8.44	6.27	4.28	8.52	6.03	4.66	3.78	2.80	2.24	2.05	1.82	1.56	1.23																
ATS000	1.70	1.05	0.79	0.64	0.48	4.53	3.09	2.36	1.90	1.38	3.23	2.13	1.54	1.26	0.91	4.53	3.31	2.53	2.05	1.49																
ATS090	6.95	3.60	1.92	1.47	1.01	15.13	8.39	5.48	4.17	2.97	6.09	4.22	3.22	2.63	1.88	2.21	1.62	1.27	1.05	0.77																
DZC180	4.68	5.70	4.19	4.69	4.01	5.63	5.03	4.23	3.37	2.38	3.58	2.51	1.97	1.62	1.19	4.20	5.17	6.50	5.63	4.25																
DZC270	14.02	20.13	8.82	4.25	1.67	47.81	25.61	19.95	13.41	8.49	34.71	22.99	17.10	13.98	10.43	28.30	21.57	16.86	13.59	9.82																
YPT060	5.30	4.18	5.37	7.14	9.53	7.32	6.09	5.88	5.34	4.30	5.59	4.45	3.58	2.98	2.18	3.11	2.30	1.83	1.61	1.20																
YPT330	24.46	5.03	5.99	9.68	11.35	15.66	10.53	10.24	9.08	7.17	10.23	8.80	7.69	6.58	5.23	5.85	5.83	4.63	3.86	2.80																
mean	11.0	10.8	5.0	3.5	2.6	15.8	10.6	7.6	4.9	3.3	13.3	10.8	7.5	5.4	3.7	10.5	7.6	5.7	4.5	3.2																
σ	10.4	20.7	6.5	3.4	2.9	16.4	12.8	8.8	4.1	2.5	15.2	13.2	8.5	5.3	3.5	12.0	7.9	5.6	4.4	3.1																
mean + σ	21.4	31.5	11.5	6.9	5.5	32.2	23.3	16.4	9.0	5.7	28.5	24.0	16.0	10.7	7.2	22.5	15.5	11.3	8.9	6.3																
COV	0.94	1.93	1.31	0.96	1.16	1.04	1.21	1.17	0.83	0.75	1.14	1.23	1.12	0.98	0.96	1.15	1.05	0.99	0.97	0.95																

Table F.19. Normalized rate-of-energy dissipated data calculated using Definition 2 and the results of unidirectional response-history analysis performed with Bin 1 ground motions.

Record	R_E^{50} / T_d (kN-m / second / second)																			
	$Q_d/W=0.03$				$Q_d/W=0.06$				$Q_d/W=0.09$				$Q_d/W=0.12$							
	T_d				T_d				T_d				T_d							
	1.5	2	2.5	3	4	1.5	2	2.5	3	4	1.5	2	2.5	3	4	1.5	2	2.5	3	4
nf01	18.7	31.6	24.0	14.2	32.2	37.8	52.2	35.0	28.9	36.7	60.5	61.1	72.6	47.9	34.9	61.8	87.1	61.8	41.1	28.4
nf02	11.7	11.3	9.8	8.8	13.9	21.3	15.0	14.1	15.1	17.9	28.0	20.4	18.3	18.2	14.8	32.4	23.8	19.3	18.1	16.3
nf03	106.7	47.6	54.5	60.9	27.9	191.3	84.1	70.2	87.5	55.0	227.4	106.7	106.1	105.3	59.7	225.7	126.8	105.9	88.4	62.2
nf04	71.2	30.3	22.1	30.6	17.0	120.2	48.5	25.7	29.5	18.9	154.9	60.2	30.3	38.4	20.3	131.8	77.6	48.7	35.4	23.7
nf05	65.0	39.5	28.1	20.5	14.4	152.8	81.8	50.0	31.5	30.4	263.4	159.1	151.3	101.7	37.5	336.8	305.1	182.3	123.0	46.2
nf06	15.9	9.9	6.6	7.2	3.5	22.8	9.9	6.2	4.3	3.0	15.6	7.6	5.4	4.3	2.9	9.5	7.2	4.7	3.8	2.7
nf07	40.1	34.8	39.0	18.7	14.9	45.9	58.5	52.3	40.2	33.7	188.6	64.1	54.3	65.9	38.5	173.1	106.8	79.4	62.5	41.6
nf08	15.5	11.6	11.0	13.0	6.2	19.0	13.6	12.9	12.4	7.0	56.8	34.5	39.6	23.9	12.9	76.9	44.8	44.6	36.1	24.4
nf09	39.6	36.2	29.3	16.4	10.5	81.0	56.5	46.6	33.4	33.4	99.4	64.2	60.1	42.5	47.3	108.9	253.5	52.0	89.1	52.9
nf10	19.3	17.6	12.9	9.2	5.7	23.7	22.2	17.2	16.5	12.3	21.9	21.2	18.0	16.6	10.7	25.2	16.6	11.7	8.8	6.0
nf11	16.3	14.0	15.5	14.6	15.9	18.6	27.9	27.2	20.1	18.6	12.6	16.1	94.1	16.7	12.9	10.4	10.7	12.4	11.4	11.2
nf12	12.0	5.1	3.2	2.3	1.7	8.5	5.2	4.1	3.4	2.5	7.5	5.7	4.6	3.8	2.8	7.8	6.0	4.8	3.9	2.9
nf13	74.6	34.1	18.0	11.6	6.7	136.4	46.8	28.5	18.1	10.9	163.8	62.2	30.6	22.3	14.4	188.4	689.5	176.7	28.4	18.0
nf14	14.2	18.4	20.3	14.3	7.2	17.8	16.5	16.6	12.4	8.3	17.5	15.4	15.2	12.4	8.6	16.9	13.7	11.3	9.4	6.9
nf15	64.1	34.6	41.1	28.3	13.6	76.2	49.0	56.9	41.1	27.0	82.7	68.3	52.0	38.1	27.1	105.9	100.6	42.5	44.3	39.5
nf16	31.0	20.1	9.4	5.9	3.8	37.0	24.9	13.7	9.9	6.6	32.3	19.9	14.4	11.1	7.7	26.8	19.2	14.3	11.3	8.0
nf17	98.6	47.0	33.6	45.7	13.3	197.9	81.0	55.8	47.1	25.0	271.6	112.7	108.1	80.9	51.4	303.7	141.3	88.9	83.7	50.7
nf18	48.7	13.6	7.7	5.6	4.1	77.2	22.8	14.2	11.3	8.1	73.9	27.8	18.2	13.8	9.5	59.1	25.5	18.2	14.1	10.1
nf19	114.6	114.6	54.7	29.9	13.6	169.1	196.4	105.4	60.7	50.6	215.8	246.2	239.0	129.1	64.9	379.6	472.7	240.3	150.6	79.5
nf20	35.7	28.9	14.8	15.9	6.5	74.5	32.8	21.3	15.7	9.6	90.2	32.5	21.1	17.4	11.5	107.3	37.5	25.5	23.3	13.3
TCU065W	34.9	57.1	13.3	10.7	18.9	35.7	40.7	16.8	13.7	14.3	27.6	19.0	13.4	13.5	9.1	17.9	11.9	10.5	9.1	6.6
TCU065N	21.5	32.8	15.3	9.0	4.8	25.7	32.4	20.1	10.8	6.5	23.9	27.8	15.1	10.3	6.5	21.7	19.5	11.6	9.0	6.3
TCU075W	6.0	13.2	6.6	11.6	14.8	5.9	9.1	10.9	12.7	12.1	4.0	5.4	5.9	5.8	5.4	3.6	4.2	4.1	3.9	2.4
TCU075N	1.8	1.4	1.3	1.1	0.8	1.5	1.2	1.0	0.8	0.5	0.9	0.7	0.6	0.5	0.3	0.6	0.4	0.3	0.3	0.2
mean	40.7	29.4	20.5	16.9	11.3	66.6	42.9	30.1	24.0	18.7	89.2	52.4	49.5	35.0	21.3	101.3	108.4	53.0	37.9	23.3
σ	32.9	23.2	15.0	13.8	7.8	61.8	40.7	24.8	20.1	14.9	88.1	56.8	56.5	35.9	19.1	112.0	168.3	64.3	41.0	22.0
mean + σ	73.6	52.6	35.5	30.7	19.2	128.3	83.6	54.9	44.1	33.6	177.3	109.2	106.0	70.9	40.4	213.4	276.7	117.3	78.9	45.3
COV	0.81	0.79	0.73	0.82	0.69	0.93	0.95	0.82	0.84	0.79	0.99	1.08	1.14	1.03	0.90	1.11	1.55	1.21	1.08	0.94

Table F.20. Normalized rate-of-energy dissipated data calculated using *Definition 2* and the results of unidirectional response-history analysis performed with Bin 2 ground motions.

Record	R_E^{50} / T_d (kN-m / second / second)																			
	$Q_d/W=0.03$				$Q_d/W=0.06$				$Q_d/W=0.09$				$Q_d/W=0.12$							
	T_d				T_d				T_d				T_d							
	1.5	2	2.5	3	4	1.5	2	2.5	3	4	1.5	2	2.5	3	4	1.5	2	2.5	3	4
G01000	2.36	1.76	1.39	1.15	0.85	4.48	3.44	2.70	2.25	1.67	6.07	4.51	3.54	2.95	2.20	8.15	6.16	4.92	4.08	3.05
G01090	10.15	6.71	5.02	3.41	2.20	19.27	13.78	10.04	8.10	5.78	26.58	19.03	15.66	12.88	9.51	33.91	24.61	19.23	15.82	11.94
SGI270	0.041	0.031	0.025	0.020	0.015	0.026	0.019	0.015	0.013	0.010	0.021	0.016	0.027	0.023	0.017	0.009	0.068	0.054	0.045	0.034
SGI360	1.144	0.815	0.639	0.521	0.373	0.053	0.039	0.032	0.026	0.020	0.042	0.032	0.026	0.022	0.016	0.042	0.057	0.045	0.038	0.028
L09000	0.71	0.52	0.41	0.34	0.25	1.38	1.02	0.81	0.67	0.50	2.25	1.67	1.37	1.14	0.85	2.67	1.96	1.57	1.31	0.98
L09090	1.00	0.73	0.58	0.48	0.36	2.24	1.65	1.28	1.03	0.73	3.47	2.56	2.00	1.66	1.25	5.98	4.99	3.98	3.32	2.48
WON095	0.59	0.42	0.32	0.27	0.20	0.44	0.33	0.27	0.22	0.17	0.33	0.25	0.20	0.17	0.13	0.27	0.20	0.16	0.14	0.10
WON185	1.24	0.81	0.62	0.51	0.36	1.09	0.73	0.56	0.45	0.33	0.61	0.50	0.39	0.35	0.26	0.31	0.22	0.18	0.15	0.11
SFL09021	0.50	0.37	0.30	0.25	0.18	0.64	0.48	0.38	0.32	0.24	0.41	0.31	0.30	0.25	0.19	0.24	0.23	0.19	0.15	0.12
SFL09291	0.28	0.21	0.17	0.14	0.10	0.30	0.22	0.18	0.15	0.11	0.33	0.24	0.19	0.16	0.12	0.31	0.24	0.20	0.16	0.12
G02000	11.88	5.96	2.76	2.06	1.48	12.18	9.87	7.49	6.16	4.44	14.63	11.13	8.26	6.77	4.96	15.25	10.17	7.95	6.53	4.87
G02090	38.36	18.08	9.43	4.79	3.16	43.95	25.78	18.22	13.11	9.25	33.74	23.22	18.87	14.24	9.62	28.66	15.97	11.27	9.28	6.83
YER270	24.11	10.08	3.77	2.95	2.53	23.44	17.33	12.27	10.98	8.33	18.56	15.77	14.67	13.06	11.21	18.28	25.71	20.99	18.03	13.48
YER360	9.50	2.97	1.82	1.41	1.13	5.14	2.66	2.03	1.57	1.13	1.91	1.46	1.25	1.05	0.78	1.24	1.02	0.82	0.69	0.52
ABN000	2.74	1.96	1.61	1.28	0.90	3.35	2.46	1.93	1.60	1.19	1.83	1.35	1.02	0.85	0.63	0.82	0.62	0.50	0.45	0.34
ABN090	2.73	2.84	2.12	1.56	0.86	2.17	1.50	1.14	0.94	0.71	1.39	1.01	0.80	0.66	0.50	1.10	0.82	0.66	0.55	0.41
A-E01140	1.06	0.79	0.62	0.51	0.37	0.407	0.311	0.250	0.210	0.382	0.110	0.083	0.041	0.034	0.026	0.066	0.004	0.003	0.002	0.002
A-E01230	0.02	0.02	0.01	0.01	0.01	0.03	0.02	0.02	0.02	0.02	0.04	0.03	0.03	0.03	0.02	0.03	0.05	0.04	0.03	0.02
CNP106	6.93	5.43	4.68	3.76	2.50	8.27	6.92	5.35	4.25	3.01	8.34	6.11	4.79	3.88	2.86	7.12	5.37	4.23	3.46	2.57
CNP196	24.27	15.50	11.85	6.29	3.15	17.89	14.06	10.71	7.50	4.65	15.69	11.14	8.70	7.06	5.14	18.34	12.45	9.63	7.77	5.82
mean	6.98	3.80	2.41	1.58	1.05	7.34	5.13	3.78	2.98	2.13	6.82	5.02	4.11	3.36	2.51	7.14	5.55	4.33	3.60	2.69
σ	10.45	5.22	3.22	1.77	1.07	11.20	7.27	5.21	4.01	2.85	9.88	7.13	5.93	4.81	3.63	10.31	8.15	6.41	5.37	4.02
mean + σ	17.43	9.02	5.62	3.36	2.12	18.54	12.40	8.99	6.99	4.99	16.69	12.15	10.04	8.17	6.14	17.45	13.70	10.74	8.97	6.71
COV	1.50	1.37	1.34	1.12	1.02	1.53	1.42	1.38	1.35	1.34	1.45	1.42	1.44	1.43	1.44	1.44	1.47	1.48	1.49	1.49

Table F.21. Normalized rate-of-energy dissipated data calculated using Definition 2 and the results of unidirectional response-history analysis performed with Bin 2M ground motions.

Record	R_E^{50} / T_d (kN-m / second / second)																			
	$Q_d/W=0.03$				$Q_d/W=0.06$				$Q_d/W=0.09$				$Q_d/W=0.12$							
	T_d				T_d				T_d				T_d							
	1.5	2	2.5	3	4	1.5	2	2.5	3	4	1.5	2	2.5	3	4	1.5	2	2.5	3	4
G01000	2.36	1.76	1.39	1.15	0.85	4.48	3.44	2.70	2.25	1.67	6.07	4.51	3.54	2.95	2.20	8.15	6.16	4.92	4.08	3.05
G01090	10.15	6.71	5.02	3.41	2.20	19.27	13.78	10.04	8.10	5.78	26.58	19.03	15.66	12.88	9.51	33.91	24.61	19.23	15.82	11.94
GBZ000	2.69	2.50	3.52	3.19	2.54	2.92	2.27	2.00	1.72	1.22	2.21	1.57	1.23	1.01	0.74	1.70	1.33	0.99	0.73	0.53
GBZ270	1.28	1.00	0.84	0.69	0.51	1.15	0.84	0.68	0.57	0.42	0.73	0.55	0.44	0.36	0.27	0.73	0.54	0.42	0.35	0.26
STG000	25.04	13.26	7.11	4.05	2.50	33.76	22.80	17.33	10.54	7.68	24.37	18.30	12.61	9.53	6.21	11.75	7.36	6.03	5.20	3.94
STG090	9.21	3.79	3.51	4.09	3.73	7.03	4.33	3.35	3.13	2.50	5.67	4.29	3.57	2.91	2.16	5.84	4.30	3.42	2.84	2.13
RIO270	17.66	5.86	3.94	2.79	1.90	25.64	14.30	7.44	5.84	4.07	26.37	15.56	10.62	8.52	6.21	21.96	17.38	13.33	10.12	6.59
RIO360	8.78	3.07	2.09	1.62	1.16	17.69	11.14	7.92	6.34	4.94	25.12	14.99	11.59	9.42	6.93	42.11	31.30	23.76	19.52	14.29
JOS000	4.21	2.36	1.64	1.27	0.89	2.70	1.71	1.27	1.02	0.74	1.31	0.90	0.71	0.57	0.41	0.44	0.32	0.25	0.20	0.14
JOS090	8.04	3.66	2.31	1.80	1.21	4.36	2.81	2.15	1.72	1.25	2.86	1.98	1.57	1.26	0.90	1.59	1.05	0.80	0.66	0.48
G02000	11.88	5.96	2.76	2.06	1.48	12.18	9.87	7.49	6.16	4.44	14.63	11.13	8.26	6.77	4.96	15.25	10.17	7.95	6.53	4.87
G02090	38.36	18.08	9.43	4.79	3.16	43.95	25.78	18.22	13.11	9.25	33.74	23.22	18.87	14.24	9.62	28.66	15.97	11.27	9.28	6.83
YER270	24.11	10.08	3.77	2.95	2.53	23.44	17.33	12.27	10.98	8.33	18.56	15.77	14.67	13.06	11.21	18.28	25.71	20.99	18.03	13.48
YER360	9.50	2.97	1.82	1.41	1.13	5.14	2.66	2.03	1.57	1.13	1.91	1.46	1.25	1.05	0.78	1.24	1.02	0.82	0.69	0.52
ABN000	2.74	1.96	1.61	1.28	0.90	3.35	2.46	1.93	1.60	1.19	1.83	1.35	1.02	0.85	0.63	0.82	0.62	0.50	0.45	0.34
ABN090	2.73	2.84	2.12	1.56	0.86	2.17	1.50	1.14	0.94	0.71	1.39	1.01	0.80	0.66	0.50	1.10	0.82	0.66	0.55	0.41
BOL000	7.3	9.1	6.2	4.7	2.5	15.0	11.6	11.7	8.0	5.3	29.3	20.2	15.4	12.7	9.2	36.4	27.2	21.4	17.1	12.8
BOL090	28.8	10.5	5.9	3.8	2.4	60.7	29.4	18.4	12.3	7.8	80.3	50.7	79.1	48.3	31.0	89.8	72.0	118.8	90.0	57.4
CNP106	6.93	5.43	4.68	3.76	2.50	8.27	6.92	5.35	4.25	3.01	8.34	6.11	4.79	3.88	2.86	7.12	5.37	4.23	3.46	2.57
CNP196	24.27	15.50	11.85	6.29	3.15	17.89	14.06	10.71	7.50	4.65	15.69	11.14	8.70	7.06	5.14	18.34	12.45	9.63	7.77	5.82
mean	12.31	6.32	4.08	2.84	1.91	15.56	9.95	7.21	5.38	3.80	16.35	11.19	10.72	7.90	5.57	17.26	13.29	13.47	10.67	7.42
σ	10.50	4.90	2.86	1.52	0.94	15.76	8.67	5.97	4.11	2.85	18.77	12.06	17.19	10.68	7.00	21.60	17.17	26.04	19.76	12.72
mean + σ	22.80	11.22	6.94	4.36	2.84	31.32	18.62	13.17	9.49	6.65	35.11	23.25	27.92	18.58	12.57	38.86	30.46	39.51	30.43	20.14
COV	0.85	0.78	0.70	0.54	0.49	1.01	0.87	0.83	0.76	0.75	1.15	1.08	1.60	1.35	1.26	1.25	1.29	1.93	1.85	1.71

Table F.22. Normalized rate-of-energy dissipated data calculated using Definition 2 and the results of unidirectional response-history analysis performed with Bin 3 ground motions.

Record	R_E^{50} / T_d (kN-m / second / second)																			
	$Q_d/W=0.03$				$Q_d/W=0.06$				$Q_d/W=0.09$				$Q_d/W=0.12$							
	T_d				T_d				T_d				T_d							
	1.5	2	2.5	3	4	1.5	2	2.5	3	4	1.5	2	2.5	3	4	1.5	2	2.5	3	4
CHY000	0.27	0.20	0.16	0.13	0.10	0.22	0.16	0.13	0.11	0.08	0.14	0.10	0.08	0.07	0.05	0.09	0.07	0.06	0.05	0.03
CHY090	0.40	0.30	0.24	0.20	0.15	0.39	0.29	0.23	0.19	0.14	0.30	0.22	0.18	0.15	0.11	0.33	0.24	0.19	0.16	0.12
29P000	0.06	0.04	0.03	0.03	0.02	0.05	0.04	0.03	0.02	0.02	0.04	0.03	0.02	0.02	0.02	0.03	0.03	0.02	0.02	0.02
29P090	0.07	0.05	0.04	0.03	0.02	0.06	0.04	0.03	0.03	0.02	0.05	0.04	0.03	0.03	0.02	0.05	0.04	0.03	0.02	0.02
MCH000	0.17	0.13	0.10	0.09	0.06	0.15	0.11	0.09	0.07	0.06	0.10	0.07	0.06	0.05	0.04	0.07	0.04	0.03	0.03	0.02
MCH090	0.25	0.19	0.15	0.12	0.09	0.23	0.17	0.14	0.12	0.09	0.08	0.06	0.17	0.15	0.11	0.05	0.07	0.05	0.05	0.01
MTW000	0.52	0.39	0.31	0.26	0.19	0.69	0.51	0.41	0.34	0.25	0.87	0.65	0.52	0.43	0.32	0.89	0.66	0.53	0.44	0.33
MTW090	0.43	0.32	0.25	0.21	0.16	0.50	0.37	0.29	0.24	0.18	0.52	0.39	0.31	0.25	0.19	0.39	0.27	0.22	0.18	0.14
GRN180	1.09	0.77	0.60	0.50	0.37	1.11	0.81	0.64	0.53	0.40	0.91	0.68	0.54	0.45	0.33	0.94	0.70	0.56	0.47	0.35
GRN270	1.46	1.02	0.80	0.65	0.48	1.55	1.16	0.94	0.78	0.59	1.41	1.08	0.85	0.74	0.56	1.44	1.08	0.87	0.72	0.54
TDO000	2.79	2.13	1.58	1.26	0.93	3.80	2.76	2.18	1.81	1.34	3.92	2.89	2.27	1.88	1.40	3.73	2.72	2.15	1.78	1.33
TDO090	1.17	0.82	0.63	0.50	0.37	1.48	1.05	0.82	0.67	0.49	1.19	0.89	0.71	0.59	0.44	0.89	0.66	0.53	0.44	0.33
PSA000	0.40	0.26	0.19	0.15	0.11	0.08	0.06	0.05	0.04	0.03	0.05	0.04	0.03	0.03	0.02	0.06	0.04	0.03	0.03	0.02
PSA090	0.50	0.37	0.30	0.24	0.17	0.11	0.09	0.07	0.07	0.05	0.06	0.04	0.04	0.03	0.02	0.05	0.04	0.03	0.03	0.02
SLC270	14.74	9.51	5.22	3.80	2.34	15.65	12.26	8.22	5.80	3.51	7.59	4.84	3.63	3.06	2.27	2.83	2.09	1.61	1.28	0.93
SLC360	5.82	4.33	2.92	2.60	1.86	4.70	3.29	3.10	2.70	2.07	9.67	6.29	5.13	4.31	3.27	10.66	8.24	6.64	5.45	4.01
CAS000	0.60	0.44	0.38	0.31	0.23	0.285	0.212	0.169	0.141	0.105	0.221	0.166	0.155	0.129	0.097	0.207	0.156	0.125	0.104	0.078
CAS270	0.42	0.31	0.25	0.21	0.15	0.61	0.45	0.35	0.29	0.21	0.27	0.20	0.16	0.14	0.10	0.56	0.38	0.30	0.25	0.19
H-VCT075	0.30	0.23	0.18	0.15	0.11	0.28	0.21	0.17	0.14	0.10	0.22	0.16	0.13	0.11	0.08	0.18	0.13	0.11	0.09	0.07
H-VCT345	0.33	0.24	0.19	0.16	0.12	0.37	0.27	0.22	0.18	0.13	0.27	0.20	0.16	0.14	0.10	0.25	0.19	0.15	0.12	0.09
mean	1.59	1.10	0.73	0.58	0.40	1.61	1.22	0.91	0.71	0.49	1.39	0.95	0.76	0.64	0.48	1.18	0.89	0.71	0.59	0.43
σ	3.36	2.21	1.25	0.96	0.62	3.53	2.75	1.89	1.37	0.87	2.65	1.72	1.36	1.14	0.86	2.44	1.87	1.51	1.23	0.91
mean + σ	4.95	3.31	1.98	1.54	1.02	5.14	3.96	2.80	2.09	1.37	4.04	2.68	2.12	1.78	1.34	3.62	2.77	2.22	1.82	1.34
COV	2.12	2.00	1.72	1.65	1.54	2.19	2.26	2.07	1.92	1.77	1.90	1.81	1.79	1.79	1.80	2.06	2.10	2.11	2.11	2.11

Table F.23. Normalized rate-of-energy dissipated data calculated using Definition 2 and the results of unidirectional response-history analysis performed with Bin 6 ground motions.

Record	R_E^{50} / T_d (kN-m / second / second)																			
	$Q_d/W=0.03$				$Q_d/W=0.06$				$Q_d/W=0.09$				$Q_d/W=0.12$							
	T_d				T_d				T_d				T_d							
	1.5	2	2.5	3	4	1.5	2	2.5	3	4	1.5	2	2.5	3	4	1.5	2	2.5	3	4
LS01C	23.3	31.5	9.2	5.2	3.1	37.3	32.9	19.4	13.7	6.3	39.0	16.6	10.3	7.7	5.2	29.6	11.5	7.5	5.8	4.0
LS02C	19.3	80.3	60.7	44.2	11.6	36.2	116.2	104.5	50.6	55.8	60.1	113.9	218.9	130.0	40.1	64.7	148.2	165.9	96.4	37.3
LS03C	8.3	20.3	54.6	66.4	31.9	18.2	64.0	85.0	95.4	114.5	37.1	79.3	124.0	124.6	85.9	51.8	119.6	156.1	134.4	71.1
LS04C	16.5	23.7	30.2	22.3	8.8	20.2	28.5	30.8	24.7	13.8	23.7	28.5	23.3	16.9	9.6	23.6	18.2	10.7	9.7	7.5
LS05C	12.9	30.2	54.7	48.5	25.2	22.9	46.5	74.8	78.5	84.9	24.7	49.8	81.6	117.6	69.6	34.7	43.0	50.7	45.6	47.1
LS06C	26.9	39.5	35.8	26.5	12.7	50.7	59.1	48.2	37.1	29.4	65.6	64.0	71.0	51.1	29.7	45.2	51.1	34.9	27.6	18.7
LS07C	29.9	19.4	12.7	27.3	10.6	34.8	13.9	8.8	7.7	5.4	48.9	18.8	5.1	4.4	3.4	41.0	22.8	16.0	12.8	9.2
LS08C	8.3	17.0	12.0	6.6	3.6	5.6	5.1	4.3	3.3	2.1	2.4	1.8	1.3	1.0	0.7	10.2	7.3	5.7	4.5	3.2
LS09C	100.3	12.3	7.9	6.5	13.1	152.9	33.6	17.3	17.7	16.8	154.1	69.2	222.2	31.2	22.2	160.9	63.4	37.8	30.1	21.9
LS10C	45.6	37.3	43.5	21.1	6.3	29.0	31.9	18.4	10.6	6.2	22.7	19.7	11.2	8.0	4.7	12.5	8.6	5.8	4.3	2.9
LS11C	56.9	45.3	22.3	16.3	6.0	47.9	56.3	45.2	33.7	23.3	78.6	72.3	68.9	43.2	28.7	75.4	82.0	54.8	41.3	30.1
LS12C	18.3	46.4	42.9	23.5	13.4	43.4	71.3	64.6	44.9	37.1	58.7	71.9	107.0	66.2	35.0	47.8	66.1	60.0	43.1	25.9
LS13C	77.1	59.8	22.5	13.0	12.6	115.4	70.1	32.1	21.9	17.0	134.6	48.5	34.7	26.4	21.0	146.6	51.0	34.8	29.9	21.4
LS14C	19.0	29.7	17.6	10.6	4.7	23.3	16.5	11.8	8.3	5.1	13.2	9.8	7.7	6.1	4.4	13.1	9.6	8.2	6.7	4.8
LS15C	61.0	42.9	23.9	11.4	8.9	99.9	46.0	39.5	31.0	12.4	113.1	84.2	309.7	157.5	60.8	169.4	556.8	284.0	183.6	97.1
LS16C	15.4	31.6	32.1	21.9	11.3	24.2	44.6	40.8	29.7	14.7	27.5	23.9	23.9	18.6	10.8	13.4	11.4	7.7	6.3	4.7
LS17C	71.2	64.3	95.1	52.2	24.4	92.5	113.3	160.1	110.2	75.8	91.2	133.8	339.5	177.4	91.2	89.8	131.0	251.3	157.1	65.9
LS18C	54.4	42.7	19.5	11.6	6.9	93.4	70.5	33.8	21.2	13.1	82.0	65.8	40.9	26.2	16.3	61.1	43.3	33.6	23.9	15.6
LS19C	56.0	42.8	31.5	18.1	8.4	99.0	65.9	43.0	27.7	18.6	121.0	79.1	92.5	54.5	30.4	121.0	127.2	84.6	56.3	49.3
LS20C	29.5	35.1	24.2	14.6	6.5	51.1	42.4	31.8	22.1	7.1	50.4	43.9	44.6	29.7	15.1	44.7	39.4	30.6	22.9	14.1
mean	37.5	37.6	32.6	23.4	11.5	54.9	51.4	45.7	34.5	28.0	62.4	54.7	91.9	54.9	29.2	62.8	80.6	67.0	47.1	27.6
σ	26.1	16.8	21.3	16.8	7.6	39.8	29.1	37.4	29.1	30.9	42.5	35.1	102.0	55.3	27.4	49.9	120.7	82.3	53.4	26.3
mean + σ	63.6	54.4	54.0	40.2	19.1	94.7	80.6	83.1	63.6	58.9	105.0	89.9	193.9	110.2	56.7	112.8	201.3	149.3	100.5	53.9
COV	0.70	0.45	0.65	0.72	0.66	0.72	0.57	0.82	0.84	1.10	0.68	0.64	1.11	1.01	0.94	0.80	1.50	1.23	1.13	0.95

Table F.24. Normalized rate-of-energy dissipated data calculated using Definition 2 and the results of unidirectional response-history analysis performed with Bin 7 ground motions.

Record	R_E^{50} / T_d (kN-m / second / second)																			
	$Q_d/W=0.03$				$Q_d/W=0.06$				$Q_d/W=0.09$				$Q_d/W=0.12$							
	T_d				T_d				T_d				T_d							
	1.5	2	2.5	3	4	1.5	2	2.5	3	4	1.5	2	2.5	3	4	1.5	2	2.5	3	4
SCTEW	11.40	109.5	44.01	17.86	6.81	18.04	88.48	62.75	26.21	9.47	33.18	63.00	58.53	33.24	17.34	26.91	21.37	12.05	8.38	8.00
SCTNS	5.24	39.78	13.98	7.53	2.44	5.41	5.77	3.73	2.42	1.34	0.14	0.15	0.15	0.07	0.06	0.00	0.00	0.00	0.00	0.00
MEN270	2.99	2.16	1.73	1.40	1.00	2.64	1.81	1.43	1.19	0.98	0.16	0.13	0.11	0.09	0.07	0.01	0.01	0.00	0.00	0.00
MEN360	5.37	3.34	2.52	1.69	0.99	4.00	2.56	1.94	1.56	1.50	1.38	1.11	0.90	0.75	0.57	0.01	0.01	0.01	0.01	0.01
EMV260	42.95	13.71	6.11	4.29	2.71	42.90	22.36	15.80	10.74	6.46	32.54	22.86	17.99	13.40	9.14	18.21	13.39	10.03	8.04	5.72
EMV350	10.74	3.63	1.75	1.28	0.87	2.23	1.64	1.22	0.99	0.75	14.44	9.73	8.57	7.01	5.00	7.16	4.60	3.56	2.92	2.30
OHW035	20.44	11.13	8.71	6.79	4.86	29.66	19.15	15.62	13.86	9.55	29.73	22.79	17.76	14.33	10.31	20.84	14.14	11.31	9.47	6.99
OHW305	31.08	12.00	5.83	3.74	2.48	21.43	14.07	8.87	6.52	4.46	21.08	12.86	8.40	6.84	4.43	49.63	47.01	31.83	22.11	15.10
RWC043	32.74	12.24	8.01	6.31	4.27	61.01	25.81	16.42	12.76	9.91	68.92	31.33	23.45	17.83	12.20	55.24	31.77	17.91	13.52	9.25
RWC233	21.32	7.55	4.39	3.35	2.28	28.55	15.30	9.06	6.46	4.35	23.23	14.39	9.42	6.92	4.75	21.78	16.04	12.49	10.29	7.53
SFA000	6.60	3.88	2.69	2.09	1.38	12.43	8.70	6.39	5.07	3.92	14.87	10.08	7.63	6.20	4.58	11.01	8.38	6.73	5.52	4.13
SFA090	9.23	4.80	3.03	2.32	1.61	18.17	14.71	8.17	6.35	4.66	20.03	15.56	12.56	10.26	6.85	17.94	12.41	9.84	8.13	6.00
TRI000	4.08	2.83	1.92	1.47	0.95	2.91	1.67	1.27	1.04	0.64	0.20	0.15	0.12	0.10	0.08	0.005	0.002	0.001	0.001	0.001
TRI090	15.69	13.03	8.24	6.20	4.50	16.67	12.80	11.20	11.12	7.70	10.30	13.08	13.62	10.95	7.71	4.32	6.47	4.94	4.53	3.33
ATS000	5.42	3.06	2.13	1.54	1.17	5.74	4.24	3.19	2.54	1.82	7.80	4.96	3.63	2.92	2.08	12.60	10.26	7.58	6.15	4.47
ATS090	18.87	7.32	4.51	3.14	2.10	17.03	9.25	5.92	4.21	2.87	6.11	4.11	3.01	2.46	1.74	1.99	1.42	1.13	1.35	1.02
DZC180	4.39	6.41	4.38	4.06	5.16	4.80	4.00	3.48	2.80	1.98	24.47	16.31	15.49	11.76	8.54	22.00	15.64	12.52	10.69	8.02
DZC270	29.34	22.04	14.52	8.61	5.06	50.98	26.61	20.62	16.82	10.75	49.08	35.44	29.11	21.74	15.13	40.26	29.59	22.40	17.82	11.57
YPT060	7.98	5.87	5.58	7.27	12.81	7.43	6.44	5.70	5.36	4.56	5.45	4.39	3.58	2.97	2.16	2.93	2.20	1.74	1.42	1.05
YPT330	31.64	8.25	8.51	11.34	12.95	20.00	10.48	8.98	8.54	8.78	12.04	10.09	8.93	8.29	5.95	6.27	5.17	4.99	4.07	2.17
mean	15.9	14.6	7.6	5.1	3.8	18.6	14.8	10.6	7.3	4.8	18.8	14.6	12.1	8.9	5.9	16.0	12.0	8.6	6.7	4.8
σ	12.0	23.9	9.3	4.1	3.5	16.8	19.1	13.5	6.4	3.4	17.7	15.2	13.6	8.4	5.0	16.6	12.5	8.4	6.1	4.2
mean + σ	27.9	38.6	17.0	9.2	7.4	35.4	33.8	24.1	13.8	8.3	36.5	29.8	25.7	17.3	11.0	32.5	24.5	16.9	12.9	9.1
COV	0.76	1.64	1.22	0.81	0.93	0.90	1.29	1.28	0.88	0.71	0.94	1.04	1.12	0.94	0.85	1.04	1.04	0.98	0.91	0.88

Table F.25. Normalized rate-of-energy dissipated data calculated using Definition 1 and the results of bi-directional response-history analysis performed with Bin 1 ground motions.

Ground motion pair	$R_{E^{90}} / T_d$ (kN-m / second / second)																			
	$Q_d/W=0.03$				$Q_d/W=0.06$				$Q_d/W=0.09$				$Q_d/W=0.12$							
	T_d				T_d				T_d				T_d							
	1.5	2	2.5	3	4	1.5	2	2.5	3	4	1.5	2	2.5	3	4	1.5	2	2.5	3	4
nf01/nf02	21.8	29.8	16.5	13.8	13.1	29.5	29.5	19.7	16.7	16.6	35.0	30.6	22.1	19.0	16.9	39.1	32.2	24.6	20.9	17.2
nf03/nf04	136.1	52.2	64.7	73.6	27.0	205.1	98.6	88.4	94.9	55.1	268.5	125.4	90.5	93.7	62.8	288.9	137.9	105.5	100.8	74.9
nf05/nf06	60.6	36.1	27.0	21.4	12.2	118.1	64.8	37.3	27.0	18.9	163.3	79.6	53.1	44.8	23.1	237.4	115.8	78.9	52.7	32.0
nf07/nf08	37.8	29.9	37.3	28.4	6.8	28.5	24.7	54.0	35.5	9.6	26.0	24.1	27.4	20.3	11.2	27.7	24.7	26.2	17.5	11.5
nf09/nf10	32.3	38.1	23.1	20.3	9.1	57.1	54.1	43.9	30.5	16.7	78.5	68.1	55.3	43.0	25.3	90.4	73.4	52.2	46.1	30.5
nf11/nf12	18.8	8.0	7.2	10.7	12.6	14.7	10.2	9.3	10.5	11.3	13.1	10.5	9.3	9.3	7.6	12.5	10.5	9.2	7.9	6.0
nf13/nf14	75.8	44.3	27.6	16.1	9.9	128.4	58.6	40.6	24.5	14.0	169.5	69.7	44.4	29.2	17.7	178.6	79.4	46.3	32.4	21.0
nf15/nf16	68.5	38.0	35.6	22.5	9.7	103.0	61.9	53.6	40.8	18.9	110.3	72.2	62.3	47.1	24.2	99.2	77.1	61.7	44.4	26.3
nf17/nf18	92.3	42.8	20.2	17.9	12.7	178.1	74.2	34.9	27.5	20.0	253.5	97.9	51.4	38.8	25.8	317.6	120.3	73.4	54.7	37.2
nf19/nf20	102.5	98.0	48.2	24.6	12.7	185.5	173.0	88.9	41.3	22.4	225.8	208.9	113.6	56.0	31.4	223.2	238.3	123.1	66.4	36.4
TCU065	53.5	71.4	22.6	18.3	21.2	69.8	69.0	33.9	23.7	20.4	71.9	53.5	35.5	27.7	18.6	60.2	41.1	30.1	24.9	17.5
TCU075	5.7	7.0	5.5	8.2	8.5	6.4	6.3	5.9	5.6	5.5	5.6	5.4	4.7	4.0	3.3	4.4	4.0	3.6	3.0	2.1
mean	58.8	41.3	28.0	23.0	13.0	93.7	60.4	42.5	31.5	19.1	118.4	70.5	47.5	36.1	22.3	131.6	79.6	52.9	39.3	26.1
σ	38.5	24.9	16.7	16.9	5.7	70.1	44.9	26.4	22.7	12.4	95.4	56.3	31.7	24.1	15.1	112.3	66.6	37.3	27.6	19.2
mean + σ	97.3	66.2	44.7	39.9	18.7	163.7	105.3	68.9	54.3	31.5	213.8	126.8	79.2	60.1	37.4	243.9	146.2	90.2	66.9	45.2
COV	0.66	0.60	0.60	0.74	0.44	0.75	0.74	0.62	0.72	0.65	0.81	0.80	0.67	0.67	0.68	0.85	0.84	0.70	0.70	0.74

Table F.26. Normalized rate-of-energy dissipated data calculated using Definition 1 and the results of bi-directional response-history analysis performed with Bin 2 ground motions.

Ground motion pair	R_E^{90} / T_d (kN-m / second / second)																			
	$Q_d/W=0.03$				$Q_d/W=0.06$				$Q_d/W=0.09$				$Q_d/W=0.12$							
	T_d				T_d				T_d				T_d							
	1.5	2	2.5	3	4	1.5	2	2.5	3	4	1.5	2	2.5	3	4	1.5	2	2.5	3	4
G01	8.32	3.41	2.17	1.68	1.22	8.69	5.85	4.42	3.56	2.57	10.98	7.69	5.81	4.78	3.55	16.50	11.21	8.79	7.26	5.41
SGL	0.18	0.13	0.10	0.08	0.06	0.06	0.04	0.03	0.03	0.02	0.04	0.03	0.02	0.02	0.01	0.03	0.02	0.02	0.02	0.01
L09	0.59	0.43	0.34	0.28	0.21	0.85	0.63	0.50	0.41	0.31	1.02	0.75	0.60	0.49	0.37	1.24	0.92	0.74	0.61	0.46
WON	1.72	1.11	0.82	0.66	0.47	1.55	1.06	0.84	0.67	0.50	1.01	0.77	0.62	0.52	0.39	0.67	0.51	0.41	0.35	0.26
SFL09	0.26	0.19	0.15	0.12	0.09	0.27	0.20	0.16	0.13	0.10	0.26	0.20	0.16	0.13	0.10	0.24	0.18	0.14	0.12	0.09
G02	46.94	8.51	3.60	2.63	1.82	55.19	20.62	10.22	6.86	4.33	44.13	28.85	17.69	13.13	9.25	41.62	25.58	19.68	15.19	10.79
YER	20.59	4.86	2.98	2.37	2.05	15.93	5.92	3.47	2.78	2.24	10.78	6.33	4.28	3.05	2.14	2.44	1.85	1.45	1.18	0.88
ABN	2.26	1.54	1.21	0.97	0.68	2.30	1.73	1.38	1.14	0.84	1.83	1.39	1.11	0.93	0.70	1.20	0.90	0.72	0.59	0.44
A-E01	0.39	0.26	0.20	0.17	0.12	0.04	0.03	0.02	0.02	0.02	0.02	0.02	0.01	0.01	0.01	0.02	0.02	0.01	0.01	0.01
CNP	18.73	19.30	9.48	4.83	2.84	20.50	16.35	12.10	8.78	5.67	22.50	16.10	12.28	9.86	7.06	21.55	15.39	11.96	9.76	7.16
mean	10.00	3.97	2.10	1.38	0.96	10.54	5.24	3.31	2.44	1.66	9.26	6.21	4.26	3.29	2.36	8.55	5.66	4.39	3.51	2.55
σ	15.12	6.02	2.88	1.53	0.98	17.30	7.39	4.42	3.11	2.00	14.30	9.47	6.12	4.65	3.30	13.93	8.83	6.82	5.35	3.85
mean + σ	25.11	9.99	4.98	2.91	1.94	27.84	12.63	7.73	5.55	3.66	23.55	15.69	10.37	7.94	5.65	22.48	14.49	11.21	8.86	6.40
COV	1.51	1.52	1.37	1.11	1.03	1.64	1.41	1.33	1.27	1.21	1.54	1.53	1.44	1.41	1.40	1.63	1.56	1.55	1.53	1.51

Table F.27. Normalized rate-of-energy dissipated data calculated using Definition 1 and the results of bi-directional response-history analysis performed with Bin 2M ground motions.

Ground motion pair	R_E^{90} / T_d (kN-m / second / second)																			
	$Q_d/W=0.03$				$Q_d/W=0.06$				$Q_d/W=0.09$				$Q_d/W=0.12$							
	T_d				T_d				T_d				T_d							
	1.5	2	2.5	3	4	1.5	2	2.5	3	4	1.5	2	2.5	3	4	1.5	2	2.5	3	4
G01	8.32	3.41	2.17	1.68	1.22	8.69	5.85	4.42	3.56	2.57	10.98	7.69	5.81	4.78	3.55	16.50	11.21	8.79	7.26	5.41
GBZ	3.48	2.90	3.02	3.48	3.93	4.54	3.94	3.33	2.85	2.15	4.85	3.61	2.82	2.32	1.72	3.36	2.41	1.90	1.60	1.19
STG	16.96	12.37	6.14	5.17	3.38	26.46	15.04	9.31	6.98	5.08	22.58	15.28	9.75	7.51	5.32	19.36	13.49	9.99	7.86	5.48
RIO	19.00	3.44	2.29	1.73	1.23	18.92	7.15	4.21	3.23	2.30	27.53	16.58	11.80	9.17	6.61	32.89	20.86	13.64	11.01	8.05
JOS	13.05	5.89	4.26	3.26	2.12	11.66	6.81	4.90	3.88	2.76	8.22	5.26	3.92	3.13	2.25	4.76	3.10	2.35	1.90	1.38
G02	46.94	8.51	3.60	2.63	1.82	55.19	20.62	10.22	6.86	4.33	44.13	28.85	17.69	13.13	9.25	41.62	25.58	19.68	15.19	10.79
YER	20.59	4.86	2.98	2.37	2.05	15.93	5.92	3.47	2.78	2.24	10.78	6.33	4.28	3.05	2.14	2.44	1.85	1.45	1.18	0.88
ABN	2.26	1.54	1.21	0.97	0.68	2.26	1.54	1.21	0.97	0.68	1.83	1.39	1.11	0.93	0.70	1.20	0.90	0.72	0.59	0.44
BOL	16.51	20.40	9.10	6.56	3.62	27.98	18.65	12.21	8.89	5.99	46.10	27.14	18.57	13.65	9.51	76.36	41.21	29.19	22.79	16.18
CNP	18.73	19.30	9.48	4.83	2.84	20.50	16.35	12.10	8.78	5.67	22.50	16.10	12.28	9.86	7.06	21.55	15.39	11.96	9.76	7.16
mean	16.58	8.26	4.42	3.27	2.29	19.21	10.19	6.54	4.88	3.38	19.95	12.82	8.80	6.75	4.81	22.01	13.60	9.97	7.92	5.70
σ	12.50	6.87	2.89	1.77	1.11	15.30	6.78	4.01	2.77	1.77	15.63	9.63	6.19	4.58	3.20	23.46	12.92	9.21	7.17	5.09
mean + σ	29.08	15.12	7.31	5.04	3.40	34.51	16.97	10.55	7.64	5.15	35.58	22.45	14.99	11.33	8.01	45.47	26.52	19.18	15.09	10.79
COV	0.75	0.83	0.65	0.54	0.49	0.80	0.67	0.61	0.57	0.52	0.78	0.75	0.70	0.68	0.66	1.07	0.95	0.92	0.91	0.89

Table F.28. Normalized rate-of-energy dissipated data calculated using Definition 1 and the results of bi-directional response-history analysis performed with Bin 3 ground motions.

Ground motion	R_E^{90} / T_d (kN-m / second / second)																			
	$Q_d/W=0.03$				$Q_d/W=0.06$				$Q_d/W=0.09$				$Q_d/W=0.12$							
	T_d				T_d				T_d				T_d							
pair	1.5	2	2.5	3	4	1.5	2	2.5	3	4	1.5	2	2.5	3	4	1.5	2	2.5	3	4
CHY	4.15	3.46	3.18	3.01	2.81	2.25	1.92	1.77	1.69	1.60	2.29	2.01	1.88	1.82	1.76	2.04	1.94	1.89	1.86	1.82
29P	8.89	9.12	9.19	8.87	8.64	7.23	6.15	5.62	5.32	5.02	3.08	2.93	2.86	2.81	2.77	2.64	2.47	2.39	2.34	2.30
MCH	3.35	2.89	2.63	2.48	2.33	2.86	2.50	2.29	2.17	2.05	1.82	1.74	1.70	1.68	1.66	1.68	1.63	1.61	1.60	1.58
MTW	5.19	5.40	5.40	5.30	5.07	3.15	3.08	3.04	3.02	3.00	3.18	3.22	3.23	3.23	3.23	2.59	2.53	2.49	2.47	2.43
GRN	5.37	5.93	5.92	5.72	5.56	2.99	2.66	2.50	2.40	2.30	2.54	2.39	2.33	2.29	2.26	2.59	2.58	2.58	2.59	2.59
TDO	6.59	4.80	4.14	3.97	3.91	4.22	3.67	3.47	3.47	3.68	3.70	3.64	3.85	4.15	3.90	4.21	4.06	3.93	3.87	3.80
PSA	4.97	4.80	4.63	4.47	4.47	1.81	1.56	1.43	1.35	1.27	3.76	3.25	2.88	2.66	2.45	2.91	2.78	2.72	2.60	2.47
SLC	2.64	2.22	2.07	2.27	2.61	2.12	1.66	1.55	1.58	1.78	1.86	1.56	1.43	1.38	1.38	1.81	1.45	1.23	1.04	0.87
CAS	6.07	5.69	5.65	5.47	5.02	4.57	4.01	3.75	3.61	3.47	2.56	2.29	2.17	2.11	2.04	2.01	1.92	1.87	1.85	1.82
H-VCT	3.31	3.05	2.95	2.88	2.78	2.93	2.77	2.70	2.66	2.33	2.09	2.00	1.96	1.93	1.91	1.43	1.37	1.35	1.33	1.32
mean	5.05	4.74	4.58	4.44	4.32	3.41	3.00	2.81	2.73	2.65	2.69	2.50	2.43	2.41	2.34	2.39	2.27	2.21	2.15	2.10
σ	1.85	2.01	2.10	2.01	1.91	1.60	1.37	1.26	1.20	1.15	0.71	0.71	0.76	0.83	0.78	0.80	0.80	0.80	0.81	0.81
mean + σ	6.90	6.74	6.68	6.46	6.23	5.01	4.36	4.07	3.92	3.80	3.40	3.22	3.19	3.24	3.11	3.19	3.08	3.01	2.96	2.92
COV	0.37	0.42	0.46	0.45	0.44	0.47	0.46	0.45	0.44	0.43	0.26	0.29	0.31	0.34	0.33	0.33	0.35	0.36	0.37	0.39

Table F.29. Normalized rate-of-energy dissipated data calculated using Definition 1 and the results of bi-idiirectional response-history analysis performed with Bin 6 ground motions.

Ground motion pair	R_E^{90} / T_d (kN-m / second / second)																			
	$Q_d/W=0.03$				$Q_d/W=0.06$				$Q_d/W=0.09$				$Q_d/W=0.12$							
	T_d				T_d				T_d				T_d							
	1.5	2	2.5	3	4	1.5	2	2.5	3	4	1.5	2	2.5	3	4	1.5	2	2.5	3	4
LS01C/S02C	29.7	68.3	34.9	39.0	6.9	35.9	114.2	50.1	50.4	10.9	43.7	116.1	65.5	43.9	14.3	62.4	88.5	59.3	41.7	23.2
LS03C/LS04C	11.6	29.5	57.4	59.9	25.7	20.8	39.0	83.7	95.0	48.3	27.0	47.6	91.5	95.6	57.7	45.2	76.4	87.6	85.6	61.6
LS05C/LS06C	20.2	35.1	60.5	45.5	23.9	38.4	65.7	90.9	80.0	41.7	54.1	80.3	94.4	90.8	53.4	63.5	84.1	90.9	85.6	58.5
LS07C/LS08C	26.9	30.6	18.2	19.5	13.9	25.6	26.9	19.7	16.6	10.7	20.2	17.1	11.4	9.2	6.5	18.0	11.4	7.6	6.3	4.4
LS09C/LS10C	113.0	38.4	32.8	16.3	13.0	148.4	53.6	35.3	24.0	16.6	133.5	47.2	26.2	19.5	16.1	94.1	42.3	24.4	19.0	14.3
LS11C/LS12C	54.4	66.5	37.6	23.3	5.7	77.7	93.3	70.2	42.3	17.3	73.0	105.7	94.2	61.9	32.0	88.6	115.6	85.6	67.3	41.3
LS13C/LS14C	66.5	66.6	26.7	18.4	12.9	122.3	84.1	42.6	31.4	18.9	141.8	81.0	50.7	35.9	26.2	149.5	69.3	52.0	38.3	27.2
LS15C/LS16C	54.4	69.4	40.0	25.4	13.5	106.7	80.9	58.0	34.1	23.0	121.1	79.8	64.1	47.3	28.1	116.5	80.2	57.4	42.9	26.8
LS17C/LS18C	79.8	65.5	81.8	43.9	17.3	134.5	124.9	138.4	90.0	46.1	163.3	171.3	170.6	120.9	65.5	173.5	187.9	181.9	133.9	79.0
LS19C/LS20C	51.4	48.1	35.5	19.8	5.7	83.2	79.6	56.0	29.5	11.8	87.6	82.0	62.1	31.8	15.8	89.8	74.8	67.8	41.4	17.3
mean	50.8	51.8	42.5	31.1	13.8	79.4	76.2	64.5	49.3	24.5	86.5	82.8	73.1	55.7	31.6	90.1	83.0	71.5	56.2	35.4
σ	30.7	17.1	18.7	14.9	7.0	47.5	31.0	33.7	28.7	15.0	51.0	42.6	44.1	36.2	20.5	47.0	46.2	47.2	37.6	24.0
mean + σ	81.5	68.9	61.3	46.0	20.8	126.8	107.2	98.2	78.0	39.5	137.5	125.4	117.2	91.8	52.0	137.1	129.2	118.7	93.8	59.3
COV	0.60	0.33	0.44	0.48	0.50	0.60	0.41	0.52	0.58	0.61	0.59	0.51	0.60	0.65	0.65	0.52	0.56	0.66	0.67	0.68

Table F.30. Normalized rate-of-energy dissipated data calculated using Definition 1 and the results of bi-directional response-history analysis performed with Bin 7 ground motions.

Ground motion pair	R_E^{90} / T_d (kN-m / second / second)																			
	$Q_d/W=0.03$				$Q_d/W=0.06$				$Q_d/W=0.09$				$Q_d/W=0.12$							
	T_d				T_d				T_d				T_d							
	1.5	2	2.5	3	4	1.5	2	2.5	3	4	1.5	2	2.5	3	4	1.5	2	2.5	3	4
SCT	10.4	129.7	39.2	13.6	5.2	17.1	90.2	40.6	20.8	9.3	23.9	48.2	34.6	20.2	10.1	28.9	36.7	21.7	12.7	3.8
MEN	4.41	2.79	2.00	1.59	1.11	3.72	2.22	1.67	1.41	1.07	0.78	0.59	0.47	0.39	0.29	0.03	0.02	0.02	0.01	0.01
EMV	47.9	9.6	5.1	3.6	2.4	43.9	18.9	9.9	7.2	4.8	35.0	27.3	18.7	13.7	8.9	31.9	20.1	14.2	10.7	7.5
OHW	36.5	14.1	5.8	3.9	2.8	42.7	22.8	10.6	6.9	4.6	45.0	29.7	21.2	15.4	10.1	52.9	29.7	21.0	16.3	11.5
RWC	20.4	6.4	4.4	3.4	2.3	55.5	21.3	14.5	10.9	7.2	65.3	31.1	20.8	15.7	10.9	62.6	32.3	21.3	16.3	11.2
SFA	6.5	3.3	2.2	1.8	1.3	10.2	6.1	4.4	3.5	2.5	14.0	8.6	6.5	5.3	3.8	17.5	12.0	9.5	7.8	5.8
TRI	13.3	13.3	7.8	4.5	3.1	18.8	13.4	11.2	7.9	5.3	13.4	9.5	7.4	6.0	4.4	2.9	2.5	3.5	3.0	2.4
ATS	5.6	3.0	1.9	1.5	1.1	21.7	11.8	7.8	5.9	4.2	17.0	10.2	7.4	5.9	4.2	7.1	5.0	3.8	3.1	2.3
DZC	15.7	26.5	11.8	8.0	5.2	18.0	18.4	12.5	8.5	5.2	27.4	16.6	22.1	17.3	10.6	36.1	28.0	22.5	20.4	15.0
YPT	21.9	8.6	8.4	18.3	15.4	26.0	16.0	15.7	18.6	20.0	18.5	15.2	13.8	13.7	12.0	15.0	12.5	10.4	8.8	6.4
mean	18.2	21.7	8.9	6.0	4.0	25.7	22.1	12.9	9.2	6.4	26.0	19.7	15.3	11.4	7.6	25.5	17.9	12.8	9.9	6.6
σ	14.2	38.6	11.1	5.7	4.3	16.4	24.8	10.6	6.2	5.3	18.5	14.2	10.1	6.5	4.0	21.0	13.3	8.6	6.6	4.8
mean + σ	32.4	60.4	20.0	11.7	8.2	42.2	46.9	23.5	15.3	11.7	44.5	33.9	25.4	17.8	11.5	46.5	31.2	21.4	16.6	11.4
COV	0.78	1.78	1.25	0.94	1.07	0.64	1.12	0.83	0.67	0.82	0.71	0.72	0.66	0.57	0.53	0.82	0.74	0.67	0.67	0.73

Table F.31. Normalized rate-of-energy dissipated data calculated using Definition 2 and the results of bi-directional response-history analysis performed with Bin 1 ground motions.

Ground motion pair	R_E^{50} / T_d (kN-m / second / second)																			
	$Q_d/W=0.03$				$Q_d/W=0.06$				$Q_d/W=0.09$				$Q_d/W=0.12$							
	T_d				T_d				T_d				T_d							
	1.5	2	2.5	3	4	1.5	2	2.5	3	4	1.5	2	2.5	3	4	1.5	2	2.5	3	4
nf01/nf02	26.5	39.6	23.3	21.1	20.3	39.8	61.7	37.7	29.4	27.7	64.5	70.1	43.2	39.4	33.8	78.4	73.9	56.5	34.3	32.2
nf03/nf04	146.6	56.2	72.6	79.9	31.2	253.5	109.1	95.5	113.7	66.5	351.4	145.6	108.1	121.2	77.8	369.8	166.8	122.3	109.3	84.1
nf05/nf06	68	42	31	23	16	157	87	53	31	34	270	161	166	106	40	341	328	194	127	48
nf07/nf08	47.4	44.8	46.3	34.8	17.1	61.3	65.1	66.0	48.5	44.8	78.4	85.0	58.4	53.8	50.6	125.3	158.4	128.0	91.8	58.4
nf09/nf10	40	41.3	32.9	20.9	13.8	75.5	71.3	64.4	45.3	37.1	98.4	93.4	84.4	57.9	42.7	95.6	105.4	76.3	58.8	46.9
nf11/nf12	25.0	15.1	15.1	15.2	16.4	32.8	22.1	27.1	21.1	22.0	22.0	18.6	103.4	21.5	16.5	19.0	17.7	16.4	14.8	11.7
nf13/nf14	74.1	46.2	28.2	16.1	11.9	146.1	61.8	42.7	27.8	15.2	187.5	74.9	48.9	37.2	19.6	208.7	86.0	57.7	35.4	21.7
nf15/nf16	81.9	43.0	42.6	29.4	14.7	123.1	67.3	63.8	47.0	25.7	136.0	81.0	65.1	54.4	25.2	112.5	86.9	61.2	46.6	30.3
nf17/nf18	110.0	51.0	31.5	20.1	15.3	234.1	93.6	62.2	50.8	27.9	340.2	127.8	102.3	106.9	37.0	365.5	183.7	112.7	85.4	55.1
nf19/nf20	125	123.0	61.4	26.1	15.6	192	214.0	114.6	54.0	33.4	238	261.4	278.0	113.7	56.0	358	439.6	285.8	131.4	75.6
TCU065	56.2	82.5	24.6	18.1	22.1	63.7	91.9	34.4	22.4	21.7	59.2	64.0	34.6	25.5	19.7	48.9	37.4	28.4	23.7	16.7
TCU075	6.5	10.5	6.1	13.5	14.4	7.5	10.2	11.7	13.4	14.8	5.9	8.2	9.0	8.1	7.2	4.8	5.9	6.4	5.3	3.1
mean	67.3	49.6	34.6	26.5	17.4	115.5	79.6	56.1	42.0	30.9	154.2	99.3	91.8	62.1	35.5	177.3	140.8	95.4	63.6	40.3
σ	43	29.5	18.7	17.9	5.1	81.5	50.9	28.7	26.2	14.3	120.8	68.2	72.0	39.6	19.7	143.9	128.9	80.4	44.0	25.4
mean + σ	110	79.0	53.3	44.4	22.5	197	130.5	84.8	68.2	45.2	275	167.5	163.7	101.7	55.3	321	269.8	175.8	107.6	65.7
COV	0.64	0.59	0.54	0.67	0.30	0.71	0.64	0.51	0.62	0.46	0.78	0.69	0.78	0.64	0.56	0.81	0.92	0.84	0.69	0.63

Table F.32. Normalized rate-of-energy dissipated data calculated using *Definition 2* and the results of bi-directional response-history analysis performed with Bin 2 ground motions.

Ground motion pair	R_E^{50} / T_d (kN-m / second / second)																			
	$Q_d/W=0.03$				$Q_d/W=0.06$				$Q_d/W=0.09$				$Q_d/W=0.12$							
	T_d				T_d				T_d				T_d							
	1.5	2	2.5	3	4	1.5	2	2.5	3	4	1.5	2	2.5	3	4	1.5	2	2.5	3	4
G01	10.98	7.65	4.89	2.36	1.85	19.58	10.39	9.53	8.79	5.58	24.63	17.87	14.97	12.21	9.08	28.68	22.97	18.01	14.84	11.03
SGL	0.75	0.55	0.43	0.36	0.27	0.10	0.08	0.06	0.05	0.04	0.07	0.05	0.04	0.04	0.03	0.06	0.07	0.05	0.05	0.03
L09	1.25	0.92	0.72	0.60	0.44	2.86	2.09	1.66	1.38	1.01	3.69	2.72	2.12	1.76	1.32	6.99	5.09	4.06	3.38	2.53
WON	1.83	1.10	0.81	0.65	0.47	1.48	1.08	0.84	0.70	0.52	1.02	0.75	0.62	0.52	0.39	0.68	0.51	0.41	0.35	0.26
SFL09	0.67	0.50	0.39	0.33	0.25	0.86	0.64	0.51	0.42	0.32	0.72	0.54	0.43	0.36	0.27	0.61	0.47	0.37	0.31	0.23
G02	47.11	19.76	8.18	5.45	3.34	59.68	31.45	20.65	8.66	8.34	54.96	37.12	30.22	22.48	14.59	43.40	30.40	25.64	20.90	15.12
YER	28.09	7.41	3.11	2.26	2.47	31.50	10.89	7.79	6.26	5.63	28.22	18.04	15.33	12.22	8.74	17.13	16.84	14.68	12.23	9.33
ABN	4.86	3.01	2.36	1.63	1.15	6.11	4.57	3.32	2.76	2.28	4.49	3.41	2.86	2.37	1.78	2.20	1.62	1.29	1.07	0.80
A-E01	1.14	0.81	0.63	0.52	0.39	0.17	0.13	0.11	0.09	0.08	0.05	0.04	0.05	0.04	0.03	0.03	0.04	0.03	0.03	0.02
CNP	30.38	22.91	14.35	7.62	3.91	25.61	19.86	14.29	9.37	6.54	24.67	18.35	14.14	11.31	7.94	25.79	18.28	13.74	11.10	7.99
mean	12.71	6.46	3.59	2.18	1.45	14.79	8.12	5.87	3.85	3.03	14.25	9.89	8.08	6.33	4.42	12.56	9.63	7.83	6.43	4.74
σ	16.56	8.32	4.53	2.47	1.37	19.59	10.42	7.08	3.96	3.16	18.37	12.48	10.18	7.75	5.22	15.43	11.41	9.38	7.67	5.62
mean + σ	29.27	14.79	8.12	4.65	2.82	34.38	18.54	12.96	7.81	6.19	32.62	22.37	18.26	14.08	9.63	27.99	21.04	17.21	14.10	10.35
COV	1.30	1.29	1.26	1.13	0.94	1.32	1.28	1.21	1.03	1.04	1.29	1.26	1.26	1.22	1.18	1.23	1.18	1.20	1.19	1.19

Table F.33. Normalized rate-of-energy dissipated data calculated using Definition 2 and the results of bi-directional response-history analysis performed with Bin 2M ground motions.

Ground motion pair	R_E^{50} / T_d (kN-m / second / second)																			
	$Q_d/W=0.03$				$Q_d/W=0.06$				$Q_d/W=0.09$				$Q_d/W=0.12$							
	T_d				T_d				T_d				T_d							
	1.5	2	2.5	3	4	1.5	2	2.5	3	4	1.5	2	2.5	3	4	1.5	2	2.5	3	4
G01	10.98	7.65	4.89	2.36	1.85	19.58	10.39	9.53	8.79	5.58	24.63	17.87	14.97	12.21	9.08	28.68	22.97	18.01	14.84	11.03
GBZ	3.30	2.96	3.66	4.56	3.74	4.63	3.46	3.23	2.76	2.37	3.39	2.54	2.01	1.65	1.22	2.40	1.77	1.39	1.13	0.84
STG	34.90	16.56	7.92	6.18	4.71	42.96	24.76	15.48	9.55	8.04	41.52	27.41	18.71	12.97	8.79	25.40	19.43	14.42	11.22	7.77
RIO	20.49	7.16	4.70	3.23	2.22	34.89	15.99	10.06	7.88	5.86	36.21	23.20	21.07	16.44	10.68	43.73	37.07	27.69	22.07	15.58
JOS	11.85	5.50	3.59	2.80	1.89	9.03	5.23	3.81	3.02	2.13	6.01	3.81	2.90	2.30	1.66	3.40	2.21	1.68	1.35	0.98
G02	47.11	19.76	8.18	5.45	3.34	59.68	31.45	20.65	8.66	8.34	54.96	37.12	30.22	22.48	14.59	43.40	30.40	25.64	20.90	15.12
YER	28.09	7.41	3.11	2.26	2.47	31.50	10.89	7.79	6.26	5.63	28.22	18.04	15.33	12.22	8.74	17.13	16.84	14.68	12.23	9.33
ABN	4.86	3.01	2.36	1.63	1.15	6.11	4.57	3.32	2.76	2.28	4.49	3.41	2.86	2.37	1.78	2.20	1.62	1.29	1.07	0.80
BOL	21.60	20.50	10.63	7.57	4.43	59.8	29.94	23.16	15.07	9.95	88.7	49.51	40.54	29.65	20.13	113.9	78.01	65.38	54.82	37.86
CNP	30.38	22.91	14.35	7.62	3.91	25.61	19.86	14.29	9.37	6.54	24.67	18.35	14.14	11.31	7.94	25.79	18.28	13.74	11.10	7.99
mean	21.36	11.34	6.34	4.37	2.97	29.37	15.65	11.13	7.41	5.67	31.28	20.13	16.27	12.36	8.46	30.60	22.86	18.39	15.08	10.73
σ	14.03	7.72	3.86	2.24	1.22	20.38	10.46	7.12	3.87	2.72	26.29	15.21	12.39	9.04	5.99	33.08	22.83	19.03	15.92	11.00
mean + σ	35.38	19.06	10.20	6.60	4.19	49.76	26.11	18.25	11.28	8.40	57.57	35.33	28.66	21.40	14.45	63.68	45.69	37.42	30.99	21.73
COV	0.66	0.68	0.61	0.51	0.41	0.69	0.67	0.64	0.52	0.48	0.84	0.76	0.76	0.73	0.71	1.08	1.00	1.03	1.06	1.02

Table F.34. Normalized rate-of-energy dissipated data calculated using Definition 2 and the results of bi-directional response-history analysis performed with Bin 3 ground motions.

Ground motion	R_E^{50} / T_d (kN-m / second / second)																			
	$Q_d/W=0.03$				$Q_d/W=0.06$				$Q_d/W=0.09$				$Q_d/W=0.12$							
	T_d				T_d				T_d				T_d							
	1.5	2	2.5	3	4	1.5	2	2.5	3	4	1.5	2	2.5	3	4	1.5	2	2.5	3	4
pair	0.69	0.51	0.40	0.33	0.25	0.67	0.50	0.40	0.34	0.25	0.48	0.36	0.28	0.24	0.18	0.44	0.32	0.26	0.21	0.16
CHY	0.12	0.09	0.07	0.06	0.04	0.12	0.09	0.07	0.06	0.04	0.10	0.08	0.06	0.05	0.04	0.09	0.07	0.05	0.05	0.03
29P	0.42	0.31	0.25	0.21	0.15	0.31	0.23	0.19	0.16	0.12	0.19	0.14	0.12	0.10	0.07	0.15	0.09	0.07	0.06	0.05
MCH	0.81	0.60	0.47	0.39	0.29	1.12	0.84	0.67	0.56	0.42	1.17	0.87	0.69	0.58	0.43	1.41	1.06	0.84	0.70	0.53
MTW	2.02	1.38	1.06	0.89	0.67	2.46	1.80	1.43	1.18	0.89	2.31	1.74	1.42	1.18	0.89	2.19	1.63	1.31	1.09	0.82
GRN	3.33	2.44	1.87	1.47	1.04	4.87	3.55	2.86	2.44	1.77	5.06	3.69	2.93	2.43	1.81	4.95	3.61	2.87	2.37	1.78
TDO	1.18	0.84	0.65	0.51	0.36	0.28	0.22	0.18	0.15	0.11	0.13	0.10	0.08	0.06	0.05	0.11	0.08	0.07	0.06	0.04
PSA	13.14	7.63	5.56	4.18	2.56	21.87	11.56	7.88	6.93	4.75	18.64	13.08	10.76	8.82	6.44	16.71	9.48	7.54	6.28	4.72
SLC	0.98	0.71	0.56	0.46	0.34	1.12	0.84	0.67	0.56	0.41	0.65	0.49	0.39	0.33	0.24	0.63	0.48	0.38	0.32	0.24
CAS	0.60	0.44	0.35	0.29	0.22	0.67	0.50	0.40	0.33	0.25	0.55	0.41	0.32	0.27	0.20	0.44	0.33	0.27	0.22	0.17
H-VCT	2.33	1.49	1.12	0.88	0.59	3.35	2.01	1.47	1.27	0.90	2.93	2.09	1.71	1.41	1.04	2.71	1.72	1.37	1.14	0.85
mean	3.91	2.26	1.64	1.23	0.75	6.66	3.51	2.40	2.11	1.45	5.72	4.02	3.30	2.71	1.98	5.14	2.94	2.34	1.94	1.46
σ	6.24	3.75	2.77	2.11	1.34	10.01	5.52	3.87	3.38	2.35	8.65	6.11	5.01	4.11	3.01	7.85	4.65	3.70	3.08	2.31
mean + σ	1.68	1.51	1.46	1.40	1.26	1.99	1.74	1.63	1.66	1.61	1.96	1.92	1.94	1.93	1.91	1.90	1.71	1.71	1.71	1.71
COV																				

Table F.35. Normalized rate-of-energy dissipated data calculated using *Definition 2* and the results of bi-directional response-history analysis performed with Bin 6 ground motions.

Ground motion pair	R_E^{50} / T_d (kN-m / second / second)																			
	$Q_d/W=0.03$				$Q_d/W=0.06$				$Q_d/W=0.09$				$Q_d/W=0.12$							
	T_d				T_d				T_d				T_d							
	1.5	2	2.5	3	4	1.5	2	2.5	3	4	1.5	2	2.5	3	4	1.5	2	2.5	3	4
LS01C/LS02C	34.7	91.3	50.6	49.1	11.8	58.6	139.4	95.6	58.9	19.2	57.4	124.6	169.2	60.2	24.2	49.5	106.8	141.4	63.7	24.5
LS03C/LS04C	13.9	33.3	68.0	73.5	33.2	31.1	77.1	107.1	118.0	67.4	50.9	100.2	122.7	119.6	83.1	61.8	103.1	123.9	119.5	83.5
LS05C/LS06C	25.2	39.9	73.3	54.1	27.7	48.3	74.4	105.9	97.3	56.7	57.2	93.5	114.5	110.5	64.2	59.7	95.9	115.1	104.7	72.5
LS07C/LS08C	32.5	29.6	25.9	39.6	18.1	23.6	22.5	16.5	14.4	8.9	38.7	14.4	8.5	7.1	5.2	52.6	36.5	22.4	17.4	12.5
LS09C/LS10C	115.7	43.0	53.3	20.7	17.1	198.4	52.8	31.1	20.4	17.9	215.0	44.6	21.6	17.0	17.0	268.1	111.0	34.4	25.0	23.0
LS11C/LS12C	71.4	75.9	46.5	27.7	12.7	74.0	104.5	90.7	60.3	35.0	93.3	146.4	108.5	76.4	44.1	116.2	149.4	114.8	81.2	41.3
LS13C/LS14C	85.4	101.5	28.5	20.1	15.1	137.4	108.5	42.0	29.3	21.8	158.9	74.4	46.6	34.8	25.9	166.6	65.1	47.5	37.2	29.1
LS15C/LS16C	64.9	79.1	41.1	29.1	19.0	114.9	83.0	68.4	46.9	26.6	134.2	83.2	66.9	51.5	30.5	160.4	80.4	56.8	43.9	30.2
LS17C/LS18C	96.7	65.8	96.9	53.2	25.2	140.9	136.9	167.2	112.7	57.8	178.8	185.9	210.7	147.8	75.5	195.0	204.0	226.9	161.8	86.6
LS19C/LS20C	62.8	55.9	41.7	23.7	9.9	123.3	95.1	65.2	40.6	14.5	159.6	110.6	81.5	53.3	28.7	177.5	122.1	89.4	63.0	35.8
mean	60.3	61.5	52.6	39.1	19.0	95.1	89.4	79.0	59.9	32.6	114.4	97.8	95.1	67.8	39.9	130.7	107.4	97.3	71.7	43.9
σ	33.3	25.1	21.6	17.9	7.5	56.7	35.9	44.2	37.5	20.7	62.7	49.0	63.6	45.8	26.1	74.6	46.0	61.3	45.7	26.8
mean + σ	93.6	86.6	74.2	57.0	26.5	151.7	125.3	123.2	97.4	53.3	177.1	146.7	158.7	113.6	65.9	205.3	153.4	158.6	117.5	70.7
COV	0.55	0.41	0.41	0.46	0.40	0.60	0.40	0.56	0.63	0.64	0.55	0.50	0.67	0.68	0.65	0.57	0.43	0.63	0.64	0.61

Table F.36. Normalized rate-of-energy dissipated data calculated using *Definition 2* and the results of bi-directional response-history analysis performed with Bin 7 ground motions.

Ground motion pair	R_E^{50} / T_d (kN-m / second / second)																			
	$Q_d/W=0.03$				$Q_d/W=0.06$				$Q_d/W=0.09$				$Q_d/W=0.12$							
	T_d				T_d				T_d				T_d							
	1.5	2	2.5	3	4	1.5	2	2.5	3	4	1.5	2	2.5	3	4	1.5	2	2.5	3	4
SCT	13.4	153.9	45.8	22.5	7.6	23.6	126.0	59.1	28.0	13.1	35.8	86.5	88.2	38.5	19.4	36.8	38.0	28.6	21.2	9.8
MEN	5.12	3.49	2.95	2.31	1.61	4.32	2.90	2.20	1.77	1.33	0.68	0.52	0.43	0.36	0.29	0.02	0.02	0.02	0.02	0.01
EMV	49.2	13.4	6.6	3.4	2.3	51.7	19.8	9.6	6.8	5.2	43.2	26.8	18.2	13.7	9.3	33.1	23.1	16.2	12.8	8.8
OHW	38.7	19.1	11.4	6.7	3.6	45.5	24.3	16.4	11.7	8.7	47.1	27.3	27.8	22.2	16.2	52.6	45.4	34.5	28.5	20.8
RWC	34.5	13.1	8.1	6.8	4.5	68.3	29.0	17.2	10.7	10.9	88.9	33.3	31.1	23.3	16.4	71.3	60.3	38.5	30.2	22.1
SFA	13.9	6.3	3.5	2.7	1.8	22.7	8.4	7.6	6.0	4.9	19.0	12.9	13.0	10.5	7.6	23.0	24.0	17.3	13.9	9.9
TRI	18.3	15.1	9.0	6.1	4.2	17.7	13.4	10.2	8.4	9.8	12.2	8.8	17.3	14.5	10.6	5.9	8.9	7.5	6.4	5.2
ATS	20.5	8.5	4.1	2.8	2.1	27.8	14.1	8.5	6.5	4.4	19.1	10.3	7.5	6.0	4.3	10.4	7.1	5.5	4.5	3.3
DZC	28.6	33.9	13.0	6.8	4.7	50.9	32.4	22.3	9.6	5.8	60.3	34.3	34.6	26.7	18.7	52.2	49.6	38.0	30.2	21.8
YPT	38.5	12.2	12.3	22.5	21.7	29.9	16.1	16.4	19.3	28.0	19.4	14.8	14.9	15.1	13.9	15.0	13.1	11.0	9.3	6.4
mean	26.1	27.9	11.7	8.3	5.4	34.2	28.6	16.9	10.9	9.2	34.6	25.5	25.3	17.1	11.6	30.0	27.0	19.7	15.7	10.8
σ	14.0	45.0	12.5	7.7	6.0	19.3	35.4	15.9	7.6	7.5	26.2	24.2	24.5	11.0	6.4	23.3	20.4	14.2	11.2	8.0
mean + σ	40.1	72.9	24.2	16.0	11.4	53.5	64.0	32.9	18.5	16.7	60.8	49.7	49.8	28.1	18.0	53.4	47.4	33.9	26.9	18.8
COV	0.54	1.62	1.07	0.93	1.11	0.56	1.24	0.94	0.70	0.81	0.76	0.95	0.97	0.64	0.55	0.78	0.76	0.72	0.71	0.74

MCEER Technical Reports

MCEER publishes technical reports on a variety of subjects written by authors funded through MCEER. These reports are available from both MCEER Publications and the National Technical Information Service (NTIS). Requests for reports should be directed to MCEER Publications, MCEER, University at Buffalo, State University of New York, Red Jacket Quadrangle, Buffalo, New York 14261. Reports can also be requested through NTIS, 5285 Port Royal Road, Springfield, Virginia 22161. NTIS accession numbers are shown in parenthesis, if available.

- NCEER-87-0001 "First-Year Program in Research, Education and Technology Transfer," 3/5/87, (PB88-134275, A04, MF-A01).
- NCEER-87-0002 "Experimental Evaluation of Instantaneous Optimal Algorithms for Structural Control," by R.C. Lin, T.T. Soong and A.M. Reinhorn, 4/20/87, (PB88-134341, A04, MF-A01).
- NCEER-87-0003 "Experimentation Using the Earthquake Simulation Facilities at University at Buffalo," by A.M. Reinhorn and R.L. Ketter, to be published.
- NCEER-87-0004 "The System Characteristics and Performance of a Shaking Table," by J.S. Hwang, K.C. Chang and G.C. Lee, 6/1/87, (PB88-134259, A03, MF-A01). This report is available only through NTIS (see address given above).
- NCEER-87-0005 "A Finite Element Formulation for Nonlinear Viscoplastic Material Using a Q Model," by O. Gyebe and G. Dasgupta, 11/2/87, (PB88-213764, A08, MF-A01).
- NCEER-87-0006 "Symbolic Manipulation Program (SMP) - Algebraic Codes for Two and Three Dimensional Finite Element Formulations," by X. Lee and G. Dasgupta, 11/9/87, (PB88-218522, A05, MF-A01).
- NCEER-87-0007 "Instantaneous Optimal Control Laws for Tall Buildings Under Seismic Excitations," by J.N. Yang, A. Akbarpour and P. Ghaemmaghami, 6/10/87, (PB88-134333, A06, MF-A01). This report is only available through NTIS (see address given above).
- NCEER-87-0008 "IDARC: Inelastic Damage Analysis of Reinforced Concrete Frame - Shear-Wall Structures," by Y.J. Park, A.M. Reinhorn and S.K. Kunnath, 7/20/87, (PB88-134325, A09, MF-A01). This report is only available through NTIS (see address given above).
- NCEER-87-0009 "Liquefaction Potential for New York State: A Preliminary Report on Sites in Manhattan and Buffalo," by M. Budhu, V. Vijayakumar, R.F. Giese and L. Baumgras, 8/31/87, (PB88-163704, A03, MF-A01). This report is available only through NTIS (see address given above).
- NCEER-87-0010 "Vertical and Torsional Vibration of Foundations in Inhomogeneous Media," by A.S. Veletsos and K.W. Dotson, 6/1/87, (PB88-134291, A03, MF-A01). This report is only available through NTIS (see address given above).
- NCEER-87-0011 "Seismic Probabilistic Risk Assessment and Seismic Margins Studies for Nuclear Power Plants," by Howard H.M. Hwang, 6/15/87, (PB88-134267, A03, MF-A01). This report is only available through NTIS (see address given above).
- NCEER-87-0012 "Parametric Studies of Frequency Response of Secondary Systems Under Ground-Acceleration Excitations," by Y. Yong and Y.K. Lin, 6/10/87, (PB88-134309, A03, MF-A01). This report is only available through NTIS (see address given above).
- NCEER-87-0013 "Frequency Response of Secondary Systems Under Seismic Excitation," by J.A. HoLung, J. Cai and Y.K. Lin, 7/31/87, (PB88-134317, A05, MF-A01). This report is only available through NTIS (see address given above).
- NCEER-87-0014 "Modelling Earthquake Ground Motions in Seismically Active Regions Using Parametric Time Series Methods," by G.W. Ellis and A.S. Cakmak, 8/25/87, (PB88-134283, A08, MF-A01). This report is only available through NTIS (see address given above).
- NCEER-87-0015 "Detection and Assessment of Seismic Structural Damage," by E. DiPasquale and A.S. Cakmak, 8/25/87, (PB88-163712, A05, MF-A01). This report is only available through NTIS (see address given above).

- NCEER-87-0016 "Pipeline Experiment at Parkfield, California," by J. Isenberg and E. Richardson, 9/15/87, (PB88-163720, A03, MF-A01). This report is available only through NTIS (see address given above).
- NCEER-87-0017 "Digital Simulation of Seismic Ground Motion," by M. Shinozuka, G. Deodatis and T. Harada, 8/31/87, (PB88-155197, A04, MF-A01). This report is available only through NTIS (see address given above).
- NCEER-87-0018 "Practical Considerations for Structural Control: System Uncertainty, System Time Delay and Truncation of Small Control Forces," J.N. Yang and A. Akbarpour, 8/10/87, (PB88-163738, A08, MF-A01). This report is only available through NTIS (see address given above).
- NCEER-87-0019 "Modal Analysis of Nonclassically Damped Structural Systems Using Canonical Transformation," by J.N. Yang, S. Sarkani and F.X. Long, 9/27/87, (PB88-187851, A04, MF-A01).
- NCEER-87-0020 "A Nonstationary Solution in Random Vibration Theory," by J.R. Red-Horse and P.D. Spanos, 11/3/87, (PB88-163746, A03, MF-A01).
- NCEER-87-0021 "Horizontal Impedances for Radially Inhomogeneous Viscoelastic Soil Layers," by A.S. Veletsos and K.W. Dotson, 10/15/87, (PB88-150859, A04, MF-A01).
- NCEER-87-0022 "Seismic Damage Assessment of Reinforced Concrete Members," by Y.S. Chung, C. Meyer and M. Shinozuka, 10/9/87, (PB88-150867, A05, MF-A01). This report is available only through NTIS (see address given above).
- NCEER-87-0023 "Active Structural Control in Civil Engineering," by T.T. Soong, 11/11/87, (PB88-187778, A03, MF-A01).
- NCEER-87-0024 "Vertical and Torsional Impedances for Radially Inhomogeneous Viscoelastic Soil Layers," by K.W. Dotson and A.S. Veletsos, 12/87, (PB88-187786, A03, MF-A01).
- NCEER-87-0025 "Proceedings from the Symposium on Seismic Hazards, Ground Motions, Soil-Liquefaction and Engineering Practice in Eastern North America," October 20-22, 1987, edited by K.H. Jacob, 12/87, (PB88-188115, A23, MF-A01). This report is available only through NTIS (see address given above).
- NCEER-87-0026 "Report on the Whittier-Narrows, California, Earthquake of October 1, 1987," by J. Pantelic and A. Reinhorn, 11/87, (PB88-187752, A03, MF-A01). This report is available only through NTIS (see address given above).
- NCEER-87-0027 "Design of a Modular Program for Transient Nonlinear Analysis of Large 3-D Building Structures," by S. Srivastav and J.F. Abel, 12/30/87, (PB88-187950, A05, MF-A01). This report is only available through NTIS (see address given above).
- NCEER-87-0028 "Second-Year Program in Research, Education and Technology Transfer," 3/8/88, (PB88-219480, A04, MF-A01).
- NCEER-88-0001 "Workshop on Seismic Computer Analysis and Design of Buildings With Interactive Graphics," by W. McGuire, J.F. Abel and C.H. Conley, 1/18/88, (PB88-187760, A03, MF-A01). This report is only available through NTIS (see address given above).
- NCEER-88-0002 "Optimal Control of Nonlinear Flexible Structures," by J.N. Yang, F.X. Long and D. Wong, 1/22/88, (PB88-213772, A06, MF-A01).
- NCEER-88-0003 "Substructuring Techniques in the Time Domain for Primary-Secondary Structural Systems," by G.D. Manolis and G. Juhn, 2/10/88, (PB88-213780, A04, MF-A01).
- NCEER-88-0004 "Iterative Seismic Analysis of Primary-Secondary Systems," by A. Singhal, L.D. Lutes and P.D. Spanos, 2/23/88, (PB88-213798, A04, MF-A01).
- NCEER-88-0005 "Stochastic Finite Element Expansion for Random Media," by P.D. Spanos and R. Ghanem, 3/14/88, (PB88-213806, A03, MF-A01).

- NCEER-88-0006 "Combining Structural Optimization and Structural Control," by F.Y. Cheng and C.P. Pantelides, 1/10/88, (PB88-213814, A05, MF-A01).
- NCEER-88-0007 "Seismic Performance Assessment of Code-Designed Structures," by H.H-M. Hwang, J-W. Jaw and H-J. Shau, 3/20/88, (PB88-219423, A04, MF-A01). This report is only available through NTIS (see address given above).
- NCEER-88-0008 "Reliability Analysis of Code-Designed Structures Under Natural Hazards," by H.H-M. Hwang, H. Ushiba and M. Shinozuka, 2/29/88, (PB88-229471, A07, MF-A01). This report is only available through NTIS (see address given above).
- NCEER-88-0009 "Seismic Fragility Analysis of Shear Wall Structures," by J-W Jaw and H.H-M. Hwang, 4/30/88, (PB89-102867, A04, MF-A01).
- NCEER-88-0010 "Base Isolation of a Multi-Story Building Under a Harmonic Ground Motion - A Comparison of Performances of Various Systems," by F-G Fan, G. Ahmadi and I.G. Tadjbakhsh, 5/18/88, (PB89-122238, A06, MF-A01). This report is only available through NTIS (see address given above).
- NCEER-88-0011 "Seismic Floor Response Spectra for a Combined System by Green's Functions," by F.M. Lavelle, L.A. Bergman and P.D. Spanos, 5/1/88, (PB89-102875, A03, MF-A01).
- NCEER-88-0012 "A New Solution Technique for Randomly Excited Hysteretic Structures," by G.Q. Cai and Y.K. Lin, 5/16/88, (PB89-102883, A03, MF-A01).
- NCEER-88-0013 "A Study of Radiation Damping and Soil-Structure Interaction Effects in the Centrifuge," by K. Weissman, supervised by J.H. Prevost, 5/24/88, (PB89-144703, A06, MF-A01).
- NCEER-88-0014 "Parameter Identification and Implementation of a Kinematic Plasticity Model for Frictional Soils," by J.H. Prevost and D.V. Griffiths, to be published.
- NCEER-88-0015 "Two- and Three- Dimensional Dynamic Finite Element Analyses of the Long Valley Dam," by D.V. Griffiths and J.H. Prevost, 6/17/88, (PB89-144711, A04, MF-A01).
- NCEER-88-0016 "Damage Assessment of Reinforced Concrete Structures in Eastern United States," by A.M. Reinhorn, M.J. Seidel, S.K. Kunnath and Y.J. Park, 6/15/88, (PB89-122220, A04, MF-A01). This report is only available through NTIS (see address given above).
- NCEER-88-0017 "Dynamic Compliance of Vertically Loaded Strip Foundations in Multilayered Viscoelastic Soils," by S. Ahmad and A.S.M. Israil, 6/17/88, (PB89-102891, A04, MF-A01).
- NCEER-88-0018 "An Experimental Study of Seismic Structural Response With Added Viscoelastic Dampers," by R.C. Lin, Z. Liang, T.T. Soong and R.H. Zhang, 6/30/88, (PB89-122212, A05, MF-A01). This report is available only through NTIS (see address given above).
- NCEER-88-0019 "Experimental Investigation of Primary - Secondary System Interaction," by G.D. Manolis, G. Juhn and A.M. Reinhorn, 5/27/88, (PB89-122204, A04, MF-A01).
- NCEER-88-0020 "A Response Spectrum Approach For Analysis of Nonclassically Damped Structures," by J.N. Yang, S. Sarkani and F.X. Long, 4/22/88, (PB89-102909, A04, MF-A01).
- NCEER-88-0021 "Seismic Interaction of Structures and Soils: Stochastic Approach," by A.S. Veletsos and A.M. Prasad, 7/21/88, (PB89-122196, A04, MF-A01). This report is only available through NTIS (see address given above).
- NCEER-88-0022 "Identification of the Serviceability Limit State and Detection of Seismic Structural Damage," by E. DiPasquale and A.S. Cakmak, 6/15/88, (PB89-122188, A05, MF-A01). This report is available only through NTIS (see address given above).
- NCEER-88-0023 "Multi-Hazard Risk Analysis: Case of a Simple Offshore Structure," by B.K. Bhartia and E.H. Vanmarcke, 7/21/88, (PB89-145213, A05, MF-A01).

- NCEER-88-0024 "Automated Seismic Design of Reinforced Concrete Buildings," by Y.S. Chung, C. Meyer and M. Shinozuka, 7/5/88, (PB89-122170, A06, MF-A01). This report is available only through NTIS (see address given above).
- NCEER-88-0025 "Experimental Study of Active Control of MDOF Structures Under Seismic Excitations," by L.L. Chung, R.C. Lin, T.T. Soong and A.M. Reinhorn, 7/10/88, (PB89-122600, A04, MF-A01).
- NCEER-88-0026 "Earthquake Simulation Tests of a Low-Rise Metal Structure," by J.S. Hwang, K.C. Chang, G.C. Lee and R.L. Ketter, 8/1/88, (PB89-102917, A04, MF-A01).
- NCEER-88-0027 "Systems Study of Urban Response and Reconstruction Due to Catastrophic Earthquakes," by F. Kozin and H.K. Zhou, 9/22/88, (PB90-162348, A04, MF-A01).
- NCEER-88-0028 "Seismic Fragility Analysis of Plane Frame Structures," by H.H-M. Hwang and Y.K. Low, 7/31/88, (PB89-131445, A06, MF-A01).
- NCEER-88-0029 "Response Analysis of Stochastic Structures," by A. Kardara, C. Bucher and M. Shinozuka, 9/22/88, (PB89-174429, A04, MF-A01).
- NCEER-88-0030 "Nonnormal Accelerations Due to Yielding in a Primary Structure," by D.C.K. Chen and L.D. Lutes, 9/19/88, (PB89-131437, A04, MF-A01).
- NCEER-88-0031 "Design Approaches for Soil-Structure Interaction," by A.S. Veletsos, A.M. Prasad and Y. Tang, 12/30/88, (PB89-174437, A03, MF-A01). This report is available only through NTIS (see address given above).
- NCEER-88-0032 "A Re-evaluation of Design Spectra for Seismic Damage Control," by C.J. Turkstra and A.G. Tallin, 11/7/88, (PB89-145221, A05, MF-A01).
- NCEER-88-0033 "The Behavior and Design of Noncontact Lap Splices Subjected to Repeated Inelastic Tensile Loading," by V.E. Sagan, P. Gergely and R.N. White, 12/8/88, (PB89-163737, A08, MF-A01).
- NCEER-88-0034 "Seismic Response of Pile Foundations," by S.M. Mamoon, P.K. Banerjee and S. Ahmad, 11/1/88, (PB89-145239, A04, MF-A01).
- NCEER-88-0035 "Modeling of R/C Building Structures With Flexible Floor Diaphragms (IDARC2)," by A.M. Reinhorn, S.K. Kunnath and N. Panahshahi, 9/7/88, (PB89-207153, A07, MF-A01).
- NCEER-88-0036 "Solution of the Dam-Reservoir Interaction Problem Using a Combination of FEM, BEM with Particular Integrals, Modal Analysis, and Substructuring," by C-S. Tsai, G.C. Lee and R.L. Ketter, 12/31/88, (PB89-207146, A04, MF-A01).
- NCEER-88-0037 "Optimal Placement of Actuators for Structural Control," by F.Y. Cheng and C.P. Pantelides, 8/15/88, (PB89-162846, A05, MF-A01).
- NCEER-88-0038 "Teflon Bearings in Aseismic Base Isolation: Experimental Studies and Mathematical Modeling," by A. Mokha, M.C. Constantinou and A.M. Reinhorn, 12/5/88, (PB89-218457, A10, MF-A01). This report is available only through NTIS (see address given above).
- NCEER-88-0039 "Seismic Behavior of Flat Slab High-Rise Buildings in the New York City Area," by P. Weidlinger and M. Ettouney, 10/15/88, (PB90-145681, A04, MF-A01).
- NCEER-88-0040 "Evaluation of the Earthquake Resistance of Existing Buildings in New York City," by P. Weidlinger and M. Ettouney, 10/15/88, to be published.
- NCEER-88-0041 "Small-Scale Modeling Techniques for Reinforced Concrete Structures Subjected to Seismic Loads," by W. Kim, A. El-Attar and R.N. White, 11/22/88, (PB89-189625, A05, MF-A01).
- NCEER-88-0042 "Modeling Strong Ground Motion from Multiple Event Earthquakes," by G.W. Ellis and A.S. Cakmak, 10/15/88, (PB89-174445, A03, MF-A01).

- NCEER-88-0043 "Nonstationary Models of Seismic Ground Acceleration," by M. Grigoriu, S.E. Ruiz and E. Rosenblueth, 7/15/88, (PB89-189617, A04, MF-A01).
- NCEER-88-0044 "SARCF User's Guide: Seismic Analysis of Reinforced Concrete Frames," by Y.S. Chung, C. Meyer and M. Shinozuka, 11/9/88, (PB89-174452, A08, MF-A01).
- NCEER-88-0045 "First Expert Panel Meeting on Disaster Research and Planning," edited by J. Pantelic and J. Stoyke, 9/15/88, (PB89-174460, A05, MF-A01).
- NCEER-88-0046 "Preliminary Studies of the Effect of Degrading Infill Walls on the Nonlinear Seismic Response of Steel Frames," by C.Z. Chrysostomou, P. Gergely and J.F. Abel, 12/19/88, (PB89-208383, A05, MF-A01).
- NCEER-88-0047 "Reinforced Concrete Frame Component Testing Facility - Design, Construction, Instrumentation and Operation," by S.P. Pessiki, C. Conley, T. Bond, P. Gergely and R.N. White, 12/16/88, (PB89-174478, A04, MF-A01).
- NCEER-89-0001 "Effects of Protective Cushion and Soil Compliancy on the Response of Equipment Within a Seismically Excited Building," by J.A. HoLung, 2/16/89, (PB89-207179, A04, MF-A01).
- NCEER-89-0002 "Statistical Evaluation of Response Modification Factors for Reinforced Concrete Structures," by H.H-M. Hwang and J-W. Jaw, 2/17/89, (PB89-207187, A05, MF-A01).
- NCEER-89-0003 "Hysteretic Columns Under Random Excitation," by G-Q. Cai and Y.K. Lin, 1/9/89, (PB89-196513, A03, MF-A01).
- NCEER-89-0004 "Experimental Study of 'Elephant Foot Bulge' Instability of Thin-Walled Metal Tanks," by Z-H. Jia and R.L. Ketter, 2/22/89, (PB89-207195, A03, MF-A01).
- NCEER-89-0005 "Experiment on Performance of Buried Pipelines Across San Andreas Fault," by J. Isenberg, E. Richardson and T.D. O'Rourke, 3/10/89, (PB89-218440, A04, MF-A01). This report is available only through NTIS (see address given above).
- NCEER-89-0006 "A Knowledge-Based Approach to Structural Design of Earthquake-Resistant Buildings," by M. Subramani, P. Gergely, C.H. Conley, J.F. Abel and A.H. Zaghaw, 1/15/89, (PB89-218465, A06, MF-A01).
- NCEER-89-0007 "Liquefaction Hazards and Their Effects on Buried Pipelines," by T.D. O'Rourke and P.A. Lane, 2/1/89, (PB89-218481, A09, MF-A01).
- NCEER-89-0008 "Fundamentals of System Identification in Structural Dynamics," by H. Imai, C-B. Yun, O. Maruyama and M. Shinozuka, 1/26/89, (PB89-207211, A04, MF-A01).
- NCEER-89-0009 "Effects of the 1985 Michoacan Earthquake on Water Systems and Other Buried Lifelines in Mexico," by A.G. Ayala and M.J. O'Rourke, 3/8/89, (PB89-207229, A06, MF-A01).
- NCEER-89-R010 "NCEER Bibliography of Earthquake Education Materials," by K.E.K. Ross, Second Revision, 9/1/89, (PB90-125352, A05, MF-A01). This report is replaced by NCEER-92-0018.
- NCEER-89-0011 "Inelastic Three-Dimensional Response Analysis of Reinforced Concrete Building Structures (IDARC-3D), Part I - Modeling," by S.K. Kunnath and A.M. Reinhorn, 4/17/89, (PB90-114612, A07, MF-A01). This report is available only through NTIS (see address given above).
- NCEER-89-0012 "Recommended Modifications to ATC-14," by C.D. Poland and J.O. Malley, 4/12/89, (PB90-108648, A15, MF-A01).
- NCEER-89-0013 "Repair and Strengthening of Beam-to-Column Connections Subjected to Earthquake Loading," by M. Corazao and A.J. Durrani, 2/28/89, (PB90-109885, A06, MF-A01).
- NCEER-89-0014 "Program EXKAL2 for Identification of Structural Dynamic Systems," by O. Maruyama, C-B. Yun, M. Hoshiya and M. Shinozuka, 5/19/89, (PB90-109877, A09, MF-A01).

- NCEER-89-0015 "Response of Frames With Bolted Semi-Rigid Connections, Part I - Experimental Study and Analytical Predictions," by P.J. DiCorso, A.M. Reinhorn, J.R. Dickerson, J.B. Radzinski and W.L. Harper, 6/1/89, to be published.
- NCEER-89-0016 "ARMA Monte Carlo Simulation in Probabilistic Structural Analysis," by P.D. Spanos and M.P. Mignolet, 7/10/89, (PB90-109893, A03, MF-A01).
- NCEER-89-P017 "Preliminary Proceedings from the Conference on Disaster Preparedness - The Place of Earthquake Education in Our Schools," Edited by K.E.K. Ross, 6/23/89, (PB90-108606, A03, MF-A01).
- NCEER-89-0017 "Proceedings from the Conference on Disaster Preparedness - The Place of Earthquake Education in Our Schools," Edited by K.E.K. Ross, 12/31/89, (PB90-207895, A012, MF-A02). This report is available only through NTIS (see address given above).
- NCEER-89-0018 "Multidimensional Models of Hysteretic Material Behavior for Vibration Analysis of Shape Memory Energy Absorbing Devices, by E.J. Graesser and F.A. Cozzarelli, 6/7/89, (PB90-164146, A04, MF-A01).
- NCEER-89-0019 "Nonlinear Dynamic Analysis of Three-Dimensional Base Isolated Structures (3D-BASIS)," by S. Nagarajaiah, A.M. Reinhorn and M.C. Constantinou, 8/3/89, (PB90-161936, A06, MF-A01). This report has been replaced by NCEER-93-0011.
- NCEER-89-0020 "Structural Control Considering Time-Rate of Control Forces and Control Rate Constraints," by F.Y. Cheng and C.P. Pantelides, 8/3/89, (PB90-120445, A04, MF-A01).
- NCEER-89-0021 "Subsurface Conditions of Memphis and Shelby County," by K.W. Ng, T-S. Chang and H-H.M. Hwang, 7/26/89, (PB90-120437, A03, MF-A01).
- NCEER-89-0022 "Seismic Wave Propagation Effects on Straight Jointed Buried Pipelines," by K. Elhmadi and M.J. O'Rourke, 8/24/89, (PB90-162322, A10, MF-A02).
- NCEER-89-0023 "Workshop on Serviceability Analysis of Water Delivery Systems," edited by M. Grigoriu, 3/6/89, (PB90-127424, A03, MF-A01).
- NCEER-89-0024 "Shaking Table Study of a 1/5 Scale Steel Frame Composed of Tapered Members," by K.C. Chang, J.S. Hwang and G.C. Lee, 9/18/89, (PB90-160169, A04, MF-A01).
- NCEER-89-0025 "DYNA1D: A Computer Program for Nonlinear Seismic Site Response Analysis - Technical Documentation," by Jean H. Prevost, 9/14/89, (PB90-161944, A07, MF-A01). This report is available only through NTIS (see address given above).
- NCEER-89-0026 "1:4 Scale Model Studies of Active Tendon Systems and Active Mass Dampers for Aseismic Protection," by A.M. Reinhorn, T.T. Soong, R.C. Lin, Y.P. Yang, Y. Fukao, H. Abe and M. Nakai, 9/15/89, (PB90-173246, A10, MF-A02). This report is available only through NTIS (see address given above).
- NCEER-89-0027 "Scattering of Waves by Inclusions in a Nonhomogeneous Elastic Half Space Solved by Boundary Element Methods," by P.K. Hadley, A. Askar and A.S. Cakmak, 6/15/89, (PB90-145699, A07, MF-A01).
- NCEER-89-0028 "Statistical Evaluation of Deflection Amplification Factors for Reinforced Concrete Structures," by H.H.M. Hwang, J-W. Jaw and A.L. Ch'ng, 8/31/89, (PB90-164633, A05, MF-A01).
- NCEER-89-0029 "Bedrock Accelerations in Memphis Area Due to Large New Madrid Earthquakes," by H.H.M. Hwang, C.H.S. Chen and G. Yu, 11/7/89, (PB90-162330, A04, MF-A01).
- NCEER-89-0030 "Seismic Behavior and Response Sensitivity of Secondary Structural Systems," by Y.Q. Chen and T.T. Soong, 10/23/89, (PB90-164658, A08, MF-A01).
- NCEER-89-0031 "Random Vibration and Reliability Analysis of Primary-Secondary Structural Systems," by Y. Ibrahim, M. Grigoriu and T.T. Soong, 11/10/89, (PB90-161951, A04, MF-A01).

- NCEER-89-0032 "Proceedings from the Second U.S. - Japan Workshop on Liquefaction, Large Ground Deformation and Their Effects on Lifelines, September 26-29, 1989," Edited by T.D. O'Rourke and M. Hamada, 12/1/89, (PB90-209388, A22, MF-A03).
- NCEER-89-0033 "Deterministic Model for Seismic Damage Evaluation of Reinforced Concrete Structures," by J.M. Bracci, A.M. Reinhorn, J.B. Mander and S.K. Kunnath, 9/27/89, (PB91-108803, A06, MF-A01).
- NCEER-89-0034 "On the Relation Between Local and Global Damage Indices," by E. DiPasquale and A.S. Cakmak, 8/15/89, (PB90-173865, A05, MF-A01).
- NCEER-89-0035 "Cyclic Undrained Behavior of Nonplastic and Low Plasticity Silts," by A.J. Walker and H.E. Stewart, 7/26/89, (PB90-183518, A10, MF-A01).
- NCEER-89-0036 "Liquefaction Potential of Surficial Deposits in the City of Buffalo, New York," by M. Budhu, R. Giese and L. Baumgrass, 1/17/89, (PB90-208455, A04, MF-A01).
- NCEER-89-0037 "A Deterministic Assessment of Effects of Ground Motion Incoherence," by A.S. Veletsos and Y. Tang, 7/15/89, (PB90-164294, A03, MF-A01).
- NCEER-89-0038 "Workshop on Ground Motion Parameters for Seismic Hazard Mapping," July 17-18, 1989, edited by R.V. Whitman, 12/1/89, (PB90-173923, A04, MF-A01).
- NCEER-89-0039 "Seismic Effects on Elevated Transit Lines of the New York City Transit Authority," by C.J. Costantino, C.A. Miller and E. Heymsfield, 12/26/89, (PB90-207887, A06, MF-A01).
- NCEER-89-0040 "Centrifugal Modeling of Dynamic Soil-Structure Interaction," by K. Weissman, Supervised by J.H. Prevost, 5/10/89, (PB90-207879, A07, MF-A01).
- NCEER-89-0041 "Linearized Identification of Buildings With Cores for Seismic Vulnerability Assessment," by I-K. Ho and A.E. Aktan, 11/1/89, (PB90-251943, A07, MF-A01).
- NCEER-90-0001 "Geotechnical and Lifeline Aspects of the October 17, 1989 Loma Prieta Earthquake in San Francisco," by T.D. O'Rourke, H.E. Stewart, F.T. Blackburn and T.S. Dickerman, 1/90, (PB90-208596, A05, MF-A01).
- NCEER-90-0002 "Nonnormal Secondary Response Due to Yielding in a Primary Structure," by D.C.K. Chen and L.D. Lutes, 2/28/90, (PB90-251976, A07, MF-A01).
- NCEER-90-0003 "Earthquake Education Materials for Grades K-12," by K.E.K. Ross, 4/16/90, (PB91-251984, A05, MF-A05). This report has been replaced by NCEER-92-0018.
- NCEER-90-0004 "Catalog of Strong Motion Stations in Eastern North America," by R.W. Busby, 4/3/90, (PB90-251984, A05, MF-A01).
- NCEER-90-0005 "NCEER Strong-Motion Data Base: A User Manual for the GeoBase Release (Version 1.0 for the Sun3)," by P. Friberg and K. Jacob, 3/31/90 (PB90-258062, A04, MF-A01).
- NCEER-90-0006 "Seismic Hazard Along a Crude Oil Pipeline in the Event of an 1811-1812 Type New Madrid Earthquake," by H.H.M. Hwang and C-H.S. Chen, 4/16/90, (PB90-258054, A04, MF-A01).
- NCEER-90-0007 "Site-Specific Response Spectra for Memphis Sheahan Pumping Station," by H.H.M. Hwang and C.S. Lee, 5/15/90, (PB91-108811, A05, MF-A01).
- NCEER-90-0008 "Pilot Study on Seismic Vulnerability of Crude Oil Transmission Systems," by T. Ariman, R. Dobry, M. Grigoriu, F. Kozin, M. O'Rourke, T. O'Rourke and M. Shinozuka, 5/25/90, (PB91-108837, A06, MF-A01).
- NCEER-90-0009 "A Program to Generate Site Dependent Time Histories: EQGEN," by G.W. Ellis, M. Srinivasan and A.S. Cakmak, 1/30/90, (PB91-108829, A04, MF-A01).
- NCEER-90-0010 "Active Isolation for Seismic Protection of Operating Rooms," by M.E. Talbott, Supervised by M. Shinozuka, 6/8/9, (PB91-110205, A05, MF-A01).

- NCEER-90-0011 "Program LINEARID for Identification of Linear Structural Dynamic Systems," by C-B. Yun and M. Shinozuka, 6/25/90, (PB91-110312, A08, MF-A01).
- NCEER-90-0012 "Two-Dimensional Two-Phase Elasto-Plastic Seismic Response of Earth Dams," by A.N. Yiagos, Supervised by J.H. Prevost, 6/20/90, (PB91-110197, A13, MF-A02).
- NCEER-90-0013 "Secondary Systems in Base-Isolated Structures: Experimental Investigation, Stochastic Response and Stochastic Sensitivity," by G.D. Manolis, G. Juhn, M.C. Constantinou and A.M. Reinhorn, 7/1/90, (PB91-110320, A08, MF-A01).
- NCEER-90-0014 "Seismic Behavior of Lightly-Reinforced Concrete Column and Beam-Column Joint Details," by S.P. Pessiki, C.H. Conley, P. Gergely and R.N. White, 8/22/90, (PB91-108795, A11, MF-A02).
- NCEER-90-0015 "Two Hybrid Control Systems for Building Structures Under Strong Earthquakes," by J.N. Yang and A. Daniellians, 6/29/90, (PB91-125393, A04, MF-A01).
- NCEER-90-0016 "Instantaneous Optimal Control with Acceleration and Velocity Feedback," by J.N. Yang and Z. Li, 6/29/90, (PB91-125401, A03, MF-A01).
- NCEER-90-0017 "Reconnaissance Report on the Northern Iran Earthquake of June 21, 1990," by M. Mehrain, 10/4/90, (PB91-125377, A03, MF-A01).
- NCEER-90-0018 "Evaluation of Liquefaction Potential in Memphis and Shelby County," by T.S. Chang, P.S. Tang, C.S. Lee and H. Hwang, 8/10/90, (PB91-125427, A09, MF-A01).
- NCEER-90-0019 "Experimental and Analytical Study of a Combined Sliding Disc Bearing and Helical Steel Spring Isolation System," by M.C. Constantinou, A.S. Mokha and A.M. Reinhorn, 10/4/90, (PB91-125385, A06, MF-A01). This report is available only through NTIS (see address given above).
- NCEER-90-0020 "Experimental Study and Analytical Prediction of Earthquake Response of a Sliding Isolation System with a Spherical Surface," by A.S. Mokha, M.C. Constantinou and A.M. Reinhorn, 10/11/90, (PB91-125419, A05, MF-A01).
- NCEER-90-0021 "Dynamic Interaction Factors for Floating Pile Groups," by G. Gazetas, K. Fan, A. Kaynia and E. Kausel, 9/10/90, (PB91-170381, A05, MF-A01).
- NCEER-90-0022 "Evaluation of Seismic Damage Indices for Reinforced Concrete Structures," by S. Rodriguez-Gomez and A.S. Cakmak, 9/30/90, PB91-171322, A06, MF-A01).
- NCEER-90-0023 "Study of Site Response at a Selected Memphis Site," by H. Desai, S. Ahmad, E.S. Gazetas and M.R. Oh, 10/11/90, (PB91-196857, A03, MF-A01).
- NCEER-90-0024 "A User's Guide to Strongmo: Version 1.0 of NCEER's Strong-Motion Data Access Tool for PCs and Terminals," by P.A. Friberg and C.A.T. Susch, 11/15/90, (PB91-171272, A03, MF-A01).
- NCEER-90-0025 "A Three-Dimensional Analytical Study of Spatial Variability of Seismic Ground Motions," by L-L. Hong and A.H.-S. Ang, 10/30/90, (PB91-170399, A09, MF-A01).
- NCEER-90-0026 "MUMOID User's Guide - A Program for the Identification of Modal Parameters," by S. Rodriguez-Gomez and E. DiPasquale, 9/30/90, (PB91-171298, A04, MF-A01).
- NCEER-90-0027 "SARCF-II User's Guide - Seismic Analysis of Reinforced Concrete Frames," by S. Rodriguez-Gomez, Y.S. Chung and C. Meyer, 9/30/90, (PB91-171280, A05, MF-A01).
- NCEER-90-0028 "Viscous Dampers: Testing, Modeling and Application in Vibration and Seismic Isolation," by N. Makris and M.C. Constantinou, 12/20/90 (PB91-190561, A06, MF-A01).
- NCEER-90-0029 "Soil Effects on Earthquake Ground Motions in the Memphis Area," by H. Hwang, C.S. Lee, K.W. Ng and T.S. Chang, 8/2/90, (PB91-190751, A05, MF-A01).

- NCEER-91-0001 "Proceedings from the Third Japan-U.S. Workshop on Earthquake Resistant Design of Lifeline Facilities and Countermeasures for Soil Liquefaction, December 17-19, 1990," edited by T.D. O'Rourke and M. Hamada, 2/1/91, (PB91-179259, A99, MF-A04).
- NCEER-91-0002 "Physical Space Solutions of Non-Proportionally Damped Systems," by M. Tong, Z. Liang and G.C. Lee, 1/15/91, (PB91-179242, A04, MF-A01).
- NCEER-91-0003 "Seismic Response of Single Piles and Pile Groups," by K. Fan and G. Gazetas, 1/10/91, (PB92-174994, A04, MF-A01).
- NCEER-91-0004 "Damping of Structures: Part 1 - Theory of Complex Damping," by Z. Liang and G. Lee, 10/10/91, (PB92-197235, A12, MF-A03).
- NCEER-91-0005 "3D-BASIS - Nonlinear Dynamic Analysis of Three Dimensional Base Isolated Structures: Part II," by S. Nagarajaiah, A.M. Reinhorn and M.C. Constantinou, 2/28/91, (PB91-190553, A07, MF-A01). This report has been replaced by NCEER-93-0011.
- NCEER-91-0006 "A Multidimensional Hysteretic Model for Plasticity Deforming Metals in Energy Absorbing Devices," by E.J. Graesser and F.A. Cozzarelli, 4/9/91, (PB92-108364, A04, MF-A01).
- NCEER-91-0007 "A Framework for Customizable Knowledge-Based Expert Systems with an Application to a KBES for Evaluating the Seismic Resistance of Existing Buildings," by E.G. Ibarra-Anaya and S.J. Fennes, 4/9/91, (PB91-210930, A08, MF-A01).
- NCEER-91-0008 "Nonlinear Analysis of Steel Frames with Semi-Rigid Connections Using the Capacity Spectrum Method," by G.G. Deierlein, S-H. Hsieh, Y-J. Shen and J.F. Abel, 7/2/91, (PB92-113828, A05, MF-A01).
- NCEER-91-0009 "Earthquake Education Materials for Grades K-12," by K.E.K. Ross, 4/30/91, (PB91-212142, A06, MF-A01). This report has been replaced by NCEER-92-0018.
- NCEER-91-0010 "Phase Wave Velocities and Displacement Phase Differences in a Harmonically Oscillating Pile," by N. Makris and G. Gazetas, 7/8/91, (PB92-108356, A04, MF-A01).
- NCEER-91-0011 "Dynamic Characteristics of a Full-Size Five-Story Steel Structure and a 2/5 Scale Model," by K.C. Chang, G.C. Yao, G.C. Lee, D.S. Hao and Y.C. Yeh," 7/2/91, (PB93-116648, A06, MF-A02).
- NCEER-91-0012 "Seismic Response of a 2/5 Scale Steel Structure with Added Viscoelastic Dampers," by K.C. Chang, T.T. Soong, S-T. Oh and M.L. Lai, 5/17/91, (PB92-110816, A05, MF-A01).
- NCEER-91-0013 "Earthquake Response of Retaining Walls; Full-Scale Testing and Computational Modeling," by S. Alampalli and A-W.M. Elgamal, 6/20/91, to be published.
- NCEER-91-0014 "3D-BASIS-M: Nonlinear Dynamic Analysis of Multiple Building Base Isolated Structures," by P.C. Tsopelas, S. Nagarajaiah, M.C. Constantinou and A.M. Reinhorn, 5/28/91, (PB92-113885, A09, MF-A02).
- NCEER-91-0015 "Evaluation of SEAOC Design Requirements for Sliding Isolated Structures," by D. Theodossiou and M.C. Constantinou, 6/10/91, (PB92-114602, A11, MF-A03).
- NCEER-91-0016 "Closed-Loop Modal Testing of a 27-Story Reinforced Concrete Flat Plate-Core Building," by H.R. Somaprasad, T. Toksoy, H. Yoshiyuki and A.E. Aktan, 7/15/91, (PB92-129980, A07, MF-A02).
- NCEER-91-0017 "Shake Table Test of a 1/6 Scale Two-Story Lightly Reinforced Concrete Building," by A.G. El-Attar, R.N. White and P. Gergely, 2/28/91, (PB92-222447, A06, MF-A02).
- NCEER-91-0018 "Shake Table Test of a 1/8 Scale Three-Story Lightly Reinforced Concrete Building," by A.G. El-Attar, R.N. White and P. Gergely, 2/28/91, (PB93-116630, A08, MF-A02).
- NCEER-91-0019 "Transfer Functions for Rigid Rectangular Foundations," by A.S. Veletsos, A.M. Prasad and W.H. Wu, 7/31/91, to be published.

- NCEER-91-0020 "Hybrid Control of Seismic-Excited Nonlinear and Inelastic Structural Systems," by J.N. Yang, Z. Li and A. Daniellians, 8/1/91, (PB92-143171, A06, MF-A02).
- NCEER-91-0021 "The NCEER-91 Earthquake Catalog: Improved Intensity-Based Magnitudes and Recurrence Relations for U.S. Earthquakes East of New Madrid," by L. Seeber and J.G. Armbruster, 8/28/91, (PB92-176742, A06, MF-A02).
- NCEER-91-0022 "Proceedings from the Implementation of Earthquake Planning and Education in Schools: The Need for Change - The Roles of the Changemakers," by K.E.K. Ross and F. Winslow, 7/23/91, (PB92-129998, A12, MF-A03).
- NCEER-91-0023 "A Study of Reliability-Based Criteria for Seismic Design of Reinforced Concrete Frame Buildings," by H.H.M. Hwang and H-M. Hsu, 8/10/91, (PB92-140235, A09, MF-A02).
- NCEER-91-0024 "Experimental Verification of a Number of Structural System Identification Algorithms," by R.G. Ghanem, H. Gavin and M. Shinozuka, 9/18/91, (PB92-176577, A18, MF-A04).
- NCEER-91-0025 "Probabilistic Evaluation of Liquefaction Potential," by H.H.M. Hwang and C.S. Lee, 11/25/91, (PB92-143429, A05, MF-A01).
- NCEER-91-0026 "Instantaneous Optimal Control for Linear, Nonlinear and Hysteretic Structures - Stable Controllers," by J.N. Yang and Z. Li, 11/15/91, (PB92-163807, A04, MF-A01).
- NCEER-91-0027 "Experimental and Theoretical Study of a Sliding Isolation System for Bridges," by M.C. Constantinou, A. Kartoum, A.M. Reinhorn and P. Bradford, 11/15/91, (PB92-176973, A10, MF-A03).
- NCEER-92-0001 "Case Studies of Liquefaction and Lifeline Performance During Past Earthquakes, Volume 1: Japanese Case Studies," Edited by M. Hamada and T. O'Rourke, 2/17/92, (PB92-197243, A18, MF-A04).
- NCEER-92-0002 "Case Studies of Liquefaction and Lifeline Performance During Past Earthquakes, Volume 2: United States Case Studies," Edited by T. O'Rourke and M. Hamada, 2/17/92, (PB92-197250, A20, MF-A04).
- NCEER-92-0003 "Issues in Earthquake Education," Edited by K. Ross, 2/3/92, (PB92-222389, A07, MF-A02).
- NCEER-92-0004 "Proceedings from the First U.S. - Japan Workshop on Earthquake Protective Systems for Bridges," Edited by I.G. Buckle, 2/4/92, (PB94-142239, A99, MF-A06).
- NCEER-92-0005 "Seismic Ground Motion from a Haskell-Type Source in a Multiple-Layered Half-Space," A.P. Theoharis, G. Deodatis and M. Shinozuka, 1/2/92, to be published.
- NCEER-92-0006 "Proceedings from the Site Effects Workshop," Edited by R. Whitman, 2/29/92, (PB92-197201, A04, MF-A01).
- NCEER-92-0007 "Engineering Evaluation of Permanent Ground Deformations Due to Seismically-Induced Liquefaction," by M.H. Baziar, R. Dobry and A-W.M. Elgamel, 3/24/92, (PB92-222421, A13, MF-A03).
- NCEER-92-0008 "A Procedure for the Seismic Evaluation of Buildings in the Central and Eastern United States," by C.D. Poland and J.O. Malley, 4/2/92, (PB92-222439, A20, MF-A04).
- NCEER-92-0009 "Experimental and Analytical Study of a Hybrid Isolation System Using Friction Controllable Sliding Bearings," by M.Q. Feng, S. Fujii and M. Shinozuka, 5/15/92, (PB93-150282, A06, MF-A02).
- NCEER-92-0010 "Seismic Resistance of Slab-Column Connections in Existing Non-Ductile Flat-Plate Buildings," by A.J. Durrani and Y. Du, 5/18/92, (PB93-116812, A06, MF-A02).
- NCEER-92-0011 "The Hysteretic and Dynamic Behavior of Brick Masonry Walls Upgraded by Ferrocement Coatings Under Cyclic Loading and Strong Simulated Ground Motion," by H. Lee and S.P. Prawl, 5/11/92, to be published.
- NCEER-92-0012 "Study of Wire Rope Systems for Seismic Protection of Equipment in Buildings," by G.F. Demetriades, M.C. Constantinou and A.M. Reinhorn, 5/20/92, (PB93-116655, A08, MF-A02).

- NCEER-92-0013 "Shape Memory Structural Dampers: Material Properties, Design and Seismic Testing," by P.R. Witting and F.A. Cozzarelli, 5/26/92, (PB93-116663, A05, MF-A01).
- NCEER-92-0014 "Longitudinal Permanent Ground Deformation Effects on Buried Continuous Pipelines," by M.J. O'Rourke, and C. Nordberg, 6/15/92, (PB93-116671, A08, MF-A02).
- NCEER-92-0015 "A Simulation Method for Stationary Gaussian Random Functions Based on the Sampling Theorem," by M. Grigoriu and S. Balopoulou, 6/11/92, (PB93-127496, A05, MF-A01).
- NCEER-92-0016 "Gravity-Load-Designed Reinforced Concrete Buildings: Seismic Evaluation of Existing Construction and Detailing Strategies for Improved Seismic Resistance," by G.W. Hoffmann, S.K. Kunnath, A.M. Reinhorn and J.B. Mander, 7/15/92, (PB94-142007, A08, MF-A02).
- NCEER-92-0017 "Observations on Water System and Pipeline Performance in the Limón Area of Costa Rica Due to the April 22, 1991 Earthquake," by M. O'Rourke and D. Ballantyne, 6/30/92, (PB93-126811, A06, MF-A02).
- NCEER-92-0018 "Fourth Edition of Earthquake Education Materials for Grades K-12," Edited by K.E.K. Ross, 8/10/92, (PB93-114023, A07, MF-A02).
- NCEER-92-0019 "Proceedings from the Fourth Japan-U.S. Workshop on Earthquake Resistant Design of Lifeline Facilities and Countermeasures for Soil Liquefaction," Edited by M. Hamada and T.D. O'Rourke, 8/12/92, (PB93-163939, A99, MF-E11).
- NCEER-92-0020 "Active Bracing System: A Full Scale Implementation of Active Control," by A.M. Reinhorn, T.T. Soong, R.C. Lin, M.A. Riley, Y.P. Wang, S. Aizawa and M. Higashino, 8/14/92, (PB93-127512, A06, MF-A02).
- NCEER-92-0021 "Empirical Analysis of Horizontal Ground Displacement Generated by Liquefaction-Induced Lateral Spreads," by S.F. Bartlett and T.L. Youd, 8/17/92, (PB93-188241, A06, MF-A02).
- NCEER-92-0022 "IDARC Version 3.0: Inelastic Damage Analysis of Reinforced Concrete Structures," by S.K. Kunnath, A.M. Reinhorn and R.F. Lobo, 8/31/92, (PB93-227502, A07, MF-A02).
- NCEER-92-0023 "A Semi-Empirical Analysis of Strong-Motion Peaks in Terms of Seismic Source, Propagation Path and Local Site Conditions, by M. Kamiyama, M.J. O'Rourke and R. Flores-Berrones, 9/9/92, (PB93-150266, A08, MF-A02).
- NCEER-92-0024 "Seismic Behavior of Reinforced Concrete Frame Structures with Nonductile Details, Part I: Summary of Experimental Findings of Full Scale Beam-Column Joint Tests," by A. Beres, R.N. White and P. Gergely, 9/30/92, (PB93-227783, A05, MF-A01).
- NCEER-92-0025 "Experimental Results of Repaired and Retrofitted Beam-Column Joint Tests in Lightly Reinforced Concrete Frame Buildings," by A. Beres, S. El-Borgi, R.N. White and P. Gergely, 10/29/92, (PB93-227791, A05, MF-A01).
- NCEER-92-0026 "A Generalization of Optimal Control Theory: Linear and Nonlinear Structures," by J.N. Yang, Z. Li and S. Vongchavalitkul, 11/2/92, (PB93-188621, A05, MF-A01).
- NCEER-92-0027 "Seismic Resistance of Reinforced Concrete Frame Structures Designed Only for Gravity Loads: Part I - Design and Properties of a One-Third Scale Model Structure," by J.M. Bracci, A.M. Reinhorn and J.B. Mander, 12/1/92, (PB94-104502, A08, MF-A02).
- NCEER-92-0028 "Seismic Resistance of Reinforced Concrete Frame Structures Designed Only for Gravity Loads: Part II - Experimental Performance of Subassemblages," by L.E. Aycaardi, J.B. Mander and A.M. Reinhorn, 12/1/92, (PB94-104510, A08, MF-A02).
- NCEER-92-0029 "Seismic Resistance of Reinforced Concrete Frame Structures Designed Only for Gravity Loads: Part III - Experimental Performance and Analytical Study of a Structural Model," by J.M. Bracci, A.M. Reinhorn and J.B. Mander, 12/1/92, (PB93-227528, A09, MF-A01).

- NCEER-92-0030 "Evaluation of Seismic Retrofit of Reinforced Concrete Frame Structures: Part I - Experimental Performance of Retrofitted Subassemblages," by D. Choudhuri, J.B. Mander and A.M. Reinhorn, 12/8/92, (PB93-198307, A07, MF-A02).
- NCEER-92-0031 "Evaluation of Seismic Retrofit of Reinforced Concrete Frame Structures: Part II - Experimental Performance and Analytical Study of a Retrofitted Structural Model," by J.M. Bracci, A.M. Reinhorn and J.B. Mander, 12/8/92, (PB93-198315, A09, MF-A03).
- NCEER-92-0032 "Experimental and Analytical Investigation of Seismic Response of Structures with Supplemental Fluid Viscous Dampers," by M.C. Constantinou and M.D. Symans, 12/21/92, (PB93-191435, A10, MF-A03). This report is available only through NTIS (see address given above).
- NCEER-92-0033 "Reconnaissance Report on the Cairo, Egypt Earthquake of October 12, 1992," by M. Khater, 12/23/92, (PB93-188621, A03, MF-A01).
- NCEER-92-0034 "Low-Level Dynamic Characteristics of Four Tall Flat-Plate Buildings in New York City," by H. Gavin, S. Yuan, J. Grossman, E. Pekelis and K. Jacob, 12/28/92, (PB93-188217, A07, MF-A02).
- NCEER-93-0001 "An Experimental Study on the Seismic Performance of Brick-Infilled Steel Frames With and Without Retrofit," by J.B. Mander, B. Nair, K. Wojtkowski and J. Ma, 1/29/93, (PB93-227510, A07, MF-A02).
- NCEER-93-0002 "Social Accounting for Disaster Preparedness and Recovery Planning," by S. Cole, E. Pantoja and V. Razak, 2/22/93, (PB94-142114, A12, MF-A03).
- NCEER-93-0003 "Assessment of 1991 NEHRP Provisions for Nonstructural Components and Recommended Revisions," by T.T. Soong, G. Chen, Z. Wu, R-H. Zhang and M. Grigoriu, 3/1/93, (PB93-188639, A06, MF-A02).
- NCEER-93-0004 "Evaluation of Static and Response Spectrum Analysis Procedures of SEAOC/UBC for Seismic Isolated Structures," by C.W. Winters and M.C. Constantinou, 3/23/93, (PB93-198299, A10, MF-A03).
- NCEER-93-0005 "Earthquakes in the Northeast - Are We Ignoring the Hazard? A Workshop on Earthquake Science and Safety for Educators," edited by K.E.K. Ross, 4/2/93, (PB94-103066, A09, MF-A02).
- NCEER-93-0006 "Inelastic Response of Reinforced Concrete Structures with Viscoelastic Braces," by R.F. Lobo, J.M. Bracci, K.L. Shen, A.M. Reinhorn and T.T. Soong, 4/5/93, (PB93-227486, A05, MF-A02).
- NCEER-93-0007 "Seismic Testing of Installation Methods for Computers and Data Processing Equipment," by K. Kosar, T.T. Soong, K.L. Shen, J.A. HoLung and Y.K. Lin, 4/12/93, (PB93-198299, A07, MF-A02).
- NCEER-93-0008 "Retrofit of Reinforced Concrete Frames Using Added Dampers," by A. Reinhorn, M. Constantinou and C. Li, to be published.
- NCEER-93-0009 "Seismic Behavior and Design Guidelines for Steel Frame Structures with Added Viscoelastic Dampers," by K.C. Chang, M.L. Lai, T.T. Soong, D.S. Hao and Y.C. Yeh, 5/1/93, (PB94-141959, A07, MF-A02).
- NCEER-93-0010 "Seismic Performance of Shear-Critical Reinforced Concrete Bridge Piers," by J.B. Mander, S.M. Waheed, M.T.A. Chaudhary and S.S. Chen, 5/12/93, (PB93-227494, A08, MF-A02).
- NCEER-93-0011 "3D-BASIS-TABS: Computer Program for Nonlinear Dynamic Analysis of Three Dimensional Base Isolated Structures," by S. Nagarajaiah, C. Li, A.M. Reinhorn and M.C. Constantinou, 8/2/93, (PB94-141819, A09, MF-A02).
- NCEER-93-0012 "Effects of Hydrocarbon Spills from an Oil Pipeline Break on Ground Water," by O.J. Helweg and H.H.M. Hwang, 8/3/93, (PB94-141942, A06, MF-A02).
- NCEER-93-0013 "Simplified Procedures for Seismic Design of Nonstructural Components and Assessment of Current Code Provisions," by M.P. Singh, L.E. Suarez, E.E. Matheu and G.O. Maldonado, 8/4/93, (PB94-141827, A09, MF-A02).
- NCEER-93-0014 "An Energy Approach to Seismic Analysis and Design of Secondary Systems," by G. Chen and T.T. Soong, 8/6/93, (PB94-142767, A11, MF-A03).

- NCEER-93-0015 "Proceedings from School Sites: Becoming Prepared for Earthquakes - Commemorating the Third Anniversary of the Loma Prieta Earthquake," Edited by F.E. Winslow and K.E.K. Ross, 8/16/93, (PB94-154275, A16, MF-A02).
- NCEER-93-0016 "Reconnaissance Report of Damage to Historic Monuments in Cairo, Egypt Following the October 12, 1992 Dahshur Earthquake," by D. Sykora, D. Look, G. Croci, E. Karaesmen and E. Karaesmen, 8/19/93, (PB94-142221, A08, MF-A02).
- NCEER-93-0017 "The Island of Guam Earthquake of August 8, 1993," by S.W. Swan and S.K. Harris, 9/30/93, (PB94-141843, A04, MF-A01).
- NCEER-93-0018 "Engineering Aspects of the October 12, 1992 Egyptian Earthquake," by A.W. Elgamal, M. Amer, K. Adalier and A. Abul-Fadl, 10/7/93, (PB94-141983, A05, MF-A01).
- NCEER-93-0019 "Development of an Earthquake Motion Simulator and its Application in Dynamic Centrifuge Testing," by I. Krstelj, Supervised by J.H. Prevost, 10/23/93, (PB94-181773, A-10, MF-A03).
- NCEER-93-0020 "NCEER-Taisei Corporation Research Program on Sliding Seismic Isolation Systems for Bridges: Experimental and Analytical Study of a Friction Pendulum System (FPS)," by M.C. Constantinou, P. Tsopelas, Y-S. Kim and S. Okamoto, 11/1/93, (PB94-142775, A08, MF-A02).
- NCEER-93-0021 "Finite Element Modeling of Elastomeric Seismic Isolation Bearings," by L.J. Billings, Supervised by R. Shepherd, 11/8/93, to be published.
- NCEER-93-0022 "Seismic Vulnerability of Equipment in Critical Facilities: Life-Safety and Operational Consequences," by K. Porter, G.S. Johnson, M.M. Zadeh, C. Scawthorn and S. Eder, 11/24/93, (PB94-181765, A16, MF-A03).
- NCEER-93-0023 "Hokkaido Nansei-oki, Japan Earthquake of July 12, 1993, by P.I. Yanev and C.R. Scawthorn, 12/23/93, (PB94-181500, A07, MF-A01).
- NCEER-94-0001 "An Evaluation of Seismic Serviceability of Water Supply Networks with Application to the San Francisco Auxiliary Water Supply System," by I. Markov, Supervised by M. Grigoriu and T. O'Rourke, 1/21/94, (PB94-204013, A07, MF-A02).
- NCEER-94-0002 "NCEER-Taisei Corporation Research Program on Sliding Seismic Isolation Systems for Bridges: Experimental and Analytical Study of Systems Consisting of Sliding Bearings, Rubber Restoring Force Devices and Fluid Dampers," Volumes I and II, by P. Tsopelas, S. Okamoto, M.C. Constantinou, D. Ozaki and S. Fujii, 2/4/94, (PB94-181740, A09, MF-A02 and PB94-181757, A12, MF-A03).
- NCEER-94-0003 "A Markov Model for Local and Global Damage Indices in Seismic Analysis," by S. Rahman and M. Grigoriu, 2/18/94, (PB94-206000, A12, MF-A03).
- NCEER-94-0004 "Proceedings from the NCEER Workshop on Seismic Response of Masonry Infills," edited by D.P. Abrams, 3/1/94, (PB94-180783, A07, MF-A02).
- NCEER-94-0005 "The Northridge, California Earthquake of January 17, 1994: General Reconnaissance Report," edited by J.D. Goltz, 3/11/94, (PB94-193943, A10, MF-A03).
- NCEER-94-0006 "Seismic Energy Based Fatigue Damage Analysis of Bridge Columns: Part I - Evaluation of Seismic Capacity," by G.A. Chang and J.B. Mander, 3/14/94, (PB94-219185, A11, MF-A03).
- NCEER-94-0007 "Seismic Isolation of Multi-Story Frame Structures Using Spherical Sliding Isolation Systems," by T.M. Al-Hussaini, V.A. Zayas and M.C. Constantinou, 3/17/94, (PB94-193745, A09, MF-A02).
- NCEER-94-0008 "The Northridge, California Earthquake of January 17, 1994: Performance of Highway Bridges," edited by I.G. Buckle, 3/24/94, (PB94-193851, A06, MF-A02).
- NCEER-94-0009 "Proceedings of the Third U.S.-Japan Workshop on Earthquake Protective Systems for Bridges," edited by I.G. Buckle and I. Friedland, 3/31/94, (PB94-195815, A99, MF-A06).

- NCEER-94-0010 "3D-BASIS-ME: Computer Program for Nonlinear Dynamic Analysis of Seismically Isolated Single and Multiple Structures and Liquid Storage Tanks," by P.C. Tsopelas, M.C. Constantinou and A.M. Reinhorn, 4/12/94, (PB94-204922, A09, MF-A02).
- NCEER-94-0011 "The Northridge, California Earthquake of January 17, 1994: Performance of Gas Transmission Pipelines," by T.D. O'Rourke and M.C. Palmer, 5/16/94, (PB94-204989, A05, MF-A01).
- NCEER-94-0012 "Feasibility Study of Replacement Procedures and Earthquake Performance Related to Gas Transmission Pipelines," by T.D. O'Rourke and M.C. Palmer, 5/25/94, (PB94-206638, A09, MF-A02).
- NCEER-94-0013 "Seismic Energy Based Fatigue Damage Analysis of Bridge Columns: Part II - Evaluation of Seismic Demand," by G.A. Chang and J.B. Mander, 6/1/94, (PB95-18106, A08, MF-A02).
- NCEER-94-0014 "NCEER-Taisei Corporation Research Program on Sliding Seismic Isolation Systems for Bridges: Experimental and Analytical Study of a System Consisting of Sliding Bearings and Fluid Restoring Force/Damping Devices," by P. Tsopelas and M.C. Constantinou, 6/13/94, (PB94-219144, A10, MF-A03).
- NCEER-94-0015 "Generation of Hazard-Consistent Fragility Curves for Seismic Loss Estimation Studies," by H. Hwang and J-R. Huo, 6/14/94, (PB95-181996, A09, MF-A02).
- NCEER-94-0016 "Seismic Study of Building Frames with Added Energy-Absorbing Devices," by W.S. Pong, C.S. Tsai and G.C. Lee, 6/20/94, (PB94-219136, A10, A03).
- NCEER-94-0017 "Sliding Mode Control for Seismic-Excited Linear and Nonlinear Civil Engineering Structures," by J. Yang, J. Wu, A. Agrawal and Z. Li, 6/21/94, (PB95-138483, A06, MF-A02).
- NCEER-94-0018 "3D-BASIS-TABS Version 2.0: Computer Program for Nonlinear Dynamic Analysis of Three Dimensional Base Isolated Structures," by A.M. Reinhorn, S. Nagarajaiah, M.C. Constantinou, P. Tsopelas and R. Li, 6/22/94, (PB95-182176, A08, MF-A02).
- NCEER-94-0019 "Proceedings of the International Workshop on Civil Infrastructure Systems: Application of Intelligent Systems and Advanced Materials on Bridge Systems," Edited by G.C. Lee and K.C. Chang, 7/18/94, (PB95-252474, A20, MF-A04).
- NCEER-94-0020 "Study of Seismic Isolation Systems for Computer Floors," by V. Lambrou and M.C. Constantinou, 7/19/94, (PB95-138533, A10, MF-A03).
- NCEER-94-0021 "Proceedings of the U.S.-Italian Workshop on Guidelines for Seismic Evaluation and Rehabilitation of Unreinforced Masonry Buildings," Edited by D.P. Abrams and G.M. Calvi, 7/20/94, (PB95-138749, A13, MF-A03).
- NCEER-94-0022 "NCEER-Taisei Corporation Research Program on Sliding Seismic Isolation Systems for Bridges: Experimental and Analytical Study of a System Consisting of Lubricated PTFE Sliding Bearings and Mild Steel Dampers," by P. Tsopelas and M.C. Constantinou, 7/22/94, (PB95-182184, A08, MF-A02).
- NCEER-94-0023 "Development of Reliability-Based Design Criteria for Buildings Under Seismic Load," by Y.K. Wen, H. Hwang and M. Shinozuka, 8/1/94, (PB95-211934, A08, MF-A02).
- NCEER-94-0024 "Experimental Verification of Acceleration Feedback Control Strategies for an Active Tendon System," by S.J. Dyke, B.F. Spencer, Jr., P. Quast, M.K. Sain, D.C. Kaspari, Jr. and T.T. Soong, 8/29/94, (PB95-212320, A05, MF-A01).
- NCEER-94-0025 "Seismic Retrofitting Manual for Highway Bridges," Edited by I.G. Buckle and I.F. Friedland, published by the Federal Highway Administration (PB95-212676, A15, MF-A03).
- NCEER-94-0026 "Proceedings from the Fifth U.S.-Japan Workshop on Earthquake Resistant Design of Lifeline Facilities and Countermeasures Against Soil Liquefaction," Edited by T.D. O'Rourke and M. Hamada, 11/7/94, (PB95-220802, A99, MF-E08).

- NCEER-95-0001 “Experimental and Analytical Investigation of Seismic Retrofit of Structures with Supplemental Damping: Part 1 - Fluid Viscous Damping Devices,” by A.M. Reinhorn, C. Li and M.C. Constantinou, 1/3/95, (PB95-266599, A09, MF-A02).
- NCEER-95-0002 “Experimental and Analytical Study of Low-Cycle Fatigue Behavior of Semi-Rigid Top-And-Seat Angle Connections,” by G. Pekcan, J.B. Mander and S.S. Chen, 1/5/95, (PB95-220042, A07, MF-A02).
- NCEER-95-0003 “NCEER-ATC Joint Study on Fragility of Buildings,” by T. Anagnos, C. Rojahn and A.S. Kiremidjian, 1/20/95, (PB95-220026, A06, MF-A02).
- NCEER-95-0004 “Nonlinear Control Algorithms for Peak Response Reduction,” by Z. Wu, T.T. Soong, V. Gattulli and R.C. Lin, 2/16/95, (PB95-220349, A05, MF-A01).
- NCEER-95-0005 “Pipeline Replacement Feasibility Study: A Methodology for Minimizing Seismic and Corrosion Risks to Underground Natural Gas Pipelines,” by R.T. Eguchi, H.A. Seligson and D.G. Honegger, 3/2/95, (PB95-252326, A06, MF-A02).
- NCEER-95-0006 “Evaluation of Seismic Performance of an 11-Story Frame Building During the 1994 Northridge Earthquake,” by F. Naeim, R. DiSulio, K. Benuska, A. Reinhorn and C. Li, to be published.
- NCEER-95-0007 “Prioritization of Bridges for Seismic Retrofitting,” by N. Basöz and A.S. Kiremidjian, 4/24/95, (PB95-252300, A08, MF-A02).
- NCEER-95-0008 “Method for Developing Motion Damage Relationships for Reinforced Concrete Frames,” by A. Singhal and A.S. Kiremidjian, 5/11/95, (PB95-266607, A06, MF-A02).
- NCEER-95-0009 “Experimental and Analytical Investigation of Seismic Retrofit of Structures with Supplemental Damping: Part II - Friction Devices,” by C. Li and A.M. Reinhorn, 7/6/95, (PB96-128087, A11, MF-A03).
- NCEER-95-0010 “Experimental Performance and Analytical Study of a Non-Ductile Reinforced Concrete Frame Structure Retrofitted with Elastomeric Spring Dampers,” by G. Pekcan, J.B. Mander and S.S. Chen, 7/14/95, (PB96-137161, A08, MF-A02).
- NCEER-95-0011 “Development and Experimental Study of Semi-Active Fluid Damping Devices for Seismic Protection of Structures,” by M.D. Symans and M.C. Constantinou, 8/3/95, (PB96-136940, A23, MF-A04).
- NCEER-95-0012 “Real-Time Structural Parameter Modification (RSPM): Development of Innervated Structures,” by Z. Liang, M. Tong and G.C. Lee, 4/11/95, (PB96-137153, A06, MF-A01).
- NCEER-95-0013 “Experimental and Analytical Investigation of Seismic Retrofit of Structures with Supplemental Damping: Part III - Viscous Damping Walls,” by A.M. Reinhorn and C. Li, 10/1/95, (PB96-176409, A11, MF-A03).
- NCEER-95-0014 “Seismic Fragility Analysis of Equipment and Structures in a Memphis Electric Substation,” by J-R. Huo and H.H.M. Hwang, 8/10/95, (PB96-128087, A09, MF-A02).
- NCEER-95-0015 “The Hanshin-Awaji Earthquake of January 17, 1995: Performance of Lifelines,” Edited by M. Shinozuka, 11/3/95, (PB96-176383, A15, MF-A03).
- NCEER-95-0016 “Highway Culvert Performance During Earthquakes,” by T.L. Youd and C.J. Beckman, available as NCEER-96-0015.
- NCEER-95-0017 “The Hanshin-Awaji Earthquake of January 17, 1995: Performance of Highway Bridges,” Edited by I.G. Buckle, 12/1/95, to be published.
- NCEER-95-0018 “Modeling of Masonry Infill Panels for Structural Analysis,” by A.M. Reinhorn, A. Madan, R.E. Valles, Y. Reichmann and J.B. Mander, 12/8/95, (PB97-110886, MF-A01, A06).
- NCEER-95-0019 “Optimal Polynomial Control for Linear and Nonlinear Structures,” by A.K. Agrawal and J.N. Yang, 12/11/95, (PB96-168737, A07, MF-A02).

- NCEER-95-0020 "Retrofit of Non-Ductile Reinforced Concrete Frames Using Friction Dampers," by R.S. Rao, P. Gergely and R.N. White, 12/22/95, (PB97-133508, A10, MF-A02).
- NCEER-95-0021 "Parametric Results for Seismic Response of Pile-Supported Bridge Bents," by G. Mylonakis, A. Nikolaou and G. Gazetas, 12/22/95, (PB97-100242, A12, MF-A03).
- NCEER-95-0022 "Kinematic Bending Moments in Seismically Stressed Piles," by A. Nikolaou, G. Mylonakis and G. Gazetas, 12/23/95, (PB97-113914, MF-A03, A13).
- NCEER-96-0001 "Dynamic Response of Unreinforced Masonry Buildings with Flexible Diaphragms," by A.C. Costley and D.P. Abrams, 10/10/96, (PB97-133573, MF-A03, A15).
- NCEER-96-0002 "State of the Art Review: Foundations and Retaining Structures," by I. Po Lam, to be published.
- NCEER-96-0003 "Ductility of Rectangular Reinforced Concrete Bridge Columns with Moderate Confinement," by N. Wehbe, M. Saiidi, D. Sanders and B. Douglas, 11/7/96, (PB97-133557, A06, MF-A02).
- NCEER-96-0004 "Proceedings of the Long-Span Bridge Seismic Research Workshop," edited by I.G. Buckle and I.M. Friedland, to be published.
- NCEER-96-0005 "Establish Representative Pier Types for Comprehensive Study: Eastern United States," by J. Kulicki and Z. Prucz, 5/28/96, (PB98-119217, A07, MF-A02).
- NCEER-96-0006 "Establish Representative Pier Types for Comprehensive Study: Western United States," by R. Imbsen, R.A. Schamber and T.A. Osterkamp, 5/28/96, (PB98-118607, A07, MF-A02).
- NCEER-96-0007 "Nonlinear Control Techniques for Dynamical Systems with Uncertain Parameters," by R.G. Ghanem and M.I. Bujakov, 5/27/96, (PB97-100259, A17, MF-A03).
- NCEER-96-0008 "Seismic Evaluation of a 30-Year Old Non-Ductile Highway Bridge Pier and Its Retrofit," by J.B. Mander, B. Mahmoodzadegan, S. Bhadra and S.S. Chen, 5/31/96, (PB97-110902, MF-A03, A10).
- NCEER-96-0009 "Seismic Performance of a Model Reinforced Concrete Bridge Pier Before and After Retrofit," by J.B. Mander, J.H. Kim and C.A. Ligozio, 5/31/96, (PB97-110910, MF-A02, A10).
- NCEER-96-0010 "IDARC2D Version 4.0: A Computer Program for the Inelastic Damage Analysis of Buildings," by R.E. Valles, A.M. Reinhorn, S.K. Kunnath, C. Li and A. Madan, 6/3/96, (PB97-100234, A17, MF-A03).
- NCEER-96-0011 "Estimation of the Economic Impact of Multiple Lifeline Disruption: Memphis Light, Gas and Water Division Case Study," by S.E. Chang, H.A. Seligson and R.T. Eguchi, 8/16/96, (PB97-133490, A11, MF-A03).
- NCEER-96-0012 "Proceedings from the Sixth Japan-U.S. Workshop on Earthquake Resistant Design of Lifeline Facilities and Countermeasures Against Soil Liquefaction, Edited by M. Hamada and T. O'Rourke, 9/11/96, (PB97-133581, A99, MF-A06).
- NCEER-96-0013 "Chemical Hazards, Mitigation and Preparedness in Areas of High Seismic Risk: A Methodology for Estimating the Risk of Post-Earthquake Hazardous Materials Release," by H.A. Seligson, R.T. Eguchi, K.J. Tierney and K. Richmond, 11/7/96, (PB97-133565, MF-A02, A08).
- NCEER-96-0014 "Response of Steel Bridge Bearings to Reversed Cyclic Loading," by J.B. Mander, D-K. Kim, S.S. Chen and G.J. Premus, 11/13/96, (PB97-140735, A12, MF-A03).
- NCEER-96-0015 "Highway Culvert Performance During Past Earthquakes," by T.L. Youd and C.J. Beckman, 11/25/96, (PB97-133532, A06, MF-A01).
- NCEER-97-0001 "Evaluation, Prevention and Mitigation of Pounding Effects in Building Structures," by R.E. Valles and A.M. Reinhorn, 2/20/97, (PB97-159552, A14, MF-A03).
- NCEER-97-0002 "Seismic Design Criteria for Bridges and Other Highway Structures," by C. Rojahn, R. Mayes, D.G. Anderson, J. Clark, J.H. Hom, R.V. Nutt and M.J. O'Rourke, 4/30/97, (PB97-194658, A06, MF-A03).

- NCEER-97-0003 "Proceedings of the U.S.-Italian Workshop on Seismic Evaluation and Retrofit," Edited by D.P. Abrams and G.M. Calvi, 3/19/97, (PB97-194666, A13, MF-A03).
- NCEER-97-0004 "Investigation of Seismic Response of Buildings with Linear and Nonlinear Fluid Viscous Dampers," by A.A. Seleemah and M.C. Constantinou, 5/21/97, (PB98-109002, A15, MF-A03).
- NCEER-97-0005 "Proceedings of the Workshop on Earthquake Engineering Frontiers in Transportation Facilities," edited by G.C. Lee and I.M. Friedland, 8/29/97, (PB98-128911, A25, MR-A04).
- NCEER-97-0006 "Cumulative Seismic Damage of Reinforced Concrete Bridge Piers," by S.K. Kunnath, A. El-Bahy, A. Taylor and W. Stone, 9/2/97, (PB98-108814, A11, MF-A03).
- NCEER-97-0007 "Structural Details to Accommodate Seismic Movements of Highway Bridges and Retaining Walls," by R.A. Imbsen, R.A. Schamber, E. Thorkildsen, A. Kartoum, B.T. Martin, T.N. Rosser and J.M. Kulicki, 9/3/97, (PB98-108996, A09, MF-A02).
- NCEER-97-0008 "A Method for Earthquake Motion-Damage Relationships with Application to Reinforced Concrete Frames," by A. Singhal and A.S. Kiremidjian, 9/10/97, (PB98-108988, A13, MF-A03).
- NCEER-97-0009 "Seismic Analysis and Design of Bridge Abutments Considering Sliding and Rotation," by K. Fishman and R. Richards, Jr., 9/15/97, (PB98-108897, A06, MF-A02).
- NCEER-97-0010 "Proceedings of the FHWA/NCEER Workshop on the National Representation of Seismic Ground Motion for New and Existing Highway Facilities," edited by I.M. Friedland, M.S. Power and R.L. Mayes, 9/22/97, (PB98-128903, A21, MF-A04).
- NCEER-97-0011 "Seismic Analysis for Design or Retrofit of Gravity Bridge Abutments," by K.L. Fishman, R. Richards, Jr. and R.C. Divito, 10/2/97, (PB98-128937, A08, MF-A02).
- NCEER-97-0012 "Evaluation of Simplified Methods of Analysis for Yielding Structures," by P. Tsopelas, M.C. Constantinou, C.A. Kircher and A.S. Whittaker, 10/31/97, (PB98-128929, A10, MF-A03).
- NCEER-97-0013 "Seismic Design of Bridge Columns Based on Control and Repairability of Damage," by C-T. Cheng and J.B. Mander, 12/8/97, (PB98-144249, A11, MF-A03).
- NCEER-97-0014 "Seismic Resistance of Bridge Piers Based on Damage Avoidance Design," by J.B. Mander and C-T. Cheng, 12/10/97, (PB98-144223, A09, MF-A02).
- NCEER-97-0015 "Seismic Response of Nominally Symmetric Systems with Strength Uncertainty," by S. Balopoulou and M. Grigoriu, 12/23/97, (PB98-153422, A11, MF-A03).
- NCEER-97-0016 "Evaluation of Seismic Retrofit Methods for Reinforced Concrete Bridge Columns," by T.J. Wipf, F.W. Klaiber and F.M. Russo, 12/28/97, (PB98-144215, A12, MF-A03).
- NCEER-97-0017 "Seismic Fragility of Existing Conventional Reinforced Concrete Highway Bridges," by C.L. Mullen and A.S. Cakmak, 12/30/97, (PB98-153406, A08, MF-A02).
- NCEER-97-0018 "Loss Assessment of Memphis Buildings," edited by D.P. Abrams and M. Shinozuka, 12/31/97, (PB98-144231, A13, MF-A03).
- NCEER-97-0019 "Seismic Evaluation of Frames with Infill Walls Using Quasi-static Experiments," by K.M. Mosalam, R.N. White and P. Gergely, 12/31/97, (PB98-153455, A07, MF-A02).
- NCEER-97-0020 "Seismic Evaluation of Frames with Infill Walls Using Pseudo-dynamic Experiments," by K.M. Mosalam, R.N. White and P. Gergely, 12/31/97, (PB98-153430, A07, MF-A02).
- NCEER-97-0021 "Computational Strategies for Frames with Infill Walls: Discrete and Smeared Crack Analyses and Seismic Fragility," by K.M. Mosalam, R.N. White and P. Gergely, 12/31/97, (PB98-153414, A10, MF-A02).

- NCEER-97-0022 "Proceedings of the NCEER Workshop on Evaluation of Liquefaction Resistance of Soils," edited by T.L. Youd and I.M. Idriss, 12/31/97, (PB98-155617, A15, MF-A03).
- MCEER-98-0001 "Extraction of Nonlinear Hysteretic Properties of Seismically Isolated Bridges from Quick-Release Field Tests," by Q. Chen, B.M. Douglas, E.M. Maragakis and I.G. Buckle, 5/26/98, (PB99-118838, A06, MF-A01).
- MCEER-98-0002 "Methodologies for Evaluating the Importance of Highway Bridges," by A. Thomas, S. Eshenaur and J. Kulicki, 5/29/98, (PB99-118846, A10, MF-A02).
- MCEER-98-0003 "Capacity Design of Bridge Piers and the Analysis of Overstrength," by J.B. Mander, A. Dutta and P. Goel, 6/1/98, (PB99-118853, A09, MF-A02).
- MCEER-98-0004 "Evaluation of Bridge Damage Data from the Loma Prieta and Northridge, California Earthquakes," by N. Basoz and A. Kiremidjian, 6/2/98, (PB99-118861, A15, MF-A03).
- MCEER-98-0005 "Screening Guide for Rapid Assessment of Liquefaction Hazard at Highway Bridge Sites," by T. L. Youd, 6/16/98, (PB99-118879, A06, not available on microfiche).
- MCEER-98-0006 "Structural Steel and Steel/Concrete Interface Details for Bridges," by P. Ritchie, N. Kaulh and J. Kulicki, 7/13/98, (PB99-118945, A06, MF-A01).
- MCEER-98-0007 "Capacity Design and Fatigue Analysis of Confined Concrete Columns," by A. Dutta and J.B. Mander, 7/14/98, (PB99-118960, A14, MF-A03).
- MCEER-98-0008 "Proceedings of the Workshop on Performance Criteria for Telecommunication Services Under Earthquake Conditions," edited by A.J. Schiff, 7/15/98, (PB99-118952, A08, MF-A02).
- MCEER-98-0009 "Fatigue Analysis of Unconfined Concrete Columns," by J.B. Mander, A. Dutta and J.H. Kim, 9/12/98, (PB99-123655, A10, MF-A02).
- MCEER-98-0010 "Centrifuge Modeling of Cyclic Lateral Response of Pile-Cap Systems and Seat-Type Abutments in Dry Sands," by A.D. Gadre and R. Dobry, 10/2/98, (PB99-123606, A13, MF-A03).
- MCEER-98-0011 "IDARC-BRIDGE: A Computational Platform for Seismic Damage Assessment of Bridge Structures," by A.M. Reinhorn, V. Simeonov, G. Mylonakis and Y. Reichman, 10/2/98, (PB99-162919, A15, MF-A03).
- MCEER-98-0012 "Experimental Investigation of the Dynamic Response of Two Bridges Before and After Retrofitting with Elastomeric Bearings," by D.A. Wendichansky, S.S. Chen and J.B. Mander, 10/2/98, (PB99-162927, A15, MF-A03).
- MCEER-98-0013 "Design Procedures for Hinge Restrainers and Hinge Sear Width for Multiple-Frame Bridges," by R. Des Roches and G.L. Fenves, 11/3/98, (PB99-140477, A13, MF-A03).
- MCEER-98-0014 "Response Modification Factors for Seismically Isolated Bridges," by M.C. Constantinou and J.K. Quarshie, 11/3/98, (PB99-140485, A14, MF-A03).
- MCEER-98-0015 "Proceedings of the U.S.-Italy Workshop on Seismic Protective Systems for Bridges," edited by I.M. Friedland and M.C. Constantinou, 11/3/98, (PB2000-101711, A22, MF-A04).
- MCEER-98-0016 "Appropriate Seismic Reliability for Critical Equipment Systems: Recommendations Based on Regional Analysis of Financial and Life Loss," by K. Porter, C. Scawthorn, C. Taylor and N. Blais, 11/10/98, (PB99-157265, A08, MF-A02).
- MCEER-98-0017 "Proceedings of the U.S. Japan Joint Seminar on Civil Infrastructure Systems Research," edited by M. Shinozuka and A. Rose, 11/12/98, (PB99-156713, A16, MF-A03).
- MCEER-98-0018 "Modeling of Pile Footings and Drilled Shafts for Seismic Design," by I. PoLam, M. Kapuskar and D. Chaudhuri, 12/21/98, (PB99-157257, A09, MF-A02).

- MCEER-99-0001 "Seismic Evaluation of a Masonry Infilled Reinforced Concrete Frame by Pseudodynamic Testing," by S.G. Buonopane and R.N. White, 2/16/99, (PB99-162851, A09, MF-A02).
- MCEER-99-0002 "Response History Analysis of Structures with Seismic Isolation and Energy Dissipation Systems: Verification Examples for Program SAP2000," by J. Scheller and M.C. Constantinou, 2/22/99, (PB99-162869, A08, MF-A02).
- MCEER-99-0003 "Experimental Study on the Seismic Design and Retrofit of Bridge Columns Including Axial Load Effects," by A. Dutta, T. Kokorina and J.B. Mander, 2/22/99, (PB99-162877, A09, MF-A02).
- MCEER-99-0004 "Experimental Study of Bridge Elastomeric and Other Isolation and Energy Dissipation Systems with Emphasis on Uplift Prevention and High Velocity Near-source Seismic Excitation," by A. Kasalanati and M. C. Constantinou, 2/26/99, (PB99-162885, A12, MF-A03).
- MCEER-99-0005 "Truss Modeling of Reinforced Concrete Shear-flexure Behavior," by J.H. Kim and J.B. Mander, 3/8/99, (PB99-163693, A12, MF-A03).
- MCEER-99-0006 "Experimental Investigation and Computational Modeling of Seismic Response of a 1:4 Scale Model Steel Structure with a Load Balancing Supplemental Damping System," by G. Pekcan, J.B. Mander and S.S. Chen, 4/2/99, (PB99-162893, A11, MF-A03).
- MCEER-99-0007 "Effect of Vertical Ground Motions on the Structural Response of Highway Bridges," by M.R. Button, C.J. Cronin and R.L. Mayes, 4/10/99, (PB2000-101411, A10, MF-A03).
- MCEER-99-0008 "Seismic Reliability Assessment of Critical Facilities: A Handbook, Supporting Documentation, and Model Code Provisions," by G.S. Johnson, R.E. Sheppard, M.D. Quilici, S.J. Eder and C.R. Scawthorn, 4/12/99, (PB2000-101701, A18, MF-A04).
- MCEER-99-0009 "Impact Assessment of Selected MCEER Highway Project Research on the Seismic Design of Highway Structures," by C. Rojahn, R. Mayes, D.G. Anderson, J.H. Clark, D'Appolonia Engineering, S. Gloyd and R.V. Nutt, 4/14/99, (PB99-162901, A10, MF-A02).
- MCEER-99-0010 "Site Factors and Site Categories in Seismic Codes," by R. Dobry, R. Ramos and M.S. Power, 7/19/99, (PB2000-101705, A08, MF-A02).
- MCEER-99-0011 "Restrainer Design Procedures for Multi-Span Simply-Supported Bridges," by M.J. Randall, M. Saiidi, E. Maragakis and T. Isakovic, 7/20/99, (PB2000-101702, A10, MF-A02).
- MCEER-99-0012 "Property Modification Factors for Seismic Isolation Bearings," by M.C. Constantinou, P. Tsopelas, A. Kasalanati and E. Wolff, 7/20/99, (PB2000-103387, A11, MF-A03).
- MCEER-99-0013 "Critical Seismic Issues for Existing Steel Bridges," by P. Ritchie, N. Kauh and J. Kulicki, 7/20/99, (PB2000-101697, A09, MF-A02).
- MCEER-99-0014 "Nonstructural Damage Database," by A. Kao, T.T. Soong and A. Vender, 7/24/99, (PB2000-101407, A06, MF-A01).
- MCEER-99-0015 "Guide to Remedial Measures for Liquefaction Mitigation at Existing Highway Bridge Sites," by H.G. Cooke and J. K. Mitchell, 7/26/99, (PB2000-101703, A11, MF-A03).
- MCEER-99-0016 "Proceedings of the MCEER Workshop on Ground Motion Methodologies for the Eastern United States," edited by N. Abrahamson and A. Becker, 8/11/99, (PB2000-103385, A07, MF-A02).
- MCEER-99-0017 "Quindío, Colombia Earthquake of January 25, 1999: Reconnaissance Report," by A.P. Asfura and P.J. Flores, 10/4/99, (PB2000-106893, A06, MF-A01).
- MCEER-99-0018 "Hysteretic Models for Cyclic Behavior of Deteriorating Inelastic Structures," by M.V. Sivaselvan and A.M. Reinhorn, 11/5/99, (PB2000-103386, A08, MF-A02).

- MCEER-99-0019 "Proceedings of the 7th U.S.- Japan Workshop on Earthquake Resistant Design of Lifeline Facilities and Countermeasures Against Soil Liquefaction," edited by T.D. O'Rourke, J.P. Bardet and M. Hamada, 11/19/99, (PB2000-103354, A99, MF-A06).
- MCEER-99-0020 "Development of Measurement Capability for Micro-Vibration Evaluations with Application to Chip Fabrication Facilities," by G.C. Lee, Z. Liang, J.W. Song, J.D. Shen and W.C. Liu, 12/1/99, (PB2000-105993, A08, MF-A02).
- MCEER-99-0021 "Design and Retrofit Methodology for Building Structures with Supplemental Energy Dissipating Systems," by G. Pekcan, J.B. Mander and S.S. Chen, 12/31/99, (PB2000-105994, A11, MF-A03).
- MCEER-00-0001 "The Marmara, Turkey Earthquake of August 17, 1999: Reconnaissance Report," edited by C. Scawthorn; with major contributions by M. Bruneau, R. Eguchi, T. Holzer, G. Johnson, J. Mander, J. Mitchell, W. Mitchell, A. Papageorgiou, C. Scaethorn, and G. Webb, 3/23/00, (PB2000-106200, A11, MF-A03).
- MCEER-00-0002 "Proceedings of the MCEER Workshop for Seismic Hazard Mitigation of Health Care Facilities," edited by G.C. Lee, M. Ettouney, M. Grigoriu, J. Hauer and J. Nigg, 3/29/00, (PB2000-106892, A08, MF-A02).
- MCEER-00-0003 "The Chi-Chi, Taiwan Earthquake of September 21, 1999: Reconnaissance Report," edited by G.C. Lee and C.H. Loh, with major contributions by G.C. Lee, M. Bruneau, I.G. Buckle, S.E. Chang, P.J. Flores, T.D. O'Rourke, M. Shinozuka, T.T. Soong, C-H. Loh, K-C. Chang, Z-J. Chen, J-S. Hwang, M-L. Lin, G-Y. Liu, K-C. Tsai, G.C. Yao and C-L. Yen, 4/30/00, (PB2001-100980, A10, MF-A02).
- MCEER-00-0004 "Seismic Retrofit of End-Sway Frames of Steel Deck-Truss Bridges with a Supplemental Tendon System: Experimental and Analytical Investigation," by G. Pekcan, J.B. Mander and S.S. Chen, 7/1/00, (PB2001-100982, A10, MF-A02).
- MCEER-00-0005 "Sliding Fragility of Unrestrained Equipment in Critical Facilities," by W.H. Chong and T.T. Soong, 7/5/00, (PB2001-100983, A08, MF-A02).
- MCEER-00-0006 "Seismic Response of Reinforced Concrete Bridge Pier Walls in the Weak Direction," by N. Abo-Shadi, M. Saiidi and D. Sanders, 7/17/00, (PB2001-100981, A17, MF-A03).
- MCEER-00-0007 "Low-Cycle Fatigue Behavior of Longitudinal Reinforcement in Reinforced Concrete Bridge Columns," by J. Brown and S.K. Kunnath, 7/23/00, (PB2001-104392, A08, MF-A02).
- MCEER-00-0008 "Soil Structure Interaction of Bridges for Seismic Analysis," I. PoLam and H. Law, 9/25/00, (PB2001-105397, A08, MF-A02).
- MCEER-00-0009 "Proceedings of the First MCEER Workshop on Mitigation of Earthquake Disaster by Advanced Technologies (MEDAT-1), edited by M. Shinozuka, D.J. Inman and T.D. O'Rourke, 11/10/00, (PB2001-105399, A14, MF-A03).
- MCEER-00-0010 "Development and Evaluation of Simplified Procedures for Analysis and Design of Buildings with Passive Energy Dissipation Systems, Revision 01," by O.M. Ramirez, M.C. Constantinou, C.A. Kircher, A.S. Whittaker, M.W. Johnson, J.D. Gomez and C. Chrysostomou, 11/16/01, (PB2001-105523, A23, MF-A04).
- MCEER-00-0011 "Dynamic Soil-Foundation-Structure Interaction Analyses of Large Caissons," by C-Y. Chang, C-M. Mok, Z-L. Wang, R. Settgast, F. Waggoner, M.A. Ketchum, H.M. Gonnermann and C-C. Chin, 12/30/00, (PB2001-104373, A07, MF-A02).
- MCEER-00-0012 "Experimental Evaluation of Seismic Performance of Bridge Restrainers," by A.G. Vlassis, E.M. Maragakis and M. Saiid Saiidi, 12/30/00, (PB2001-104354, A09, MF-A02).
- MCEER-00-0013 "Effect of Spatial Variation of Ground Motion on Highway Structures," by M. Shinozuka, V. Saxena and G. Deodatis, 12/31/00, (PB2001-108755, A13, MF-A03).
- MCEER-00-0014 "A Risk-Based Methodology for Assessing the Seismic Performance of Highway Systems," by S.D. Werner, C.E. Taylor, J.E. Moore, II, J.S. Walton and S. Cho, 12/31/00, (PB2001-108756, A14, MF-A03).

- MCEER-01-0001 “Experimental Investigation of P-Delta Effects to Collapse During Earthquakes,” by D. Vian and M. Bruneau, 6/25/01, (PB2002-100534, A17, MF-A03).
- MCEER-01-0002 “Proceedings of the Second MCEER Workshop on Mitigation of Earthquake Disaster by Advanced Technologies (MEDAT-2),” edited by M. Bruneau and D.J. Inman, 7/23/01, (PB2002-100434, A16, MF-A03).
- MCEER-01-0003 “Sensitivity Analysis of Dynamic Systems Subjected to Seismic Loads,” by C. Roth and M. Grigoriu, 9/18/01, (PB2003-100884, A12, MF-A03).
- MCEER-01-0004 “Overcoming Obstacles to Implementing Earthquake Hazard Mitigation Policies: Stage 1 Report,” by D.J. Alesch and W.J. Petak, 12/17/01, (PB2002-107949, A07, MF-A02).
- MCEER-01-0005 “Updating Real-Time Earthquake Loss Estimates: Methods, Problems and Insights,” by C.E. Taylor, S.E. Chang and R.T. Eguchi, 12/17/01, (PB2002-107948, A05, MF-A01).
- MCEER-01-0006 “Experimental Investigation and Retrofit of Steel Pile Foundations and Pile Bents Under Cyclic Lateral Loadings,” by A. Shama, J. Mander, B. Blabac and S. Chen, 12/31/01, (PB2002-107950, A13, MF-A03).
- MCEER-02-0001 “Assessment of Performance of Bolu Viaduct in the 1999 Duzce Earthquake in Turkey” by P.C. Roussis, M.C. Constantinou, M. Erdik, E. Durukal and M. Dicleli, 5/8/02, (PB2003-100883, A08, MF-A02).
- MCEER-02-0002 “Seismic Behavior of Rail Counterweight Systems of Elevators in Buildings,” by M.P. Singh, Rildova and L.E. Suarez, 5/27/02. (PB2003-100882, A11, MF-A03).
- MCEER-02-0003 “Development of Analysis and Design Procedures for Spread Footings,” by G. Mylonakis, G. Gazetas, S. Nikolaou and A. Chauncey, 10/02/02, (PB2004-101636, A13, MF-A03, CD-A13).
- MCEER-02-0004 “Bare-Earth Algorithms for Use with SAR and LIDAR Digital Elevation Models,” by C.K. Huyck, R.T. Eguchi and B. Houshmand, 10/16/02, (PB2004-101637, A07, CD-A07).
- MCEER-02-0005 “Review of Energy Dissipation of Compression Members in Concentrically Braced Frames,” by K.Lee and M. Bruneau, 10/18/02, (PB2004-101638, A10, CD-A10).
- MCEER-03-0001 “Experimental Investigation of Light-Gauge Steel Plate Shear Walls for the Seismic Retrofit of Buildings” by J. Berman and M. Bruneau, 5/2/03, (PB2004-101622, A10, MF-A03, CD-A10).
- MCEER-03-0002 “Statistical Analysis of Fragility Curves,” by M. Shinozuka, M.Q. Feng, H. Kim, T. Uzawa and T. Ueda, 6/16/03, (PB2004-101849, A09, CD-A09).
- MCEER-03-0003 “Proceedings of the Eighth U.S.-Japan Workshop on Earthquake Resistant Design of Lifeline Facilities and Countermeasures Against Liquefaction,” edited by M. Hamada, J.P. Bardet and T.D. O’Rourke, 6/30/03, (PB2004-104386, A99, CD-A99).
- MCEER-03-0004 “Proceedings of the PRC-US Workshop on Seismic Analysis and Design of Special Bridges,” edited by L.C. Fan and G.C. Lee, 7/15/03, (PB2004-104387, A14, CD-A14).
- MCEER-03-0005 “Urban Disaster Recovery: A Framework and Simulation Model,” by S.B. Miles and S.E. Chang, 7/25/03, (PB2004-104388, A07, CD-A07).
- MCEER-03-0006 “Behavior of Underground Piping Joints Due to Static and Dynamic Loading,” by R.D. Meis, M. Maragakis and R. Siddharthan, 11/17/03, (PB2005-102194, A13, MF-A03, CD-A00).
- MCEER-03-0007 “Seismic Vulnerability of Timber Bridges and Timber Substructures,” by A.A. Shama, J.B. Mander, I.M. Friedland and D.R. Allicock, 12/15/03.
- MCEER-04-0001 “Experimental Study of Seismic Isolation Systems with Emphasis on Secondary System Response and Verification of Accuracy of Dynamic Response History Analysis Methods,” by E. Wolff and M. Constantinou, 1/16/04 (PB2005-102195, A99, MF-E08, CD-A00).

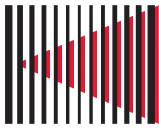
- MCEER-04-0002 "Tension, Compression and Cyclic Testing of Engineered Cementitious Composite Materials," by K. Kesner and S.L. Billington, 3/1/04, (PB2005-102196, A08, CD-A08).
- MCEER-04-0003 "Cyclic Testing of Braces Laterally Restrained by Steel Studs to Enhance Performance During Earthquakes," by O.C. Celik, J.W. Berman and M. Bruneau, 3/16/04, (PB2005-102197, A13, MF-A03, CD-A00).
- MCEER-04-0004 "Methodologies for Post Earthquake Building Damage Detection Using SAR and Optical Remote Sensing: Application to the August 17, 1999 Marmara, Turkey Earthquake," by C.K. Huyck, B.J. Adams, S. Cho, R.T. Eguchi, B. Mansouri and B. Houshmand, 6/15/04, (PB2005-104888, A10, CD-A00).
- MCEER-04-0005 "Nonlinear Structural Analysis Towards Collapse Simulation: A Dynamical Systems Approach," by M.V. Sivaselvan and A.M. Reinhorn, 6/16/04, (PB2005-104889, A11, MF-A03, CD-A00).
- MCEER-04-0006 "Proceedings of the Second PRC-US Workshop on Seismic Analysis and Design of Special Bridges," edited by G.C. Lee and L.C. Fan, 6/25/04, (PB2005-104890, A16, CD-A00).
- MCEER-04-0007 "Seismic Vulnerability Evaluation of Axially Loaded Steel Built-up Laced Members," by K. Lee and M. Bruneau, 6/30/04, (PB2005-104891, A16, CD-A00).
- MCEER-04-0008 "Evaluation of Accuracy of Simplified Methods of Analysis and Design of Buildings with Damping Systems for Near-Fault and for Soft-Soil Seismic Motions," by E.A. Pavlou and M.C. Constantinou, 8/16/04, (PB2005-104892, A08, MF-A02, CD-A00).
- MCEER-04-0009 "Assessment of Geotechnical Issues in Acute Care Facilities in California," by M. Lew, T.D. O'Rourke, R. Dobry and M. Koch, 9/15/04, (PB2005-104893, A08, CD-A00).
- MCEER-04-0010 "Scissor-Jack-Damper Energy Dissipation System," by A.N. Sigaher-Boyle and M.C. Constantinou, 12/1/04 (PB2005-108221).
- MCEER-04-0011 "Seismic Retrofit of Bridge Steel Truss Piers Using a Controlled Rocking Approach," by M. Pollino and M. Bruneau, 12/20/04 (PB2006-105795).
- MCEER-05-0001 "Experimental and Analytical Studies of Structures Seismically Isolated with an Uplift-Restraint Isolation System," by P.C. Roussis and M.C. Constantinou, 1/10/05 (PB2005-108222).
- MCEER-05-0002 "A Versatile Experimentation Model for Study of Structures Near Collapse Applied to Seismic Evaluation of Irregular Structures," by D. Kusumastuti, A.M. Reinhorn and A. Rutenberg, 3/31/05 (PB2006-101523).
- MCEER-05-0003 "Proceedings of the Third PRC-US Workshop on Seismic Analysis and Design of Special Bridges," edited by L.C. Fan and G.C. Lee, 4/20/05, (PB2006-105796).
- MCEER-05-0004 "Approaches for the Seismic Retrofit of Braced Steel Bridge Piers and Proof-of-Concept Testing of an Eccentrically Braced Frame with Tubular Link," by J.W. Berman and M. Bruneau, 4/21/05 (PB2006-101524).
- MCEER-05-0005 "Simulation of Strong Ground Motions for Seismic Fragility Evaluation of Nonstructural Components in Hospitals," by A. Wanitkorkul and A. Filiatrault, 5/26/05 (PB2006-500027).
- MCEER-05-0006 "Seismic Safety in California Hospitals: Assessing an Attempt to Accelerate the Replacement or Seismic Retrofit of Older Hospital Facilities," by D.J. Alesch, L.A. Arendt and W.J. Petak, 6/6/05 (PB2006-105794).
- MCEER-05-0007 "Development of Seismic Strengthening and Retrofit Strategies for Critical Facilities Using Engineered Cementitious Composite Materials," by K. Kesner and S.L. Billington, 8/29/05 (PB2006-111701).
- MCEER-05-0008 "Experimental and Analytical Studies of Base Isolation Systems for Seismic Protection of Power Transformers," by N. Murota, M.Q. Feng and G-Y. Liu, 9/30/05 (PB2006-111702).
- MCEER-05-0009 "3D-BASIS-ME-MB: Computer Program for Nonlinear Dynamic Analysis of Seismically Isolated Structures," by P.C. Tsopelas, P.C. Roussis, M.C. Constantinou, R. Buchanan and A.M. Reinhorn, 10/3/05 (PB2006-111703).

- MCEER-05-0010 “Steel Plate Shear Walls for Seismic Design and Retrofit of Building Structures,” by D. Vian and M. Bruneau, 12/15/05 (PB2006-111704).
- MCEER-05-0011 “The Performance-Based Design Paradigm,” by M.J. Astrella and A. Whittaker, 12/15/05 (PB2006-111705).
- MCEER-06-0001 “Seismic Fragility of Suspended Ceiling Systems,” H. Badillo-Almaraz, A.S. Whittaker, A.M. Reinhorn and G.P. Cimellaro, 2/4/06 (PB2006-111706).
- MCEER-06-0002 “Multi-Dimensional Fragility of Structures,” by G.P. Cimellaro, A.M. Reinhorn and M. Bruneau, 3/1/06 (PB2007-106974, A09, MF-A02, CD A00).
- MCEER-06-0003 “Built-Up Shear Links as Energy Dissipators for Seismic Protection of Bridges,” by P. Dusicka, A.M. Itani and I.G. Buckle, 3/15/06 (PB2006-111708).
- MCEER-06-0004 “Analytical Investigation of the Structural Fuse Concept,” by R.E. Vargas and M. Bruneau, 3/16/06 (PB2006-111709).
- MCEER-06-0005 “Experimental Investigation of the Structural Fuse Concept,” by R.E. Vargas and M. Bruneau, 3/17/06 (PB2006-111710).
- MCEER-06-0006 “Further Development of Tubular Eccentrically Braced Frame Links for the Seismic Retrofit of Braced Steel Truss Bridge Piers,” by J.W. Berman and M. Bruneau, 3/27/06 (PB2007-105147).
- MCEER-06-0007 “REDARS Validation Report,” by S. Cho, C.K. Huyck, S. Ghosh and R.T. Eguchi, 8/8/06 (PB2007-106983).
- MCEER-06-0008 “Review of Current NDE Technologies for Post-Earthquake Assessment of Retrofitted Bridge Columns,” by J.W. Song, Z. Liang and G.C. Lee, 8/21/06 06 (PB2007-106984).
- MCEER-06-0009 “Liquefaction Remediation in Silty Soils Using Dynamic Compaction and Stone Columns,” by S. Thevanayagam, G.R. Martin, R. Nashed, T. Shenthan, T. Kanagalingam and N. Ecemis, 8/28/06 06 (PB2007-106985).
- MCEER-06-0010 “Conceptual Design and Experimental Investigation of Polymer Matrix Composite Infill Panels for Seismic Retrofitting,” by W. Jung, M. Chiewanichakorn and A.J. Aref, 9/21/06 (PB2007-106986).
- MCEER-06-0011 “A Study of the Coupled Horizontal-Vertical Behavior of Elastomeric and Lead-Rubber Seismic Isolation Bearings,” by G.P. Warn and A.S. Whittaker, 9/22/06 (PB2007-108679).
- MCEER-06-0012 “Proceedings of the Fourth PRC-US Workshop on Seismic Analysis and Design of Special Bridges: Advancing Bridge Technologies in Research, Design, Construction and Preservation,” Edited by L.C. Fan, G.C. Lee and L. Ziang, 10/12/06 (PB2007-109042).
- MCEER-06-0013 “Cyclic Response and Low Cycle Fatigue Characteristics of Plate Steels,” by P. Dusicka, A.M. Itani and I.G. Buckle, 11/1/06 06 (PB2007-106987).
- MCEER-06-0014 “Proceedings of the Second US-Taiwan Bridge Engineering Workshop,” edited by W.P. Yen, J. Shen, J-Y. Chen and M. Wang, 11/15/06.
- MCEER-06-0015 “User Manual and Technical Documentation for the REDARS™ Import Wizard,” by S. Cho, S. Ghosh, C.K. Huyck and S.D. Werner, 11/30/06 (PB2007-114766).
- MCEER-06-0016 “Hazard Mitigation Strategy and Monitoring Technologies for Urban and Infrastructure Public Buildings: Proceedings of the China-US Workshops,” edited by X.Y. Zhou, A.L. Zhang, G.C. Lee and M. Tong, 12/12/06 (PB2008-500018).
- MCEER-07-0001 “Static and Kinetic Coefficients of Friction for Rigid Blocks,” by C. Kafali, S. Fathali, M. Grigoriu and A.S. Whittaker, 3/20/07 (PB2007-114767).

- MCEER-07-0002 “Hazard Mitigation Investment Decision Making: Organizational Response to Legislative Mandate,” by L.A. Arendt, D.J. Alesch and W.J. Petak, 4/9/07 (PB2007-114768).
- MCEER-07-0003 “Seismic Behavior of Bidirectional-Resistant Ductile End Diaphragms with Unbonded Braces in Straight or Skewed Steel Bridges,” by O. Celik and M. Bruneau, 4/11/07 (PB2008-105141).
- MCEER-07-0004 “Modeling Pile Behavior in Large Pile Groups Under Lateral Loading,” by A.M. Dodds and G.R. Martin, 4/16/07(PB2008-105142).
- MCEER-07-0005 “Experimental Investigation of Blast Performance of Seismically Resistant Concrete-Filled Steel Tube Bridge Piers,” by S. Fujikura, M. Bruneau and D. Lopez-Garcia, 4/20/07 (PB2008-105143).
- MCEER-07-0006 “Seismic Analysis of Conventional and Isolated Liquefied Natural Gas Tanks Using Mechanical Analogs,” by I.P. Christovasilis and A.S. Whittaker, 5/1/07.
- MCEER-07-0007 “Experimental Seismic Performance Evaluation of Isolation/Restraint Systems for Mechanical Equipment – Part 1: Heavy Equipment Study,” by S. Fathali and A. Filiatrault, 6/6/07 (PB2008-105144).
- MCEER-07-0008 “Seismic Vulnerability of Timber Bridges and Timber Substructures,” by A.A. Sharma, J.B. Mander, I.M. Friedland and D.R. Allicock, 6/7/07 (PB2008-105145).
- MCEER-07-0009 “Experimental and Analytical Study of the XY-Friction Pendulum (XY-FP) Bearing for Bridge Applications,” by C.C. Marin-Artieda, A.S. Whittaker and M.C. Constantinou, 6/7/07.
- MCEER-07-0010 “Proceedings of the PRC-US Earthquake Engineering Forum for Young Researchers,” Edited by G.C. Lee and X.Z. Qi, 6/8/07.
- MCEER-07-0011 “Design Recommendations for Perforated Steel Plate Shear Walls,” by R. Purba and M. Bruneau, 6/18/07.
- MCEER-07-0012 “Performance of Seismic Isolation Hardware Under Service and Seismic Loading,” by M.C. Constantinou, A.S. Whittaker, Y. Kalpakidis, D.M. Fenz and G.P. Warn, 8/27/07.
- MCEER-07-0013 “Experimental Evaluation of the Seismic Performance of Hospital Piping Subassemblies,” by E.R. Goodwin, E. Maragakis and A.M. Itani, 9/4/07.
- MCEER-07-0014 “A Simulation Model of Urban Disaster Recovery and Resilience: Implementation for the 1994 Northridge Earthquake,” by S. Miles and S.E. Chang, 9/7/07.
- MCEER-07-0015 “Statistical and Mechanistic Fragility Analysis of Concrete Bridges,” by M. Shinozuka, S. Banerjee and S-H. Kim, 9/10/07.
- MCEER-07-0016 “Three-Dimensional Modeling of Inelastic Buckling in Frame Structures,” by M. Schachter and AM. Reinhorn, 9/13/07.
- MCEER-07-0017 “Modeling of Seismic Wave Scattering on Pile Groups and Caissons,” by I. Po Lam, H. Law and C.T. Yang, 9/17/07.
- MCEER-07-0018 “Bridge Foundations: Modeling Large Pile Groups and Caissons for Seismic Design,” by I. Po Lam, H. Law and G.R. Martin (Coordinating Author), 12/1/07.
- MCEER-07-0019 “Principles and Performance of Roller Seismic Isolation Bearings for Highway Bridges,” by G.C. Lee, Y.C. Ou, Z. Liang, T.C. Niu and J. Song, 12/10/07.
- MCEER-07-0020 “Centrifuge Modeling of Permeability and Pinning Reinforcement Effects on Pile Response to Lateral Spreading,” by L.L. Gonzalez-Lagos, T. Abdoun and R. Dobry, 12/10/07.
- MCEER-07-0021 “Damage to the Highway System from the Pisco, Perú Earthquake of August 15, 2007,” by J.S. O’Connor, L. Mesa and M. Nykamp, 12/10/07.
- MCEER-07-0022 “Experimental Seismic Performance Evaluation of Isolation/Restraint Systems for Mechanical Equipment – Part 2: Light Equipment Study,” by S. Fathali and A. Filiatrault, 12/13/07.


MCEER-07-0023 "Fragility Considerations in Highway Bridge Design," by M. Shinozuka, S. Banerjee and S.H. Kim, 12/14/07.

MCEER-07-0024 "Performance Estimates for Seismically Isolated Bridges," by G.P. Warn and A.S. Whittaker, 12/30/07.



MCEER
EARTHQUAKE ENGINEERING TO EXTREME EVENTS

University at Buffalo, The State University of New York
Red Jacket Quadrangle ▪ Buffalo, New York 14261
Phone: (716) 645-3391 ▪ Fax: (716) 645-3399
E-mail: mceer@buffalo.edu ▪ WWW Site <http://mceer.buffalo.edu>



University at Buffalo *The State University of New York*

ISSN 1520-295X